



QA: QA

TDR-MGR-HS-000002 REV 01

February 2007

## **Thermal Testing Measurements Report**

Prepared for:  
U.S. Department of Energy  
Office of Civilian Radioactive Waste Management  
Office of Repository Development  
1551 Hillshire Drive  
Las Vegas, Nevada 89134-6321

Prepared by:  
Sandia National Laboratories  
OCRWM Lead Laboratory for Repository Systems  
1180 Town Center Drive  
Las Vegas, Nevada 89144

Under Contract Number  
DE-AC04-94AL85000

#### **DISCLAIMER**


This report was prepared as an account of work sponsored by an agency of the United States Government. Neither the United States Government nor any agency thereof, nor any of their employees, nor any of their contractors, subcontractors or their employees, makes any warranty, express or implied, or assumes any legal liability or responsibility for the accuracy, completeness, or any third party's use or the results of such use of any information, apparatus, product, or process disclosed, or represents that its use would not infringe privately owned rights. Reference herein to any specific commercial product, process, or service by trade name, trademark, manufacturer, or otherwise, does not necessarily constitute or imply its endorsement, recommendation, or favoring by the United States Government or any agency thereof or its contractors or subcontractors. The views and opinions of authors expressed herein do not necessarily state or reflect those of the United States Government or any agency thereof.

Originator:

  
\_\_\_\_\_  
R.L. Jones

2-19-2007  
Date

Checker:

  
\_\_\_\_\_  
A. Sanchez

2-19-2007  
Date

QCS/Lead Lab QA Reviewer:

  
\_\_\_\_\_  
C. Beach

2-19-2007  
Date

Responsible Manager:

  
\_\_\_\_\_  
G. Freeze

2/19/07  
Date

INTENTIONALLY LEFT BLANK

## CHANGE HISTORY

<u>Revision Number</u>	<u>Interim Change No.</u>	<u>Date</u>	<u>Description of Change</u>
00		September 2004	Initial issue. Although this is the initial issue of this report number, this report is a rewrite of ANL-NBS-HS-000041, Rev. 00 to correct identified deficiencies. These deficiencies were documented in BSC Audit Report BQAP-BSC-03-02, Deficiency Reports BSC(B)-03-D-043 and BSC(B)-03-D-045 and Condition Reports 165, 288 657 and 1936. The report also contains an expanded discussion on introduced materials to DST waters.
01		February 2007	TDR-MGR-HS-000002 is being revised to incorporate a review of data collected from the DST cooling phase. Discussion of the cooling phase data has been added to the report, along with new graphics and charts depicting DST data histories of both the heating and cooling phases. Discussion of major test events and/or anomalies has also been added. This revision also addresses condition description #3 from CR 5383. Table 6.3-32 entries for samples BH 59-2, dated 5/23/00, and BH 59-4, dated 1/26/99, were added to the table because they were inadvertently left off the original version. Tables 4-4, 4-5, and 4-6 were removed from the report because their content was irrelevant to the purpose and objective of this revision. Finally, the report has been reorganized and reformatted, with figures and tables co-located with the text, and minor editorial corrections have been made. Certain elements of this revision were begun under TWP-MGR-PA-000019 (REV 01), and the report sent into review, prior to the addition of new work scope described in the current TWP (TWP-NBS-HS-000017 REV 00). The sequence of draft designators has been maintained to reflect those circumstances.

INTENTIONALLY LEFT BLANK

# CONTENTS

	<b>Page</b>
ACRONYMS AND ABBREVIATIONS .....	xxiii
1. PURPOSE.....	1-1
2. QUALITY ASSURANCE.....	2-1
2.1 PROCEDURAL COMPLIANCE.....	2-1
3. USE OF SOFTWARE .....	3-1
4. INPUTS.....	4-1
4.1 LARGE BLOCK TEST .....	4-1
4.2 SINGLE HEATER TEST .....	4-1
4.3 DRIFT SCALE TEST.....	4-1
4.4 CRITERIA .....	4-1
4.5 CODES AND STANDARDS.....	4-3
5. ASSUMPTIONS.....	5-1
5.1 AIR PERMEABILITY ANALYSIS.....	5-1
6. DISCUSSION OF MEASUREMENTS .....	6-1
6.1 LARGE BLOCK TEST .....	6-2
6.1.1 LBT Thermal Measurements .....	6-11
6.1.1.1 Heater Power .....	6-11
6.1.1.1.1 Results: Heater Power.....	6-11
6.1.1.1.2 Measurement Uncertainty: Heater Power .....	6-12
6.1.1.2 Temperatures .....	6-12
6.1.1.2.1 Results: Temperatures.....	6-13
6.1.1.2.2 Measurement Uncertainty: Temperatures.....	6-15
6.1.2 LBT Hydrological Measurements.....	6-15
6.1.2.1 Electrical Resistance Tomography .....	6-15
6.1.2.1.1 Data Processing.....	6-17
6.1.2.1.2 Results: ERT .....	6-18
6.1.2.1.3 Measurement Uncertainty: ERT .....	6-21
6.1.2.2 Neutron Logging .....	6-21
6.1.2.2.1 Results: Neutron Logging.....	6-22
6.1.2.2.2 Measurement Uncertainty: Neutron Logging .....	6-25
6.1.2.3 Passive Monitoring—Gas Pressure and Relative Humidity.....	6-25
6.1.2.3.1 Results: Gas Pressure and Relative Humidity.....	6-26
6.1.2.3.2 Measurement Uncertainty: Relative Humidity .....	6-28
6.1.2.4 Laboratory Parameters—Matrix Permeability, Density, Porosity, Micro-Pore Structure, Fracture Flow, and Matrix Imbibition Visualization.....	6-28

## CONTENTS (Continued)

	<b>Page</b>
6.1.2.4.1	Results: Matrix Permeability, Density, Porosity, Micro-Pore Structure, Fracture Flow, and Matrix Imbibition Visualization..... 6-29
6.1.2.4.2	Measurement Uncertainty: Matrix Permeability, Density, Porosity, Fracture Flow, and Matrix Imbibition Visualization ..... 6-33
6.1.3	LBT Mechanical Measurements ..... 6-33
6.1.3.1	Multipoint Borehole Extensometer Displacements..... 6-33
6.1.3.1.1	Results: MPBX Displacements..... 6-34
6.1.3.1.2	Measurement Uncertainty: MPBX Displacements ..... 6-35
6.1.3.2	Fracture Monitoring ..... 6-36
6.1.3.2.1	Results: Fracture Monitoring ..... 6-36
6.1.3.2.2	Measurement Uncertainty: Fracture Monitoring ..... 6-37
6.1.4	LBT Miscellaneous Measurements and Observations..... 6-37
6.1.4.1	Fracture Mapping ..... 6-37
6.1.4.1.1	Results: Fracture Mapping..... 6-37
6.1.4.1.2	Measurement Uncertainty: Fracture Mapping ..... 6-38
6.1.4.2	Video Observation of Boreholes ..... 6-38
6.1.4.2.1	Results: Video Observation of Boreholes..... 6-38
6.1.4.2.2	Measurement Uncertainty: Video Observation of Boreholes ..... 6-38
6.1.4.3	Microbial Observation..... 6-38
6.1.4.3.1	Results: Microbial Observation ..... 6-39
6.1.4.3.2	Measurement Uncertainty: Microbial Observation ..... 6-39
6.2	SINGLE HEATER TEST ..... 6-39
6.2.1	SHT Thermal Measurements ..... 6-51
6.2.1.1	Heater Power ..... 6-51
6.2.1.1.1	Results: Heater Power..... 6-52
6.2.1.1.2	Measurement Uncertainty: Heater Power ..... 6-52
6.2.1.2	Temperatures ..... 6-52
6.2.1.2.1	Results: Temperatures..... 6-53
6.2.1.2.2	Measurement Uncertainty: Temperatures..... 6-56
6.2.1.3	Laboratory Thermal Conductivity..... 6-56
6.2.1.3.1	Results: Laboratory Thermal Conductivity..... 6-57
6.2.1.3.2	Measurement Uncertainty: Laboratory Thermal Conductivity..... 6-57
6.2.2	SHT Hydrological Measurements..... 6-57
6.2.2.1	Electrical Resistance Tomography ..... 6-58
6.2.2.1.1	Results: ERT ..... 6-58
6.2.2.1.2	Measurement Uncertainty: ERT ..... 6-61
6.2.2.2	Ground Penetrating Radar ..... 6-61



## CONTENTS (Continued)

	<b>Page</b>
6.2.2.2.1	Results: GPR..... 6-62
6.2.2.2.2	Measurement Uncertainty: GPR..... 6-66
6.2.2.3	Neutron Logging ..... 6-66
6.2.2.3.1	Results: Neutron Logging ..... 6-67
6.2.2.3.2	Measurement Uncertainty: Neutron Logging ..... 6-68
6.2.2.4	Active Pneumatic Testing and Passive Hydrological Monitoring..... 6-68
6.2.2.4.1	Results: Active Pneumatic Testing and Passive Hydrological Monitoring ..... 6-70
6.2.2.4.2	Measurement Uncertainty: Active Pneumatic Testing and Passive Hydrological Monitoring..... 6-78
6.2.2.5	Laboratory Parameters—Saturation, Porosity, Density, Moisture Retention Curves..... 6-79
6.2.2.5.1	Results: Laboratory Parameters—Saturation, Porosity, Density, Moisture Retention Curves..... 6-80
6.2.2.5.2	Measurement Uncertainty: Laboratory Parameters—Saturation, Porosity, Density, Moisture Retention Curves ..... 6-85
6.2.3	SHT Mechanical Measurements ..... 6-86
6.2.3.1	MPBX Displacements ..... 6-87
6.2.3.1.1	Results: MPBX Displacements..... 6-90
6.2.3.1.2	Measurement Uncertainty: MPBX Displacements ..... 6-93
6.2.3.2	Borehole Jack ..... 6-95
6.2.3.2.1	Results: Borehole Jack ..... 6-95
6.2.3.2.2	Measurement Uncertainty: Borehole Jack ..... 6-96
6.2.3.3	Rock Bolt Load ..... 6-96
6.2.3.3.1	Results: Rock Bolt Load ..... 6-97
6.2.3.3.2	Measurement Uncertainty: Rock Bolt Load ..... 6-98
6.2.3.4	Laboratory Parameters—Thermal Expansion, Young’s Modulus, Poisson’s Ratio, and Peak Stress..... 6-99
6.2.3.4.1	Results: Laboratory Parameters—Thermal Expansion, Young’s Modulus, Poisson’s Ratio, Peak Stress, and Axial Strain at Peak Stress..... 6-99
6.2.3.4.2	Measurement Uncertainty: Laboratory Parameters—Thermal Expansion, Young’s Modulus, Poisson’s Ratio, and Peak Stress ..... 6-105
6.2.3.4.3	Measurement Uncertainty: Rock Mass Thermal Expansion..... 6-105
6.2.4	SHT Chemical Measurements ..... 6-105
6.2.4.1	Aqueous Chemistry ..... 6-105
6.2.4.1.1	Field Sampling..... 6-106
6.2.4.1.2	Results: Aqueous Chemistry..... 6-106

## CONTENTS (Continued)

	<b>Page</b>
6.2.4.1.3	Measurement Uncertainty: Aqueous Chemistry ..... 6-107
6.2.4.2	Mineralogic and Petrologic Analyses..... 6-107
6.2.4.2.1	Results: Mineralogy of the Preheating Natural Fracture System..... 6-109
6.2.4.2.2	Results: Evidence of Mineral Deposition ..... 6-112
6.2.4.2.3	Measurement Uncertainty: Mineralogic and Petrologic Analyses..... 6-113
6.2.5	SHT Miscellaneous Measurements and Observations..... 6-113
6.2.5.1	Fracture Mapping ..... 6-114
6.2.5.1.1	Results: Fracture Mapping..... 6-114
6.2.5.1.2	Measurement Uncertainty: Fracture Mapping ..... 6-115
6.2.5.2	Infrared Imaging..... 6-115
6.2.5.2.1	Results: Infrared Imaging..... 6-116
6.2.5.2.2	Measurement Uncertainty: Infrared Imaging..... 6-116
6.2.5.3	Borehole Video Logging..... 6-116
6.2.5.3.1	Results: Borehole Video Logging..... 6-116
6.2.5.3.2	Measurement Uncertainty: Borehole Video Logging ..... 6-116
6.3	DRIFT SCALE TEST ..... 6-117
6.3.1	DST Thermal Measurements ..... 6-153
6.3.1.1	Heater Power ..... 6-153
6.3.1.1.1	Results: Heater Power..... 6-154
6.3.1.1.2	Measurement Uncertainty: Heater Power ..... 6-155
6.3.1.2	Temperatures ..... 6-155
6.3.1.2.1	Results: Temperatures..... 6-156
6.3.1.2.2	Measurement Uncertainty: Temperatures..... 6-163
6.3.1.2.3	RTD Failures..... 6-163
6.3.1.3	Laboratory Parameter: Thermal Conductivity ..... 6-163
6.3.1.3.1	Results: Thermal Conductivity ..... 6-164
6.3.1.3.2	Measurement Uncertainty: Thermal Conductivity..... 6-166
6.3.1.4	Field Parameters (REKA–Thermal Conductivity and Thermal Diffusivity)..... 6-166
6.3.1.4.1	Results: Field Thermal Conductivity and Thermal Diffusivity..... 6-167
6.3.1.4.2	Measurement Uncertainty: Field Thermal Conductivity and Thermal Diffusivity..... 6-168
6.3.2	DST Hydrological Measurements..... 6-168
6.3.2.1	Electrical Resistance Tomography ..... 6-168
6.3.2.1.1	Results: ERT ..... 6-169
6.3.2.1.2	Measurement Uncertainty: ERT Saturation Changes..... 6-177
6.3.2.2	Ground Penetrating Radar ..... 6-177

## CONTENTS (Continued)

	<b>Page</b>
6.3.2.2.1	Results: GPR..... 6-178
6.3.2.2.2	Measurement Uncertainty: GPR..... 6-180
6.3.2.3	Neutron Logging ..... 6-180
6.3.2.3.1	Results: Neutron Logging ..... 6-180
6.3.2.3.2	Measurement Uncertainty: Moisture Content Determined by Neutron Logging ..... 6-182
6.3.2.4	Active Pneumatic Testing and Passive Hydrological Monitoring Measurements ..... 6-183
6.3.2.4.1	Results: Active Pneumatic Testing and Passive Hydrological Monitoring ..... 6-186
6.3.2.4.2	Measurement Uncertainty: Active Pneumatic Testing and Passive Hydrological Monitoring Measurements ..... 6-194
6.3.2.5	Laboratory Hydrological Parameters ..... 6-194
6.3.2.5.1	Results: Laboratory Hydrological Parameters ..... 6-194
6.3.2.5.2	Measurement Uncertainty: Laboratory Hydrological Parameters..... 6-200
6.3.2.6	Heat and Mass Flow through the Bulkhead ..... 6-201
6.3.3	DST Mechanical Measurements ..... 6-203
6.3.3.1	Multipoint Borehole Extensometers..... 6-203
6.3.3.1.1	Results: MPBX Displacements..... 6-206
6.3.3.1.2	Measurement Uncertainty: MPBX Displacements ..... 6-212
6.3.3.2	Cross-Drift Extensometers ..... 6-216
6.3.3.2.1	Results: CDEX Displacements ..... 6-217
6.3.3.2.2	Measurement Uncertainty: CDEX Displacements ..... 6-218
6.3.3.3	Strains..... 6-218
6.3.3.3.1	Results: Strains..... 6-221
6.3.3.3.2	Measurement Uncertainty: Strains..... 6-223
6.3.3.4	Acoustic Emission..... 6-224
6.3.3.4.1	Results: Acoustic Emissions ..... 6-224
6.3.3.4.2	Measurement Uncertainty: Acoustic Emissions ..... 6-227
6.3.3.5	Laboratory Mechanical Parameters..... 6-227
6.3.3.5.1	Results: Thermal Expansion ..... 6-227
6.3.3.5.2	Results: Elastic Constants and Strength Parameters of DST Intact Rock ..... 6-228
6.3.3.5.3	Results: Elastic Constants and Strength Properties of Cast-in-Place Concrete Samples..... 6-229
6.3.3.5.4	Measurement Uncertainty: Laboratory Mechanical Parameters ..... 6-231
6.3.3.6	Field Mechanical Parameters ..... 6-232
6.3.3.6.1	Results: Plate Loading Test..... 6-232

## CONTENTS (Continued)

	<b>Page</b>
6.3.3.6.2	Results: In Situ Stress Measurements ..... 6-232
6.3.3.6.3	Results: Rock Mass Thermal Expansion ..... 6-233
6.3.3.6.4	Measurement Uncertainty: Field Mechanical Parameters ..... 6-234
6.3.3.7	Scaling along the Roof of the Heated Drift ..... 6-235
6.3.3.7.1	Background ..... 6-235
6.3.3.7.2	Observations ..... 6-235
6.3.3.7.3	Conclusions ..... 6-237
6.3.3.7.4	Records ..... 6-237
6.3.4	DST Chemical Measurements ..... 6-239
6.3.4.1	DST Aqueous Chemistry ..... 6-239
6.3.4.1.1	Sampling Procedures ..... 6-241
6.3.4.1.2	Results: Aqueous Chemistry ..... 6-243
6.3.4.1.3	Measurement Uncertainty: Aqueous Chemistry ..... 6-272
6.3.4.1.4	CHEMSAMP Water Sample Chemistry ..... 6-274
6.3.4.2	Gas Chemistry ..... 6-285
6.3.4.2.1	Gas Sampling ..... 6-285
6.3.4.2.2	Results: CO <sub>2</sub> Concentration ..... 6-286
6.3.4.2.3	Results: Isotopic Composition of CO <sub>2</sub> ..... 6-301
6.3.4.2.4	Results: Isotopic Analyses of Vapor Condensate Samples ..... 6-301
6.3.4.2.5	Measurement Uncertainty: Concentration and Isotopic Ratios ..... 6-310
6.3.4.3	DST Mineralogic and Petrologic Analyses ..... 6-312
6.3.4.3.1	Results: Mineralogy of the Preheating Natural Fracture System ..... 6-313
6.3.4.3.2	Results: Evidence of Mineral Deposition ..... 6-314
6.3.4.3.3	Results: Evidence of Mineral Dissolution ..... 6-314
6.3.4.3.4	Results: Mineral Deposition Associated with Man-Made Materials Interactions ..... 6-315
6.3.4.3.5	Measurement Uncertainty: Mineralogic and Petrologic Analyses ..... 6-315
6.3.4.4	Strontium and Uranium in Water Samples ..... 6-316
6.3.4.4.1	Results: Strontium and Uranium in Water Samples ..... 6-316
6.3.4.4.2	Measurement Uncertainty: Strontium and Uranium in Water Samples ..... 6-320
6.3.4.5	Chemical Effects of Introduced Materials in the DST ..... 6-320
6.3.4.5.1	Thermal Environments of Sample Collection ..... 6-321
6.3.4.5.2	Aqueous Geochemistry of Materials Interaction ..... 6-321
6.3.4.5.3	Experimental Verification of Materials Interactions ..... 6-338
6.3.4.5.4	Summary and Conclusions ..... 6-344

## CONTENTS (Continued)

	<b>Page</b>
6.3.5 DST Miscellaneous Measurements.....	6-344
6.3.5.1 Fracture Mapping .....	6-344
6.3.5.1.1 Results: Fracture Mapping .....	6-345
6.3.5.1.2 Measurement Uncertainty: Fracture Mapping .....	6-345
6.3.5.2 Borehole Video Logging.....	6-345
6.3.5.2.1 Results: Borehole Video Logging.....	6-345
6.3.5.2.2 Measurement Uncertainty: Borehole Video Logging .....	6-345
6.3.5.3 Waste Package Materials.....	6-345
6.3.5.4 Microbiological Investigations.....	6-346
7. SUMMARY .....	7-1
7.1 DISCUSSION .....	7-1
7.2 YUCCA MOUNTAIN REVIEW PLAN CRITERIA ASSESSMENT.....	7-2
8. INPUTS AND REFERENCES.....	8-1
8.1 DOCUMENTS CITED .....	8-1
8.2 CODES, STANDARDS, REGULATIONS, AND PROCEDURES.....	8-7
8.3 SOURCE DATA, LISTED BY DATA TRACKING NUMBER .....	8-9
8.4 SUMMARY DATA, LISTED BY DATA TRACKING NUMBER.....	8-32

INTENTIONALLY LEFT BLANK

## FIGURES

	<b>Page</b>
6.1-1. LBT Block of Topopah Spring Tuff at Fran Ridge .....	6-4
6.1-2. LBT Vertical Boreholes Drilled from the Top of the Block.....	6-5
6.1-3. LBT Sensor Boreholes Drilled from the North Side of the Block.....	6-6
6.1-4. LBT Boreholes Drilled from the East Side of the Block.....	6-7
6.1-5. LBT Sensor Boreholes Drilled from the West Side of the Block.....	6-8
6.1-6. Power History of LBT Heater EH1 .....	6-12
6.1-7. Temperature History at LBT TT1-14 .....	6-14
6.1-8. Temperature History at LBT TT2-14 .....	6-14
6.1-9. LBT Layout of ERT Electrodes.....	6-16
6.1-10. Distribution of Moisture Content in Two Horizontal Planes from LBT ERT.....	6-19
6.1-11. Distribution of Moisture Content in Two Vertical Planes in LBT .....	6-20
6.1-12. Initial Fraction Volume Water Content Measured in LBT Vertical Borehole TN3 Using Neutron Logging (Preheating/Baseline).....	6-23
6.1-13. Difference Fraction Volume Water Content Measured in LBT Borehole TN3 Using Neutron Logging (March 11 to June 11, 1997).....	6-24
6.1-14. Difference Fraction Volume Water Content Measured in LBT Borehole TN3 Using Neutron Logging (July 8, 1997, to September 15, 1998).....	6-25
6.1-15. Temperature Measured in LBT Borehole WH-2 as a Function of Time.....	6-27
6.1-16. Relative Humidity Measured by the Humicap in LBT Borehole WH-2 as a Function of Time.....	6-27
6.1-17. Images of Imbibition under Thermal Gradient: 0.26 m Water Head at 7.2 Hours (left) and 0.46 m Water Head at 0.67 Hours (right).....	6-32
6.1-18. MPBX Borehole Locations, Viewed from the South Face.....	6-34
6.1-19. East–West Displacement for WM-2 Anchor 4 and Temperature at Depth of 1.2 m.....	6-35
6.2-1. Schematic Plan View of ESF Thermal Test Facility Including the SHT .....	6-40
6.2-2. Schematic SHT Layout of the Instrumentation Boreholes .....	6-41
6.2-3. SHT Power History.....	6-52
6.2-4. Temperature History for SHT Borehole 15 at Select Locations.....	6-54
6.2-5. Temperature Profile for SHT Borehole 15 at Select Times.....	6-55
6.2-6. Temperature History for SHT Borehole 8 at Select Locations.....	6-55
6.2-7. Temperature Profile for SHT Borehole 8 at Select Times.....	6-56
6.2-8. Interpretation of ERT Moisture Data during the SHT Heating Phase.....	6-59
6.2-9. Interpretation of ERT Moisture Data during the SHT Cooling Phase.....	6-60
6.2-10. Two Typical SHT GPR Receiver Gathers for the 15-17 Borehole Pair on January 16, 1997 .....	6-63
6.2-11. SHT GPR Velocity Tomograms for Borehole Pair 15-17 .....	6-64
6.2-12. SHT GPR Velocity Difference Tomograms for Borehole Pair 15-17.....	6-65
6.2-13. Smoothed Difference Fraction Volume Water Content Measured in SHT Borehole 15 Using Neutron Logging (April 30 and May 21, 1997) .....	6-67
6.2-14. Smoothed Difference Fraction Volume Water Content Measured in SHT Borehole 15 Using Neutron Logging (November 24 and December 17, 1997).....	6-68

## FIGURES (Continued)

	Page
6.2-15. SHT Permeability Changes for Boreholes 16 and 18 as a Ratio of Transient Permeabilities to the Baseline Permeability Estimate .....	6-73
6.2-16. Passive Monitoring Temperature Data in SHT Boreholes 16 and 18.....	6-74
6.2-17. Passive Monitoring Relative Humidity Data in SHT Boreholes 16 and 18 .....	6-75
6.2-18. Passive Monitoring Pressure Data in SHT Boreholes 16 and 18.....	6-76
6.2-19. Average Moisture Retention Curves for 11 SHT Samples at 25.1°C.....	6-84
6.2-20. Plan View Showing Locations of the SHT Mechanical Boreholes .....	6-88
6.2-21. Cross Section Showing Locations of the SHT Mechanical Boreholes.....	6-89
6.2-22. Displacement History for SHT MPBX-3 Borehole .....	6-91
6.3-1. DST As-Built Plan View with Two-Dimensional Coordinates of Key Locations .....	6-119
6.3-2. Drifts and Boreholes of the DST .....	6-120
6.3-3. Temperature (RTD) Boreholes of the DST .....	6-120
6.3-4. Hydrology Boreholes of the DST .....	6-121
6.3-5. Mechanical (MPBX) Boreholes of the DST .....	6-121
6.3-6. Neutron GPR Boreholes of the DST.....	6-122
6.3-7. Chemical (SEAMIST) Boreholes of the DST .....	6-122
6.3-8. ERT Boreholes of the DST .....	6-123
6.3-9. Total Power and Representative Drift Wall Temperature (TC-19) during the DST Heating Phase .....	6-154
6.3-10. Temperature Profile along DST Borehole 79 at Select Times .....	6-158
6.3-11. Temperature Profile along DST Borehole 80 at Select Times .....	6-158
6.3-12. Temperature Histories for DST Borehole 158 at Selected Locations.....	6-159
6.3-13. Temperature Profile along DST Borehole 158 at Select Times .....	6-160
6.3-14. Temperature Histories for DST Borehole 164 at Select Locations .....	6-161
6.3-15. Temperature Profile along DST Borehole 164 at Select Times .....	6-162
6.3-16. Vertical Slice through the Mid-length of the DST Heated Drift Showing 96°C Temperature Contours after 1, 2, 3, and 4 Years of Heating.....	6-162
6.3-17. DST ERT Resistivity Ratios of the 1/10/00 Measurement to the Preheating Measurement.....	6-171
6.3-18. DST Saturation Ratio Calculated from the 1/10/00 Resistivity Ratio .....	6-172
6.3-19. Saturation Estimates Corresponding to February 2002, Shortly after Heating Phase Ended.....	6-173
6.3-20. Saturation Estimates Corresponding to June 2002, Approximately Five Months after Heating Phase Ended.....	6-174
6.3-21. Saturation Estimates Corresponding to October 2002, When a Large Region of Increased Saturation Reappeared below the Heated Drift .....	6-175
6.3-22. Saturation Estimates Corresponding to June 2005, Approximately 3.5 Years after the End of the Heating Phase.....	6-176
6.3-23. GPR Difference Velocity Tomograms for DST Borehole Pairs 51-50 and 50-49 .....	6-179
6.3-24. Difference Fraction Volume Water Content Measured in DST Borehole 66 Using Neutron Logging (November 19, 1998, to December 11, 2001) .....	6-181



## FIGURES (Continued)

	Page
6.3-25. Rock Moisture Content as a Function of Temperature as Measured from Neutron Logging of Boreholes 79 and 80 during the DST Heating Phase.....	6-182
6.3-26. Changes in Permeability Displayed as a Ratio to the Preheating Permeability Estimate for DST Boreholes 57 through 61.....	6-190
6.3-27. Changes in Permeability Displayed as a Ratio to the Preheating Permeability Estimate for DST Boreholes 74 through 78.....	6-190
6.3-28. Changes in Permeability Displayed as a Ratio to the Preheating Permeability Estimate for DST Boreholes 185 and 186 .....	6-191
6.3-29. Passive Monitoring Temperature Data for DST Borehole 186 .....	6-193
6.3-30. Electrical Resistivity of DST Samples as Function of Saturation in the Drying Cycle at 50°C .....	6-199
6.3-31. Relative Permittivity of the DST Samples as a Function of Saturation in the Drying Cycle at 50°C.....	6-200
6.3-32. MPBX Layout for the Drift Scale Test.....	6-204
6.3-33. Corrected Displacements Measured for ESF-HD-81-MPBX1 .....	6-207
6.3-34. Corrected Displacements Measured for ESF-HD-147-MPBX3.....	6-208
6.3-35. Corrected Displacements Measured for ESF-HD-154-MPBX7.....	6-209
6.3-36. Corrected Displacements Measured for ESF-HD-155-MPBX8.....	6-210
6.3-37. Corrected Displacements Measured for ESF-HD-156-MPBX9.....	6-211
6.3-38. Corrected Displacements Measured for ESF-HD-157-MPBX10.....	6-212
6.3-39. Corrected Displacements Measured for ESF-HD-CDEX-1 and -2 .....	6-218
6.3-40. Layout and Location of Strain Gage Rosettes on the Concrete Liner .....	6-220
6.3-41. Axial Strains Measured by the Strain Gages on the DST Concrete Liner.....	6-222
6.3-42. Strain Gages Operating Past Epoxy Degradation Point.....	6-223
6.3-43. Location of DST Microseismic Activity (Acoustic Emissions) between December 21, 1998, and July 2, 2000.....	6-226
6.3-44. Three Arrays of DST Hydrology Boreholes Showing Relative Packer Positions and Fluid Sampling Zones .....	6-242
6.3-45. Cross Section of the Drift Scale Test at the Plane Containing the CHEMSAMP Boreholes.....	6-274
6.3-46. Moisture Content (wt % water) for Samples from Borehole HD-CHEMSAMP-1 ..	6-275
6.3-47. Box and Whisker Plots Comparing the Distribution of Chemical Constituents in Water Extracted from HD-CHEMSAMP-1 (N = 4) and HD-CHEMSAMP-3 (N = 13) with Water Extracted from HD-PERM Core (N = 3; Table 6.3-25).....	6-277
6.3-48. Moisture Content (in wt % water) of Core Samples from HD-CHEMSAMP-3 as a Function of Distance into the Borehole (upper plot), and Na/Ca Ratio (by weight), Also as a Function of Distance into the Borehole (lower plot).....	6-284
6.3-49. Uranium Concentrations and Isotopic Compositions of Water Samples Collected from the DST .....	6-317
6.3-50. U Concentration (upper) and <sup>234</sup> U/ <sup>238</sup> U Activity Ratios (lower) in DST Samples Plotted versus Collection Date.....	6-318
6.3-51. Strontium Isotope Ratio Compositions of Water Samples Collected from DST Boreholes Compared to Compositions of Pore Water, Rock, Calcite, and Grout....	6-319

## FIGURES (Continued)

	<b>Page</b>
6.3-52. Thermal History and Water Recovery in Borehole 75, Zone 2 .....	6-322
6.3-53. Sodium versus Chloride for Water Analyses from the DST.....	6-337
6.3-54. pH Values of Water Samples from the Flow-Through Test.....	6-343
6.3-55. Chloride Concentrations for Water Samples from the Flow-Through Test .....	6-343

## TABLES

	<b>Page</b>
4-1. Input DTNs for the Large Block Test .....	4-4
4-2. Input DTNs for the Single Heater Test .....	4-5
4-3. Input DTNs for the Drift Scale Test .....	4-7
6.1-1. DTNs for the Large Block Test .....	6-3
6.1-2. XYZ Coordinates of the Collar and Bottom of LBT Boreholes .....	6-9
6.1-3. LBT Permeability Measurements on Intact Core Sample SPC00504573.4 .....	6-30
6.1-4. Density and Porosity of LBT Samples Determined by Gravimetric Method .....	6-30
6.2-1. DTNs for the Single Heater Test .....	6-42
6.2-2. SHT Borehole Information .....	6-45
6.2-3. SHT Post-Testing Borehole Information .....	6-51
6.2-4. SHT Thermal Conductivity Laboratory Data for Four Specimens from Heater Borehole 1 .....	6-57
6.2-5. Parameters for the Estimation of Preheating SHT Air Permeability, k, around Injection Zones for Various Boreholes .....	6-71
6.2-6. Input Parameters and Estimated Preheating Air Permeability, k(m <sup>2</sup> ), for Consecutive 0.69-m Zones from Injection Tests between Straddle Packers in SHT Borehole 6 .....	6-72
6.2-7. Postcooling Air Permeability, k(m <sup>2</sup> ), for SHT Boreholes 1, 3, 6, 7, 16, 18, 19 .....	6-77
6.2-8. Comparison of Preheating and Postcooling Air Permeability Measurements for SHT Boreholes 3, 6, 7, 16, 18, 19 .....	6-77
6.2-9. SHT Gas Tracer Test Results .....	6-78
6.2-10. SHT Preheating Laboratory Hydrological Measurement of Wet-Drilled Cores .....	6-81
6.2-11. Preheating Laboratory Hydrological Measurement of Grab Samples from Wet Excavation of the Observation Drift of the ESF Thermal Test Facility .....	6-82
6.2-12. SHT Bulk Densities and Porosity of Cores from Boreholes CHE-1 and CHE-2 .....	6-82
6.2-13. SHT Laboratory Hydrological Measurements of Postcooling Dry-Drilled Cores .....	6-85
6.2-14. Wire Extensometer Data .....	6-92
6.2-15. Tape Extensometer Measurements for the SHT .....	6-93
6.2-16. Summary of SNL-Installed Measurement System Specifications .....	6-94
6.2-17. Estimated Rock Mass Modulus in Borehole ESF-TMA-BJ-1 (Goodman/Borehole Jack) .....	6-96
6.2-18. Rock Bolt Load Cells, Load versus Time .....	6-97
6.2-19. Mean Coefficients of Thermal Expansion during First Cycle Heating of Postcooling SHT Characterization Specimens .....	6-100
6.2-20. Mean Coefficients of Thermal Expansion during First Cycle Cooling of Postcooling SHT Characterization Specimens .....	6-102
6.2-21. Summary Data: SHT Postcooling Characterization Unconfined Compression Tests .....	6-104
6.2-22. Chemistry Analysis of SHT Borehole 16-4 Waters with Reported In Situ Waters from the General Area .....	6-108
6.2-23. SHT Stellerite Abundance on Fractures, Preheating Drill Core ESF-TMA-MPBX-1 .....	6-109

## TABLES (Continued)

	Page
6.2-24. Summary Descriptions of SHT Natural-Fracture Mineral and Test-Product XRD Samples.....	6-110
6.2-25. Semiquantitative XRD Identification of SHT Natural-Fracture Minerals and Test Products.....	6-111
6.3-1. DTNs for the Drift Scale Test.....	6-124
6.3-2. DST Borehole Information .....	6-145
6.3-3. Summary of Thermal Conductivity Data for Saturated Specimens from the DST Block .....	6-165
6.3-4. Thermal Conductivity as a Function of Saturation State .....	6-166
6.3-5. REKA Results with No Background Temperature Correction.....	6-167
6.3-6. REKA Results with Background Temperature Correction.....	6-167
6.3-7. Estimated Local Permeability for 41 Packed-off Zones in 14 Boreholes during DST Preheating (November/December 1996 and February/March 1997) .....	6-186
6.3-8. Parameters Used in Equation 5.2-1 for the Estimation of Local Permeability during DST Preheating (July 1997) .....	6-187
6.3-9. Parameters Used in Equation 5.2-1 for the Estimation of Local DST Permeability during Preheating (November 1997) .....	6-188
6.3-10. Date of Pneumatic Packer Deflation in the DST Hydrology Boreholes.....	6-192
6.3-11. Laboratory Measurement of Dry-Drilled Cores from DST Permeability Boreholes (182, 183, and 184).....	6-195
6.3-12. Laboratory Measurement of Wet-Drilled Cores from DST Boreholes (81, 52, 53, and 56) .....	6-196
6.3-13. Summary of SNL-Installed Measurement System Specifications for the DST.....	6-213
6.3-14. Data Quality Grades for Each MPBX Displacement Gage .....	6-213
6.3-15. Summary of Thermal Expansion Data for Specimens from the DST Block for the First Heating Cycle .....	6-228
6.3-16. Summary of the Mean Thermal Expansion Coefficients for Specimens from DST Block for the First Cooling Cycle .....	6-228
6.3-17. Tabulation of DST Unconfined Compression Tests.....	6-229
6.3-18. Summary of Results for DST Reinforced Concrete .....	6-230
6.3-19. Summary of Results for Nonreinforced Concrete .....	6-231
6.3-20. DST PLT Results from October 2000 and April 2003 .....	6-232
6.3-21. Rock Mass Thermal Expansion Coefficients from DST MPBX Data .....	6-234
6.3-22. Video Tapes in the YMP Records Center.....	6-237
6.3-23. Special Instruction Sheets for Video Tapes in the YMP Records Center.....	6-238
6.3-24. Summary of DST Water Samples, Field Data, and Observations through December 31, 2005 .....	6-245
6.3-25. Chemical Analyses of DST Borehole Water Samples.....	6-261
6.3-26. Moisture Content of HD-CHEMSAMP Core Samples .....	6-278
6.3-27. Chemical Analyses of Water Extracted from CHEMSAMP Core Samples.....	6-282
6.3-28. Concentration and Isotopic Compositions of CO <sub>2</sub> in Gas Samples Collected during the DST Heating and Cooling Phases .....	6-287

**TABLES (Continued)**

	<b>Page</b>
6.3-29. Hydrogen ( $\delta D$ ) and Oxygen ( $\delta^{18}O$ ) Isotope Compositions of Steam Condensed from Gas Samples Collected during the DST Heating and Cooling Phases.....	6-301
6.3-30. Mineral Coverage on Fractures, Drill Core ESF-HD-TEMP-2 .....	6-313
6.3-31. Field and Laboratory Analytical Data for Borehole 75-2 Water Samples.....	6-323
6.3-32. Assessment of Effects of Introduced Materials on Water Chemistry .....	6-325
6.3-33. Field Measurements and F-Content of Condensates Sampled during the HF Field Tests.....	6-339
6.3-34. Fluoride Concentrations (ppm)/pH from Gas Flow-Through Experiments .....	6-341
6.3-35. Isothermal Degradation Rates of BH 60 and BH 72 Fluoroelastomer .....	6-342

INTENTIONALLY LEFT BLANK

## ACRONYMS AND ABBREVIATIONS

AES	Atomic Emission Spectroscopy
ASTM	American Society for Testing and Materials
CDEX	cross-drift extensometers
CIP	cast-in-place
DCS	Data Collection System
DOE	U.S. Department of Energy
DST	Drift Scale Test
EC	electrical conductivity
EDX	energy-dispersive x-ray
ERT	electrical resistivity tomography
ESF	Exploratory Studies Facility
FKM	fluoroelastomer
FM	fracture monitoring
FSO	full scale output
GPR	ground penetrating radar
GPa	giga Pascal
HF	hydrogen fluoride
IC	Ion Chromatography
ICP	Inductively Coupled Plasma
LANL	Los Alamos National Laboratory
LBNL	Lawrence Berkeley National Laboratory
LBT	Large Block Test
LLNL	Lawrence Livermore National Laboratory
LT	low temperature
LVDT	linear variable displacement transducer
MCTE	mean coefficient of thermal expansion
$\mu\text{D}$	micro Darcy
$\mu\text{m}$	micrometer
MPa	mega Pascal
MPBX	multipoint borehole extensometers
PLT	Plate Loading Test
RBLC	rock bolt load cells
REKA	Rapid Evaluation of K and Alpha
RH	relative humidity
RPC	Records Processing Center

## ACRONYMS AND ABBREVIATIONS (Continued)

RTD	resistance temperature detector
SEM	scanning electron microscopy/microscope
SHT	Single Heater Test
SLPM	standard liters per minute
SMF	Sample Management Facility
SNL	Sandia National Laboratories
TCA	thermocouple apparatus
TDIF	Technical Data Information Form
TDMS	Technical Data Management System
TDS	total dissolved solids
TH	thermal-hydrological
USBR	U.S. Bureau of Reclamation
USGS	U.S. Geological Survey
XRD	X-ray diffraction
YMP	Yucca Mountain Project



## 1. PURPOSE

The purpose of this technical report is to address deficiencies in the original version of *Thermal Testing Measurements Report* (BSC 2002 [DIRS 160771]). These deficiencies were documented in audit report BQAP-BSC-03-02 (BSC 2003 [DIRS 170669]); Deficiency Reports BSC(B)-03-D-043 (Krisha 2002 [DIRS 170840]) and BSC(B)-03-D-045 (BSC 2003 [DIRS 170670]); and in Condition Reports 165, 288, 657, 1936, and 5383. The identified deficiencies included:

- Data tracking numbers (DTNs) that were not populated with data in the Technical Data Management System (TDMS)
- Software discussed in the report, but not addressed in Section 3 of the report
- Unqualified input sources to product output DTNs
- Insufficient or excessive numbers of data sources listed in the report for certain product output DTNs
- Various errors in Technical Data Information Forms (TDIFs)
- Basis for data selection not discussed.

Full details of the deficiencies can be found in the audit, deficiency, and condition reports referenced above.

The purpose of the original version of *Thermal Testing Measurements Report* (BSC 2002 [DIRS 160771]) was to document, in one report, the comprehensive set of measurements taken within the Yucca Mountain Project (YMP) Thermal Testing Program since its inception in 1996. This technical report substantially retains the documentation and discussion from the original version of *Thermal Testing Measurements Report* (BSC 2002 [DIRS 160771]).

Since either detailed reports exist or the measurements are straightforward, only brief discussions are provided for each data set. These brief discussions for different data sets are intended to impart a clear sense of applicability of data, so that they will be used properly within the context of measurement uncertainty. As appropriate, thermal testing data currently residing in the TDMS were reorganized and reformatted into summary DTNs. These summary DTNs provide a readily usable data structure, including graphical displays and comprehensive spreadsheets. Summary DTNs were developed only for data acquired during the heating phase. In some cases, there was no need to reformat or restructure input DTNs, so they remained unchanged. Although the DTNs in this report are characterized as input DTNs and summary DTNs, all DTNs discussed are in fact input to this report.

Thermal testing measurement data come from the characterization (preheating/baseline and postcooling) and testing (heating and cooling) phases of the Large Block Test (LBT), the Single Heater Test (SHT), and the Drift Scale Test (DST). Since the LBT and SHT are completed, all phases of those two tests are addressed. DST measurements addressed in this report include preheating tests, the entire four-year heating phase, which ended January 14, 2002, and the cooling phase, which ended December 31, 2005. The objective of the YMP Thermal Testing

Program is to gain a more in-depth understanding of the coupled thermal, hydrological, mechanical, and chemical processes. Satisfaction of this objective will ultimately lead to better understanding of how thermally driven coupled processes would affect the performance of the waste packages and the flow and transport of radionuclides (and consequently, the performance of the repository). The YMP Thermal Testing Program was initially described in *Site Characterization Plan Yucca Mountain Site, Nevada Research and Development Area, Nevada* (DOE 1988 [DIRS 100282]). The plan identified seven types of tests. In 1994, the YMP Thermal Testing Program was reevaluated, resulting in two phases of test planning. The first phase, documented in the report entitled *In-Situ Thermal Testing Program Strategy* (DOE 1995 [DIRS 130104]), presented five types of in situ thermal tests, including the LBT and the SHT. The second phase of test planning, documented in the report entitled *Updated In Situ Thermal Testing Program Strategy* (CRWMS M&O 1997 [DIRS 111106]), was a more fundamental approach that included consideration of thermally driven coupled processes and related parameters. Additional scope included laboratory tests, analogues, modeling, performance confirmation monitoring, and a restructured suite of in situ thermal tests. The DST was developed from this second phase of test consolidation.

The LBT, located in Fran Ridge, southeast of Yucca Mountain, is described in *Large Block Test Final Report* (Lin et al. 2001 [DIRS 159069]). The heating phase of the LBT started in February 1997 and continued until March 1998, at which time the heaters were turned off. Cooling-phase measurements at the LBT were made until September 1998. Upon completion of the postcooling characterization of the LBT block, a final report was prepared (Lin et al. 2001 [DIRS 159069]).

The SHT, located in Alcove No. 5 of the Exploratory Studies Facility (ESF), is described in *Characterization of the ESF Thermal Test Area* (CRWMS M&O 1996 [DIRS 101428]), *Single Heater Test Status Report* (CRWMS M&O 1997 [DIRS 101540]), and *Single Heater Test Final Report* (CRWMS M&O 1999 [DIRS 129261]). The heating phase of the SHT started in August 1996 and continued for 275 days until May 1997. The cooling phase continued until January 1998, at which time postcooling characterization of the test block commenced. Laboratory tests, modeling, analyses, and documentation were completed, and the final report (CRWMS M&O 1999 [DIRS 129261]) was submitted to the U.S. Department of Energy (DOE) in October 1999.

The DST, also located in Alcove No. 5 of the ESF, is described in the following reports: *Drift Scale Test Design and Forecast Results* (CRWMS M&O 1997 [DIRS 146917]) and *Drift Scale Test As-Built Report* (CRWMS M&O 1998 [DIRS 111115]). The results from characterizing the test block are contained in *Ambient Characterization of the Drift Scale Test Block* (CRWMS M&O 1997 [DIRS 101539]). Early results of the DST are discussed in *Drift Scale Test Progress Report No. 1* (CRWMS M&O 1998 [DIRS 108306]). The heating phase of the DST started in December 1997 and lasted approximately four years until January 14, 2002. The cooling phase started January 14, 2002, and lasted until December 31, 2005, when most of the measurement ceased. DST measurements through the entire eight-year period are presented in this technical report.

Discussion of the thermal testing measurements in this report is organized first under the heading of the three tests: LBT, SHT, and DST; and then under the four processes: thermal, hydrological, mechanical, and chemical. Miscellaneous measurements and observations are also discussed. Although the list of measurement types is comprehensive, it is neither practical (because of finite

report length) nor necessary to thoroughly discuss all data sets. For example, the DST measured temperatures come from nearly 2,700 thermal sensors distributed throughout the test block and collected hourly, resulting in approximately 100 million measurements. Therefore, as appropriate for each measurement type, only a representative discussion of the test data behavior is presented. Readers are referred to summary DTNs for comprehensive data sets that include complementary graphics.

The depth of the following discussions concerning the 12 basic measurement groups (three thermal tests and four processes) is dictated by their respective data characteristics. In general, discussions of thermal and mechanical measurements tend to be comparatively short, although the respective summary DTNs contain comparatively large amounts of data. This condition reflects the inherent simplicity or straightforwardness of temperature and displacement measurements that are recorded frequently (hourly) on a data acquisition system. Conversely, discussions of hydrological and chemical measurements tend to be lengthier, while their summary DTNs are comparatively small. The smaller output data sets result from measurements collected comparatively infrequently (monthly or longer) on a nonintegrated data acquisition system. The more lengthy discussion in the chemical measurements sections relates to sampling procedures that have considerable relevance to the data collected. Also, in certain hydrological measurements, detailed explanations are needed for the complex data reduction that occurs as the data are transformed from input DTN data into more useful and functional summary DTN data. Furthermore, since other technical documents exist (see prior comments on LBT, SHT, and DST reports), discussion of the measurement process was intentionally limited. More specifically, discussions of calibration, of measurement technique, and of scientific notebook entries, for the most part, were not included in this report. Uncertainty associated with most measurements is also discussed. These discussions are restricted to actual measurements and data reduction. If quantifiable uncertainties were cited, then either references to equipment manufacturers' specifications were provided or they were referred to as "estimates." Standard error analyses (mean and standard deviation) were provided for applicable measurements such as repetitive measurements of laboratory or field parameters. Test measurements of a response for a specific location and time are not applicable for standard error analyses. Additional information on measurement uncertainties can be located via directions in DTNs cited in the footnotes of Tables 4-1, 4-2, and 4-3. This information, among other things, provides detailed discussions of scientific notebooks and calibration relationships relevant to uncertainties of thermal testing measurements. Also included in this report are summaries of three "white papers" involving in-depth investigations of unexpected or unusual behavior. The summaries are in Sections 6.3.2.6 and 6.3.4.5.

This report is written in accordance with LS-PRO-001, *Technical Reports*, and *Technical Work Plan for: Revising the Thermal Testing Measurements Report* (BSC 2006 [DIRS 178175]). The technical work plan (TWP) states that no acceptance criteria from *Yucca Mountain Review Plan, Final Report* (NRC 2003 [DIRS 163274]) are applicable to this report. This report deviates from the TWP in that several acceptance criteria from *Yucca Mountain Review Plan, Final Report* (NRC 2003 [DIRS 163274]) are addressed herein. It should also be noted that this technical report is a summarization of field thermal testing data.

For this particular revision of the report, the TWP (BSC 2006 [DIRS 178175], Section 1.2) identifies the following primary tasks:

1. A review of data collected from the DST cooling phase to verify that these data exist in TDMS, and that the qualification status is appropriately identified. To address this task, discussion of the cooling phase data has been added to the report, along with new graphics and charts depicting DST data histories of both heating and cooling phases. Discussion of major test events and/or anomalies has also been added.
2. Correction of a deficiency identified in Condition Report 5383. Specifically, entries for samples BH 59-2, dated 5/23/00, and BH 59-4, dated 1/26/99, have been added to Table 6.3-32 of the report because they were inadvertently omitted from the original version (BSC 2002 [DIRS 160771]).
3. Reorganization, reformatting, and editing of the report to achieve greater transparency and readability. Specifically, figures and tables have been co-located with the text, and minor editorial corrections identified in the TWP (BSC 2006 [DIRS 178175], Section 1.2) have been made.

The product output DTNs from the original version of *Thermal Testing Measurements Report* (BSC 2002 [DIRS 160771]) have been retained unless supersession was necessary. In some cases, the data in the original product output DTN was found to be in error, and the source input DTNs were used in lieu of the original product output DTNs (see Section 4). The status of the original product output DTNs has been changed to non-product output and their qualification status has been changed to reflect the qualification status of their source input DTNs (i.e., an unqualified source DTN would make the original product output DTN unqualified as well). The DTN numbers from the original version of *Thermal Testing Measurements Report* (BSC 2002 [DIRS 160771]) have been retained in the present report. These DTNs are characterized as summary DTNs in this report since their product output status has been removed.

*Technical Work Plan for: Unsaturated Zone Sections of License Application Chapters 8 and 12* (BSC 2002 [DIRS 159051]) contained the work packages for the DST and the test was conducted in accordance with *Test Plan for: Drift Scale Test* (BSC 2002 [DIRS 158190]).

The report is organized as follows: Section 2 addresses quality assurance. Section 3 discusses the use of software. Section 4 provides a tabulation of input DTNs. Assumptions are documented in Section 5. Discussion of the thermal test measurements for each of the three thermal tests is provided in Section 6. A summary is provided in Section 7, and references are presented in Section 8.

## 2. QUALITY ASSURANCE

### 2.1 PROCEDURAL COMPLIANCE

The activities documented in this technical report are subject to the requirements of *Quality Assurance Requirements and Description* (DOE 2006 [DIRS 177092]). This report was prepared in accordance with LS-PRO-001. The summarization of thermal test measurements reported in the original version of *Thermal Testing Measurements Report* (BSC 2002 [DIRS 160771]) is consistent with the direction delineated in *Test Plan for: Drift Scale Test* (BSC 2002 [DIRS 158190]). The activities to address deficiencies in the original version of *Thermal Testing Measurements Report* (BSC 2002 [DIRS 160771]) are delineated in *Technical Work Plan for: Near-Field Environment Thermal Properties Model and Analysis Reports Integration* (BSC 2005 [DIRS 175829]). Activities for the current revision are delineated in *Technical Work Plan for: Revising the Thermal Testing Measurements Report* (BSC 2006 [DIRS 178175]).

Input DTNs were documented in accordance with SCI-PRO-004, *Managing Technical Product Inputs*. Data submittals to the TDMS were done in accordance with one of the appropriate and relevant predecessors to TST-PRO-001, *Submittal and Incorporation of Data to the Technical Data Management System*. Process controls on specific uses of electronically stored information, including information residing in an electronic information management system or on electronic media, were evaluated.

The methods used for control of electronic management of data were in accordance with those specified in *Technical Work Plan for: Revising the Thermal Testing Measurements Report* (BSC 2006 [DIRS 178175]). Electronic management of information was also controlled under the following organization-specific procedures: YMP-LBNL-QIP-SV.0, *Management of YMP-LBNL Electronic Data*, for Lawrence Berkeley National Laboratory (LBNL); 033-YMP-QP-3.8, *Control of the Electronic Management of Data*, for Lawrence Livermore National Laboratory (LLNL); and LANL-YMP-QP-S5.01, *Electronic Information Management*, for Los Alamos National Laboratory (LANL).

The remainder of this section is provided for informational purposes and discusses the quality assurance controls for activities supporting the original version of *Thermal Testing Measurements Report* (BSC 2002 [DIRS 160771]).

For work done by the U. S. Geological Survey (USGS), four electronic databases on workstations/personal computers were used by the USGS Environmental Science Team. The databases were backed up on a fixed schedule and whenever blocks of new data were added. Backed-up files were stored on fixed and removable magnetic media and removable optical media. Backup media were kept in secure areas remote from the workstations/personal computers. Backup was also provided by hard copies of original raw data and by laboratory notebooks. Data were subjected to multiple checking steps. A final check was attained by retrieving data from the database and physically checking it against the original input records. Errors were corrected and the records were rechecked after correction. Records of this checking process were maintained. Data packages submitted to the TDMS were prepared by outputting the data from the databases, commonly through spreadsheets. For work done by Sandia National

Laboratories (SNL), the requirements of IM-PRO-002 were met by the following measures: Computers used for processing and storing information were password-protected. All files were backed up on magnetic media monthly or more often if needed. Backup media were labeled with the date and time of backup, DOE serial number of the computer backed up, system utility used to perform the backup, and format of the magnetic media. Information transfers from one computer to another were done by magnetic media, Internet, or local network, using file transfer protocol (FTP) or attachments to e-mail on the same system. In most cases, such transfers were between computers that use a common operating system and storage format. In these cases, the name, date, and file size were visually checked. ASCII files were also verified by visual comparison of the data.

For work done by Integrated Science Solutions, Inc., the requirement of IM-PRO-002 was met by the following measures: Computers used for processing and storing information were password-protected. All files were backed up on magnetic media monthly or more often if needed. Backup media was labeled with the date and time of backup, DOE serial number of the computer backed up, system utility used to perform the backup, and format of the magnetic media. Information transfers from one computer to another were done by magnetic media, Internet, or local network, using FTP or attachments to e-mail on the same system. In most cases, such transfers were between computers that use a common operating system and storage format. In these cases, the name, date, and file size were visually checked. ASCII files were also verified by visual comparison of the data.

### 3. USE OF SOFTWARE

The process of restructuring groups of DTNs into summary DTNs involved the limited use of commercial off-the-shelf graphics packages and spreadsheet software exempt from the control requirements of IM-PRO-003, *Software Management*. The software used included Microsoft EXCEL, Versions 97 and 2000; and operating systems Windows 98, Windows NT, and Windows 2000. AutoCAD software was used to provide the graphical displays in Figures 6.3.1.2-7 and 6.3.1.2-8. Software code CA-DISSPLA was used to provide the graphical displays in Figures 6.2.2.2-2, 6.2.2.2-3, and 6.3.2.2-1. Both AutoCAD and CA-DISSPLA are commercial off-the-shelf software codes, and their use in this report is for display purposes only. They are therefore exempt from the software qualification requirements per Section 2 of IM-PRO-003.

The following summary DTNs use Excel spreadsheets containing macros written to sort and/or chart data:

- LB0208AIRKDSTH.001 [DIRS 160897]
- LL020710523142.025 [DIRS 164182] (unqualified)
- MO0208RESTRSHT.002 [DIRS 170582]
- MO0208RESTRDST.002 [DIRS 161129].

The macros in the above DTNs are not required to be qualified in accordance with IM-PRO-003 per the exemptions stated in Section 2 of that procedure.

INTENTIONALLY LEFT BLANK



## 4. INPUTS

There are no direct inputs to this technical report as none of the data presented are being used to produce output from the report. As such, all inputs are indirect inputs. This section provides a listing of input and summary DTNs for measurements of characterization and test data from each of the three thermal tests: LBT, SHT, and DST. Although this report identifies DTNs as input DTNs and summary DTNs, both types are inputs to this report. Since many of these DTNs were developed in an incremental manner during the duration of each test, several DTNs need to be accessed to examine measurements for the duration of the already completed thermal tests (LBT and SHT) and the four-year heating phase of the DST. Many of the input DTNs have been restructured into summary DTNs listed here and in Tables 6.1-1, 6.2-1, and 6.3-1. These summary DTNs retain the same DTN identifiers as the product output DTNs from the original version of *Thermal Testing Measurements Report* (BSC 2002 [DIRS 160771]), with the following exceptions. Product output DTNs: SN0208F3511695.011 and LB0208ISODSTHP.001, from the original version of the report (BSC 2002 [DIRS 160771]), were not used as summary DTN inputs to this report due to errors found in these DTNs. Also, product output DTN: SN0208F3912298.039, also from the original version of the report (BSC 2002 [DIRS 160771]), was superseded by summary DTN: SN0407F3912298.060 [DIRS 170627]. As stated in Section 1, product output DTNs from the original version of *Thermal Testing Measurements Report* (BSC 2002 [DIRS 160771]) have had their status changed to non-product output, and are now characterized as summary DTNs.

### 4.1 LARGE BLOCK TEST

Table 4-1 lists DTNs for characterization and test measurements from the LBT. In the third column under the heading “Type,” the data are identified according to the four processes: thermal, hydrological, mechanical, and chemical, plus a fifth category, “general.”

### 4.2 SINGLE HEATER TEST

Table 4-2 lists DTNs for characterization and test measurements from the SHT. In the third column under the heading “Type,” the data are identified according to the four processes: thermal, hydrological, mechanical, and chemical, plus a fifth category, “general.”

### 4.3 DRIFT SCALE TEST

Table 4-3 lists DTNs for characterization and test measurements from the DST. In the third column under the heading “Type,” the data are identified according to the four processes: thermal, hydrological, mechanical, and chemical, plus a fifth category, “general.”

### 4.4 CRITERIA

The following acceptance criteria from Section 2.2.1.3.3.3 of *Yucca Mountain Review Plan, Final Report* (NRC 2003 [DIRS 163274]) have been identified as being applicable to this report.

### **Acceptance Criterion 1 – System Description and Model Integration Are Adequate**

- (4) Spatial and temporal abstractions appropriately address physical couplings (thermal-hydrologic-mechanical-chemical). For example, the U.S. Department of Energy evaluates the potential for focusing of water flow into drifts, caused by coupled thermal-hydrologic-mechanical-chemical processes.
- (5) Sufficient technical bases and justification are provided for total system performance assessment assumptions and approximations for modeling coupled thermal-hydrologic-mechanical-chemical effects on seepage and flow, the waste package chemical environment, and the chemical environment for radionuclide release. The effects of distribution of flow on the amount of water contacting the engineered barriers and waste forms are consistently addressed, in all relevant abstractions.
- (8) Adequate technical bases are provided, including activities such as independent modeling, laboratory or field data, or sensitivity studies, for inclusion of any thermal-hydrologic-mechanical-chemical couplings and features, events, and processes.
- (9) Performance-affecting processes that have been observed in thermal-hydrologic tests and experiments are included into the performance assessment. For example, the U.S. Department of Energy either demonstrates that liquid water will not reflux into the underground facility or incorporates refluxing water into the performance assessment calculation, and bounds the potential adverse effects of alteration of the hydraulic pathway that result from refluxing water.

### **Acceptance Criterion 2 – Data Are Sufficient for Model Justification**

- (1) Geological, hydrological, and geochemical values used in the license application are adequately justified. Adequate description of how the data were used, interpreted, and appropriately synthesized into the parameters is provided
- (2) Sufficient data were collected on the characteristics of the natural system and engineered materials to establish initial and boundary conditions for conceptual models of thermal-hydrologic-mechanical-chemical coupled processes, that affect seepage and flow and the engineered barrier chemical environment.
- (3) Thermal-hydrologic tests were designed and conducted with the explicit objectives of observing thermal-hydrologic processes for the temperature ranges expected for repository conditions and making measurements for mathematical models. Data are sufficient to verify that thermal-hydrologic conceptual models address important thermal-hydrologic phenomena.
- (4) Sufficient information to formulate the conceptual approach(es) for analyzing water contact with the drip shield, engineered barriers, and waste forms is provided.

### **Acceptance Criterion 3 – Data Uncertainty Is Characterized and Propagated Through the Model Abstraction**

- (4) Adequate representation of uncertainties in the characteristics of the natural system and engineered materials is provided in parameter development for conceptual models, process-level models, and alternative conceptual models. The U.S. Department of Energy may constrain these uncertainties using sensitivity analyses or conservative limits. For example, the U.S. Department of Energy demonstrates how parameters used to describe flow through the engineered barrier system bound the effects of backfill and excavation-induced changes.

### **Acceptance Criterion 5 – Model Abstraction Output Is Supported by Objective Comparisons**

- (3) Accepted and well-documented procedures are used to construct and test the numerical models that simulate coupled thermal-hydrologic-mechanical-chemical effects on seepage and flow, engineered barrier chemical environment, and the chemical environment for radionuclide release. Analytical and numerical models are appropriately supported. Abstracted model results are compared with different mathematical models, to judge robustness of results.

## **4.5 CODES AND STANDARDS**

No specific formally established codes and standards have been identified as applying to this report. Although some standards were used to obtain thermal testing measurements, this activity was prior to DTN submittal, and therefore outside the scope of this report (see Section 1). Also, refer to key references cited in Section 1 and corresponding background discussion in the input DTNs for information on applicable standards.

Table 4-1. Input DTNs for the Large Block Test

Input DTN	Description	Type	Q Status
LL980918904244.074 [DIRS 135872]	Heater power, temperature, relative humidity, and gas pressure	T, H	UQ
LL980919404244.076 [DIRS 148630]	Rock mass displacements	M	Q
LA0106FH831151.002 [DIRS 158230]	Data Collection System data	T, M	UQ
LA0106FH831151.003 [DIRS 158229]	Data Collection System data	T, M	UQ
LL981110704244.085 [DIRS 169259]	Large Block Test report, chapter 4	G	UQ
LL980913304244.072 [DIRS 145385]	Electrical resistance tomograms	H	Q
LL981001604244.079 [DIRS 158261]	Electrical resistivity	H	Q
LL980919304244.075 [DIRS 145099]	Neutron logging	H	Q
LL971204304244.047 [DIRS 113894]	Neutron logging	H	Q
LL970803404244.040 [DIRS 113889]	Data on moisture content in the LBT	H	Q
LL950812704242.017 [DIRS 158237]	Porosity, saturated and dry density	H	UQ
LL960905204244.022 [DIRS 158244]	Laboratory matrix permeability	H	Q
LL981208404244.092 [DIRS 158263]	X-ray radiography	H	UQ
LL960400404244.012 [DIRS 158271]	Fracture mapping	G	Q
LL960400504244.013 [DIRS 158274]	Fracture mapping	G	Q
LL960400604244.014 [DIRS 158275]	Fracture mapping	G	Q
LL981202305912.004 [DIRS 158270]	Bacterial transport	C	UQ
LL960400704244.015 [DIRS 158276]	Fracture mapping	G	Q
LL020710523142.025 [DIRS 164182]	Temperatures, heater powers, and rock displacements of the LBT	T, M	UQ

NOTES: All input DTNs are indirect inputs.

DTNs: LA0106FH831151.002 [DIRS 158230] and LA0106FH831151.003 [DIRS 158229] provide access via the Records Processing Center (RPC) to all thermal and mechanical data collected in the LBT Data Collection System (original/electrical and converted/engineering units). These unqualified DTNs also provide access (via the RPC) to pertinent supporting material such as scientific notebooks and calibration relationships.

T = thermal, H = hydrological, M = mechanical, C = chemical, G = general/miscellaneous.

Q = qualified, UQ = unqualified. Data sets listed as UQ should be used only for corroborative purposes.

Table 4-2. Input DTNs for the Single Heater Test

Input DTN	Description	Type	Q Status
LA0009SL831151.001 [DIRS 153485]	Fracture mineralogy	C	Q
LA0002FH6001WP.001 [DIRS 158278]	Data Collection System data	T,H,M,C	UQ
LL970805504244.043 [DIRS 158313]	XYZ coordinates of boreholes and sensors	T,H,M,C	Q
SNF35110695001.001 [DIRS 158315]	XYZ coordinates of boreholes and sensors	T,H,M,C	Q
SNL22080196001.001 [DIRS 109722]	Thermal conductivity, thermal expansion	T	Q
LL970101004244.026 [DIRS 158281]	Electrical resistance tomography	H	Q
LL970505404244.031 [DIRS 148609]	Electrical resistance tomography	H	Q
LL971002904244.044 [DIRS 158286]	Electrical resistance tomography	H	Q
LL980105204244.049 [DIRS 148610]	Electrical resistance tomography	H	Q
LB980901123142.003 [DIRS 119016]	Ground penetrating radar data	H	Q
LL980106904244.051 [DIRS 118963]	Neutron logging	H	Q
LB960500834244.001 [DIRS 105587]	Preheating air injection	H	Q
LB980120123142.008 [DIRS 158280]	Air injections in boreholes 16 and 18, part 1 of 4	H	Q
LB970500123142.001 [DIRS 158293]	Air injections in boreholes 16 and 18, part 2 of 4	H	Q
LB0204SHAIRK3Q.001 [DIRS 159543]	Air injections in boreholes 16 and 18, part 3 of 4	H	Q
LB971000123142.001 [DIRS 118965]	Air injections in boreholes 16 and 18, part 4 of 4	H	Q
LB980901123142.001 [DIRS 118999]	Postcooling air injection and gas tracer testing	H	Q
LB980901123142.002 [DIRS 119009]	Temperature, relative humidity, gauge pressure (passive monitoring)	T, H	Q
LB970500123142.003 [DIRS 131500]	Preheating laboratory saturation, porosity, bulk density gravimetric water content	H	Q
LL020506123142.021 [DIRS 169256]	Preheating laboratory porosity, relative humidity, and water saturation	H	Q
LB970100123142.001 [DIRS 158287]	Air injections in boreholes 16 and 18	H	Q
LB980901123142.006 [DIRS 119029]	Postcooling laboratory saturation, porosity, bulk density gravimetric water content	H	Q
SN0401F3511695.012 [DIRS 169262]	Thermal and thermal-mechanical data	M	Q
SN0401F3511695.013 [DIRS 169263]	Thermal and thermal-mechanical data	M	Q

Table 4-2. Input DTNs for the Single Heater Test (Continued)

Input DTN	Description	Type	Q Status
LL980109904243.015 [DIRS 158299]	Optical MPBX displacements	M	Q
SNF35110695001.010 [DIRS 158300]	Rock mass deformation modulus – borehole (Goodman) jack	M	Q
SNL22080196001.002 [DIRS 158306]	Preheating laboratory unconfined compressive strength, dry bulk density, Poisson's ratio, Young's modulus, saturated bulk density, seismic velocity	M	Q
SNL22080196001.003 [DIRS 119042]	Postcooling laboratory thermal conductivity, thermal expansion, unconfined compressive strength, dry bulk density, Poisson's ratio, Young's modulus	T, M	Q
LL970101104244.027 [DIRS 158309]	chemical abundance data	C	UQ
LL970409604244.030 [DIRS 111481]	Chemical abundance data	C	UQ
LL970703904244.034 [DIRS 111482]	Chemical abundance data	C	UQ
LL971006604244.046 [DIRS 148611]	Chemical abundance data	C	UQ
GS951108312271.006 [DIRS 169244]	Chemical abundance data	C	UQ
LB970700123142.002 [DIRS 158295]	Infrared images, part 3 of 5	T, H	Q
LB980120123142.001 [DIRS 158297]	Infrared images, part 5 of 5	T, H	Q
MO0208RESTRSHT.002 [DIRS 170582]	Restructured SHT heating phase power and temperature data	T	Q
LL020801823142.029 [DIRS 170581]	Electrical resistance tomographs of the SHT august 1996 through December 1997	H	UQ
LB0208GPRSHTTCP.001 [DIRS 170578]	Ground penetrating radar for the heating and cooling phases of the SHT	H	Q
LB0208AIRKSHTC.001 [DIRS 170576]	Air permeability data for the heating and cooling phases of the SHT	H	Q

NOTES: All input DTNs are indirect inputs.

DTN: LA0002FH6001WP.001 [DIRS 158278] provides access via the RPC to all thermal and mechanical data collected in the SHT Data Collection System (original/electrical and converted/engineering units). This unqualified DTN also provides access (via the RPC) to pertinent supporting material such as scientific notebooks and calibration relationships. These data should only be used for corroborative purposes.

T = thermal, H = hydrological, M = mechanical, C = chemical, G = general/miscellaneous.

Q = qualified, UQ = unqualified. Data sets listed as UQ should be used only for corroborative purposes.

Table 4-3. Input DTNs for the Drift Scale Test

Input DTN	Description	Type	Q Status
MO0002ABBLSLDS.000 [DIRS 147304]	XYZ coordinates of boreholes and sensors	T,H,M,C	Q
MO9807DSTSET01.000 [DIRS 113644]	Heater, power, current, voltage, temperature: November 7, 1997, to May 1998	T	Q
MO9810DSTSET02.000 [DIRS 113662]	Heater, power, current, voltage, temperature: June 1998 to August 1998	T	Q
MO9906DSTSET03.000 [DIRS 113673]	Heater, power, current, voltage, temperature: September 1998 to May 1999	T	Q
MO0001SEPDSTPC.000 [DIRS 153836]	Heater, power, current, voltage, temperature: June 1999 to October 1999	T	Q
MO0007SEPDSTPC.001 [DIRS 153707]	Heater, power, current, voltage, temperature: November 1999 to May 2000	T	Q
MO0012SEPDSTPC.002 [DIRS 153708]	Heater, power, current, voltage, temperature: June 2000 to November 2000	T	Q
MO0107SEPDSTPC.003 [DIRS 158321]	Heater, power, current, voltage, temperature: December 2000 to May 2001	T	Q
MO0202SEPDSTTV.001 [DIRS 158320]	Heater, power, current, voltage, temperature: June 2001 to January 14, 2002	T	Q
MO0208SEPDSTTD.001 [DIRS 161767]	DST temperature data for January 15, 2002, through June 30, 2002.	T	Q
MO0303SEPDSTTM.000 [DIRS 165698]	DST Temperature Data for July 1, 2002, through December 31, 2002.	T	Q
MO0307SEPDST31.000 [DIRS 165699]	DST temperature data for January 1, 2003, through June 30, 2003.	T	Q
MO0403SEPDST32.000 [DIRS 177813]	DST temperature data for July 1, 2003, through December 31, 2003.	T	Q
MO0408SEPDSTTD.000 [DIRS 177814]	DST temperature data for January 1, 2004, through June 30, 2004.	T	Q
MO0509SEPDSTTD.000 [DIRS 177815]	DST temperature data for July 1, 2004, through June 30, 2005.	T	Q
MO0603SEPDSTTD.000 [DIRS 177816]	DST temperature data for July 1, 2005, through December 31, 2005.	T	Q
MO0603SEPDSTTB.002 [DIRS 178054]	DST temperature borehole RTD status as of December 31, 2005.	T	Q
SNF39012298002.004 [DIRS 153837]	MPBX and CDEX displacement corrected for thermal expansion November 9, 1997, to May 1998	M	Q
SNF39012298002.008 [DIRS 153839]	MPBX and CDEX displacement corrected for thermal expansion June 1998 to August 1998	M	Q
SNF39012298002.012 [DIRS 153840]	MPBX and CDEX displacement corrected for thermal expansion September 1998 to May 1999	M	Q
SN0001F3912298.016 [DIRS 153842]	MPBX and CDEX displacement corrected for thermal expansion June 1999 to October 1999	M	Q

Table 4-3. Input DTNs for the Drift Scale Test (Continued)

Input DTN	Description	Type	Q Status
SN0007F3912298.020 [DIRS 158388]	MPBX and CDEX displacement corrected for thermal expansion November 1999 to May 2000	M	Q
SN0101F3912298.026 [DIRS 158402]	MPBX and CDEX displacement corrected for thermal expansion June 2000 to November 2000	M	Q
SN0107F3912298.031 [DIRS 158413]	MPBX and CDEX displacement corrected for thermal expansion December 2000 to May 2001	M	Q
SNL22100196001.003 [DIRS 111068]	Thermal expansion of carbon fiber and Invar rods	M	Q
SN0203F3912298.035 [DIRS 158363]	MPBX and CDEX displacement corrected for thermal expansion June 2001 to January 14, 2002	M	Q
SN0209F3912298.042 [DIRS 177941]	Measurements of displacement data for the DST corrected for thermal expansion (with results from January 15, 2002, through June 30, 2002)	M	Q
SN0303F3912298.046 [DIRS 177945]	Measurements of displacement data for the DST corrected for thermal expansion (with results from July 1, 2002, through December 31, 2002)	M	Q
SN0308F3912298.052 [DIRS 177946]	Measurements of displacement data for the DST corrected for thermal expansion (with results from January 1, 2003, through June 30, 2003)	M	Q
SN0403F3912298.057 [DIRS 177948]	Measurements of displacement data for the DST corrected for thermal expansion (with results from July 1, 2003, through December 31, 2003)	M	Q
SN0410F3912298.063 [DIRS 177973]	Measurements of displacement data for the DST corrected for thermal expansion (with results from January 1, 2004, through June 30, 2004)	M	Q
SN0601F3912298.067 [DIRS 178005]	Measurements of displacement data for the DST corrected for thermal expansion (with results from July 1, 2004, through June 30, 2005)	M	Q
SN0608F3912298.071 [DIRS 177975]	Measurements of displacement data for the DST corrected for thermal expansion (with results from July 1, 2005, through June 30, 2006)	M	Q
LB990630123142.005 [DIRS 129274]	Ground penetrating radar data	H	Q
LB000121123142.004 [DIRS 158338]	Ground penetrating radar data	H	Q
LB000718123142.004 [DIRS 153354]	Ground penetrating radar data	H	Q
LB0101GPRDST01.001 [DIRS 158346]	Ground penetrating radar data	H	Q
LB0203GPRDSTE01.001 [DIRS 158350]	Ground penetrating radar data	H	Q
LB0108GPRDST05.001 [DIRS 158440]	Ground penetrating radar data	H	Q
LB0210GPRDSTHP.001 [DIRS 160895]	DST ground penetrating radar monitoring of water content over time (heating phase)	H	Q
LB0209GPRDSTCP.001 [DIRS 177817]	Ground penetrating radar for the cooling phase of the DST	H	Q



Table 4-3. Input DTNs for the Drift Scale Test (Continued)

Input DTN	Description	Type	Q Status
LB0210GPRDSTCP.001 [DIRS 160896]	DST ground penetrating radar monitoring of water content over time (cooling phase)	H	Q
LB0303GPRDSTCP.001 [DIRS 177822]	Ground penetrating radar for the cooling phase of the DST: processed data	H	Q
LB0309GPRDSTCP.001 [DIRS 177823]	Ground penetrating radar for the cooling phase of the DST: processed data	H	Q
LB0403GPRDSTCP.001 [DIRS 177824]	Ground penetrating radar for the cooling phase of the DST: processed data	H	Q
LB0509GPRDSTCP.001 [DIRS 177825]	Ground penetrating radar data for the cooling phase of the DST	H	Q
LB0603GPRDSTCP.001 [DIRS 177826]	Ground penetrating radar data for the cooling phase of the DST	H	Q
LB980120123142.004 [DIRS 105590]	Active baseline air injections in boreholes 57-61, 74-78, 185-186	H	Q
LB980420123142.002 [DIRS 113706]	Active hydrology testing for boreholes 57-61, 74-78, 185-186; air injection and gas tracer tests	H	Q
LB980715123142.002 [DIRS 113742]	Active hydrology testing data (air injection) collected from 12 hydrology boreholes: March 1998 to May 1998	H	Q
LB0101AIRKDST1.001 [DIRS 158345]	Active hydrology testing data (air injection) collected from 12 hydrology boreholes: June 1, 2000, to November 30, 2000	H	Q
LB981016123142.002 [DIRS 129245]	Active hydrology testing for boreholes 57-61, 74-78, 185-186; air injection tests: June 1998 to August 1999	H	Q
LB990630123142.001 [DIRS 129247]	Active hydrology testing by air injection: September 1998 to May 1999	H	Q
LB000121123142.002 [DIRS 158337]	Active hydrology testing by air injection: June 1999 to October 1999	H	Q
LB000718123142.002 [DIRS 158341]	Active hydrology testing data (air injection) collected from 12 hydrology holes: November 1, 1999, to May 31, 2000	H	Q
LB0108AIRKDST5.001 [DIRS 158438]	Active hydrology testing data (air injection) collected from 12 hydrology boreholes: December 1, 2000, to May 31, 2001	H	Q
LB0203AIRKDSTE.001 [DIRS 158348]	Active hydrology testing data (air injection) collected from 12 hydrology boreholes: June 1, 2001, to January 2002	H	Q
LB0209AIRKDSTC.001 [DIRS 177869]	Air pressure data for the cooling phase of the DST	H	Q
LB0303AIRKDSTC.001 [DIRS 177870]	Air pressure data for the cooling phase of the DST	H	Q
LB0309AIRKDSTC.001 [DIRS 177871]	Air pressure data for the cooling phase of the DST	H	Q
LB0403AIRKDSTC.001 [DIRS 177872]	Air pressure data for the cooling phase of the DST	H	Q
LB0410AIRKDSTC.001 [DIRS 177886]	Air pressure data for the cooling phase of the DST	H	Q
LB0509AIRKDSTC.001 [DIRS 177887]	Air pressure data for the cooling phase of the DST	H	Q

Table 4-3. Input DTNs for the Drift Scale Test (Continued)

Input DTN	Description	Type	Q Status
LB0603AIRKDSTC.001 [DIRS 178559]	Air pressure data for the cooling phase of the DST	H	Q
SNF39012298002.002 [DIRS 159114]	Measurements of displacement data for the DST (with results from November 1 1997, through May 31, 1998)	M	Q
SNF39012298002.010 [DIRS 158367]	MPBX and CDEX displacement September 1998 to May 1999	M	Q
SN0001F3912298.014 [DIRS 153841]	MPBX and CDEX displacement June 1999 to October 1999	M	Q
SN0007F3912298.018 [DIRS 158374]	MPBX and CDEX displacement November 1999 to May 2000	M	Q
SN0101F3912298.024 [DIRS 158400]	MPBX and CDEX displacement June 2000 to November 2000	M	Q
SN0107F3912298.029 [DIRS 158408]	MPBX and CDEX displacement December 2000 to May 2001	M	Q
SN0203F3912298.033 [DIRS 158361]	MPBX and CDEX displacement June 2001 to January 14, 2002	M	Q
SN0209F3912298.040 [DIRS 178009]	Measurements of displacement data for the DST (with results from January 15, 2002 through June 30, 2002)	M	Q
SN0303F3912298.044 [DIRS 178010]	Measurements of displacement data for the DST (with results from July 1, 2002, through December 31, 2002)	M	Q
SN0308F3912298.050 [DIRS 178011]	Measurements of displacement data for the DST (with results from January 1, 2003, through June 30, 2003)	M	Q
SN0403F3912298.055 [DIRS 178012]	Measurements of displacement data for the DST (with results from July 1, 2003, through December 31, 2003)	M	Q
SN0410F3912298.061 [DIRS 178013]	Measurements of displacement data for the DST (with results from January 1, 2004, through June 30, 2004)	M	Q
SN0601F3912298.065 [DIRS 178014]	Measurements of Displacement Data for the DST (with Results from July 1, 2004, through June 30, 2005)	M	Q
SN0608F3912298.069 [DIRS 178015]	Measurements of displacement data for the DST (with results from July 1, 2005, through June 30, 2006)	M	Q
MO0207AL5WATER.001 [DIRS 159300]	Water sampling in Alcove 5 (results from February 4, 1997, through April 20, 1999)	C	Q
MO0101SEPFDDST.000 [DIRS 153711]	Field measured data of water samples from the DST	C	Q
SN0203F3903102.001 [DIRS 159133]	DST water sampling (with results from April 17, 2001, through January 14, 2002)	C	Q
SN0210F3903102.004 [DIRS 170573]	DST water sampling (results from January 16, 2002, through April 4, 2002)	C	Q
SN0211F3903102.005 [DIRS 170574]	DST water sampling (results from April 25, 2002, through August 28, 2002)	C	Q
SN0303F3903102.006 [DIRS 178034]	DST water sampling (results from October 7, 2002, through February 18, 2003)	C	Q
SN0311F3903102.007 [DIRS 178035]	DST water sampling in Alcove 5 (results from April 3, 2003, through October 7, 2003)	C	Q

Table 4-3. Input DTNs for the Drift Scale Test (Continued)

Input DTN	Description	Type	Q Status
SN0411F3903102.009 [DIRS 178036]	DST water sampling in Alcove 5 on May 11, 2004, and September 16, 2004	C	Q
SN0507F3903102.010 [DIRS 178037]	DST water sampling in Alcove 5 on January 27, 2004	C	Q
SN0510F3903102.012 [DIRS 178038]	DST water sampling in Alcove 5 on January 25, 2005, and June 2, 2005	C	Q
SN0511F3903102.013 [DIRS 178039]	DST water sampling in Alcove 5 on November 8, 2005	C	Q
MO0005PORWATER.000 [DIRS 150930]	Perm-Sample pore water data	C	Q
LL001100931031.008 [DIRS 153288]	Aqueous chemistry of water sampled from boreholes of the DST	C	Q
LL001200231031.009 [DIRS 153616]	Aqueous chemistry of water sampled from boreholes of the DST	C	UQ
LL020302223142.015 [DIRS 159134]	Aqueous geochemistry of DST samples collected from HYD boreholes	C	Q
LL021107623121.014 [DIRS 169257]	Aqueous geochemistry of DST samples collected between April 20, 1999, and January 25, 2000	C	Q
LL030107523142.031 [DIRS 169258]	Anion concentrations of two DST samples collected between June 4, 1998, and March 30, 1999	C	UQ
LL990702804244.100 [DIRS 144922]	Borehole and pore water data	C	UQ
LB0011CO2DST08.001 [DIRS 153460]	Isotope data for CO <sub>2</sub> from gas samples collected from DST hydrology holes	C	Q
LB980420123142.005 [DIRS 111471]	Isotope data for CO <sub>2</sub> from gas samples collected from DST: February 1998	C	Q
LB980715123142.003 [DIRS 111472]	Isotope data for CO <sub>2</sub> from gas samples collected from DST: June 4, 1998	C	Q
LB0404ISODSTHP.003 [DIRS 169254]	Third submittal of CO <sub>2</sub> /H <sub>2</sub> O isotope data for the heating phase of the DST	C	Q
LB990630123142.003 [DIRS 111476]	Isotope data for CO <sub>2</sub> from gas and water samples: September 1998 to May 1999	C	Q
LB000121123142.003 [DIRS 146451]	Isotope data for CO <sub>2</sub> gas samples collected from the hydrology boreholes: August 9, 1999, through November 30, 1999	C	Q
LB000718123142.003 [DIRS 158342]	Isotope data for CO <sub>2</sub> gas samples collected from the hydrology boreholes: April 18, 2000, through April 19, 2000	C	Q
LB0102CO2DST98.001 [DIRS 159306]	Concentration and isotope data for CO <sub>2</sub> and H <sub>2</sub> O from gas samples collected from hydrology boreholes: May and August 1999, April 2000, January and April 2001	C	Q
LB0108CO2DST05.001 [DIRS 156888]	Concentration and isotope data for CO <sub>2</sub> and H <sub>2</sub> O from gas samples collected from hydrology boreholes: May and August 1999, April 2000, January and April 2001	C	Q
LB0203CO2DSTE.001 [DIRS 158349]	Concentration/isotope data for CO <sub>2</sub> /H <sub>2</sub> O from gas samples collected from hydrology boreholes up to end of heating	C	Q

Table 4-3. Input DTNs for the Drift Scale Test (Continued)

Input DTN	Description	Type	Q Status
LB0303ISODSTCP.001 [DIRS 177538]	Isotope data and CO <sub>2</sub> analysis for the cooling phase of the DST	C	Q
LB0309ISODSTCP.001 [DIRS 177539]	Isotope data and CO <sub>2</sub> analysis for the cooling phase of the DST	C	Q
LB0403ISODSTCP.001 [DIRS 177540]	Isotope data and CO <sub>2</sub> analysis for the cooling phase of the DST	C	Q
LB0410ISODSTCP.001 [DIRS 177541]	Isotope data and CO <sub>2</sub> analysis for the cooling phase of the DST	C	Q
LB0509ISODSTCP.001 [DIRS 177542]	Isotope data and CO <sub>2</sub> analysis for the cooling phase of the DST	C	Q
LB0206C14DSTEH.001 [DIRS 159303]	Carbon 14 isotope data from CO <sub>2</sub> gas samples collected from DST	C	Q
GS010808312322.004 [DIRS 156007]	Uranium and uranium isotope data for water samples from wells and springs in the Yucca Mountain vicinity collected between December 1996 and December 1997	C	Q
GS011108312322.008 [DIRS 159136]	Uranium concentrations and <sup>234</sup> U/ <sup>238</sup> U activity ratios analyzed between February 1, 1999, and August 1, 2001, for drift-scale heater test water collected between June 1998 and April 2001, and pore water collected between March 1996 and April 1999	C	Q
GS010608315215.002 [DIRS 156187]	Uranium and thorium isotope data for waters analyzed between January 18, 1994, and September 14, 1996	C	Q
GS011108312322.009 [DIRS 159137]	Strontium isotope ratios and strontium concentrations in water samples from the DST analyzed from March 16, 1999, to June 27, 2001	C	Q
GS960908315215.012 [DIRS 169552]	Strontium isotope ratios and isotope dilutions data for strontium analyzed July 6, 1995, to August 5, 1996	C	Q
GS010908315215.005 [DIRS 169553]	Strontium isotope ratios and strontium concentrations in calcite samples from the ESF analyzed from May 25, 2000, to June 5, 2001	C	Q
GS990308315215.004 [DIRS 145711]	Strontium isotope ratios and strontium concentrations in rock core samples and leachates from USW SD-9 and USW SD-12	C	Q
GS040508312272.002 [DIRS 169629]	Strontium isotope ratios and strontium concentrations on introduced materials to the ESF tunnel	C	UQ
GS990308315215.003 [DIRS 145707]	X-ray fluorescence elemental compositions of rock core samples from USW SD-9 and USW SD-12	C	Q
LL020405123142.019 [DIRS 159307]	Aqueous geochemistry of condensed fluids collected during studies of introduced materials	C	Q
LA0108FH831151.001 [DIRS 158316]	Data Collection System data	T,H,M,C	UQ
LA0111FH831151.001 [DIRS 169386]	Data Collection System data	T,H,M,C	UQ
LA0111FH831151.003 [DIRS 158318]	Data Collection System data	T,H,M,C	UQ
LA9908FH6001WP.001 [DIRS 158319]	Data Collection System data	T,H,M,C	UQ
LA0111FH831151.002 [DIRS 158317]	Data Collection System data	T,H,M,C	UQ

Table 4-3. Input DTNs for the Drift Scale Test (Continued)

Input DTN	Description	Type	Q Status
LA0208FH831151.001 [DIRS 159515]	Data Collection System data	T,H,M,C	UQ
LA0208FH831151.002 [DIRS 159308]	Data Collection System data	T,H,M,C	UQ
SNL22100196001.006 [DIRS 158213]	Thermal conductivity as function of saturation	T	Q
SN0203L2210196.007 [DIRS 158322]	Thermal expansion thermal conductivity DST specimens	T,M	Q
LL980411004244.060 [DIRS 159107]	DST baseline REKA probe measurements. Temperature measurements using REKA probes: November 14, 1997, to July 31, 1998.	T	Q
LL980902104244.070 [DIRS 159109]	DST baseline REKA probe measurements for thermal conductivity and diffusivity. Probe 1 from borehole 153, probe 2 from borehole 152, probe 3 from borehole 151.	T	Q
UN0106SPA013GD.003 [DIRS 159115]	DST REKA probe acquired data for thermal conductivity and diffusivity: May 1, 1998, to April 30, 2001	T	Q
UN0106SPA013GD.004 [DIRS 159116]	DST REKA probe developed data for thermal conductivity and diffusivity: May 1, 1998, to April 30, 2001	T	Q
UN0109SPA013GD.005 [DIRS 159117]	DST REKA probe acquired data for thermal conductivity and diffusivity: May 1, 2001, to August 31, 2001	T	Q
UN0112SPA013GD.006 [DIRS 159118]	DST REKA probe acquired data for thermal conductivity and diffusivity: September 1, 2001, to December 31, 2001	T	Q
UN0201SPA013GD.007 [DIRS 159119]	DST REKA probe developed data for thermal conductivity and diffusivity: May 1, 2001, to December 31, 2001	T	Q
LL000804023142.009 [DIRS 158325]	Water saturation	H	Q
LL980108804244.052 [DIRS 158332]	Electrical resistivity	H	Q
LL980406404244.057 [DIRS 113782]	Electrical resistance tomography	H	Q
LL990702704244.099 [DIRS 113872]	Electrical resistivity	H	Q
LL980808604244.065 [DIRS 113791]	Electrical resistance tomography	H	UQ
LL020307723142.018 [DIRS 177795]	Liquid saturation tomographs for the DST determined from electrical resistance tomography	H	Q
LL030606723142.035 [DIRS 177798]	Saturation and resistivity ratio tomographs from the DST for the period February 5, 2002, through October 1, 2002	H	Q
LL030906923142.038 [DIRS 177803]	Electrical resistivity and saturation ratio tomographs of the DST, March 4, 2003, through May 21, 2003	H	Q
LL040307423142.072 [DIRS 177806]	Electrical resistivity and saturation ratio tomographs of the DST for November 18-19, 2003	H	Q
LL041000223142.045 [DIRS 177807]	Saturation ratio and resistivity ratio tomographs from the DST for the period January 1, 2004, through June 30, 2004	H	Q

Table 4-3. Input DTNs for the Drift Scale Test (Continued)

Input DTN	Description	Type	Q Status
LL050902223142.048 [DIRS 177809]	Saturation Ratio and resistivity ratio tomographs from the DST for the period January 1, 2005, through June 30, 2005	H	Q
LL060303223142.051 [DIRS 177810]	Saturation ratio tomographs from the DST for the period July 1, 2005, through December 31, 2005	H	UQ
LL020710223142.024 [DIRS 159551]	Neutron logging	H	Q
LL030309723122.022 [DIRS 165700]	Moisture content of rock from neutron logging activities in the DST: July 2002 through November 2002	H	Q
LL030709023122.032 [DIRS 165701]	Moisture content of rock from neutron logging activities in the DST: January 2003 through May 2003	H	Q
LL040308623122.043 [DIRS 177827]	Moisture content of rock from neutron logging activities in the DST: May 2003 through November 2003	H	Q
LL041001623122.052 [DIRS 177831]	Moisture content of rock from neutron logging activities in the DST: January 1, 2004 through June 30, 2004	H	Q
LL050206323122.057 [DIRS 177829]	Moisture content of rock from neutron logging activities in the DST: July 1, 2004 through December 31, 2004	H	Q
LL060101523122.066 [DIRS 177833]	Moisture content of rock from neutron logging activities in the DST: February 2005 through September 2005	H	Q
LL060302423122.067 [DIRS 177834]	Moisture content of rock from neutron logging activities in the DST: October 2005 through December 2005	H	Q
LB970600123142.001 [DIRS 105589]	Active DST preheating air injection, part 1 of 2	H	Q
LB980120123142.005 [DIRS 114134]	Active DST preheating air injection, part 2 of 2	H	Q
LB0401PRTDSTHP.001 [DIRS 169251]	Passive monitoring data for boreholes 57-61, 74-78, 185-186: November 1997 to February 1998	H	Q
LB0401PRTDSTHP.002 [DIRS 169252]	Passive monitoring data collected from 12 hydrology boreholes: March 1998 to May 1998	H	Q
LB0401PRTDSTHP.003 [DIRS 169253]	Passive monitoring data for boreholes 57-61, 74-78, 185-186 taken from June 1998 to August 1998, Third Quarter	H	Q
LB0401PRTDSTHP.004 [DIRS 169255]	Passive monitoring data (pressure and temperature): September 1998 to May 1999	H	Q
LB0401PRTDSTHP.005 [DIRS 169246]	Passive monitoring data (pressure and temperature): June 1 through October 31, 1999	H	Q
LB0401PRTDSTHP.006 [DIRS 169247]	Passive monitoring data collected from 12 hydrology boreholes test: November 1, 1999, to May 31, 2000	H	Q
LB0401PRTDSTHP.007 [DIRS 169248]	Passive monitoring data collected from 12 hydrology boreholes: June 1, 2000, to November 30, 2000	H	Q
LB0401PRTDSTHP.008 [DIRS 169249]	Passive monitoring data collected from 12 hydrology boreholes: December 1, 2000, to May 31, 2001	H	Q
LB0401PRTDSTHP.009 [DIRS 169250]	Passive monitoring data collected from 12 hydrology boreholes: June 1, 2001, through end of heating phase January 14, 2002	H	Q
LB0401PRTDSTCP.001 [DIRS 170568]	Passive monitoring data (temperature and pressure) for the DST (January 15, 2002, through June 30, 2002)	H	Q

Table 4-3. Input DTNs for the Drift Scale Test (Continued)

Input DTN	Description	Type	Q Status
LB0401PRTDSTCP.002 [DIRS 170569]	Passive monitoring data (temperature and pressure) for the DST (July 1, 2002, through December 31, 2002)	H	Q
LB0309H2ODSTCP.001 [DIRS 177905]	Passive temperature and pressure monitoring data for the cooling phase of the DST	H	Q
LB0403PRTDSTCP.001 [DIRS 177906]	Passive monitoring data (temperature and pressure) for the DST	H	Q
LB0410PRTDSTCP.001 [DIRS 177907]	Passive temperature and pressure monitoring data for the cooling phase of the DST (January 1, 2004, through June 30, 2004)	H	Q
LB0609PRTDSTCP.001 [DIRS 177908]	Passive temperature and pressure monitoring data for the cooling phase of the DST (July 1, 2004, through June 30, 2005)	H	Q
LB0609PRTDSTCP.002 [DIRS 177909]	Passive temperature and pressure monitoring data for the cooling phase of the DST (July 1, 2005, through December 31, 2005)	H	Q
LB0401RHMDSTHP.001 [DIRS 177911]	Passive monitoring data (relative humidity) for the DST (November 1, 1997, through February 28, 1998)	H	UQ
LB0401RHMDSTHP.002 [DIRS 177914]	Passive monitoring data (relative humidity) for the DST (March 1, 1998, through May 31, 1998)	H	UQ
LB0401RHMDSTHP.003 [DIRS 177915]	Passive monitoring data (relative humidity) for the DST (June 1, 1998, through August 31, 1998)	H	UQ
LB0401RHMDSTHP.004 [DIRS 177916]	Passive monitoring data (relative humidity) for the DST (September 1, 1998, through May 31, 1999)	H	UQ
LB0401RHMDSTHP.005 [DIRS 177918]	Passive monitoring data (relative humidity) for the DST (June 1, 1999, through October 31, 1999)	H	UQ
LB0401RHMDSTHP.006 [DIRS 177920]	Passive monitoring data (relative humidity) for the DST (November 1, 1999, through May 31, 2000)	H	UQ
LB0401RHMDSTHP.007 [DIRS 177921]	Passive monitoring data (relative humidity) for the DST (June 1, 2000, through November 30, 2000)	H	UQ
LB0401RHMDSTHP.008 [DIRS 177922]	Passive monitoring data (relative humidity) for the DST (December 1, 2000, through May 31, 2001)	H	UQ
LB0401RHMDSTHP.009 [DIRS 177924]	Passive monitoring data (relative humidity) for the DST (June 1, 2001, through January 14, 2002)	H	UQ
LB0401RHMDSTCP.001 [DIRS 177929]	Passive monitoring data (relative humidity) for the DST (January 15, 2002, through June 30, 2002)	H	UQ
LB0401RHMDSTCP.002 [DIRS 177930]	Passive monitoring data (relative humidity) for the DST (July 1, 2002, through December 31, 2002)	H	UQ
LB0311RHMDSTCP.001 [DIRS 177932]	Passive relative humidity monitoring data for the cooling phase of the DST	H	UQ
LB0403RHMDSTCP.001 [DIRS 177933]	Passive monitoring data (relative humidity) for the DST	H	UQ
LB0410RHMDSTCP.001 [DIRS 177935]	Passive relative humidity monitoring data for the cooling phase of the DST (January 1, 2004, through June 30, 2004)	H	UQ
LB0509RHMDSTCP.001 [DIRS 177937]	Passive relative humidity monitoring data for the cooling phase of the DST (July 1, 2004, through June 30, 2005)	H	UQ
LB0603RHMDSTCP.001 [DIRS 177938]	Passive relative humidity monitoring data for the cooling phase of the DST (July 1, 2005, through December 31, 2005)	H	UQ

Table 4-3. Input DTNs for the Drift Scale Test (Continued)

Input DTN	Description	Type	Q Status
LB970500123142.003 [DIRS 131500]	Laboratory saturation, porosity, bulk density, particle density, gravimetric water content data from dry-drilled and wet-drilled cores in the DST and SHT	H	Q
LL020506123142.021 [DIRS 169256]	Laboratory moisture retention and porosity	H	Q
LL020502523142.020 [DIRS 159105]	Laboratory measured electrical properties of the DST samples as a function of saturation at 95°C	H	Q
LL981109904242.072 [DIRS 118959]	Saturated and dry bulk density permittivity	H	Q
LL980411104244.061 [DIRS 159111]	DST baseline REKA probe measurements for thermal conductivity and diffusivity; VA supporting data	T	Q
SNF39012298002.006 [DIRS 158419]	MPBX and CDEX displacement June 1998 to August 1998	M	Q
SNF38040197001.001 [DIRS 159130]	Strain-gage and anchor locations	M	Q
SNF39012298002.003 [DIRS 158417]	Ground support system strain: November 9, 1997, to May 1998	M	Q
SNF39012298002.007 [DIRS 158365]	Ground support system strain: June 1998 to August 1998	M	Q
SNF39012298002.011 [DIRS 158368]	Ground support system strain: September 1998 to May 1999	M	Q
SN0001F3912298.015 [DIRS 158372]	Ground support system strain: June 1999 to October 1999	M	Q
SN0007F3912298.019 [DIRS 158387]	Ground support system strain: November 1999 to May 2000	M	Q
SN0101F3912298.025 [DIRS 158401]	Ground support system strain: June 2000 to November 2000	M	Q
SN0107F3912298.030 [DIRS 158409]	Ground support system strain: December 2000 to May 2001	M	Q
SN0203F3912298.034 [DIRS 158362]	Ground support system strain: June 2001 to January 14, 2002	M	Q
SN0209F3912298.041 [DIRS 178019]	Measurements of strain data for the DST (with results from January 15, 2002, through June 30, 2002)	M	Q
SN0303F3912298.045 [DIRS 178020]	Measurements of strain data for the DST (with results from July 1, 2002, through December 31, 2002)	M	Q
SN0308F3912298.051 [DIRS 178021]	Measurements of strain data for the DST (with results from January 1, 2003, through June 30, 2002)	M	Q
SN0403F3912298.056 [DIRS 178022]	Measurements of strain data for the DST (with results from July 1, 2003, through December 31, 2003)	M	Q
SN0410F3912298.062 [DIRS 178023]	Measurements of strain data for the DST (with results from January 1, 2004, through June 30, 2004)	M	Q
SN0601F3912298.066 [DIRS 178024]	Measurements of strain data for the DST (with results from July 1, 2004, through June 30, 2005)	M	Q
SN0608F3912298.070 [DIRS 178025]	Measurements of strain data for the DST (with results from July 1, 2005, through June 30, 2006)	M	Q



Table 4-3. Input DTNs for the Drift Scale Test (Continued)

Input DTN	Description	Type	Q Status
SNF39012298002.005 [DIRS 158418]	Ground support system strain corrected for thermal expansion: November 9, 1997, to May 1998	M	Q
SNF39012298002.013 [DIRS 158369]	Ground support system strain corrected for thermal expansion: September 1998 to May 1999	M	Q
SN0001F3912298.017 [DIRS 158373]	Ground support system strain corrected for thermal expansion: June 1999 to October 1999	M	Q
SN0007F3912298.021 [DIRS 158391]	Ground support system strain corrected for thermal expansion: November 1999 to May 2000	M	Q
SN0101F3912298.027 [DIRS 158407]	Ground support system strain corrected for thermal expansion: June 2000 to November 2000	M	Q
SN0107F3912298.032 [DIRS 158414]	Ground support system strain corrected for thermal expansion: December 2000 to May 2001	M	Q
SN0203F3912298.036 [DIRS 158364]	Ground support system strain corrected for thermal expansion: June 2001 to January 14, 2002	M	Q
SN0209F3912298.043 [DIRS 178027]	Measurements of strain data for the DST (with results from January 15, 2002, through June 30, 2002)	M	Q
SN0303F3912298.047 [DIRS 178028]	Measurements of strain data for the DST (with results from July 1, 2002, through December 31, 2002)	M	Q
SN0308F3912298.053 [DIRS 178029]	Measurements of strain data for the DST (with results from January 1, 2003, through June 30, 2003)	M	Q
SN0403F3912298.058 [DIRS 178030]	Measurements of strain data for the DST (with results from July 1, 2003, through December 31, 2003)	M	Q
SN0410F3912298.064 [DIRS 178031]	Measurements of strain data for the DST (with results from January 1, 2004, through June 30, 2004)	M	Q
SN0601F3912298.068 [DIRS 178032]	Measurements of strain data for the DST (with results from July 1, 2004, through June 30, 2005)	M	Q
SN0608F3912298.072 [DIRS 178033]	Measurements of strain data for the DST (with results from July 1, 2005, through June 30, 2006)	M	Q
LB980120123142.007 [DIRS 158352]	Acoustic emissions: baseline and heating	M	Q
LB980420123142.004 [DIRS 113717]	Acoustic emissions: baseline and heating	M	Q
LB000121123142.005 [DIRS 158339]	Acoustic emissions: baseline and heating	M	Q
LB000718123142.005 [DIRS 158343]	Acoustic emissions: baseline and heating	M	Q
LB0101ACEMDST1.001 [DIRS 158344]	Acoustic emissions: baseline and heating	M	Q
LB0108ACEMDST5.001 [DIRS 158437]	Acoustic emissions: baseline and heating	M	Q
SNF39012298002.009 [DIRS 158366]	Ground support system strain corrected for thermal expansion: June 1998 to August 1998	M	Q
SNL02100196001.001 [DIRS 158420]	Elastic constants and strength properties	M	Q

Table 4-3. Input DTNs for the Drift Scale Test (Continued)

Input DTN	Description	Type	Q Status
SNL23030598001.001 [DIRS 158370]	Elastic constants and strength of concrete	M	Q
SN0011F3912298.022 [DIRS 158392]	Rock mass displacement pressure data plate load test October 16 and 17, 2000	M	Q
SN0011F3912298.023 [DIRS 158399]	Rock mass displacement pressure data in modulus October 16 and 17, 2000	M	Q
SN0306F3912298.048 [DIRS 165416]	Plate-loading measured displacement and test pressure data for 2003 (with Results from April 30, 2003)	M	Q
SN0310F3912298.054 [DIRS 168527]	Updated plate-loading rock mass modulus data for 2003	M	Q
LA9912SL831151.002 [DIRS 146449]	Percent coverage by fracture-coating minerals in core ESF-HD-TEMP-2	C	Q
LA0201SL831225.001 [DIRS 158426]	Chemical, textural, and mineralogical characteristics of sidewall samples from the DST	C	Q
LA0303WS831151.001 [DIRS 169378]	Amorphous Silica in DST sidewall samples	C	Q
LA0009SL831151.001 [DIRS 153485]	Fracture mineralogy of the ESF Single Heater Test Block, Alcove 5	C	Q
LA0609SL831322.001 [DIRS 178052]	Mineralogy of red spot deposit from DST	C	Q
GS970608314244.006 [DIRS 158429]	Fracture mapping	G	Q
LARO831422AQ97.002 [DIRS 158431]	DST borehole video logging	G	Q
GS020808312272.004 [DIRS 166569]	Analysis of water-quality samples July 1999 to July 2002	C	UQ
GS030408312272.002 [DIRS 165226]	Analysis of water-quality samples July 2002 to November 2002	C	Q
GS031008312272.008 [DIRS 166570]	Analysis of pore water and miscellaneous water samples for the period from December 2002 to July 2003	C	Q
GS041108312272.005 [DIRS 178057]	Analysis of pore water and miscellaneous water samples for the period from July 2003 to September 2004	C	Q
GS040308312272.001 [DIRS 178056]	Gravimetric moisture content measurements for HD-CHEMSAMP cores for the period from June 2002 to January 2004	C	Q
LB0211DSTRBRDG.001 [DIRS 170566]	DST packer materials investigation	C	Q
LB0302NEOPDGRD.001 [DIRS 170567]	Neoprene degradation experiments	C	Q
LB980912332245.002 [DIRS 105593]	Gas tracer data from Niche 3 (Also referred to as Niche 3107) of the ESF	C	Q
LL030305023121.023 [DIRS 170570]	Aqueous geochemistry of DST water samples collected February and March 2002 from borehole 75, zone 2	C	UQ
LL030310023121.024 [DIRS 170571]	Chemical composition of water samples collected from hydraulic boreholes of the DST	C	UQ

Table 4-3. Input DTNs for the Drift Scale Test (Continued)

Input DTN	Description	Type	Q Status
LL030605512251.064 [DIRS 170572]	Thermogravimetric analysis on the thermal decomposition of fluoroelastomer samples taken from boreholes 60 and 72	C	UQ
LB0208ACEMDSTH.001 [DIRS 170575]	Acoustic emission for the heating phase of the DST	M	Q
LB0208GPRDSTHP.001 [DIRS 170577]	Ground penetrating radar for the heating phase of the DST	H	Q
LB0208AIRKDSTH.001 [DIRS 160897]	Air permeability data for the heating phase of the DST	H	Q
LB0208H2ODSTHP.001 [DIRS 170579]	Passive hydrological data for the heating phase of the DST	H	Q
LB0208ISODSTHP.001 [DIRS 161638]	Gas chemistry (CO <sub>2</sub> concentration and isotopic data) for the heating phase of the DST.	C	Q
LL020709923142.023 [DIRS 161677]	Aqueous geochemistry of borehole waters collected in the heating phase of the DST	C	Q
LL020801723142.028 [DIRS 170580]	Electrical resistance tomographs of the DST November 1997 through December 2001	H	UQ
MO0208RESTRDST.002 [DIRS 161129]	Restructured DST heating phase power and temperature data	T	Q
MO0406SEPDSTHP.000 [DIRS 170615]	DST heating phase power and reference temperature data	T	Q
MO0406SEPTVDST.000 [DIRS 170616]	Temperature and volume water content for DST heating phase for boreholes 79 and 80	T	Q
SN0208F3903102.002 [DIRS 161246]	Summary of thermal test water samples and field measurements through January 14, 2002	C	Q
SN0208F3903102.003 [DIRS 170620]	Field measurements and Fluoride content from Hydrogen Fluoride tests	C	Q
SN0208F3912298.038 [DIRS 170610]	Summary of smoothed measurements of strain data for the heating phase of the DST	M	UQ
SN0407F3912298.060 [DIRS 170627]	Rock mass thermal expansion coefficients for the DST compared with in situ measurements	M	Q

NOTES: All input DTNs are indirect input.

DTNs: LA9908FH6001WP.001 [DIRS 158319], LA0111FH831151.002 [DIRS 158317], LA0208FH831151.001 [DIRS 159515], LA0108FH831151.001 [DIRS 158316], LA0111FH831151.001 [DIRS 169386], LA0111FH831151.003 [DIRS 158318], and LA0208FH831151.002 [DIRS 159308] provide access via the RPC to all thermal and mechanical data collected in the DST Data Collection System (original/electrical and converted/engineering units). These unqualified DTNs also provide access (via the RPC) to pertinent supporting material such as scientific notebooks and calibration relationships.

T = thermal, H = hydrological, M = mechanical, C = chemical, G = general/miscellaneous.

Q = qualified, UQ = unqualified. Data sets listed as UQ should be used only for corroborative purposes.

CDEX = cross-drift extensometer; MPBX = multipoint borehole extensometer; REKA = Rapid Evaluation of K and Alpha.

INTENTIONALLY LEFT BLANK

## 5. ASSUMPTIONS

The following assumption is listed for informational purposes only. This assumption was included in the original version of *Thermal Testing Measurements Report* (BSC 2002 [DIRS 160771]) and has been preserved in this revision because it discusses measurements requiring complex data reduction.

### 5.1 AIR PERMEABILITY ANALYSIS

**Assumption:** The development of air permeabilities from air-injection flow rates and pressure responses assumes that (a) air behaves as an ideal gas, (b) a finite line source can represent a borehole injection interval, and (c) air flows are governed by Darcy's law.

**Basis:** The following discussion pertains to measurements described in Sections 6.2.2.4 and 6.3.2.4. Based on the detailed discussion below, further confirmation of this assumption is not required.

During air-injection testing, local permeability is estimated from the steady-state pressure response to a constant flow rate gas injection. An analytical solution for the steady-state pressure response of a constant flow rate injection in a finite line source is applied to estimate gas permeability near the well bore. The solution was adapted from the steady-state analytical solution for ellipsoidal flow of incompressible fluid from a finite line source (Hvorslev 1951 [DIRS 101868]) in an infinite medium ( $L/r_w \gg 1$ ) and is as follows:

$$k = \frac{P_{SC} Q_{SC} \mu \ln\left(\frac{L}{r_w}\right) T_f}{\pi L (P_2^2 - P_1^2) T_{SC}} \quad (\text{Eq. 5.1-1})$$

where:

$k$	=	permeability ( $\text{m}^2$ )
$P_{SC}$	=	pressure at standard conditions ( $1.013 \times 10^5$ Pa)
$Q_{SC}$	=	flowrate at standard conditions ( $\text{m}^3/\text{s}$ )
$\mu$	=	dynamic viscosity of air ( $1.81 \times 10^{-5}$ Pa · s at 20°C)
$L$	=	length of air injection zone (m)
$r_w$	=	radius of borehole (m)
$T_f$	=	temperature of formation (K)
$P_2$	=	steady state pressure (Pa)
$P_1$	=	ambient pressure (Pa)
$T_{SC}$	=	temperature at standard conditions (293.16 K)

Equation 5.1-1 is discussed in Section 8.1.1.1 of *Single Heater Test Final Report* (CRWMS M&O 1999 [DIRS 129261]). It assumes a finite length and finite radius cylindrical injection source, surrounded by a homogeneous medium of infinite extent. In cases where the assumptions of an effective continuum are not valid, Equation 5.1-1 still yields a useful quantitative value that reflects the rock-mass gas injectivity. Here injectivity is defined as a measure of the formation's ability to permit gas flow. Changes in permeability (or formation injectivity) during heating and cooling are indicative of changes in fracture liquid saturation, or opening and closing of fractures from thermal-hydrological-mechanical coupling. As fracture saturation increases or fractures close, gas injectivity decreases. Similarly, a decrease in fracture liquid saturation or increase in fracture opening will lead to an increase in gas injectivity. For both the SHT and DST, changes in permeability will be reported as a ratio of measured permeability to the baseline value, established prior to the start of heating.

The user of the permeability estimates should understand the limitations of a continuum model in interpreting measurements performed in a heterogeneous formation, such as the Topopah Spring middle nonlithophysal tuff. An example of model limitations is a block of rock that contains only a single transmissive feature. An injection test can be performed with a straddle packer that spans length  $L$  of a formation that includes this single transmissive feature, leading to an estimate of permeability,  $k$ . If a shorter injection interval is tested, for example  $L/10$ , where this same single transmissive feature is straddled, it is erroneous to assume that Equation 5.1-1 will provide an accurate estimate of formation permeability. However, by repeatedly performing measurements using the same testing configuration, changes in permeability can be tracked as thermal testing proceeds. For both the SHT and the DST, the air permeability test intervals were kept fixed between quarterly air-injection tests, excluding the DST zones that varied as a result of pneumatic-packer failures.

## 6. DISCUSSION OF MEASUREMENTS

In general, the discussions that follow were taken from the original version of *Thermal Testing Measurements Report* (BSC 2002 [DIRS 160771]) and modified as necessary for this version of the report.

The scientific phenomena investigated are the thermal-hydrological-mechanical-chemical behaviors measured in each of the three thermal tests: the Large Block Test (LBT), the Single Heater Test (SHT), and the Drift Scale Test (DST). Parameters in this report reflect laboratory and field measurements that characterized the respective test blocks for each of the three thermal tests. As discussed in Section 1, data collected within the Yucca Mountain Project (YMP) Thermal Testing Program must be readily usable to end users. Since either detailed YMP reports exist or the measurements are straightforward, only brief discussions are provided for each data set. These brief discussions for different data sets are intended to impart a clear sense of applicability of data, so that end users will be able to use and interpret these data properly within the context of measurement uncertainty. This approach also keeps the report to a manageable size, an important consideration since it encompasses nearly all measurements for three long-term thermal tests. As appropriate, thermal testing data currently residing in the Technical Data Management System (TDMS) have been reorganized and reformatted into summary DTNs. In many cases, these summary DTNs contain test data sampled on a more infrequent basis (e.g., every 10 days) than the actual data obtained from testing (e.g., every hour). This serves to make the summary DTN data sets more manageable when used for modeling purposes. In some cases, there was no need to reformat or restructure existing DTNs, so they remained unchanged.

Discussion of the thermal testing measurements in this report is organized first under the heading of the three tests: LBT, SHT, and DST; and then under the four processes: thermal, hydrological, mechanical, and chemical. Miscellaneous measurements and observations are also discussed. Although the list of measurement types is comprehensive, it is neither practical (because of finite report length) nor necessary to thoroughly discuss all data sets. For example, the DST-measured temperatures come from nearly 2,700 thermal sensors distributed throughout the test block and collected on an hourly basis, resulting in approximately 100 million measurements. Therefore, as appropriate for each measurement type, only a representative discussion of the test data behavior is presented. Readers are referred to the summary DTNs for comprehensive data sets that include complementary graphics.

The following discussions concerning the 12 basic measurement groups (three thermal tests and four processes) are dictated by their respective data characteristics. In general, discussions of thermal and mechanical measurements tend to be comparatively short, although the respective summary DTNs contain comparatively large amounts of data. This condition reflects the inherent straightforwardness of temperature and displacement measurements that are recorded frequently (hourly) on a data acquisition system. Conversely, discussions of hydrological and chemical measurements tend to be lengthier, while their summary DTNs are comparatively small. The smaller output data sets result from measurements collected comparatively infrequently (monthly or longer) on a nonintegrated data acquisition system. The more lengthy discussion in the chemical measurements sections relates to sampling procedures that have relevance to the data collected. Also, in certain hydrological measurements, detailed

explanations are needed for the complex reduction that occurs as the data are transformed into summary DTNs.

In addition, uncertainty associated with most measurements is discussed. These discussions of uncertainty are restricted to actual measurements and data reduction. Standard error analyses (mean and standard deviation) were provided for applicable measurements such as repetitive measurements of laboratory or field parameters. Test measurements of a response for a specific location and time are not applicable for standard error analyses. Additional information on measurement uncertainties can be located via directions in DTNs cited in the first footnote of Tables 4-1, 4-2, and 4-3. This information, among other things, provides detailed discussions of scientific notebooks and calibration relationships relevant to uncertainties of thermal testing measurements. The approach taken provides sufficient discussion of uncertainties for end-users of thermal testing measurements such as process modelers. In cases where uncertainty is redundant among two or all three thermal tests, the initial discussion of uncertainty is referenced. Also included in this report are summaries of three “white papers” involving in-depth investigations of unexpected or unusual DST behavior. Summaries are found in Sections 6.3.2.6 and 6.3.4.5.

## **6.1 LARGE BLOCK TEST**

The Large Block Test (LBT) was a controlled test to provide data for a better understanding of the coupled thermal-hydrologic-mechanical-chemical processes in a heated unsaturated rock mass. The LBT was conducted at the outcrop of the middle nonlithophysal unit of the Topopah Spring Tuff (Ttptmn) at Fran Ridge, Nevada. A column of the rock mass  $3 \times 3 \times 4.5$  m high was isolated from the outcrop at the eastern slope of Fran Ridge (see Figure 6.1-1). The base of the column is still connected to the ground. The block was heated from February 28, 1997, to March 10, 1998. A natural cooling phase started on March 10, 1998, until the termination of the data acquisition on September 30, 1998.

Tables 4-1 and 6.1-1 provide a listing of LBT input DTNs and summary DTNs, respectively. The summary DTNs provide either test measurements or parameter values and related graphics and coordinates of the sensors used in the test measurements. Table 4-1 also provides the qualification status of the measurements. For ease of thermal modeling, a one-dimensional thermal field (having a thermal gradient dependent only on the z direction) within the block was created by line heaters used to simulate a planar heat source located at a height of approximately one-third of the total height of the block (1.75 m from the base of the block). A heat exchanger system was used to maintain a constant temperature, about 60°C, on the top surface of the block. This system consisted of an aluminum plate fitted with heating/cooling coils mounted on the top of the block. This plate was connected to a heat exchanger to allow thermal control of the top surface.

To achieve a one-dimensional thermal-hydrological (TH) process in the z (up) direction, a layer of room-temperature vulcanized rubber and Viton was installed on the block sides to minimize moisture flux. Three layers of thermal-insulation materials were installed on the outside of the moisture barrier. All of the sensor boreholes were sealed by cement grout, packers, or a room-temperature vulcanized rubber/Teflon membrane.



Table 6.1-1. DTNs for the Large Block Test

Input DTN	Input DTN Description	Input DTN Text Location	Summary DTN	Summary DTN Description
LA0106FH831151.002 <sup>a</sup> [DIRS 158230]	Data Collection System data	6.1	Unchanged DTN	Unchanged DTN
LA0106FH831151.003 <sup>a</sup> [DIRS 158229]	Data Collection System data	6.1	Unchanged DTN	Unchanged DTN
LL981110704244.085 <sup>b</sup> [DIRS 169259]	Large Block Test Report, Chapter 4	6.1	Unchanged DTN	Unchanged DTN
LL980918904244.074 <sup>b</sup> [DIRS 135872]	Heater power, temperature, relative humidity, and gas pressure	6.1.1.1 6.1.1.2 6.1.2.3	LL020710523142.025 <sup>b</sup> [DIRS 164182]	Heater power, temperature, and displacement data
LL980919404244.076 [DIRS 148630]	Rock mass displacements	6.1.3.1 6.1.3.2		
LL980913304244.072 [DIRS 145385]	Electrical resistance tomograms	6.1.2.1	Unchanged DTN	Unchanged DTN
LL981001604244.079 [DIRS 158261]	Electrical resistivity	6.1.2.1	Unchanged DTN	Unchanged DTN
LL980919304244.075 [DIRS 145099]	Neutron logging	6.1.2.2	Unchanged DTN	Unchanged DTN
LL971204304244.047 [DIRS 113894]	Neutron logging	6.1.2.2	Unchanged DTN	Unchanged DTN
LL970803404244.040 [DIRS 113889]	Data on moisture content in the LBT	6.1.2.2	Unchanged DTN	Unchanged DTN
LL950812704242.017 <sup>b</sup> [DIRS 158237]	Porosity, saturated and dry density	6.1.2.4	Unchanged DTN	Unchanged DTN
LL960905204244.022 [DIRS 158244]	Laboratory matrix permeability	6.1.2.4	Unchanged DTN	Unchanged DTN
LL981208404244.092 <sup>b</sup> [DIRS 158263]	X-ray radiography	6.1.2.4	Unchanged DTN	Unchanged DTN
LL960400404244.012 [DIRS 158271]	Fracture mapping	6.1.4.1	Unchanged DTN	Unchanged DTN
LL960400504244.013 [DIRS 158274]	Fracture mapping	6.1.4.1		
LL960400604244.014 [DIRS 158275]	Fracture mapping	6.1.4.1		
LL960400704244.015 [DIRS 158276]	Fracture mapping	6.1.4.1		
LL981202305912.004 <sup>b</sup> [DIRS 158270]	Bacterial transport	6.1.4.3	Unchanged DTN	Unchanged DTN

<sup>a</sup> DTNs: LA0106FH831151.002 [DIRS 158230] and LA0106FH831151.003 [DIRS 158229] provide access (via the RPC) to all thermal and mechanical data collected in the LBT Data Collection System (original/electrical and converted/engineering units). These unqualified DTNs also provide access (via the RPC) to pertinent measurement information such as scientific notebooks and calibration procedures. These DTNs should be used for corroborative purposes only.

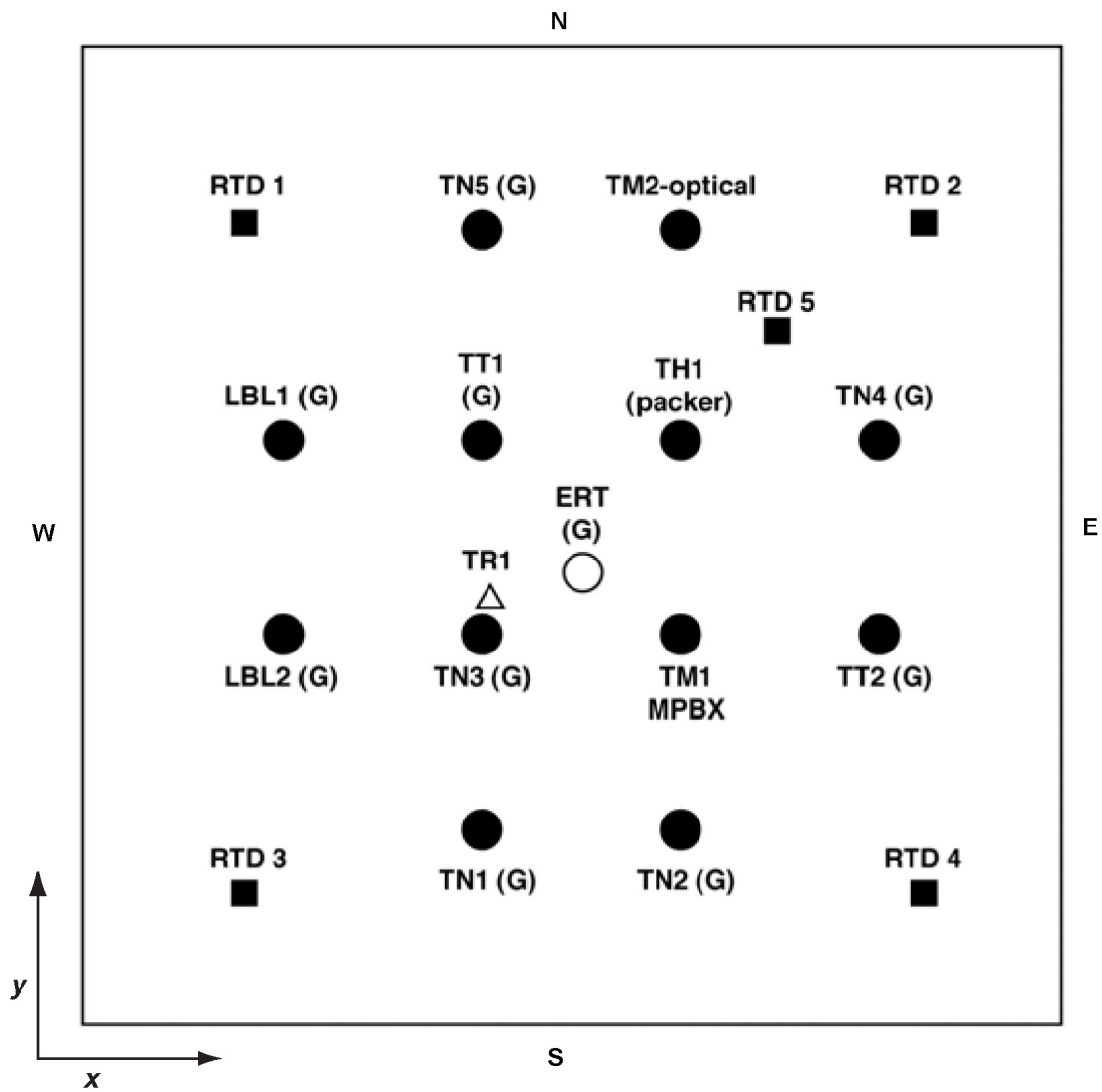
<sup>b</sup> These unqualified DTNs should be used for corroborative purposes only.



Source: Lin et al. 2001 [DIRS 159069].

Figure 6.1-1. LBT Block of Topopah Spring Tuff at Fran Ridge

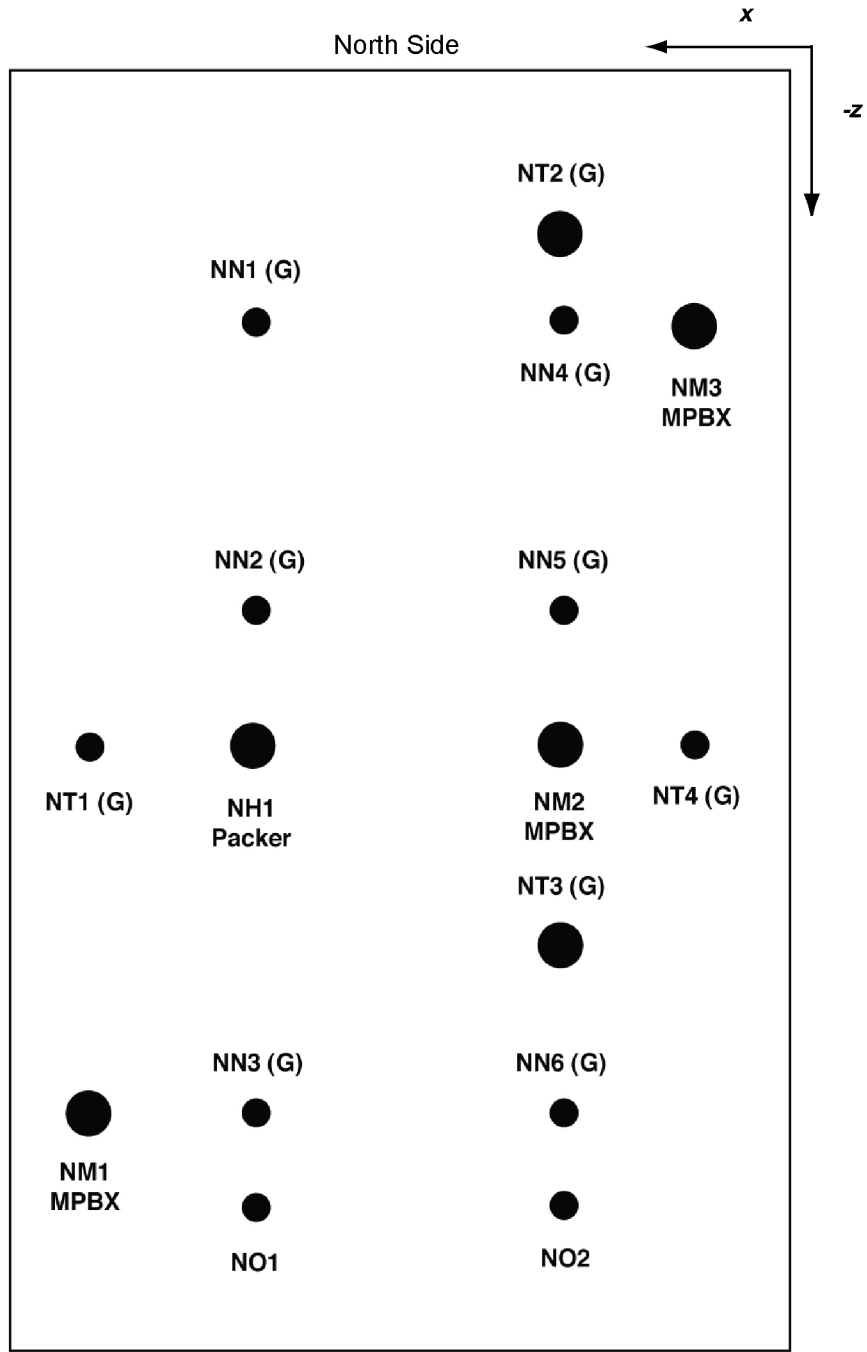
Sensors in the block measured heater power, temperature, moisture content, mechanical deformations, thermal conductivity and diffusivity, relative humidity, and gas pressure. Air permeability was measured before the heating and at the end of the heating phase. Figures 6.1-2 through 6.1-5 (DTN: LL981110704244.085 [DIRS 169259], unqualified) show the sensor boreholes in the top and sides of the block. There are no sensor boreholes in the south side of the block. The assessment of the chemical process in the block was achieved by comparing the mineralogical changes in the core samples obtained before and after the test. Small blocks of the rock were obtained from the proximity of the large block for conducting laboratory tests to determine hydrologic and mechanical properties. Microbial survivability and migration were also investigated. These measurements and observations are described in greater detail in the following sections. Table 6.1-2 shows the XYZ coordinates of the collar and bottom of all of the boreholes in the LBT.



- TT# - Temperature measurements - borehole
- RTD# - Temperature - Surface-mounted RTD
- LBL# - Open holes used by LBNL for air and then grouted
- TN# - Neutron holes lined and grouted
- TR1 - REKA probe - grouted
- TM# - Mechanical - MPBX borehole
- ERT - ERT electrode hole, grouted
- TH - Hydrologic hole with packers
- G - Grouted

Source: DTN: LL981110704244.085 [DIRS 169259] (unqualified).

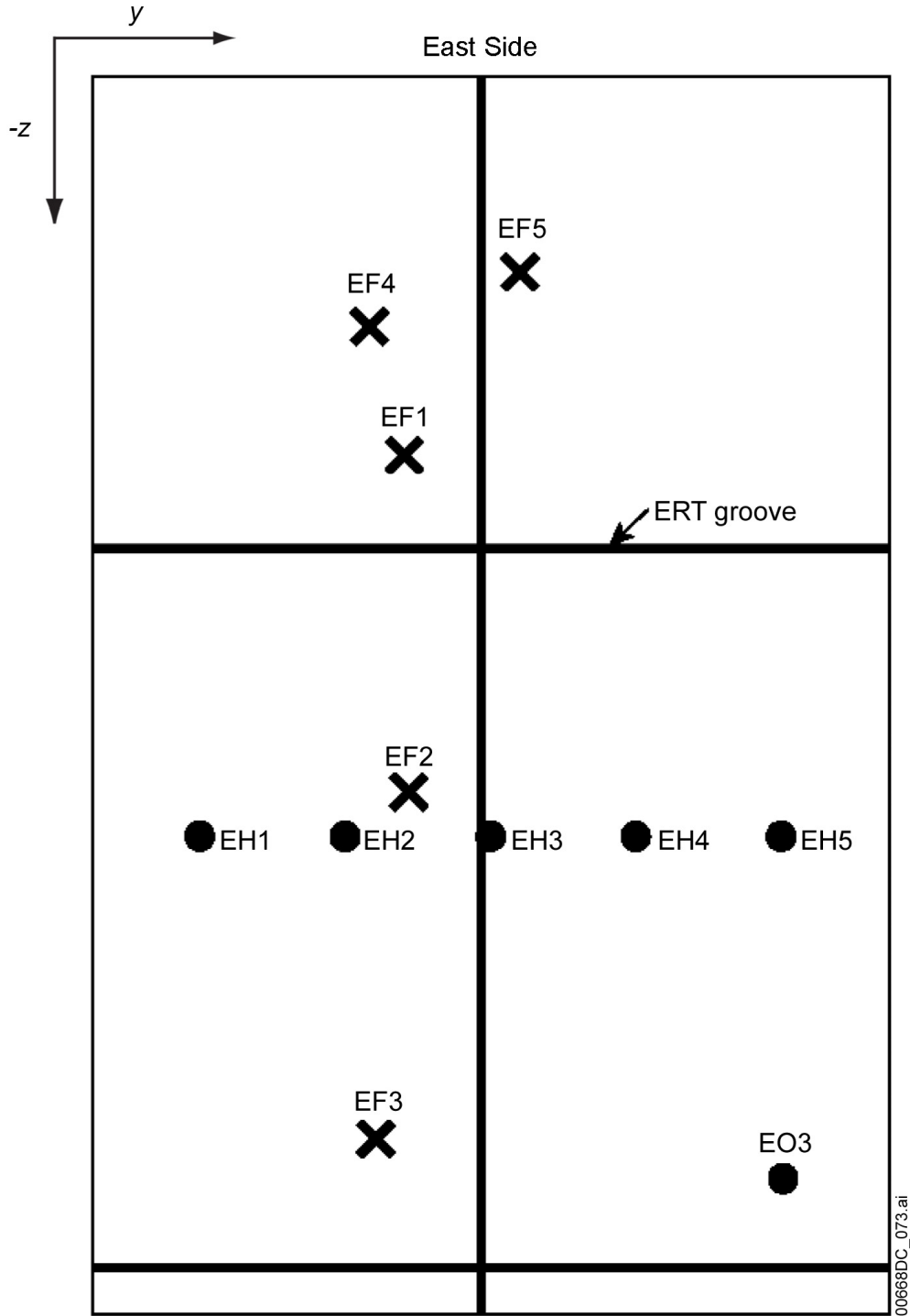
Figure 6.1-2. LBT Vertical Boreholes Drilled from the Top of the Block



- NN# – North side neutron hole – lined and grouted
- NT# – North side temperature (RTD bundle) all grouted
- NM# – North side mechanical
- NO# – North side observation hole
- NH# – North side hydrology – packer assembly installed

Source: DTN: LL981110704244.085 [DIRS 169259] (unqualified).

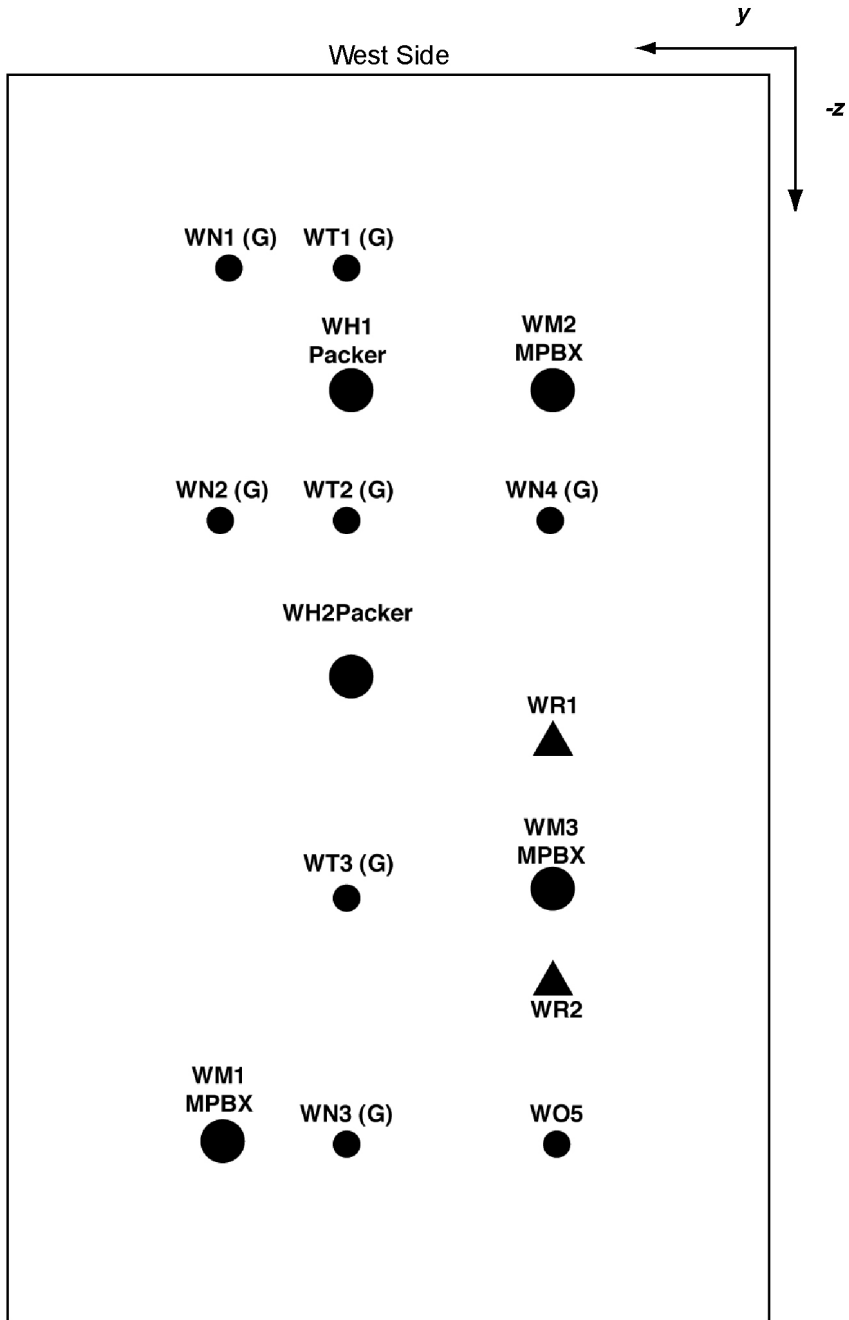
Figure 6.1-3. LBT Sensor Boreholes Drilled from the North Side of the Block



EH# – East heater hole (heater assembly with ERT)  
 EO – East observation  
 EF# – Fracture monitors

Source: DTN: LL981110704244.085 [DIRS 169259] (unqualified).

Figure 6.1-4. LBT Boreholes Drilled from the East Side of the Block



- WN# – West side neutron hole – lined and grouted
- WT# – West side temperature (RTD bundle) grouted
- WH# – West side horizontal – packer assembly installed
- WM# – West side mechanical (MPBX) hole – grouted
- WO# – West side observation hole
- WR# – West side REKA borehole

Source: DTN: LL981110704244.085 [DIRS 169259] (unqualified).

Figure 6.1-5. LBT Sensor Boreholes Drilled from the West Side of the Block

Table 6.1-2. XYZ Coordinates of the Collar and Bottom of LBT Boreholes

Borehole ID (Alt. ID)	X-Collar (m)	Y-Collar (m)	Z-Collar (m)	X-Bottom (m)	Y-Bottom (m)	Z-Bottom (m)	Borehole Type	
eh1 (EH1)	3.05	0.30	-2.74	0.30	0.30	-2.74	Heater	
eh2 (EH2)	3.05	0.91	-2.74	0.30	0.91	-2.74		
eh3 (EH3)	3.05	1.52	-2.74	0.30	1.52	-2.74		
eh4 (EH4)	3.05	2.13	-2.74	0.30	2.13	-2.74		
eh5 (EH5)	3.05	2.74	-2.74	0.30	2.74	-2.74		
e7 (TT1)	1.22	1.83	0.00	1.22	1.83	-5.51	RTD	
e1 (TT2)	2.44	1.22	0.00	2.40	1.19	-5.38		
nt1 (NT1)	2.74	3.05	-2.44	2.74	0.30	-2.44		
nt2 (NT2)	0.91	3.05	-0.61	0.91	0.30	-0.61		
nt3 (NT3)	0.91	3.05	-3.20	0.91	0.30	-3.20		
nt4 (NT4)	0.30	3.05	-2.44	0.30	0.30	-2.44		
wt1 (WT1)	0.00	1.68	-0.76	2.74	1.68	-0.76		
wt2 (WT2)	0.00	1.68	-1.68	2.74	1.68	-1.68		
wt3 (WT3)	0.00	1.68	-3.05	2.74	1.68	-3.05		
tr1 (TR1)	1.27	1.32	0.00	1.27	1.32	-1.42		REKA
wr1 (WR1)	0.00	0.63	-1.86	1.75	0.63	-1.86		
wr2 (WR2)	0.00	0.91	-3.32	1.75	0.91	-3.32		
te1 (ERT)	1.52	1.37	0.00	1.52	1.37	-3.96	ERT	
e5 (TN1)	1.22	0.61	0.00	1.18	0.57	-5.64	Neutron	
e3 (TN2)	1.83	0.61	0.00	1.83	0.62	-3.75		
e6 (TN3)	1.22	1.22	0.00	1.21	1.16	-5.64		
e2 (TN4)	2.44	1.83	0.00	2.41	1.82	-5.44		
e8 (TN5)	1.22	2.44	0.00	1.21	2.45	-5.21		
nn1 (NN1)	2.13	3.05	-0.91	2.13	0.30	-0.91		
nn2 (NN2)	2.13	3.05	-1.98	2.13	0.30	-1.98		
nn3 (NN3)	2.13	3.05	-3.81	2.13	0.30	-3.81		
nn4 (NN4)	0.91	3.05	-0.91	0.91	0.30	-0.91		
nn5 (NN5)	0.91	3.05	-1.98	0.91	0.30	-1.98		
nn6 (NN6)	0.91	3.05	-3.81	0.91	0.30	-3.81		
wn1 (WN1)	0.00	2.13	-0.76	2.74	2.13	-0.76		
wn2 (WN2)	0.00	2.13	-1.68	2.74	2.13	-1.68		
wn3 (WN3)	0.00	1.68	-3.96	2.74	1.68	-3.96		
wn4 (WN4)	0.00	0.91	-1.68	2.74	0.91	-1.68		
n1 (TH1)	1.83	1.83	0.00	1.81	1.76	-4.01	Hydrology	
nh1 (NH1)	0.00	3.05	-2.44	2.13	0.30	-2.44		
wh1 (WH1)	0.00	1.68	-1.22	2.74	1.68	-1.22		
wh2 (WH2)	0.00	1.68	-2.29	2.74	1.68	-2.29		
no1 (NO1)	2.13	3.05	-4.11	2.13	0.30	-4.11	Observation	
no2 (NO2)	0.91	3.05	-4.11	0.91	0.30	-4.11		
eo3 (EO3)	3.05	2.74	-3.96	0.30	2.74	-3.96		
wo5 (WO5)	0.00	0.91	-3.96	2.74	0.91	-3.96		

Table 6.1-2. XYZ Coordinates of the Collar and Bottom of LBT Boreholes (Continued)

Borehole ID (Alt. ID)	X-Collar (m)	Y-Collar (m)	Z-Collar (m)	X-Bottom (m)	Y-Bottom (m)	Z-Bottom (m)	Borehole Type
n2 (TM1)	1.83	1.22	0.00	1.82	1.21	-4.05	Mechanical
n3 (TM2)	1.83	2.44	0.00	1.78	2.42	-4.09	
nm1 (NM1)	2.74	3.05	-3.81	2.74	0.30	-3.81	
nm2 (NM2)	0.91	3.05	-2.44	0.91	0.30	-2.44	
nm3 (NM3)	0.30	3.05	-0.91	0.30	0.30	-0.91	
wm1 (WM1)	0.00	2.13	-3.96	2.74	2.13	-3.96	
wm2 (WM2)	0.00	0.91	-1.22	2.74	0.91	-1.22	
wm3 (WM3)	0.00	0.91	-3.05	2.74	0.91	-3.05	
n4	1.52	3.05	0.00	1.52	3.05	-6.4	
n5	0	1.52	0	0	1.52	-6.4	
n6	1.52	0	0	1.52	0	-6.4	
n7	3.05	1.52	0	3.05	1.52	-6.4	
PTC#1	1.22	3.05	-2.29	1.22	0.00	-2.29	Postcooling
PTC#2	1.22	3.05	-2.02	1.22	0.00	-1.48	
PTC#3	1.22	3.05	-2.56	1.22	0.00	-3.09	
PTC#4	1.22	3.05	-1.73	1.22	0.00	-0.62	
PTC#5	1.22	3.05	-2.84	1.22	0.00	-3.95	
PTC#6	1.22	3.05	-1.41	1.22	0.00	0.35	
PTC#7	1.22	3.05	-3.76	1.22	0.00	-6.70	
PTC#8	1.22	3.05	-1.01	1.22	0.00	1.55	
PTC#9	1.22	3.05	-2.29	2.53	0.00	-2.29	
PTC#10	0.00	1.83	-1.09	3.05	1.83	1.29	
PTC#11	0.00	1.83	-1.30	3.05	1.83	0.68	
PTC#12	0.00	1.83	-1.51	3.05	1.83	0.04	
PTC#13	0.00	1.83	-1.73	3.05	1.83	-0.62	
PTC#14	0.00	1.83	-1.91	3.05	1.83	-1.15	
PTC#15	0.00	1.83	-2.26	3.05	1.83	-2.21	
PTC#16	0.00	1.83	-2.55	3.05	1.83	-3.09	
PTC#17	0.00	1.83	-2.84	3.05	1.83	-3.95	
PTC#18	0.00	1.83	-3.35	3.05	1.83	-5.49	
PTC#19	0.00	1.83	-2.18	3.05	1.83	-1.97	
PTC#19a	0.00	1.83	-2.29	3.05	0.52	-2.29	
e10 (LBL1)	0.61	1.83	0.00	0.55	1.81	-4.00	Micro.
e9 (LBL2)	0.61	1.22	0.00	0.61	1.22	-3.98	

Source: Lin et al. 2001 [DIRS 159069].

NOTE: ERT = electrical resistance tomography; REKA = Rapid Evaluation of K and Alpha; RTD = resistance temperature detector.



The LBT Data Collection System (DCS) recorded thermal and mechanical data hourly for the most part. The acquired data consist of both original (measured electronic) values and converted (engineering units) values. Two packages of data were submitted to the RPC, and corresponding DTNs (LA0106FH831151.002 [DIRS 158230] and LA0106FH831151.003 [DIRS 158229]) were also obtained. These DCS DTNs are unqualified. The DCS DTNs also identify scientific notebooks that provide details of LBT measurements including calibration information. DCS DTNs are reduced and re-structured and periodically submitted to the TDMS, resulting in many of the input DTNs introduced below and listed in Table 4-1. As discussed in Section 1 and the introduction to Section 6, these input DTNs are further refined, reduced, and restructured before being resubmitted to the TDMS as summary DTNs (see Table 6.1-1).

### **6.1.1 LBT Thermal Measurements**

The block was heated by electrical heaters in the five heater boreholes, which formed a horizontal plane 1.75 m from the base of the block. The heater boreholes are EH1 to EH5 as shown in Figure 6.1-4. The temperature was measured in boreholes within the block as well as on the block surfaces. The temperature boreholes within the block are shown as TT1 and TT2 in Figure 6.1-2, NT1 to NT4 in Figure 6.1-3, and WT1 to WT3 in Figure 6.1-5. In situ thermal conductivity [ $k$ ] and diffusivity [ $\alpha$ ] were measured by using Rapid Evaluation of K and Alpha (REKA) probes in three boreholes. The REKA boreholes are TR1 in Figure 6.1-2 and WR1 and WR2 in Figure 6.1-5. The following sections present the heater power, temperature, and thermal conductivity and diffusivity of the block.

A detailed discussion of the LBT thermal measurements is provided in Section 5 of *Large Block Test Final Report* (Lin et al. 2001 [DIRS 159069]). Input DTNs and summary DTNs for thermal measurements are provided in Tables 4-1 and 6.1-1, respectively.

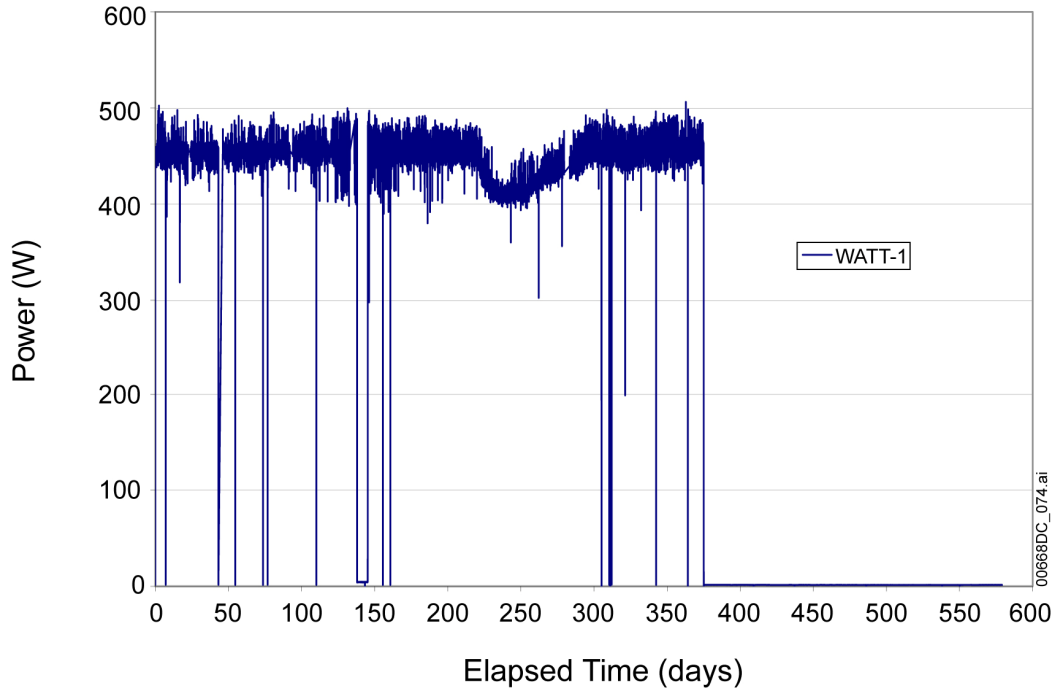
#### **6.1.1.1 Heater Power**

##### **6.1.1.1.1 Results: Heater Power**

The heater in each of the five heater boreholes (EH1 to EH5 as in Figure 6.1-4) was energized to 450 W on February 28, 1997. The power output of one of those heaters as a function of time is shown in Figure 6.1-6, as an example. The power output of the other heaters was similar to this one. Spikes in this figure were due to short-duration power outages, which did not affect the test significantly. Data gaps were caused by malfunction of the data acquisition unit. The power was maintained approximately constant, at about 450 W, until about day 222, when the power was reduced to reach a near steady-state temperature in the block. The temperature at TT1-14 was maintained fairly constant at about 135°C (see Figure 6.1-7) for the remainder of the test. Toward the end of the test, the power had to be increased back to nearly 450 W to maintain the 135°C temperature in the test block. This may have been caused by a cooler ambient temperature at that time. The heater power data are in the TDMS under DTN: LL980918904244.074 [DIRS 135872]. This DTN is unqualified and should only be used for corroborative purposes.

### 6.1.1.1.2 Measurement Uncertainty: Heater Power

The accuracy of the watt transducers used in measuring the heater power is conservatively estimated to be within 2% at 500 W full span. This degree of uncertainty is considered typical. The uncertainty is less than the power fluctuations associated with routine oscillations of power supply from the local utility, as shown in Figure 6.1-6.



Source: DTN: LL980918904244.074 [DIRS 135872] (unqualified).

Figure 6.1-6. Power History of LBT Heater EH1

### 6.1.1.2 Temperatures

The temperature measurements included the spatial and temporal variation of the temperature in the block and the thermal gradient on the block surfaces. Resistance temperature devices (RTDs) were used to measure temperatures in the block and on the block surface. Within the block, temperature was measured in nine RTD boreholes and five heater boreholes: TT1 and TT2, NT1 to NT4, EH1 to EH5, and WT1 to WT3, as shown in Figures 6.1-2 to 6.1-5, respectively. The RTD boreholes were instrumented with RTDs at 20-cm spacing. This was accomplished by grouting a bundle of RTDs with cement in each of the temperature boreholes. The RTD numbering always started from the bottom of a borehole. For example, TT1-1 is the RTD at the bottom of the vertical RTD borehole TT1, and NT1-14 is the RTD near the collar of the horizontal RTD borehole NT1, which was drilled from the north face of the block to a distance of about 30 cm from the south face of the block. In addition, five RTDs were placed in a thin-walled stainless-steel tube to test the feasibility of their being calibrated or replaced during the test. The stainless-steel tube was grouted along with the RTD bundle in borehole TT1. Three RTDs were placed in each of the five heater boreholes approximately 0.6, 1.5, and 2.4 m from the collar. The thermal gradient to determine heat flux out of the block across the block

surface was measured by a pair of RTDs on both sides of a 1.2-cm-thick Ultratemp insulation panel. Ultratemp panels were mounted in zones on the four vertical faces of the block, on the outside of the Viton sheet. Temperature measurements on the top of the block were performed to verify that the heat exchanger controlled the top temperature at about 60°C during the test.

For the discussion of the temperatures within the block during the test, only the temperature measured in the grouted boreholes will be used because they directly measure thermal behavior of the rock. The entire set of the temperature data is available in the TDMS under DTN: LL980918904244.074 [DIRS 135872]. This DTN is unqualified and should only be used for corroborative purposes.

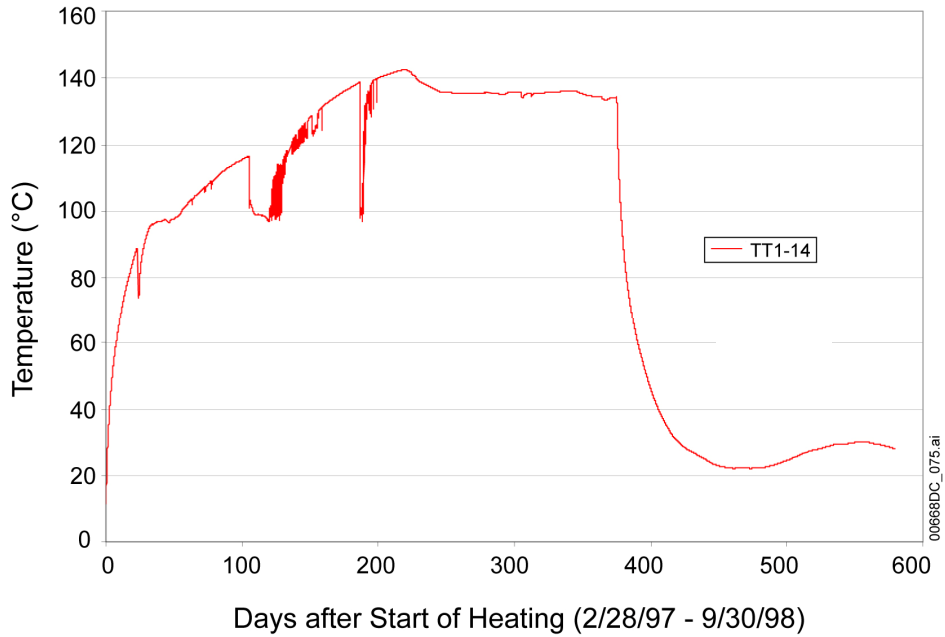
#### **6.1.1.2.1 Results: Temperatures**

The spatial distribution of the temperature in the LBT shows that the block was heated nearly unidirectionally in the z direction. The temperature in the two vertical RTD boreholes will be used to illustrate the temperature history in the block during the test. Figures 6.1-7 and 6.1-8 show the temperature history at RTDs TT1-14 and TT2-14, respectively. TT1-14 and TT2-14 are at 5 and 10 cm below the heater plane, respectively. The location of boreholes TT1 and TT2 can be found in Figure 6.1-2. The temperatures at TT1-14 are about 10°C higher than those at TT2-14, mainly because TT1-14 is about 5 cm closer to the heater plane than TT2-14. Sharp drops in temperature that occurred before 100 days since heating began are related to power outages. An anomalous reading of -246.9°C was noted for TT2-14 on the 145th day of heating. TT1-14 represents the highest measured temperature in the rock of the LBT.

As shown in Figure 6.1-7, the temperature at TT1-14 increased rapidly with time at the early stages of the heating. The temperature increased mainly from heat conduction. Rate of increase for the temperature decreased with time, mainly because of the decrease in thermal gradient at the RTD location as the thermal front expanded with time. When the temperature reached the boiling point of water, which is about 96°C at the elevation of Fran Ridge, the rate of temperature increase was significantly decreased. This decrease was caused by consumption of energy in the vaporization of the pore water in the rock. During the 20-day period between day 30 and day 50, the temperature at TT1-14 increased from about 96°C to about 98°C. After day 50, the temperature at TT1-14 increased faster with time, indicating that most of the pore water had vaporized. Then, at day 105 (June 13, 1997) the temperature dropped to near the boiling point of water. This is the onset of the first of the two TH events corresponding to rain storms and power outages (see Hardin 1998 [DIRS 100123]). The second TH event occurred at day 186 (September 2, 1997). The temperature fluctuations in those TH events indicated condensate refluxing. On day 220 (October 6, 1997), the heater power started to ramp down to keep the TT1-14 temperature at approximately 137°C. The heaters were turned off on March 10, 1998, to start a natural cooling phase. The data acquisition was terminated on September 30, 1998.

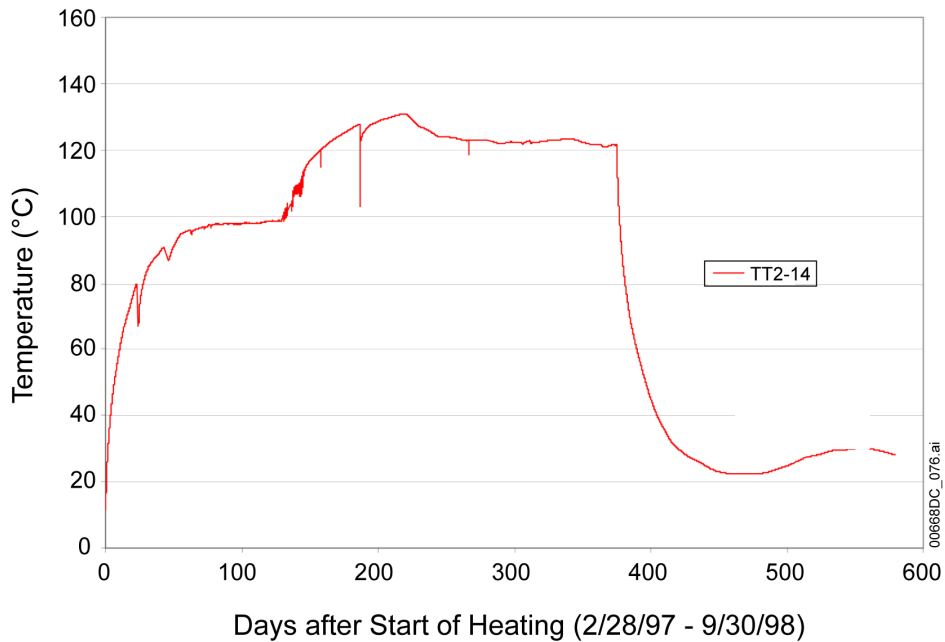
Figure 6.1-8 shows a temperature history at TT2-14 similar to that of TT1-14. The temperature at TT2-14 remained at 97.4°C for about 37 days (day 75 to day 112). Then the temperature increased to, and remained at, about 99°C for 16 days. Because the temperature at TT2-14 was at the boiling point of water when the first TH event occurred, the temperature at TT2-14 was not

affected by that event. The rest of the temperature history at TT2-14 was very similar to that at TT1-14.



Source: DTN: LL980918904244.074 [DIRS 135872] (unqualified), SEP Tables S98461\_033, S98461\_034, and S98461\_035.

Figure 6.1-7. Temperature History at LBT TT1-14



Source: DTN: LL980918904244.074 [DIRS 135872] (unqualified), SEP Tables S98461\_033, S98461\_034, and S98461\_035.

Figure 6.1-8. Temperature History at LBT TT2-14

### 6.1.1.2.2 Measurement Uncertainty: Temperatures

The accuracy of the RTD is within 0.3°C (CRWMS M&O 1997 [DIRS 101540], Section 5.1). With consideration of other factors, such as the location of the RTDs, the accuracy of the measured temperature in the LBT is estimated to be within 1.5°C. The RTD bundles were grouted in the boreholes; therefore, some of the RTDs may not have had direct contact with the borehole wall. Additional uncertainty may be introduced into the heat flux calculation. The heat flux of a region is represented only by the measurement at one point.

## 6.1.2 LBT Hydrological Measurements

The hydrologic measurements presented in this section include the field-measured moisture content, gas pressure, relative humidity, air permeability, and the laboratory-determined hydrologic parameters. The moisture content in the block was determined by electrical resistance tomography (ERT) and neutron logging. Neutron logging provides accurate determination of the moisture content within about a 10-cm radius distance from a borehole. The ERT provides two-dimensional distribution of the moisture content on a larger scale with less accuracy. The two methods were used to complement each other. Neutron logging was conducted periodically in 15 neutron boreholes: TN1-TN5 (Figure 6.1-2), NN1-NN6 (Figure 6.1-3), and WN1-WN4 (Figure 6.1-5). ERT electrodes were mounted in the vertical ERT borehole near the center of the block top and on the block sides. ERT was also conducted on the large block periodically. Gas pressure and relative humidity were monitored in the four hydrologic boreholes: TH1 (Figure 6.1-2), NH1 (Figure 6.1-3), and WH1-WH2 (Figure 6.1-5). Air permeability was measured in the hydrologic borehole TH1 before the block was cut, before the heating started, and at the end of the heating phase. Cross-borehole permeability between some of the boreholes was also measured before heating.

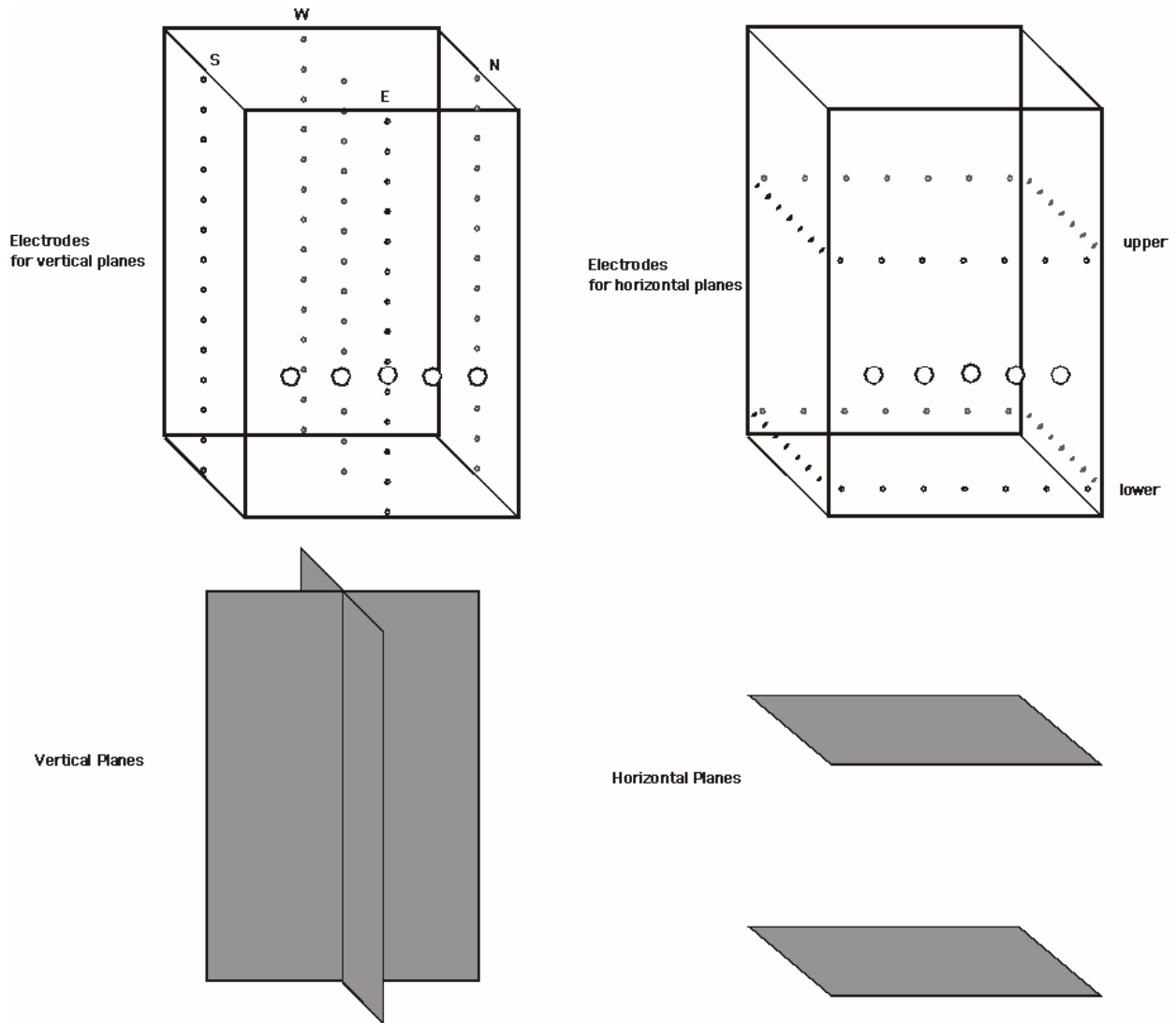
Small blocks of the rock were collected in the proximity of the large block for laboratory tests of parameters. These include density, porosity, water permeability, moisture-retention curves, and fracture flow and matrix-imbibition visualization using X-ray radiography.

A detailed discussion of the LBT hydrological measurements is provided in Section 6 of *Large Block Test Final Report* (Lin et al. 2001 [DIRS 159069]). Input DTNs and summary DTNs for hydrological measurements are provided in Tables 4-1 and 6.1-1, respectively.

### 6.1.2.1 Electrical Resistance Tomography

ERT is a geophysical imaging technique that can be used to map subsurface resistivity (Daily and Owen 1991 [DIRS 159126]; Lin et al. 2001 [DIRS 159069], pp. 6-3 and 6-6). The ERT measurements consisted of a series of voltage and current measurements from buried electrodes, using an automated data collection system. The data were then processed to produce ERT tomograms. The images of resistivity change can be used, along with the measured temperature field and what is known of initial conditions in the rock mass, to estimate moisture change during heating. ERT electrodes were placed at approximately 0.3-m spacing in horizontal and vertical grooves on all four sides of the block, as shown in Figures 6.1-9 and 6.1-4, and along the ERT borehole (Figure 6.1-2). This arrangement of electrodes allowed imaging of two

intersecting perpendicular vertical planes and two parallel horizontal planes, about 1.25 m above and below the horizontal heater plane.



Source: Lin et al. 2001 [DIRS 159069].

Figure 6.1-9. LBT Layout of ERT Electrodes

The ERT tomograms can be found in the TDMS under DTNs: LL980913304244.072 [DIRS 145385] and LL981001604244.079 [DIRS 158261], and represent data obtained between February 1997 and March 1998. Some of the resistivity images reconstructed late in the experiment (and the moisture changes inferred from them) are questionable because of the sparse data. As the rock mass dehydrated, the contact impedance between the electrodes and the rock increased significantly, and data quality declined. Having fewer usable data results in a poorly constrained reconstruction that might look smeared or washed out. This is particularly noticeable in the vertical planes beginning early in 1998.

#### 6.1.2.1.1 Data Processing

Section 6.1.2.1 of *Large Block Test Final Report* (Lin et al. 2001 [DIRS 159069]) provides detailed descriptions of the ERT methodology and data reduction procedures. Some of the important features of the two-dimensional algorithm used for ERT are briefly described. The algorithm (LaBrecque et al. 1996 [DIRS 159047]) solves both the forward and inverse problems to find the smoothest resistivity model that fits the field data to a prescribed tolerance. Resistivity values assigned in this way to each pixel in the mesh constitute the ERT tomograms. Although the mesh is of a large region around the electrode arrays, only the region inside the ERT electrode array is used in the calculations of moisture content, because the region outside the array is poorly constrained by the data.

The ratio of the measured electrical resistivity data during the test (both the heating phase and the cooling phase) to that of the preheating phase is chosen to represent the changes in the rock's electrical resistivity. This was done pixel by pixel within the image plane.

Resistivity of the rock is influenced by changes in moisture content, porosity, cation exchange capacity, solutes in the pore water, and temperature. Moisture content and temperature effects are expected to be most significant. An increase in temperature or moisture causes a resistivity decrease. However, there may be regions where the increasing temperature and decreasing pore-water resistivity were opposed by the rock mass drying, which increases the resistivity. The goal in this section is to use the images of resistivity change along with the measured temperature to estimate moisture change during the test. See Section 6.1.2.1.2 of *Large Block Test Final Report* (Lin et al. 2001 [DIRS 159069]) for a detailed description of how the changes in moisture content were calculated from the resistivity changes.

Waxman and Thomas (1974 [DIRS 101736]) describe a model for electrical conduction in partially saturated shaly sands typical of oil reservoirs (intended for oil field data) that accounts for conduction through the bulk pore water as well as conduction through the electrical double layer near the pore surface. This model can predict temperature dependence of the resistivity, but several of the model parameters must be empirically determined and are not available for tuff. Roberts and Lin (1997 [DIRS 101710]) suggest that the Waxman-Thomas model provides reasonably good estimates of resistivity for saturations greater than 20%.

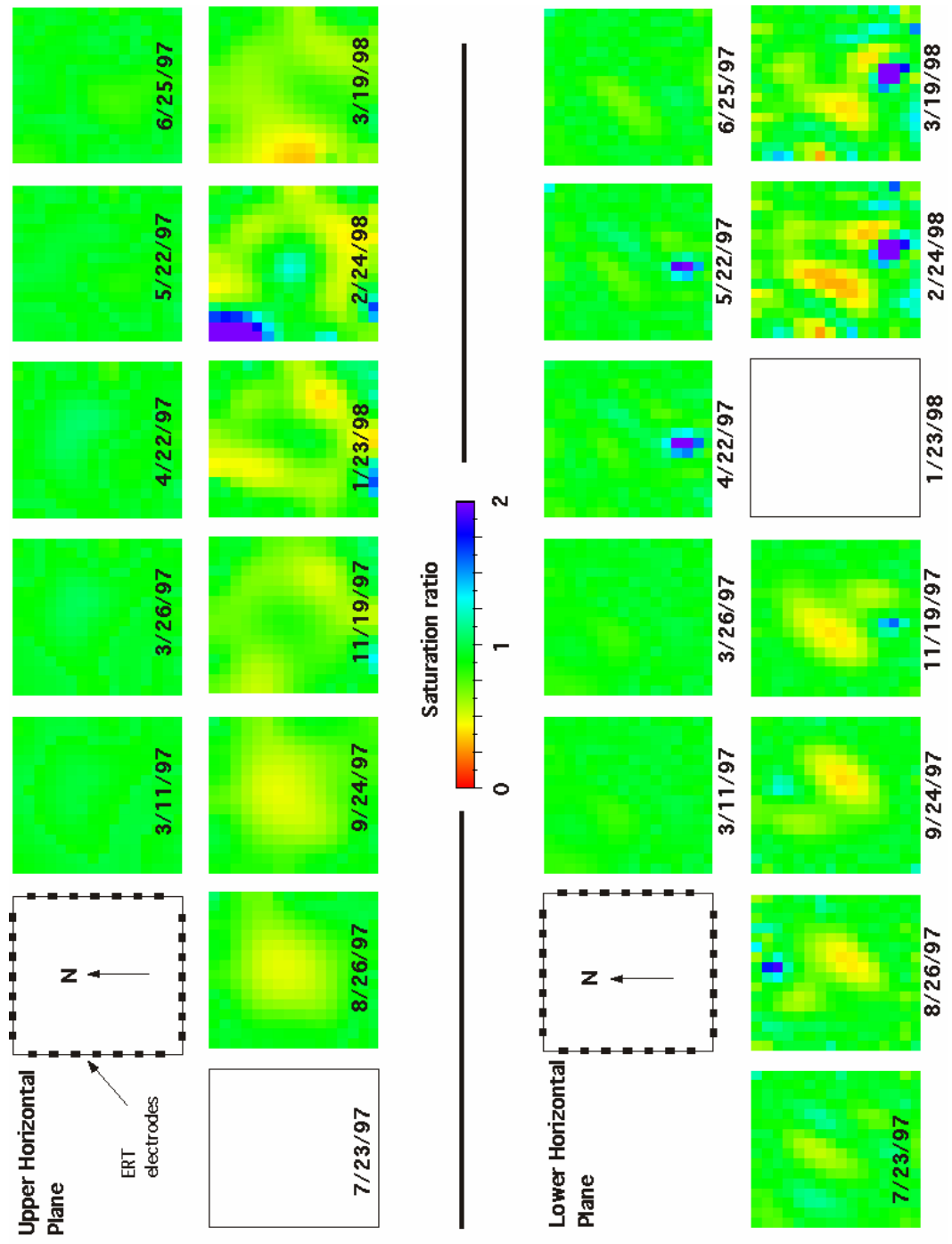
Changes in saturation are estimated by using both models 1 and 2 (Waxman and Thomas 1974 [DIRS 101736]). This approach should provide bounds to the domain of possible saturations that may be present. However, if the cation exchange capacity, porosity, or water resistivity varies significantly across the ERT image plane, it is possible that model 1 results would be more accurate. Model 1 is believed to be more representative of the rock mass for two reasons. First, the saturation estimates based on this model are in better agreement with those of the neutron log where those data are available. Second, model 2 occasionally predicts a saturation greater than 1, a nonphysical result. For that reason, only the saturation change tomograms of model 1 are presented in DTN: LL980913304244.072 [DIRS 145385].

#### 6.1.2.1.2 Results: ERT

Figure 6.1-10 shows the saturation ratios (defined as current moisture content to preheating initial moisture content) in the two horizontal planes. Blank spaces indicate data sets that did not converge. The changes in moisture content initially are very small and increase in magnitude and extent as the test proceeds. Through June 25, 1997 (117 days into heating), the upper plane (above the heater elevation) shows significantly less change from initial conditions than the lower plane. This asymmetry possibly resulted from heterogeneities in the block. Drying started to appear as early as May 22, 1997, in the lower plane.

Figure 6.1-11 shows the changes in the moisture content in the two vertical planes. As expected, the most obvious feature is the drying zone surrounding the heaters. Although drying is not clearly associated with the heaters until May 22, 1997 (about 83 days into heating), once formed, the drying zone is the dominant feature in either image plane all the way through the last data of cool-down (March 19, 1998). This large dry zone around the heater persists until the late heating phase in February 1998. Once formed, the heater dry zone is not smooth and planar. Instead, it is very irregular in shape, with many appendages. There is also a tendency for the dry zone to be relatively flat on top and bottom early in the test, but convex on top and concave on the bottom late in the test.





Source: DTN: LL980913304244.072 [DIRS 145385].

Figure 6.1-10. Distribution of Moisture Content in Two Horizontal Planes from LBT ERT

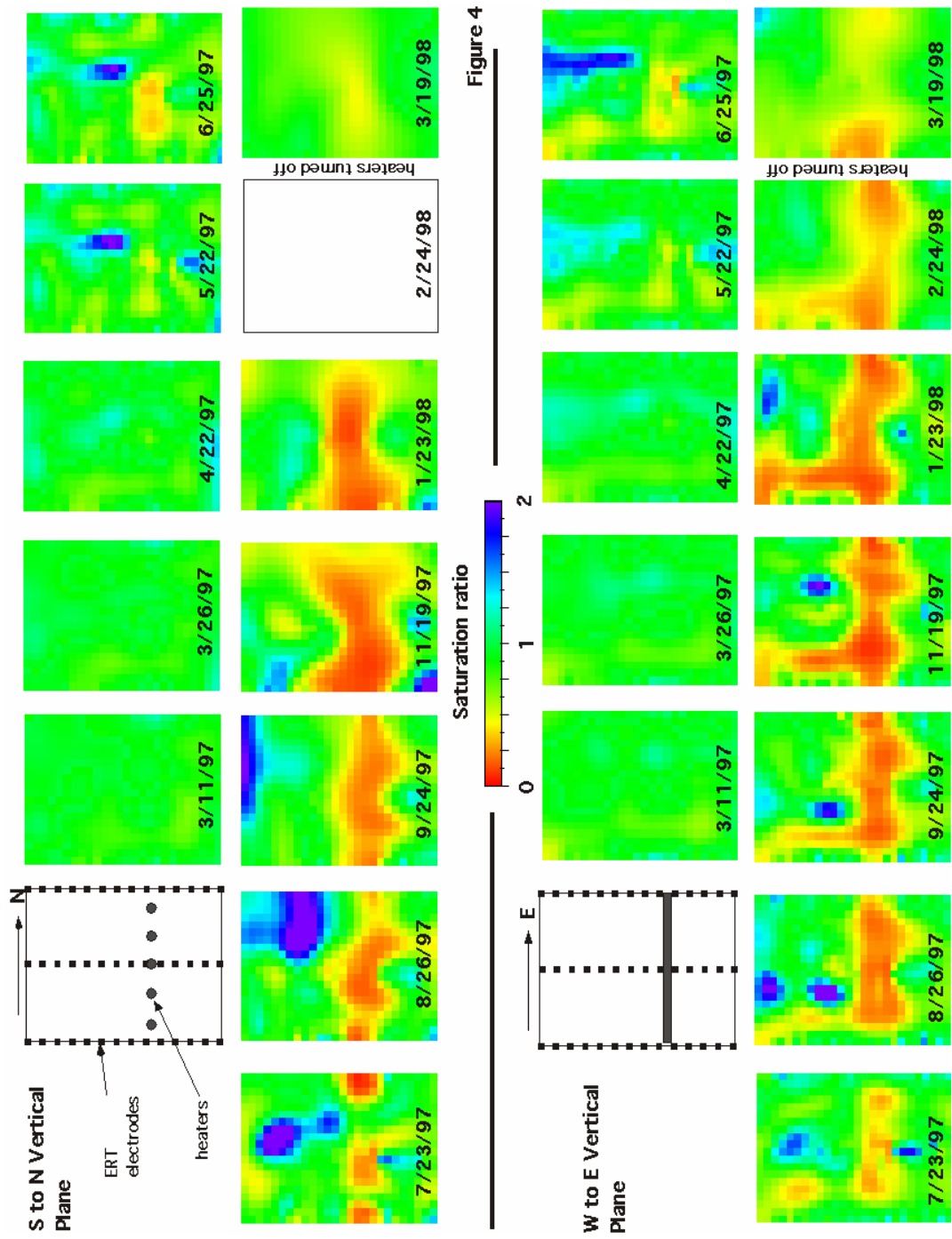


Figure 4

Source: DTN: LL980913304244.072 [DIRS 145385].

Figure 6.1-11. Distribution of Moisture Content in Two Vertical Planes in LBT

### 6.1.2.1.3 Measurement Uncertainty: ERT

Geophysical methods, including ERT, are intended to give qualitative estimates of drying and wetting. The ERT image represents integration of the saturation distribution over a relatively large area, and is therefore less accurate than neutron logging. There are many factors that affect the uncertainty of the ERT results:

- The measurements of electrical voltage and current in the field are accurate, relative to other factors.
- Measured temperatures within the image region are used for the ERT data reduction. Although the temperature can be measured very accurately at the RTD locations, interpolations are necessary to provide a two-dimensional temperature field suitable for the ERT. The interpolation will introduce uncertainty in the temperature field, especially with significant heterogeneity in the rock mass.
- The current ERT data reduction does not directly consider the cation exchange capacity of the rock. The cation exchange capacity is indirectly considered when the laboratory measured relationship among the electrical resistivity, water saturation, and temperature is used to check the Waxman-Thomas model of electrical resistivity and water saturation, which was developed for the case of shale sands.
- The laboratory resistivity data of welded tuff indicate that the Waxman-Thomas model tends to overpredict dryness for saturations less than 20%.
- The inversion algorithm used to reconstruct the tomographs smoothes the data. Therefore, the structures observed are “smeared” versions of the true target.
- The effect of the thermal fracturing on the electrical resistivity was not considered by the Waxman-Thomas model.
- The resistivity ratios were calculated using a two-dimensional algorithm; natural heterogeneities such as fractures tend to be three-dimensional. Changes in resistivity occurring along fractures may be distorted by use of the two-dimensional algorithm.
- Metallic sensors in the block may reduce sensitivity to resistivity changes occurring in the block.
- The Waxman-Thomas models do not account for changes in water resistivity caused by rock/water chemical interactions. If chemical reactions cause changes in the concentration or types of ions in the water, or change the porosity because of mineral precipitation or dissolution, the estimated saturation changes will be in error.

### 6.1.2.2 Neutron Logging

Neutron logging was used to measure the moisture content in the rock through the various phases of the LBT. The neutron probe contains a source of high-energy neutrons and a detector for slow

(thermal) neutrons. Neutron counts were measured in each borehole at 10-cm intervals. The hydrogen in the water in the rocks slows down the neutrons, making them detectable. Thus, higher counts (or a positive difference in counts relative to background or preheating levels) indicate higher water content (or increased water content over background). Known moisture contents were used to calibrate the neutron tool in liner-grout and liner-RTD-grout assemblies (identical to those used in the boreholes). Water content is calculated from the neutron counts using the calibration results. Under ambient conditions, the sampling volume surrounding the probe has a diameter of approximately 12 cm (Lin et al. 2001 [DIRS 159069], Section 6.1.2.1.2); this volume diameter increases as moisture content decreases.

Neutron logging was conducted in some of the vertical boreholes in the potential location of the block, before the boundary of the block was cut. This was to assess the initial moisture content in the outcrop. Then, after the cutting of the block boundary, the neutron logging was repeated to assess the changes in the moisture content resulting from the cutting. Cutting the block boundary using water had no significant effect on the moisture content of the block. Background moisture saturation levels were determined to be about 60% to 80%, for a laboratory-determined porosity of about 11%. Before the heating was started, the baseline moisture content in every neutron borehole was established. Then, during the heating phase and the consequent cooling phase of the test, neutron logging was conducted about once per month. In all cases, neutron counts were obtained at every 10-cm spacing in each borehole. The neutron counts were converted to fraction volume water content by using calibration results.

Neutron logging was conducted in the five vertical boreholes (TN1 to TN5, as shown in Figure 6.1-2), six horizontal boreholes from the north face (NN1 to NN6 in Figure 6.1-3), and four horizontal boreholes from the west face (WN1 to WN4 in Figure 6.1-5) after the completion of the installation of sensors (preheating) in February 1997. The neutron boreholes were equipped with a Teflon liner, and the space between the liner and the borehole wall was sealed with cement grout. Moisture content was determined with both the Teflon liner and the cement grout in place. The preheating measurement established the baseline so that the effect of heating the block on its moisture content could be determined. The neutron tool was calibrated in a 3.81-cm diameter borehole, with the Teflon liner/grout assembly exactly the same as in the neutron boreholes of the LBT. The neutron tool was calibrated both with and without Teflon liner and cement grout conditions. It was determined that the Teflon liner/grout assembly had no major effect on the determined moisture content. This is not surprising because the neutron boreholes in the LBT are designed in such a way that the thickness of the annular cement grout is minimal, only about 0.3 cm (Lin et al. 2001 [DIRS 159069], p. 6-14).

A complete set of the raw neutron counts, the location of measurements in each borehole, and the converted difference fraction volume water content are in the TDMS under DTNs: LL980919304244.075 [DIRS 145099] and LL970803404244.040 [DIRS 113889].

#### **6.1.2.2.1 Results: Neutron Logging**

The difference fraction volume water content in TN3 during the test is presented in this section in graphical form, so that the process of moisture movement can be analyzed. The difference fraction volume water was calculated by subtracting the baseline fraction volume water from that measured during the test.

Figure 6.1-12 shows the preheating (baseline) fraction volume water content in TN3 as a function of depth from the borehole collar. This is an example of the baseline water content in the neutron borehole. Generally, the initial moisture content in the region near the collar is less than that in the borehole. The variation in the initial moisture content in each borehole is probably caused by heterogeneity in the rock mass.



Source: DTN: LL970803404244.040 [DIRS 113889].

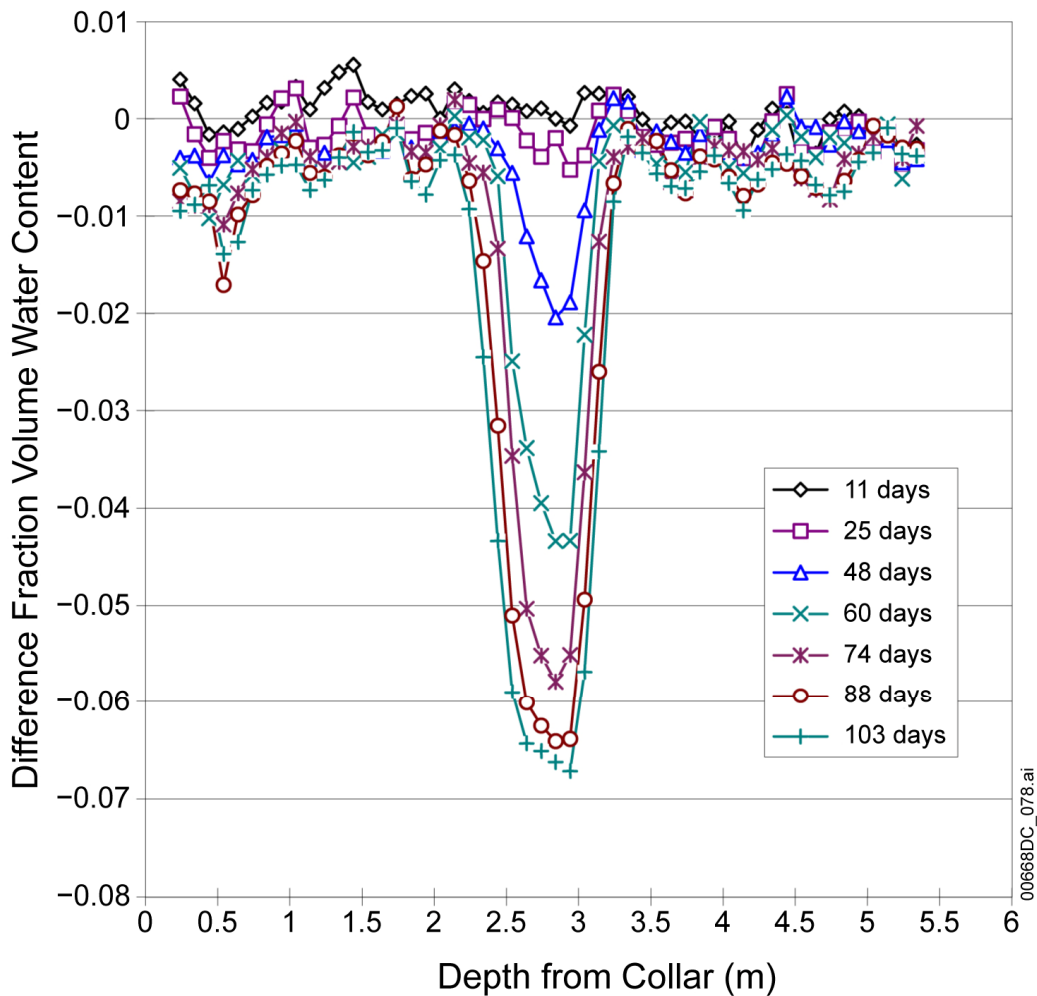
Figure 6.1-12. Initial Fraction Volume Water Content Measured in LBT Vertical Borehole TN3 Using Neutron Logging (Preheating/Baseline)

Figures 6.1-13 and 6.1-14 show the difference fraction volume water in borehole TN3, as a function of depth from the borehole collar. These are examples to illustrate the variation in the moisture content in the block as measured by neutron logging. Data for the other boreholes can be found in DTNs: LL971204304244.047 [DIRS 113894] and LL970803404244.040 [DIRS 113889]. In these figures, the positive fraction volume water means gaining moisture content; the negative fraction volume water means losing moisture content. Generally, the vertical boreholes have a well-defined dryout zone developed after 48 days of heating at the heater plane, which was at about 2.74 m from the top of the block. The dryout zone widened with time, and the extent of the drying also increased with time, because of the continuous heating. The widths of the maximum dryout zones, as measured at the half of the depth of the dryness in the five vertical boreholes, ranged from 1.49 to 1.69 m. The width of the dryout zone is quite uniform. There was not much change in the extent of the dryness after day 361 of heating. There were some variations in the shape of the tip of the dryout zone among those five vertical neutron boreholes. The dryness in those five vertical boreholes ranged from  $-0.07$

to  $-0.09$  fraction volume. Those variations among the five vertical boreholes illustrate the effect of heterogeneity in the block on the movement of moisture. Those figures do not show significant rewetting during the cooldown phase.

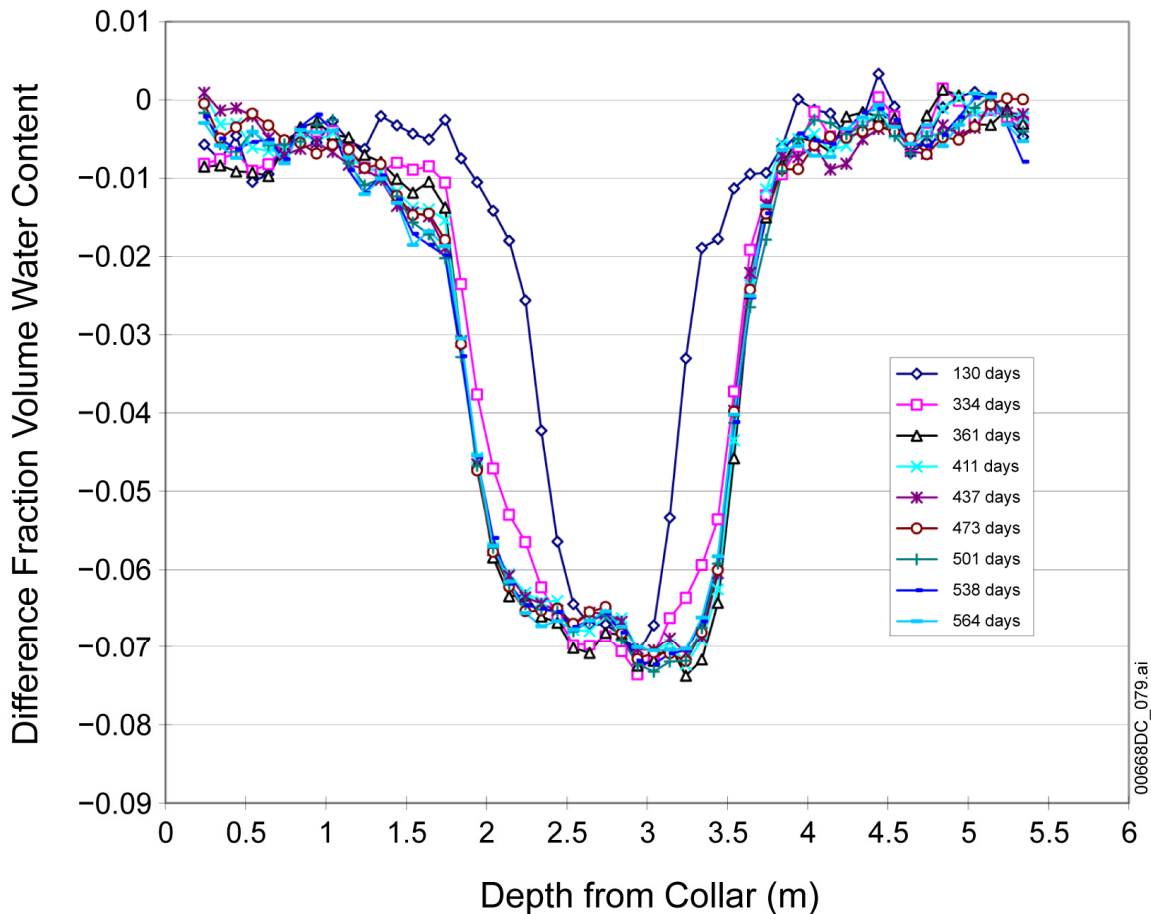
The variation of the moisture content among the north-face neutron boreholes and the west-face neutron boreholes is similar, and is consistent with that shown in TN3. Generally, the variation of the moisture content was uniform across the block. The variation of the moisture content in the horizontal neutron boreholes depends on the vertical location of the borehole.

The data also showed that the moisture movement in the block was almost one-dimensional. A well-defined dryout zone was developed at the heater plane. The neutron results did not show significant rewetting during the cooldown phase. Fractures have important roles in the localized movement of the moisture (Lin et al. 2001 [DIRS 159069], pp. 6-14 and 6-16).



Source: DTN: LL970803404244.040 [DIRS 113889].

Figure 6.1-13. Difference Fraction Volume Water Content Measured in LBT Borehole TN3 Using Neutron Logging (March 11 to June 11, 1997)



Source: DTN: LL970803404244.040 [DIRS 113889].

Figure 6.1-14. Difference Fraction Volume Water Content Measured in LBT Borehole TN3 Using Neutron Logging (July 8, 1997, to September 15, 1998)

#### 6.1.2.2.2 Measurement Uncertainty: Neutron Logging

Neutron logging provides an accurate measurement of water content but the volume or cross-sectional area covered by the neutron measurement extends only about 15 cm into the rock. The variation of the moisture content in the cement grout between the Teflon liner and the borehole wall may have some effect on the neutron counts, but the effect is small in the LBT because the thickness of the grout column is only about 0.3 cm.

#### 6.1.2.3 Passive Monitoring—Gas Pressure and Relative Humidity

Gas pressure and relative humidity were measured in the four hydrology boreholes: TH1, NH1, WH1, and WH2. Packers were installed in those boreholes to pack off zones for the measurements. Each pack-off zone was about 0.46 m in length. One Humicap was installed in each pack-off zone, and a pressure line was installed to bring the gas pressure to a pressure transducer outside of the block. There were three pack-off zones in TH1: one each in NH1, WH1, and WH2. Detailed discussion of these measurements can be found in Section 9.2 of

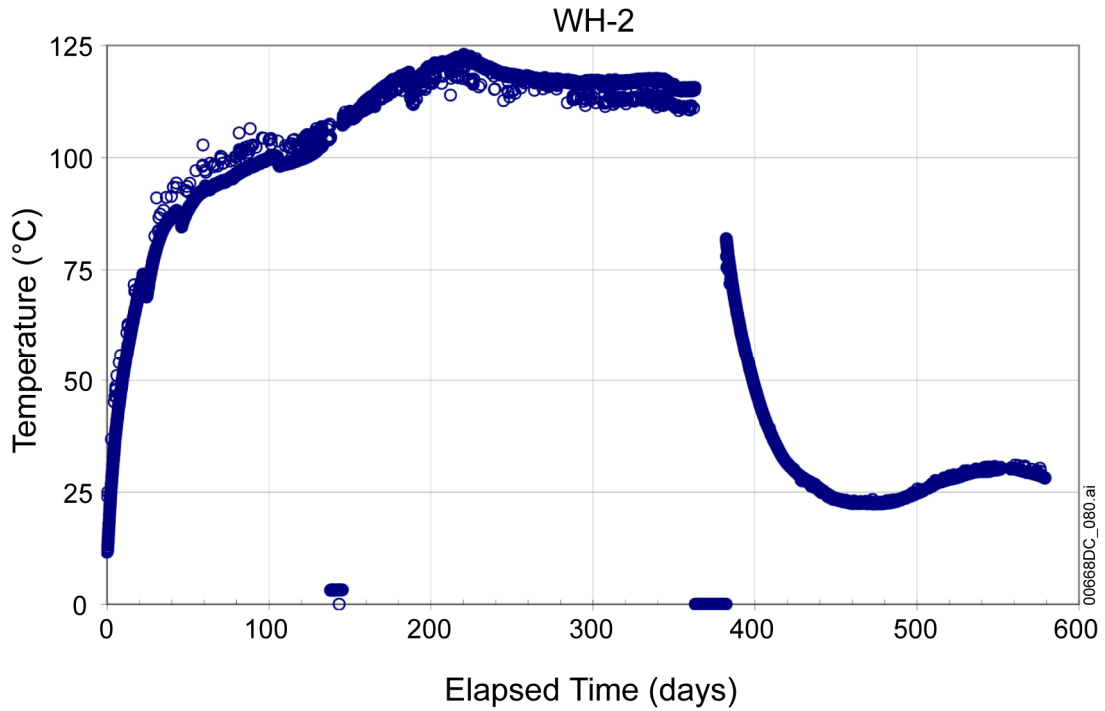
*Large Block Test Final Report* (Lin et al. 2001 [DIRS 159069]). The gas pressure and the relative humidity data can be found in the TDMS under DTN: LL980918904244.074 [DIRS 135872]. This DTN is unqualified and should only be used for corroborative purposes.

#### **6.1.2.3.1 Results: Gas Pressure and Relative Humidity**

Since the pressure transducer outputs were all noisy, only the relative humidity and temperature measured by the Humicap sensors will be presented. The Humicap sensors in the first two packed-off zones of the vertical borehole (TH1) also performed unreliably during the LBT. The discussion below, therefore, focuses on the third zone of the vertical borehole and the horizontal boreholes. The Humicaps in WH1 and WH2 are the only two sensors that performed for the entire test period. Figures 6.1-15 and 6.1-16 show the temperature and relative humidity, respectively, as measured in WH2 (borehole WH2 is at about 0.5 m above the heater plane). These figures are used as examples of the humidity sensor data. Other humidity sensors functioned similarly.

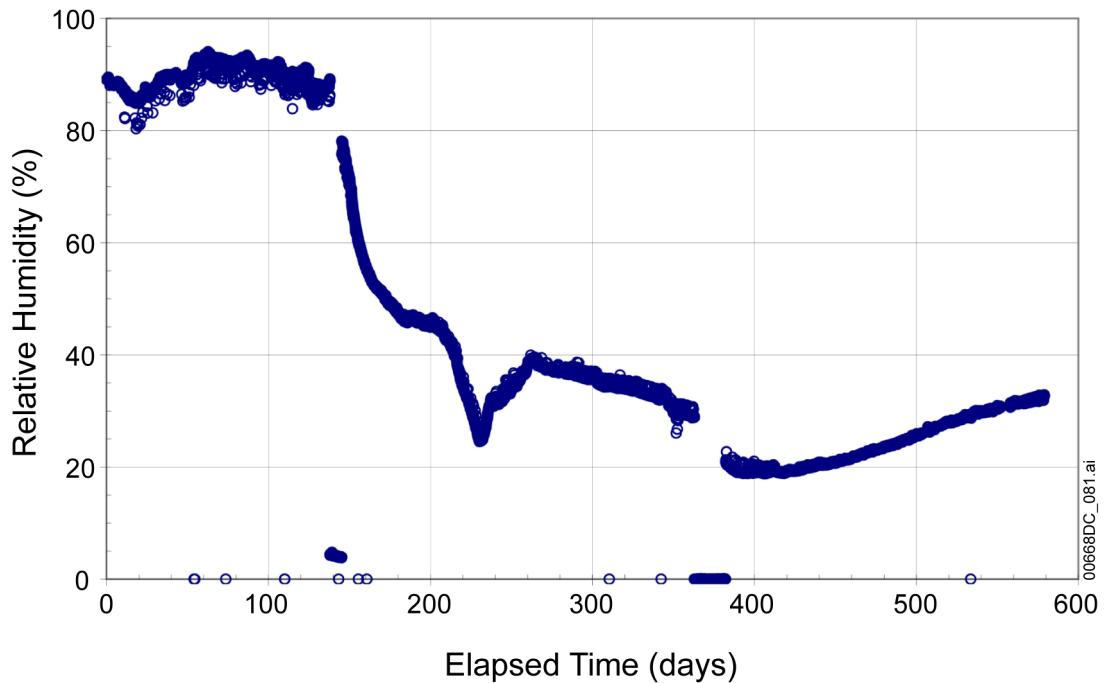
The WH2 temperature results (Figure 6.1-15) agree well with the temperatures measured by the RTDs. The initial relative humidity was about 90% and remained high until slightly past 125 days (Figure 6.1-16). The relative humidity values fell to about 25% by about 230 days. This decrease is consistent with the moisture content measured by neutron logging. Neutron logging in TN3 (Figure 6.1-14) shows that more than 3% fraction volume water was lost between 130 days and 334 days of heating. This amount of moisture loss was almost half of the total moisture loss at that location in that borehole. The small number of humidity sensors deployed in the LBT limited the conclusive information about the TH process. However, the temperature and relative humidity records from borehole WH2 clearly show that a dry zone extended 0.5 m or more above the heater plane after 135 days. Higher in the block, at 1.5 m above the heater plane (borehole WH-1), boiling conditions were never reached, and relative humidity remained high throughout the LBT. Data also show that rewetting of the dry zone was slow following heater turn-off.





Source: DTN: LL980918904244.074 [DIRS 135872] (unqualified).

Figure 6.1-15. Temperature Measured in LBT Borehole WH-2 as a Function of Time



Source: DTN: LL980918904244.074 [DIRS 135872] (unqualified).

Figure 6.1-16. Relative Humidity Measured by the Humicap in LBT Borehole WH-2 as a Function of Time

#### 6.1.2.3.2 Measurement Uncertainty: Relative Humidity

The humidity measurement is accurate to within 2% to 3% and the RTD temperature measured by the humidity sensor is accurate to within 0.3°C (CRWMS M&O 1997 [DIRS 101540], Section 5.1). Another source of uncertainty in the measurement can result from the conditions in the borehole, such as the sealing of the packer. In a highly fractured rock mass, sealing of a borehole by packers may be incomplete. Quantitative uncertainty cannot be established for relative humidity measurements obtained where there is packer leakage.

#### 6.1.2.4 Laboratory Parameters—Matrix Permeability, Density, Porosity, Micro-Pore Structure, Fracture Flow, and Matrix Imbibition Visualization

Small blocks of the rock at the LBT site were collected for laboratory testing of hydrologic properties and processes. Those hydrologic properties include density, porosity, water permeability, and moisture-retention curves. The hydrologic process investigated was fracture flow and matrix imbibition. Section 3.5.1.3 of *Large Block Test Final Report* (Lin et al. 2001 [DIRS 159069]) carries the description of the laboratory tests in greater detail. Here, the methods of the laboratory tests are briefly discussed and the results summarized.

##### Matrix Permeability

The water permeability of the Topopah Spring Tuff samples obtained from Fran Ridge was measured in the laboratory as a function of temperature. The technique of measuring the permeability was the steady-state flow-through method. Core samples of about 2.54 cm in diameter and 5.1 cm in length were prepared from small block sample SPC00504573 collected at Fran Ridge during the excavation of the large block, with core identification numbers SPC00504573.4 and SPC00504573.5. The test sample was first saturated with water. Then the sample was encapsulated in a membrane, which separated the sample from the confining pressure fluid. The sample assembly was placed within a pressure vessel with independently controlled confining pressure, pore-water pressure, and temperature. The sample was brought to an equilibrium of certain temperature, confining pressure, and pore pressure.

A differential pressure across the length of the sample was created to cause a flow. The steady-state flow rate was measured. Permeability was calculated using a one-dimensional form of Darcy's Law. Darcy's Law applies because it relates permeability to differential pressure, flow rate, and flow length. The measurement equipment used in the permeability measurement included a confining pressure transducer, pore pressure transducer, differential pressure transducer, and thermocouple to measure temperature. Flow rate was determined by letting water flow into a container on a balance. The weight of the balance corresponded to the volume of water that has flowed through the sample and is recorded by a computer, along with all the other data such as time, temperature, differential pressure, pore pressures, and confining pressure. Because the flow rate was low, it was necessary to consider the rate of evaporation from the collection bottle. This was found to be linear with time over a period of about one week. The water lost due to evaporation was 4.13 mg/hr. This lost water was added to the balance reading for a specific period of time when calculating permeability. The matrix permeability data can be found under DTN: LL960905204244.022 [DIRS 158244] in the TDMS.

### Density, Porosity, and Micro-Pore Structure

Section 3.5.1.3.3 of *Large Block Test Final Report* (Lin et al. 2001 [DIRS 159069]) presents the porosity and the micro-pore structure of the LBT samples. The porosity was determined by calculating the difference between the dry density and the water-saturated wet density, divided by the water density (the Gravimetric method). The micro-pore size distribution was determined by mercury-injection porosimetry, another conventional method in the study of rock pore structure. The density and porosity data from the dry-and-saturation method can be found in the TDMS under DTN: LL950812704242.017 [DIRS 158237]. Note that these data are unqualified and should only be used for corroborative purposes.

### Fracture Flow and Matrix Imbibition Visualization

Section 3.5.1.3.4 of *Large Block Test Final Report* (Lin et al. 2001 [DIRS 159069]) presents the laboratory experiments using X-ray radiography to visualize fracture flow and matrix imbibition. The samples used in those visualizations were machined from small blocks obtained at the LBT site. A vertical tensile fracture was induced in the middle of the sample block of 2.5 cm thickness, oriented so that the plane of the fracture was parallel to the direction of X-ray transmission. At the top and bottom of the sample were chambers for ponding and collection of water. X-ray radiographs were taken periodically to image water movement into the fracture and rock matrix. A total of seven experiments were conducted. The experimental conditions included isothermal with and without shim, and at thermal gradients with shim. (The role of the shim is to increase the aperture of the induced fracture.) The X-ray radiograph data can be found in the TDMS under DTN: LL981208404244.092 [DIRS 158263]. Note that this DTN is unqualified and should only be used for corroborative purposes.

#### **6.1.2.4.1 Results: Matrix Permeability, Density, Porosity, Micro-Pore Structure, Fracture Flow, and Matrix Imbibition Visualization**

### Matrix Permeability

The water/matrix permeability data of intact core sample SPC00504573.4 are summarized in Table 6.1-3. The permeability of the intact Topopah Spring Tuff sample was less than  $10^{-18}$  m<sup>2</sup>. This permeability value is consistent with that measured in cores from Yucca Mountain (Lin and Daily 1984 [DIRS 101393]). It is also shown in Table 6.1-3 that intact sample permeability was not a strong function of temperature. This finding is also consistent with the results reported by Lin and Daily (1984 [DIRS 101393]).

Table 6.1-3. LBT Permeability Measurements on Intact Core Sample SPC00504573.4

Temperature (°C)	Confining Pressure (MPa)	Differential Pressure (MPa)	Permeability (μD)
23	5.06	1.92	0.12
25	5.07	2.47	0.14
53	5.06	2.42	0.11
53	5.06	1.91	0.15
91	5.06	2.17	0.14
92	5.06	1.60	0.14
154	5.06	1.61	0.09
130	5.05	1.46	0.13
130	5.05	2.04	0.11
83	5.06	2.02	0.17
26	5.06	2.59	0.67
26	5.06	2.61	0.20

Source: DTN: LL960905204244.022 [DIRS 158244].

*Density, Porosity, and Micro-Pore Structure*

Table 6.1-4 shows the porosity of the LBT samples. The porosity ranged from 0.08 to 0.14, with a mean of 0.104 for the 36 samples. The porosity of the 33 samples determined from the mercury-injection porosimetry ranged from 0.08 to 0.20 with a mean of 0.115, which agreed well with that determined by the dry-and-saturation method.

Table 6.1-4. Density and Porosity of LBT Samples Determined by Gravimetric Method

Sample <sup>a</sup>	Sample ID	Depth (m)	Dry Weight (g)	Wet Weight (g)	Dry Density (g/cm <sup>3</sup> )	Wet Density (g/cm <sup>3</sup> )	Porosity
N1-6.3	0032079.3	1.92	1.5352	1.6111	2.23	2.35	0.110
N1-6.3A	0032079.3A	1.92	1.7890	1.8680	2.26	2.36	0.0997
N1-6.3B	0032079.3B	1.92	1.6358	1.7098	2.28	2.39	0.103
N1-11.0	0032081.3	3.35	1.6352	1.7181	2.25	2.37	0.114
N1-11.0A	0032081.3A	3.35	1.5920	1.6734	2.26	2.38	0.116
N1-11.0B	0032081.3B	3.35	1.6762	1.7525	2.30	2.41	0.105
N1-13.45	0032082.3	4.10	1.4982	1.5752	2.27	2.39	0.117
N1-13.45A	0032082.3A	4.10	1.7118	1.7951	2.27	2.38	0.110
N1-13.45B	0032082.3B	4.10	1.6954	1.7781	2.26	2.37	0.110
N1-16.9	0032083.3	5.15	1.6499	1.7522	2.20	2.33	0.136
N1-16.9A	0032083.3A	5.15	1.6094	1.6987	2.23	2.35	0.124
N1-16.9B	0032083.3B	5.15	1.6885	1.7670	2.27	2.38	0.106
N1-20.3	0032084.3	6.19	1.5438	1.6133	2.22	2.32	0.0998
N1-20.3A	0032084.3A	6.19	1.5567	1.6244	2.26	2.36	0.0982
N1-20.3B	0032084.3B	6.19	1.5109	1.5849	2.21	2.32	0.108

Table 6.1-4. Density and Porosity of LBT Samples Determined by Gravimetric Method (Continued)

Sample <sup>a</sup>	Sample ID	Depth (m)	Dry Weight (g)	Wet Weight (g)	Dry Density (g/cm <sup>3</sup> )	Wet Density (g/cm <sup>3</sup> )	Porosity
N4-11.6	0032104.3	3.54	1.5429	1.6036	2.26	2.34	0.0887
N4-11.6A	0032104.3A	3.54	1.6222	1.6864	2.24	2.33	0.0886
N4-11.6B	0032104.3B	3.54	1.6375	1.6969	2.27	2.35	0.0823
N5-4.9	0032107.3	1.49	1.6998	1.7687	2.25	2.34	0.0911
N5-4.9A	0032107.3A	1.49	1.6501	1.7104	2.28	2.37	0.0834
N5-4.9B	0032107.3B	1.49	1.8818	1.9569	2.31	2.40	0.0922
N5-20.4	0032111.3	6.22	1.5230	1.5909	2.22	2.32	0.0992
N5-20.4A	0032111.3A	6.22	1.4883	1.5593	2.21	2.32	0.106
N5-20.4B	0032111.3B	6.22	1.4765	1.5463	2.22	2.32	0.105
N6-4.75	0032112.3	1.43	1.7549	1.8228	2.25	2.33	0.0869
N6-4.75A	0032112.3A	1.43	1.6761	1.7374	2.29	2.37	0.0837
N6-4.75B	0032112.3B	1.43	1.7136	1.7755	2.27	2.35	0.0819
N6-14.2	0032116.3	4.33	1.6590	1.7398	2.26	2.37	0.110
N6-14.2A	0032116.3A	4.33	1.6869	1.7706	2.24	2.35	0.111
N6-14.2B	0032116.3B	4.33	1.6285	1.7137	2.23	2.35	0.117
N7-5.7	0032120.3	1.74	1.6161	1.7003	2.24	2.36	0.117
N7-5.7A	0032120.3A	1.74	1.6320	1.7051	2.29	2.39	0.102
N7-5.7B	0032120.3B	1.74	1.7091	1.7834	2.28	2.38	0.0991
N7-11.0	0032123.3	3.35	1.5850	1.6705	2.25	2.37	0.121
N7-11.0A	0032123.3A	3.35	1.6353	1.7171	2.26	2.38	0.113
N7-11.0B	0032123.3B	3.35	1.6318	1.7112	2.27	2.38	0.110
Mean <sup>b</sup> (36 samples)					2.25±0.03	2.36±0.02	0.104±0.013

DTN: LL950812704242.017 [DIRS 158237] (unqualified).

<sup>a</sup> Sample name consists of borehole designation followed by depth in feet below the template used to locate vertical boreholes.

<sup>b</sup> Statistical mean for 36 samples. Errors represent one standard deviation for all samples collectively.

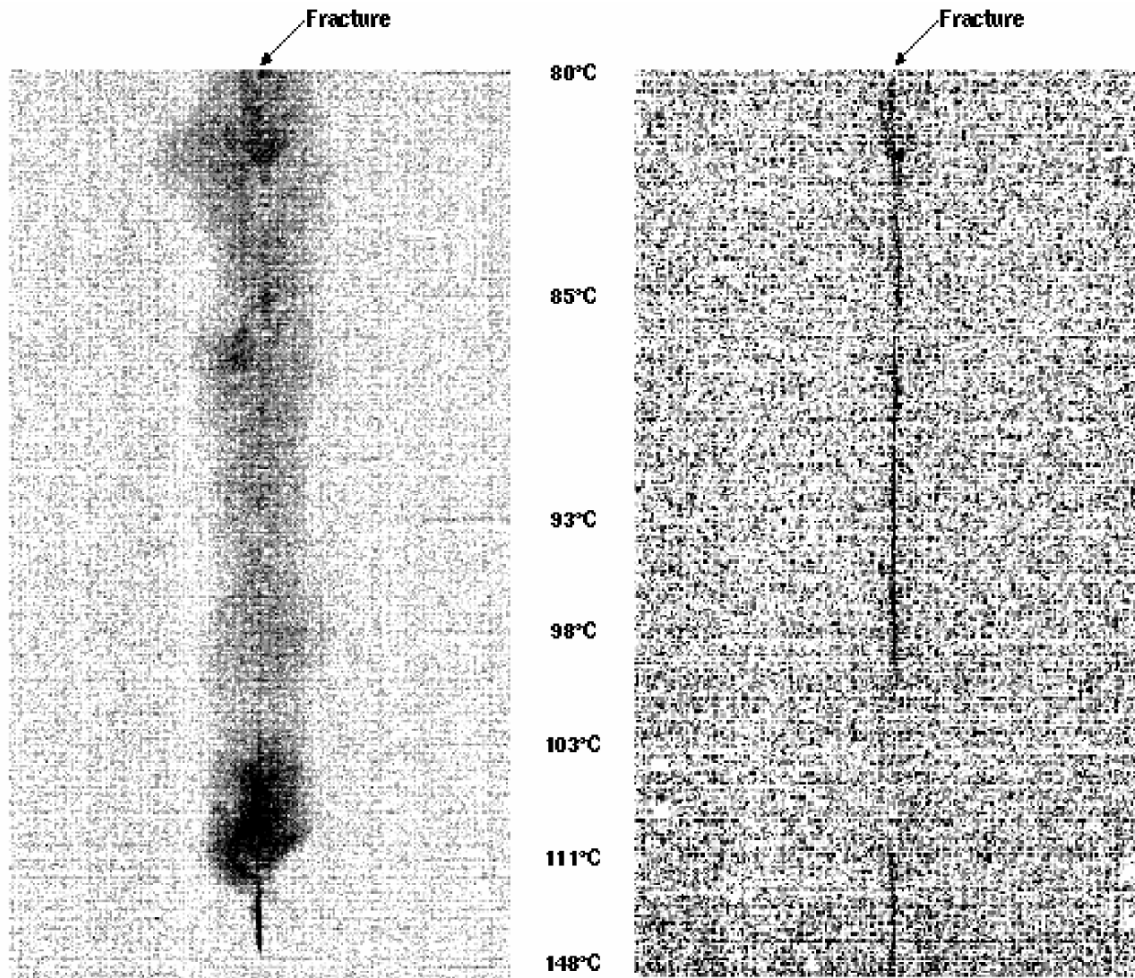
### Fracture Flow and Matrix Imbibition Visualization

At room temperature, imbibition occurred chiefly through the matrix for the unshimmed fracture, with a roughly V-shaped wetting front. During the shimmed fracture experiment, water flowed along the fracture length first, then imbibed horizontally into the matrix.

Under a thermal gradient, water flowed down the fracture quickly. There was significant lateral imbibition into the matrix from the fracture. Penetration of the boiling zone by the water depends on the water head.

Figure 6.1-17 shows two images to illustrate the effect of water head on the fracture flow and matrix imbibition. In those two cases, the lower portion of the sample was the boiling zone. The

convention used for the difference images is that darker colors or shades indicate relatively high X-ray attenuation and the presence of water, while the lighter areas correspond to lower attenuation and relatively dry areas. For a small water head of about 0.26 m, the water wetted almost the entire fracture first, followed by imbibition into the matrix, as shown in Figure 6.1-17 (left image). Within 7.2 hours of ponding, the water penetrated about 3 cm into the boiling zone. Figure 6.1-17 (right image) shows that when the water head was increased to 0.46 m, the water flowed through the entire length of the fracture within minutes and continued to flow through the boiling region. Not much imbibition into the matrix was observed in this case. The difference in water head was enough to force water through the boiling zone without significant imbibition.



Source: Lin et al. 2001 [DIRS 159069].

Figure 6.1-17. Images of Imbibition under Thermal Gradient: 0.26 m Water Head at 7.2 Hours (left) and 0.46 m Water Head at 0.67 Hours (right)

#### **6.1.2.4.2 Measurement Uncertainty: Matrix Permeability, Density, Porosity, Fracture Flow, and Matrix Imbibition Visualization**

##### Matrix Permeability

The factors contributing to permeability uncertainty include the measurement accuracy of flow rate, differential pressure, and temperature. The inaccuracy in these measurements is small. The propagated error in the permeability through Darcy's equation is also small.

##### Density and Porosity

The uncertainty of determining the density and porosity of a sample includes the uncertainty in the sample weight and volume.

##### Fracture Flow and Matrix Imbibition Visualization

The fracture flow and matrix imbibition experiments were qualitative observations. The main source of uncertainty is the similar X-ray attenuation caused by either increased water content or the formation of potassium iodide crystals.

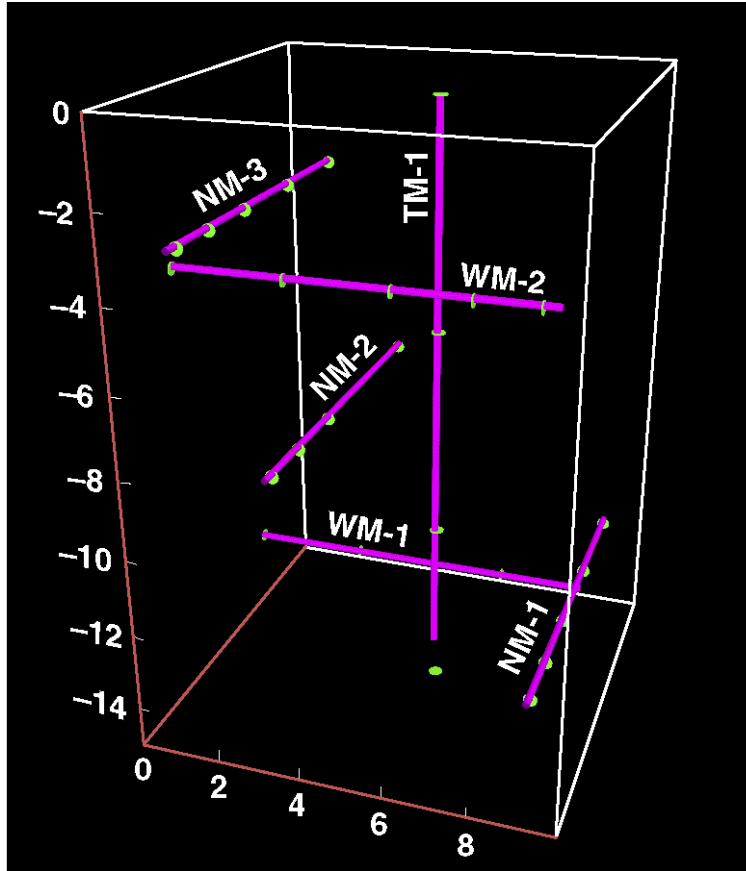
### **6.1.3 LBT Mechanical Measurements**

#### **6.1.3.1 Multipoint Borehole Extensometer Displacements**

The three-dimensional view of the six multipoint borehole extensometer (MPBX) boreholes in the block is shown in Figure 6.1-18. For the location of those boreholes in the top, north, and west sides of the block, see Figures 6.1-2, 6.1-3, and 6.1-5, respectively. Section 7.1.1 of *Large Block Test Final Report* (Lin et al. 2001 [DIRS 159069]) presents the MPBX measurements in detail. Each extensometer consists of three or four borehole anchors connected to linear variable displacement transducers (LVDTs) at the collar by Invar rods. The anchors are numbered such that anchor 1 is nearest and anchor 4 is farthest from the collar. The anchors are spring-loaded to the borehole wall. Each anchor is connected to an LVDT at the collar by one invar rod. Any movement of the rock at an anchor is transferred to the LVDT at the collar. Therefore, the extensometers measure linear displacement relative to the surface collar. In the data reduction, the thermal expansion of the invar rod was corrected from the raw displacement data by using the manufacturer's invar rod thermal-expansion coefficient and the measured temperatures in TT1 and TT2.

Preheating MPBX measurements were conducted for several days before the heaters were energized on February 28, 1997. The LVDTs were zeroed before the heating was started. All of the extensometers performed well during the first few weeks, but problems developed over time, beginning with NM-2, which is located near the heater plane. NM2 failed after about 40 days of heating. About 100 days into the heating phase, two more MPBXs (TM1 and NM1) failed. Before the heating phase ended, at about 375 days, TM1 and NM1 were repaired. Three out of the six MPBXs provided complete sets of displacement data for the entire duration of the test.

A detailed discussion of the LBT mechanical measurements is provided in Section 7.1 of *Large Block Test Final Report* (Lin et al. 2001 [DIRS 159069]). The input DTNs for mechanical measurements are provided in Table 4-1. The input DTN for these MPBX displacements is LL980919404244.076 [DIRS 148630].



Source: Lin et al. 2001 [DIRS 159069].

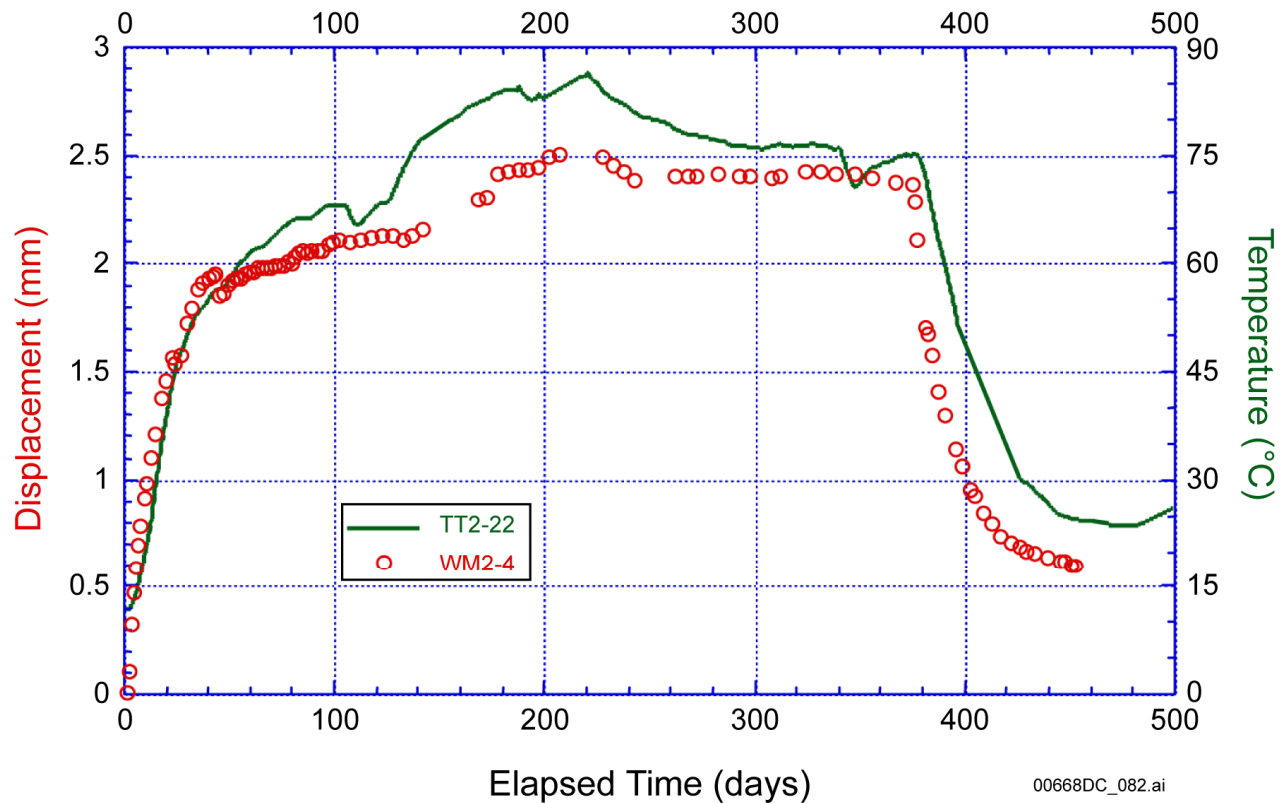
Figure 6.1-18. MPBX Borehole Locations, Viewed from the South Face

### 6.1.3.1.1 Results: MPBX Displacements

Figure 6.1-19 shows a typical example of the displacement data as a function of time. This is the displacement measured at the #4 anchor of WM2. Also shown in the figure is the temperature measured at TT2-22, which was about the same distance from the heater plane as WM2. Positive displacement means expansion; negative displacement means contraction. The measured displacement in the block tracked the temperature well, indicating that the block expanded as a result of heating.

The horizontal displacements near the base of the block were small, essentially the same in the two horizontal directions, and were recovered during cool-down. The horizontal displacements near the top of the block were large, isotropic, and were only partially recovered. The vertical displacement was fairly small but only partially recovered during cooldown.





Source: DTNs: LL980919404244.076 [DIRS 148630]; LL980918904244.074 [DIRS 135872] (unqualified).

NOTE: The temperature data shown in green are from DTN: LL980918904244.074 [DIRS 135872].

Figure 6.1-19. East–West Displacement for WM-2 Anchor 4 and Temperature at Depth of 1.2 m

### 6.1.3.1.2 Measurement Uncertainty: MPBX Displacements

There are several potential sources for measurement uncertainty in the displacement measurements presented in this section. These uncertainties, quantifiable and nonquantifiable, are listed below:

#### Quantifiable

- The accuracy of the instrumentation.
- The conversion of the electrical output to engineering units. The uncertainty from these equations, and the computational (round-off) error inherent in the data conversion software, are negligible.
- The physical location of the gages in the test region. The location uncertainty is particularly important in regions of high temperature gradient, where hydrological and thermal expansion behavior are thought to be strong functions for certain temperature ranges.

- The uncertainty related to the choice of method for computing thermal expansion of Invar rods based on measured temperatures along MPBXs. Although uncertainty is difficult to estimate, the magnitude of any discretization error is likely not large enough to affect the general trends in thermal-mechanical deformation of the rock.

### Nonquantifiable

- Electrical interference, such as spurious signals from power surges, which can cause low-magnitude noise, unexplained meandering in the data, or high-magnitude spikes.
- Unidentified sensor or MPBX assembly stability issues, which caused a few LVDTs or vibrating wire gages either to produce “bad” data for an extended period of time before returning “good” data, or to have an unexplained shift in magnitude while maintaining expected rates of behavior on both sides of the shift.
- Degradation or failure of the instrumentation.

Nonquantifiable uncertainties are usually addressed by removing questionable data from the data set prior to its use in analysis and modeling activities.

### **6.1.3.2 Fracture Monitoring**

Deformations of several major fractures that intersect the surface of the LBT block were monitored using three-component fracture monitors. The purpose of these sensors was to monitor the movement of fractures to gain information about the magnitude and direction of fracture deformation during the test, especially as it relates to TH behavior.

Linear variable displacement transducers were used to measure the displacements in the three-component surface fracture monitor. The sensors were mounted in T-shaped slots cut into the block, visible in Figure 6.1-1. The slots were cut so that one LVDT would measure aperture change or deformation across the fracture in the plane of the face, while the other two LVDTs would measure sliding in orthogonal directions, parallel and perpendicular to the face. The fractures chosen were oriented perpendicular to the face as much as possible; thus, the information can be used to supply estimates of fracture deformation parameters, such as dilation with sliding. See Section 7.1.3 of *Large Block Test Final Report* (Lin et al. 2001 [DIRS 159069]) for detailed discussion of fracture monitoring. The input DTN for fracture monitoring is LL980919404244.076 [DIRS 148630].

#### **6.1.3.2.1 Results: Fracture Monitoring**

The fracture monitoring (FM) data show that the vertical and horizontal fractures responded somewhat differently. The major horizontal fracture near the top opened coincidentally with the TH event at day 105. Both vertical and horizontal fractures showed closing during the thermal recovery from the TH events, that is, during periods of apparent condensate refluxing. Initial response for several of the FM readings was associated with temperature at the heater plane. FM data indicate that the top of the block moved to the east. Most of the FM deformation was not recovered. The FM data are somewhat inconsistent with the MPBX data, as FM results indicate

more deformation in lower portions of the block and less deformation in the upper portions of the block. The FM and MPBX results are given in DTN: LL980919404244.076 [DIRS 148630].

#### **6.1.3.2.2 Measurement Uncertainty: Fracture Monitoring**

Factors contributing to uncertainty in fracture monitoring include the rigidity of the mounting brackets, the limited number of monitoring points, the effects of the environmental conditions on the fracture monitor, the heterogeneity in the rock, and the apparent movement on the block surface.

#### **6.1.4 LBT Miscellaneous Measurements and Observations**

Fracture mapping and qualitative observations were included in the LBT. Observations from boreholes included assessments of fracture flows and microbial survivability and migration. Fracture mapping and the activities in the observation boreholes, as well as microbial survivability and migration, are summarized here. A detailed discussion of the LBT miscellaneous measurements is provided in *Large Block Test Final Report* (Lin et al. 2001 [DIRS 159069]).

##### **6.1.4.1 Fracture Mapping**

Fracture mapping served to characterize the test block, help interpret test results, and compare with the fracture characteristics of the Exploratory Studies Facility (ESF). Section 4 of *Large Block Test Final Report* (Lin et al. 2001 [DIRS 159069]) presents the fractures mapped in the block. Fractures were carefully mapped on the block surface (four sides and top). Information on the fractures was also collected from video logs of boreholes. On the block surface, fractures were mapped using a 30-by-30-cm grid system on all four vertical sides and the top of the block. The fracture locations were digitized, and fracture segment nodes were assigned x-y-z values. From the borehole video logs, the depths at which the fracture enters and exits the borehole were recorded, as well as the strike, dip, dip direction, aperture, and magnitude of the features. Appendix C of *Large Block Test Final Report* (Lin et al. 2001 [DIRS 159069]) includes information from all borehole video logs. The fracture information can be found in the TDMS under the following DTNs:

- LL960400404244.012 [DIRS 158271]
- LL960400504244.013 [DIRS 158274]
- LL960400604244.014 [DIRS 158275]
- LL960400704244.015 [DIRS 158276].

##### **6.1.4.1.1 Results: Fracture Mapping**

Major fractures were identified based on size, extent, continuity, and other considerations. The major fractures were then grouped into six systems according to their strike and dip. The fractures in the LBT were dominated by high-angle fractures. This is similar to the fractures in the ESF of Yucca Mountain.

#### **6.1.4.1.2 Measurement Uncertainty: Fracture Mapping**

The fractures were mapped by hand with tape measures and by viewing video logs, which have a measuring tape in the image. The accuracy of the measured location and extent of the fractures are a few millimeters. The major uncertainty is in the continuity of the fractures within the block.

#### **6.1.4.2 Video Observation of Boreholes**

Four observation boreholes, NO1, NO2, EO3, and WO5, were installed near the bottom of the block. See Figures 6.1-3, 6.1-4, and 6.1-5, respectively, for the location of these boreholes.

##### **6.1.4.2.1 Results: Video Observation of Boreholes**

Section 9.1 of *Large Block Test Final Report* (Lin et al. 2001 [DIRS 159069]) describes the observations performed in these boreholes. Observation boreholes were equipped with a Pyrex tube. The Pyrex tube was put in a half section of PVC pipe, cushioned by one piece of white cloth. The Pyrex tube was to allow access to a video camera for viewing fracture flows in a borehole. The ink marks on the Pyrex tube and the white cloth under the tube were to provide markers of fracture flow. Observations were performed periodically. It was obvious very early that the moisture in the tube prohibited any meaningful direct observation by a video camera. Most of the observations were performed by examining the ink marks on the tube and the ink stains on the white cloth. Many discrete markers (ink stains) were observed in the white cloth, but it was also obvious that condensation on the tube dissolved away a significant portion of the ink marks. Therefore, the video observation results are considered to be of little value.

##### **6.1.4.2.2 Measurement Uncertainty: Video Observation of Boreholes**

These observations have qualitative uncertainties, which are inherent to visual observations of geologic features.

#### **6.1.4.3 Microbial Observation**

Section 9.3 of *Large Block Test Final Report* (Lin et al. 2001 [DIRS 159069]) provides a detailed summary of the findings concerning microbial survivability and migration. Microbes were collected from the rock at the LBT site and cultured to be double-drug resistant. The labeled microbes were placed in the heater boreholes and the two vertical boreholes identified as LBL-1 and LBL-2 in Figure 6.1-2. The purpose was to test the survivability of the microbes and their migration in the heated, partially saturated rock environment. The observation performed was to periodically sample the moisture on the Pyrex tube and the white cloth cushion in the observation boreholes mentioned above. The data on the microbial types, abundance, and growth rates can be found in the TDMS under DTN: LL981202305912.004 [DIRS 158270]. Note that these data are unqualified and should only be used for corroborative purposes.

#### 6.1.4.3.1 Results: Microbial Observation

The microbes were found in the observation boreholes, which were about 1.5 m below the heater boreholes. This observation indicates that the microbes survived the heating and traveled with drainage water to the observation boreholes.

#### 6.1.4.3.2 Measurement Uncertainty: Microbial Observation

The microbial observation was qualitative and scoping. Uncertainty assessment for the qualitative activity is not meaningful.

### 6.2 SINGLE HEATER TEST

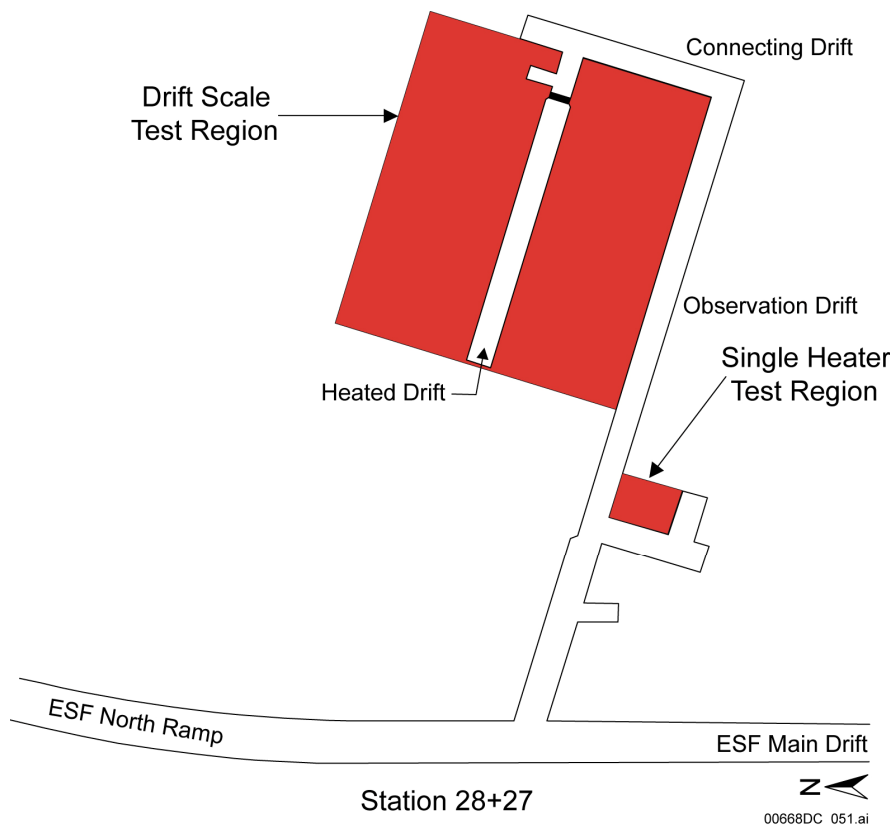
The Single Heater Test (SHT) was the first of several in situ thermal tests planned and conducted to investigate coupled processes in the local rock mass surrounding the repository. These coupled processes are thermally driven by heat released from an electrical heater that simulates heat from emplaced nuclear waste. The SHT is located in the same rock unit (Ttpmn) as the LBT, but the LBT block is from a surface outcrop while the SHT (and the DST) are in situ or underground. More specifically, the SHT is located in Alcove 5 in the ESF as shown in Figure 6.2-1. The heating phase of the SHT started in August 1996 and continued for nine months until May 1997. The cooling phase continued for seven months until January 1998, at which time postcooling characterization of the test block commenced. A detailed description of the SHT is presented in *Single Heater Test Final Report* (CRWMS M&O 1999 [DIRS 129261]).

The test block was characterized under ambient conditions prior to heater activation. Characterization included testing in the laboratory for thermal, mechanical, and hydrological properties, mineralogic-petrologic characteristics, as well as field measurements of permeabilities and fracture characteristics (CRWMS M&O 1996 [DIRS 101428]).

SHT input DTNs are tabulated in Table 4-2. SHT summary DTNs are tabulated in Table 6.2-1.

A plan and cross section of the SHT are shown in Figure 6.2-2. The SHT block was approximately 12.9 m wide, 9.5 m deep, and 5.5 m high. Forty-one boreholes with total length of 230 m were drilled into the block. Borehole 1 (shown in red in Figure 6.2-2) contained the single 5-m-long heater capable of generating nominal 4 kW of heat. The other boreholes were installed with various equipment systems and sensors to monitor the thermal, mechanical, hydrological, and chemical responses of the rock as it was heated and cooled. Detailed description of the SHT as-built borehole locations is provided in Table 6.2-2. Coordinates of the various SHT sensors are provided in Appendix G of *Single Heater Test Final Report* (CRWMS 1999 [DIRS 129261]) and the respective summary DTNs identified in Table 6.2-1. The origin of the SHT XYZ coordinate system is the center of the collar for the heater borehole. The X-axis is horizontal and positive to the right when facing the heater borehole, the Y-axis is also horizontal and follows the longitudinal direction of the heater borehole, and the Z-axis is vertical and positive in the upward direction. The borehole numbers in Figure 6.2-2 correspond to those in Table 6.2-2. Table 6.2-2 gives the sensor type or type of measurement for which any particular borehole is used. A total of 530 sensors were placed in the boreholes. Several

boreholes were drilled for postcooling characterization. The coordinates of the additional boreholes in the SHT block are shown in Table 6.2-3.



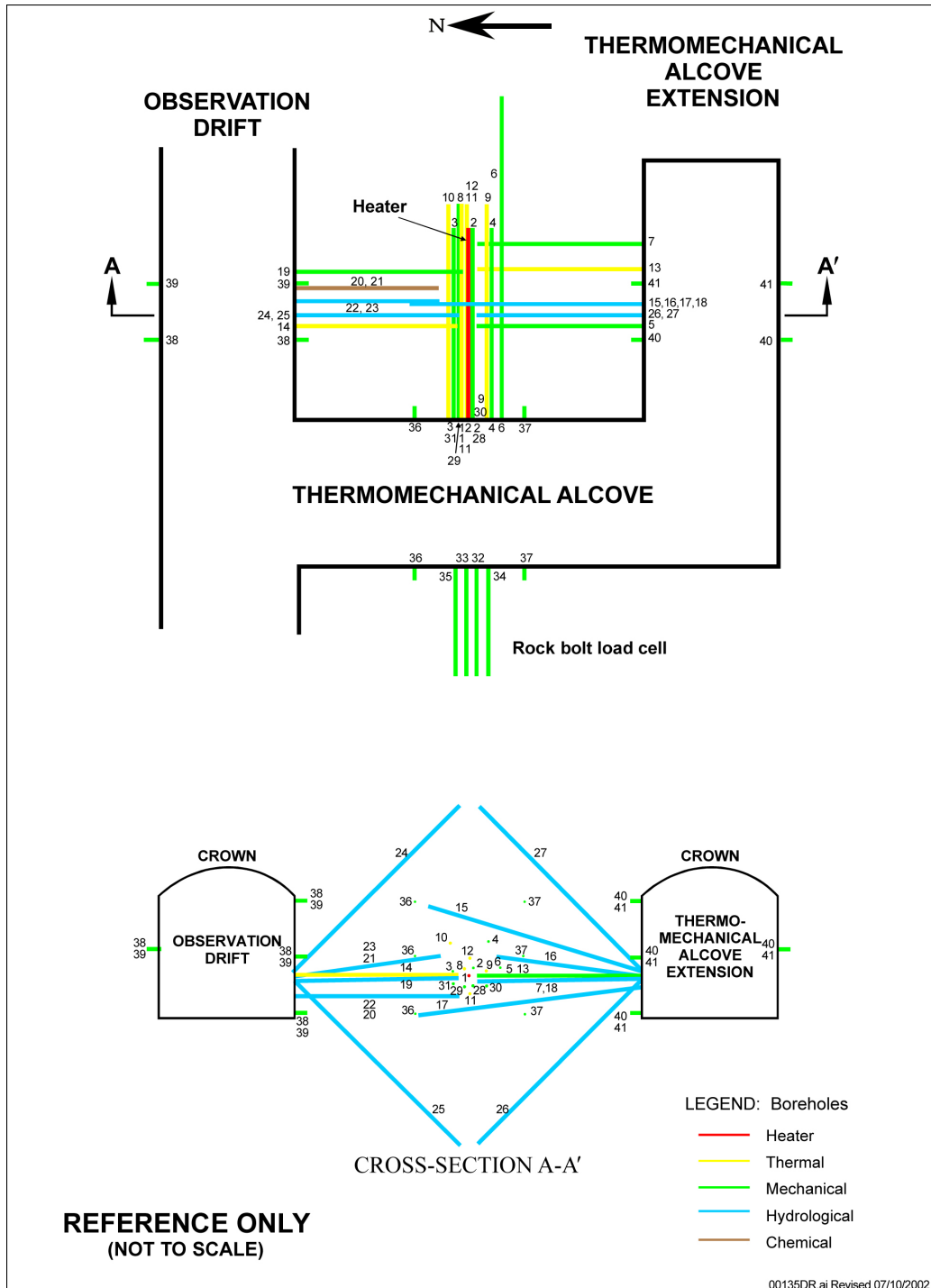
Source: CRWMS M&O 1999 [DIRS 129261].

Figure 6.2-1. Schematic Plan View of ESF Thermal Test Facility Including the SHT

Most of the measurements made by the sensors were scanned and recorded by an automated data collection system. The central component of the DCS was a Geomation Model 2380 Measurement and Control Unit (MCU) in a NEMA-12 enclosure with a capacity of 640 channels. The DCS recorded the heater power and the readings of the thermocouples mounted on the heater itself every 15 minutes. The readings of the other sensors were recorded hourly. Certain measurements that were not recorded by the DCS included electrical resistivity tomography (ERT), neutron logging, ground penetrating radar (GPR), Goodman Jack (borehole jack), pneumatic permeability, and infrared imaging.

The SHT DCS recorded thermal, hydrological (partial), and mechanical data, for the most part, on an hourly basis (heater power and temperature recorded every 15 minutes). The acquired data consists of both original (measured electronic values) and converted (engineering units). A package of data was submitted to the RPC and a corresponding DTN (LA0002FH6001WP.001 [DIRS 158278]) was also obtained. This DCS DTN also identifies scientific notebooks that provide details of SHT measurements including calibration information. DCS DTNs are reduced and restructured and periodically submitted to the TDMS, resulting in many of the input DTNs introduced below and listed in Table 4-2. As discussed in Section 1 and the introduction to

Section 6, these input DTNs are further refined, reduced, and restructured before being resubmitted to the TDMS as summary DTNs (see Table 6.2-1).



Source: CRWMS M&O 1999 [DIRS 129261].

Figure 6.2-2. Schematic SHT Layout of the Instrumentation Boreholes

Table 6.2-1. DTNs for the Single Heater Test

Input DTN	Input DTN Description	Input DTN Text Location	Summary DTN	Summary DTN Description
LA002FH6001WP.001 <sup>a</sup> [DIRS 158278]	Data Collection System data	Section 6.2	Unchanged DTN	Unchanged DTN
SN0401F3511695.012 [DIRS 169262]	Thermal and thermal-mechanical data	Section 6.2.1.1	MO208RESTRSHT.002 [DIRS 170582]	Power and Temperature Data
SN0401F3511695.013 [DIRS 169263]	Thermal and thermal-mechanical data	Section 6.2.1.2		
SNF35110695001.001 [DIRS 158315]	XYZ coordinates of boreholes and sensors	Section 6.2		
LL970805504244.043 [DIRS 158313]	XYZ coordinates of boreholes and sensors	Section 6.2		
SNL22080196001.001 [DIRS 109722]	Thermal conductivity	Section 6.2.1.3	Unchanged DTN	Unchanged DTN
LL970101004244.026 [DIRS 158281]	Electrical resistance tomography	Section 6.2.2.1	LL020801823142.029 [DIRS 170581]	ERT Tomograms
LL970505404244.031 [DIRS 148609]	Electrical resistance tomography	Section 6.2.2.1		
LL971002904244.044 [DIRS 158286]	Electrical resistance tomography	Section 6.2.2.1		
LL980105204244.049 [DIRS 148610]	Electrical resistance tomography	Section 6.2.2.1		
LB980901123142.003 [DIRS 119016]	Ground penetrating radar data	Section 6.2.2.2	LB0208GPRSHTCP.001 [DIRS 170578]	GPR Velocity Tomograms
LL980106904244.051 [DIRS 118963]	Neutron logging	Section 6.2.2.3	Unchanged DTN	Unchanged DTN
LB970100123142.001 [DIRS 158287]	Air injections in boreholes 16 and 18	Section 6.2.2.4	Unchanged DTN	Unchanged DTN
LB960500834244.001 [DIRS 105587]	Preheating air injection	Section 6.2.2.4	Unchanged DTN	Unchanged DTN



Table 6.2-1. DTNs for Single Heater Test (Continued)

Input DTN	Input DTN Description	Input DTN Text Location	Summary DTN	Summary DTN Description
LB980120123142.008 [DIRS 158280]	Air injections in boreholes 16 and 18, part 1 of 4	Section 6.2.2.4	LB0208AIRKSHTC.001 [DIRS 170576]	Permeability Data (Boreholes 16 and 18)
LB970500123142.001 [DIRS 158293]	Air injections in boreholes 16 and 18, part 2 of 4	Section 6.2.2.4		
LB0204SHAIRK3Q.001 [DIRS 159543]	Air injections in boreholes 16 and 18, part 3 of 4	Section 6.2.2.4		
LB971000123142.001 [DIRS 118965]	Air injections in boreholes 16 and 18, part 4 of 4	Section 6.2.2.4		
LB980901123142.001 [DIRS 118999]	Postcooling air injection and gas tracer testing	Section 6.2.2.4	Unchanged DTN	Unchanged DTN
LB980901123142.002 [DIRS 119009]	Temperature, relative humidity, gauge pressure (passive monitoring)	Section 6.2.2.4	Unchanged DTN	Unchanged DTN
LB970500123142.003 [DIRS 131500]	Preheating laboratory saturation, porosity, bulk density gravimetric water content	Section 6.2.2.5	Unchanged DTN	Unchanged DTN
LL020506123142.021 [DIRS 169256]	Preheating laboratory porosity, relative humidity, and water saturation	Section 6.2.2.5	Unchanged DTN	Unchanged DTN
LB980901123142.006 [DIRS 119029]	Postcooling laboratory saturation, porosity, bulk density gravimetric water content	Section 6.2.2.5	Unchanged DTN	Unchanged DTN
SN0401F3511695.012 [DIRS 169262]	Thermal and thermal-mechanical data	Section 6.2.3.1	Unchanged DTN	Unchanged DTN
SN0401F3511695.013 [DIRS 169263]	Thermal and thermal-mechanical data	Section 6.2.3.1	Unchanged DTN	Unchanged DTN
LL980109904243.015 [DIRS 158299]	Optical MPBX displacements	Section 6.2.3.1	Unchanged DTN	Unchanged DTN
SNF35110695001.010 [DIRS 158300]	Rock mass deformation modulus – borehole (Goodman) jack	Section 6.2.3.2	Unchanged DTN	Unchanged DTN
SN0401F3511695.012 [DIRS 169262]	Thermal and thermal-mechanical data	Section 6.2.3.3	Unchanged DTN	Unchanged DTN
SN0401F3511695.013 [DIRS 169263]	Thermal and thermal-mechanical data	Section 6.2.3.3	Unchanged DTN	Unchanged DTN
SNL22080196001.001 [DIRS 109722]	Laboratory thermal expansion	Section 6.2.3.4	Unchanged DTN	Unchanged DTN

Table 6.2-1. DTNs for Single Heater Test (Continued)

Input DTN	Input DTN Description	Input DTN Text Location	Summary DTN	Summary DTN Description
SNL22080196001.002 [DIRS 158306]	Preheating laboratory unconfined compressive strength, dry bulk density, Poisson's ratio, Young's modulus, saturated bulk density, seismic velocity	Section 6.2.3.4	Unchanged DTN	Unchanged DTN
SNL22080196001.003 [DIRS 119042]	Postcooling laboratory thermal conductivity, thermal expansion, unconfined compressive strength, dry bulk density, Poisson's ratio, Young's modulus	Section 6.2.3.4	Unchanged DTN	Unchanged DTN
LL970101104244.027 <sup>b</sup> [DIRS 158309]	Chemical abundance data	Section 6.2.4.1	Unchanged DTN	Unchanged DTN
LL970409604244.030 <sup>b</sup> [DIRS 111481]	Chemical abundance data	Section 6.2.4.1	Unchanged DTN	Unchanged DTN
LL970703904244.034 <sup>b</sup> [DIRS 111482]	Chemical abundance data	Section 6.2.4.1	Unchanged DTN	Unchanged DTN
LL971006604244.046 <sup>b</sup> [DIRS 148611]	Chemical abundance data	Section 6.2.4.1	Unchanged DTN	Unchanged DTN
GS951108312271.006 <sup>b</sup> [DIRS 169244]	Chemical abundance data	Section 6.2.4.1	Unchanged DTN	Unchanged DTN
LA0009SL831151.001 [DIRS 153485]	Fracture mineralogy	Section 6.2.4.2	Unchanged DTN	Unchanged DTN
LB970700123142.002 [DIRS 158295]	Infrared images, part 3 of 5	Section 6.2.5.2	Unchanged DTN	Unchanged DTN
LB980120123142.001 [DIRS 158297]	Infrared images, part 5 of 5	Section 6.2.5.2	Unchanged DTN	Unchanged DTN

<sup>a</sup> DTN: LA0002FH6001WP.001 [DIRS 158278] provides access via the RPC to all thermal and mechanical data collected in SHT DCS (original/electrical and converted/engineering units). This unqualified DTN also provides access (via the RPC) to pertinent supporting material such as scientific notebooks and calibration relationships. These data should only be used for corroborative purposes.

<sup>b</sup> These data are unqualified and should only be used for corroborative purposes.

Table 6.2-2. SHT Borehole Information

Borehole Number	Borehole Identification	Primary Purpose	Collar Coordinates (m)			Bottom Coordinates (m)			Orientation Degree	Diameter (cm)	Length (m)	Volume (m <sup>3</sup> )	Thermo-Couples	RTD	Thermistors	Lead Coll (Average)	Anchor in MPBX	Type/Wire Extensometer	Humidity Sensor	Pressure Transducer	Electrode Sensor (ERT)	Chemistry Absorbing Pad	Comments
			X	Y	Z	X	Y	Z															
			X	Y	Z	X	Y	Z															
1	ESF-TMA-H-1	Heater	0.01	0.04	-0.03	0.00	6.97	-0.01	0.5	9.60	7.00	0.05	27	—	—	—	—	—	—	—	—	5-in-long heater with metallic spring centralizers	
2	ESF-TMA-MPBX-1	MPBX – Rock Mass Displacement	0.18	0.08	0.27	0.14	6.99	0.28	0.5	7.57	7.00	0.03	9	—	—	6	—	—	—	—	—	Thermocouple sensors between and at anchors in MPBX	
3	ESF-TMA-MPBX-2	MPBX - Rock Mass Displacement	-0.62	0.23	0.21	-0.62	7.25	0.25	0.5	7.57	7.00	0.03	13	—	—	7	—	—	—	—	—	Thermocouple sensors between and at anchors in MPBX	
4	ESF-TMA-MPBX-3	MPBX – Rock Mass Displacement	0.75	0.10	0.24	0.78	7.00	1.29	0.5	7.57	7.00	0.03	9	—	—	6	—	—	—	—	—	Thermocouple sensors between and at anchors in MPBX	
5	ESF-TMA-MPBX-4	MPBX – Rock Mass Displacement	6.43	3.50	-0.11	0.40	3.50	-0.21	0.5	7.57	6.20	0.03	12	—	—	6	—	—	—	—	—	Thermocouple sensors between and at anchors in MPBX	
6	ESF-TMA-OMPBX-1	Optical MPBX	1.19	-0.05	0.28	1.21	11.99	0.13	-0.5	7.57	12.00	0.05	—	—	—	—	—	—	—	—	—	Laser reflection MPBX system	
7	ESF-TMA-OMPBX-2	Optical MPBX	6.20	6.49	-0.17	0.30	6.45	0.27	-0.5	7.57	6.20	0.03	—	—	—	—	—	—	—	—	—	Laser reflection MPBX system	
8	ESF-TMA-TC-1	Thermocouple	-0.18	0.15	0.28	-0.27	7.85	0.34	0.0	4.80	8.00	0.01	15	—	—	—	—	—	—	—	—	Thermocouple probes grouted in borehole	
9	ESF-TMA-TC-2	Thermocouple	0.63	0.06	0.21	0.62	8.15	0.26	0.0	4.80	8.00	0.01	15	—	—	—	—	—	—	—	—	Thermocouple probes grouted in borehole	
10	ESF-TMA-TC-3	Thermocouple	-0.75	0.23	1.26	-0.71	8.05	1.31	0.0	4.80	8.00	0.01	15	—	—	—	—	—	—	—	—	Thermocouple probes grouted in borehole	
11	ESF-TMA-TC-4	Thermocouple	-0.02	0.03	0.69	-0.09	5.49	-0.77	0.0	4.80	8.00	0.01	15	—	—	—	—	—	—	—	—	Thermocouple probes grouted in borehole	
12	ESF-TMA-TC-5	Thermocouple	0.00	0.16	0.65	-0.04	6.84	0.68	0.0	4.80	8.00	0.01	15	—	—	—	—	—	—	—	—	Thermocouple probes grouted in borehole	
13	ESF-TMA-TC-6	Thermocouple	6.26	5.49	-0.01	1.87	5.46	-0.04	0.0	4.80	6.20	0.01	10	—	—	—	—	—	—	—	—	Thermocouple probes grouted in borehole	
14	ESF-TMA-TC-7	Thermocouple	-6.59	3.46	-0.01	-0.34	3.43	-0.02	0.0	6.00	6.20	0.02	10	—	—	—	—	—	—	—	—	Thermocouple probes grouted in borehole	
15	ESF-TMA-NEU-1	Neutron Probe and Temp	6.10	4.29	0.33	-1.60	4.28	2.74	17.0	7.57	8.50	0.04	—	27	—	—	—	—	—	—	—	RTDs grouted between hole and Teflon tube	
16	ESF-TMA-NEU-2	Hydrology	6.10	4.30	0.04	1.14	4.32	0.71	7.5	7.57	5.50	0.02	—	4	—	—	4	—	—	—	—	Pressure, RTD, and humidity sensors in packer systems	
17	ESF-TMA-NEU-3	Neutron Probe and Temp	6.16	4.30	-0.45	-1.78	4.31	-1.47	-7.0	7.57	8.50	0.04	—	29	—	—	—	—	—	—	—	RTDs grouted between borehole and Teflon tube	
18	ESF-TMA-NEU-4	Hydrology	6.17	4.29	-0.22	1.51	4.28	-0.28	-0.5	7.57	5.00	0.02	—	4	—	—	4	—	—	—	—	Pressure, RTD, and humidity sensors in packer systems	
19	ESF-TMA-BJ-1	Borehole Jack	-6.55	5.52	-0.14	-0.34	5.51	-0.07	0.5	7.57	6.20	0.03	—	—	—	—	—	—	—	—	—	Open hole for borehole jack	
20	ESF-TMA-CHE-1	Chemistry – SEAMIST	-6.64	4.91	-0.66	-1.51	4.93	-0.77	-0.5	7.57	5.00	0.02	—	—	—	—	—	—	—	—	—	SEAMIST system with chemical sensors, 45 sensors failed	

INTENTIONALLY LEFT BLANK

Table 6.2-2. SHT Borehole Information (Continued)

Borehole Number	Borehole Identification	Primary Purpose	Collar Coordinates (m)			Bottom Coordinates (m)			Orientation Degree	Diameter (cm)	Length (m)	Volume (m <sup>3</sup> )	Thermo-Couples	RTD	Thermistors	Load Cell (Average)	Anchor in MPBX	Type/Wire Extensometer	Humidity Sensor	Pressure Transducer	Electrode Sensor (ERT)	Chemistry Absorbing Pad	Comments
			X	Y	Z	X	Y	Z															
21	ESF-TMA-CHE-2	Chemistry - SEAMIST	-6.59	5.01	-0.01	-1.06	5.10	0.63	7.5	7.57	5.50	0.02	—	—	—	—	—	—	—	50	—	SEAMIST system with chemical sensors, 45 sensors failed	
22	ESF-TMA-HYD-1	Neutron Probe and Temp	-6.60	4.43	-0.86	-1.56	4.39	-0.74	-0.5	7.57	5.00	0.02	—	20	—	—	—	—	—	—	—	RTDs grouted between borehole and Teflon tube	
23	ESF-TMA-HYD-2	Neutron Probe and Temp	-6.57	4.43	0.00	-1.31	4.42	0.65	7.5	7.57	5.50	0.02	—	19	—	—	—	—	—	—	—	RTDs grouted between borehole and Teflon tube	
24	ESF-TMA-ERT-1	Electrical Resistivity Tomography	-6.56	3.89	0.12	-0.41	3.82	6.28	45.0	7.57	8.70	0.04	—	—	—	—	—	—	—	—	—	Electrical resistivity tomography, electrode sensor on 1-m intervals	
25	ESF-TMA-ERT-2	Electrical Resistivity Tomography	-6.57	3.91	-0.13	-0.29	4.07	-6.22	-45.0	7.57	8.70	0.04	—	—	—	—	—	—	—	—	—	Electrical resistivity tomography, electrode sensor on 1-m intervals	
26	ESF-TMA-ERT-3	Electrical Resistivity Tomography	6.25	3.89	-0.36	1.15	3.85	-5.71	-45.0	7.57	8.70	0.04	—	—	—	—	—	—	—	—	—	Electrical resistivity tomography, electrode sensor on 1 m intervals	
27	ESF-TMA-ERT-4	Electrical Resistivity Tomography	6.25	3.90	0.36	0.38	3.97	6.29	45.0	7.57	8.70	0.04	—	—	—	—	—	—	—	—	—	Electrical resistivity tomography, electrode sensor on 1-m intervals	
28	ESF-TMA-RB-1	Rock Bolt w/Load Cell	0.14	0.05	-0.38	0.26	4.21	-0.38	0.0	5.72	4.00	0.01	—	—	1	—	—	—	—	—	—	Vibrating wire load cell on head of rock bolt	
29	ESF-TMA-RB-2	Rock Bolt w/Load Cell	-0.23	0.00	-0.35	-0.18	4.22	-0.42	0.0	5.72	4.00	0.01	—	—	1	—	—	—	—	—	—	Vibrating wire load cell on head of rock bolt	
30	ESF-TMA-RB-3	Rock Bolt w/Load Cell	0.59	0.10	-0.31	0.60	4.03	-0.35	0.0	5.72	4.00	0.01	—	—	1	—	—	—	—	—	—	Vibrating wire load cell on head of rock bolt	
31	ESF-TMA-RB-4	Rock Bolt w/Load Cell	-0.68	0.13	-0.29	-0.59	4.18	-0.23	0.0	5.72	4.00	0.01	—	—	1	—	—	—	—	—	—	Vibrating wire load cell on head of rock bolt	
32	ESF-TMA-RB-5	Rock Bolt w/Load Cell	0.14	-5.37	-0.39	0.06	-9.47	-0.41	0.0	5.72	4.00	0.01	—	—	1	—	—	—	—	—	—	Vibrating wire load cell on head of rock bolt	
33	ESF-TMA-RB-6	Rock Bolt w/Load Cell	-0.20	-5.45	-0.42	-0.21	-9.45	-0.42	0.0	5.72	40.00	0.01	—	—	1	—	—	—	—	—	—	Vibrating wire load cell on head of rock bolt	
34	ESF-TMA-RB-7	Rock Bolt w/Load Cell	0.59	-5.49	-0.30	0.64	-9.60	-0.36	0.0	5.72	4.00	0.01	—	—	1	—	—	—	—	—	—	Vibrating wire load cell on head of rock bolt	
35	ESF-TMA-RB-8	Rock Bolt w/Load Cell	-0.64	-5.38	-0.31	-0.73	-9.43	-0.45	0.0	5.72	4.00	0.01	—	—	1	—	—	—	—	—	—	Vibrating wire load cell on head of rock bolt	
36	ESF-TMA-TE-1	Tape Extensometer Array 3	-2.00	0.00	Multiple	—	—	—	0.0	2.54	Up to 0.5	—	—	—	—	—	—	—	—	—	—	4-pin tape extensometer array	
37	ESF-TMA-TE-2	Tape Extensometer Array 3	2.00	0.00	Multiple	—	—	—	0.0	2.54	Up to 0.5	—	—	—	—	—	—	—	—	—	—	4-pin tape extensometer array	

INTENTIONALLY LEFT BLANK

Table 6.2-2. SHT Borehole Information (continued)

Borehole Number	Borehole Identification	Primary Purpose	Collar Coordinates (m)			Bottom Coordinates (m)			Orientation Degree	Diameter (cm)	Length (m)	Volume (m <sup>3</sup> )	Thermo-Couples	RTD	Thermistors	Load Cell (Average)	Anchor in MPBX	Type/Wire Extensometer	Humidity Sensor	Pressure Transducer	Electrode Sensor (ERT)	Chemistry Absorbing Pad	Comments
			X	Y	Z	X	Y	Z															
38	ESF-TMA-TE-3	Tape Extensometer Array 3	-6.50	3.00	Multiple	-	-	-	0.0	2.54	Up to 0.5	-	-	-	-	-	1	-	-	-	-	4-pin tape extensometer array	
39	ESF-TMA-TE-4	Tape Extensometer Array 3	-6.50	5.10	Multiple	-	-	-	0.0	2.54	Up to 0.5	-	-	-	-	-	1	-	-	-	-	4-pin tape extensometer array	
40	ESF-TMA-TE-5	Tape Extensometer Array 3	6.50	3.00	Multiple	-	-	-	0.0	2.54	Up to 0.5	-	-	-	-	-	1	-	-	-	-	4-pin tape extensometer array	
41	ESF-TMA-TE-6	Tape Extensometer Array 3	6.50	5.00	Multiple	-	-	-	0.0	2.54	Up to 0.5	-	-	-	-	-	1	-	-	-	-	4-pin tape extensometer array	
	ESF-TMA-IN-THRM-1 through 15	Thermistors	-	-	-	-	-	-	-	-	-	-	-	15	-	-	-	-	-	-	-	5 thermistors in the insulation of each rib	
	ESF-TMA-STC-1 through 36	Thermocouple	-	-	-	-	-	-	-	-	-	-	36	-	-	-	-	-	-	-	-	Surface thermocouples located on each rib	
	ESF-ATC-1 through 3	Thermocouple	-	-	-	-	-	-	-	-	-	-	3	-	-	-	-	-	-	-	-	Surface thermocouples located on each rib	
	ESF-TMA-WX-1 through 6	Wire Extensometer	-	-	-	-	-	-	-	-	-	-	-	-	-	-	6	-	-	-	-	6 sets of strain measurements on rib	
TOTAL										226.30	0.84	204	103	26	8	25	12	8	8	36	100	530	

TOTAL NUMBER OF SENSORS (ALL TYPES):

Source: CRWMS M&O 1999 [DIRS 129261].

NOTE: Borehole coordinates are referenced to a 0.0.0 coordinate located at the center of the collar for the heater borehole.

INTENTIONALLY LEFT BLANK



Table 6.2-3. SHT Post-Testing Borehole Information

Borehole Number	Borehole ID (ESF-TMA)	Primary Purpose	Collar Coordinates (Cartesian) <sup>a</sup>			Orientation (azim/decline)	Hole Diameter (cm)	Hole Length (m)
			X (m)	Y (m)	Z (m)			
194	PTC-H-1	Overcore Heater	0.00	0.00	0.00	az -288/ 0.5 deg	25.40	7.00
195 - Deleted	PTC-RB-1	Overcore Rock Bolt	0.18	0.00	-0.37	az -288/ 0.0 deg	15.24	4.00
196	PTC-MPBX-1	Overcore MPBX	0.18	0.00	0.29	az -288/ 0.5 deg	15.24	7.00
197	PTC-NEU-2	Overcore Hyd.	6.50	4.30	0.00	az 18/ 7.5 deg	15.24	6.00
198	PTC-TC-6	Overcore TC	6.50	5.50	0.00	az 18/ 0.0 deg	15.24	6.50
199	PTC-1	Observation	6.50	4.70	0.53	az 18/ 0.0 deg	7.57	7.50
200	PTC-2	Observation	6.50	4.70	0.26	az 18/ -7.94 deg	7.57	8.10
201	PTC-3	Observation	6.50	4.70	-0.28	az 18/ -22.68 deg	7.57	8.10
202	PTC-4	Observation	-0.31	0.00	0.18	az -288/ 0.0 deg	7.57	8.00
203	PTC-5	Observation	0.40	0.00	0.25	az -288/ 0.0 deg	7.57	8.00
204	PTC-6	Observation	1.14	0.00	0.50	az -288/ 9.8 deg	7.57	8.00

Source: CRWMS M&O 1999 [DIRS 129261].

<sup>a</sup> +X-direction azimuth = 18 degrees (N);  
 +Y-direction azimuth = 288 degrees (W);  
 +Z-direction azimuth = vertically.

NOTE: From field survey.

## 6.2.1 SHT Thermal Measurements

Thermal measurements include the heater power and the temperatures at various locations in the test block. A detailed description of the thermal measurements discussed below can be found in Section 7.2 of *Single Heater Test Final Report* (CRWMS M&O 1999 [DIRS 129261]).

Input DTNs and associated summary DTNs for SHT power and thermal measurements are listed in Tables 4-2 and 6.2-1, respectively.

### 6.2.1.1 Heater Power

The heater assembly for the SHT consisted of two single-ended 4,000-watt heating elements centered in a 5.4-cm (2.125-in.) diameter copper tube with a copper end cap at the bottom end. The two heating elements were contained in a nominally 2.5-cm (1-in.) diameter carbon-steel inner casing. The heating elements were made of nichrome and were each 5 m long, with a 180° bend at the bottom end. The design of the SHT heater allowed for one of the heating elements to act as a secondary heating source in the event that the other failed, or if additional heat needed to be added to the rock. The heater included a control loop that allowed for automatic switching from the primary element to the secondary element if the heater power dropped below a prescribed set point. Throughout the test, the heating elements were operated one at a time.

The heater power, voltage, and current were monitored using a Magtrol power monitor. The SHT heater power was nominally 4,000 watts for a period of nine months, followed by a

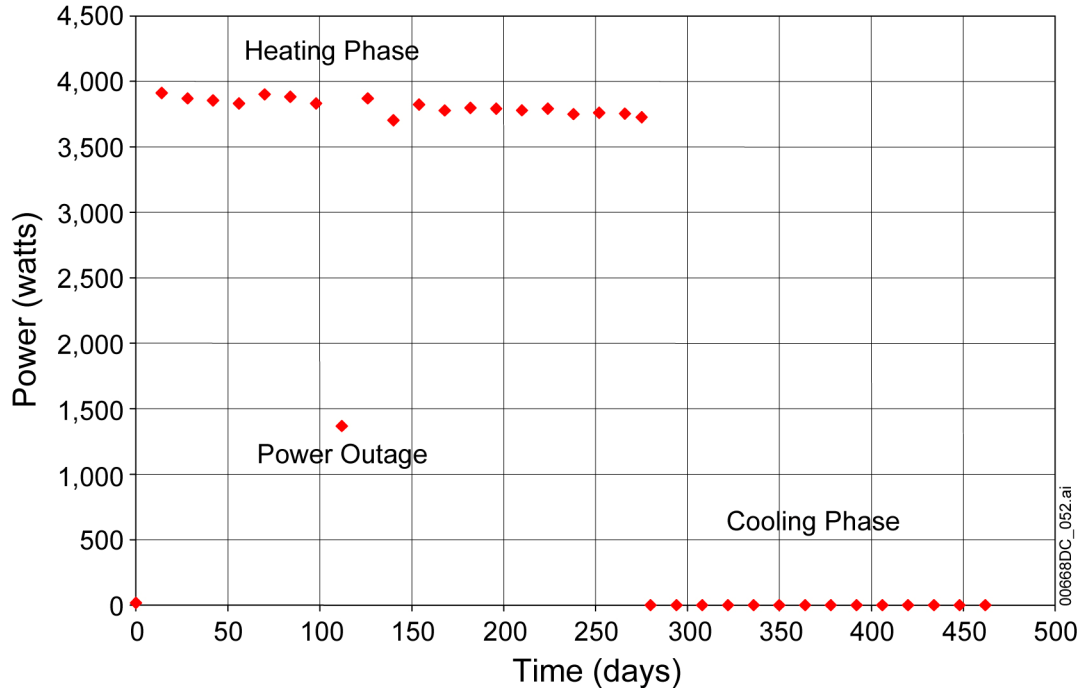
cooldown period with the heater off completely. The cooldown period lasted approximately seven months.

The SHT power data may be found in input DTN: SN0401F3511695.012 [DIRS 169262].

### 6.2.1.1.1 Results: Heater Power

The heater power history for the SHT over time periods of two weeks is illustrated in Figure 6.2-3. Power was applied to the heater starting on August 26, 1996, at 18:30:30 Universal Coordinated Time, time zero in Figure 6.2-3 showing the elapsed time from the activation of the heater. Between the time of activation and May 28, 1997, but omitting the anomalous data intervals and heater down times, the heater power output averaged approximately 3,800 watts.

The data indicate that the power output of the heater under normal operation declined by approximately 130 watts (3%) over the nine months that it was in operation. The heater was deactivated 275 days after being activated.



Source: DTN: MO0208RESTRSHT.002 [DIRS 170582].

Figure 6.2-3. SHT Power History

### 6.2.1.1.2 Measurement Uncertainty: Heater Power

The uncertainty in SHT power is similar to that discussed for the LBT in Section 6.1.1.1.2.

### 6.2.1.2 Temperatures

The thermocouple probes used in the SHT consist of Type-K thermocouples enclosed within 304 stainless steel, 0.64-cm (0.25-in.) diameter sheaths. The thermocouples within the sheaths

were insulated from each other with magnesium oxide. Thermocouple probes were installed in seven boreholes in the rock mass around the heater to monitor temperature changes away from the heater. Three additional thermocouple probes were installed on the top, side, and bottom of the heater canister to monitor heater surface temperatures.

Five of the boreholes (boreholes 8 through 12) were drilled roughly parallel to the heater axis to a depth slightly exceeding the planned heater installation depth. Within these five boreholes, probes TMA-TC-1, TMA-TC-2, TMA-TC-3, TMA-TC-4, and TMA-TC-5 were located at nominal radial distances from the heater borehole of 0.4 m, 0.7 m, and 1.5 m, roughly corresponding to the numerically predicted temperature isotherms of 200°C, 150°C, and 100°C, respectively (CRWMS M&O 1996 [DIRS 101375], pp. 3-2 and 3-5). Within each of these five boreholes, two thermocouple probes were installed. Two probes were required during test planning because the drift width was too narrow to allow installation of 8 m long thermocouple probes. Therefore, for each of these boreholes, two probes were used: one approximately 6 m long with ten Type-K thermocouple junctions spaced along its length (designated probe “A” for each borehole), and one approximately 2 m long with five Type-K thermocouple junctions spaced along its length (designated probe “B” for each borehole). The other two thermocouple probes (TMA-TC-6 and TMA-TC-7) were drilled perpendicular to the heater borehole from the Observation Drift and the Thermal-Mechanical Alcove Extension.

Temperatures were also measured on each of the free surfaces of the SHT block, using individual Type-K thermocouple junctions. Twelve individual thermocouples were installed on each face of the SHT block.

Temperatures were measured between the two layers of insulation on each of the three free surfaces of the SHT block, using individual thermistors. Five individual thermistors were installed between the layers of insulation on each face of the SHT block

The complete set of temperature data is provided in the summary DTN identified in Table 6.2-1. The temperatures measured in the rock mass are organized into a series of EXCEL workbooks, one for each borehole, with temperatures sampled every fourteen days. Each of the workbooks contains two charts, with the data on an accompanying worksheet. The first chart shows the temperature history for thermocouples or resistance temperature devices (RTDs). The second chart shows temperature profiles as a function of a spatial coordinate at various times during the SHT heating and cooling phases. The coordinates for borehole endpoints and corresponding sensors are also provided in the workbooks.

The SHT temperature data may be found in input DTNs: SN0401F3511695.012 [DIRS 169262] and SN0401F3511695.013 [DIRS 169263].

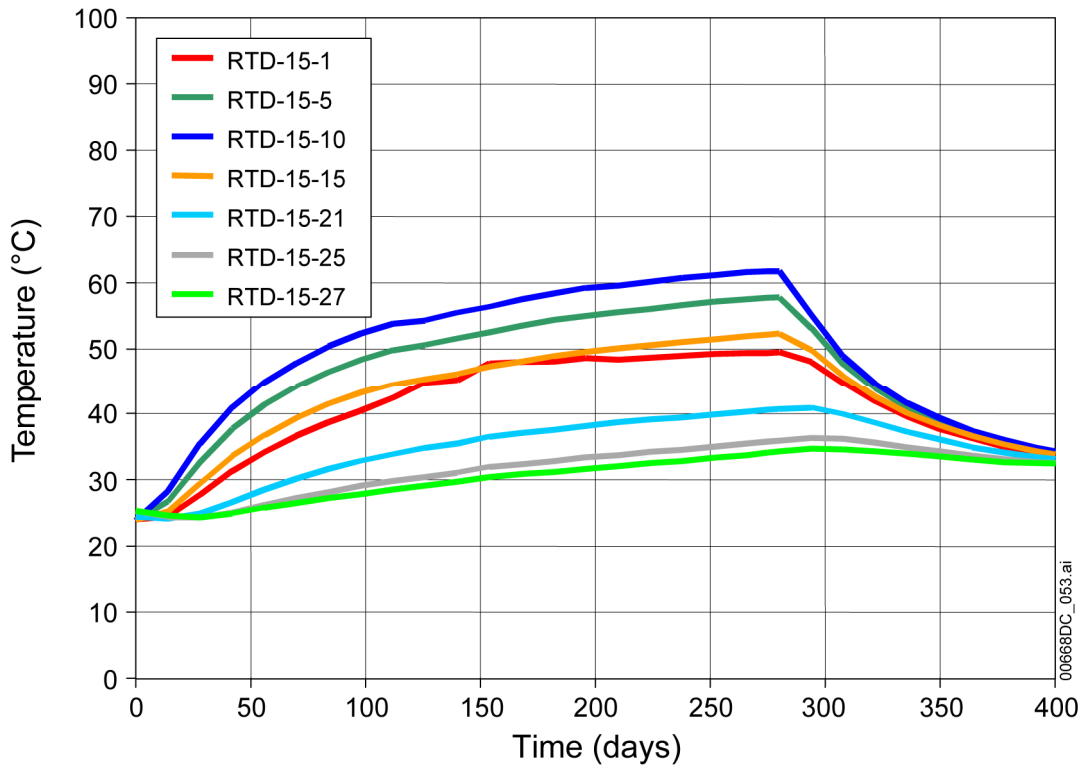
#### **6.2.1.2.1 Results: Temperatures**

Because of the abundance of SHT temperature measurements, only representative discussion and graphics are provided below. All temperature data can be accessed in the summary DTN (MO0208RESTRSHT.002) identified in Table 6.2-1. This summary DTN is also supported by input DTNs: SNF35110695001.001 [DIRS 158315] and LL970805504244.043 [DIRS 158313].

A complete discussion of the SHT temperature data is provided in *Single Heater Test Final Report* (CRWMS M&O 1999 [DIRS 129261]).

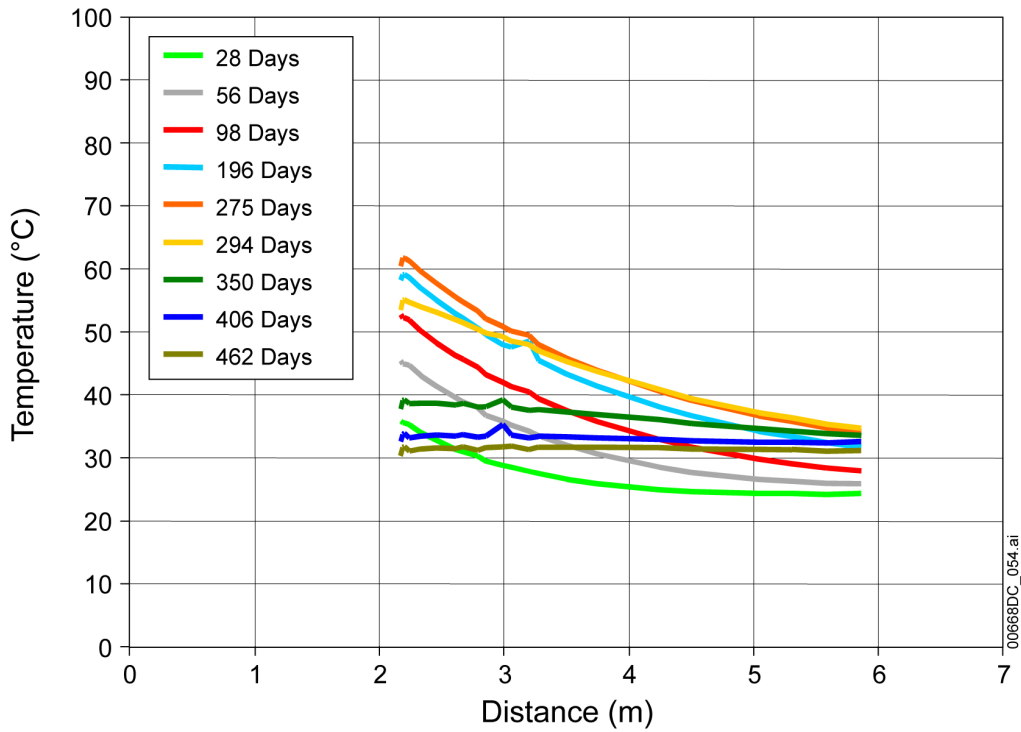
The following discussion uses borehole 15 and borehole 8 to illustrate how temperature results are displayed in the output workbooks for individual boreholes. borehole 15 is parallel to the x-direction and angles upward such that it extends above and beyond the heater as shown in Figure 6.2-2. Figures 6.2-4 and 6.2-5 present typical temperature history and temperature profile results for temperature sensors located in borehole 15. Figures 6.2-6 and 6.2-7 present the temperature history and temperature profile for borehole 8, respectively.

Interruptions to heater power slightly reduced the rock temperature. When the heater was turned off after 275 days, the temperatures of the sensors dropped rapidly. The temperatures recorded by sensors closest to the center of the heater, which recorded the warmest temperatures, dropped more rapidly than the sensors further from the center of the heater. By 523 days after heater activation (after 248 days of cooling), the temperature recorded by the sensors in borehole 8 had cooled to between 23°C and 32°C.



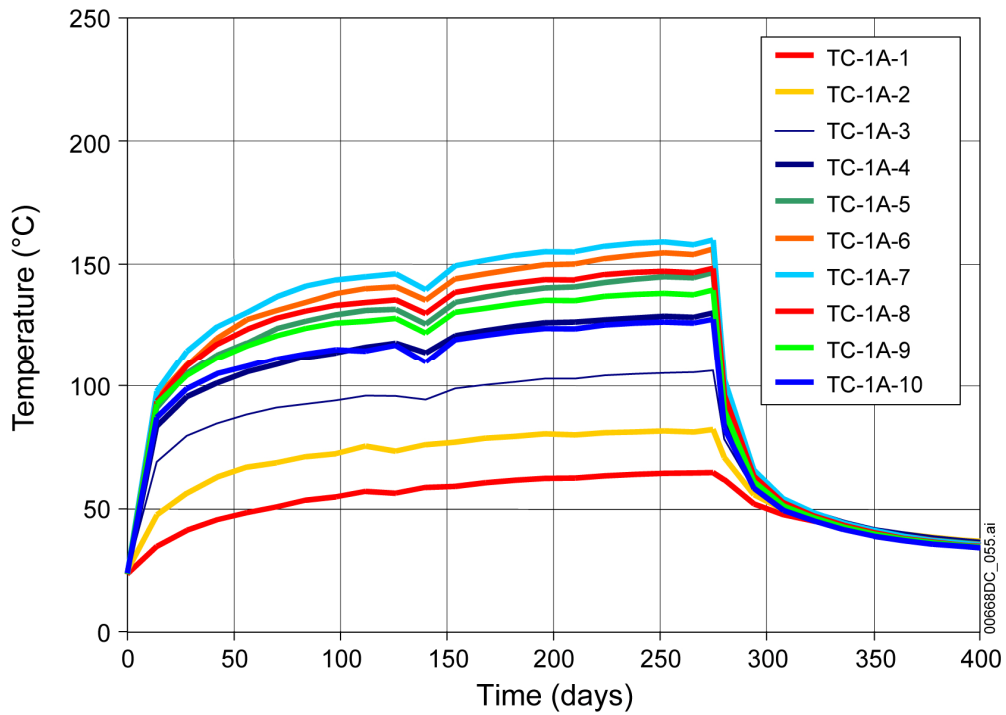
Source: DTN: MO0208RESTRSHT.002 [DIRS 170582].

Figure 6.2-4. Temperature History for SHT Borehole 15 at Select Locations



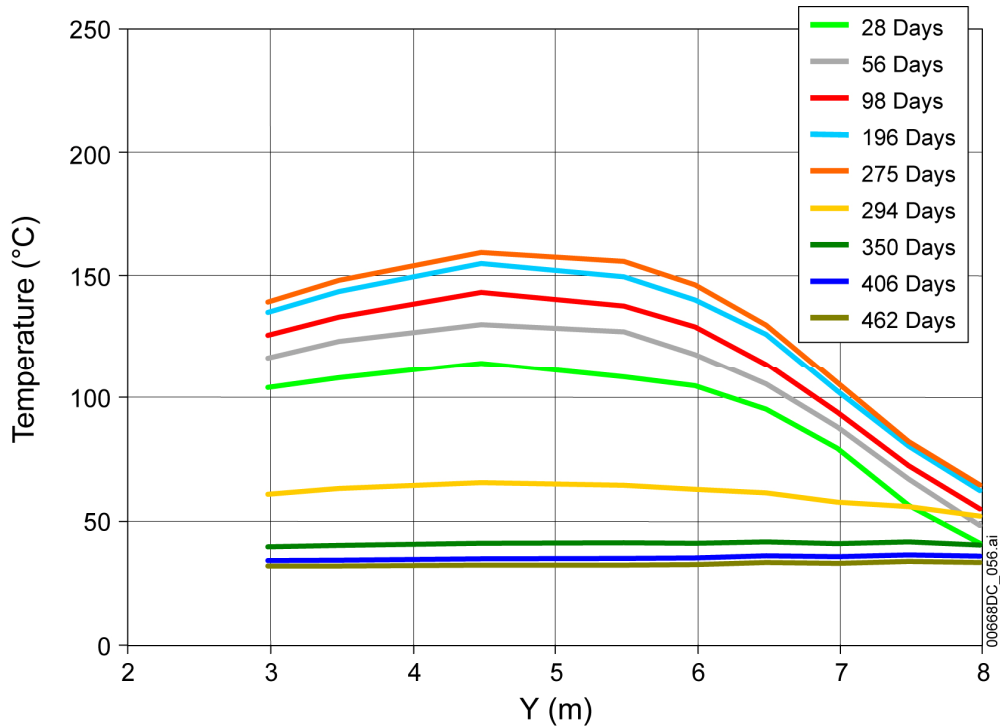
Source: DTN: MO0208RESTRSHT.002 [DIRS 170582].

Figure 6.2-5. Temperature Profile for SHT Borehole 15 at Select Times



Source: DTN: MO0208RESTRSHT.002 [DIRS 170582].

Figure 6.2-6. Temperature History for SHT Borehole 8 at Select Locations



Source: DTN: MO0208RESTRSHT.002 [DIRS 170582].

Figure 6.2-7. Temperature Profile for SHT Borehole 8 at Select Times

### 6.2.1.2.2 Measurement Uncertainty: Temperatures

The uncertainty in SHT temperature measurements involves both RTDs and thermocouples. In general in the SHT, RTDs measured temperatures in the neutron boreholes and thermocouples measured temperatures in most other boreholes.

The RTD is accurate within 0.3°C (CRWMS M&O 1997 [DIRS 101540], Section 5.1). With consideration of other factors, such as uncertainty in the location of the RTDs, the accuracy of the RTD-measured temperature in the SHT is estimated to be within 2°C. The RTD bundles were grouted in the boreholes; consequently, some of the RTDs may not have had direct contact with the borehole wall. There may also have been some time delay between the temperature variations in the rock and that measured by the RTDs. It is believed that this time delay was small because the rock mass was heated slowly. The thermocouple is accurate within 2.2°C (CRWMS M&O 1997 [DIRS 101540], Section 5.1). With consideration of other factors, such as uncertainty in the location, the overall accuracy of the measured temperatures in the SHT is estimated to be within 3.5°C.

### 6.2.1.3 Laboratory Thermal Conductivity

Four thermal conductivity tests and nine thermal expansion tests were performed (CRWMS M&O 1996 [DIRS 101428]). The specimens tested represent Topopah Spring welded tuff specimens. Cores from boreholes drilled into the SHT test block were used to prepare specimens for both mechanical and thermal properties testing in the laboratory.

The laboratory-measured thermal conductivity from the SHT may be found in input DTN: SNL22080196001.001 [DIRS 109722].

### 6.2.1.3.1 Results: Laboratory Thermal Conductivity

Thermal conductivity data are tabulated in Table 6.2-4. The mean thermal conductivity and standard deviation about the mean are given at each temperature. It appears that temperature dependence on thermal conductivity is small. The sharp increase in thermal conductivity at 70°C reflects a change in instrumentation at that temperature. A low temperature (LT) device was used for testing at 70°C and below; a thermocouple apparatus (TCA) was used for 70°C and above.

Table 6.2-4. SHT Thermal Conductivity Laboratory Data for Four Specimens from Heater Borehole 1

Apparatus <sup>a</sup>	Temperature (°C)	Thermal Conductivity (W/(m-K))				Mean	Standard Deviation
		ESF-H1-0.6-B	ESF-H1-11.3-B	ESF-H1-11.6-B	ESF-H1-19.9-B		
LT	30	1.50	1.76	1.37	1.76	1.60	0.20
LT	50	1.52	1.79	1.40	1.77	1.62	0.19
LT	70	1.54	1.81	1.44	1.77	1.64	0.18
TCA	70	1.58	1.96	1.61	1.89	1.76	0.19
TCA	110	1.56	1.88	1.57	1.80	1.70	0.16
TCA	155	1.61	1.85	1.62	1.79	1.72	0.12
TCA	200	1.60	1.82	1.59	1.78	1.70	0.12
TCA	245	1.57	1.81	1.60	1.75	1.68	0.12
TCA	289	1.48	1.76	1.56	1.69	1.62	0.13
Mean	—	1.55	1.83	1.53	1.78	1.67	N/A
Standard Deviation		0.04	0.06	0.10	0.05	N/A	0.15

Source: DTN: SNL22080196001.001[DIRS 109722].

<sup>a</sup> An LT device was used for testing at 70°C and below; a TCA was used for 70°C and above.

### 6.2.1.3.2 Measurement Uncertainty: Laboratory Thermal Conductivity

Uncertainty in the laboratory measurement of thermal conductivity includes heterogeneity in the rock sample, temperature and insulator control, moisture determination, temperature effects, changes in instrumentation, and machine calibration. Most of these uncertainties are unquantifiable. In the case of machine calibration, if the error reached 4%, then the device was recalibrated (CRWMS M&O 1996 [DIRS 101428], p. 3-6).

## 6.2.2 SHT Hydrological Measurements

To assess the thermal-hydrologic processes in the SHT, the spatial distribution and the temporal variations of the moisture content in the rock mass were monitored. Electrical resistance tomography, GPR, and neutron logging were used to monitor the moisture content. Air permeability was measured periodically to assess the changes in the fracture permeability during the test. Core samples collected from the SHT region were tested in the laboratory for some hydrological properties, such as porosity, density, and moisture retention curves. These will be presented in the following corresponding sections.

Detailed discussion of SHT hydrological measurements is provided in Sections 6.3 and 8 of *Single Heater Test Final Report* (CRWMS M&O 1999 [DIRS 129261]). SHT hydrologic input DTNs and summary DTNs are presented in Tables 4-2 and 6.2-1, respectively.

### **6.2.2.1 Electrical Resistance Tomography**

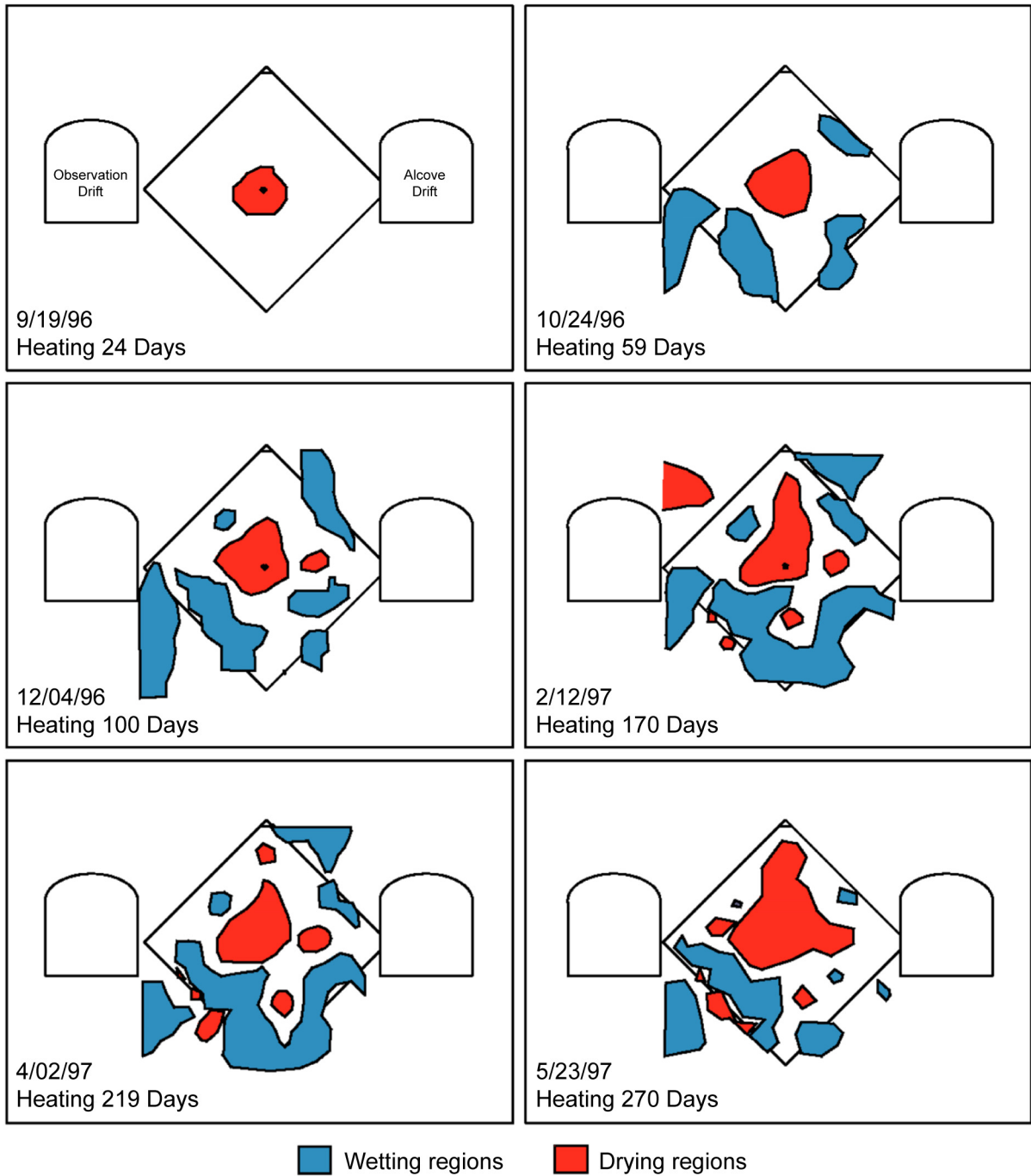
This section describes ERT surveys made during the SHT heating and cooling phases to map the changes in moisture content caused by heating. Of particular interest are the formation and movement of condensate within the fractured rock mass. Figure 6.2-2 shows the relative position of the ERT (hydrological) boreholes in the SHT. Four inclined boreholes (24-27), forming a plane perpendicular to the heater axis, were used to position electrodes around the region of interest; this plane intersects the heater near its midpoint. Twenty-eight electrodes, equally spaced within the four boreholes, were used to conduct ERT surveys around the heater. The electrode spacing was about 30 cm with the electrodes grouted in the boreholes. Section 8.5 of *Single Heater Test Final Report* (CRWMS M&O 1999 [DIRS 129261]) describes the ERT in detail. All of the SHT ERT data can be found in the TDMS under the following input DTNs: LL970101004244.026 [DIRS 158281], LL970505404244.031 [DIRS 148609], LL971002904244.044 [DIRS 158286], and LL980105204244.049 [DIRS 148610].

#### **6.2.2.1.1 Results: ERT**

The discussion of the ERT data reduction can be found in Section 6.1.2.1.1. The saturation estimates produced by data reduction model 2 are presented below. The interpretation of ERT results of the SHT is shown in Figures 6.2-8 and 6.2-9, for the heating phase and the cooling phase respectively. The drying and wetting regions in these figures are based on hand tracings made over the model 2 saturation estimates.

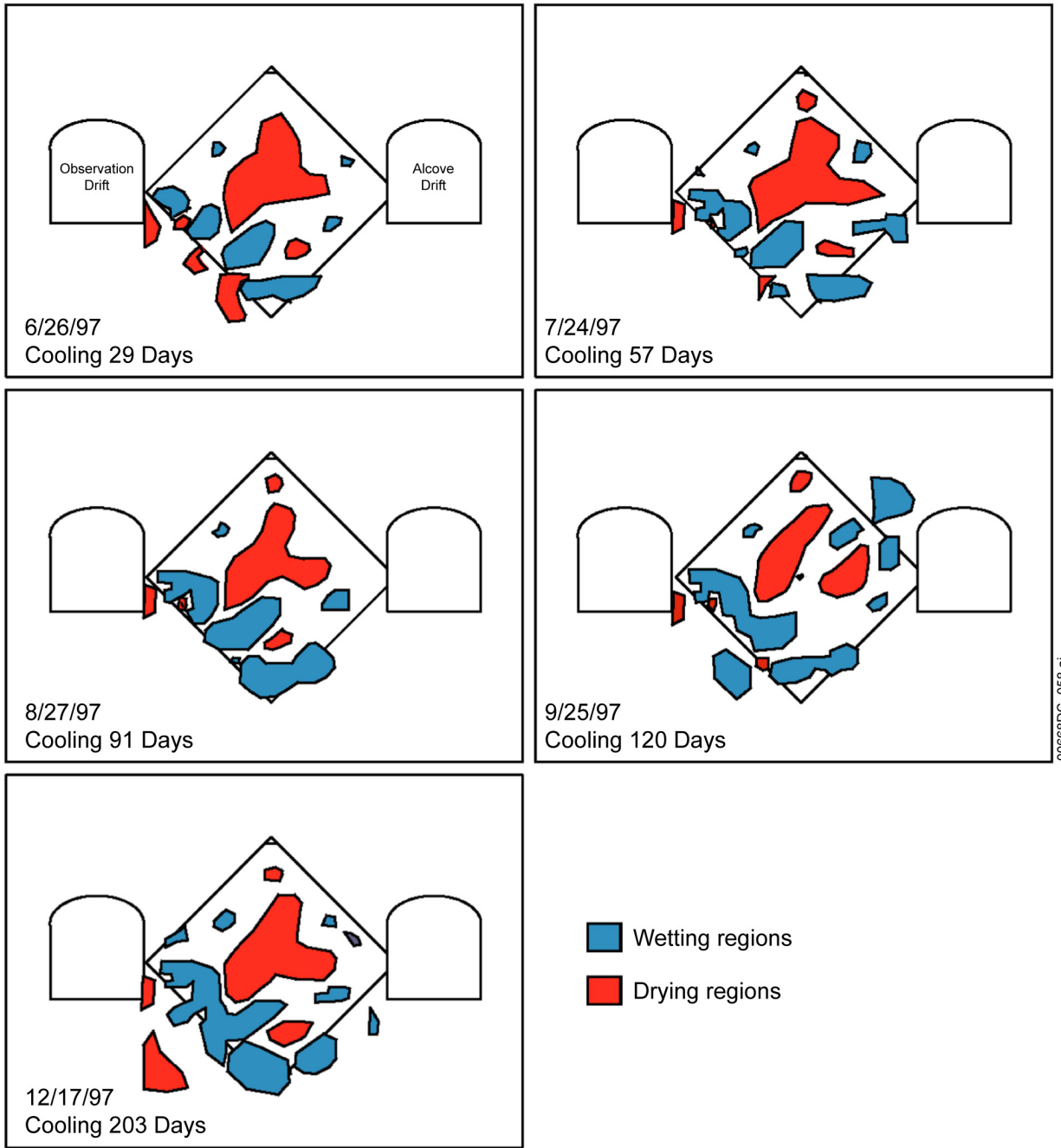
In general, the outline of the drying and wetting regions roughly coincides with saturations equal to 70% or less for the drying zone and 98% or more for the wetting zone. A significant region of drying is present around the heater. The dry zone is not centered on the heater and is not symmetric about the heater. The pattern suggests a distribution of moisture that is strongly controlled by fractures. As time increases, the drying zone appears to propagate upward, especially after 219 days of heating; also, the minimum saturation estimate was near 10%. During the cooling phase, the dry zone around the heater appears to remain relatively stable; an exception to this observation is the result from September 25, 1997, which showed a change in the dry zone near the heater's location. At the end of the cooling phase, the image (December 17, 1997) still shows a clear dry zone around the heater and significant wetting regions on the lower left flank of the heater.





Source: DTN: LL02080123142.029 [DIRS 170581].

Figure 6.2-8. Interpretation of ERT Moisture Data during the SHT Heating Phase



Source: DTN: LL02080123142.029 [DIRS 170581].

Figure 6.2-9. Interpretation of ERT Moisture Data during the SHT Cooling Phase

### 6.2.2.1.2 Measurement Uncertainty: ERT

Many factors may contribute to the uncertainty in the saturation changes in the rock mass estimated from ERT. The measurements of the voltage and current at the electrodes are fairly accurate. More importantly, the saturation estimates presented here are impacted by one or more of the following factors:

- The accuracy of the temperature maps in the vertical direction is limited by the sparse vertical coverage of the temperature sensors. Errors in the interpolated/extrapolated temperature maps will result in erroneous saturation estimates.
- The presence of metal in the SHT block such as the heater resulted in measurement interference.
- Other uncertainty factors that impact the ERT are similar to those listed in Section 6.1.2.1.3.

### 6.2.2.2 Ground Penetrating Radar

This section describes the borehole radar tomography experiment conducted in the SHT block. In the borehole radar method, high frequency electromagnetic signals are transmitted from modified GPR antennas in one borehole through subsurface material to a receiving antenna in another borehole. Moisture content in the rock strongly influences the propagation of the signal, i.e., whether it travels at a high or low velocity or whether it is highly attenuated. The high dielectric permittivity of water—in contrast to dry rock—typically results in greatly reduced signal velocities. The cross-borehole transmitted signals may be represented as multiple raypaths crossing through the zone of interest. If sufficient raypaths are recorded, a tomographic image may be obtained through computer processing. The processed tomogram, containing the transit time (which depends on the wave velocity) and the amplitude (which depends on the wave attenuation), offers a high-resolution approach to monitoring the thermally induced spatial redistribution of the moisture content within the rock mass. The effect of temperature on radar measurements and its impact on moisture content estimation are included in the processing methodology.

The borehole radar field surveys were conducted in boreholes 15, 17, 22, and 23 (see Figure 6.2-2). These same boreholes are used for neutron logging as discussed in Section 6.2.3. Boreholes 22 and 23 are collared from the Observation Drift and boreholes 15 and 17 are collared from the Thermal-Mechanical Alcove Extension. The boreholes are drilled several degrees off horizontal into the drift, cased with a Teflon liner, and grouted into place. Each pair of boreholes defines a two-dimensional plane transverse to the heater assembly at mid-length and trending towards this assembly. In the case of boreholes 15 and 17, this plane actually extends across the strike of the heater. This is not the case with boreholes 22 and 23, which stop just short of the heater.

A Pulse EKKO 100 radar system was used for the radar data acquisition in the SHT. Section 8.3 of *Single Heater Test Final Report* (CRWMS 1999 [DIRS 129261]) presents the GPR data acquisition in detail. Five separate surveys were performed using the borehole pairs. The first

data set was acquired on August 22, 1996, before the heater was turned on (time = T0). Three data sets were acquired during heating: on January 15, 1997, three months after heating began (T1); on March 12, 1997, five months after heating began (T2); and on May 29, 1997, nine months after heating and one day into cooling (T3). The fifth data set was acquired on January 7, 1998, a little over seven months after the heater was turned off (T4). The complete set of GPR data for borehole pair 15 to 17<sup>1</sup> can be found in input DTN: LB980901123142.003 [DIRS 119016].

The crosshole radar data collection was performed using two acquisition modes. The first was a zero offset profile, in which the transmitter and receiver antennas were positioned within the boreholes at equal depths such that there was no vertical offset. The second was a multiple offset profile, in which the receiving antenna remained at a fixed depth while the transmitter antenna was moved incrementally in the second borehole. Each multiple offset profile constitutes a “receiver gather.” In the SHT surveys, the transmitter and receiver intervals were located every 0.25 meters. Each of the necessary raypaths was collected and recorded for the subsequent tomographic processing.

Over the course of the heater experiment, the radar system was operated by using identical acquisition parameters for each of the five field surveys. No adjustments, filters, or gains were applied to the stored raw data. Therefore, data acquisition (and hence data repeatability) was the same regardless of who operated the system and when—so long as the antenna configuration was the same. Data repeatability is essential to successful tomographic differencing and interpretation. Small deviations in experimental methodology at such close spacing can result in large discrepancies in data processing.

Further, accurate transport times between the transmitter and receiver antennas must be obtained from the radar data to invert for the velocity structure between boreholes. Hence, it is necessary to know the precise time when the transmitter fires (known as zero time). An accurate measure of zero time throughout the surveys was obtained by direct airwave measurements (the signal from transmitter antenna to receiver antenna in air) with the antennas held together in air and at the borehole collars in air.

#### **6.2.2.2.1 Results: GPR**

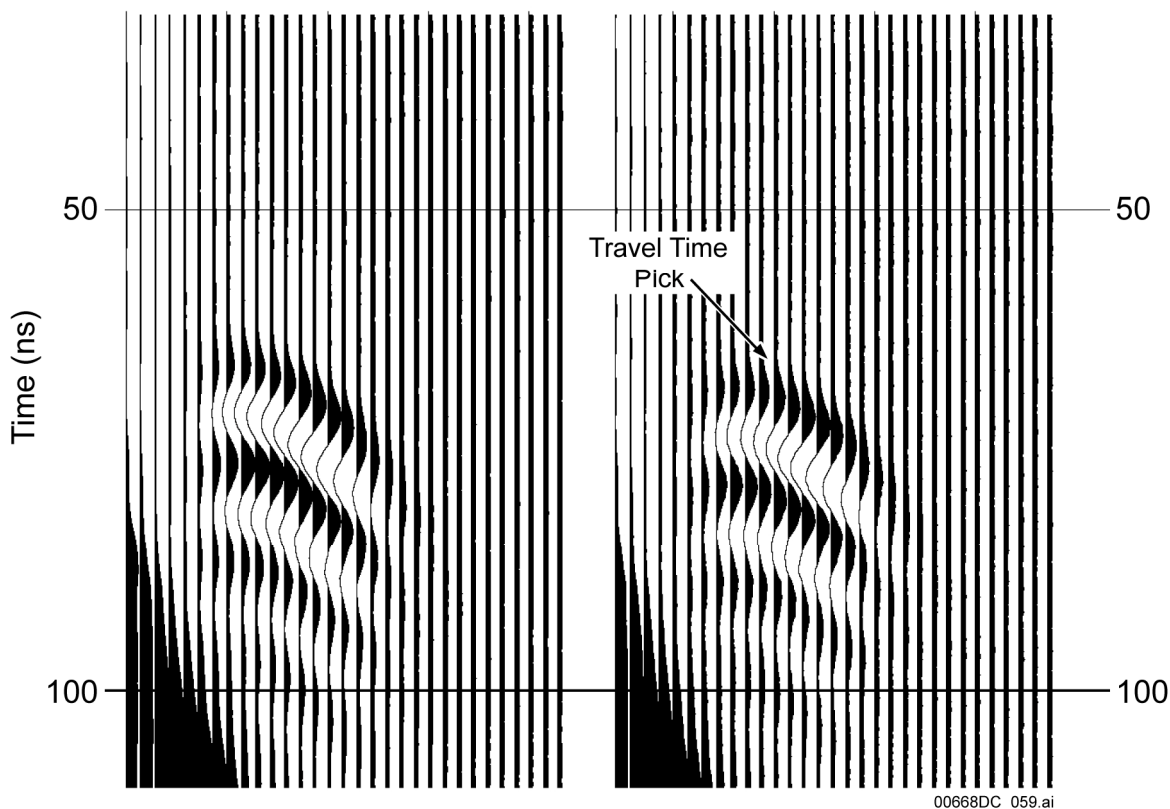
Boreholes 15 and 17 are 0.785 m apart at their collars at the alcove wall and deviate to approximately 4.0 m at their endpoints while remaining in the same plane. Accurate coordinates for each transmitter and receiver point (which are at 0.25-m intervals) were determined using the surveyed borehole coordinates. Each multiple offset profile constitutes a “receiver gather” (one receiver depth and many transmitter depths), and a series of these gathers are used to construct tomographic images.

Figure 6.2-10 shows two typical receiver gathers for the 15-17 borehole pair. The time scale along each trace is in nanoseconds. The transport times are picked at the moment of first arrival

---

<sup>1</sup> Radar data for the SHT started out as a scoping study to test out feasibility of the method. When the data from borehole pair 22 to 23 were found similar to that from borehole pair 15 to 17, data acquisition in the former pair was stopped after the first three surveys.

of energy, as marked for example in Figure 6.2-10. The data (DTN: LB980901123142.003 [DIRS 119016]) consist of the XYZ coordinates of the transmitter (borehole 15) and receiver (borehole 17) and the respective picked transport times for each survey.



Source: CRWMS M&O 1999 [DIRS 129261].

NOTE: Shown are gathers for receivers at 2.37 and 2.61 m down Borehole 15.

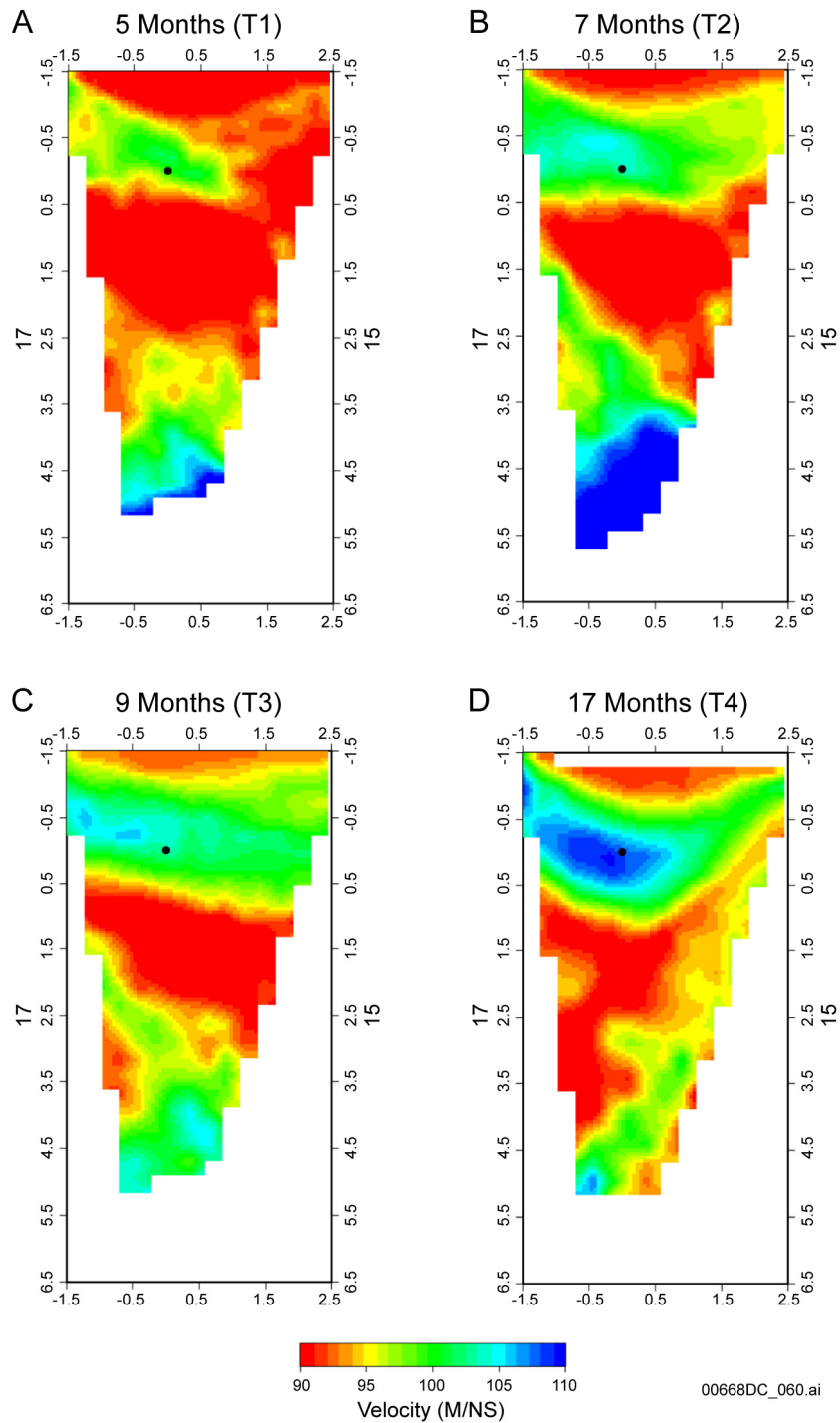
Figure 6.2-10. Two Typical SHT GPR Receiver Gathers for the 15-17 Borehole Pair on January 16, 1997

Figure 6.2-11 shows the velocity (in a 4-m × 8-m field in the plane of boreholes 15 and 17) for the surveys taken 5, 7, 9, and 17 months after the start of heating.

Changes in moisture content (rather than the absolute moisture content) are of primary interest. Therefore, it is useful to subtract the velocity values between two tomograms since velocities relate directly to liquid saturation. The baseline velocity tomogram is subtracted from the four postheating velocity tomograms, producing four velocity-difference tomograms: T1-T0, T2-T0, T3-T0, and T4-T0. The difference tomograms are shown in Figure 6.2-12. The tomograms all show significant velocity increases and decreases. In general, radar velocities increase with water content decrease.

The derived tomograms are submitted under summary DTN: LB0208GPRSHTCP [DIRS 170578], as identified in Table 6.2-1.

## Velocity Tomograms

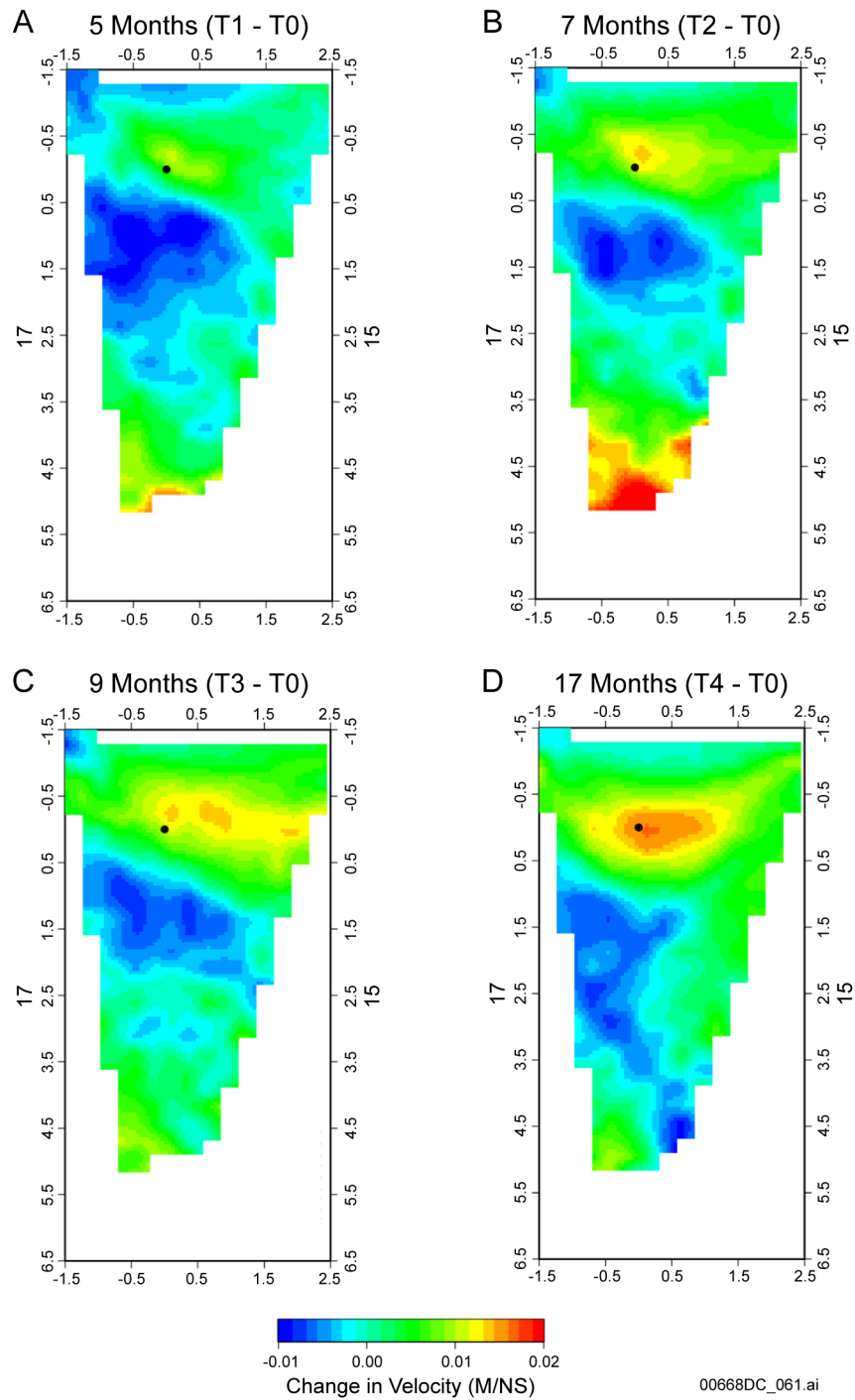


Source: DTN: LB0208GPRSHTCP.001 [DIRS 170578].

NOTE: (A) survey taken January 15, 1997; (B) survey taken March 12, 1997; (C) survey taken May 29, 1997; and (D) survey taken January 7, 1998.

Figure 6.2-11. SHT GPR Velocity Tomograms for Borehole Pair 15-17

## Velocity Tomograms



Source: DTN: LB0208GPRSHTCP.001 [DIRS 170578].

NOTE: Each tomogram is a difference from the baseline tomogram after (A) 5 months, (B) 7 months, (C) 9 months, and (D) 17 months.

Figure 6.2-12. SHT GPR Velocity Difference Tomograms for Borehole Pair 15-17

#### 6.2.2.2.2 Measurement Uncertainty: GPR

The uncertainties associated with data acquisition and processing include:

- Relocation errors of the transmitters and receivers for each survey. The antennas were relocated to within one centimeter.
- Zero time shift. The methodology employed reduced zero time errors to less than 0.5 ns.
- Transport time picking errors less than one sample, or 0.2 ns. The transport times must be picked very accurately; due to the short distance between boreholes, small errors in geometry and travel-time picks can have a significant effect on the results. The accuracy and repeatability of the picks is better than one sample (0.2 ns) over a 20 ns transport time. Despite the low signal amplitudes, a sufficient number of transport times could be picked to obtain an estimate of the two-dimensional interborehole velocity structure, based on an inversion as described by Peterson (1986 [DIRS 101698]). An error in picking is dependent primarily on the zero time adjustment and the repeatability of transmitter/receiver locations. These are both accurate.
- Inversion errors, which can be calculated to be less than 0.03 ns.

Though the results presented here in terms of difference in velocities are accurate, converting these results to water content and liquid saturation would involve assumptions regarding porosity, temperature, and locations of the radar survey.

#### 6.2.2.3 Neutron Logging

Neutron logging is used to determine moisture content in rocks and soils. Neutron logging was used to monitor moisture content in boreholes 15, 17, 22, and 23 (see Figure 6.2-2) during the SHT. The neutron probe used in this test is a Campbell Pacific Nuclear Model 503DR. A 3.81-cm (1.5-in.) diameter probe (serial number H37067677) was used for the SHT. Under ambient conditions, the sampling volume surrounding the probe has a diameter of approximately 15 cm; this volume diameter increases as moisture content decreases.

For the SHT, a Teflon tube, with an RTD bundle mounted on its outside, was inserted into the boreholes and grouted into place. The Teflon tube permitted easy insertion, placement, and removal of the tool. Neutron counts were measured in each borehole at 10-cm intervals. Calibrations to known moisture contents were conducted for the neutron tool in a liner-RTD-grout assembly identical to that used in the SHT boreholes. Water content was calculated from the neutron counts using the calibration results.

The preheating neutron loggings were conducted on August 21, 1996, prior to initiation of heating (August 26, 1996). A total of eighteen neutron loggings were conducted in each of the four neutron boreholes in the SHT. Section 8.6 of *Single Heater Test Final Report* (CRWMS 1999 [DIRS 129261]) carries detailed descriptions of the neutron logging. The SHT neutron data can be found in the TDMS under input DTN: LL980106904244.051 [DIRS 118963].

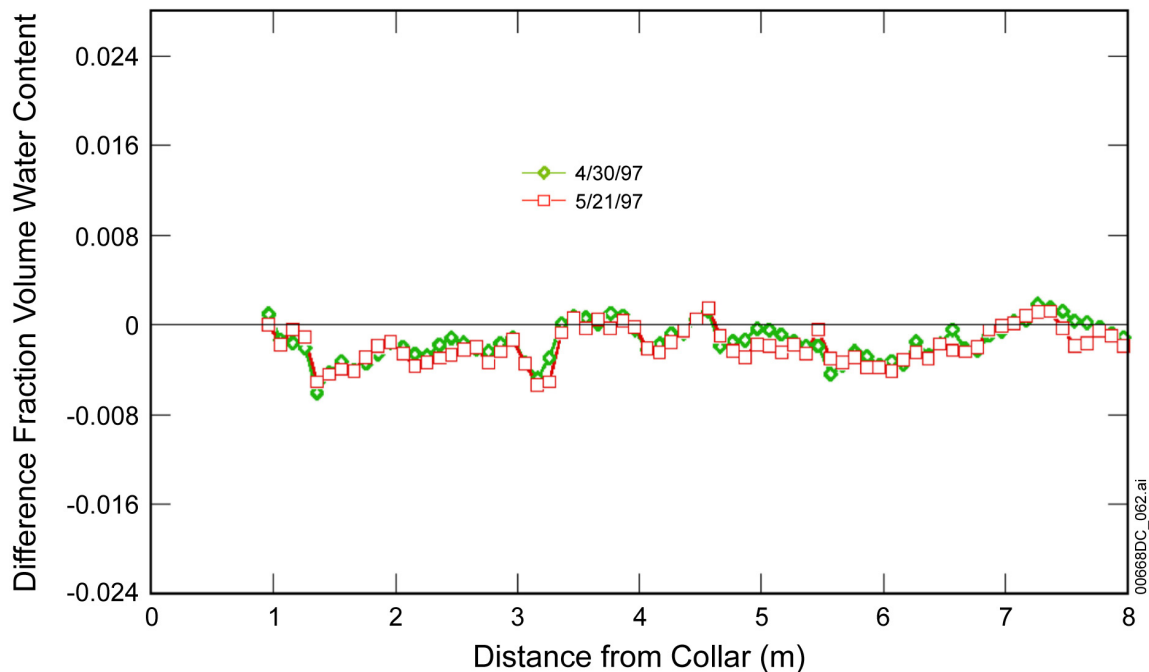


### 6.2.2.3.1 Results: Neutron Logging

The neutron results are presented as the difference in water content between the heating/cooling measurements and the preheating baselines. Positive difference fraction volume water means gaining moisture content; negative difference fraction volume water means drying. To calculate water saturation, one can simply divide the fraction volume water content by the porosity. All of the neutron results were smoothed to remove some variations, but without changing their amplitudes significantly.

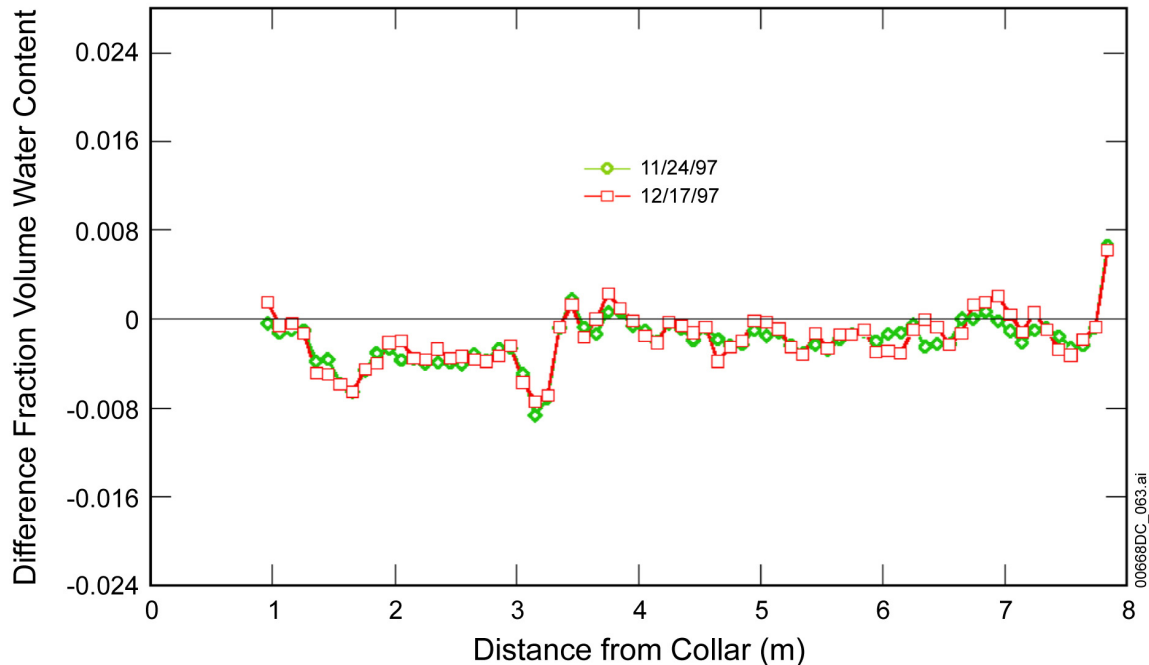
As examples of the neutron results in the SHT, Figures 6.2-13 and 6.2-14 show smoothed data for the difference fraction volume water in borehole 15 as a function of depth from the collar, at the end of the heating phase and the end of the cooling phase, respectively. The shortest distance between the borehole and the heater is about 2.07 m, at approximately 5.75 m from the collar of the borehole. The peak temperature in this borehole before the heater was de-energized was approximately 62°C. During the cooling phase, the neutron results show a slight rewetting, especially at the closest point between the heater and the borehole.

The neutron logging in the SHT region displayed changes in the moisture content in the heated rock mass. The degree of drying seemed in good correlation with the temperatures in the rock. The decreases in water content for the drying regions were small, because the neutron logging boreholes were not close to the heater. Rewetting was observed at a few localized regions during the cooling phase.



Source: DTN: LL980106904244.051 [DIRS 118963].

Figure 6.2-13. Smoothed Difference Fraction Volume Water Content Measured in SHT Borehole 15 Using Neutron Logging (April 30 and May 21, 1997)



Source: DTN: LL980106904244.051 [DIRS 118963].

Figure 6.2-14. Smoothed Difference Fraction Volume Water Content Measured in SHT Borehole 15 Using Neutron Logging (November 24 and December 17, 1997)

#### 6.2.2.3.2 Measurement Uncertainty: Neutron Logging

The uncertainty of the neutron logging itself is about 0.1% volume water content. Measurements are sensitive to the presence of elements, such as chlorine and boron, which have large neutron capture cross sections. The uncertainty caused by those minerals is difficult to assess, but probably not significant in the tuff.

Under ambient conditions, the sampling volume surrounding the probe has a diameter of approximately 15 cm; this volume diameter increases as moisture content decreases. The neutron tool was calibrated to the exact liner-RTD bundle-grout, but variations in the grout volume along a borehole (possibly caused by changes in the borehole diameter, breakout regions, etc.) will introduce uncertainty in the measured results. Changes in the water content of the grout annulus are not distinguishable from the water content of the surrounding rock during the course of the test. Therefore, if the temperature causes the grout to dehydrate, it will affect the neutron logging results, because the neutron tool is very close to the grout column.

#### 6.2.2.4 Active Pneumatic Testing and Passive Hydrological Monitoring

##### Preheating Air Injection

Characterization by means of air injection tests, prior to the onset of heating, provides an estimate of the fracture permeability in the test block. Air permeability testing in the SHT block was performed prior to the heating phase in boreholes 1 through 31 as shown in Figure 6.2-2. The preheating air injection data, which have been submitted under input

DTN: LB960500834244.001 [DIRS 105587], contain 47 files of pressure, temperature, and flow data from each air-injection test, located in TDMS data tables S97535\_001 through S97535\_047. Data include the change in pressure from initial pressure in each borehole ( $\Delta kPa$ ), as well as columns of data containing the injection flow rate (SLPM for standard liters per minute), the barometric pressure (kPa), the relative humidity (percent), and temperature ( $^{\circ}C$ ). Permeabilities estimated from injection tests performed in a short straddle packer in borehole 6 are found in TDMS data table S97535\_048. Permeabilities estimated from injection tests performed in SHT boreholes isolated by a single pneumatic packer at the collar of the borehole are found in TDMS data table S97535\_049.

### Heating/Cooling Air Injection and Passive Monitoring

During the heating and subsequent cooling phase, air injection tests were periodically performed in boreholes 16 and 18 to provide information on the changes in flow arising from coupled TH processes. In boreholes 16 and 18 are strings of four pneumatically inflated packers to isolate the borehole into different instrumented intervals, numbered from the closest to the collar of the borehole (1) to the deepest (4). Behind each packer are relative humidity, temperature, and pressure transducers. The eight instrumented intervals are referred to by borehole number followed by the instrument interval number, i.e., 18-3 is the third instrument cluster from the collar in borehole 18. Injection tests were performed in three zones: (1) zone 1 between inflated packers 1 and 3 with packer 2 deflated, (2) zone 2 between inflated packers 2 and 4 with packer 3 deflated, and (3) zone 3 between inflated packer 4 and borehole bottom with all packers inflated. Measurement data associated with the quarterly injection tests were submitted to the TDMS under the following input DTNs:

- LB970100123142.001 [DIRS 158287]
- LB980120123142.008 [DIRS 158280]
- LB970500123142.001 [DIRS 158293]
- LB0204SHAIK3Q.001 [DIRS 159543]
- LB971000123142.001 [DIRS 118965].

The heading of the data reports contains a description of the data in comma-separated format.

When air injection testing was not in progress, the packers in boreholes 16 and 18 were left inflated, and pressure, temperature, and relative humidity sensors were used for passive monitoring of the heater test. Passive monitoring data from August 1996 through December 1997 can be found in input DTN: LB980901123142.002 [DIRS 119009].

### Postcooling Air Injection Characterization and Tracer Tests

Postcooling characterization by air injection was done during the third and fourth weeks of January 1998. Of the original 31 SHT boreholes, only boreholes 1, 3, 6, 7, and 19 were available for postcooling air injection testing. The other 26 boreholes contained grouted instrumentation and were not accessible. The postcooling characterization strategy was to duplicate the preheating characterization test conditions when feasible. Therefore, inflatable packers were installed near the collar of boreholes 3, 6, 7, and 19 to depths identical to those of their preheating characterization positions. The hydrology boreholes 16 and 18 were

already equipped with packer strings for the duration of the SHT and were not modified for postcooling characterization.

As part of the postcooling characterization, gas tracer tests were conducted between borehole 1, the heater borehole, and boreholes 16 and 18. The purpose of the tracer tests was to gain a better understanding of the hydrological conditions that permitted rapid vapor transport from the heater borehole 1 vicinity into borehole 16, resulting in water accumulation in borehole 16. The gas tracer testing data, together with the postcooling air injection data, are located under input DTN: LB980901123142.001 [DIRS 118999] in the TDMS.

The results of the pneumatic tests and passive monitoring data will be briefly summarized in Section 6.2.2.4.1. For a more detailed description and discussion of the measurements and results, readers are referred to Sections 8.1 and 8.2 of *Single Heater Test Final Report* (CRWMS M&O 1999 [DIRS 129261]), and the references therein. The summary DTN is listed in Table 6.2-1.

#### **6.2.2.4.1 Results: Active Pneumatic Testing and Passive Hydrological Monitoring**

Estimated permeabilities from preheating air-injection tests have been calculated using Equation 5.1-1 and appear in Tables 6.2-5 and 6.2-6. The three orders of magnitude range in the permeability values can be attributed to flow through fractures of hierarchical scales, with the microfractures accounting for the lower values, and longer fractures (a few meters in extent) responsible for the higher values.

Changes in the permeabilities for boreholes 16 and 18 during heating and cooling are shown in Figure 6.2-15 as a ratio of transient permeabilities to preheating (baseline) value. For both 16-4 and 18-4, a decrease in permeability is shown after the initiation of heating, followed by an increase after heating has concluded. This decrease is interpreted as an increase in fracture liquid saturation, decreasing the relative gas-phase permeability. Similarly, the increase is attributed to the drainage of the water from the fractures. The increase between the baseline permeability and postcooling estimates in the back zone of boreholes 16 and 18 may result from lower fracture saturations after heating, because of the reduced saturation in the vicinity of the heater borehole, or to overall opening of fractures.

Pressure, temperature, and relative humidity in boreholes 16 and 18 were continuously monitored during heating and cooling. Figures 6.2-16, 6.2-17, and 6.2-18 show the temperature, humidity and pressure data, respectively. The pressure buildup in sensor 16-4 reflects accumulation of water in borehole 16 during the heating phase. A rise in pressure was discernable after only a few days of heating, indicating that water was rapidly mobilized from very near heater borehole 1 to 16-4. Each drop in pressure at 16-4 shown in Figure 6.2-18 data reflects the sampling of water that had accumulated in the borehole.

Table 6.2-5. Parameters for the Estimation of Preheating SHT Air Permeability, k, around Injection Zones for Various Boreholes

Borehole and Data File ID	Borehole Length (m)	Borehole Radius (cm)	Packed Zone, L (m)	Constant Flow Rate, Q(SLPM)	P <sub>2</sub> -P <sub>1</sub> (kPa)	Estimated Permeability k(m <sup>2</sup> )
Borehole 1 (5/24-03)	7.00	4.8	1.73	53.	35.0	1.5E-13
Borehole 1 (5/28-08)	7.00	4.8	1.73	50.	32.5	1.5E-13
Borehole 1 (5/30-14)	7.00	4.8	2.70	22.	9.5	1.8E-13
Borehole 2 (5/28-06)	6.91	3.79	6.00	22.	13.4	7.2E-14
Borehole 3 (5/28-02)	7.02	3.79	6.11	100.	22.3	1.8E-13
Borehole 4 (5/28-03)	6.89	3.79	5.98	22.	77.0	9.2E-15
Borehole 6 (5/30-07)	11.99	3.79	11.07	40.	20.0	5.1E-14
Borehole 7 (5/31-01)	5.91	3.79	5.00	360.	10.7	1.7E-12
Borehole 7 (5/31-07)	5.91	3.79	2.26	500.	16.0	2.9E-12
Borehole 10 (5/24-02)	8.00	2.4	7.09	3.	10.6	1.2E-14
Borehole 11 (5/28-04)	6.80	2.4	5.89	300.	3.0	5.2E-12
Borehole 12 (5/28-05)	7.67	2.4	6.76	200.	37.0	2.1E-13
Borehole 13 (5/30-08)	5.95	3.79	5.04	22.	16.5	6.6E-14
Borehole 15 (5/29-14)	8.18	3.79	7.09	20.	48.0	1.4E-14
Borehole 16 (5/30-09)	5.18	3.79	3.94	11.	64.0	8.3E-15
Borehole 17 (5/28-07)	8.00	3.79	6.91	100.	1.5	2.8E-12
Borehole 18 (5/30-10)	4.86	3.79	3.59	21.	15.5	8.8E-14
Borehole 19 (5/31-04)	5.79	3.79	4.88	20.	6.6	1.6E-13
Borehole 22 (5/29-02)	5.00	3.79	4.09	1.	6.4	9.9E-15
Borehole 23 (5/29-01)	5.50	3.79	4.59	1.	11.0	5.0E-15
Borehole 24 (5/31-03)	8.71	3.79	7.44	5.	15.7	1.2E-14
Borehole 25 (5/31-02)	8.74	3.79	7.82	100.	7.8	4.6E-13
Borehole 26 (5/31-05)	8.70	3.79	7.73	200.	6.8	1.1E-12
Borehole 27 (5/30-13)	8.70	3.79	7.43	4.5	30.0	5.1E-15

Source: DTN: LB960500834244.001 [DIRS 105587].

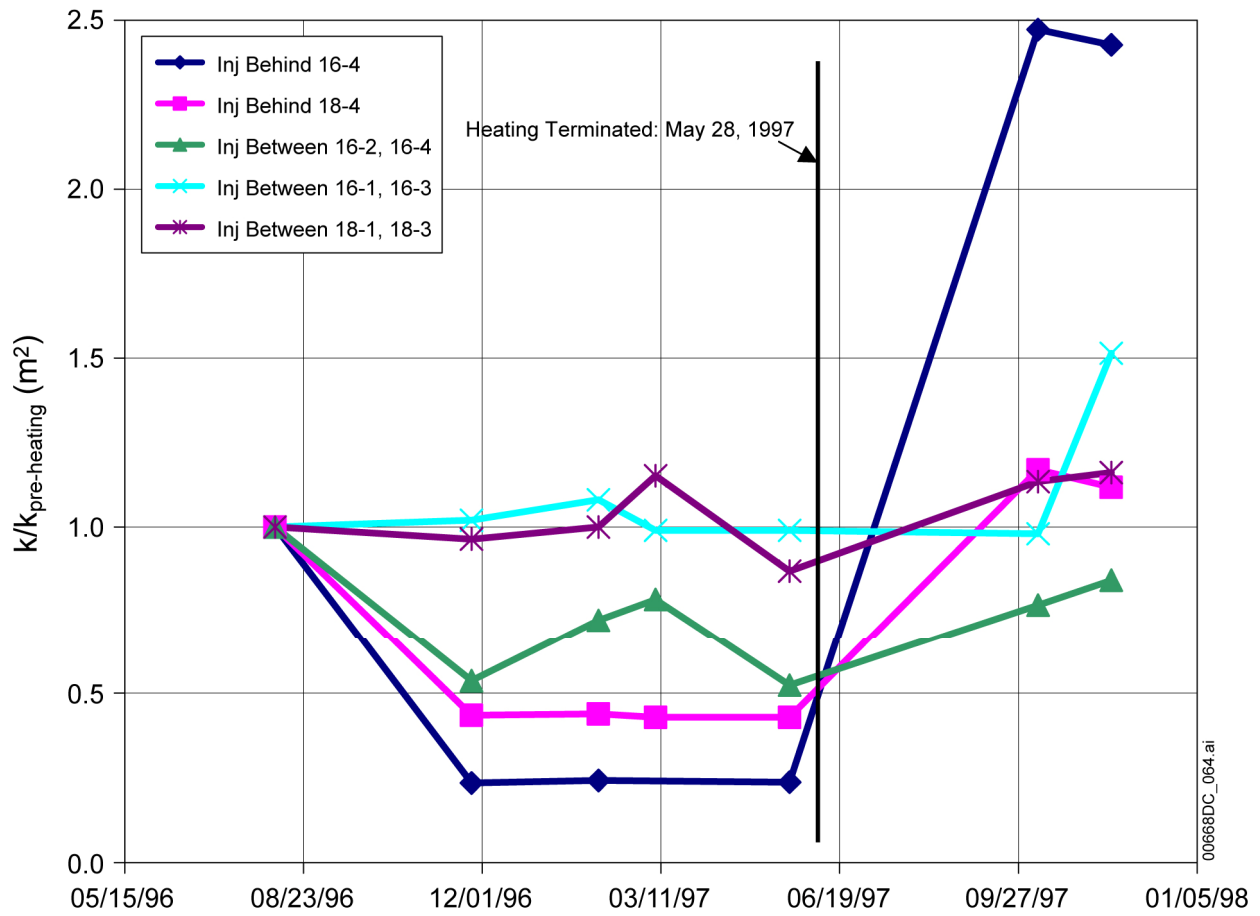
SLPM = standard liter per minute.

Table 6.2-6. Input Parameters and Estimated Preheating Air Permeability,  $k(m^2)$ , for Consecutive 0.69-m Zones from Injection Tests between Straddle Packers in SHT Borehole 6

Borehole 6 Data File and Straddle Zone ID	Mid-zone Location from Collar (m)	Constant Flow Rate, Q(SLPM)	$P_2-P_1$ (kPa)	Permeability $k(m^2)$
(5/29-03) 3'-5'	1.22	1.03	47.00	4.0E-15
(5/29-04) 5'-7'	1.83	0.39	65.00	1.0E-15
(5/29-05) 7'-9'	2.44	0.62	57.20	1.9E-15
(5/29-06) 9'-11'	3.05	0.62	58.00	1.9E-15
(5/29-07) 11'-13'	3.66	0.62	*	*
(5/29-08) 13'-15'	4.27	2.04	*	*
(5/29-09) 15'-17'	4.88	2.01	58.00	6.1E-15
(5/29-10) 17'-19'	5.49	2.01	24.50	1.7E-14
(5/29-11) 19'-21'	6.10	2.01	28.00	1.4E-14
(5/29-12) 21'-23'	6.71	4.00	17.20	5.0E-14
(5/30-06) 23'-25'	7.32	4.02	8.00	1.1E-13
(5/29-13) 25'-27'	7.92	42.00	25.00	3.4E-13
(5/30-01) 25'-27'	7.92	40.50	25.20	3.3E-13
(5/31-06) 25'-27'	7.92	41.00	27.00	3.1E-13
(5/30-02) 27'-29'	8.53	2.00	6.20	7.3E-14
(5/30-03) 29'-31'	9.14	2.03	13.00	3.4E-14
(5/30-04) 31'-33'	9.75	2.03	14.00	3.1E-14
(5/30-05) 33'-35'	10.36	2.00	0.75	6.2E-13

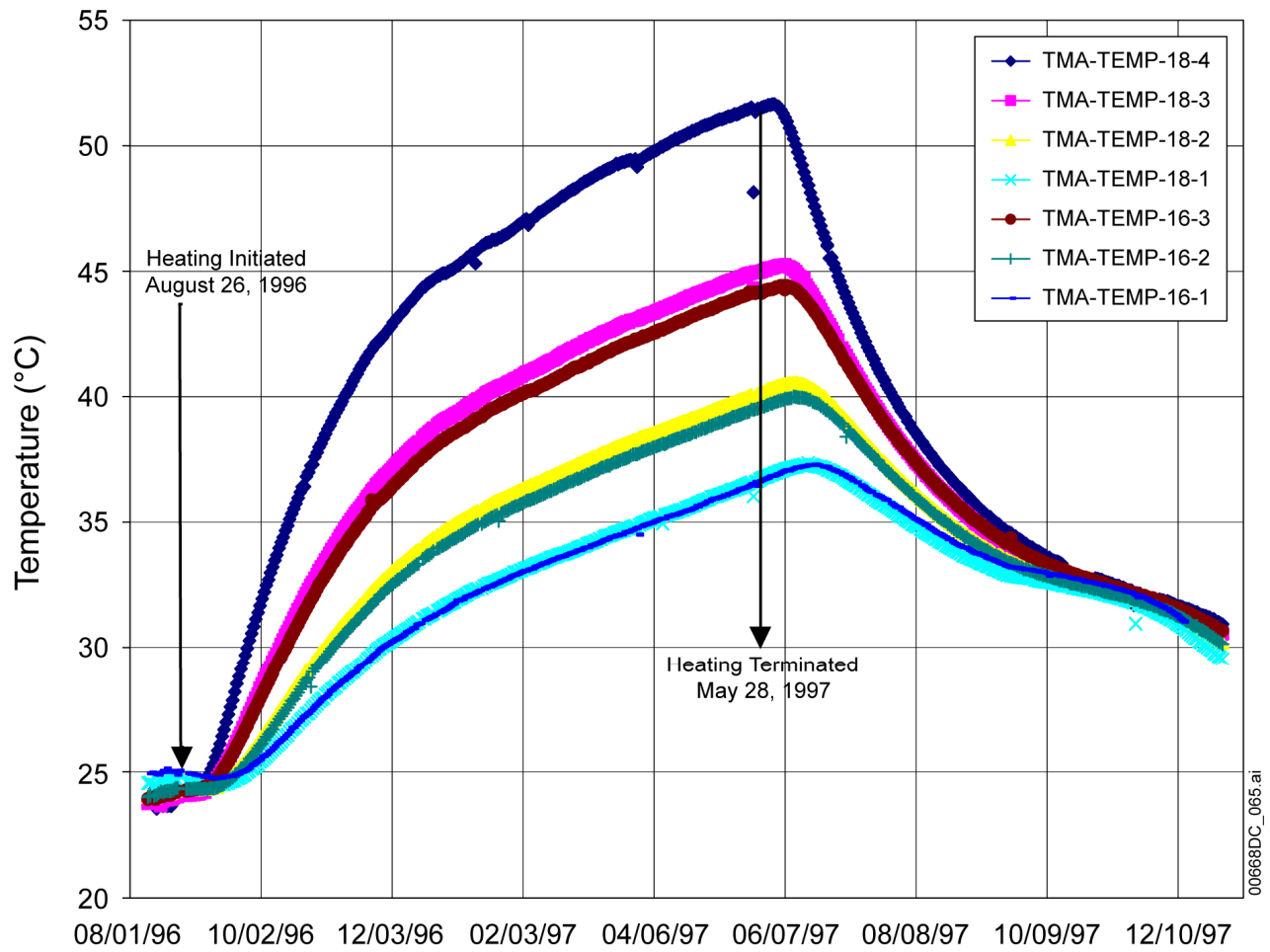
Source: DTN: LB960500834244.001 [DIRS 105587].

NOTE: Entries containing an asterisk (\*) indicate that the pressure response to the constant injection flow rate is linear with time, indicative of injection into a nearly closed system: in other words, formation of a very low permeability.



Source: DTN: LB0208AIRKSHTC.001 [DIRS 170576].

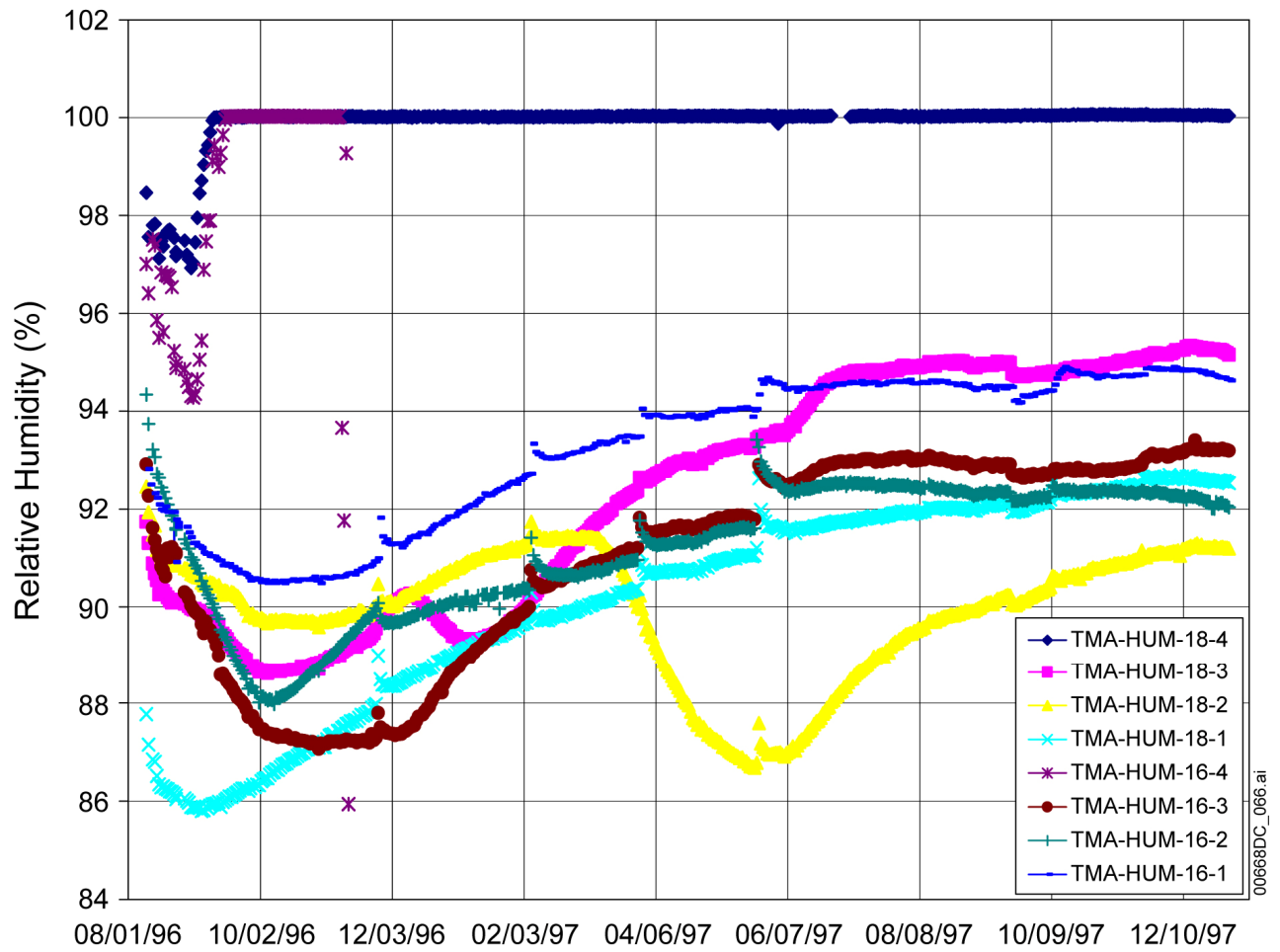
Figure 6.2-15. SHT Permeability Changes for Boreholes 16 and 18 as a Ratio of Transient Permeabilities to the Baseline Permeability Estimate



Source: DTN: LB980901123142.002 [DIRS 119009].

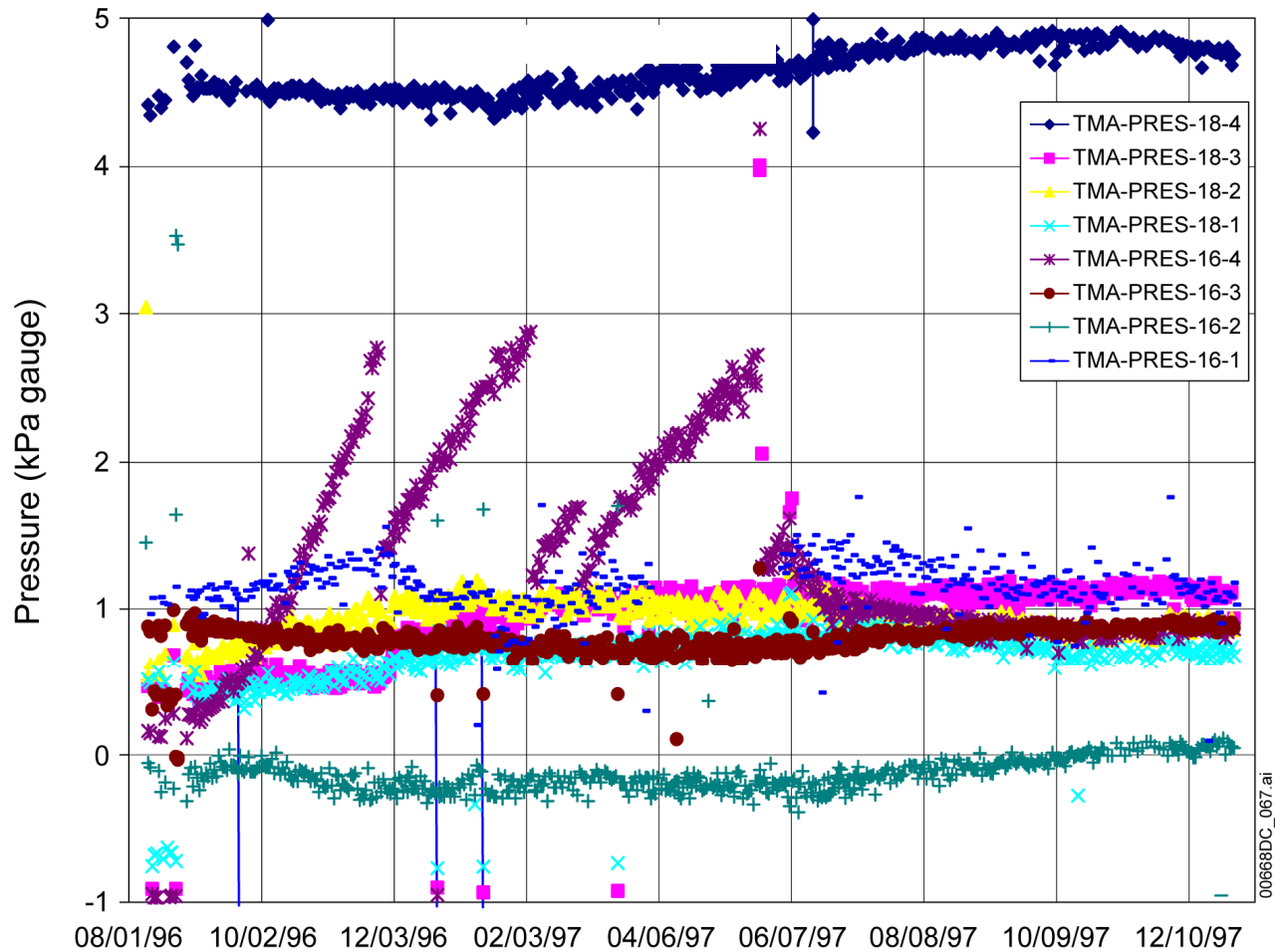
Figure 6.2-16. Passive Monitoring Temperature Data in SHT Boreholes 16 and 18





Source: DTN: LB980901123142.002 [DIRS 119009].

Figure 6.2-17. Passive Monitoring Relative Humidity Data in SHT Boreholes 16 and 18



Source: DTN: LB980901123142.002 [DIRS 119009].

Figure 6.2-18. Passive Monitoring Pressure Data in SHT Boreholes 16 and 18

Postcooling site characterization activities began in January 1998. Table 6.2-7 shows the postcooling air permeability values of various injection zones estimated using Equation 5.2-1. Table 6.2-8 shows a comparison of permeability estimates from preheating and postcooling measurements using data from injections into boreholes 3, 6, 7, 16, 18, and 19. Direct comparison is possible in these boreholes because of the identical preheating and postcooling packer configurations. The postcooling and preheating permeability values in these boreholes have the same order of magnitude. Furthermore, a study of the cross-borehole steady-state pressure response shows that they are also comparable under preheating and postcooling conditions (i.e., the data do not reveal that the pneumatic connectivity between the boreholes tested had been significantly altered by heating and cooling). The ratios of post to preheating permeability values (Table 6.2-8), however, show a consistent upward trend in the permeability values from preheating to postcooling. This increase in permeability, ranging from a factor of 1.2 to a factor of 3.5, may be attributed to opening of fractures from heating.

Table 6.2-7. Postcooling Air Permeability,  $k(m^2)$ , for SHT Boreholes 1, 3, 6, 7, 16, 18, 19

Injection Zone and Datafile ID	Packed Zone L (m)	Constant Flowrate Q(SLPM)	$P_2-P_1$ (kPa)	$k(m^2)$ Assuming $T_f=30.6^\circ C$
Borehole 1-Zone 1 (Jan21-08)	0.59	1	1.62	1.5E-13
Borehole 1-Zone 2 (Jan21-09)	0.59	10	3.48	6.8E-13
Borehole 1-Zone 3 (Jan21-10)	0.59	10	2.3	1.0E-12
Borehole 1-Zone 4 (Jan21-11)	0.59	10	2.36	1.0E-12
Borehole 1-Zone 5 (Jan21-13)	0.59	10	0.46	5.2E-12
Borehole 1-Zone 6 (Jan21-12)	1.34	10	0.972	1.4E-12
Borehole 3 (21Jan03)	6.11	40	3.22	5.7E-13
Borehole 6 (21Jan04)	11.07	40	14.8	7.2E-14
Borehole 7 (21Jan05)	5.00	100	2.17	2.5E-12
Borehole 7-back zone (22Jan01)	2.43	100	2.15	4.5E-12
Borehole 16 Zone 3 (Jan2106)	2.10	1	2.71	3.9E-14
Borehole 18 Zone 3 (Jan2107)	1.55	10	4.9	2.7E-13
Borehole 19 (21Jan02)	4.88	20	3.37	3.3E-13

Source: DTN: LB980901123142.001 [DIRS 118999].

Table 6.2-8. Comparison of Preheating and Postcooling Air Permeability Measurements for SHT Boreholes 3, 6, 7, 16, 18, 19

Preheating Air Permeability (Assume $T_f=24.6^\circ C$ )			Postcooling Air Permeability (Assume $T_f=30.6^\circ C$ )			Postcooling/ Preheating Ratio
Borehole and Datafile ID	L (m)	$k(m^2)$	Borehole and Datafile ID	L (m)	$k(m^2)$	
Borehole 3 (5/28-02)	6.11	1.8E-13	3 (21Jan-03)	6.11	5.7E-13	3.1
Borehole 6 (5/30-07)	11.07	5.1E-14	6 (21Jan-04)	11.07	7.2E-14	1.4
Borehole 7 (5/31-01)	5.00	1.7E-12	7 (21Jan-05)	5.00	2.5E-12	1.5
Borehole 7 (5/31-07)	2.26	2.9E-12	7 (22Jan-01)	2.43	4.5E-12	1.6
16 Zone 3 (Aug 7,8, 1996)	2.10	1.1E-14	16-Zone 3 (Jan21-06)	2.10	3.9E-14	3.5
18 Zone 3 (Aug 7,8, 1996)	1.55	2.3E-13	18-Zone 3 (Jan21-07)	1.55	2.7E-13	1.2
Borehole 19 (5/31-04)	4.88	1.6E-13	19 (21Jan-02)	4.88	3.3E-13	2.0

Source: DTNs: LB960500834244.001 [DIRS 105587]; LB980901123142.001 [DIRS 118999].

Postcooling air injection tests were also utilized to test the hypothesis that a fast path for vapor transport exists between heater borehole 1 and borehole 16, and that it was responsible for the accumulation of condensed water in borehole 16, zone 3. With this in mind, air permeability tests were carried out in a multizone configuration for boreholes 1, 16, and 18. Specifically, injection testing was conducted in six consecutive zones in the heater borehole 1, and the cross-borehole pressure response in the zones behind the fourth packer (referred to as zone 3 earlier) in boreholes 16 and 18 was measured to identify plausible fast-path connections. Upon conclusion of air permeability tests, gas tracer tests were also performed between the heater borehole 1 and boreholes 16 and 18 to investigate the possible presence of fast paths for vapor transport.

For the gas tracer tests, zone 3, behind the 4th packer in boreholes 16 and 18, was chosen as the tracer withdrawal interval, and borehole 1 was chosen as the tracer injection borehole. Based on the results of the postcooling air permeability tests, two intervals in borehole 1 that gave the largest cross-borehole pressure response were selected for gas tracer injections. The first interval, extending from 3.83 m to 4.42 m from the collar of the borehole, produced a strong pressure response in zone 3 of borehole 16 and a much weaker response in zone 3 of borehole 18. The second interval, between 5.05 m and 5.64 m as measured from the collar of the borehole, produced a stronger response in zone 3 of borehole 18 than in zone 3 of borehole 16.

The perpendicular layout between borehole 1 and boreholes 16 and 18, which significantly complicates transport geometry, made the test results less amenable to detailed transport analysis. The purpose of the tracer testing was to gain an understanding of the rapid gas flux that gave rise to the observed presence of water (condensate) in the back of borehole 16, as opposed to borehole 18, from which no condensate had been sampled. Thus, it was decided to focus on the first arrival of tracer and qualitatively examine the rate at which cumulative mass recovery occurred.

The results of five gas tracer tests are shown in Table 6.2-9. Tracer transport from zone 3 of borehole 1 to zone 3 of borehole 16 was extremely rapid, with 100% tracer recovery occurring within 30 minutes from injection. First arrival of tracer to zone 3 of borehole 18 took more than twice as long and 100% tracer recovery took approximately 15 hours. The differences in the transport times and recovery efficiencies suggests that the path between zone 3 of borehole 18 and borehole 1 is much more tortuous and indirect than the path between zone 3 of borehole 16 and borehole 1. This, together with the results of air permeability tests, supports the hypothesis of a direct fracture connection between borehole 1 and zone 3 of borehole 16 that allows for rapid vapor transport. This direct fracture connection was subsequently confirmed by visual inspection of the overcores of borehole 16.

Table 6.2-9. SHT Gas Tracer Test Results

Tracer Injection (Borehole 1, Location w.r.t. Collar)	Withdrawal Location Borehole Number - Zone	First Arrival Time	Mass Recovery (Qualitative Analysis)
3.93 m – 4.42 m	16-Zone 3	3 minutes	100% within 30 minutes
3.93 m – 4.42 m	16-Zone 3	3 minutes	100% within 30 minutes
3.93 m – 4.42 m	18-Zone 3	7 minutes	100% within 15 hours
5.05 m – 5.64 m	16-Zone 3	12 minutes	50% within 1 hour
5.05 m – 5.64 m	18-Zone 3	8 minutes	No analysis made

Source: DTN: LB980901123142.001 [DIRS 118999].

#### 6.2.2.4.2 Measurement Uncertainty: Active Pneumatic Testing and Passive Hydrological Monitoring

Assumptions about the validity and accuracy of the acquired data of humidity, temperature, gas flow-rate, and pressure vary, depending on the sensor and the method by which the sensor is used to perform the measurement. Accuracy as used here is defined as combined nonlinearity, hysteresis, and nonrepeatability. The data acquisition equipment used to record the sensor signal can introduce an inaccuracy into the measurement of the sensor output. However, here the

accuracy and repeatability of the acquisition system (Keithley Model 2001 Digital Multimeters were used) far exceeds the limitations of the sensors being employed. The accuracy of the Keithley 2001 Digital Multimeter is approximately 25 ppm (where 10,000 ppm = 1%) of the full-scale output (FSO) for voltage measurements and 56 ppm of the FSO for resistance measurements. Limitations of the data acquisition systems can therefore be neglected in further discussion.

In the preheating and postheating air-injection testing, pressure measurements were performed using Setra Model 204C pressure sensors. These sensors have an accuracy of 0.2% FSO. Boreholes 16 and 18 used Endevco Model 8520A-50 sensors, which also have an accuracy of 0.2% FSO. However, heating/cooling measurements of pressure by the eight Endevco sensors installed in the heated region indicated a significant thermal shift, ranging from 1 to 1.5% over the temperature range of 10°C to 150°C. Vaisala Model HMP235-A humidity sensors were used to monitor temperature and relative humidity within boreholes 16 and 18. The humidity measurement has a tolerance of  $\pm 1.0\%$  relative humidity below 90% relative humidity and an accuracy of  $\pm 2.0\%$  relative humidity above 90% relative humidity. The temperature measurement performed with the HMP235-A has an accuracy of  $\pm 0.2^\circ\text{C}$ . Sierra Instruments Model 840 mass flow controllers were used to monitor gas injection flow rates. Sierra Instruments specifies an accuracy of  $\pm 1.0\%$  FSO. However, in thermal testing field conditions, the accuracy is derated to  $\pm 10.0\%$  FSO. This derating of performance reflects the sensitivity of the mass flow controller to the shock, vibration, and dust that it is subjected to during underground testing.

Short-circuiting of gas flow caused by the high density of boreholes within the test block may increase the estimated permeability. The degree to which borehole short-circuiting of fractures influences the estimated permeability is difficult to estimate. However, the range of values obtained here does not significantly differ from values obtained in the Drift Scale Test (Section 6.3.2.4) or from surface-based boreholes.

#### **6.2.2.5 Laboratory Parameters—Saturation, Porosity, Density, Moisture Retention Curves**

##### *Preheating*

As part of the preheating characterization, laboratory measurements of saturation, porosity, bulk density, particle density, and gravimetric water content for cores from the SHT area were conducted. These studies determine the amount of pore water available for evaporation and boiling during the heating phase. Hydrological laboratory measurements were carried out for grab samples from wet excavation of the Observation Drift, and for cores, wrapped in sealed packets after coring from three wet-drilled boreholes (boreholes 1, 6, 5) in the SHT block. The grab samples, nominally 12"  $\times$  12"  $\times$  6" in size, were broken open with a jackhammer to retrieve samples (200 to 700 g in mass) from the interior regions away from drying surfaces. The results of these measurements have been submitted to the TDMS under DTN: LB970500123142.003 [DIRS 131500]. Detailed discussion of these measurements can be found in *Single Heater Test Final Report* (CRWMS M&O 1999 [DIRS 129261]).

In addition to the above parameters, moisture retention curves were also determined, at temperatures of 25.1°C, 49.6°C, and 93.7°C for 11 SHT core samples from boreholes 20 (CHE-1) and 21 (CHE-2). Prior to the retention-curve determination, the dry bulk density, saturated bulk density, and porosity of these samples were determined at room temperature. The results of these measurements are extracted from a report by Lin et al. (2002 [DIRS 159099]). Data for 25.1°C before heating can be found in the TDMS under input DTN: LL020506123142.021 [DIRS 169256].

### Postcooling

A number of boreholes were dry-drilled following the termination of the cooling phase of the SHT for postcooling characterization. In particular, protected (wrapped and sealed) cores from three dry-drilled boreholes (boreholes 199, 200, and 201) were tested for porosity, density, and water content or liquid saturation. The locations of these protected cores (Table 6.2-3) were designed to pass through both the anticipated “dryout” and “condensing” regions developing in the SHT block as a result of the heating. While the quantities measured and the methodology of these postcooling laboratory measurements remain the same as their preheating counterparts, the focus in the postcooling effort is substantially different. In the preheating results, the intent is to estimate an average initial liquid saturation of the matrix cores; in the postcooling results, the focus is on the change from their initial value as a result of TH coupled processes, and more importantly, the spatial location of the cores (with respect to the heater) where changes have occurred. The data have been submitted to the TDMS under input DTN: LB980901123142.006 [DIRS 119029].

#### **6.2.2.5.1 Results: Laboratory Parameters—Saturation, Porosity, Density, Moisture Retention Curves**

### Preheating

The measurements of wet-drilled cores from boreholes 1, 6, and 5 of the SHT are shown in Table 6.2-10. These laboratory measurements were conducted following the technical implementation procedure YMP-LBNL-TIP-AFT 2.0. Samples were placed in containers with tight-fitting lids and immediately weighed. The samples were subsequently oven-dried at a temperature between 100°C and 110°C, until they reached a constant weight (from several weighings). They were then placed in a desiccator, cooled, and weighed to determine the gravimetric water content. The samples were then water-saturated in a vacuum chamber, after which they were weighed following the method of Archimedes (i.e., immersed in air and water) to determine the weight under conditions of full saturation and the sample bulk volume. Knowledge of the dry weight, saturated weight, and sample bulk volume was used to calculate bulk density, porosity, and particle density.

Table 6.2-10 shows that saturation is approximately 95%. The variability of rock properties is evident. In the core processing procedure, any observation of factors potentially affecting the results is recorded. The abbreviated description for each core with abnormal features is included in the table footnotes. This “soft” information forms the basis for distinguishing cores that yield reliable weight measurement from cores that give potentially abnormal and inaccurate measurements. Large fractures with porous infill material generally introduce greater inaccuracy

into the weight measurement. In the resaturation step needed to determine total pore volume with cores stored in water, debris is sometimes observed. Cyclic resaturation steps are used to quantify and to compensate for solid losses.

Table 6.2-10. SHT Preheating Laboratory Hydrological Measurement of Wet-Drilled Cores

<b>Borehole 1, ESF-TMA-H1</b>					
<b>Sample Location (m)</b>	<b>Saturation (%)</b>	<b>Porosity (%)</b>	<b>Bulk Density (g/cc)</b>	<b>Particle Density (g/cc)</b>	<b>Gravimetric Water Content (g/g)</b>
1.0	89.46	10.66	2.25	2.51	0.043
2.5 <sup>a</sup>	88.04	13.30	2.18	2.52	0.054
3.7	93.60	8.87	2.29	2.52	0.036
4.7	97.27	11.83	2.22	2.51	0.051
5.7	93.97	13.83	2.16	2.51	0.061
6.7	96.03	11.89	2.21	2.51	0.052
<b>Borehole 6, ESF-TMA-OMPBX-1</b>					
0.2	94.82	11.00	2.24	2.51	0.047
2.4	94.75	10.43	2.25	2.51	0.044
4.4	93.58	10.18	2.26	2.51	0.042
7.5 <sup>b</sup>	96.87	23.62	1.96	2.57	0.104
Subcore	—	20.44	2.02	2.53	—
9.3	96.17	11.55	2.22	2.52	0.050
11.3	93.07	9.74	2.27	2.51	0.040
<b>Borehole 5, ESF-TMA-MPBX-4</b>					
0.7 <sup>c</sup>	95.85	17.03	2.05	2.48	0.079
2.1 <sup>c</sup>	101.61	9.69	2.25	2.49	0.044
2.6 <sup>d</sup>	102.17	13.33	2.17	2.50	0.063
3.8 <sup>d</sup>	96.74	10.58	2.24	2.50	0.046
Subcore	—	10.44	2.24	2.50	—
5.4	97.65	9.60	2.27	2.51	0.040
<b>Borehole Summary</b>					
<b>SHT Average:</b>	95.39	12.53	2.20	2.51	0.053
<b>Standard Deviation</b>	3.56	3.89	0.09	0.02	0.017

Source: DTN: LB970500123142.003 [DIRS 131500].

<sup>a</sup> Contains small voids.

<sup>b</sup> Split along axis during oven drying.

<sup>c</sup> Contains open fractures and large vugs.

<sup>d</sup> Received in fragments.

The data from two grab samples from the wet excavation of the Observation Drift near the SHT block are shown in Table 6.2-11. Five subsamples were tested.

One of the subsamples had an 81% saturation, while the saturation of the other four subsamples was 94% or higher. These measurements provide the only site-specific data for liquid saturation at the onset of the SHT. Consequently, those values resulted in using 92% initial saturation in modeling of the SHT.

Table 6.2-11. Preheating Laboratory Hydrological Measurement of Grab Samples from Wet Excavation of the Observation Drift of the ESF Thermal Test Facility

Observation Drift Grab Samples					
Sample Location (m)	Saturation (%)	Porosity (%)	Bulk Density (g/cc)	Particle Density (g/cc)	Gravimetric Water Content (g/g)
30.0	99.00	8.60	2.26	2.47	0.038
Subsample	94.90	8.30	2.27	2.47	0.035
40.0	95.40	9.30	2.27	2.50	0.039
Subsample	93.80	10.10	2.24	2.49	0.042
Subsample	80.50	10.40	2.24	2.50	0.037
Observation Drift Grab Sample Summary					
<b>Average</b>	92.72	9.34	2.26	2.49	0.038
<b>Standard Deviation</b>	7.10	0.91	0.02	0.02	0.003

Source: DTN: LB970500123142.003 [DIRS 131500].

Bulk density and porosity of the 11 core samples intended for moisture retention curves are shown in Table 6.2-12. These specimens have no obvious large cavities or inhomogeneous inclusions. The specimens were dried in a vacuum oven at a temperature of about 35°C until their weights became constant for several days. Dry bulk density was calculated by dividing the dry weight with the specimen volume. The specimens were then saturated with water under vacuum condition and remained in water until their weights were constant for several days. Saturated bulk density was calculated from the saturated weights. Porosity was calculated by subtracting the dry density from the saturated density, and dividing by the density of water. The average porosity for these samples is  $11.1 \pm 1.1\%$ .

Table 6.2-12. SHT Bulk Densities and Porosity of Cores from Boreholes CHE-1 and CHE-2

Sample ID	Boreholes CHE-1 and CHE-2	Depth (m)	Wet Bulk Density (g/cm <sup>3</sup> )	Dry Bulk Density (g/cm <sup>3</sup> )	Effective Porosity
0047525.2	CHE-1	0.7	2.348	2.247	0.102
0047525.2A	CHE-1	0.7	2.350	2.249	0.102
0047526.2	CHE-1	1.4	2.349	2.240	0.109
0047527.2	CHE-1	2.5	2.345	2.246	0.0998
0047528.2	CHE-1	3.8	2.331	2.224	0.107
0047529.2	CHE-1	4.3	2.344	2.235	0.109
0047530.2A	CHE-2	4.5	2.294	2.167	0.127
0047531.2	CHE-2	1.5	2.332	2.222	0.111
0047533.2	CHE-2	3.9	2.290	2.156	0.135
0047534.2	CHE-2	4.6	2.331	2.229	0.103
0047535.2	CHE-2	5.4	2.314	2.195	0.119
Mean <sup>a</sup>	—	3.0	2.33 ± 0.02	2.22 ± 0.03	0.111 ± 0.011

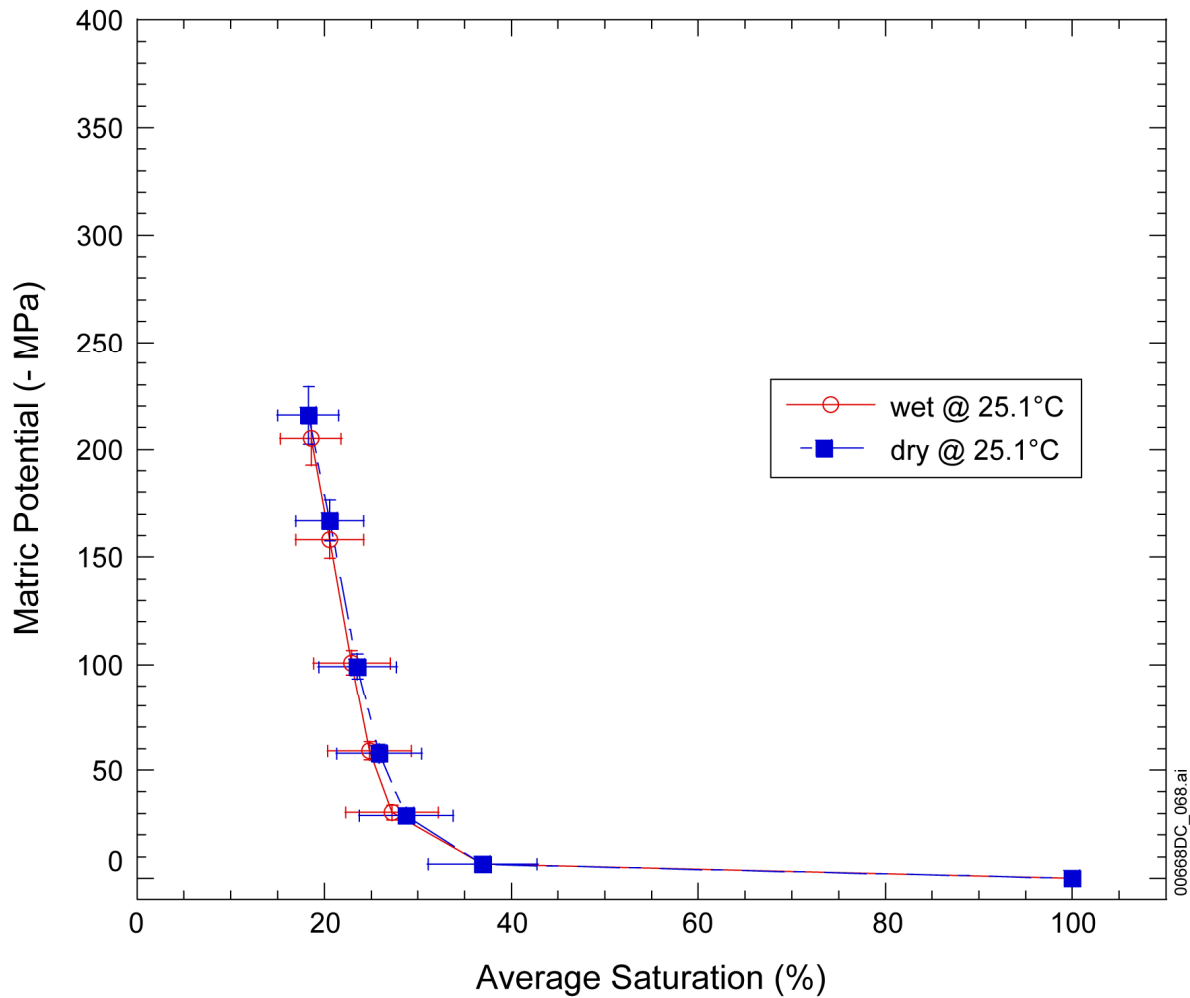
Source: DTN: LL020506123142.021 [DIRS 169256].

<sup>a</sup> Statistical mean for 11 samples; errors represent one standard deviation for all samples collectively.



To start the moisture retention curve measurement in the wetting cycle at room temperature, the specimens were dried and placed in the relative humidity chamber at about 25°C and 20% relative humidity. The samples were weighed daily until they held a constant value for several days. Once equilibrium was established, the sample weights were used to calculate the saturation level at that relative humidity condition. Saturation was calculated by comparing the measured weights with dry weights and taking into account porosity. Then the relative humidity was increased to 35%, and the procedures were repeated. This was repeated for the higher relative humidity levels at 50%, 65%, 80%, and 95%. After this, the relative humidity was decreased according to the following steps: 80%, 65%, 50%, 35%, and 20% to start the measurements in the drying cycle at room temperature. The maximum saturation achieved at the highest relative humidity was between 30% and 40% (see below). The process was then repeated for the drying portion of the measurement. This cycle of measurement was repeated at different temperatures, 50°C and 94°C, without the measurements at 35% and 65% relative humidity.

Moisture retention curves of the SHT specimens at a temperature of 25.1°C are shown in Figure 6.2-19. Only the “average” properties are shown for clarity. The averages are the mean saturation and matric potential of all 11 specimens. The error bars for saturation are the standard deviation from the average saturation at a matric potential level of all samples. There is little hysteresis at all temperatures.



Source: DTN: LL020506123142.021 [DIRS 169256].

NOTE: Lines connect the points and do not represent curve fits. The point at 100% saturation is inferred.

Figure 6.2-19. Average Moisture Retention Curves for 11 SHT Samples at 25.1°C

### Postcooling

Table 6.2-13 presents laboratory-determined saturation, porosity, and particle density. Average porosity and particle density values are given at the end of the table. An average value for liquid saturation is not a meaningful parameter in these postcooling cores, because liquid saturation of the cores reflects the TH processes that have taken place in the SHT, and their importance lies in their spatial variability with respect to the heat source. The porosity of three core samples (local ID H-1, H-22, and H-27) is exceptionally high, and is attributed to visible evidence of fractures. In turn, the liquid saturation of these samples would be less reliable.

Table 6.2-13. SHT Laboratory Hydrological Measurements of Postcooling Dry-Drilled Cores

Sample ID	LBNL ID	Saturation	Porosity	Bulk Density (g/cc)	Particle Density (g/cc)	Gravimetric Water Content (g/g)
SPC01009880	H-1	0.50	0.169	1.96	2.36	0.043
SPC01009882	H-2	0.79	0.105	2.19	2.44	0.038
SPC01009884	H-3	0.75	0.115	2.16	2.44	0.040
SPC01009885	H-4	0.44	0.099	2.20	2.44	0.020
SPC01009887	H-5	0.19	0.101	2.18	2.42	0.009
SPC01009888	H-6	0.32	0.110	2.17	2.43	0.016
SPC01009889	H-7	0.80	0.104	2.19	2.45	0.038
SPC01009806	H-8	0.80	0.098	2.19	2.43	0.035
SPC01009807	H-9	0.61	0.099	2.19	2.43	0.027
SPC01009808	H-10	0.82	0.090	2.21	2.43	0.033
SPC01009809	H-11	0.78	0.092	2.20	2.42	0.033
SPC01009810	H-12	0.53	0.105	2.16	2.41	0.026
SPC01009811	H-13	0.38	0.097	2.19	2.43	0.017
SPC01009812	H-14	0.41	0.089	2.21	2.43	0.016
SPC01009890	H-15	0.76	0.090	2.21	2.43	0.031
SPC01009891	H-16	0.87	0.102	2.17	2.42	0.041
SPC01009892	H-17	0.89	0.101	2.18	2.42	0.041
SPC01009893	H-18	0.94	0.093	2.20	2.43	0.040
SPC01009894	H-19	0.83	0.106	2.17	2.43	0.041
SPC01009895	H-20	0.85	0.087	2.24	2.45	0.033
SPC01009896	H-21	0.89	0.082	2.22	2.42	0.033
SPC01009897	H-22	0.73	0.131	2.12	2.44	0.044
SPC01009898	H-23	0.86	0.104	2.17	2.42	0.041
SPC01009899	H-24	0.86	0.099	2.20	2.44	0.039
SPC01009900	H-25	0.82	0.117	2.15	2.44	0.045
SPC01009901	H-26	0.86	0.103	2.20	2.45	0.040
SPC01009902	H-27	0.77	0.143	2.09	2.44	0.053
SPC01009903	H-28	0.88	0.087	2.23	2.44	0.034
<b>Average:</b>			0.104	2.18	2.43	
<b>Standard Deviation:</b>			0.018	0.05	0.02	

Source: DTN: LB980901123142.006 [DIRS 119029].

#### 6.2.2.5.2 Measurement Uncertainty: Laboratory Parameters—Saturation, Porosity, Density, Moisture Retention Curves

A balance with a sensitivity of 0.01 mg calibrated to a traceable standard was used to weigh the samples. Saturation was calculated by comparing weights with dry weights and taking porosity into account. One difficulty was the establishment of steady weight values at the highest humidities, particularly at high temperatures. The reasons for this difficulty are that the relative humidity is difficult to control at high humidities and the weight of the samples is more sensitive to changes in relative humidity when the relative humidity is high. Refinement of the control parameters on the humidity chambers aided in solving this problem. The measurement

uncertainty involved in determining the moisture-retention curves includes the measurements of weights, relative humidity, and sample size. The sample dimensions are used to determine sample wet and dry densities. It is estimated that the thickness of the sample can be determined to  $\pm 0.005$  mm and diameter to  $\pm 0.05$  mm. This results in an error in sample volume of approximately  $\pm 0.3\%$ . The uncertainty in dry weight is estimated to be approximately 0.00002 g and for wet weight approximately 0.0001 g. The error in the wet weight is higher than that of the dry condition because of the difficulty in achieving and maintaining saturation levels of 100%. These uncertainties result in errors in dry and wet densities of approximately 0.3%.

When repetitive measurements are made on samples over a period of several days, such as the determination of weights at a specified relative humidity, the uncertainty in the measurement is often less than the statistical uncertainty in the mean of the measured parameter. In such cases, the error is taken as one standard deviation of the mean. The errors in saturation determined at specific temperature and relative humidity are estimated to vary from approximately 0.07% to 0.5% water saturation, which includes errors associated with dry and wet densities discussed above. Thus, the relative uncertainty is estimated to be between approximately 1% and 10%, with a 1% to 2% error most common.

The uncertainty in the relative humidity is approximately  $\pm 2\%$ . When propagated through Kelvin's equation to matric potential, the absolute uncertainties are fairly low, but the relative uncertainties are high at the matric potentials closest to zero (as much as 200% at a matric potential of  $-1.36 \pm 2.73$  MPa).

Other factors that can affect accuracy of laboratory measurements include:

- Ability to account for all moisture in the rock sample because of the condensation of water on walls of core container. These are estimated by absorbing water from the container with a paper cloth and weighing the cloth.
- Large fractures and cores with infill material generally introduce greater inaccuracy in the weight measurements.
- Averages and standard deviations introduce a measure of data uncertainty.

### **6.2.3 SHT Mechanical Measurements**

The discussion of mechanical data for the SHT has been divided into several subsections, based on the type of measurement:

- Multipoint borehole extensometer (MPBX) displacements were measured within the rock mass surrounding the SHT. These measurements were used to evaluate numerical models related to thermal-hydrological-mechanical coupling as well as to provide data for determination of rock mass thermal expansion.
- Wire and tape extensometer measurements were used to measure movement of the free surfaces of the SHT block.

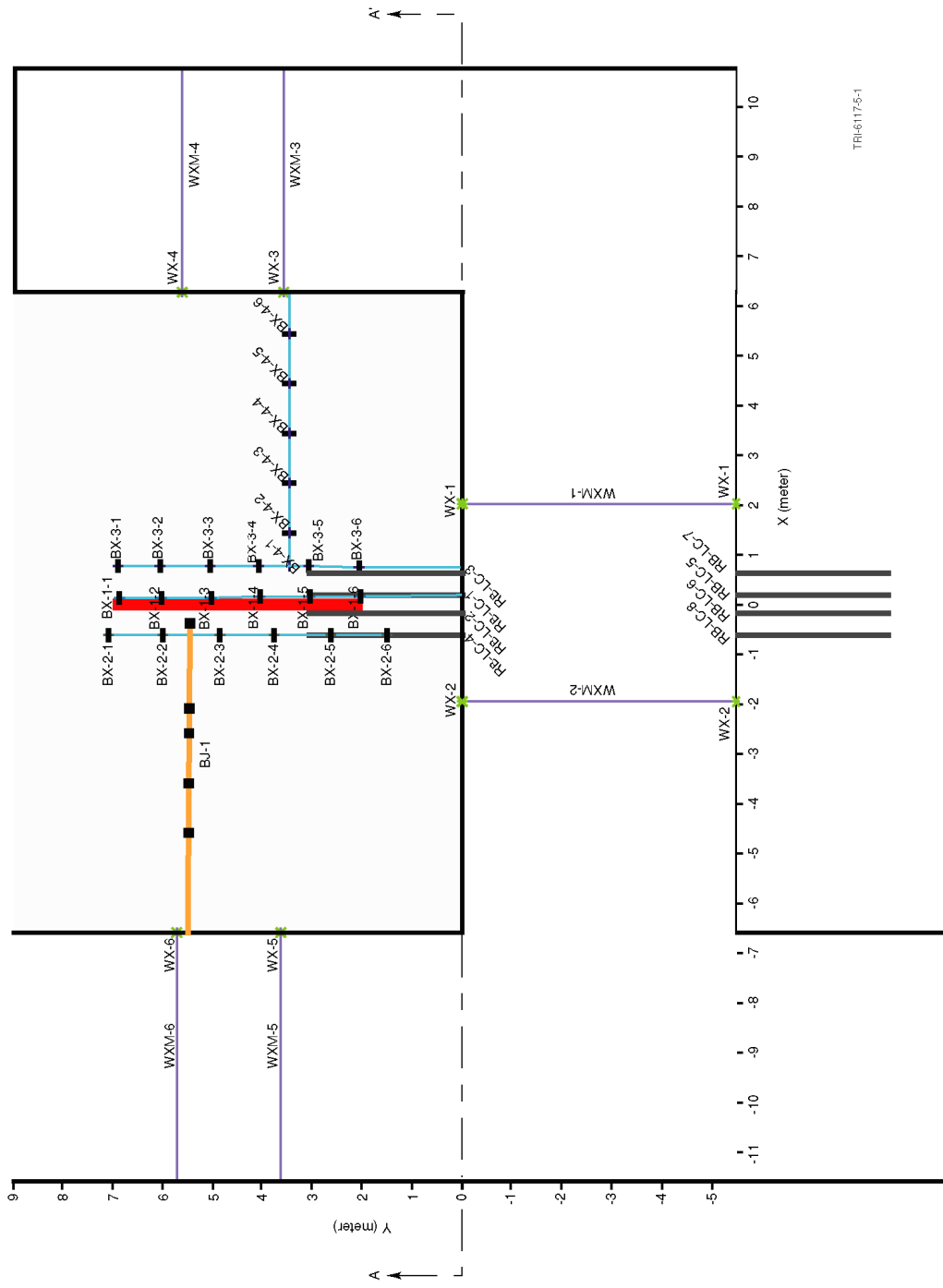
- Borehole jack tests were performed to measure rock mass modulus at ambient and elevated temperatures.
- Rock-bolt loading tests were performed to evaluate qualitatively the effects of elevated temperature on rock bolt performance.
- Laboratory properties/parameters such as elastic modulus, Poisson's ratio, and thermal expansion were measured.
- Field properties/parameters, including rock-mass thermal expansion estimations from the MPBX displacement data, were measured.

Detailed descriptions of all SHT mechanical measurements may be found in Section 9 of *Single Heater Test Final Report* (CRWMS M&O 1999 [DIRS 129261]). SHT mechanical measurement input DTNs and summary DTNs are listed in Tables 4-2 and 6.2-1, respectively.

### 6.2.3.1 MPBX Displacements

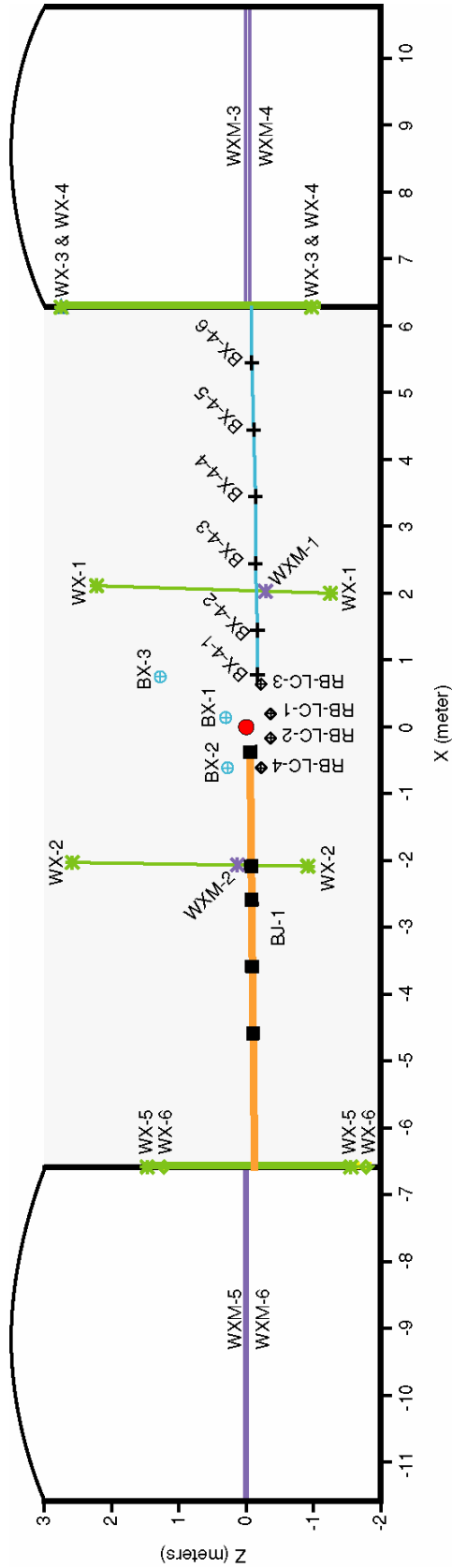
Displacements were measured both within and on the surfaces of the SHT block. These measurements support numerical model evaluations related to thermal-mechanical-hydrological coupling and also provide data for determination of rock-mass thermal expansion. All displacements reported in this document follow the convention of extension positive. Four boreholes were instrumented with MPBXs: three boreholes drilled parallel to the heater axis and one borehole drilled perpendicular to the heater axis. The MPBXs include six or seven anchors spaced along the length of the borehole. Displacements were measured using high temperature linear variable displacement transducers (LVDTs) and vibrating wire displacement transducers.

Wire extensometers and tape extensometer pins were installed on the three free surfaces of the SHT block (see Figures 6.2-20 and 6.2-21). Note that the legend for the abbreviations in these two figures is as follows: BX is multiple-point borehole extensometer, WX and WXM are wire extensometers, RB-LC is rock bolt load cell, and BJ is borehole jack. The wire extensometers consist of spring-loaded linear potentiometers mounted on brackets welded to steel rebar segments. These segments are grouted into the rock near the top of the SHT block at six locations (two on each of the three free surfaces of the SHT block). These surface displacements are intended to augment the displacement data collected from the MPBXs. Detailed discussion of the SHT displacements is presented in Sections 9 and 11.2 of *Single Heater Test Final Report* (CRWMS M&O 1999 [DIRS 129261]). SHT displacement data can be found in the TDMS under input DTNs: SN0401F3511695.012 [DIRS 169262], SN0401F3511695.013 [DIRS 169263], and LL980109904243.015 [DIRS 158299]. Because of the abundance of SHT displacement data, only representative discussion and graphics are provided. All displacement data and graphics can be accessed in the summary DTN identified in Table 6.2-1.



Source: CRWMS M&O 1999 [DIRS 129261].

Figure 6.2-20. Plan View Showing Locations of the SHT Mechanical Boreholes



Source: CRWMS M&O 1999 [DIRS 129261].

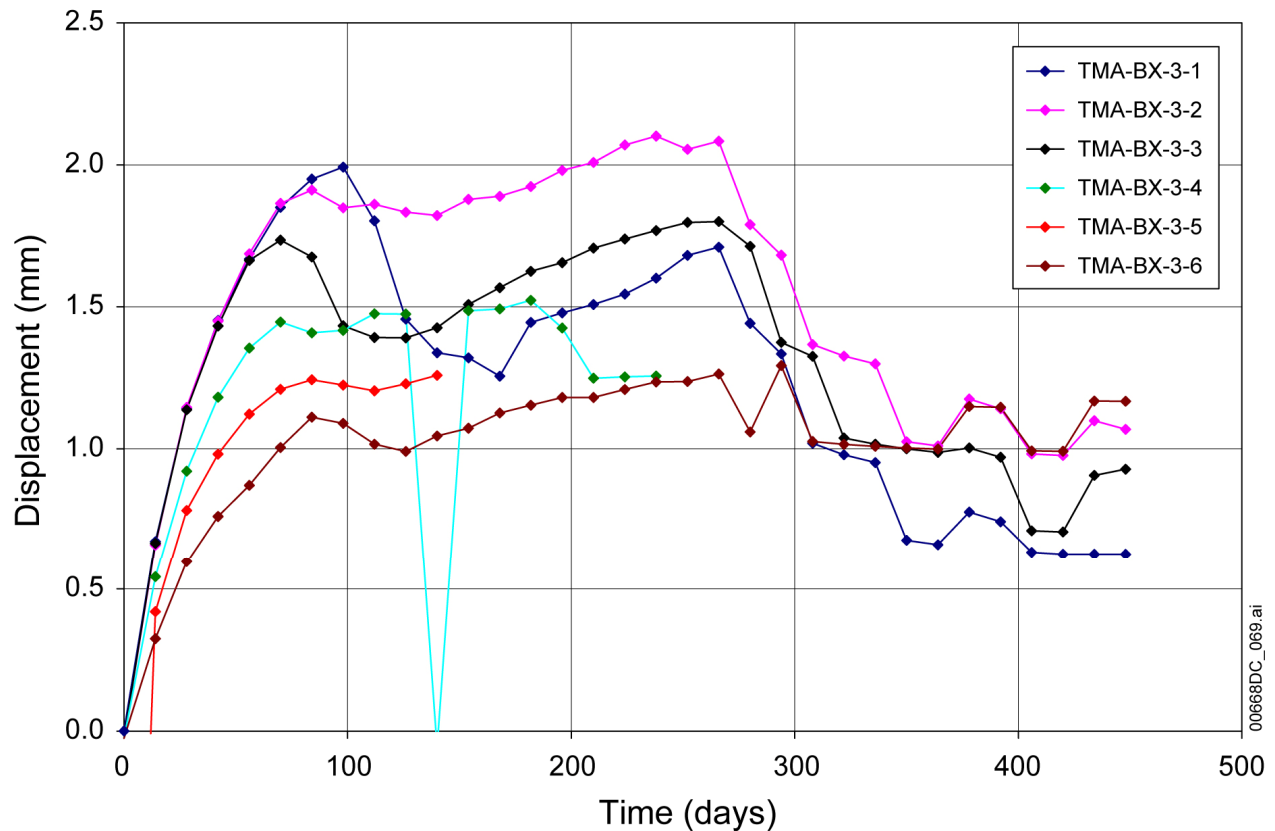
Figure 6.2-21. Cross Section Showing Locations of the SHT Mechanical Boreholes

### 6.2.3.1.1 Results: MPBX Displacements

Representative discussion and graphics are presented here. Figure 6.2-22 shows displacement data for MPBX-3, which is located approximately 1.5 m from the heater, above and to the right (south). The data from MPBX-3 show an increase in gage length (extension) for all anchor positions through about the first 70 days. From 70 to about 100 days, all anchors exhibit a gradual decrease in gage length. After about 100 days, all anchors except MPBX-3-1 reverse trend and increase extension through the second quarter of heating. Anchor MPBX-3-1 continues the relative compression from day 100 through about day 180, when it experiences a sudden extensional jump followed by continued extension throughout the fourth quarter of heating. The extensional jump at about day 180 is seen only in anchor MPBX-3-1; therefore, it is likely that it results from discrete movement along a fracture or system of fractures located between anchors MPBX-3-2 and MPBX-3-1. This region corresponds to similar presumed behavior near anchor MPBX-1-1 (MPBX-1) near day 210. The change in slope for most of the anchor responses after about 70 days may be the result of matrix thermal expansion closing existing fractures, thus limiting additional thermally driven displacements until a greater volume of rock is heated. Thus, three-dimensional confinement effects may influence the response of some anchors.

The cooldown data for MPBX-3 are also included in Figure 6.2-22 (cooling starts at day 275). Four gages in MPBX-3 are operational; gages MPBX-3-4 and MPBX-3-5 are suspected to have failed from unknown causes during heating. MPBX-3 exhibits step-like decreases in all operational gages during cool down. As with MPBX-1, this type of behavior may be characteristic of the rock mass deformation associated with normal and shear deformation of fractures in the cooling rock mass. This type of behavior should not be unexpected in a fractured rock mass.





Source: DTNs: SN0401F3511695.012 [DIRS 169262]; SN0401F3511695.013 [DIRS 169263].

Figure 6.2-22. Displacement History for SHT MPBX-3 Borehole

Wire and tape extensometer pins were placed on the three free surfaces of the SHT block (see Figures 6.2-20 and 6.2-21). Because the measurements are made from short pins installed near the rock surface, they can be influenced by discrete block movement. All the wire extensometer stations show displacement changes of over several millimeters, with the exception of WX-4, which experienced displacements of less than 1 mm throughout the test. The data from the wire extensometers are provided in tabular form in Table 6.2-14. The data from the manual tape-extensometer measurements are given in Table 6.2-15. The data show that the horizontal cross-drift measurements are largest for WXM-1, WXM-2, and WXM-3, with all measurements compressive (i.e., shortening of the gage length). In other words, the surface pins are moving away from the SHT block in all cases. These displacements are consistent with the gross displacements measured using the MPBXs. In addition, the tape extensometer results for WXM-2 are consistent with the large displacements measured by the wire extensometer station WX-2. This suggests gross surface displacements near the surface of the SHT block to the left of the heater. It is likely that either or both of the WXM-2 pins are located in a loose block of rock, which appears to have loosened almost immediately during the SHT. The subsequent data suggest that the block(s) stabilized somewhat, with only minor additional displacement after September 24, 1996.

Table 6.2-14. Wire Extensometer Data

Gage	Days after Startup									
	0	14	28	42	56	70	84	98	112	126
TMA-WX-1	0	-0.1	0.08	0.02	0.03	0.27	0.2	0.33	0.49	0.47
TMA-WX-2	0	-0.14	-0.15	-0.12	3.16	3.21	3.26	3.27	3.29	3.27
TMA-WX-3	0	-0.03	-0.09	0.01	0.01	0.2	0.25	0.31	0.33	0.41
TMA-WX-4	0	-0.83	-0.78	-0.78	-0.78	-0.58	-0.49	-0.66	-0.63	-0.31
TMA-WX-5	0	-0.61	-0.66	-0.58	-0.52	-0.5	-0.44	-0.67	-0.4	-0.58
TMA-WX-6	0	-2.45	-2.46	-1.98	-1.88	-1.89	-1.83	-2.95	-2.97	-2.97
Gage	Days after Startup									
	140	154	168	182	196	210	224	238	252	266
TMA-WX-1	0.39	0.66	0.66	0.55	0.55	0.55	0.55	0.55	0.44	0.59
TMA-WX-2	3.17	3.52	3.51	3.51	3.51	3.5	3.5	3.5	3.41	3.38
TMA-WX-3	0.28	0.69	-23.92	-23.92	-23.84	-23.99	-24.08	-24.08	-24	-24.03
TMA-WX-4	-0.59	-0.2	-0.21	-0.04	-0.04	-0.09	-0.09	-0.1	-0.1	-0.12
TMA-WX-5	-0.89	-0.48	-0.59	-0.65	-0.78	-0.82	-0.82	-0.83	-0.81	-0.82
TMA-WX-6	-3.21	-2.75	-2.91	-2.74	-2.74	-3.06	-3.06	-3.06	-2.96	-2.92
Gage	Days after Startup									
	280	294	308	322	336	350	364	378	392	406
TMA-WX-1	0.46	0.22	0.01	-0.05	-5.89	-5.89	-6.4	-6.56	-6.63	-6.40
TMA-WX-2	4.49	4.49	4.22	4.22	3.99	4.11	4.04	4.04	3.93	2.97
TMA-WX-3	-23.91	-24.16	-24.16	-23.91	-24.42	-24.42	-24.42	-24.68	-24.66	-24.67
TMA-WX-4	-0.17	-0.17	-0.17	-0.17	-0.68	-0.42	-0.68	-0.90	-0.91	-0.68
TMA-WX-5	-0.69	-0.69	-0.95	-0.95	-0.95	-1.2	-38.29	-38.61	-38.65	-38.54
TMA-WX-6	-2.99	-3.25	-3.5	-3.5	-3.75	-3.75	-3.5	-3.77	-3.83	—
Gage	Days after Startup									
	420	434	448	462	476	490	504	518	—	—
TMA-WX-1	-6.65	-3.93	-5.52	-5.54	-4.11	-2.31	-2.01	-2.39	—	—
TMA-WX-2	2.97	2.85	0.37	0.67	0.22	-21.04	-20.51	-20.89	—	—
Gage	Days after Startup									
	420	434	448	462	476	490	504	518	—	—
TMA-WX-3	-24.67	-24.72	-24.71	-24.65	-24.65	1.19	1.92	1.46	—	—
TMA-WX-4	-0.68	-0.91	-0.91	-0.89	-0.87	-53.45	-53.42	-53.48	—	—
TMA-WX-5	-38.54	-38.72	-38.76	-38.98	-38.99	1.72	1.55	-3.99	—	—
TMA-WX-6	—	-3.75	-3.50	-3.80	-3.79	-3.74	-3.71	-3.6	—	—

Source: DTNs: SN0401F3511695.012 [DIRS 169262]; SN0401F3511695.013 [DIRS 169263].

NOTE: Wire extensometer data given in mm. Extension is positive.

Table 6.2-15. Tape Extensometer Measurements for the SHT

Gage No.	Initial Reading (m)	Displ. 9/24/96 (mm)	Displ. 10/21/96 (mm)	Displ. 12/19/96 (mm)	ΔDispl. 1/7/97 (mm)	Displ. 2/11/97 (mm)	Displ. 3/10/97 (mm)
WXM-1	5.40439	-0.48	-0.78	-0.86	-0.76	-1.14	-1.19
WXM-2	5.08585	-3.20	-3.20	-1.17	-3.71	-3.71	-3.71
WXM-3 <sup>a</sup>	—	4.67249	0.33	Erroneous	0.08	-1.93	2.24
WXM-4	4.33635	-0.46	-0.21	-0.56	-0.64	-0.84	Erroneous
WXM-5	5.87639	-0.04	-0.32	-0.49	-0.57	-0.37	-0.82
WXM-6	5.83158	-0.29	-0.129	-0.17	-0.39	-0.72	-0.80
Gage No.	Displ. 4/21/97 (mm)	Displ. 5/6/97 (mm)	Displ. 6/25/97 (mm)	Displ. 7/24/97 (mm)	Displ. 8/20/97 (mm)	Displ. 7/15/97 (mm)	
WXM-1	-1.27	-0.86	-1.39	-1.52	-1.34	-1.16	
WXM-2	Erroneous	-4.39	-4.21	-4.21	-4.21	-3.71	
WXM-3 <sup>b</sup>	0.26	0.31	-0.17	2.29	-0.07	0.26	
WXM-4	-0.36	-0.18	-1.17	-1.22	-1.20	-1.50	
WXM-5	-0.72	-0.79	-0.88	-0.95	-0.62	-0.60	
WXM-6	-0.64	-0.31	-1.15	-0.95	-0.21	-0.64	

Source: DTN: SN0401F3511695.012 [DIRS 169262].

<sup>a</sup> Extension is positive.

<sup>b</sup> WXM-3 initial reading suspect. Change in displacement from 9/24/96.

### 6.2.3.1.2 Measurement Uncertainty: MPBX Displacements

There are several potential sources for measurement uncertainty in the displacement measurements presented in this section. These uncertainties, quantifiable and nonquantifiable, are listed below:

#### Quantifiable

- The accuracy of the instrumentation itself. The gage range and accuracy of SHT displacement-related instrumentation are presented in Table 6.2-16.
- The conversion of the electrical output to engineering units. The uncertainty from these equations and the round-off error inherent in the data conversion are negligible.

#### Nonquantifiable

- Electrical interference, such as spurious signals from power surges, can cause low-magnitude noise, unexplained meandering in the data, or high-magnitude spikes.
- Unidentified sensor or MPBX assembly stability issues have caused a few LVDTs or vibrating wire gages to either produce “bad” data for an extended period of time before returning “good” data, or to have an unexplained shift in magnitude while maintaining expected rates of behavior on both sides of the shift.

- The physical location of the gages in the test region is difficult to precisely determine. The location uncertainty is particularly important in regions of high temperature gradient, of which hydrological and thermal expansion behavior are thought to be strong functions for certain temperature ranges.
- The uncertainty related to the choice of method for computing thermal expansion of Invar rods, based on measured temperatures along MPBXs, is difficult to estimate. Piecewise linear discretization using average temperature values and a 4th-order polynomial for thermal expansion as a function of temperature were used for the SHT. The choice of another method (e.g., an integral function along the length of the rods) requires different assumptions that may be as reasonable as the method chosen. The magnitude of any discretization error is likely not large enough to affect the general trends in thermal-mechanical deformation of the rock illustrated by the data.
- Instruments can degrade or fail.
- Anchors can slip (considered possible but unlikely).
- The temperature change near the anchor heads could affect LVDT calibration constants. This uncertainty is anticipated to be negligible.

Table 6.2-16. Summary of SNL-Installed Measurement System Specifications

Measurement System	Manufacturer	Gage Accuracy, Range, and Precision
Type-K Thermocouples (Chromel-Alumel)	STI (probes) Omega	±2.2°C max 1280°C
Vibrating Wire Displacement Transducers	GeoKon	1 in. full range Resolution: .02%
High-Temp LVDT	RDP	±0.5% of full range = ±19 mm @200°C
Wire Extensometer	Houston Scientific, Inc.	0.1% resolution 2-in. range
Vibrating Wire Load Cell	GeoKon	60,000 lb max ±0.5% full range
Tape Extensometer	GeoKon	±0.127 mm
Goodman Jack –Readout Box –Near LVDT –Far LVDT –Pressure Gage –Enerpak Pump	Sinco	Range: pressure: 0 to 10,000 psi displacement: –0.25 to +0.25 in. Accuracy: pressure: ±0.2% displacement: ±0.005 in.
Power Monitor	Magtrol	Volts (0.2% of reading +0.2% of range) 0 to 600 volts Amps (0.22% of reading +0.25% of range) 0 to 50 amps Watts (0.2% of reading +0.3% of range)
Thermistors	Omega	±0.2°C 100°C range

Source: CRWMS M&O 1999 [DIRS 129261].

### 6.2.3.2 Borehole Jack

Borehole jack tests were performed in ESF-TMA-BJ-1 (borehole 19). Detailed discussion of the borehole jack tests is presented in Sections 9.2 and 11.2 of *Single Heater Test Final Report* (CRWMS M&O 1999 [DIRS 129261]). Because the rock-mass modulus measured using the borehole jack is directional (perpendicular to the borehole), an estimate of horizontal modulus anisotropy was not possible. It is likely that some anisotropy in modulus exists locally because of differences in fracture stiffness for each set of fractures present in the SHT block. Also, it is likely that the rock-mass modulus varies across the repository block. These measurements, which included 15 ambient and 10 elevated-temperature measurements, were taken at five locations within the testing borehole at nine different times during the heating and cooling phases of the SHT. Consequently, the effects of temperature on rock-mass modulus were examined.

Borehole jack data may be found in input DTN: SNF35110695001.010 [DIRS 158300].

#### 6.2.3.2.1 Results: Borehole Jack

The results from the borehole-jack testing show that the measured rock mass modulus ranges from about 3 to 23 GPa where the higher values were generally associated with increases in temperature. The highest value is for the deepest measurement location in the borehole (approximately 6.2 m from the collar). This location corresponds to roughly 0.33 m from the heater borehole, about 1.5 m from the end of the heater. Measurement at this location approximately 110 days before and 190 days after resulted in moduli of approximately 8.5 and 9.2 GPa, respectively. This high value of 23 GPa may be due to measurement error. All the other borehole-jack data are relatively low, less than 12 GPa.

The data presented in Table 6.2-17 include italicized results in which the two LVDT readings (far and near) differ by slightly greater than 0.02 in. at the maximum test pressure. According to the American Society for Testing and Materials (ASTM) (ASTM D4971-89 [DIRS 101786], p. 3), these data should be discarded because of uneven loading. The fractured nature of the rock surrounding the borehole made it difficult in some cases to “set” the borehole jack at those locations. However, the data presented represent only slight deviation from the ASTM criteria (ASTM D4971-89 [DIRS 101786], p. 3) and are presented to qualitatively assess modulus difference along borehole BJ-1. The italicized data should not be used in calculations requiring rock mass modulus.

Table 6.2-17. Estimated Rock Mass Modulus in Borehole ESF-TMA-BJ-1 (Goodman/Borehole Jack)

	Distance from Collar				
	2.0 m	3.0 m	4.0 m	4.51 m	6.2 m
Date	Rock Mass Modulus-GPa (Temp °C)				
8/26/96	6.9 (25)	3.71 (25)	No test	No test	No test
10/10/96	10.3 (27.5)	10.3 (27.7)	8.3 (30.2)	6.0 (34)	No test
11/26/96	<i>Results discarded (31.1)</i>	10.2 (35.9)	5.71 (46.4)	5.01 (55.4)	8.4 (141.8)
3/18/97	<i>Results discarded (35)</i>	6.3 (41)	10.3 (52)	5.7 (58.7)	22.8 (143.1)
10/23/97 1st run	No test	No test	6.28 (Ambient)	Discarded	8.28 (Ambient)
10/23/97 2nd run	No test	No test	8.97 (Ambient)	7.1 (Ambient)	10.0 (Ambient)
1/29/98 1st run	5.47 (Ambient)	9.67 (Ambient)	8.28 (Ambient)	7.60 (Ambient)	Not calculated
1/29/98 2nd run	No test	No test	No test	No test	11.72 (Ambient)
1/29/98 3rd run	No test	No test	No test	No test	11.72 (Ambient)

Source: DTN: SNF35110695001.010 [DIRS 158300].

NOTE: Italicized calculated moduli are based on field data in which the difference between the two borehole jack LVDT readings slightly exceeded the limits set in ASTM D 4971-89 [DIRS 101786]. The fractured nature of the rock made setting the jack difficult. Discarded results were for data that far exceeded ASTM D 4971-89 [DIRS 101786] limits.

#### 6.2.3.2.2 Measurement Uncertainty: Borehole Jack

Measurement uncertainties in SHT borehole-jack measurements include those associated with accuracy and precision (as tabulated in Table 6.2-16) and proximity to fractures. The borehole jack is better suited for local regions that are intact rather than fractured rock. Also, elevated temperatures, especially near peak temperatures in the SHT block, may affect the performance of the borehole jack.

#### 6.2.3.3 Rock Bolt Load

Eight rock bolt load cells were installed on Williams B7X Hollow Core rock bolts as part of the SHT mechanical testing program. The objective was to evaluate qualitatively the effects of elevated temperature on bolt performance by (1) monitoring load changes during the test, (2) evaluations of the bolt/grout/rock interface following heating and cooling, and (3) pull-testing selected bolts to failure after heating and subsequent cooling. Each rock bolt included one vibrating wire load cell (load washer) that was installed between cover plates and adjustable angled washers. This entire assembly was bolted to the Williams bolt on the cold side of the insulation.

Four of the rock bolts were installed on the heated side of the Thermal-Mechanical Alcove below the level of the heater. Another four rock bolts were installed on the opposite cold side of the Thermal-Mechanical Alcove. The rock bolts and load cells were installed during July 1996. Initial readings were taken using a hand-held Geokon readout box, prior to connection to the DCS. The load cells each contain three strain gages, and the total load acting on the cell is calculated by averaging the measurements from all three. The locations of the rock bolts instrumented with rock bolt load cells (RBLCs) are shown in Figures 6.2-20 and 6.2-21. Four RBLCs were installed on the heated side of the west face of the SHT block (RB-1, RB-2, RB-3,

and RB-4), and four were installed on the opposite ambient side of the Thermal-Mechanical Alcove (RB-5, RB-6, RB-7, and RB-8).

Detailed discussion of the SHT rock bolt load testing is presented in Section 9.3 of *Single Heater Test Final Report* (CRWMS M&O 1999 (129261)). SHT rock bolt load data may be found in input DTNs: SN0401F3511695.012 [DIRS 169262] and SN0401F3511695.013 [DIRS 169263].

### 6.2.3.3.1 Results: Rock Bolt Load

The data are presented in tabular form in Table 6.2-18 as load (lb) versus time from the start of heating. The data show a general decline in load measured in all the RBLCs through the end of heating. Three of the four heated rock bolts (RB-2, RB-3, and RB-4) show an increase in load after the heater is turned off, and RB-1 exhibits a stabilization of the previously observed load decrease. The increase is only up to 100 lb, or 0.7% of the load measured in the bolt. The load increase is likely caused by thermal-contraction effects in the bolt itself, which likely has a higher thermal expansion/contraction coefficient than the rock mass surrounding it. The ambient rock bolts continue to experience a decrease in load throughout the reporting period.

Table 6.2-18. Rock Bolt Load Cells, Load versus Time

TMA RBLC Gage	Days after Startup									
	0	14	28	42	56	70	84	98	112	126
RB-LC-1-AVG	22662	22262.8	22158	21732.3	21537.1	21444.1	21407.5	21380.8	21340.3	21308.5
RB-LC-2-AVG	14859.4	14739.7	14708.6	14680.1	14643.7	14597	14559.8	14522.5	14496.5	14449.6
RB-LC-3-AVG	22428	22402.2	22378.7	22348.4	22317.5	22281	22262.3	22243.2	22231	22224.1
RB-LC-4-AVG	16663.9	16602.8	16580.3	16558.8	16522.1	16496.6	16467.4	16446.3	16424.2	16407.5
RB-LC-5-AVG	25971.9	25928.5	25887	25856.6	25829.3	25802.6	25783.4	25765.5	25748.7	25738.1
RB-LC-6-AVG	14642.7	14633.2	14632.7	14627.3	14619.4	14609.5	14601.2	14595.9	14589.2	14573.7
RB-LC-7-AVG	4932.6	4921.1	4919.7	4911.8	4904.3	4893.6	4890.9	4883.8	4877.5	4873
RB-LC-8-AVG	16862.8	16818.5	16783.6	16758.7	16738.7	16605	16592.7	16575.4	16566	16561.5
TMA RBLC Gage	Days after Startup									
	140	154	168	182	196	210	224	238	252	266
RB-LC-1-AVG	21279.7	21254.3	21206.3	21176.9	21161.2	21145.9	21127.1	21112.2	21100.9	21102.1
RB-LC-2-AVG	14422.7	14405.6	14389.9	14378.6	14369.9	14365.5	14353.4	14349	14342	14341.1
RB-LC-3-AVG	22214.2	22206.8	22201.1	22194.3	22189.6	22183.4	22176.4	22171.7	22165.3	22158.4
RB-LC-4-AVG	16394.3	16377.4	16361.5	16350.8	16340.4	16331	16320.2	16316.8	16312.1	16310.9
RB-LC-5-AVG	25728.1	25722.2	25714.1	25705.1	25698.3	25692.7	25683.1	25676	25665.6	25652
RB-LC-6-AVG	14567.1	14563.5	14562.3	14557.4	14553.9	14551.2	14549.3	14543.8	14543.4	14538.9
RB-LC-7-AVG	4866.9	4866.7	4867.2	4866.6	4868.2	4865.2	4863.2	4863.9	4864.1	4867.1
RB-LC-8-AVG	16552.8	16544.8	16538	16533.3	16528.6	16522.3	16516.4	16514	16503.2	16501.5

Table 6.2-18. Rock Bolt Load Cells, Load versus Time (Continued)

TMA RBLC Gage	Days after Startup									
	280	294	308	322	336	350	364	378	392	406
RB-LC-1-AVG	21090.8	21092.2	21097.1	21090.6	21081.3	21070.5	21066.3	21073.0	21072.7	21080.6
RB-LC-2-AVG	14354.1	14380.2	14391.6	14396.8	14404.6	14409	14412.4	14416.8	14421.9	14439.3
RB-LC-3-AVG	22160.3	22171.6	22179.8	22180.8	22182.1	22179.1	22180.2	22177.4	22179.1	22183.0
RB-LC-4-AVG	16315.9	16332.3	16338.5	16340.7	16346.6	16348.2	16350.4	16354.0	16358.0	16366.6
RB-LC-5-AVG	25641.1	25617.7	25604.4	25589.9	25581.9	25573.8	25571.5	25561.4	25555.1	25548.7
RB-LC-6-AVG	14538.6	14538.2	14536.1	14534.8	14531.9	14531.1	14529.5	14528.5	14530.7	14534.1
RB-LC-7-AVG	4865	4858.2	4857.6	4856.9	4851	4850.2	4850.1	4852.8	4853.3	4856.6
RB-LC-8-AVG	16497.8	16491.7	16491.7	16488.4	16487	16484.6	16477.2	16480.8	16475.8	16476.1
TMA RBLC Gage	Days after Startup									
	420	434	448	462	476	490	504	518	—	—
RB-LC-1-AVG	21074.6	21058.0	21019.0	20999.9	20964.1	20943.1	20933.8	20928.1	—	—
RB-LC-2-AVG	14435.0	14432.4	14419.5	14391.8	14352.8	14338.9	14347.6	14346.7	—	—
RB-LC-3-AVG	22179.8	22177.4	22168.4	22150.2	22111.5	22097.6	22099.3	22096.8	—	—
RB-LC-4-AVG	16360.9	16354.1	16345.6	16330.8	16282.0	16234.2	16268.6	16278.5	—	—
RB-LC-5-AVG	25535.6	25525.3	25515.4	25496.9	25457.7	25444.7	25445.6	25445.2	—	—
RB-LC-6-AVG	14533.1	14532.5	14528.0	14521.6	14503.0	14493.0	14492.2	14490.9	—	—
RB-LC-7-AVG	4860.1	4858.9	4854.8	4842.0	4808.4	4796.1	4795.0	4680.1	—	—
RB-LC-8-AVG	16468.7	16462.1	16454.2	16079.7	16060.3	16052.3	16056.2	16058.1	—	—

Source: DTNs: SN0401F3511695.012 [DIRS 169262]; SN0401F351695.013 [DIRS 169263].

NOTE: TMA = Thermal-Mechanical Alcove. Load cell data are for average load and are given in lbs.

Loads were measured in rock bolts installed on both the heated side of the SHT block and on the opposite ambient rib of the Thermal-Mechanical Alcove. The rock bolts were installed to evaluate the longer-term effects of elevated temperature on this type of rock anchorage. Results show that loads are decreasing in all load cells; however, the decrease is greatest in those rock bolts on the heated side of the SHT. Alternatively, there could also be some load loss caused by creep of the anchorage, which is composed of the steel bolt and mechanical anchor, the surrounding grout, and the rock itself. The fact that load decreases were about 1% to 2% for all rock bolts, except RB-1 and RB-2, which decreased about 7% and 4% respectively, appears to indicate: (1) the influence of anchorage creep on all the bolts and (2) the effect of temperature on the creep of the rock bolts, because rock bolts with the highest temperatures had the most load decrease.

### 6.2.3.3.2 Measurement Uncertainty: Rock Bolt Load

Measurement uncertainties in SHT rock bolt measurements are similar to many of those discussed in Section 6.2.3.1.2. Additional uncertainties include those associated with accuracy and precision as tabulated in Table 6.2-16.



#### **6.2.3.4 Laboratory Parameters—Thermal Expansion, Young’s Modulus, Poisson’s Ratio, and Peak Stress**

The SHT includes preheating planning, test design, preheating analyses, preheating characterization, test implementation, heating-phase testing, cooling-phase testing, and postcooling characterization and instrumentation/equipment evaluations. This section discusses the postcooling characterization activities for mechanical processes after the cooling phase of the SHT was completed. Specifically, the activity described here is the use of postcooling borehole and intact rock sample locations for laboratory determination of thermal-mechanical properties. A detailed discussion for all SHT laboratory mechanical parameters is presented in Section 6.2 of *Single Heater Test Final Report* (CRWMS M&O 1999 [DIRS 129261]) and Section 4 of *Characterization of the ESF Thermal Test Area* (CRWMS M&O 1996 [DIRS 101428]). SHT preheating and postcooling laboratory parameter data may be found in input DTNs: SNL22080196001.002 [DIRS 158306] and SNL22080196001.003 [DIRS 119042].

##### **6.2.3.4.1 Results: Laboratory Parameters—Thermal Expansion, Young’s Modulus, Poisson’s Ratio, Peak Stress, and Axial Strain at Peak Stress**

The mean coefficients of thermal expansion (MCTEs) are summarized in Tables 6.2-19 and 6.2-20 for heating and cooling, respectively, during the first thermal cycle. Data are categorized as being either from within or outside the maximum extent of the 100°C isotherm, and either perpendicular or parallel to the heater. The mean MCTEs and standard deviations about each mean are given at each temperature for each category. Summary data for the entire test suite are given with standard deviations and 95% confidence limits at the bottom of each table. All specimens show steep increases in MCTE beginning at approximately 150°C to 200°C and continuing until approximately 300°C. The steepest increases are between 250°C and 300°C. This steep increase is attributed to phase changes in the silica mineral phases. The MCTEs calculated over the temperature interval of 300°C to 325°C decrease as the phase change is completed. The specimens with lower MCTEs are primarily from within the approximate maximum extent of the 100°C isotherm. The SHT preheating characterization data and data from within the approximate maximum extent of the 100°C isotherm continue to track one another and fall below the remaining data sets.

Fourteen specimens were tested in unconfined compression and the experimental data are summarized in Table 6.2-21. Mean values, standard deviations, and 95% confidence limits are given for Young’s modulus, Poisson’s ratio, peak stress, and axial strain at peak stress. Young’s moduli ranged from 20.1 to 37.0 GPa, with a mean value of 31.6 GPa. The standard deviation was  $\pm 4.8$  GPa, and the 95% confidence limit was  $\pm 2.5$  GPa. Poisson’s ratio ranged from 0.12 to 0.39 with a mean value of 0.20. The standard deviation was  $\pm 0.07$ , and the 95% confidence limit was  $\pm 0.03$ . Peak stress ranged from 34 to 246 MPa, with a mean value of 134 MPa. The standard deviation was  $\pm 70$  MPa, and the 95% confidence limit was  $\pm 37$  MPa. Axial strain at peak stress ranged from 0.11% to 0.89%, with a mean value of 0.47%. The standard deviation was  $\pm 0.25\%$ , and the 95% confidence limit was  $\pm 0.13\%$ .

Table 6.2-19. Mean Coefficients of Thermal Expansion during First Cycle Heating of Postcooling SHT Characterization Specimens

Specimen ID	Distance from Collar (ft)	Max. Temp. (°C)	Mean CTE on Heat-up (10 <sup>-6</sup> /°C)											
			25 to 50	50 to 75	75 to 100	100 to 125	125 to 150	150 to 175	175 to 200	200 to 225	225 to 250	250 to 275	275 to 300	300 to 325
<b>Perpendicular to Heater, Outside 100°C Isotherm</b>														
PTC1-A 2.9-B	2.9	322	8.7	9.6	9.8	11.2	12.3	13.1	14.6	19.4	32.7	56.3	75.0	52.3
PTC1-A 16.8-B	16.8	321	9.1	11.0	9.6	10.4	11.3	12.5	12.3	15.8	20.3	33.2	62.1	49.8
PTC2-B 4.1-B	4.1	321	9.2	10.5	9.9	10.3	11.1	12.3	12.8	16.4	23.8	43.1	61.4	45.6
		N =	3	3	3	3	3	3	3	3	3	3	3	3
		Mean =	9.0	10.4	9.8	10.7	11.6	12.6	13.2	17.2	25.6	44.2	66.2	49.2
		STD =	0.3	0.7	0.1	0.5	0.7	0.4	1.2	1.9	6.4	11.6	7.7	3.4
<b>Perpendicular to Heater, Inside 100°C Isotherm</b>														
PTC1-B19.0-B	19.0	322	9.0	10.1	8.9	9.4	10.8	12.9	13.5	16.0	20.4	30.6	51.4	54.0
<b>Parallel to Heater, Outside 100°C Isotherm</b>														
PTC4-A 4.6 B	4.6	321	8.8	10.0	8.3	9.5	10.5	11.9	11.2	13.9	20.1	34.1	81.4	69.0
PTC5-B 4.1-B	4.6	321	8.7	10.4	8.9	9.6	10.6	11.6	11.7	14.5	34.2	38.5	57.0	63.1
PTC5-B 24.4-B	4.6	321	8.9	10.5	8.6	9.4	10.2	11.2	11.1	14.1	17.9	26.7	47.5	52.9
PTC5-B 24.4-C	4.6	331	8.8	9.9	8.5	9.3	10.2	11.4	12.6	17.2	21.5	34.5	59.9	45.1
		N =	4	4	4	4	4	4	4	4	4	4	4	4
		Mean =	8.8	10.2	8.6	9.5	10.4	11.5	11.7	14.9	23.4	33.5	61.5	57.5
		STD =	0.1	0.3	0.3	0.1	0.2	0.3	0.7	1.5	7.3	4.9	14.3	10.6
<b>Parallel to Heater, Inside 100°C Isotherm</b>														
PTC4-A 6.8-B	6.8	318	7.9	8.8	9.1	9.4	10.5	11.1	12.4	15.4	24.3	38.0	70.2	73.0
PTC4-B 14.8-B	14.8	321	9.0	10.3	8.6	9.3	10.4	12.0	12.4	15.0	19.2	28.1	45.8	52.2
PTC4-A 19.0-B	19.0	319	8.1	8.9	8.9	9.2	10.1	11.1	12.4	14.5	17.5	28.0	51.0	56.9
PTC4-B 19.8-B	19.8	318	8.4	9.1	9.4	9.8	10.6	11.5	12.9	15.4	19.2	27.8	44.2	44.4
PTC H1-A 15.6-B	15.6	322	7.66	9.48	8.24	9.11	10.19	10.65	11.05	12.33	14.63	22.02	41.38	54.172
PTC MPBX1 14.2-B	14.2	322	8.51	9.64	8.49	9.04	9.86	11.50	11.82	15.29	20.75	28.98	50.49	55.86
		N =	6	6	6	6	6	6	6	6	6	6	6	6
		Mean =	8.2	9.4	8.8	9.3	10.3	11.3	12.2	14.7	19.3	28.8	50.5	56.1
		STD =	0.5	0.6	0.4	0.3	0.3	0.5	0.6	1.2	3.2	5.1	10.3	9.4

Table 6.2-19. Mean Coefficients of Thermal Expansion during First Cycle Heating of Postcooling SHT Characterization Specimens (Continued)

Specimen ID	Distance from Collar (ft)	Max. Temp. (°C)	Mean CTE on Heat-up (10 <sup>-6</sup> /°C)													
			25 to 50	50 to 75	75 to 100	100 to 125	125 to 150	150 to 175	175 to 200	200 to 225	225 to 250	250 to 275	275 to 300	300 to 325		
<b>All Data Outside 100°C Isotherm</b>																
		N =	7	7	7	7	7	7	7	7	7	7	7	7	7	7
		Mean =	8.9	10.3	9.1	10.0	10.9	12.0	12.3	15.9	24.4	38.1	63.5	54.0		
		STD =	0.2	0.4	0.7	0.7	0.8	0.7	1.2	2.0	6.5	9.5	11.3	8.9		
<b>All Data Inside 100°C Isotherm</b>																
		N =	7	7	7	7	7	7	7	7	7	7	7	7	7	7
		Mean =	8.3	9.5	8.8	9.3	10.4	11.5	12.3	14.9	19.4	29.1	50.6	55.8		
		STD =	0.5	0.6	0.4	0.2	0.3	0.8	0.8	1.2	3.0	4.7	9.4	8.6		
<b>All Data</b>																
		N =	14	14	14	14	14	14	14	14	14	14	14	14	14	14
		Mean =	8.6	9.9	9.0	9.6	10.6	11.8	12.3	15.4	21.9	33.6	57.1	54.9		
		STD =	0.5	0.7	0.6	0.6	0.6	0.7	1.0	1.7	5.5	8.6	12.0	8.5		
		95%	0.2	0.3	0.3	0.3	0.3	0.4	0.5	0.9	2.9	4.5	6.3	4.5		

Source: DTN: SNL22080196001.003 [DIRS 119042].

NOTE: N = Number of samples; STD = Standard deviation; 95% = 95% Confidence Limit; Lithostratigraphic Unit: Tptpmn; Thermal/mechanical Unit TSw2; Air dried.

Table 6.2-20. Mean Coefficients of Thermal Expansion during First Cycle Cooling of Postcooling SHT Characterization Specimens

Specimen ID	Distance from Collar (ft)	Max. Temp. (°C)	Mean CTE on Cool-Down (10 <sup>-6</sup> /°C)											
			325 to 300	300 to 275	275 to 250	250 to 225	225 to 200	200 to 175	175 to 150	150 to 125	125 to 100	100 to 75	75 to 50	50 to 30
<b>Perpendicular to Heater, Outside 100°C Isotherm (without cooling outlier PTC1-A 2.9B)</b>														
PTC1-A 2.9-B	2.9	322	12.2	16.5	31.8	21.6	67.2	35.4	22.1	15.2	13.2	15.0	11.6	11.4
PTC1-A 16.8-B	16.8	321	16.1	30.2	42.1	39.5	26.3	19.2	15.1	12.9	12.1	10.7	10.2	9.7
PTC2-B 4.1-B	4.1	321	14.9	27.8	43.8	48.0	30.1	20.4	15.6	13.3	12.3	10.8	10.2	9.6
		N =	2	2	2	2	2	2	2	2	2	2	2	2
		Mean =	15.5	29.0	42.9	43.7	28.2	19.8	15.4	13.1	12.2	10.7	10.2	9.6
		STD =	0.9	1.7	1.2	6.0	2.7	0.9	0.4	0.3	0.1	0.1	0.0	0.1
<b>Perpendicular to Heater, Inside 100°C Isotherm</b>														
PTC1-B19.0-B	19.0	322	18.8	32.2	38.3	32.9	22.9	18.0	15.0	12.7	12.3	10.3	10.2	9.1
<b>Parallel to Heater, Outside 100°C Isotherm</b>														
PTC4-A 4.6 B	4.6	321	14.2	29.3	50.7	53.8	29.6	20.7	15.8	13.7	12.6	11.5	10.4	10.4
PTC5-B 4.1-B	4.6	321	15.1	31.8	43.4	40.4	29.2	31.2	17.1	13.5	12.7	11.2	10.4	9.9
PTC5-B 24.4-B	4.6	321	19.1	29.9	35.9	32.0	21.9	16.6	14.0	11.9	11.5	10.2	9.7	9.1
PTC5-B 24.4-C	4.6	331	18.6	28.1	40.9	41.1	27.8	22.1	15.8	12.9	11.9	10.5	9.8	9.2
		N =	4	4	4	4	4	4	4	4	4	4	4	4
		Mean =	16.8	29.8	42.7	41.8	27.1	22.7	15.7	13.0	12.2	10.8	10.1	9.7
		STD =	2.5	1.5	6.1	9.0	3.6	6.2	1.3	0.8	0.6	0.6	0.4	0.6
<b>Parallel to Heater, Inside 100°C Isotherm</b>														
PTC4-A 6.8-B	6.8	318	12.2	26.6	39.0	45.8	33.5	26.0	17.5	14.0	12.2	11.9	10.4	9.8
PTC4-B 14.8-B	14.8	321	16.6	29.5	36.5	33.1	23.7	18.1	14.6	12.5	11.8	10.4	9.9	9.3
PTC4-A 19.0-B	19.0	319	16.9	29.2	38.3	34.6	23.4	17.5	13.7	12.3	11.2	9.7	9.7	10.0
PTC4-B 19.8-B	19.8	318	19.8	26.6	31.2	29.8	22.5	18.2	14.0	12.3	11.4	10.8	10.0	9.4
PTC H1-A 15.6-B	15.6	322	19.33	30.87	32.25	24.14	18.09	14.42	12.59	11.20	10.55	10.03	9.29	20.154
PTC MPBX1 14.2-B	14.2	322	17.89	30.67	39.41	33.88	23.31	18.80	15.12	12.42	11.60	10.27	9.79	8.99
		N =	6	6	6	6	6	6	6	6	6	6	6	6
		Mean =	17.1	28.9	36.1	33.6	24.1	18.9	14.6	12.5	11.5	10.5	9.9	11.3
		STD =	2.7	1.9	3.6	7.1	5.1	3.8	1.7	0.9	0.6	0.8	0.4	4.4

Table 6.2-20. Mean Coefficients of Thermal Expansion during First Cycle Cooling of Postcooling SHT Characterization Specimens (Continued)

Specimen ID	Distance from Collar (ft)	Max. Temp. (°C)	Mean CTE on Cool-Down (10 <sup>-6</sup> /°C)												
			325 to 300	300 to 275	275 to 250	250 to 225	225 to 200	200 to 175	175 to 150	150 to 125	125 to 100	100 to 75	75 to 50	50 to 30	
<b>All Data Outside 100°C Isotherm (without cooling outlier PTC1-A 2.9-B)</b>															
		N =	6	6	6	6	6	6	6	6	6	6	6	6	6
		Mean =	16.3	29.5	42.8	42.4	27.5	21.7	15.6	13.0	12.2	10.8	10.1	9.7	
		STD =	2.1	1.4	4.8	7.6	3.1	5.0	1.0	0.6	0.4	0.5	0.3	0.5	
<b>All Data Inside 100°C Isotherm</b>															
		N =	7	7	7	7	7	7	7	7	7	7	7	7	7
		Mean =	17.4	29.4	36.4	33.5	23.9	18.7	14.7	12.5	11.6	10.5	9.9	11.0	
		STD =	2.5	2.1	3.4	6.5	4.7	3.5	1.5	0.8	0.6	0.7	0.4	4.1	
<b>All Data (without cooling outlier PTC1-A 2.9-B)</b>															
		N =	13	13	13	13	13	13	13	13	13	13	13	13	13
		Mean =	16.9	29.4	39.4	37.6	25.6	20.1	15.1	12.7	11.8	10.6	10.0	10.4	
		STD =	2.3	1.8	5.1	8.2	4.3	4.4	1.4	0.8	0.6	0.6	0.3	3.0	
		95%	1.3	1.0	2.8	4.4	2.3	2.4	0.7	0.4	0.3	0.3	0.2	1.6	

Source: DTN: SNL22080196001.003 [DIRS 119042].

NOTE: N = Number of samples; STD = Standard deviation; 95% = 95% Confidence Limit; Lithostratigraphic Unit: Tptpmn; Thermal/mechanical Unit TSw2; Air dried.

Table 6.2-21. Summary Data: SHT Postcooling Characterization Unconfined Compression Tests

		Specimen ID <sup>a</sup>										
		PTC4-B 9.2	PTC4-B 4.3	PTC4-B 6.6	PTC4 11.8	PTC4 17.4	PTC4 20.9	PTC4-B 26.0	PTC2-B 10.8	PTCH1 8.6		
Date Tested		21-07-98	22-07-98	22-07-98	23-07-98	23-07-98	23-07-98	24-07-98	24-07-98	24-07-98		
Thermal / Mechanical Unit		Tsw2	Tsw2	Tsw2	Tsw2	Tsw2	Tsw2	Tsw2	Tsw2	Tsw2		
Lithostratigraphic Unit		Tptpmn	Tptpmn	Tptpmn	Tptpmn	Tptpmn	Tptpmn	Tptpmn	Tptpmn	Tptpmn		
Dry Bulk Density		2.25	2.27	2.26	2.32	2.30	2.32	2.31	2.21	2.30		
Moisture Content (%)		1.1	1.0	0.8	0.9	1.1	1.1	1.1	1.0	1.0		
Confining Pressure		0	0	0	0	0	0	0	0	0		
<b>Static Young's Modulus (GPa)</b>		<b>34.4</b>	<b>33.4</b>	<b>32.3</b>	<b>37.0</b>	<b>34.0</b>	<b>34.4</b>	<b>32.9</b>	<b>20.1</b>	<b>34.3</b>		
<b>Static Poisson's Ratio</b>		<b>0.185</b>	<b>0.168</b>	<b>0.166</b>	<b>0.259</b>	<b>0.182</b>	<b>0.187</b>	<b>0.178</b>	<b>0.251</b>	<b>0.159</b>		
<b>Peak Stress</b>		<b>175.4</b>	<b>34.3</b>	<b>113.9</b>	<b>144.9</b>	<b>240.5</b>	<b>245.7</b>	<b>191.4</b>	<b>51.8</b>	<b>80.5</b>		
<b>Axial Strain at Peak Stress</b>		<b>0.005274</b>	<b>0.001138</b>	<b>0.003637</b>	<b>0.008941</b>	<b>0.007924</b>	<b>0.007909</b>	<b>0.006003</b>	<b>0.00213</b>	<b>0.002629</b>		
		Specimen ID <sup>a</sup>										
					PTC MPBX1-B 14.4					PTC1-B 15.7		
Date Tested		27-07-98	28-07-98	29-07-98	29-07-98	30-07-98						
Thermal/Mechanical Unit		Tsw2	Tsw2	Tsw2	Tsw2	Tsw2						
Lithostratigraphic Unit		Tptpmn	Tptpmn	Tptpmn	Tptpmn	Tptpmn						
Dry Bulk Density		2.23	2.28	2.29	2.31	2.21						
Moisture Content (%)		1.3	0.9	1.1	0.9	0.9						
Confining Pressure		0	0	0	0	0						
<b>Static Young's Modulus (GPa)</b>		<b>24.2</b>	<b>34.2</b>	<b>26.6</b>	<b>35.4</b>	<b>28.9</b>						
<b>Static Poisson's Ratio</b>		<b>0.123</b>	<b>0.173</b>	<b>0.393</b>	<b>0.168</b>	<b>0.183</b>						
<b>Peak Stress</b>		<b>38.7</b>	<b>137.0</b>	<b>78.7</b>	<b>183.5</b>	<b>159.2</b>						
<b>Axial Strain at Peak Stress</b>		<b>0.002316</b>	<b>0.004349</b>	<b>0.001641</b>	<b>0.005806</b>	<b>0.005614</b>						
		<b>Statistical Summary</b>										
					Mean	Standard Deviation	Count	95% Confidence Limit				
					31.6	4.8	14	2.5				
					0.198	0.066	14	0.034				
					134.0	70.2	14	36.8				
					0.004665	0.002521	14	0.001321				

DTN: SNL22080196001.003 [DIRS 119042].

<sup>a</sup> The distance from the borehole collar (in feet) is given as part of the specimen identification number.

#### **6.2.3.4.2 Measurement Uncertainty: Laboratory Parameters—Thermal Expansion, Young’s Modulus, Poisson’s Ratio, and Peak Stress**

The uncertainty in the unconfined compressive testing of intact rock samples, which results in the measurement of Young’s modulus, Poisson’s ratio, and peak stress, includes the accuracy of the load cell, the accuracy of the LVDT, specimen alignment, changes in the specimen cross-section area during the test, specimen variation, and anisotropy of the rock. Among these factors, the greatest uncertainty is with the specimen variation. The heterogeneity in the rock mass will have significant effects on its compressive strength and moduli. Many of these uncertainties also apply to thermal expansion of intact samples. In addition, temperature control contributes to uncertainties in thermal expansion. Additional discussion of the uncertainties associated with these measurements can be found in Sections 9 and 11.2 of *Single Heater Test Final Report* (CRWMS M&O 1999 [DIRS 129261]).

#### **6.2.3.4.3 Measurement Uncertainty: Rock Mass Thermal Expansion**

Measurement uncertainty of the rock mass thermal expansion is dependent on the uncertainties of the original field measurements (MPBX displacements and temperatures), and in the discretization error associated with the available lengths over which to measure these values (primarily deviation from a constant temperature).

### **6.2.4 SHT Chemical Measurements**

This section presents the results from geochemical studies of water samples collected during the SHT and mineralogical studies of preheating borehole cores and postcooling overcores from the test block. The study of the geochemical composition of the water collected during the test provides insight into thermally driven geochemical processes. The mineralogical studies present information on the rock, providing a necessary starting point for the study of rock and water evolution with temperature and time. The aqueous geochemistry is discussed in Section 6.2.4.1. Mineralogical and petrologic studies are covered in Section 6.2.4.2.

A detailed description of SHT chemical measurements is documented in Sections 6.4 and 10 of *Single Heater Test Final Report* (CRWMS M&O 1999 [DIRS 129261]). SHT chemical measurement input DTNs and summary DTNs are listed in Tables 4-2 and 6.2-1, respectively.

#### **6.2.4.1 Aqueous Chemistry**

Samples of water were collected from borehole 16-4 (see Figure 6.2-2) on four occasions during the course of the SHT and were distributed for analysis. Water collected in the field was tested for pH, filtered to 0.45  $\mu\text{m}$ , and splits for analyses were prepared for distribution. Each field sample was also given a unique identification number, which was tracked by the Sample Management Facility (SMF). Samples were designated for analysis of metals, anions, and stable isotopes. The metals samples were stabilized by acidifying the water with  $\text{HNO}_3$  and stored in polyethylene bottles. The anion samples were also stored in polyethylene, and the stable isotope samples were stored in glass. All bottles were filled to minimize headspace and tightly capped to reduce evaporation. The samples were maintained under refrigeration at the SMF until they were shipped.

The cation analyses were performed at LLNL by Inductively Coupled Plasma (ICP) and Atomic Emission Spectroscopy (AES). Total dissolved metals of Al, B, Ca, Fe, Mg, Li, Na, K, S, Si, and Sr were measured. Anions were measured by Ion Chromatography; anions measured included F<sup>-</sup>, Cl<sup>-</sup>, Br<sup>-</sup>, NO<sub>2</sub><sup>-</sup>, NO<sub>3</sub><sup>-</sup>, PO<sub>4</sub><sup>3-</sup>, and SO<sub>4</sub><sup>2-</sup>. Bicarbonate (HCO<sub>3</sub><sup>-</sup>) was computed by charge balance, using the measured pH to indicate actual hydrogen activity at the time of sampling. The analytical aqueous chemistry results are in the TDMS under DTNs: LL970101104244.027 [DIRS 158309], LL970409604244.030 [DIRS 111481], LL970703904244.034 [DIRS 111482], and LL971006604244.046 [DIRS 148611]. These represent quarterly results for the four sampling activities. DTN: GS951108312271.006 [DIRS 169244] also contains data related to aqueous geochemistry. Note that these five DTNs are unqualified and should only be used for corroborative purposes.

#### **6.2.4.1.1 Field Sampling**

Among the boreholes instrumented with various monitoring systems shown in Figure 6.2-2, boreholes 20 (ESF-TMA-CHE-1) and 21 (ESF-TMA-CHE-2) were designed to collect aqueous chemical data from specific locations in the thermal test block. One borehole was instrumented with a suite of solid-state chemical sensors for in situ, real-time geochemical assessment of the contacting waters. Early in the SHT, however, the sensors' performance was inconsistent with the manufacturer's specifications. Subsequent laboratory testing demonstrated significant compositional dependencies; consequently, the sensors were determined unsuitable for monitoring the water chemistry. The second borehole was fitted with absorbent pads that could be collected in the field and returned to the lab for analytical testing. Several pads were removed, examined, and found to be relatively dry. Nevertheless, an extraction process was developed in which pads were soaked in de-ionized water (dilution). The process was followed by sampling and filtering the solution. A clean-pad blank was also run to provide baseline corrections (per gram weight of fabric). The resulting solution chemistries were determined to be very dilute, with a high uncertainty arising from scatter in the background contributions as well as imprecise weight corrections.

Borehole 16 (ESF-TMA-NEU-2), which was drilled and instrumented for hydrology studies (see Sections 6.2.2.3 and 6.2.2.4), proved to be important to collecting SHT water for analysis. The borehole was instrumented with a string of high-temperature, inflatable packers, which isolated four open zones. The inflated packers, which straddled fractured regions, also provided a means of containing mobilized water entering an open zone. One zone in particular, zone 4 of borehole 16 (at a depth of 3 m), yielded a significant and steady supply of water for chemical analyses starting in November 1996 and continuing throughout the heating phase of the SHT.

#### **6.2.4.1.2 Results: Aqueous Chemistry**

The results of chemical analyses for the four suites of SHT water are presented in Table 6.2-22. For comparative purposes, data from several relevant water sources (other than the SHT) have been included, and their respective sources are cited among the footnotes. The reported temperatures are those downloaded from the Data Acquisition System at time of sampling. The pH measurement is a field value taken at the time of sample collection. The one exception is for the initial sample (collected November 25, 1996); the pH value reported was for a sample measured about 30 days after collection.



Table 6.2-22 clearly shows that the SHT water is more dilute than other in situ waters from the general vicinity. Trends in the SHT water indicate that Na and Si are the dominant metals, followed by Ca, with other cations and anions in considerably lower abundances. The same general patterns are observed in both saturated and unsaturated zone waters sampled from the region. Over time, the concentrations of Na, Ca, Mg, and Sr are seen to systematically decrease, whereas all other elements exhibit nonsystematic variation. SHT waters are slightly acidic with pH values between 6.2 and 6.9. These measured pH readings may have indicated elevated CO<sub>2</sub> partial pressures in equilibrium with the water in the packed-off interval.

#### **6.2.4.1.3 Measurement Uncertainty: Aqueous Chemistry**

Input DTNs: LL970101104244.027 [DIRS 158309], LL970409604244.030 [DIRS 111481], LL970703904244.034 [DIRS 111482], LL971006604244.046 [DIRS 148611] and GS951108312271.006 [DIRS 169244] are unqualified due to a lack of data traceability. These data should only be used for corroborative purposes.

#### **6.2.4.2 Mineralogic and Petrologic Analyses**

The SHT served as a prototype test for the larger DST. Techniques were developed to produce a quantitative inventory of natural minerals in the fracture network of the test block. Continuous characterization over meter-scale distances was essential to provide estimated mineral abundances of general validity as input to numerical geochemical models of thermal tests. Collection of data on this scale also would document the existence of variability in the mineral content of the fracture network. Data for natural mineral abundances were obtained from cores drilled prior to heating. Data on stellerite abundance (fracture-surface coverage) in fractures have been submitted to the TDMS under input DTN: LA0009SL831151.001 [DIRS 153485].

The ability to identify and document test-related mineralogic reactions was a key to assessing the reliability of computational models of coupled thermal-hydrologic-chemical processes. Two types of postcooling (following heating and cooling) sampling were employed: overcoring of preheating boreholes and drilling of new continuously cored boreholes. Both coring and overcoring were performed after the field test was completed. Identification of preheating and postcooling minerals was verified by X-ray diffraction analysis (XRD), scanning-electron microscopy (SEM), and energy-dispersive X-ray (EDX) analysis. A summary of preheating fracture minerals and postcooling products can be found in the TDMS under input DTN: LA0009SL831151.001 [DIRS 153485].

Table 6.2-22. Chemistry Analysis of SHT Borehole 16-4 Waters with Reported In Situ Waters from the General Area

BH 16-4	SPC00521206 Suite 1	SPC00521245 Suite 2	SPC00521252 Suite 3	SPC00522238 Suite 4	Perched Water UZ-14 PT-4	SZ Ground- water J-13	Rainier Mesa Fractur e Water	SZ Ground- water G-4
Collection Date	11/25/96	02/04/97	02/27/97	05/22/97				
DCS Temp (°C)	N/A	46.9	47.6	51.20				
	LLNL	LLNL	LLNL	LLNL				
Na (mg/L)	16	13.9	12.20	11.00	34.0	45.8	35	57
Si (mg/L)	16.8	17.4	14.50	15.20	32.1	28.5	25	21
Ca (mg/L)	13	9.76	8.65	7.70	27.0	13	8.4	13
K (mg/L)	2.5	2.5	3.30	2.30	1.8	5	4.7	2.1
Mg (mg/L)	1.63	1.16	1.01	0.92	2.1	2.01	1.5	0.20
pH	6.2	6.9	6.80	6.55	—	7.4	7.5	7.7
HCO <sub>3</sub> (mg/L)	188	—	—	—	141.5	129	98	139
F <sup>-</sup> (mg/L)	0.44	0.12	<0.5	<0.50	—	2.18	0.25	2.5
Cl <sup>-</sup> (mg/L)	2.54	1.45	1.00	2.20	6.7	7.1	8.5	5.9
S (mg/L)	0.71	—	0.20	0.21	—	—	—	—
SO <sub>4</sub> <sup>2-</sup> (mg/L)	1.83	0.42	<2	<2	14.1	18.4	15	19
PO <sub>4</sub> <sup>3-</sup> (mg/L)	<0.03	<0.4	<2	<2	—	<10	—	—
NO <sub>2</sub> <sup>-</sup> (mg/L)	<0.01	0.15	<2	<2	—	—	—	—
NO <sub>3</sub> <sup>-</sup> (mg/L)	1.1	<0.4	<2	<2	14.5	8.8	—	—
Li (mg/L)	<0.03	<0.03	<0.01	<0.01	—	0.048	—	—
B (mg/L)	0.37	0.74	0.66	0.93	—	0.134	—	—
Al (mg/L)	<0.06	<0.06	<0.06	<0.06	0.0	0.02	—	—
Fe (mg/L)	0.74	0.13	0.30	0.03	—	—	—	—
Sr (mg/L)	0.2	0.14	0.12	0.11	—	0.04	—	—
Br <sup>-</sup> (mg/L)	<0.02	<0.4	<2	<2	0.1	—	—	—
δ D	-101.7	-99.6	—	—	-97.3	-98	—	-103
δ <sup>18</sup> O	-12.9	-12.9	—	—	-13.4	-13	—	-13.8
Tritium	0.44 ± 0.19 TU	—	—	—	0.0	—	—	—
<sup>87</sup> Sr/ <sup>86</sup> Sr	—	0.7124	—	—	—	—	—	—

DTNs: LL970101104244.027 [DIRS 158309]; LL970409604244.030 [DIRS 111481]; LL970703904244.034 [DIRS 111482]; LL971006604244.046 [DIRS 148611]; GS951108312271.006 [DIRS 169244].

NOTE: All data in this table are considered unqualified and should only be used for corroborative purposes.

### 6.2.4.2.1 Results: Mineralogy of the Preheating Natural Fracture System

Time constraints precluded completion of an inventory for all fracture-coating minerals. Instead, a survey of stellerite abundance in macroscopically visible fractures was undertaken for preheating drill core MPBX-1 (borehole 2 as shown in Figure 6.2-2). Stellerite, a zeolite, was chosen because it can be identified with a high level of confidence based on stereomicroscopic examination. Visual-recognition criteria of crystal morphology, luster, and hardness were verified by XRD of typical deposits. Because stellerite is a major fracture-coating mineral in the SHT block, quantification of its abundance was especially useful input for geochemical modeling.

The survey was conducted piece by piece for the MPBX-1 core. For each fracture, the percent of fracture surface covered by stellerite was estimated by comparison with standard abundance diagrams like those of Compton (1962 [DIRS 101588], pp. 332 to 333). The observed or calculated coverage of a fracture by stellerite is defined for this estimation as an attribute shared by the opposing surfaces of an intact fracture. For partly sealed fractures, the estimated percent stellerite coverage of nonsealed fracture area was treated as an attribute of the entire fracture. Matching fracture faces at the ends of adjacent core pieces count as a single fracture, with percent zeolite coverage equal to the higher of the values estimated for each face. The results of this inventory are presented in Table 6.2-23.

Table 6.2-23. SHT Stellerite Abundance on Fractures, Preheating Drill Core ESF-TMA-MPBX-1

<b>Total number of fractures examined</b>	75
<b>Number of fractures with stellerite</b>	58
<b>Average percent coverage of fractures by stellerite</b>	31%
Drill hole characteristics: 7 m long, 0.5° dip toward bottom of hole (eastward) Core interval examined: 0 to 4.33 m, minus 0.49 m unrecovered or removed for thermal/mechanical measurements	

Source: DTN: LA0009SL831151.001 [DIRS 153485].

Additional natural-fracture minerals, as identified by XRD in two samples from drill core ESF-TMA-H-1 (borehole 1 as shown in Figure 6.2-2), include smectite, feldspar, and quartz (Tables 6.2-24 and 6.2-25).

Table 6.2-24. Summary Descriptions of SHT Natural-Fracture Mineral and Test-Product XRD Samples

Sample Identifier	Borehole	Depth (ft)	Description of Sample
LANL 3052, p1	1	2.3 to 2.4	Natural fracture coating. Centimeter-scale vapor-phase pocket with zeolite-cemented breccia. Sample is mostly zeolite, with some brecciated tuff.
LANL 3054, p1	1	13.0 to 13.2	Natural fracture coating, ~0.1 mm thick, of microcrystalline zeolite, deposited directly on smooth, planar cooling-joint surface.
LANL 3006, p1	16	16.5 to 17.0	Test products, small white mounds on original borehole surface with minor bedrock impurities, orientation of sample unknown.
LANL 3004, SSL08p1	16	15.5 to 16.5	Post-test sample, outermost 0.5 mm of original borehole surface, orientation of sample site unknown.
LANL 3003	16	12.0 to 12.1	Test products, cohesive brownish particulate layer peeled from bottom of original preheating borehole.
LANL 3000, SSL02	2	2.9 to 3.4	Test products, silica scale, maximum thickness 0.2 mm, on bottom of original borehole surface. Impurities of bedrock and brownish particulates.

Source: DTN: LA0009SL831151.001 [DIRS 153485].

Table 6.2-25. Semiquantitative XRD Identification of SHT Natural-Fracture Minerals and Test Products

Sample Identifier	Borehole	Depth (ft)	Smectite	Zeolite	Amorphous	Calcite	Gypsum	Feldspar	Tridymite	Cristobalite	Quartz	Hematite	Other
<b>Natural Fracture Minerals</b>													
LANL 3052, p1	1	2.3 to 2.4	minor	major <sup>a</sup>	—	—	—	minor	—	—	major	—	—
LANL 3054, p1	1	13.0 to 13.2	trace	major <sup>a</sup>	—	—	—	—	—	—	—	—	—
<b>Test Products</b>													
LANL 3006, p1	16	16.5 to 17.0	—	minor	major <sup>b</sup>	major	minor	minor	—	—	trace	—	minor <sup>c</sup>
LANL 3004, SSL08p1	16	15.5 to 16.5	minor	minor	—	minor	minor	major	—	major	major	trace	major Al metal
LANL 3003	16	12.0 to 12.1	trace	trace	—	minor	—	major	minor	major	major	—	—
LANL 3000, SSL02	2	2.9 to 3.4	minor	—	minor <sup>b</sup>	minor	—	major	minor	major	major	minor	minor mica

Source: DTN: LA0009SL831151.001 [DIRS 153485].

<sup>a</sup> Stellerite.

<sup>b</sup> Identified on the basis of XRD and SEM-EDX as opal-A.

<sup>c</sup> Unidentified mineral, possibly a sulfate-bearing phase.

NOTE: Approximate limits of semiquantitative descriptors, all in wt %: major = >20%, minor = <20%, trace = <1%, "—" = not detected.

#### 6.2.4.2.2 Results: Evidence of Mineral Deposition

Alteration products of the SHT resulting from fluid/rock interaction have been identified in the overcores of borehole 16 (ESF-TMA-PTC-NEU-2) and borehole 2 (ESF-TMA-PTC-MPBX-1). The new mineral deposits are of three general varieties, described here from the occurrences in the ESF-TMA-PTC-NEU-2 borehole. This borehole was inclined upward from the surface of the test block, so that the “bottom” of the borehole was above the heater. Water that entered the borehole from fractures near the bottom flowed downslope along the wellbore. Small white mounds and patches,  $\leq 1$  mm across, of gypsum  $\pm$  calcite  $\pm$  opal-A are present on natural fracture surfaces and preheating borehole 16 surfaces near the bottom of the ESF-TMA-PTC-NEU-2 overcore. Some of the mounds are concentrated along the traces of very tight fractures intersecting the borehole or fracture surfaces on which the mounds were deposited. Glassy scale deposits, mostly silica, are especially abundant on the bottom of the preheating borehole 2. Some scale deposits take the form of dried drip marks on the sides of the borehole.

##### Gypsum

The identification of gypsum is based on XRD of white deposits from preheating borehole surface and adjoining fractures in the 15.5- to 16.5-ft (4.72- to 5.03-m) interval of ESF-TMA-PTC-NEU-2. Only one core fragment contained enough material to collect about a milligram for XRD analysis. Smaller deposits on other core pieces are identified as gypsum on the basis of similar crystal morphology observed in SEM images and the Ca+S peaks in the energy-dispersive X-ray spectrum.

##### Opal-A and Other Silica

Opal-A in the white deposits from PTC-NEU-2 (preheating overcore borehole 16) was identified by a combination of XRD and SEM-EDX. A broad peak, characteristic of structurally amorphous material, was observed in the XRD pattern from the white deposits. SEM-EDX examination of the deposits revealed the presence of nearly pure silica (Si peak on the EDX spectrum) in portions of the deposits with no discernible crystal form.

Some opal-rich areas of the white mounds contain masses of minute silica tubules projecting up to about 5  $\mu\text{m}$  from the surface of the deposit. A few tubules are straight, but most have variably tortuous shapes. Outside diameters of the tubules range from about 0.3 to 0.7  $\mu\text{m}$ , whereas inside diameters vary from less than 0.1 to about 0.3  $\mu\text{m}$ .

Deposits of glassy silica scale  $\leq 0.2$  mm thick were observed on the preheating wellbore surface of ESF-TMA-PTC-MPBX-1, a horizontal borehole close to the heater borehole. There is a 2- to 3-cm-wide zone of silica deposition along what is inferred to be the bottom of the wellbore surface. In addition, silica scale deposits define elongated drip marks on the inferred lower half of the wellbore surface. The silica scale generally consists of two texturally distinct components. At the base of the deposits are aggregates of platy silica particles about 1 to 5  $\mu\text{m}$  across, silica rods 1 to 2  $\mu\text{m}$  across and up to about 15  $\mu\text{m}$  long, and a few round particles 1 to 2  $\mu\text{m}$  across. Overlying the silica particles are cracked silica sheets about 2  $\mu\text{m}$  thick. The siliceous composition of the scale was documented by EDX.

Sampling the silica scale for mineralogic analysis was complicated by the small quantities of material and the difficulty in removing the scale from the wellbore surface while minimizing the incorporation of bedrock. Some of the thickest scale deposits were laid down on top of 0.1-mm-thick fine particulate layers, to which the scale adheres. The milligram sample collected for XRD was estimated by visual examination to contain about 20% silica scale. Because of the high impurity content, identification of the scale mineralogy on the basis of XRD is very uncertain. Of the silica phases identified in the sample (cristobalite, quartz, tridymite, and opal-A), the opal-A is most likely to be solely a test product. The ESF-TMA-MPBX-1 borehole (borehole 2), where this material was deposited, was heated to more than 150°C during the test. In comparison, the maximum temperature was slightly less than 80°C (DTN: SN0401F3511695.012 [DIRS 169262]) in borehole 16 where opal-A without platy morphology was deposited.

### Calcite

Calcite has been documented by XRD as a constituent of the white mounds deposited on natural fracture surfaces and on the preheating borehole surface of overcore ESF-TMA-PTC-NEU-2 (borehole 16) in the 15.5- to 17.0-ft (4.72- to 5.18-m) interval. The mineral is also part of the thin, nearly invisible coatings present on the preheating wellbore surface in the same interval. A thin, brown particulate deposit on the bottom of the wellbore also contains calcite. In overcore ESF-TMA-PTC-MPBX-1, calcite occurs with silica scale, fine particulate deposits, or other deposits on the preheating wellbore. Discrete calcite crystals have not been documented by SEM-EDX studies of these deposits, due perhaps to spectroscopic interference from other calcium-rich phases such as gypsum and stellerite, or to overgrowths of other minerals.

#### **6.2.4.2.3 Measurement Uncertainty: Mineralogic and Petrologic Analyses**

A formal error analysis was not performed for the exploratory research technique employed to obtain the stellerite abundance in fractures presented in Table 6.2-23. The principal sources of error lie in estimating the percent zeolite coverage of a fracture and in estimating the portion of a fracture sealed by vapor-phase minerals. The loss of small amounts of core on account of nonrecovery or sample removal is an additional source of uncertainty not related to errors of measurement.

#### **6.2.5 SHT Miscellaneous Measurements and Observations**

This section discusses additional SHT measurements not covered in the prior four SHT sections. Specifically, fracture mapping, infrared imaging, and borehole video logging are discussed. Detailed discussion on these measurements is documented in *Characterization of the ESF Thermal Test Area* (CRWMS M&O 1996 [DIRS 101428]). SHT miscellaneous measurement input DTNs and associated summary DTNs are listed in Tables 4-2 and 6.2-1, respectively.

### 6.2.5.1 Fracture Mapping

The objective of geologic mapping in the SHT area was to determine the vertical and horizontal variability of fracture networks, to characterize any faults and fault zones, to map the lithostratigraphic features of geologic subunits and the abundance and character of lithophysal zones, and to assist in selection of test locations. Two data collection techniques were used: full-periphery mapping and detailed line surveys.

Mapping in the Thermal Test Alcove was carried out by the U.S. Geological Survey (USGS) and the U.S. Bureau of Reclamation (USBR). It was done essentially to the same standards used in the ESF main drift, using Technical Procedure NWM-USGS-G-32, R0. From these procedures, the USGS/USBR used full-periphery mapping techniques and detailed line surveys to characterize the rock and fractures in the alcove.

Geologic mapping included recording lithostratigraphic and structural features on 1:125 scale drawings. Maps were developed in the full-periphery style, in which the tunnel walls were unrolled to produce a flat map of the tunnel periphery. Discontinuities and lithostratigraphic contacts with trace lengths longer than 1 m were recorded on the field sheets. The orientation of geologic features was determined using a goniometer for strike azimuth and a Brunton compass for dip values. Discontinuity orientations were recorded using the right-hand rule, where dip direction is 90 degrees to the right (clockwise) of strike. Traces of lithostratigraphic and structural features were sketched onto the geologic drawings and later digitized with AutoCAD.

Detailed discussion, including a full-periphery geotechnical map for Alcove 5, is presented in Section 7 of the report entitled *Characterization of the ESF Thermal Test Area* (CRWMS M&O 1996 [DIRS 101428]).

#### 6.2.5.1.1 Results: Fracture Mapping

Thermal Test Alcove 5 was excavated at Station 28+27, near the base of the ESF north ramp and at the beginning of the main drift. It was excavated in an easterly direction off the north-south trending main drift and at a downward angle of approximately 10 to 15°.

The lithology of the unit consists of densely welded, devitrified tuff of rhyolitic composition, containing vapor-phase minerals and about 1% phenocrysts, chiefly feldspar and biotite. Lithophysae are rare (less than 1%), and range in size up to 80 mm, with vapor-phase minerals and very light gray rims and spots. Short (10 to 20 cm), discontinuous, subhorizontal vapor phase partings are present throughout the unit, while the more developed subhorizontal partings form bedding plane features on the order of meters apart.

Fractures in this unit are generally moderately to widely spaced (30 cm to 2 m), slightly to moderately continuous (1 m to 10 m), and slightly open to tight. A series of low angle shears strikes through the area of the alcove in an east-west direction and dips to the north. These shears form local subhorizontal breccia zones or wedges where they intercept the more predominant vapor phase partings and bedding planes.



Results of detailed line surveys indicated three prominent joint sets in the Thermal Test Facility. These joint sets correspond to similar sets observed in the Tptpmn in the main drift. Joint Set 1 (JS1) and Joint Set 2 (JS2) are both near vertical, relatively long (3 to 4 m in length), had relatively smooth surfaces (Brown 1981 [DIRS 102003], pp. JRC 4 to JRC 6), and relatively small variations in amplitudes normal to the joint surfaces (0.05 to 0.2 m). Joint apertures are typically 1 to 2 mm, open, and with little or no infilling. Joint Set 1 has a dip direction of approximately 40° and a dip angle of 70° to 85°. Joint Set 2 has a dip direction of approximately 130° and a dip angle of 70° to 90°. Joint Set 1 and 2 are difficult to observe because their orientation was subparallel to the walls.

Joint Set 3 (JS3) is a relatively low-angle vapor-phase parting surface, with a dip direction of approximately 300° and a dip angle of 15° to 40°. Compared to Joint Set 1 and Joint Set 2, the parting surfaces of Joint Set 3 are generally shorter (1.0 m to 1.3 m), have more irregular surfaces (Brown 1981 [DIRS 102003], pp. JRC 10 to JRC 16), and have larger variations in amplitudes normal to the joint surfaces (0.2 m to 0.3 m). The apertures for Joint Set 3 are generally wider, 3 to 5 mm, and are filled with vapor-phase calcite and quartz and occasionally Fe-Mn oxides. The joint density is approximately seven fractures per cubic meter.

#### **6.2.5.1.2 Measurement Uncertainty: Fracture Mapping**

Uncertainty associated with SHT fracture mapping is similar to that discussed in Section 6.1.4.1.2.

#### **6.2.5.2 Infrared Imaging**

The objective of infrared imaging of rock surfaces prior to the onset of heating was to establish the initial conditions on the drift walls around the SHT region, specifically the temperature distributions at the outlets of potential pathways for fluids. During the heating period, thermally induced flow can change the wall temperature. A set of reconnaissance surveys was conducted on April 11 and 12, 1996, after excavation of the drifts around the SHT region. Similar images were taken on other walls surrounding the SHT region and on the ceilings. Additional surveys were also carried out in June 1996, with essentially uniform temperatures on the walls observed. These images were digitized and later compared with the images taken at the same location during and following the SHT heating phase. For the end wall of the alcove extension, an aluminum grid was installed on the wall so that human body heat would not distort the infrared images in later surveys.

Detailed discussion of SHT infrared imaging is presented in Section 9.2 of *Characterization of the ESF Thermal Test Area* (CRWMS M&O 1996 [DIRS 101428]) and Section 8.4 of *Single Heater Test Final Report* (CRWMS M&O 1999 [DIRS 129261]). SHT infrared images and accompanying data may be found in input DTNs: LB970700123142.002 [DIRS 158295] and LB980120123142.001 [DIRS 158297].

#### **6.2.5.2.1 Results: Infrared Imaging**

Wet (cool) surfaces appear in infrared images near the invert where some remaining muck is piled against the wall. In the corresponding infrared images, the muck pile is colder than the wall surface above. On the wall, there are slightly cooler areas corresponding to the apparently wet areas. “Hot” spots show up in the infrared images of the SHT wall above and below the mid-height between the invert and the drift crown.

The “hot” spots in the rock could be associated with pathways through the rock masses behind the wall. The pneumatic pathways are likely along heterogeneous channels through the fracture network and exit at “spots.”

#### **6.2.5.2.2 Measurement Uncertainty: Infrared Imaging**

Uncertainty in the infrared measurements includes parallax changes to the images, subjective interpretation of temperature differences along the surface of the image, and natural variations along a surface.

#### **6.2.5.3 Borehole Video Logging**

The objective of borehole video logs was to provide descriptive visual information from boreholes in the DST block and to supplement other available characterization data. Borehole video logs were also used to help select appropriate depths for packer settings for air permeability testing.

The borehole television camera consists of the downhole video camera system, monitor, and VCR. The TV/VCR was first configured to record, and then the camera was inserted into the borehole. The camera was paused as needed. The videotape was viewed to ensure visibility and adequacy. The process was repeated if the video information was inadequate. Any unusable entries or videos were identified as inadequate. The following information was recorded in the scientific notebook: borehole identifier, date, measuring and test equipment serial numbers if applicable, the location of the zero datum point, traceability between the notebook and the video, depth-correction measurements if applicable, and the total depth reached.

#### **6.2.5.3.1 Results: Borehole Video Logging**

Borehole video logs provide visual information regarding fractures, including aperture size, fracture frequency, and fracture orientation. Video logs, which are documented by Mitchell (1996 [DIRS 159518]), include visual descriptions of the boreholes in the SHT region.

#### **6.2.5.3.2 Measurement Uncertainty: Borehole Video Logging**

These observations are inherently subjective, and determination of orientation and location may be subjected to multiple interpretations.

### 6.3 DRIFT SCALE TEST

The Drift Scale Test (DST) is the third and largest of the in situ thermal tests planned and conducted to investigate coupled processes in the local rock-mass surrounding the repository. These coupled processes are thermally driven by heat released from electrical heaters that simulate heat from emplaced nuclear waste. A block of rock, approximately 60 m wide, 50 m deep, and 50 m high, includes 9 floor/canister heaters in a 5-m-diameter drift and 50 wing heaters installed in horizontal boreholes drilled perpendicular to the drift into the rock. Numerous sensors located in the DST block measure thermal-hydrological-mechanical-chemical behavior. The heating of the DST began on December 3, 1997, and continued through January 14, 2002. As of that date, the test entered a planned 4-year cooling phase that concluded on January 14, 2006. Heaters were turned off and the heat in the test block was allowed to dissipate without recourse to deliberate ventilation. A detailed description of the DST is provided in the following two reports: *Drift Scale Test Design and Forecast Results* (CRWMS M&O 1997 [DIRS 146917]) and *Drift Scale Test As-Built Report* (CRWMS M&O 1998 [DIRS 111115]).

DST input DTNs are tabulated in Table 4-3. DST summary DTNs are tabulated in Table 6.3-1.

The general layout and plan view of the Exploratory Studies Facility (ESF) Thermal Test Facility and DST area are shown in Figures 6.2-1 and 6.3-1. The configuration for the DST, as shown in Figure 6.2-1, includes a declining observation drift driven mostly east in a downward slope. The breakout, near the intersection of the ESF north ramp and main drift, is 2,827 m from the north ramp portal. The downward slope of the observation drift ensures a minimum 10 m of Tptpmn rock (Tertiary (Period), Paintbrush (Group), Topopah Spring Tuff (Formation), Crystal-Poor (Member), Middle Nonlithophysal (Zone)) overlying the DST heated drift. The Tptpmn represents one of the three geologic units targeted to host the repository. The Auxiliary Testing Niche is located along the observation drift as shown in Figure 6.3-1. Although not denoted, the Data Collection System Niche is located at the far right of the observation drift as it is shown in Figure 6.3-1.

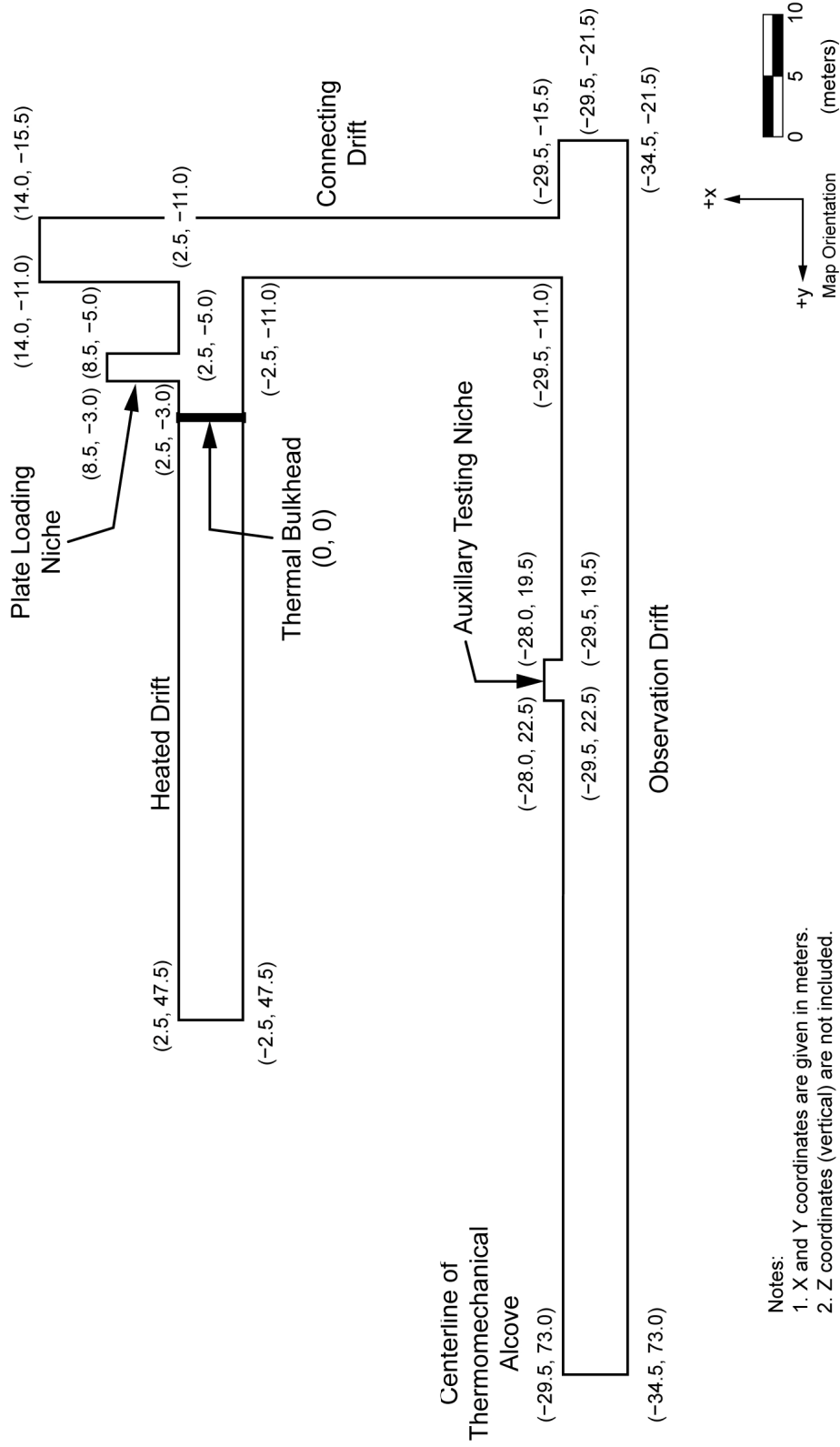
Figure 6.3-1 shows that the DST includes a 47.5-m-long, 5-m-diameter heated drift. The heated drift is complemented by an 11-m-long entry from the connecting drift of similar diameter. Other components include plate loading and Data Collection System (DCS) niches. Figures 6.3-2 through 6.3-8 provide three-dimensional perspectives of the thermal, mechanical, hydrological, and chemical boreholes. Since some boreholes contain multiple types of sensors, only the primary usage of the borehole was highlighted. The boreholes are color coded to identify the wing heaters and the primary processes (thermal, hydrological, mechanical, chemical) measured in each of the 147 boreholes. The DST borehole numbering system begins at 42 because the initial 41 boreholes correspond to the Single Heater Test (which is co-located in the Thermal Test Facility).

The as-built locations of the 147 boreholes drilled into the DST block are listed in Table 6.3-2. All coordinates are based on a local right-hand coordinate system in which 0,0,0 is the center of the bulkhead on the cool side. The positive X-, Y-, and Z-directions are generally northward (away from the observation drift), westward (away from the connecting drift), and upward, respectively. The last 12.5 m of the heated drift (starting from Y = 35 m) is lined with concrete

in order to evaluate the feasibility of concrete liner as ground support for waste emplacement drifts in the repository.

The DST DCS recorded thermal, hydrological (partial), and mechanical data, for the most part on an hourly basis. The acquired data consists of both original (measured electronic values) and converted (engineering units) data.

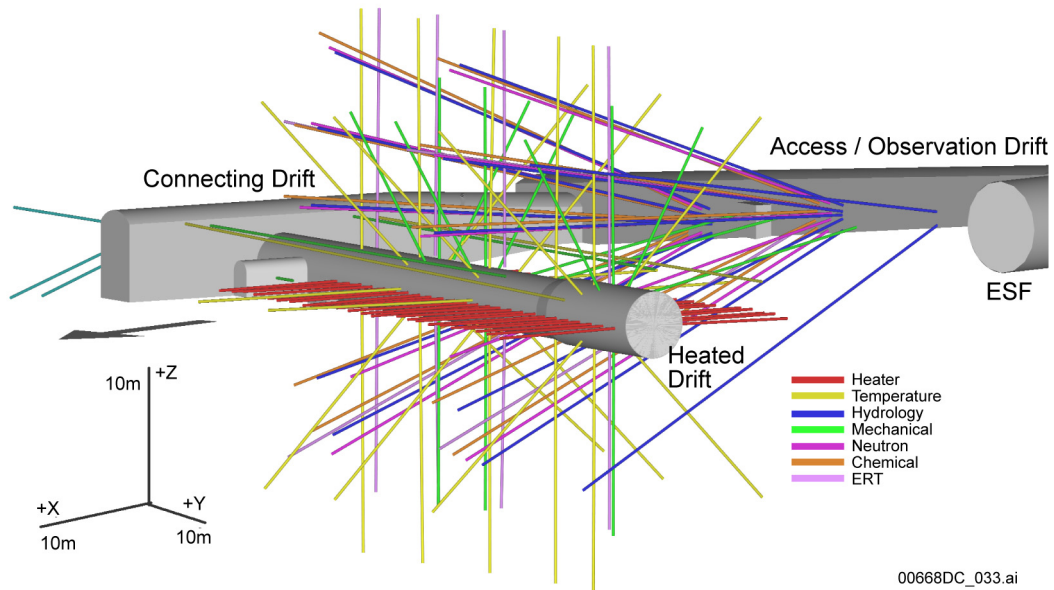
The DCS DTNs were reviewed and restructured and periodically submitted to the Technical Data Management System (TDMS), resulting in many of the input DTNs introduced below and listed in Table 4-3. As discussed in Section 1 and the introduction to Section 6, these input DTNs were further refined, reduced, and restructured and then resubmitted to the TDMS as summary DTNs (see Table 6.3-1). As mentioned in Section 6.1, the end user has access to three levels of data for DST thermal, hydrological (partial), and mechanical measurements: DCS DTNs, input DTNs, and summary DTNs.



- Notes:
1. X and Y coordinates are given in meters.
  2. Z coordinates (vertical) are not included.
  3. Only key locations are provided.
  4. Coordinates are based on design with the following as-builts tolerances:  
 Horizontal alignment = 0 to + 0.5m  
 All other = -0 to = 0.3m

Source: CRWMS M&O 1998 [DIRS 111115], Section 3.1.

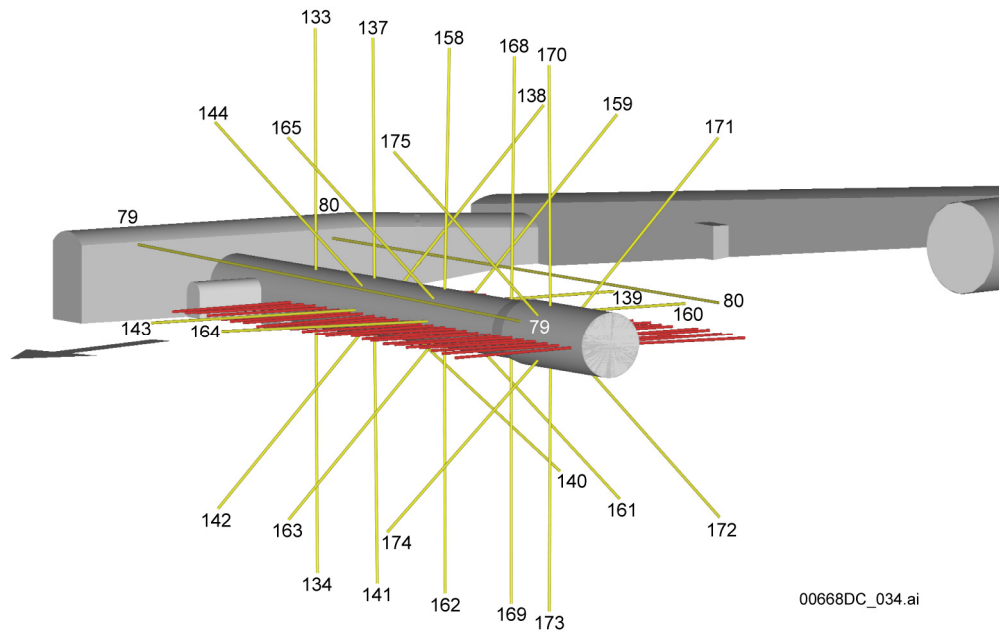
Figure 6.3-1. DST As-Built Plan View with Two-Dimensional Coordinates of Key Locations



Source: DTN: MO0002ABBLSLDS.000 [DIRS 147304].

NOTE: Schematic is prepared from coordinates based on an origin located at the center of the heated drift bulkhead.

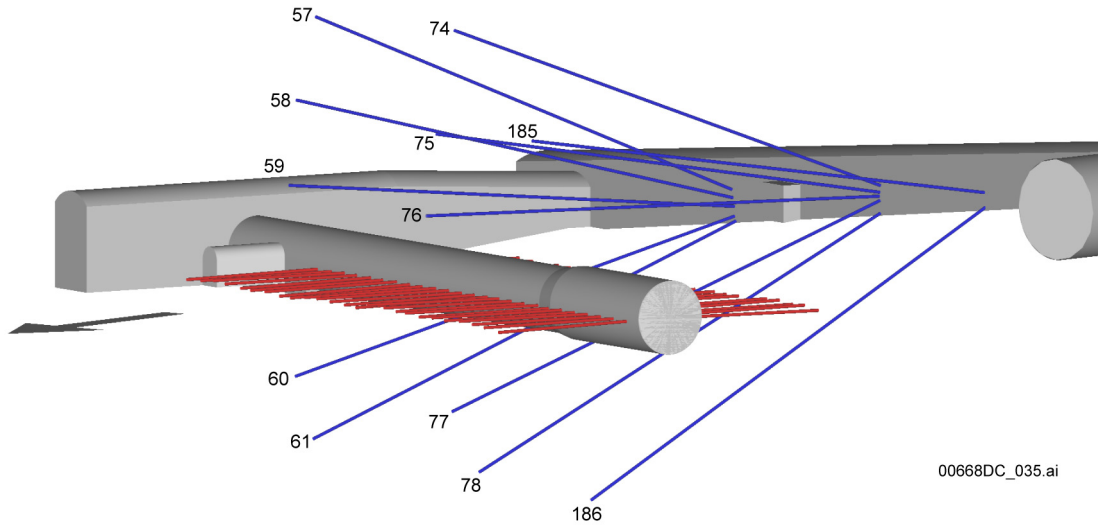
Figure 6.3-2. Drifts and Boreholes of the DST



Source: DTN: MO0002ABBLSLDS.000 [DIRS 147304].

NOTE: Schematic is prepared from coordinates based on an origin located at the center of the heated drift bulkhead.

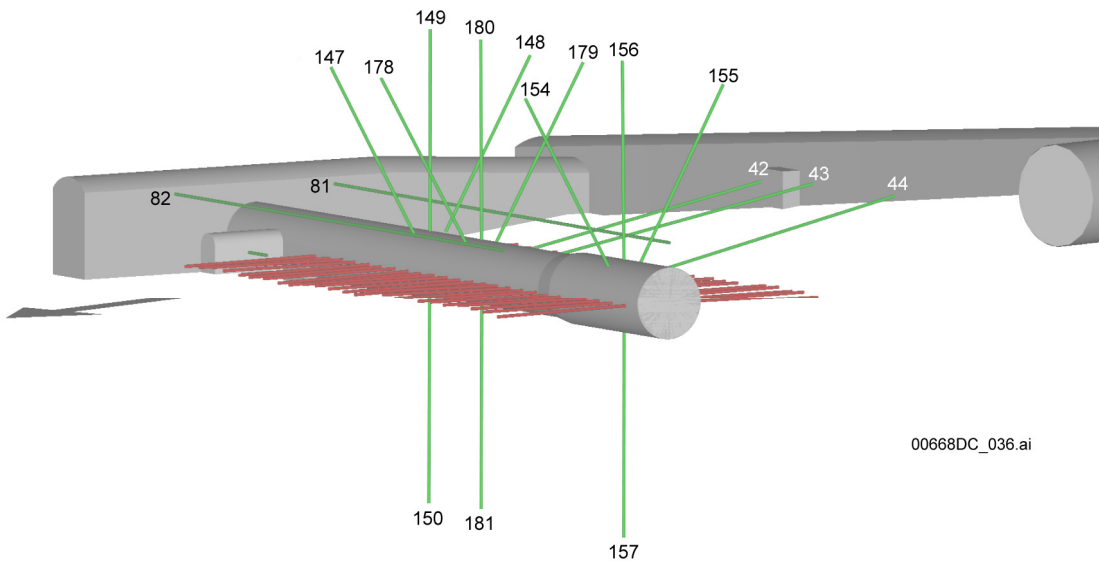
Figure 6.3-3. Temperature (RTD) Boreholes of the DST



Source: DTN: MO0002ABBLSLDS.000 [DIRS 147304].

NOTE: Schematic is prepared from coordinates based on an origin located at the center of the heated drift bulkhead.

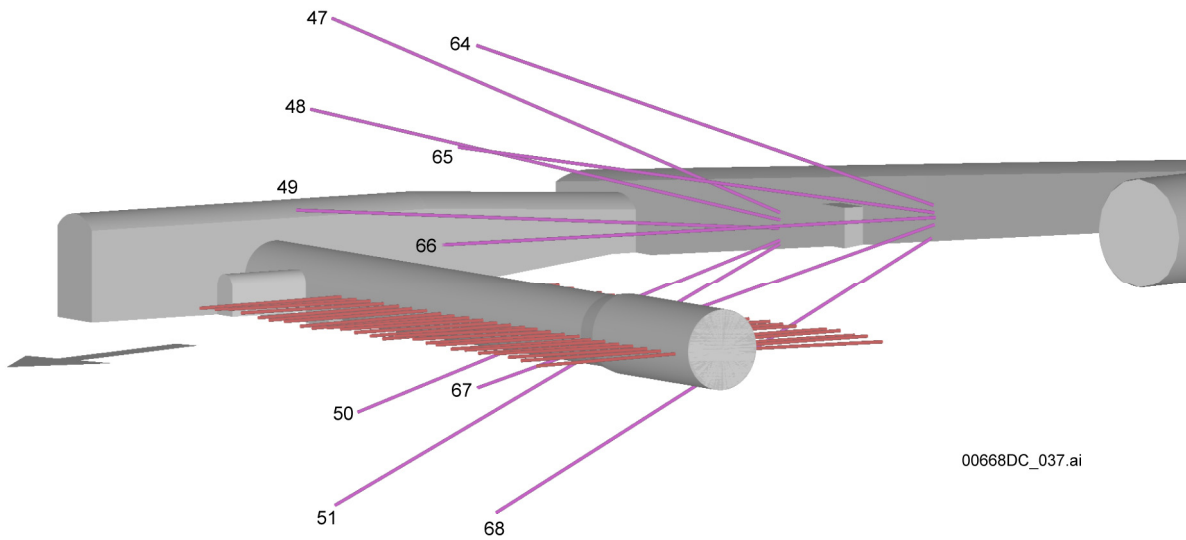
Figure 6.3-4. Hydrology Boreholes of the DST



Source: DTN: MO0002ABBLSLDS.000 [DIRS 147304].

NOTE: Schematic is prepared from coordinates based on an origin located at the center of the heated drift bulkhead.

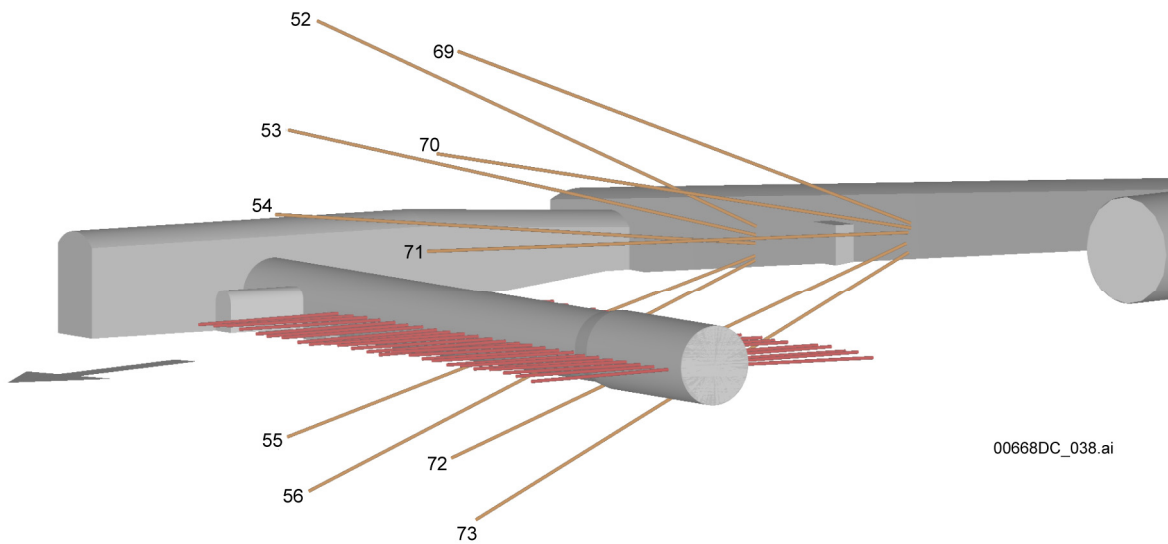
Figure 6.3-5. Mechanical (MPBX) Boreholes of the DST



Source: DTN: MO0002ABBLSLDS.000 [DIRS 147304].

NOTE: Schematic is prepared from coordinates based on an origin located at the center of the heated drift bulkhead.

Figure 6.3-6. Neutron GPR Boreholes of the DST

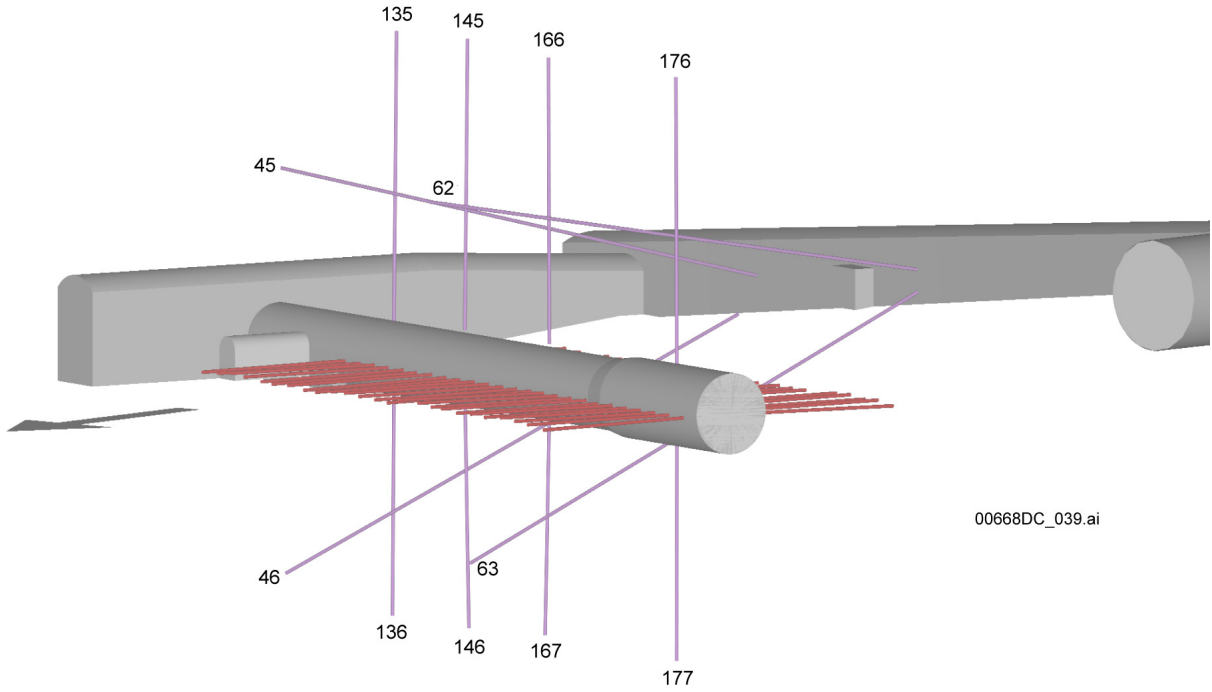


Source: DTN: MO0002ABBLSLDS.000 [DIRS 147304].

NOTE: Schematic is prepared from translated coordinates based on an origin located at the center of the heated drift bulkhead.

Figure 6.3-7. Chemical (SEAMIST) Boreholes of the DST





Source: DTN: MO0002ABBLSLDS.000 [DIRS 147304].

NOTE: Schematic is prepared from translated coordinates based on an origin located at the center of the heated drift bulkhead.

Figure 6.3-8. ERT Boreholes of the DST

Table 6.3-1. DTNs for the Drift Scale Test

Input DTN	Input DTN Description	Input DTN Text Location	Summary DTN	Summary DTN Description
LA908FH6001WP.001 <sup>a</sup> [DIRS 158319]	Data Collection System data	6.3	Unchanged DTN	Unchanged DTN
LA0111FH831151.002 <sup>a</sup> [DIRS 158317]	Data Collection System data	6.3	Unchanged DTN	Unchanged DTN
LA0208FH831151.001 <sup>a</sup> [DIRS 159515]	Data Collection System data	6.3	Unchanged DTN	Unchanged DTN
LA0208FH831151.002 <sup>a</sup> [DIRS 159308]	Data Collection System data	6.3	Unchanged DTN	Unchanged DTN
LA0108FH831151.001 <sup>a</sup> [DIRS 158316]	Data Collection System data	6.3	Unchanged DTN	Unchanged DTN
LA0111FH831151.001 <sup>a</sup> [DIRS 169386]	Data Collection System data	6.3	Unchanged DTN	Unchanged DTN
LA0111FH831151.003 <sup>a</sup> [DIRS 158318]	Data Collection System data	6.3	Unchanged DTN	Unchanged DTN
MO0002ABBLSDS.000 [DIRS 147304]	XYZ coordinates of boreholes and sensors	6.3	Unchanged DTN	Unchanged DTN
MO9807DSTSET01.000 [DIRS 113644]	Heater, power, current, voltage, temperature: November 7, 1997, to May 1998	6.3.1.1 6.3.1.2	MO0208RESTRDST.002 [DIRS 161129]	Heater power and temperature data
MO9810DSTSET02.000 [DIRS 113662]	Heater, power, current, voltage, temperature: June 1998 to August 1998	6.3.1.1 6.3.1.2		
MO9906DSTSET03.000 [DIRS 113673]	Heater, power, current, voltage, temperature: September 1998 to May 1999	6.3.1.1 6.3.1.2		
MO0001SEPDSTPC.000 [DIRS 153836]	Heater, power, current, voltage, temperature: June 1999 to October 1999	6.3.1.1 6.3.1.2		
MO0007SEPDSTPC.001 [DIRS 153707]	Heater, power, current, voltage, temperature: November 1999 to May 2000	6.3.1.1 6.3.1.2		
MO0012SEPDSTPC.002 [DIRS 153708]	Heater, power, current, voltage, temperature: June 2000 to November 2000	6.3.1.1 6.3.1.2		
MO0107SEPDSTPC.003 [DIRS 158321]	Heater, power, current, voltage, temperature: December 2000 to May 2001	6.3.1.1 6.3.1.2		
MO0202SEPDSTTV.001 [DIRS 158320]	Heater, power, current, voltage, temperature: June 2001 to January 14, 2002	6.3.1.1 6.3.1.2		

Table 6.3-1. DTNs for the Drift Scale Test (Continued)

Input DTN	Input DTN Description	Input DTN Text Location	Summary DTN	Summary DTN Description
MO0208SEPDSTTD.001 [DIRS 161767]	DST temperature data for January 15, 2002 through June 30, 2002	6.3.1.2	Unchanged DTN	Unchanged DTN
MO0303SEPDSTTM.000 [DIRS 165698]	DST temperature data for July 1, 2002 through December 31, 2002	6.3.1.2	Unchanged DTN	Unchanged DTN
MO0307SEPDST31.000 [DIRS 165699]	DST temperature data for January 1, 2003 through June 30, 2003	6.3.1.2	Unchanged DTN	Unchanged DTN
MO0403SEPDST32.000 [DIRS 177813]	DST temperature data for July 1, 2003 through December 31, 2003	6.3.1.2	Unchanged DTN	Unchanged DTN
MO0408SEPDSTTD.000 [DIRS 177814]	DST temperature data for January 1, 2004 through June 30, 2004	6.3.1.2	Unchanged DTN	Unchanged DTN
MO0509SEPDSTTD.000 [DIRS 177815]	DST temperature data for July 1, 2004 through June 30, 2005	6.3.1.2	Unchanged DTN	Unchanged DTN
MO0603SEPDSTTD.000 [DIRS 177816]	DST temperature data for July 1, 2005 through December 31, 2005	6.3.1.2	Unchanged DTN	Unchanged DTN
MO0603SEPDSTTB.002 [DIRS 178054]	DST temperature borehole RTD status as of December 31, 2005	6.3.1.2.3	Unchanged DTN	Unchanged DTN
SNL22100196001.006 [DIRS 158213]	Thermal conductivity as function of saturation	6.3.1.3	Unchanged DTN	Unchanged DTN
SN0203L2210196.007 [DIRS 158322]	Thermal expansion thermal conductivity DST specimens	6.3.1.3	Unchanged DTN	Unchanged DTN
LL980411004244.060 [DIRS 159107]	DST baseline REKA probe measurements. Temperature measurements using REKA probes: November 14, 1997, to July 31, 1998	6.3.1.4	Unchanged DTN	Unchanged DTN
LL980411104244.061 [DIRS 159111]	DST baseline REKA probe measurements for thermal conductivity and diffusivity. VA-supporting data	6.3.1.4	Unchanged DTN	Unchanged DTN
LL980902104244.070 [DIRS 159109]	DST baseline REKA probe measurements for thermal conductivity and diffusivity: probe 1 from borehole 153, probe 2 from borehole 152, probe 3 from borehole 151	6.3.1.4	Unchanged DTN	Unchanged DTN
UN0106SPA013GD.003 [DIRS 159115]	DST REKA probe acquired data for thermal conductivity and diffusivity: May 1, 1998, to April 30, 2001	6.3.1.4	Unchanged DTN	Unchanged DTN

Table 6.3-1. DTNs for the Drift Scale Test (Continued)

Input DTN	Input DTN Description	Input DTN Text Location	Summary DTN	Summary DTN Description
UN0109SPA013GD.005 [DIRS 159117]	DST REKA probe acquired data for thermal conductivity and diffusivity: May 1, 2001, to August 31, 2001	6.3.1.4	Unchanged DTN	Unchanged DTN
UN0112SPA013GD.006 [DIRS 159118]	DST REKA probe acquired data for thermal conductivity and diffusivity: September 1, 2001, to December 31, 2001	6.3.1.4	Unchanged DTN	Unchanged DTN
UN0201SPA013GD.007 [DIRS 159119]	DST REKA probe developed data for thermal conductivity and diffusivity: May 1, 2001, to December 31, 2001	6.3.1.4	Unchanged DTN	Unchanged DTN
UN0106SPA013GD.004 [DIRS 159116]	DST REKA probe developed data for thermal conductivity and diffusivity: May 5, 1998, to April 30, 2001	6.3.1.4	Unchanged DTN	Unchanged DTN
LL000804023142.009 [DIRS 158325]	Water saturation	6.3.2.1	LL020801723142.028 <sup>b</sup> [DIRS 170580]	ERT tomograms
LL980406404244.057 [DIRS 113782]	Electrical resistance tomography	6.3.2.1		
LL990702704244.099 [DIRS 113872]	Electrical resistivity	6.3.2.1		
LL980808604244.065 <sup>b</sup> [DIRS 113791]	Electrical resistance tomography	6.3.2.1		
LL020307723142.018 [DIRS 177795]	Liquid saturation tomographs for the ESF DST Determined from ERT	6.3.2.1	Unchanged DTN	Unchanged DTN
LL030606723142.035 [DIRS 177798]	Saturation and resistivity ratio tomographs from the DST for the period February 5, 2002 through October 1, 2002	6.3.2.1	Unchanged DTN	Unchanged DTN
LL030906923142.038 [DIRS 177803]	Electrical resistivity and saturation ratio tomographs of the DST, March 4, 2003 through May 21, 2003	6.3.2.1	Unchanged DTN	Unchanged DTN
LL040307423142.072 [DIRS 177806]	Electrical resistivity and saturation ratio tomographs of the DST for November 18-19, 2003	6.3.2.1	Unchanged DTN	Unchanged DTN

Table 6.3-1. DTNs for the Drift Scale Test (Continued)

Input DTN	Input DTN Description	Input DTN Text Location	Summary DTN	Summary DTN Description
LL041000223142.045 [DIRS 177807]	Saturation ratio and resistivity ratio tomographs from the DST for the period January 1, 2004 through June 30, 2004	6.3.2.1	Unchanged DTN	Unchanged DTN
LL050902223142.048 [DIRS 177809]	Saturation ratio and resistivity ratio tomographs from the DST for the period January 1, 2005 through June 30, 2005	6.3.2.1	Unchanged DTN	Unchanged DTN
LL060303223142.051 <sup>b</sup> [DIRS 177810]	Saturation ratio tomographs from the DST for the period July 1, 2005 through December 31, 2005	6.3.2.1	Unchanged DTN	Unchanged DTN
LB990630123142.005 [DIRS 129274]	Ground penetrating radar data	6.3.2.2	LB0208GPRDSTHP.001 [DIRS 170577]	GPR velocity tomograms
LB000121123142.004 [DIRS 158338]	Ground penetrating radar data	6.3.2.2		
LB000718123142.004 [DIRS 153354]	Ground penetrating radar data	6.3.2.2		
LB0203GPRDSTEH.001 [DIRS 158350]	Ground penetrating radar data	6.3.2.2		
LB0101GPRDST01.001 [DIRS 158346]	Ground penetrating radar data	6.3.2.2		
LB0108GPRDST05.001 [DIRS 158440]	Ground penetrating radar data	6.3.2.2		
LB0210GPRDSTHP.001 [DIRS 160895]	DST GPR monitoring of water content over time (heating phase)	6.3.2.2	Unchanged DTN	Unchanged DTN
LB0209GPRDSTCP.001 [DIRS 177817]	GPR for the cooling phase of the DST	6.3.2.2	Unchanged DTN	Unchanged DTN
LB0210GPRDSTCP.001 [DIRS 160896]	DST GPR monitoring of water content over time (cooling phase)	6.3.2.2	Unchanged DTN	Unchanged DTN
LB0303GPRDSTCP.001 [DIRS 177822]	GPR for the cooling phase of the DST: processed data	6.3.2.2	Unchanged DTN	Unchanged DTN
LB0309GPRDSTCP.001 [DIRS 177823]	GPR for the cooling phase of the DST: processed data	6.3.2.2	Unchanged DTN	Unchanged DTN
LB0403GPRDSTCP.001 [DIRS 177824]	GPR for the cooling phase of the DST: processed data	6.3.2.2	Unchanged DTN	Unchanged DTN

Table 6.3-1. DTNs for the Drift Scale Test (Continued)

Input DTN	Input DTN Description	Input DTN Text Location	Summary DTN	Summary DTN Description
LB0509GPRDSTPC.001 [DIRS 177825]	Ground penetrating radar data for the cooling phase of the DST	6.3.2.2	Unchanged DTN	Unchanged DTN
LB0603GPRDSTPC.001 [DIRS 177826]	Ground penetrating radar data for the cooling phase of the DST	6.3.2.2	Unchanged DTN	Unchanged DTN
LL020710223142.024 [DIRS 159551]	Neutron logging	6.3.2.3	MO0406SEPTVDST.000 [DIRS 170616]	Temperature and volume water content
MO0001SEPDSTPC.000 [DIRS 153836]	Heater, power, current, voltage, temperature: June 1999 to October 1999	6.3.2.3		
MO0007SEPDSTPC.001 [DIRS 153707]	Heater, power, current, voltage, temperature: November 1999 to May 2000	6.3.2.3		
MO0012SEPDSTPC.002 [DIRS 153708]	Heater, power, current, voltage, temperature: June 2000 to November 2000	6.3.2.3		
MO0107SEPDSTPC.003 [DIRS 158321]	Heater, power, current, voltage, temperature: December 2000 to May 2001	6.3.2.3		
MO0202SEPDSTTV.001 [DIRS 158320]	Heater, power, current, voltage, temperature: June 2001 to January 14, 2002	6.3.2.3		
MO9807DSTSET01.000 [DIRS 113644]	Heater, power, current, voltage, temperature: November 7, 1997, to May 1998	6.3.2.3		
MO9810DSTSET02.000 [DIRS 113662]	Heater, power, current, voltage, temperature: June 1998 to August 1998	6.3.2.3		
MO9906DSTSET03.000 [DIRS 113673]	Heater, power, current, voltage, temperature: September 1998 to May 1999	6.3.2.3		
LL030309723122.022 [DIRS 165700]	Moisture content of rock from neutron logging activities in the DST: July 2002 through November 2002	6.3.2.3	Unchanged DTN	Unchanged DTN
LL030709023122.032 [DIRS 165701]	Moisture content of rock from neutron logging activities in the DST: January 2003 through May 2003	6.3.2.3	Unchanged DTN	Unchanged DTN
LL040308623122.043 [DIRS 177827]	Moisture content of rock from neutron logging activities in the DST: May 2003 through November 2003	6.3.2.3	Unchanged DTN	Unchanged DTN

Table 6.3-1. DTNs for the Drift Scale Test (Continued)

Input DTN	Input DTN Description	Input DTN Text Location	Summary DTN	Summary DTN Description
LL041001623122.052 [DIRS 177831]	Moisture content of rock from neutron logging activities in the DST: January 1, 2004 through June 30, 2004	6.3.2.3	Unchanged DTN	Unchanged DTN
LL050206323122.057 [DIRS 177829]	Moisture content of rock from neutron logging activities in the DST: July 1, 2004 through December 31, 2004	6.3.2.3	Unchanged DTN	Unchanged DTN
LL060101523122.066 [DIRS 177833]	Moisture content of rock from neutron logging activities in the DST: February 2005 through September 2005	6.3.2.3	Unchanged DTN	Unchanged DTN
LL060302423122.067 [DIRS 177834]	Moisture content of rock from neutron logging activities in the DST: October 2005 through December 2005	6.3.2.3	Unchanged DTN	Unchanged DTN
LB980912332245.002 [DIRS 105593]	Gas tracer data from Niche 3 (also referred to as Niche 3107) of the ESF	6.3.2.4	Unchanged DTN	Unchanged DTN
LB970600123142.001 [DIRS 105589]	Air permeability	6.3.2.4	Unchanged DTN	Unchanged DTN
LB980120123142.005 [DIRS 114134]	Active DST preheating air injection, Part 2 of 2	6.3.2.4	Unchanged DTN	Unchanged DTN
LB980120123142.004 [DIRS 105590]	Active baseline air injections in boreholes 57-61, 74-78, and 185-186	6.3.2.4	LB0208AIRKDSTH.001 [DIRS 160897]	Permeability data
LB980420123142.002 [DIRS 113706]	Active hydrology testing for boreholes 57-61, 74-78, and 185-186; air injection and gas tracer tests	6.3.2.4		
LB980715123142.002 [DIRS 113742]	Active hydrology testing data (air injection) collected from 12 hydrology boreholes: March 1998 to May 1998	6.3.2.4		
LB981016123142.002 [DIRS 129245]	Active hydrology testing for boreholes 57-61, 74-78, and 185-186; air injection tests: June 1998 to August 1999	6.3.2.4		
LB990630123142.001 [DIRS 129247]	Active hydrology testing by air injection: September 1998 to May 1999	6.3.2.4		
LB000121123142.002 [DIRS 158337]	Active hydrology testing by air injection: June 1999 to October 1999	6.3.2.4		

Table 6.3-1. DTNs for the Drift Scale Test (Continued)

Input DTN	Input DTN Description	Input DTN Text Location	Summary DTN	Summary DTN Description
LB0203AIRKDSTE.001 [DIRS 158348]	Active hydrology testing data (air injection) collected from 12 hydrology boreholes: June 1, 2001 to January 2002	6.3.2.4	LB0208AIRKDSTH.001 [DIRS 160897] (continued)	Permeability data (continued)
LB0108AIRKDST5.001 [DIRS 158438]	Active hydrology testing data (air injection) collected from 12 hydrology boreholes: December 1, 2000, to May 31, 2001	6.3.2.4		
LB0101AIRKDST1.001 [DIRS 158345]	Active hydrology testing data (air injection) collected from 12 hydrology boreholes: June 1, 2000, to November 30, 2000	6.3.2.4		
LB000718123142.002 [DIRS 158341]	Active hydrology testing data (air injection) collected from 12 hydrology boreholes: November 1, 1999, to May 31, 2000	6.3.2.4		
LB0209AIRKDSTC.001 [DIRS 177869]	Air pressure data for the cooling phase of the DST	6.3.2.4	Unchanged DTN	Unchanged DTN
LB0303AIRKDSTC.001 [DIRS 177870]	Air pressure data for the cooling phase of the DST	6.3.2.4	Unchanged DTN	Unchanged DTN
LB0309AIRKDSTC.001 [DIRS 177871]	Air pressure data for the cooling phase of the DST	6.3.2.4	Unchanged DTN	Unchanged DTN
LB0403AIRKDSTC.001 [DIRS 177872]	Air pressure data for the cooling phase of the DST	6.3.2.4	Unchanged DTN	Unchanged DTN
LB0410AIRKDSTC.001 [DIRS 177886]	Air pressure data for the cooling phase of the DST	6.3.2.4	Unchanged DTN	Unchanged DTN
LB0509AIRKDSTC.001 [DIRS 177887]	Air pressure data for the cooling phase of the DST	6.3.2.4	Unchanged DTN	Unchanged DTN
LB0603AIRKDSTC.001 [DIRS 178559]	Air pressure data for the cooling phase of the DST	6.3.2.4	Unchanged DTN	Unchanged DTN
LB0401PRDSTHP.001 [DIRS 169251]	Passive monitoring data for boreholes 57-61, 74-78, and 185-186: November 1997 to February 1998	6.3.2.4	LB0208H2ODSTHP.001 [DIRS 170579]	Passive hydrological monitoring data of temperature, relative humidity and pressure in the hydrology boreholes
LB0401PRDSTHP.002 [DIRS 169252]	Passive monitoring data collected from 12 hydrology boreholes: March 1998 to May 1998	6.3.2.4		
LB0401PRDSTHP.009 [DIRS 169250]	Passive monitoring data collected from 12 hydrology boreholes: June 1, 2001, through end of heating phase (January 14, 2002)	6.3.2.4		



Table 6.3-1. DTNs for the Drift Scale Test (Continued)

Input DTN	Input DTN Description	Input DTN Text Location	Summary DTN	Summary DTN Description
LB0401PRTDSTHP.003 [DIRS 169253]	Passive monitoring data for boreholes 57-61, 74-78, and 185-186 taken from June 1998 to August 1998	6.3.2.4	LB0208H2ODSTHP.001 [DIRS 170579] (continued)	Passive hydrological monitoring data of temperature, relative humidity and pressure in the hydrology boreholes (continued)
LB0401PRTDSTHP.004 [DIRS 169255]	Passive monitoring data (relative humidity, pressure, temperature): September 1998 to May 1999	6.3.2.4		
LB0401PRTDSTHP.005 [DIRS 169246]	Passive monitoring data (relative humidity, pressure, temperature): June 1 through October 31, 1999	6.3.2.4		
LB0401PRTDSTHP.006 [DIRS 169247]	Passive monitoring data collected from 12 hydrology boreholes: November 1, 1999, to May 31, 2000	6.3.2.4		
LB0401PRTDSTHP.007 [DIRS 169248]	Passive monitoring data collected from 12 hydrology boreholes: June 1, 2000, to November 30, 2000	6.3.2.4		
LB0401PRTDSTHP.008 [DIRS 169249]	Passive monitoring data collected from 12 hydrology boreholes: December 1, 2000, to May 31, 2001	6.3.2.4		
LB0401PRTDSTCP.001 [DIRS 170568]	Passive monitoring data (temperature and pressure) for the DST (January 15, 2002, through June 30, 2002)	6.3.2.4	Unchanged DTN	Unchanged DTN
LB0401PRTDSTCP.002 [DIRS 170569]	Passive monitoring data (temperature and pressure) for the DST (July 1, 2002, through December 31, 2002)	6.3.2.4	Unchanged DTN	Unchanged DTN
LB0309H2ODSTCP.001 [DIRS 177905]	Passive temperature and pressure monitoring data for the cooling phase of the DST	6.3.2.4	Unchanged DTN	Unchanged DTN
LB0403PRTDSTCP.001 [DIRS 177906]	Passive monitoring data (temperature and pressure) for the DST	6.3.2.4	Unchanged DTN	Unchanged DTN
LB0410PRTDSTCP.001 [DIRS 177907]	Passive temperature and pressure monitoring data for the cooling phase of the DST (January 1, 2004, through June 30, 2004)	6.3.2.4	Unchanged DTN	Unchanged DTN
LB0609PRTDSTCP.001 [DIRS 177908]	Passive temperature and pressure monitoring data for the cooling phase of the DST (July 1, 2004, through June 30, 2005)	6.3.2.4	Unchanged DTN	Unchanged DTN

Table 6.3-1. DTNs for the Drift Scale Test (Continued)

Input DTN	Input DTN Description	Input DTN Text Location	Summary DTN	Summary DTN Description
LB0609PRTDSTCP.002 [DIRS 177909]	Passive temperature and pressure monitoring data for the cooling phase of the DST (July 1 2005, through December 31, 2005)	6.3.2.4	Unchanged DTN	Unchanged DTN
LB0401RHMDSTHP.001 <sup>b</sup> [DIRS 177911]	Passive monitoring data (relative humidity) for the DST (November 1, 1997, through February 28, 1998)	6.3.2.4	Unchanged DTN	Unchanged DTN
LB0401RHMDSTHP.002 <sup>b</sup> [DIRS 177914]	Passive monitoring data (relative humidity) for the DST (March 1, 1998, through March 31, 1998)	6.3.2.4	Unchanged DTN	Unchanged DTN
LB0401RHMDSTHP.003 <sup>b</sup> [DIRS 177915]	Passive monitoring data (relative humidity) for the DST (June 1, 1998, through August 31, 1998)	6.3.2.4	Unchanged DTN	Unchanged DTN
LB0401RHMDSTHP.004 <sup>b</sup> [DIRS 177916]	Passive monitoring data (relative humidity) for the DST (September 1, 1998, through May 31, 1999)	6.3.2.4	Unchanged DTN	Unchanged DTN
LB0401RHMDSTHP.005 <sup>b</sup> [DIRS 177918]	Passive monitoring data (relative humidity) for the DST (June 1, 1999, through October 31, 1999)	6.3.2.4	Unchanged DTN	Unchanged DTN
LB0401RHMDSTHP.006 <sup>b</sup> [DIRS 177920]	Passive monitoring data (relative humidity) for the DST (November 1, 1999, through May 31, 2000)	6.3.2.4	Unchanged DTN	Unchanged DTN
LB0401RHMDSTHP.007 <sup>b</sup> [DIRS 177921]	Passive monitoring data (relative humidity) for the DST (June 1, 2000, through November 30, 2000)	6.3.2.4	Unchanged DTN	Unchanged DTN
LB0401RHMDSTHP.008 <sup>b</sup> [DIRS 177922]	Passive monitoring data (relative humidity) for the DST (December 1, 2000, through May 31, 2001)	6.3.2.4	Unchanged DTN	Unchanged DTN
LB0401RHMDSTHP.009 <sup>b</sup> [DIRS 177924]	Passive monitoring data (relative humidity) for the DST (June 1, 2001, through January 14, 2002)	6.3.2.4	Unchanged DTN	Unchanged DTN
LB0401RHMDSTCP.001 <sup>b</sup> [DIRS 177929]	Passive monitoring data (relative humidity) for the DST (January 15, 2002, through June 30, 2002)	6.3.2.4	Unchanged DTN	Unchanged DTN
LB0401RHMDSTCP.002 <sup>b</sup> [DIRS 177930]	Passive monitoring data (relative humidity) for the DST (July 1, 2002, through December 31, 2002)	6.3.2.4	Unchanged DTN	Unchanged DTN

Table 6.3-1. DTNs for the Drift Scale Test (Continued)

Input DTN	Input DTN Description	Input DTN Text Location	Summary DTN	Summary DTN Description
LB031RHMDSTCP.001 <sup>b</sup> [DIRS 177932]	Passive relative humidity monitoring data for the cooling phase of the DST	6.3.2.4	Unchanged DTN	Unchanged DTN
LB0403RHMDSTCP.001 <sup>b</sup> [DIRS 177933]	Passive monitoring data (relative humidity) for the DST	6.3.2.4	Unchanged DTN	Unchanged DTN
LB0410RHMDSTCP.001 <sup>b</sup> [DIRS 177935]	Passive relative humidity monitoring data for the cooling phase of the DST (January 1, 2004, through June 30, 2004)	6.3.2.4	Unchanged DTN	Unchanged DTN
LB0509RHMDSTCP.001 <sup>b</sup> [DIRS 177937]	Passive relative humidity monitoring data for the cooling phase of the DST (July 1, 2004, through June 30, 2005)	6.3.2.4	Unchanged DTN	Unchanged DTN
LB0603RHMDSTCP.001 <sup>b</sup> [DIRS 177938]	Passive relative humidity monitoring data for the cooling phase of the DST (July 1, 2005, through December 31, 2005)	6.3.2.4	Unchanged DTN	Unchanged DTN
LB970500123142.003 [DIRS 131500]	Laboratory saturation, porosity, bulk density, particle density, gravimetric water content data from dry-drilled and wet-drilled cores in the DST and SHT	6.3.2.5	Unchanged DTN	Unchanged DTN
LL020506123142.021 [DIRS 169256]	Laboratory moisture retention and porosity	6.3.2.5	Unchanged DTN	Unchanged DTN
LL020502523142.020 [DIRS 159105]	Laboratory-measured electrical properties of the DST samples as a function of saturation at 95°C	6.3.2.5	Unchanged DTN	Unchanged DTN
LL981109904242.072 [DIRS 118959]	Saturated and dry bulk density permittivity	6.3.2.5	Unchanged DTN	Unchanged DTN
SNF39012298002.002 [DIRS 159114]	Measurements of displacement data for the DST (with results from November 1, 1997, through May 31, 1998)	6.3.3.1 6.3.3.2	Unchanged DTN	Unchanged DTN
SNF39012298002.006 [DIRS 158419]	MPBX and CDEX displacement, June 1998 to August 1998	6.3.3.1 6.3.3.2	Unchanged DTN	Unchanged DTN
SNF39012298002.010 [DIRS 158367]	MPBX and CDEX displacement, September 1998 to May 1999	6.3.3.1 6.3.3.2	Unchanged DTN	Unchanged DTN
SN0001F3912298.014 [DIRS 153841]	MPBX and CDEX displacement, June 1999 to October 1999	6.3.3.1 6.3.3.2	Unchanged DTN	Unchanged DTN
SN0203F3912298.033 [DIRS 158361]	MPBX and CDEX displacement, June 2001 to January 2002	6.3.3.1 6.3.3.2	Unchanged DTN	Unchanged DTN

Table 6.3-1. DTNs for the Drift Scale Test (Continued)

Input DTN	Input DTN Description	Input DTN Text Location	Summary DTN	Summary DTN Description
SNF39012298002.002 [DIRS 159114]	MPBX and CDEX displacement, November 1997 to May 1998	6.3.3.1 6.3.3.2	Unchanged DTN	Unchanged DTN
SN0007F3912298.018 [DIRS 158374]	MPBX and CDEX displacement, November 1999 to May 2000	6.3.3.1 6.3.3.2	Unchanged DTN	Unchanged DTN
SN0101F3912298.024 [DIRS 158400]	MPBX and CDEX displacement, June 2000 to November 2000	6.3.3.1 6.3.3.2	Unchanged DTN	Unchanged DTN
SN0107F3912298.029 [DIRS 158408]	MPBX and CDEX displacement, December 2000 to May 2001	6.3.3.1 6.3.3.2	Unchanged DTN	Unchanged DTN
SN0209F3912298.040 [DIRS 178009]	Measurements of displacement data for the DST (with results from January 15, 2002, through June 30, 2002)	6.3.3.1 6.3.3.2	Unchanged DTN	Unchanged DTN
SN0303F3912298.044 [DIRS 178010]	Measurements of displacement data for the DST (with results from July 1, 2002, through December 31, 2002)	6.3.3.1 6.3.3.2	Unchanged DTN	Unchanged DTN
SN0308F3912298.050 [DIRS 178011]	Measurements of displacement data for the DST (with results from January 1, 2003, through June 30, 2003)	6.3.3.1 6.3.3.2	Unchanged DTN	Unchanged DTN
SN0403F3912298.055 [DIRS 178012]	Measurements of displacement data for the DST (with results from July 1, 2003, through December 31, 2003)	6.3.3.1 6.3.3.2	Unchanged DTN	Unchanged DTN
SN0410F3912298.061 [DIRS 178013]	Measurements of displacement data for the DST (with results from January 1, 2004, through June 30, 2004)	6.3.3.1 6.3.3.2	Unchanged DTN	Unchanged DTN
SN0601F3912298.065 [DIRS 178014]	Measurements of displacement data for the DST (with results from July 1, 2004, through June 30, 2005)	6.3.3.1 6.3.3.2	Unchanged DTN	Unchanged DTN
SN0608F3912298.069 [DIRS 178015]	Measurements of displacement data for the DST (with results from July 1, 2005, through June 30, 2006)	6.3.3.1 6.3.3.2	Unchanged DTN	Unchanged DTN
MO0002ABBLSLDS.000 [DIRS 147304]	DST borehole and sensor locations	6.3.2.4	SN0407F3912298.060 [DIRS 170627]	Rock mass thermal expansion
MO0012SEPDSTPC.002 [DIRS 153708]	DST heater power and temperature	6.3.1.1 6.3.1.2		
MO0202SEPDSTTV.001 [DIRS 158320]	DST heater power and temperature	6.3.1.1 6.3.1.2		

Table 6.3-1. DTNs for the Drift Scale Test (Continued)

Input DTN	Input DTN Description	Input DTN Text Location	Summary DTN	Summary DTN Description
MO9807DSTSET01.000 [DIRS 113644]	DST heater power and temperature	6.3.1.1 6.3.1.2	SN0407F3912298.060 [DIRS 170627]	Rock mass thermal expansion (continued)
MO9810DSTSET02.000 [DIRS 113662]	DST heater power and temperature	6.3.1.1 6.3.1.2	(continued)	
MO9906DSTSET03.000 [DIRS 113673]	DST heater power and temperature	6.3.1.1 6.3.1.2		
MO0001SEPDSTPC.000 [DIRS 153836]	DST heater power and temperature	6.3.1.1 6.3.1.2		
MO0007SEPDSTPC.001 [DIRS 153707]	DST heater power and temperature	6.3.1.1 6.3.1.2		
MO0012SEPDSTPC.002 [DIRS 153708]	DST heater power and temperature	6.3.1.1 6.3.1.2		
MO0107SEPDSTPC.003 [DIRS 158321]	DST heater power and temperature	6.3.1.1 6.3.1.2		
MO0202SEPDSTTV.001 [DIRS 158320]	DST heater power and temperature	6.3.1.1 6.3.1.2		
SNL22100196001.003 [DIRS 111068]	Thermal expansion of carbon fiber and Invar rods	6.3.3.1 6.3.3.2		
MO0002ABBLSDS.000 [DIRS 147304]	DST borehole and sensor locations	6.3.2.4		
SNF39012298002.004 [DIRS 153837]	MPBX and CDEX displacement corrected for thermal expansion, November 1997 to May 1998	6.3.3.1 6.3.3.2		
SNF39012298002.008 [DIRS 153839]	MPBX and CDEX displacement corrected for thermal expansion, June 1998 to August 1998	6.3.3.1 6.3.3.2		
SN0001F3912298.016 [DIRS 153842]	MPBX and CDEX displacement corrected for thermal expansion, June 1999 to October 1999	6.3.3.1 6.3.3.2		
SN0101F3912298.026 [DIRS 158402]	MPBX and CDEX displacement corrected for thermal expansion, June 2000 to November 2000	6.3.3.1 6.3.3.2		
SNF39012298002.012 [DIRS 153840]	MPBX and CDEX displacement corrected for thermal expansion, November 1997 to May 1998	6.3.3.1 6.3.3.2		

Table 6.3-1. DTNs for the Drift Scale Test (Continued)

Input DTN	Input DTN Description	Input DTN Text Location	Summary DTN	Summary DTN Description
SN0107F3912298.031 [DIRS 158413]	MPBX and CDEX displacement corrected for thermal expansion, December 2000 to May 2001	6.3.3.1 6.3.3.2	SN0407F3912298.060 [DIRS 170627] (continued)	Rock mass thermal expansion (continued)
SN0203F3912298.035 [DIRS 158363]	MPBX and CDEX displacement corrected for thermal expansion, June 2001 to January 2002	6.3.3.1 6.3.3.2	Unchanged DTN	Unchanged DTN
SN0007F3912298.020 [DIRS 158388]	MPBX and CDEX displacement corrected for thermal expansion, November 1999 to May 2000	6.3.3.1 6.3.3.2	Unchanged DTN	Unchanged DTN
SN0209F3912298.042 [DIRS 177941]	Measurements of displacement data for the DST corrected for thermal expansion (with results from January 15, 2002, through June 30, 2002)	6.3.3.1 6.3.3.2	Unchanged DTN	Unchanged DTN
SN0303F3912298.046 [DIRS 177945]	Measurements of displacement data for the DST corrected for thermal expansion (with results from July 1, 2002, through December 31, 2002)	6.3.3.1 6.3.3.2	Unchanged DTN	Unchanged DTN
SN0308F3912298.052 [DIRS 177946]	Measurements of displacement data for the DST corrected for thermal expansion (with results from January 1, 2003, through June 30, 2003)	6.3.3.1 6.3.3.2	Unchanged DTN	Unchanged DTN
SN0403F3912298.057 [DIRS 177948]	Measurements of displacement data for the DST corrected for thermal expansion (with results from July 1, 2003, through December 31, 2003)	6.3.3.1 6.3.3.2	Unchanged DTN	Unchanged DTN
SN0410F3912298.063 [DIRS 177973]	Measurements of displacement data for the DST corrected for thermal expansion (with results from January 1, 2004, through June 30, 2004)	6.3.3.1 6.3.3.2	Unchanged DTN	Unchanged DTN
SN0601F3912298.067 [DIRS 178005]	Measurements of displacement data for the DST corrected for thermal expansion (with results from 7/1/2004 through 6/30/2005)	6.3.3.1 6.3.3.2	Unchanged DTN	Unchanged DTN
SN0608F3912298.071 [DIRS 177975]	Measurements of displacement data for the DST corrected for thermal expansion (with results from July 1, 2005, through June 30, 2006)	6.3.3.1 6.3.3.2	Unchanged DTN	Unchanged DTN
SNF38040197001.001 [DIRS 159130]	Strain-gage and anchor locations	6.3.3.3	Unchanged DTN	Unchanged DTN
SNF39012298002.003 [DIRS 158417]	Ground support system strain: November 1997 to May 1998	6.3.3.3	Unchanged DTN	Unchanged DTN
SNF39012298002.007 [DIRS 158365]	Ground support system strain: June 1998 to August 1998	6.3.3.3	Unchanged DTN	Unchanged DTN

Table 6.3-1. DTNs for the Drift Scale Test (Continued)

Input DTN	Input DTN Description	Input DTN Text Location	Summary DTN	Summary DTN Description
SNF39012298002.011 [DIRS 158368]	Ground support system strain: September 1998 to May 1999	6.3.3.3	Unchanged DTN	Unchanged DTN
SN0001F3912298.015 [DIRS 158372]	Ground support system strain: June 1999 to October 1999	6.3.3.3	Unchanged DTN	Unchanged DTN
SN0007F3912298.019 [DIRS 158387]	Ground support system strain: November 1999 to May 2000	6.3.3.3	Unchanged DTN	Unchanged DTN
SN0101F3912298.025 [DIRS 158401]	Ground support system strain: June 2000 to November 2000	6.3.3.3	Unchanged DTN	Unchanged DTN
SN0107F3912298.030 [DIRS 158409]	Ground support system strain: December 2000 to May 2001	6.3.3.3	Unchanged DTN	Unchanged DTN
SN0203F3912298.034 [DIRS 158362]	Ground support system strain: June 2001 to January 14, 2002	6.3.3.3	Unchanged DTN	Unchanged DTN
SN0209F3912298.041 [DIRS 178019]	Measurements of strain data for the DST (with results from January 15 2002, through June 30, 2002)	6.3.3.3	Unchanged DTN	Unchanged DTN
SN0303F3912298.045 [DIRS 178020]	Measurements of strain data for the DST (with results from July 1, 2002, through December 31, 2002)	6.3.3.3	Unchanged DTN	Unchanged DTN
SN0308F3912298.051 [DIRS 178021]	Measurements of strain data for the DST (with results from January 1, 2003, through June 30, 2003)	6.3.3.3	Unchanged DTN	Unchanged DTN
SN0403F3912298.056 [DIRS 178022]	Measurements of strain data for the DST (with results from July 1, 2003, through December 31, 2003)	6.3.3.3	Unchanged DTN	Unchanged DTN
SN0410F3912298.062 [DIRS 178023]	Measurements of strain data for the DST (with results from January 1, 2004, through June 30, 2004)	6.3.3.3	Unchanged DTN	Unchanged DTN
SN0601F3912298.066 [DIRS 178024]	Measurements of strain data for the DST (with results from July 1, 2004, through June 30, 2005)	6.3.3.3	Unchanged DTN	Unchanged DTN
SN0608F3912298.070 [DIRS 178025]	Measurements of strain data for the DST (with results from July 1, 2005, through June 30, 2006)	6.3.3.3	Unchanged DTN	Unchanged DTN

Table 6.3-1. DTNs for the Drift Scale Test (Continued)

Input DTN	Input DTN Description	Input DTN Text Location	Summary DTN	Summary DTN Description
SNF39012298002.005 [DIRS 158418]	Ground support system strain corrected for thermal expansion: November 9, 1997, to May 1998	6.3.3.3	SN0208F3912298.038 <sup>b</sup> [DIRS 170610]	Smoothed strain data
SNF39012298002.009 [DIRS 158366]	Ground support system strain corrected for thermal expansion: June 1998 to August 1998	6.3.3.3		
SNF39012298002.013 [DIRS 158369]	Ground support system strain corrected for thermal expansion: September 1998 to May 1999	6.3.3.3		
SN0001F3912298.017 [DIRS 158373]	Ground support system strain corrected for thermal expansion: June 1999 to October 1999	6.3.3.3		
SN0007F3912298.021 [DIRS 158391]	Ground support system strain corrected for thermal expansion: November 1999 to May 2000	6.3.3.3		
SN0101F3912298.027 [DIRS 158407]	Ground support system strain corrected for thermal expansion: June 2000 to November 2000	6.3.3.3		
SN0107F3912298.032 [DIRS 158414]	Ground support system strain corrected for thermal expansion: December 2000 to May 2001	6.3.3.3		
SN0203F3912298.036 [DIRS 158364]	Ground support system strain corrected for thermal expansion: June 2001 to January 14, 2002	6.3.3.3		
SN0209F3912298.043 [DIRS 178027]	Measurements of strain data for the DST (with results from January 15, 2002, through June 30, 2002)	6.3.3.3	Unchanged DTN	Unchanged DTN
SN0303F3912298.047 [DIRS 178028]	Measurements of strain data for the DST (with results from July 1, 2002, through, December 31, 2002)	6.3.3.3	Unchanged DTN	Unchanged DTN
SN0308F3912298.053 [DIRS 178029]	Measurements of strain data for the DST (with results from January 1, 2003, through June 30, 2003)	6.3.3.3	Unchanged DTN	Unchanged DTN
SN0403F3912298.058 [DIRS 178030]	Measurements of strain data for the DST (with results from July 1, 2003, through December 31, 2003)	6.3.3.3	Unchanged DTN	Unchanged DTN



Table 6.3-1. DTNs for the Drift Scale Test (Continued)

Input DTN	Input DTN Description	Input DTN Text Location	Summary DTN	Summary DTN Description
SN0410F3912298.064 [DIRS 178031]	Measurements of strain data for the DST (with results from January 1, 2004, through June 30, 2004)	6.3.3.3	Unchanged DTN	Unchanged DTN
SN0601F3912298.068 [DIRS 178032]	Measurements of strain data for the DST (with results from July 1, 2004, through June 30, 2005)	6.3.3.3	Unchanged DTN	Unchanged DTN
SN0608F3912298.072 [DIRS 178033]	Measurements of strain data for the DST (with results from July 1, 2005, through June 30, 2006)	6.3.3.3	Unchanged DTN	Unchanged DTN
LB980120123142.007 [DIRS 158352]	Acoustic emissions: baseline and heating	6.3.3.4	LB0208ACEMDSTH.001 [DIRS 170575]	Acoustic emissions: baseline and heating
LB980420123142.004 [DIRS 113717]	Acoustic emissions: baseline and heating	6.3.3.4		
LB000121123142.005 [DIRS 158339]	Acoustic emissions: baseline and heating	6.3.3.4		
LB000718123142.005 [DIRS 158343]	Acoustic emissions: baseline and heating	6.3.3.4		
LB0101ACEMDST1.001 [DIRS 158344]	Acoustic emissions: baseline and heating	6.3.3.4		
LB0108ACEMDST5.001 [DIRS 158437]	Acoustic emissions: baseline and heating	6.3.3.4		
SN0203L2210196.007 [DIRS 158322]	Laboratory thermal expansion	6.3.3.5	Unchanged DTN	Unchanged DTN
SNL02100196001.001 [DIRS 158420]	Elastic constants and strength properties	6.3.3.5	Unchanged DTN	Unchanged DTN
SNL23030598001.001 [DIRS 158370]	Elastic constants and strength of concrete	6.3.3.5	Unchanged DTN	Unchanged DTN
SN0011F3912298.022 [DIRS 158392]	Rock mass displacement pressure data plate load test, October 16 and 17, 2000	6.3.3.6	Unchanged DTN	Unchanged DTN
SN0011F3912298.023 [DIRS 158399]	Rock mass displacement pressure data in modulus, October 16 and 17, 2000	6.3.3.6	Unchanged DTN	Unchanged DTN
SN0306F3912298.048 [DIRS 165416]	Plate-loading measured displacement and test pressure data for 2003 (with results from April 30, 2003)	6.3.3.6	Unchanged DTN	Unchanged DTN
SN0310F3912298.054 [DIRS 168527]	Updated plate-loading rock mass modulus data for 2003	6.3.3.6	Unchanged DTN	Unchanged DTN

Table 6.3-1. DTNs for the Drift Scale Test (Continued)

Input DTN	Input DTN Description	Input DTN Text Location	Summary DTN	Summary DTN Description
MO0207AL5WATER.001 [DIRS 159300]	Water sampling in Alcove 5 (results from February 4, 1997, through April 20, 1999)	6.3.4.1	SN0208F3903102.002 [DIRS 161246]	Field water sampling and chemistry
MO0101SEPFDDST.000 [DIRS 153711]	Field-measured data of water samples from the DST	6.3.4.1		
SN0203F3903102.001 [DIRS 159133]	DST water sampling (with results from April 17, 2001, through January 14, 2002)	6.3.4.1		
SN0210F3903102.004 [DIRS 170573]	DST water sampling (results from January 16, 2002, through April 4, 2002)	6.3.4.1 6.3.4.5	Unchanged DTN	Unchanged DTN
SN0211F3903102.005 [DIRS 170574]	DST water sampling (results from April 25, 2002, through August 28, 2002)	6.3.4.1 6.3.4.5	Unchanged DTN	Unchanged DTN
SN0303F3903102.006 [DIRS 178034]	DST water sampling (results from October 7, 2002, through February 18, 2003)	6.3.4.1	Unchanged DTN	Unchanged DTN
SN0311F3903102.007 [DIRS 178035]	DST water sampling in Alcove 5 (results from April 3, 2003, through October 7, 2003)	6.3.4.1	Unchanged DTN	Unchanged DTN
SN0411F3903102.009 [DIRS 178036]	DST water sampling in Alcove 5 on May 11, 2004, and September 16, 2004)	6.3.4.1	Unchanged DTN	Unchanged DTN
SN0507F3903102.010 [DIRS 178037]	DST water sampling in Alcove 5 on January 27, 2004	6.3.4.1	Unchanged DTN	Unchanged DTN
SN0510F3903102.012 [DIRS 178038]	DST water sampling in Alcove 5 on January 25, 2005, and June 2, 2005	6.3.4.1	Unchanged DTN	Unchanged DTN
SN0511F3903102.013 [DIRS 178039]	DST water sampling in Alcove 5 on November 8, 2005	6.3.4.1	Unchanged DTN	Unchanged DTN
LL001100931031.008 [DIRS 153288]	Aqueous chemistry of water sampled from boreholes of the DST	6.3.4.1	LL020709923142.023 <sup>b</sup> [DIRS 161677]	Water chemistry
LL001200231031.009 <sup>b</sup> [DIRS 153616]	Aqueous chemistry of water sampled from boreholes of the DST	6.3.4.1		
LL020302223142.015 [DIRS 159134]	Aqueous geochemistry of DST samples collected from HYD boreholes	6.3.4.1		
MO0005PORWATER.000 [DIRS 150930]	Perm-sample pore water data	6.3.4.1		

Table 6.3-1. DTNs for the Drift Scale Test (Continued)

Input DTN	Input DTN Description	Input DTN Text Location	Summary DTN	Summary DTN Description
LL021107623121.014 [DIRS 169257]	Aqueous geochemistry of DST samples collected between April 20, 1999, and January 25, 2000	6.3.4.1	LL020709923142.023 <sup>b</sup> [DIRS 161677]	Water chemistry (continued)
LL030107523142.031 <sup>b</sup> [DIRS 169258]	Anion concentrations of two DST samples collected between June 4, 1998, and March 30, 1999	6.3.4.1	(continued)	
LL990702804244.100 <sup>b</sup> [DIRS 144922]	Borehole and pore water data	6.3.4.1		
GS040308312272.001 [DIRS 178056]	Gravimetric moisture content measurements for HD-CHEMSAMP cores for the period from June 2002 to January 2004	6.3.4.1.4	Unchanged DTN	Unchanged DTN
GS030408312272.002 [DIRS 165226]	Analysis of water-quality samples for the period from July 2002 to November 2002	6.3.4.1.4 6.3.4.5.2	Unchanged DTN	Unchanged DTN
GS031008312272.008 [DIRS 166570]	Analysis of pore water and miscellaneous water samples for the period from December 2002 to July 2003	6.3.4.1.4	Unchanged DTN	Unchanged DTN
GS041108312272.005 [DIRS 178057]	Analysis of pore water and miscellaneous water samples for the period from July 2003 to September 2004	6.3.4.1.4	Unchanged DTN	Unchanged DTN
LB980420123142.005 [DIRS 111471]	Isotope data for CO <sub>2</sub> from gas samples collected from the DST: February 1998	6.3.4.2	LB0208ISODSTHP.001 [DIRS 161638]	Gas Chemistry
LB980715123142.003 [DIRS 111472]	Isotope data for CO <sub>2</sub> from gas samples collected from the DST: June 4, 1998	6.3.4.2		
LB0404ISODSTHP.003 [DIRS 169254]	Third submittal of CO <sub>2</sub> /H <sub>2</sub> O isotope data for the heating phase of the DST	6.3.4.2		
LB990630123142.003 [DIRS 111476]	Isotope data for CO <sub>2</sub> from gas and water samples: September 1998 to May 1999	6.3.4.2		
LB000121123142.003 [DIRS 146451]	Isotope data for CO <sub>2</sub> gas samples collected from the hydrology boreholes: August 9, 1999, through November 30, 1999	6.3.4.2		
LB000718123142.003 [DIRS 158342]	Isotope data for CO <sub>2</sub> gas samples collected from hydrology boreholes: April 18, 2000, through April 19, 2000	6.3.4.2		
LB0011CO2DST08.001 [DIRS 153460]	Isotope data for CO <sub>2</sub> from gas samples collected from hydrology boreholes	6.3.4.2		

Table 6.3-1. DTNs for the Drift Scale Test (Continued)

Input DTN	Input DTN Description	Input DTN Text Location	Summary DTN	Summary DTN Description
LB0102CO2DST98.001 [DIRS 159306]	Concentration and isotope data for CO <sub>2</sub> and H <sub>2</sub> O from gas samples collected from hydrology boreholes: May and August 1999, April 2000, January and April 2001	6.3.4.2	LB0208ISODSTHP.001 [DIRS 161638] (continued)	Gas Chemistry (continued)
LB0108CO2DST05.001 [DIRS 156888]	Concentration and isotope data for CO <sub>2</sub> and H <sub>2</sub> O from gas samples collected from hydrology boreholes: May and August 1999, April 2000, January and April 2001	6.3.4.2		
LB0203CO2DSTEH.001 [DIRS 158349]	Concentration and isotope data for CO <sub>2</sub> and H <sub>2</sub> O from gas samples collected from hydrology boreholes up to end of heating	6.3.4.2		
LB0206C14DSTEH.001 [DIRS 159303]	Carbon 14 isotope data from CO <sub>2</sub> gas samples collected from DST	6.3.4.2		
LB0303ISODSTCP.001 [DIRS 177538]	Isotope data and CO <sub>2</sub> analysis for the cooling phase of the DST	6.3.4.2	Unchanged DTN	Unchanged DTN
LB0309ISODSTCP.001 [DIRS 177539]	Isotope data and CO <sub>2</sub> analysis for the cooling phase of the DST	6.3.4.2	Unchanged DTN	Unchanged DTN
LB0403ISODSTCP.001 [DIRS 177540]	Isotope data and CO <sub>2</sub> analysis for the cooling phase of the DST	6.3.4.2	Unchanged DTN	Unchanged DTN
LB0410ISODSTCP.001 [DIRS 177541]	Isotope data and CO <sub>2</sub> analysis for the cooling phase of the DST	6.3.4.2	Unchanged DTN	Unchanged DTN
LB0509ISODSTCP.001 [DIRS 177542]	Isotope data and CO <sub>2</sub> analysis for the cooling phase of the DST	6.3.4.2	Unchanged DTN	Unchanged DTN
LA9912SL831151.002 [DIRS 146449]	Percent coverage by fracture-coating minerals in core ESF-HD-TEMP-2	6.3.4.3	Unchanged DTN	Unchanged DTN
LA0009SL831151.001 [DIRS 153485]	Fracture mineralogy of the ESF Single Heater Test block, Alcove 5	6.3.4.3	Unchanged DTN	Unchanged DTN
LA0303WS831151.001 [DIRS 169378]	Amorphous silica in DST sidewall samples	6.3.4.3	Unchanged DTN	Unchanged DTN
LA0201SL831225.001 [DIRS 158426]	Chemical, textural, and mineralogical characteristics of sidewall samples from the DST	6.3.4.3	Unchanged DTN	Unchanged DTN
LA0609SL831322.001 [DIRS 178052]	Mineralogy of red spot deposit from DST	6.3.4.3	Unchanged DTN	Unchanged DTN

Table 6.3-1. DTNs for the Drift Scale Test (Continued)

Input DTN	Input DTN Description	Input DTN Text Location	Summary DTN	Summary DTN Description
GS01108312322.008 [DIRS 159136]	Uranium concentrations and $^{234}\text{U}/^{238}\text{U}$ activity ratios analyzed between February 1, 1999, and August 1, 2001 for drift-scale heater test water collected between June 1998 and April 2001, and pore water collected between March 1996 and April 1999	6.3.4.4	Unchanged DTN	Unchanged DTN
GS010808312322.004 [DIRS 156007]	Uranium and uranium isotope data for water samples from wells and springs in the Yuucca Mountain vicinity collected between December 1996 and December 1997	6.3.4.4	Unchanged DTN	Unchanged DTN
GS010608315215.002 [DIRS 156187]	Uranium and thorium isotope data for waters analyzed between January 18, 1994, and September 14, 1996	6.3.4.4	Unchanged DTN	Unchanged DTN
GS01108312322.009 [DIRS 159137]	Strontium isotope ratios and strontium concentrations in water samples from the DST analyzed from March 16, 1999, to June 27, 2001	6.3.4.4	Unchanged DTN	Unchanged DTN
GS960908315215.012 [DIRS 169552]	Strontium isotope ratios and isotope dilutions data for strontium analyzed from July 6, 1995, to August 5, 1996	6.3.4.4	Unchanged DTN	Unchanged DTN
GS010908315215.005 [DIRS 169553]	Strontium isotope ratios and strontium concentrations in calcite samples from the ESF analyzed from May 25, 2000, to June 5, 2001	6.3.4.4	Unchanged DTN	Unchanged DTN
GS990308315215.004 [DIRS 145711]	Strontium isotope ratios and strontium concentrations in rock core samples and leachates from USW SD-9 and USW SD-12	6.3.4.4	Unchanged DTN	Unchanged DTN
GS040508312272.002 <sup>b</sup> [DIRS 169629]	Strontium isotope ratios and strontium concentrations on introduced materials to the ESF tunnel	6.3.4.4	Unchanged DTN	Unchanged DTN
GS990308315215.003 [DIRS 145707]	X-ray fluorescence elemental compositions of rock core samples from USW SD-9 and USW SD-12	6.3.4.4	Unchanged DTN	Unchanged DTN
SN0203F3903102.001 [DIRS 159133]	DST water sampling (with results from April 17, 2001, through January 14, 2002)	6.3.4.5	SN0208F3903102.003 [DIRS 170620]	Field hydrogen fluoride (HF) data
LL020405123142.019 [DIRS 159307]	Aqueous geochemistry of condensed fluids collected during studies of introduced materials	6.3.4.5		

Table 6.3-1. DTNs for the Drift Scale Test (Continued)

Input DTN	Input DTN Description	Input DTN Text Location	Summary DTN	Summary DTN Description
LB0211DSTRBRDG.001 [DIRS 170566]	DST packer materials investigation	6.3.4.5	Unchanged DTN	Unchanged DTN
LB0302NEOPDGRD.001 [DIRS 170567]	Neoprene degradation experiments	6.3.4.5	Unchanged DTN	Unchanged DTN
LL030305023121.023 [DIRS 170570]	Aqueous geochemistry of DST water samples collected in February and March of 2002 from borehole 75, zone 2	6.3.4.5	Unchanged DTN	Unchanged DTN
LL030310023121.024 <sup>b</sup> [DIRS 170571]	Chemical composition of water samples collected from hydrology boreholes of the DST	6.3.4.5	Unchanged DTN	Unchanged DTN
LL030605512251.064 <sup>b</sup> [DIRS 170572]	Thermogravimetric analysis data on the thermal decomposition of fluoroelastomer samples taken from borehole 60 and borehole 72 of the DST	6.3.4.5	Unchanged DTN	Unchanged DTN
GS020808312272.004 <sup>b</sup> [DIRS 166569]	Analysis of water-quality samples, July 1999 to July 2002	6.3.4.5	Unchanged DTN	Unchanged DTN
GS970608314224.006 [DIRS 158429]	Fracture mapping	6.3.5.1	Unchanged DTN	Unchanged DTN
LARO831422AQ97.002 [DIRS 158431]	DST borehole video logging	6.3.5.2	Unchanged DTN	Unchanged DTN

<sup>a</sup> DTNs: LA9908FH6001WP.001 [DIRS 158319], LA0111FH831151.002 [DIRS 158317], LA0208FH831151.001 [DIRS 159515], LA0108FH831151.001 [DIRS 158316], LA0111FH831151.001 [DIRS 169386], LA0111FH831151.003 [DIRS 158318] and LA0208FH831151.002 [DIRS 159308] provide access via RPC to all thermal and mechanical data collected in DST DCS (original/electrical and converted/engineering units). These unqualified DTNs also provides access (via the RPC) to pertinent supporting material such as scientific notebooks and calibration relationships.

<sup>b</sup> These data are unqualified and should only be used for corroborative purposes.

Table 6.3-2. DST Borehole Information

Borehole Number	Borehole Identification	Primary Purpose	Collar Coordinates (m) x/y/z	Bottom Coordinates (m) x/y/z	Diameter (cm)
42	ESF-SDM-MPBX-1	MPBX – Rock Mass Displacement	-29.304/13.820/4.631	-3.555/13.688/-0.371	7.70
43	ESF-SDM-MPBX-2	MPBX – Rock Mass Displacement	-29.166/21.062/5.073	-3.424/20.743/0.356	7.70
44	ESF-SDM-MPBX-3	MPBX – Rock Mass Displacement	-29.539/32.079/5.137	-3.600/32.192/-0.372	7.70
45	ESF-HD-ERT-1	Electrical Resistivity Tomography	-28.875/4.577/4.118	9.565/4.674/13.693	7.70
46	ESF-HD-ERT-2	Electrical Resistivity Tomography	-27.408/4.572/1.533	9.093/4.533/-14.333	7.70
47	ESF-HD-NEU-1	Neutron Probe	-29.114/6.385/4.636	7.166/6.338/21.099	7.70
48	ESF-HD-NEU-2	Neutron Probe	-29.051/6.391/4.042	9.515/6.260/13.545	7.70
49	ESF-HD-NEU-3	Neutron Probe	-29.039/6.377/3.435	10.841/6.703/7.714	7.70
50	ESF-HD-NEU-4	Neutron Probe	-29.012/6.395/2.558	9.680/6.419/-8.126	7.70
51	ESF-HD-NEU-5	Neutron Probe	-28.993/6.414/2.254	8.072/6.687/-11.996	7.70
52	ESF-HD-CHE-1	Chemistry – SEAMIST	-29.211/8.247/4.540	7.045/8.293/20.070	10.00
53	ESF=HD-CHE-2	Chemistry – SEAMIST	-29.232/8.258/4.014	9.415/8.702/13.889	10.00
54	ESF-HD-CHE-3	Chemistry – SEAMIST	-29.139/8.227/3.434	10.332/8.375/6.906	10.00
55	ESF-HD-CHE-4	Chemistry – SEAMIST	-29.233/8.224/2.583	5.087/7.976/-7.547	10.00
56	ESF-HD-CHE-5	Chemistry – SEAMIST	-29.223/8.248/2.322	7.264/8.456/-13.833	10.00
57	ESF-HD-HYD-1	Hydrology	-28.841/10.054/4.748	7.773/9.825/19.805	7.70
58	ESF-HD-HYD-2	Hydrology	-28.951/10.017/4.114	9.567/9.961/13.730	7.70
59	ESF-HD-HYD-3	Hydrology	-29.071/10.044/3.453	10.248/10.045/7.227	7.70
60	ESF-HD-HYD-4	Hydrology	-29.107/10.003/2.707	9.213/9.259/-7.328	7.70
61	ESF-HD-HYD-5	Hydrology	-29.193/10.062/2.337	8.215/10.184/-12.022	7.70
62	ESF-HD-ERT-3	Electrical Resistivity Tomography	-29.238/24.703/6.307	10.095/24.853/13.169	7.70
63	ESF-HD-ERT-4	Electrical Resistivity Tomography	-29.284/24.690/4.730	7.004/25.015/-11.927	7.70
64	ESF-HD-NEU-6	Neutron Probe	-29.311/26.519/6.639	8.073/26.437/20.795	7.70
65	ESF-HD-NEU-7	Neutron Probe	-29.341/26.524/6.310	9.937/26.650/13.715	7.70
66	ESF-HD-NEU-8	Neutron Probe	-29.118/26.506/5.999	10.682/26.580/6.890	7.70
67	ESF-HD-NEU-9	Neutron Probe	-28.974/26.489/5.222	8.262/25.877/-7.953	7.70

Table 6.3-2. DST Borehole Information (Continued)

Borehole Number	Borehole Identification	Primary Purpose	Collar Coordinates (m) x/y/z	Bottom Coordinates (m) x/y/z	Diameter (cm)
68	ESF-HD-NEU-10	Neutron Probe	-29.116/26.550/4.588	6.847/26.856/-12.272	7.70
69	ESF-HD-CHE-6	Chemistry – SEAMIST	-29.199/28.368/6.842	8.312/28.683/20.044	7.70
70	ESF-HD-CHE-7	Chemistry – SEAMIST	-29.261/28.373/6.315	10.024/29.034/13.092	7.70
71	ESF-HD-CHE-8	Chemistry – SEAMIST	-29.393/28.345/5.964	10.664/27.898/6.244	10.00
72	ESF-HD-CHE-9	Chemistry – SEAMIST	-29.289/28.385/5.467	8.353/28.822/-8.384	10.00
73	ESF-HD-CHE-10	Chemistry – SEAMIST	-29.062/28.375/4.546	6.628/28.542/-12.589	7.70
74	ESF-HD-HYD-6	Hydrology	-29.380/30.194/6.811	8.168/30.068/20.601	7.70
75	ESF-HD-HYD-7	Hydrology	-29.306/30.215/6.303	10.024/30.485/12.913	7.70
76	ESF-HD-HYD-8	Hydrology	-29.295/30.177/6.002	10.731/30.178/6.737	7.70
77	ESF-HD-HYD-9	Hydrology	-29.331/30.210/5.672	8.268/29.906/-8.208	7.70
78	ESF-HD-HYD-10	Hydrology	-29.376/30.191/4.702	6.467/30.359/-12.931	7.70
79	ESF-HD-TEMP-1	Temperature	9.460/-11.022/3.752	9.459/48.478/2.706	10.00
80	ESF-HD-TEMP-2	Temperature	-9.486/-11.059/3.228	-9.903/48.570/3.162	10.00
81	ESF-HD-MPBX-1	MPBX – Rock Mass Displacement	6.994/-11.130/3.463	6.781/34.945/3.326	7.70
82	ESF-HD-MPBX-2	MPBX – Rock Mass Displacement	-7.028/-10.958/3.451	-7.675/35.252/3.128	7.70
83	ESF-HD-WH-1	Wing Heater	-2.483/1.837/-0.259	-14.005/1.848/-0.325	10.00
84	ESF-HD-WH-2	Wing Heater	-2.488/3.645/-0.239	-14.030/3.676/-0.182	10.00
85	ESF-HD-WH-3	Wing Heater	-2.470/5.498/-0.248	-14.050/5.529/-0.255	10.00
86	ESF-HD-WH-4	Wing Heater	-2.491/7.310/-0.251	-13.908/7.190/-0.353	10.00
87	ESF-HD-WH-5	Wing Heater	-2.605/9.154/-0.251	-13.963/9.334/-0.233	10.00
88	ESF-HD-WH-6	Wing Heater	-2.567/10.984/-0.242	-14.007/10.946/-0.249	10.00
89	ESF-HD-WH-7	Wing Heater	-2.778/12.816/-0.239	-14.001/12.881/-0.270	10.00
90	ESF-HD-WH-8	Wing Heater	-2.517/14.602/-0.269	-14.088/14.507/-0.381	10.00
91	ESF-HD-WH-9	Wing Heater	-2.512/16.482/-0.234	-13.791/16.640/-0.188	10.00
92	ESF-HD-WH-10	Wing Heater	-2.537/18.280/-0.260	-14.051/18.171/-0.342	10.00
93	ESF-HD-WH-11	Wing Heater	-2.447/20.108/-0.274	-13.970/20.104/-0.475	10.00
94	ESF-HD-WH-12	Wing Heater	-2.475/21.958/-0.246	-13.928/22.088/-0.237	10.00



Table 6.3-2. DST Borehole Information (Continued)

Borehole Number	Borehole Identification	Primary Purpose	Collar Coordinates (m) x/y/z	Bottom Coordinates (m) x/y/z	Diameter (cm)
95	ESF-HD-WH-13	Wing Heater	-2.575/23.777/-0.253	-14.065/23.777/-0.293	10.00
96	ESF-HD-WH-14	Wing Heater	-2.603/25.617/-0.278	-14.092/25.653/-0.550	10.00
97	ESF-HD-WH-15	Wing Heater	-2.541/27.451/-0.234	-14.051/27.619/-0.350	10.00
98	ESF-HD-WH-16	Wing Heater	-2.445/29.241/-0.238	-13.642/29.156/-0.254	10.00
99	ESF-HD-WH-17	Wing Heater	-2.584/31.126/-0.260	-14.038/31.267/-0.263	10.00
100	ESF-HD-WH-18	Wing Heater	-2.466/32.933/-0.247	-13.995/33.022/-0.311	10.00
101	ESF-HD-WH-19	Wing Heater	-2.715/34.732/-0.262	-14.062/34.660/-0.281	10.00
102	ESF-HD-WH-20	Wing Heater	-2.595/36.571/-0.283	-14.000/36.407/-0.621	10.00
103	ESF-HD-WH-21	Wing Heater	-2.597/38.409/-0.246	-14.167/38.457/-0.160	10.00
104	ESF-HD-WH-22	Wing Heater	-2.613/40.230/-0.250	-14.133/40.306/-0.099	10.00
105	ESF-HD-WH-23	Wing Heater	-2.588/42.092/-0.272	-14.109/42.233/-0.246	10.00
106	ESF-HD-WH-24	Wing Heater	-2.590/43.875/-0.239	-14.109/43.911/-0.155	10.00
107	ESF-HD-WH-25	Wing Heater	-2.567/45.734/-0.260	-14.150/45.795/-0.384	10.00
108	ESF-HD-WH-26	Wing Heater	2.593/45.737/-0.278	14.083/45.805/-0.489	10.00
109	ESF-HD-WH-27	Wing Heater	2.581/43.876/-0.251	14.099/43.790/-0.302	10.00
110	ESF-HD-WH-28	Wing Heater	2.582/42.065/-0.258	14.106/42.121/-0.216	10.00
111	ESF-HD-WH-29	Wing Heater	2.586/40.216/-0.236	14.099/40.278/-0.133	10.00
112	ESF-HD-WH-30	Wing Heater	2.561/38.385/-0.262	14.178/38.316/-0.269	10.00
113	ESF-HD-WH-31	Wing Heater	2.576/36.561/-0.245	14.141/36.476/-0.212	10.00
114	ESF-HD-WH-32	Wing Heater	2.850/34.787/-0.273	14.325/34.970/-0.276	10.00
115	ESF-HD-WH-33	Wing Heater	2.593/32.913/-0.232	14.115/32.667/-0.194	10.00
116	ESF-HD-WH-34	Wing Heater	2.668/31.081/-0.254	13.903/31.031/-0.229	10.00
117	ESF-HD-WH-35	Wing Heater	2.646/29.228/-0.241	13.813/29.165/-0.129	10.00
118	ESF-HD-WH-36	Wing Heater	2.609/27.420/-0.207	14.168/27.390/-0.048	10.00
119	ESF-HD-WH-37	Wing Heater	2.498/25.603/-0.256	14.100/25.657/-0.406	10.00
120	ESF-HD-WH-38	Wing Heater	2.509/23.775/-0.267	13.979/23.831/-0.377	10.00
121	ESF-HD-WH-39	Wing Heater	2.451/21.940/-0.272	14.077/21.945/-0.299	10.00

Table 6.3-2. DST Borehole Information (Continued)

Borehole Number	Borehole Identification	Primary Purpose	Collar Coordinates (m) x/y/z	Bottom Coordinates (m) x/y/z	Diameter (cm)
122	ESF-HD-WH-40	Wing Heater	2.482/20.114/-0.249	14.082/20.122/-0.232	10.00
123	ESF-HD-WH-41	Wing Heater	2.490/18.287/-0.248	14.050/18.275/-0.297	10.00
124	ESF-HD-WH-42	Wing Heater	2.529/16.434/-0.273	14.025/16.280/-0.514	10.00
125	ESF-HD-WH-43	Wing Heater	2.509/14.643/-0.288	13.977/14.678/-0.523	10.00
126	ESF-HD-WH-44	Wing Heater	2.511/12.801/-0.245	14.145/12.865/-0.342	10.00
127	ESF-HD-WH-45	Wing Heater	2.578/10.949/-0.272	14.056/10.705/-0.441	10.00
128	ESF-HD-WH-46	Wing Heater	2.515/9.141/-0.260	14.012/9.212/-0.419	10.00
129	ESF-HD-WH-47	Wing Heater	2.612/7.313/-0.245	14.069/7.108/-0.272	10.00
130	ESF-HD-WH-48	Wing Heater	2.561/5.504/-0.230	14.011/5.350/-0.177	10.00
131	ESF-HD-WH-49	Wing Heater	2.567/3.672/-0.277	14.078/3.705/-0.326	10.00
132	ESF-HD-WH-50	Wing Heater	2.648/1.816/-0.264	14.000/1.583/-0.444	10.00
133	ESF-HD-TEMP-3	Temperature	0.749/2.736/2.397	0.878/2.834/22.465	7.70
134	ESF-HD-TEMP-4	Temperature	0.736/2.734/-1.603	0.635/2.787/-22.938	7.70
135	ESF-HD-ERT-5	Electrical Resistivity Tomography	-0.763/2.709/2.397	-0.957/2.756/22.399	7.70
136	ESF-HD-ERT-6	Electrical Resistivity Tomography	-0.758/2.740/-1.615	-0.707/2.625/-17.953	7.70
137	ESF-HD-TEMP-5	Temperature	0.775/11.918/2.510	0.880/11.840/22.463	7.70
138	ESF-HD-TEMP-6	Temperature	-1.983/11.880/1.958	-15.960/11.516/15.926	7.70
139	ESF-HD-TEMP-7	Temperature	-2.569/11.891/-0.017	-22.536/11.953/0.149	7.70
140	ESF-HD-TEMP-8	Temperature	-1.911/11.907/-1.599	-17.366/11.791/-14.661	7.70
141	ESF-HD-TEMP-9	Temperature	0.764/11.893/-1.637	0.570/12.034/-22.973	7.70
142	ESF-HD-TEMP-10	Temperature	1.617/11.912/-1.639	16.017/11.903/-15.924	7.70
143	ESF-HD-TEMP-11	Temperature	2.665/11.890/-0.008	22.513/11.918/0.022	7.70
144	ESF-HD-TEMP-12	Temperature	2.009/11.915/1.982	16.394/12.063/16.351	7.70
145	ESF-HD-ERT-7	Electrical Resistivity Tomography	-0.757/11.892/2.579	-0.899/12.019/22.667	7.70
146	ESF-HD-ERT-8	Electrical Resistivity Tomography	-0.757/11.894/-1.613	-1.065/11.929/-18.014	7.70
147	ESF-HD-MPBX-3	MPBX – Rock Mass Displacement	1.284/13.706/2.213	8.682/13.653/15.233	7.70
148	ESF-HD-MPBX-4	MPBX – Rock Mass Displacement	-1.390/13.725/2.387	-8.864/13.700/15.172	7.70
149	ESF-HD-MPBX-5	MPBX – Rock Mass Displacement	-0.028/13.697/2.484	-0.097/13.608/17.594	7.70

Table 6.3-2. DST Borehole Information (Continued)

Borehole Number	Borehole Identification	Primary Purpose	Collar Coordinates (m) x/y/z	Bottom Coordinates (m) x/y/z	Diameter (cm)
150	ESF-HD-MPBX-6	MPBX – Rock Mass Displacement	0.006/13.693/-1.639	0.145/13.807/-18.008	7.70
151	ESF-HD-REKA-1	Thermal Conductivity and Diffusivity	-0.027/17.352/2.669	-0.049/17.348/12.705	4.80
152	ESF-HD-REKA-2	Thermal Conductivity and Diffusivity	-2.437/17.359/0.017	-12.528/17.234/0.078	4.80
153	ESF-HD-REKA-3	Thermal Conductivity and Diffusivity	-1.603/17.359/-1.603	-9.199/17.241/-9.312	4.80
154	ESF-HD-MPBX-7	MPBX a – Rock Mass Displacement	1.285/21.020/2.186	8.867/21.011/15.099	7.70
155	ESF-HD-MPBX-8	MPBX – Rock Mass Displacement	-1.317/21.006/2.270	-9.016/20.919/15.268	7.70
156	ESF-HD-MPBX-9	MPBX – Rock Mass Displacement	-0.013/21.001/2.504	0.028/20.944/17.482	7.70
157	ESF-HD-MPBX-10	MPBX – Rock Mass Displacement	-0.004/21.037/-1.624	0.031/21.014/-17.820	7.70
158	ESF-HD-TEMP-13	Temperature	0.757/22.847/2.565	0.412/23.021/22.599	7.70
159	ESF-HD-TEMP-14	Temperature	-1.949/22.876/1.931	-16.007/22.892/16.157	7.70
160	ESF-HD-TEMP-15	Temperature	-2.502/22.871/-0.004	-22.615/22.956/0.107	7.70
161	ESF-HD-TEMP-16	Temperature	-1.607/22.883/-1.605	-16.040/23.241/-15.875	7.70
162	ESF-HD-TEMP-17	Temperature	0.769/22.850/-1.623	0.828/23.004/-22.820	7.70
163	ESF-HD-TEMP-18	Temperature	1.515/22.828/-1.597	15.772/22.510/-15.913	7.70
164	ESF-HD-TEMP-19	Temperature	2.489/22.869/0.016	22.586/23.017/0.299	7.70
165	ESF-HD-TEMP-20	Temperature	1.862/22.845/1.882	16.004/22.754/16.020	7.70
166	ESF-HD-ERT-9	Electrical Resistivity Tomography	-0.735/22.845/2.566	-0.558/23.020/22.390	7.70
167	ESF-HD-ERT-10	Electrical Resistivity Tomography	-0.772/22.810/-1.637	-0.458/22.747/-17.522	7.70
168	ESF-HD-TEMP-21	Temperature	-0.071/31.952/2.451	-0.335/31.978/22.650	7.70
169	ESF-HD-TEMP-22	Temperature	-0.003/32.007/-1.629	0.259/32.435/-22.894	7.70
170	ESF-HD-TEMP-23	Temperature	0.751/39.306/2.488	0.746/39.115/22.604	7.70
171	ESF-HD-TEMP-24	Temperature	-1.853/39.313/1.817	-15.619/39.292/15.716	7.70
172	ESF-HD-TEMP-25	Temperature	-1.581/39.291/-1.571	-16.011/38.870/-16.010	7.70
173	ESF-HD-TEMP-26	Temperature	0.758/39.324/-1.623	0.715/39.104/-22.887	7.70
174	ESF-HD-TEMP-27	Temperature	1.584/39.306/-1.586	16.413/38.942/-15.444	7.70
175	ESF-HD-TEMP-28	Temperature	1.880/39.320/1.843	15.914/39.177/16.275	7.70
176	ESF-HD-ERT-11	Electrical Resistivity Tomography	-0.750/39.296/2.463	-0.779/39.120/22.462	7.70
177	ESF-HD-ERT-12	Electrical Resistivity Tomography	-0.739/39.327/-1.623	-0.749/39.263/-17.823	7.70

Table 6.3-2. DST Borehole Information (Continued)

Borehole Number	Borehole Identification	Primary Purpose	Collar Coordinates (m) x/y/z	Bottom Coordinates (m) x/y/z	Diameter (cm)
178	ESF-HD-MPBX-11	MPBX – Rock Mass Displacement	1.297/41.138/2.249	8.693/41.103/15.341	7.70
179	ESF-HD-MPBX-12	MPBX – Rock Mass Displacement	-1.319/41.143/2.279	-8.785/41.067/15.433	7.70
180	ESF-HD-MPBX-13	MPBX – Rock Mass Displacement	0.010/41.134/2.597	0.121/41.079/17.687	7.70
181	ESF-HD-MPBX-14	MPBX – Rock Mass Displacement	0.035/41.194/-1.658	0.083/41.211/-18.122	7.70
182	ESF-HD-PERM-1	Ambient Characterization	11.616/-15.677/2.284	11.954/-34.533/-4.367	7.70
183	ESF-HD-PERM-2	Ambient Characterization	10.716/-15.649/3.045	10.861/-35.731/3.003	7.70
184	ESF-HD-PERM-3	Ambient Characterization	8.853/-15.678/2.298	8.856/-34.504/-4.376	7.70
185	ESF-HD-HYD-11	Hydrology	-29.488/44.728/7.563	10.084/44.145/13.613	7.70
186	ESF-HD-HYD-12	Hydrology	-29.609/44.774/6.470	5.008/44.352/-13.807	7.70
187	ESF-PL-MPBX-1	MPBX – Rock Mass Displacement	5.499/-5.137/-0.286	5.464/-8.529/-0.358	7.70
188	ESF-PL-MPBX-2	MPBX – Rock Mass Displacement	5.502/-2.759/-0.262	5.458/0.471/-0.270	7.70
	ESF-HD-CAN1 <sup>a</sup>	Floor Heater	-0.144/0.565/-0.218	-0.144/5.213/-0.218	N/A
	ESF-HD-CAN2 <sup>a</sup>	Floor Heater	-0.156/5.848/-0.237	-0.156/10.496/-0.237	N/A
	ESF-HD-CAN3 <sup>a</sup>	Floor Heater	-0.139/11.013/-0.236	-0.139/15.661/-0.236	N/A
	ESF-HD-CAN4 <sup>a</sup>	Floor Heater	-0.177/16.305/-0.250	-0.177/20.953/-0.250	N/A
	ESF-HD-CAN5 <sup>a</sup>	Floor Heater	-0.165/21.544/-0.251	-0.165/26.192/-0.251	N/A
	ESF-HD-CAN6 <sup>a</sup>	Floor Heater	-0.176/26.892/-0.246	-0.176/31.540/-0.246	N/A
	ESF-HD-CAN7 <sup>a</sup>	Floor Heater	-0.167/32.077/-0.237	-0.167/36.725/-0.237	N/A
	ESF-HD-CAN8 <sup>a</sup>	Floor Heater	-0.148/37.375/-0.225	-0.148/42.023/-0.225	N/A
	ESF-HD-CAN9 <sup>a</sup>	Floor Heater	-0.163/42.664/-0.235	-0.163/47.312/-0.235	N/A
	ESF-HD-83-WH1	Wing Heater	-4.263/1.839/-0.269	-14.093/1.848/-0.326	N/A
	ESF-HD-84-WH2	Wing Heater	-4.208/3.650/-0.231	-14.038/3.676/-0.182	N/A
	ESF-HD-85-WH3	Wing Heater	-4.250/5.503/-0.249	-14.080/5.529/-0.255	N/A
	ESF-HD-86-WH4	Wing Heater	-4.081/7.293/-0.265	-13.910/7.190/-0.353	N/A
	ESF-HD-87-WH5	Wing Heater	-4.175/9.179/-0.249	-14.004/9.335/-0.233	N/A
	ESF-HD-88-WH6	Wing Heater	-4.137/10.979/-0.243	-13.967/10.946/-0.249	N/A
	ESF-HD-89-WH7	Wing Heater	-4.348/12.825/-0.243	-14.178/12.882/-0.270	N/A
	ESF-HD-90-WH8	Wing Heater	-4.267/14.588/-0.286	-14.096/14.507/-0.381	N/A

Table 6.3-2. DST Borehole Information (Continued)

Borehole Number	Borehole Identification	Primary Purpose	Collar Coordinates (m) x/y/z	Bottom Coordinates (m) x/y/z	Diameter (cm)
	ESF-HD-91-WH9	Wing Heater	-4.292/16.507/-0.227	-14.121/16.645/-0.187	N/A
	ESF-HD-92-WH10	Wing Heater	-4.237/18.264/-0.272	-14.066/18.171/-0.342	N/A
	ESF-HD-93-WH11	Wing Heater	-4.127/20.107/-0.303	-13.955/20.104/-0.475	N/A
	ESF-HD-94-WH12	Wing Heater	-4.035/21.976/-0.245	-13.864/22.087/-0.237	N/A
	ESF-HD-95-WH13	Wing Heater	-4.255/23.777/-0.259	-14.085/23.777/-0.293	N/A
	ESF-HD-96-WH14	Wing Heater	-4.233/25.622/-0.317	-14.060/25.653/-0.549	N/A
	ESF-HD-97-WH15	Wing Heater	-3.691/27.468/-0.246	-13.519/27.611/-0.345	N/A
	ESF-HD-98-WH16	Wing Heater	-4.115/29.228/-0.240	-13.945/29.154/-0.254	N/A
	ESF-HD-99-WH17	Wing Heater	-4.184/31.146/-0.260	-14.013/31.267/-0.263	N/A
	ESF-HD-100-WH18	Wing Heater	-4.186/32.946/-0.257	-14.015/33.022/-0.311	N/A
	ESF-HD-101-WH19	Wing Heater	-4.215/34.722/-0.265	-14.045/34.660/-0.281	N/A
	ESF-HD-102-WH20	Wing Heater	-4.204/36.548/-0.331	-14.029/36.407/-0.622	N/A
	ESF-HD-103-WH21	Wing Heater	-4.267/38.416/-0.234	-14.097/38.457/-0.161	N/A
	ESF-HD-104-WH22	Wing Heater	-4.313/40.241/-0.228	-14.142/40.306/-0.099	N/A
	ESF-HD-105-WH23	Wing Heater	-4.018/42.109/-0.269	-13.847/42.230/-0.247	N/A
	ESF-HD-106-WH24	Wing Heater	-4.260/43.880/-0.227	-14.090/43.911/-0.155	N/A
	ESF-HD-107-WH25	Wing Heater	-4.267/45.743/-0.278	-14.096/45.795/-0.383	N/A
	ESF-HD-108-WH26	Wing Heater	4.263/45.747/-0.309	14.091/45.805/-0.489	N/A
	ESF-HD-109-WH27	Wing Heater	4.211/43.864/-0.258	14.041/43.790/-0.302	N/A
	ESF-HD-110-WH28	Wing Heater	4.202/42.073/-0.252	14.032/42.121/-0.216	N/A
	ESF-HD-111-WH29	Wing Heater	4.226/40.225/-0.221	14.055/40.278/-0.133	N/A
	ESF-HD-112-WH30	Wing Heater	4.311/38.375/-0.263	14.141/38.316/-0.269	N/A
	ESF-HD-113-WH31	Wing Heater	4.296/36.548/-0.240	14.126/36.476/-0.212	N/A
	ESF-HD-114-WH32	Wing Heater	4.450/34.813/-0.273	14.279/34.969/-0.276	N/A
	ESF-HD-115-WH33	Wing Heater	4.233/32.878/-0.227	14.060/32.668/-0.194	N/A
	ESF-HD-116-WH34	Wing Heater	4.018/31.075/-0.251	13.848/31.031/-0.229	N/A
	ESF-HD-117-WH35	Wing Heater	3.946/29.221/-0.228	13.775/29.165/-0.129	N/A

Table 6.3-2. DST Borehole Information (Continued)

Borehole Number	Borehole Identification	Primary Purpose	Collar Coordinates (m) x/y/z	Bottom Coordinates (m) x/y/z	Diameter (cm)
	ESF-HD-118-WH36	Wing Heater	4.219/27.416/-0.185	14.048/27.390/-0.050	N/A
	ESF-HD-119-WH37	Wing Heater	4.268/25.611/-0.279	14.097/25.657/-0.406	N/A
	ESF-HD-120-WH38	Wing Heater	4.009/23.782/-0.281	13.838/23.830/-0.376	N/A
	ESF-HD-121-WH39	Wing Heater	4.251/21.941/-0.276	14.081/21.945/-0.299	N/A
	ESF-HD-122-WH40	Wing Heater	3.162/20.114/-0.248	12.992/20.121/-0.234	N/A
	ESF-HD-123-WH41	Wing Heater	4.130/18.285/-0.255	13.960/18.275/-0.297	N/A
	ESF-HD-124-WH42	Wing Heater	4.328/16.410/-0.311	14.155/16.278/-0.517	N/A
	ESF-HD-125-WH43	Wing Heater	4.299/14.648/-0.325	14.127/14.678/-0.526	N/A
	ESF-HD-126-WH44	Wing Heater	4.131/12.810/-0.259	13.960/12.864/-0.340	N/A
	ESF-HD-127-WH45	Wing Heater	4.287/10.913/-0.297	14.114/10.704/-0.442	N/A
	ESF-HD-128-WH46	Wing Heater	4.115/9.151/-0.282	13.944/9.212/-0.418	N/A
	ESF-HD-129-WH47	Wing Heater	3.922/7.290/-0.248	13.750/7.114/-0.271	N/A
	ESF-HD-130-WH48	Wing Heater	4.161/5.482/-0.223	13.990/5.350/-0.177	N/A
	ESF-HD-131-WH49	Wing Heater	3.067/3.673/-0.279	12.897/3.702/-0.321	N/A
	ESF-HD-132-WH50	Wing Heater	4.287/1.782/-0.290	14.114/1.581/-0.446	N/A
	ESF-HD-CDEX-MPBX-1	Cross Extensometer	0.427/42.357/2.510	0.409/42.357/-1.250	N/A
	ESF-HD-CDEX-MPBX-2	Cross Extensometer	2.547/42.268/-0.019	-2.547/42.277/0.011	N/A

Source: DTN: M00002ABBLSLDS.000 [DIRS 147304].

<sup>a</sup> Canister heater coordinates are for the approximate longitudinal centerline of the two ends.

NOTE: Borehole coordinates are referenced to 0,0,0 coordinate located at the center of the bulkhead in the heated drift.

### 6.3.1 DST Thermal Measurements

The following sections present discussions on the power and temperature histories of the DST during the four-year heating phase. Discussion includes measurements of heater power and rock-mass temperatures, as well as parameters derived from laboratory and field measurements.

Detailed discussion of DST power and thermal measurements is provided in Sections 6.2 and 8 of *Drift Scale Test Design and Forecast Results* (CRWMS M&O 1997 [DIRS 146917]), in Sections 5.1.1, 6, and 9 of *Drift Scale Test As-Built Report* (CRWMS M&O 1998 [DIRS 111115]), and in Sections 3 and 10.2 of *Ambient Characterization of the Drift Scale Test Block* (CRWMS M&O 1997 [DIRS 101539]). The input and summary DTNs for DST power and thermal measurements are listed in Tables 4-3 and 6.3-1.

#### 6.3.1.1 Heater Power

Heat was generated from 50 wing heaters and 9 floor (canister) heaters. These two types of electrical heaters had a combined power output of approximately 280 kW when operating at full capacity. The nine canister heaters were located in the center of the drift along a distance of approximately 47 m. The wing heaters were inserted in horizontal boreholes in the wall of the heated drift perpendicular to the longitudinal axis of the heated drift. These wing heaters were evenly distributed on 1.83 m spacings in boreholes located on both walls of the heated drift. Each wing heater had 10 m of heated length evenly divided between inner and outer heating elements of 1.145-kW and 1.719-kW capacity, respectively.

Each of the nine canister heaters in the heated drift has 60 heating elements, only 30 of which were on at any given time (the other 30 elements were backups). To estimate the power supplied to each canister, the current being supplied to all the heating elements in a given canister was summed and the result multiplied by the canister heater voltage. Note that for the first 20 days of the test, only 28 heating elements in canister #8 were active. A 29th heating element was activated on day 20 and the 30th heating element on day 40.

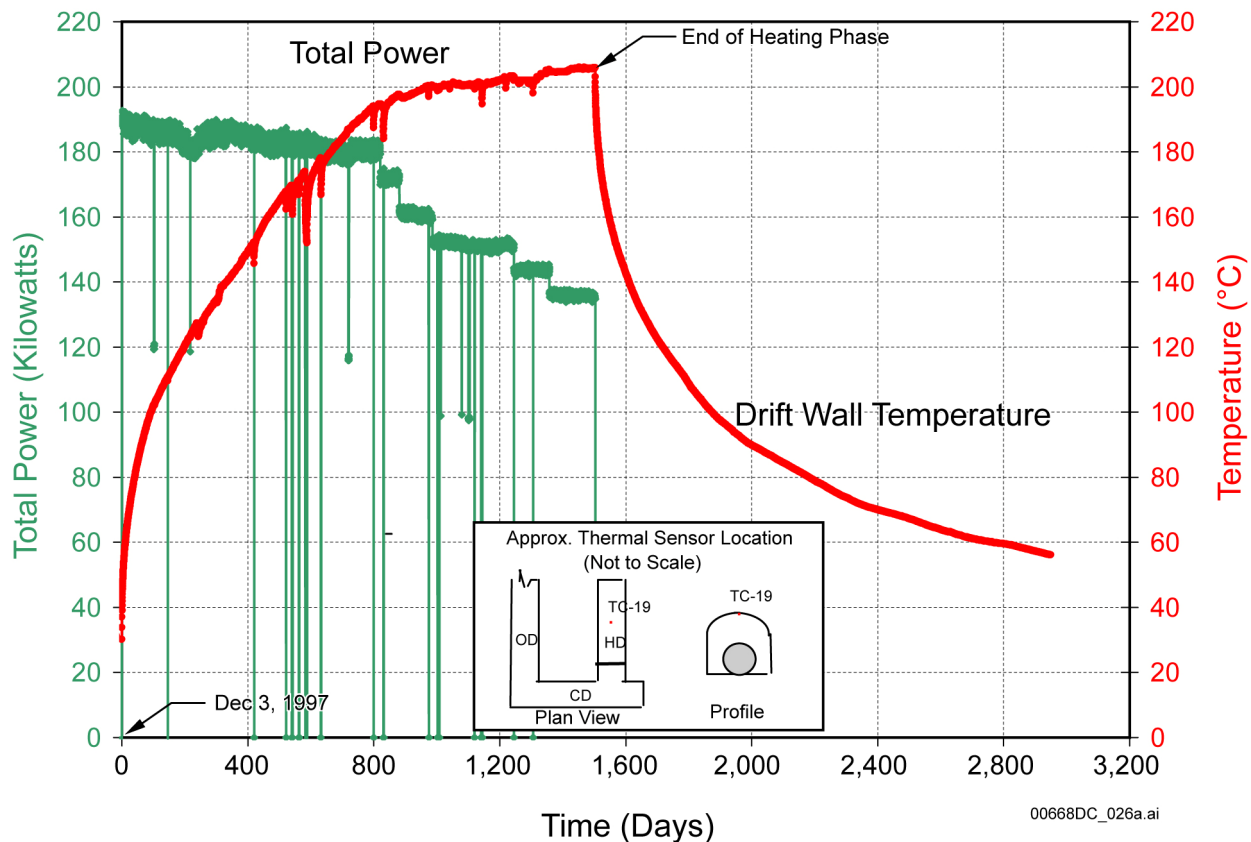
The DST wing heater, canister heater, and total power data may be found in the following input DTNs:

- MO9807DSTSET01.000 [DIRS 113644]
- MO9810DSTSET02.000 [DIRS 113662]
- MO9906DSTSET03.000 [DIRS 113673]
- MO0001SEPDSTPC.000 [DIRS 153836]
- MO0007SEPDSTPC.001 [DIRS 153707]
- MO0012SEPDSTPC.002 [DIRS 153708]
- MO0107SEPDSTPC.003 [DIRS 158321]
- MO0202SEPDSTTV.001 [DIRS 158320].

### 6.3.1.1.1 Results: Heater Power

Because of the numerous DST power measurements, only representative discussion and graphics are provided. DST power measurements and graphics can be accessed in the summary DTNs identified in Table 6.3-1.

Figure 6.3-9 shows the total power applied to the wing heaters and the canister heaters, as a function of time. For the first 800 days, average total power to the wing heaters is approximately 135 kW, average total power to the canister heaters is approximately 52 kW, and average sum of the wing and canister power is approximately 187 kW. The voltage applied to the wing and canister heaters is also recorded. Average wing and canister heater voltages have been stable at approximately 212 and 189 volts, respectively.



Source: DTNs: MO0001SEPDSTPC.000 [DIRS 153836]; MO0007SEPDSTPC.001 [DIRS 153707]; MO0012SEPDSTPC.002 [DIRS 153708]; MO0107SEPDSTPC.003 [DIRS 158321]; MO0202SEPDSTTV.001 [DIRS 158320]; MO0208SEPDSTTD.001 [DIRS 161767]; MO0303SEPDSTTM.000 [DIRS 165698]; MO0307SEPDST31.000 [DIRS 165699]; MO0403SEPDST32.000 [DIRS 177813]; MO0408SEPDSTTD.000 [DIRS 177814]; MO0509SEPDSTTD.000 [DIRS 177815]; MO0603SEPDSTTD.000 [DIRS 177816]; MO9807DSTSET01.000 [DIRS 113644]; MO9810DSTSET02.000 [DIRS 113662]; MO9906DSTSET03.000 [DIRS 113673].

Figure 6.3-9. Total Power and Representative Drift Wall Temperature (TC-19) during the DST Heating Phase



For the first 820 days of the test, the power was nearly constant, dropping from an initial value of approximately 188 kW to approximately 178 kW. On March 3, 2000, the first of five intentional interim power reductions was implemented to maintain drift wall temperature near 200°C (see temperature plot at drift crown in Figure 6.3-9). The fifth and final interim power reduction occurred on August 22, 2001. After these five interim reductions, the total power was approximately 140 kW, or approximately 75% of its initial level. On January 14, 2002, all heaters to the DST were reduced to zero power.

Of the 100 wing-heater elements, 5 failed. Both elements of wing heater 29 failed after 185 days of heating, the outer element of wing heater 26 failed after 211 days of heating, the outer element of wing heater 9 failed after 412 days of heating, and the outer element of wing heater 16 failed after 622 days of heating.

#### **6.3.1.1.2 Measurement Uncertainty: Heater Power**

The accuracy of the watt transducers used in measuring the heater power is conservatively estimated to be within 2%. Refer to Section 6.1.1.1.2 for additional discussion of uncertainty related to heater power.

#### **6.3.1.2 Temperatures**

Temperatures of the rock in the DST were measured from approximately 1,950 resistance temperature devices (RTDs). Temperatures elsewhere in the DST, including the heated drift, wing-heater boreholes, and multipoint borehole extensometer (MPBX) boreholes, were measured with approximately 700 thermocouples as described in *Drift Scale Test As-Built Report* (CRWMS M&O 1998 [DIRS 111115]). Temperature boreholes in the DST were designed to ensure three-dimensional measurement of the thermal field. RTD sensors, which were used to measure rock-mass temperature, were bundled together with a uniform spacing of 30 cm between sensor tips. The spatial density of thermocouple sensors along an instrument borehole is higher in regions where greater thermal gradients are expected. The spatial density is also higher in regions where transition between dryout and condensation is expected to develop during the tests.

The range of temperature in the DST depended on the location of the measurement and the duration of heating. The highest temperatures were encountered in the vicinity of the heat sources (i.e., wing heaters). In these regions, the range of temperature varied from ambient to about 300°C. To properly cover the expected range of temperatures, sensors with the capability of measuring temperatures to at least 300°C were used. RTDs and thermocouples are commercially available for the expected temperature range, and are reliable for long term monitoring.

The heating-phase temperature data in the summary DTN for approximately 1,950 RTDs are organized into individual EXCEL workbooks corresponding to each temperature borehole. Each workbook contains spreadsheets and charts. On one EXCEL spreadsheet, the data are organized with each RTD temperature history in each column in ten-day intervals for the duration of the heating phase. In general, there are approximately 70 RTDs for most of the temperature boreholes. Individual columns can be hidden or revealed for graphical display or usage.

Another EXCEL spreadsheet in the workbook contains, for each temperature borehole, the coordinates for the respective temperature sensors. Two types of thermal graphs are developed in two separate charts. The first chart shows temperature history. The second chart shows temperature profiles as a function of a spatial coordinate at various times during the DST heating phase. These two types of graphics are intended to facilitate comparison with simulations for the validation of thermal-hydrological process models.

The DST heating phase temperature data may be found in the following DTNs:

- MO9807DSTSET01.000 [DIRS 113644]
- MO9810DSTSET02.000 [DIRS 113662]
- MO9906DSTSET03.000 [DIRS 113673]
- MO0001SEPDSTPC.000 [DIRS 153836]
- MO0007SEPDSTPC.001 [DIRS 153707]
- MO0012SEPDSTPC.002 [DIRS 153708]
- MO0107SEPDSTPC.003 [DIRS 158321]
- MO0202SEPDSTTV.001 [DIRS 158320].

The DST cooling phase temperature data may be found in the following DTNs:

- MO0208SEPDSTTD.001 [DIRS 161767]
- MO0303SEPDSTTM.000 [DIRS 165698]
- MO0307SEPDST31.000 [DIRS 165699]
- MO0403SEPDST32.000 [DIRS 177813]
- MO0408SEPDSTTD.000 [DIRS 177814]
- MO0509SEPDSTTD.000 [DIRS 177815]
- MO0603SEPDSTTD.000 [DIRS 177816].

### **6.3.1.2.1 Results: Temperatures**

Because of the numerous DST temperature measurements, only representative discussion and graphics are provided. DST temperature measurements and graphics can be accessed in the summary DTN identified in Table 6.3-1.

Figure 6.3-9 presents the temperature response for a single thermocouple (TC-19) located near the center of the heated drift during the heating phase of the DST. The temperature response at the drift wall follows an expected response, in that temperatures initially rise rapidly in response to switching on the heaters over a period of approximately 50 days. As time passes, the temperatures rise gradually, then the rate of rise decreases and the temperatures tend to remain flat as a result of the five interim power reductions during the final two years of the heating phase. After all heaters are switched off, the drift surface temperature, including TC-19, decreases rapidly. Gradually the rate of cooling slows with only the seasonal influences changing the smooth temperature decrease.

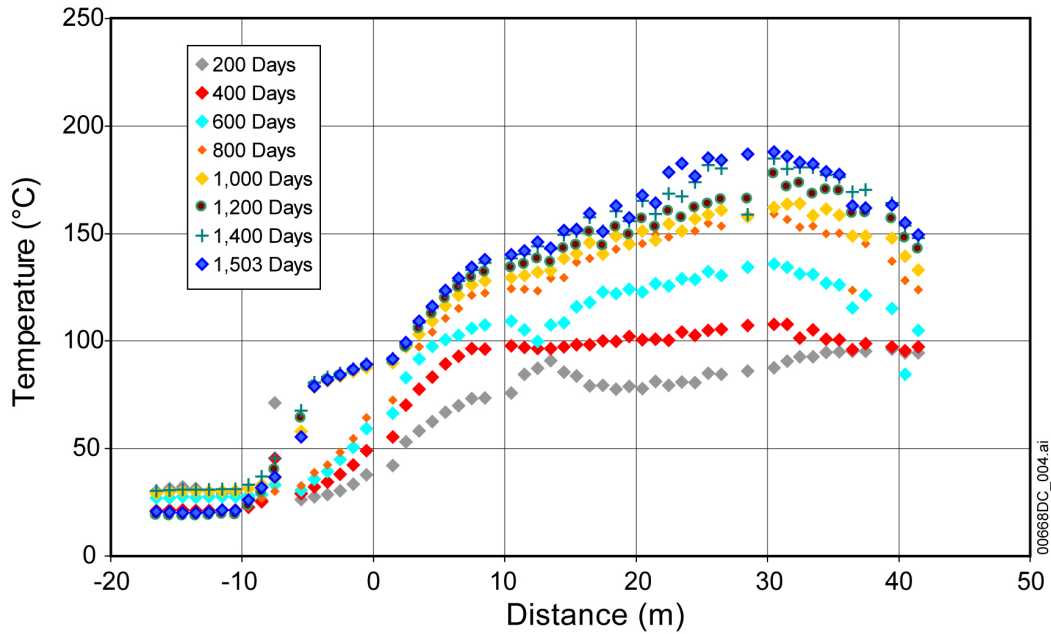
Thermocouples installed on the drift walls, at the drift crown (roof), and at the ribs (elevation of the wing heaters) recorded lower temperatures near both ends of the heated drift and higher temperatures at the mid-length of the heated drift. For a given distance along the heated drift

length, temperature is consistently higher at the wing-heater elevation. Boreholes 79 and 80 are parallel to the heated drift (Figure 6.3-3) and at an elevation of approximately 10 m from the centerline of the DST, above the horizontal boreholes that house the wing heaters. The temperature profiles (heating phase only) for boreholes 79 and 80 are presented in Figures 6.3-10 and 6.3-11, respectively. These temperatures are higher over the central part of the DST and lower over the unheated portion (the 11-m entry into the bulkhead of the heated drift). Also, note that the temperatures in borehole 79 are somewhat higher than those in borehole 80. This is because the elevation of borehole 79 could not be maintained during drilling because of its extreme length, causing it to be closer to the wing heaters than planned.

There are two notable thermal behaviors evident in borehole 79. The first is the tendency of the curves to flatten at an approximate temperature of 96°C, the boiling point of water at the site elevation. This phenomenon occurs because the temperature rise pauses temporarily at the boiling point as the water in the rock vaporizes due to the latent heat of vaporization as water changes phase from liquid to gas. The other notable thermal signature evident in borehole 79 is the temperature behavior near Y = 13 m (Figure 6.3-10). At sub-boiling temperatures, the rock near this location was substantially warmer than the rock on either side of it. Near the boiling point, the temperature profile was essentially constant, and at temperatures exceeding the boiling point, the rock near this location was somewhat cooler than the surrounding rock. This may be explained by the existence of a vertical fracture near this location. When the rock temperature was below boiling (i.e., the rock still contained liquid water), steam generated below this location (closer to the heater) may have been rising along the fracture, elevating the temperature of the rock near the fracture to levels exceeding those of adjacent rocks. At boiling, everything was isothermal for a while as water in the rock evaporated. After all the water in the rock had boiled off, the temperature of most of the rock started to increase again. Near the fracture, however, the temperature remained somewhat cooler than that of the surrounding rock. It may be that a lot of water condensed in this region when the temperature was sub-boiling, and additional heat was required to evaporate that water when the temperature in the vicinity of the fracture first reached and then exceeded the boiling temperature. Alternatively, the anomalous cool temperature near the fracture could reflect cool moisture flowing downward in the fracture toward the heated region.

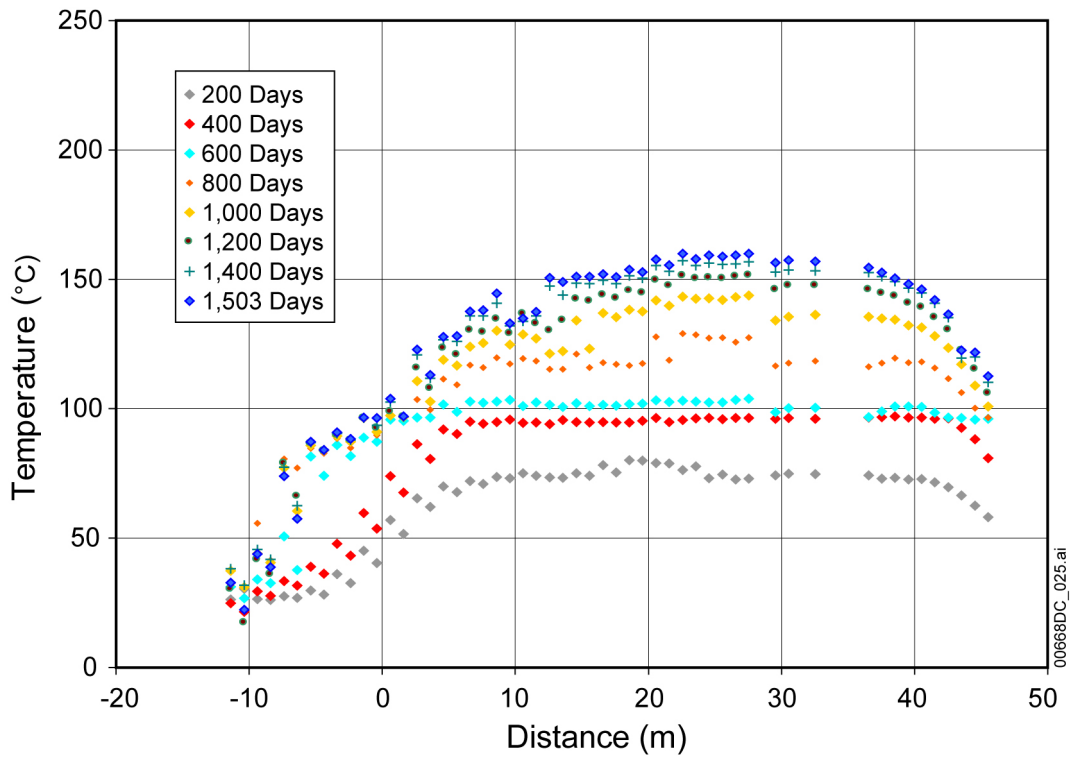
The other thermal DST boreholes were drilled radially away from the heated drift centerline at a fixed Y station. Figures 6.3-12 through 6.3-15 present temperature histories and temperature profiles for boreholes 158 and 164, respectively. Borehole 158 is orientated vertically up in the crown of the heated drift near its midlength. Borehole 164 is a horizontal borehole that parallels the wing heater boreholes. The temperature distribution shows the boiling phenomenon discussed above, as well as comparatively high rock temperatures characteristic of rock-mass in close proximity to the wing heaters.

Figure 6.3-16 provides the approximate location of the 96°C temperature contours after four years of heating in a vertical slice through the mid-length of the heated drift. These contours approximately define the dryout zone. The dryout zone is estimated to be 24,000 cubic meters at the end of the four-year heating phase.



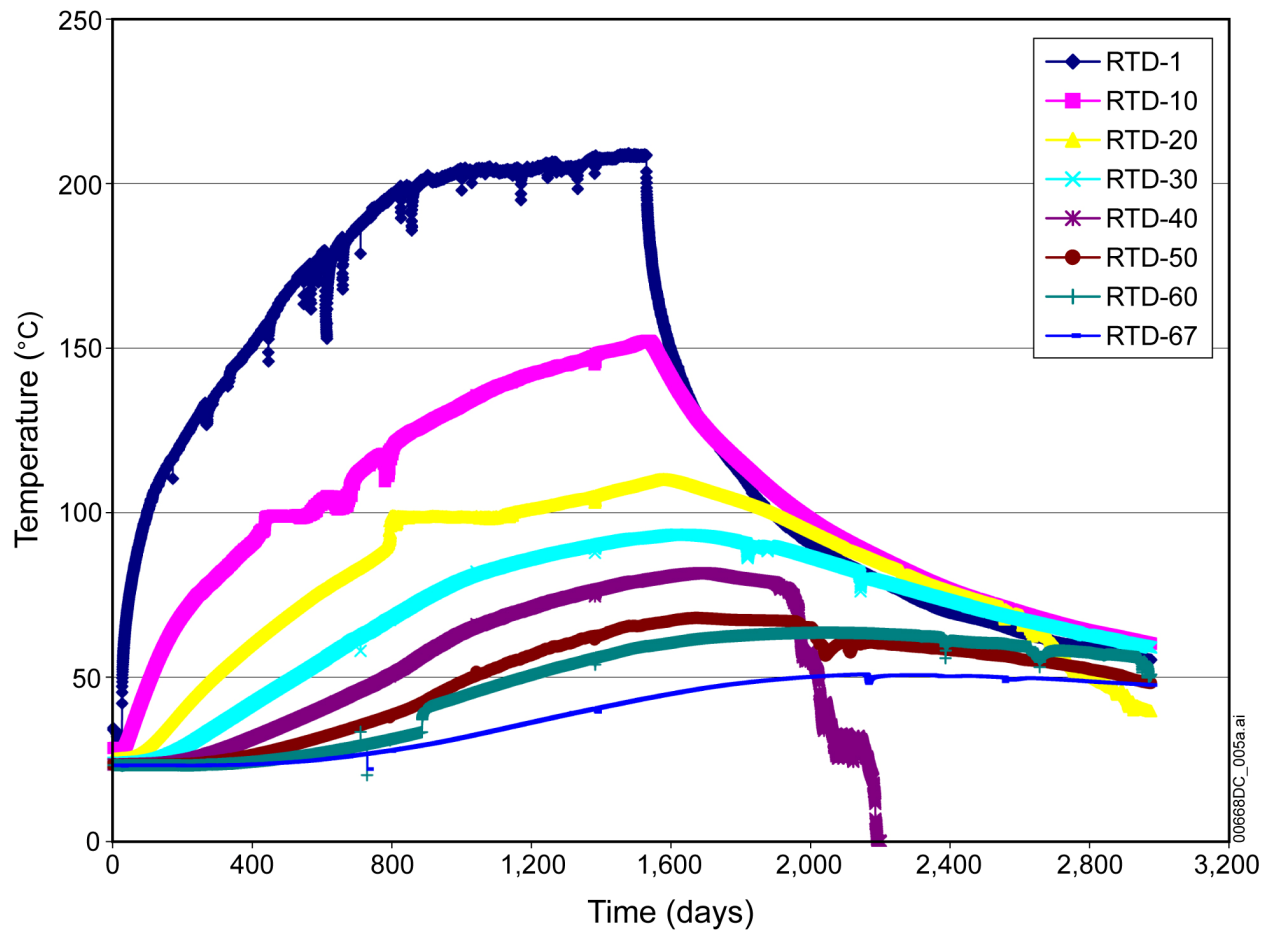
Source: DTN: MO0208RESTRDST.002 [DIRS 161129].

Figure 6.3-10. Temperature Profile along DST Borehole 79 at Select Times



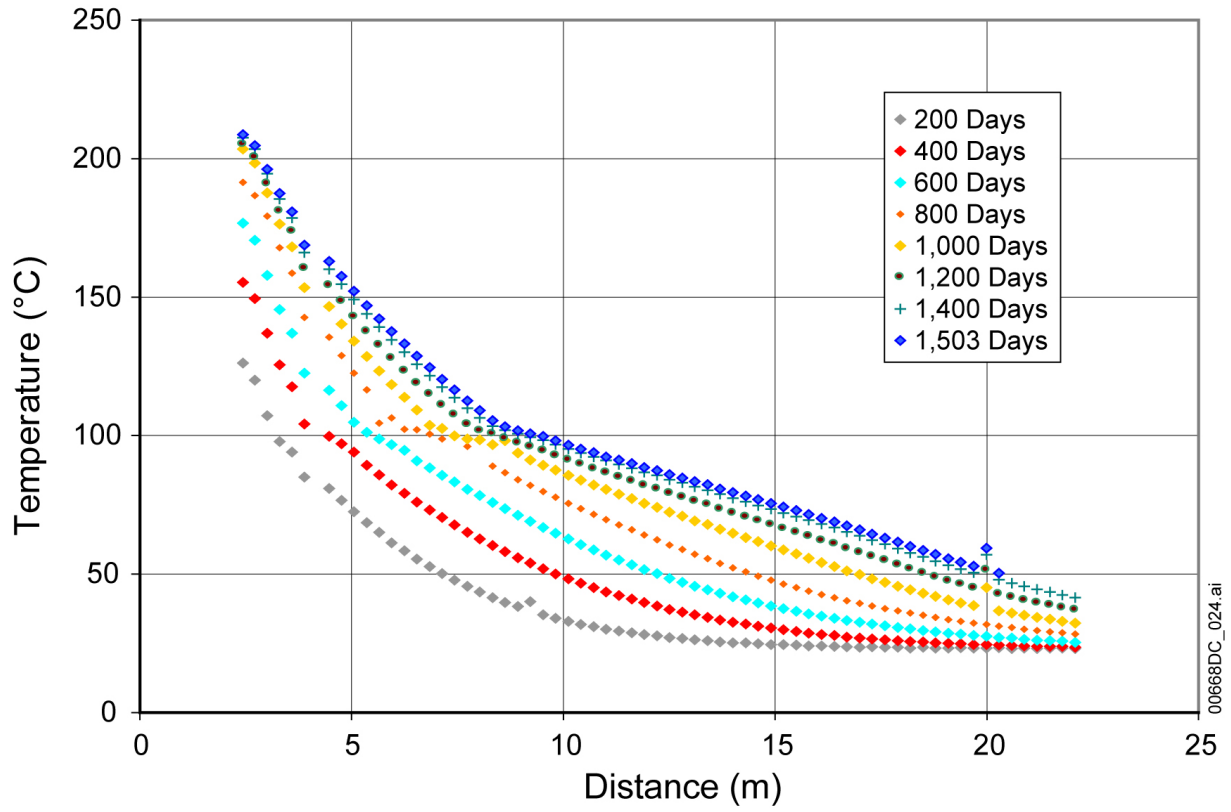
Source: DTN: MO0208RESTRDST.002 [DIRS 161129].

Figure 6.3-11. Temperature Profile along DST Borehole 80 at Select Times



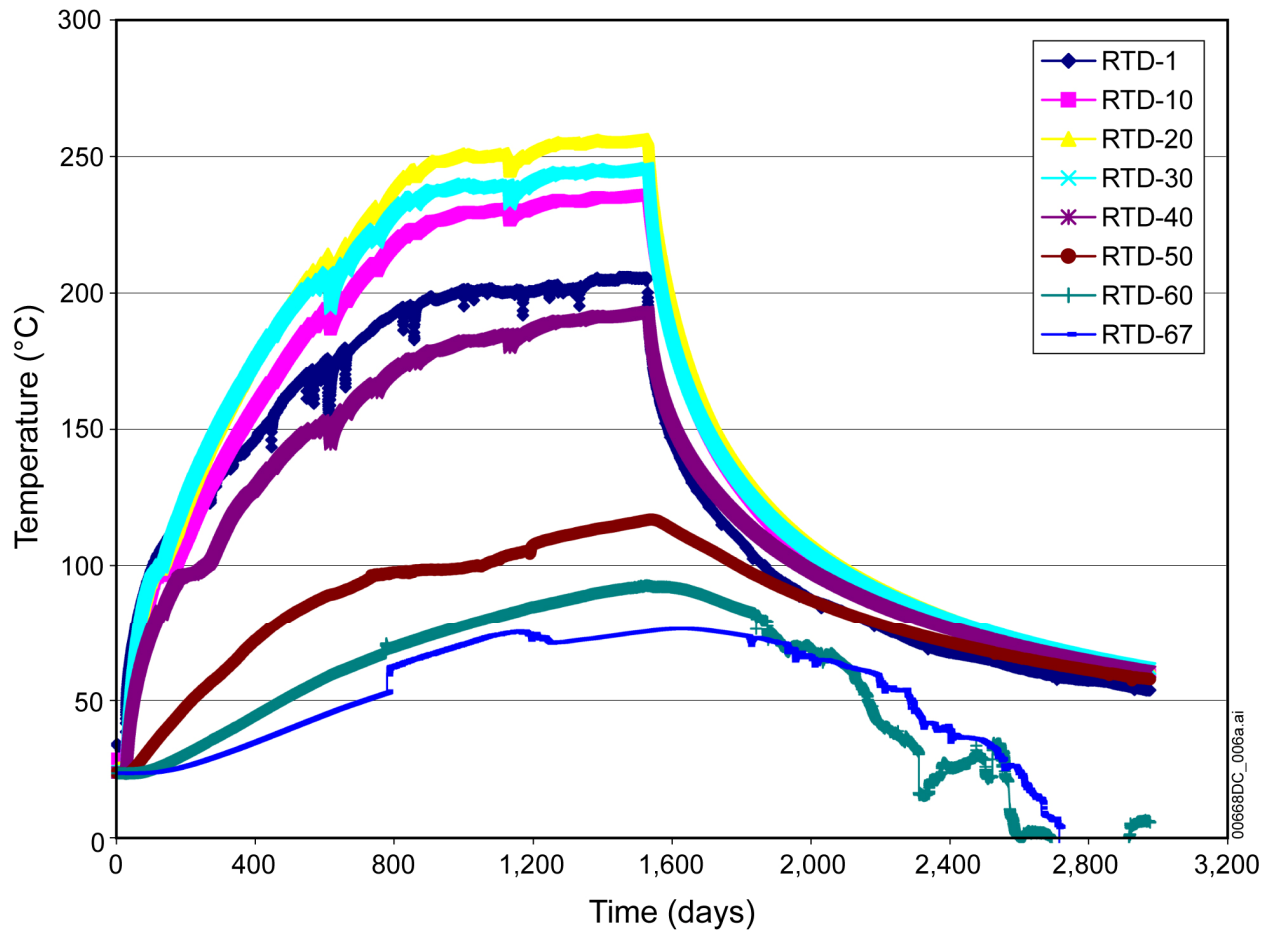
Source: DTNs: MO0001SEPDSTPC.000 [DIRS 153836]; MO0007SEPDSTPC.001 [DIRS 153707];  
 MO0012SEPDSTPC.002 [DIRS 153708]; MO0107SEPDSTPC.003 [DIRS 158321];  
 MO0202SEPDSTTV.001 [DIRS 158320]; MO0208SEPDSTTD.001 [DIRS 161767];  
 MO0303SEPDSTTM.000 [DIRS 165698]; MO0307SEPDST31.000 [DIRS 165699];  
 MO0403SEPDST32.000 [DIRS 177813]; MO0408SEPDSTTD.000 [DIRS 177814];  
 MO0509SEPDSTTD.000 [DIRS 177815]; MO0603SEPDSTTD.000 [DIRS 177816];  
 MO9807DSTSET01.000 [DIRS 113644]; MO9810DSTSET02.000 [DIRS 113662]; MO9906DSTSET03.000  
 [DIRS 113673].

Figure 6.3-12. Temperature Histories for DST Borehole 158 at Selected Locations



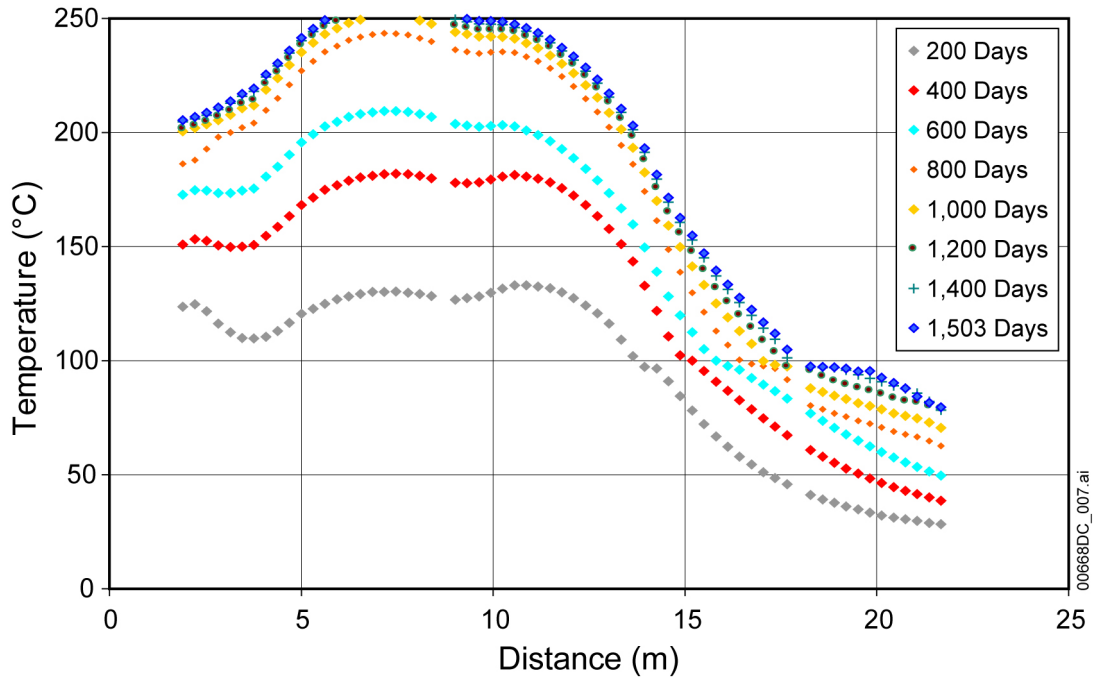
Source: DTN: MO0208RESTRDST.002 [DIRS 161129].

Figure 6.3-13. Temperature Profile along DST Borehole 158 at Select Times



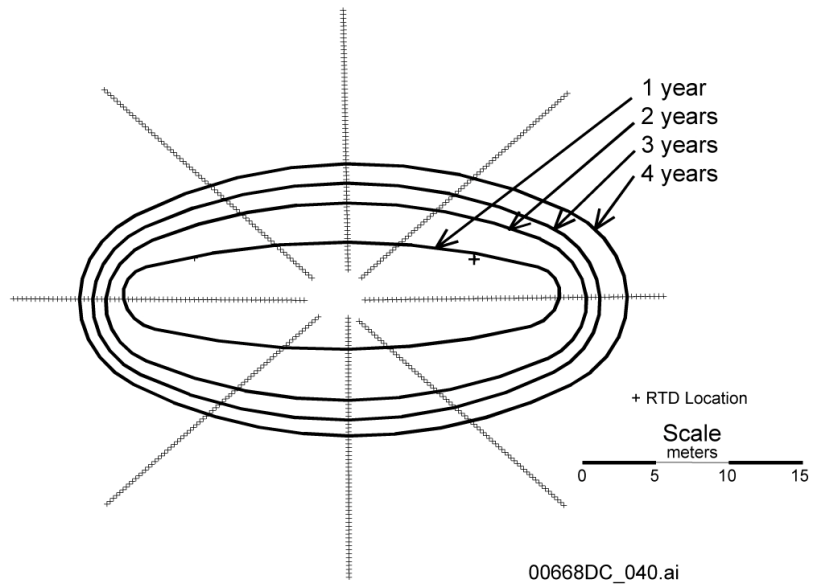
Source: DTNs: MO0001SEPDSTPC.000 [DIRS 153836]; MO0007SEPDSTPC.001 [DIRS 153707]; MO0012SEPDSTPC.002 [DIRS 153708]; MO0107SEPDSTPC.003 [DIRS 158321]; MO0202SEPDSTTV.001 [DIRS 158320]; MO0208SEPDSTTD.001 [DIRS 161767]; MO0303SEPDSTTM.000 [DIRS 165698]; MO0307SEPDST31.000 [DIRS 165699]; MO0403SEPDST32.000 [DIRS 177813]; MO0408SEPDSTTD.000 [DIRS 177814]; MO0509SEPDSTTD.000 [DIRS 177815]; MO0603SEPDSTTD.000 [DIRS 177816]; MO9807DSTSET01.000 [DIRS 113644]; MO9810DSTSET02.000 [DIRS 113662]; MO9906DSTSET03.000 [DIRS 113673].

Figure 6.3-14. Temperature Histories for DST Borehole 164 at Select Locations



Source: DTN: MO0208RESTRDST.002 [DIRS 161129].

Figure 6.3-15. Temperature Profile along DST Borehole 164 at Select Times



Source: DTN: MO0208RESTRDST.002 [DIRS 161129].

Figure 6.3-16. Vertical Slice through the Mid-length of the DST Heated Drift Showing 96°C Temperature Contours after 1, 2, 3, and 4 Years of Heating



### 6.3.1.2.2 Measurement Uncertainty: Temperatures

The uncertainty in DST temperature measurements involved both RTDs and thermocouples. The RTD was accurate within 0.3°C (CRWMS M&O 1997 [DIRS 101540], Section 5.1). With consideration of other factors, such as the location of the RTDs, measured temperature in the DST by the RTDs was estimated to be accurate within 2°C. The RTD bundles were grouted in the boreholes; consequently, some of the RTDs might not have had direct contact with the borehole wall. There might have been some time delay between the temperature variations in the rock and that measured by the RTDs, but it is believed that this time delay was small because the rock-mass was heated slowly.

The thermocouple was accurate within 2.2°C (CRWMS M&O 1997 [DIRS 101540], Section 5.1). With consideration of other factors, such as location, the accuracy of the measured temperature in the DST by the thermocouples was estimated to be within 3.5°C.

### 6.3.1.2.3 RTD Failures

A total of 1,861 RTDs were installed in 28 boreholes providing most of the rock mass temperatures measurements (BSC 2004 [DIRS 178055]). Over approximately eight years of testing, some of the RTDs produced unreasonable temperature values displaying one of two characteristic behaviors. As of December 31, 2005, 119 RTDs had failed due to mechanical connection faults, exhibited by open electrical circuits; 1,126 had failed due to electrical leakage to ground; and 616 were still functioning, probably with acceptable tolerance (DTN: MO0603SEPDSTTB.002 [DIRS 178054]). Generally, the failures that demonstrated open electrical circuits occurred relatively early in the test and did not occur with any spatial preference. The failures that demonstrated electrical leakage to ground displayed both a temporal and spatial preference occurring only during the cooling period and generally in a borehole at a depth deeper than the location where the “boiling front” was present longest.

Physical inspection of similar sensors used elsewhere underground, the employment of Time Domain Reflectometer techniques, and analysis of the failures suggest that all of the failures in a given bundle (two bundles per borehole) (BSC 2004 [DIRS 178055]) likely occurred at a single location within the bundle.

### 6.3.1.3 Laboratory Parameter: Thermal Conductivity

Thermal conductivity measurements on core samples were performed using the Guarded Heat Flow Meter test method (Brodsky et al. 1997 [DIRS 100653], pp. 11 to 14) as described in Section 3 of *Ambient Characterization of the Drift Scale Test Block* (CRWMS M&O 1997 [DIRS 101539]). The apparatus functioned by placing a specimen between two heater plates controlled at different temperatures, producing heat flow through the specimen. A heat flux transducer (HFT) located between the specimen and one heater plate measured heat flow. Since this heat flux transducer is in series with the specimen and between both heater plates, the resulting temperatures on each side of the specimen, along with knowledge of the specimen thickness, allowed the thermal conductivity of the specimen to be determined.

Two series of tests were performed to measure thermal conductivity. In the first test series, samples recovered from the DST block were tested over the temperature range of 30°C to 300°C. The test specimens were placed between two heater plates controlled at different temperatures, and the heat flow was measured. Radial heat flow losses were minimized by using a cylindrical guard heater. Moisture contents were either air dry (as received), oven dry, vacuum saturated, or partially saturated (intermediate between air dry and vacuum saturated). The moisture contents of the specimens tested as received were not indicative of in situ conditions. Laboratory specimens were cored under water and dried out in storage. In a second series of tests, the relationship between thermal conductivity and saturation was determined (SNL 1998 [DIRS 118788]). Welded tuff was taken from Alcove 5 of the DST, and nonwelded tuffs from four lithostratigraphic units were obtained from three surface drill holes. Thermal conductivities were measured for six welded and six nonwelded specimens under dry, saturated, and approximately ten intermediate moisture conditions (SNL 1998 [DIRS 118788]). All thermal conductivity tests were conducted at 30°C and at atmospheric pressure.

The DST thermal conductivity data may be found in the following input DTNs: SNL22100196001.006 [DIRS 158213] and SN0203L2210196.007 [DIRS 158322].

#### **6.3.1.3.1 Results: Thermal Conductivity**

A complete listing of DST thermal conductivity for different temperatures and saturation is provided in the summary DTN identified in Table 6.3-1. A small subset is presented in Tables 6.3-3 and 6.3-4.

The thermal conductivity data over a range of temperatures from 30°C to 70°C are summarized in Table 6.3-3. Thermal conductivity values were relatively uniform throughout the sampling volume. The mean thermal conductivities and standard deviations about the mean are given at each temperature. No temperature dependence is observed. Thermal conductivities ranged from 1.9 to 2.3 W/(m-K) with an average thermal conductivity of  $2.1 \pm 0.1$  W/(m-K) over this range of temperatures.

The distribution of thermal conductivity results obtained at 30°C provides a visual indication of the central tendency of the data. No analysis was performed to determine the best-fit distribution curve. Results show that the individual specimens with thermal conductivities farther than one standard deviation from the mean did not cluster in particular locations. The highest thermal conductivity, 2.3 W/(m-K), was obtained for HDFR1-97.5-C, which is from either the lower portion of the Tptpmn or the upper portion of the Tptpll unit. The mean thermal conductivity for each individual borehole was 2.1 W/(m-K).

Results for the second series of tests in which thermal conductivities were determined for a range of saturation are illustrated in Table 6.3-4. A linear and commonly used nonlinear curve were fitted to the data and the goodness of fit determined. The linear relationship provides a better fit to the data, as indicated by the sum of the squared errors.

Table 6.3-3. Summary of Thermal Conductivity Data for Saturated Specimens from the DST Block

Distance from collar (ft)	Max. Temp. (°C)	Thermal Conductivity (W/m-K)					
		30°C	50°C	70°C	Mean	STD	N
<b>ESF-SDM-MPBX1-C</b>							
1.0	70	2.2	2.2	2.2	2.2	0.0	3
32.1	70	2.2	2.2	2.1	2.2	0.0	3
40.6	70	2.1	2.1	2.1	2.1	0.0	3
62.0	70	2.2	2.2	2.2	2.2	0.0	3
80.5	70	2.15	2.1	2.1	2.1	0.0	3
	N =	5	5	5	—	—	—
	Mean =	2.2	2.2	2.1			
	STD =	0.1	0.0	0.0			
<b>ESF-SDM-MPBX2-C</b>							
13.0	70	2.1	2.1	2.1	2.1	0.0	3
29.0	70	2.1	2.1	2.1	2.1	0.0	3
48.4	70	2.0	2.0	2.0	2.0	0.0	3
71.5	70	2.3	2.3	2.3	2.3	0.0	3
84.6	70	2.0	2.0	2.1	2.0	0.1	3
	N =	5	5	5	—	—	—
	Mean =	2.1	2.1	2.1			
	STD =	0.1	0.1	0.1			
<b>ESF-SDM-MPBX3-C</b>							
3.0	70	1.9	1.9	1.9	1.9	0.0	3
17.7	70	2.1	2.1	2.1	2.1	0.0	3
38.7	70	2.2	2.2	2.2	2.2	0.0	3
72.0	70	2.2	2.2	2.2	2.2	0.0	3
85.3	70	2.1	2.1	2.1	2.1	0.0	3
	N =	5	5	5	—	—	—
	Mean =	2.1	2.1	2.1			
	STD =	0.1	0.1	0.1			
<b>ESF-AOD-HDFR1-C</b>							
8.6	70	2.0	2.0	2.0	2.0	0.0	3
32.2	70	2.1	2.1	2.1	2.1	0.0	3
48.7	70	1.9	1.9	2.0	1.9	0.0	3
68.8	70	2.1	2.1	2.0	2.1	0.0	3
97.5	70	2.3	2.3	2.3	2.3	0.0	3
	N =	5	5	5	—	—	—
	Mean =	2.1	2.1	2.1			
	STD =	0.2	0.1	0.1			
<b>All DST Characterization Boreholes</b>							
	N =	20	20	20	—	—	—
	Mean =	2.1	2.1	2.1			
	STD =	0.1	0.1	0.1			
<b>All Specimens, All Temperatures</b>							
	N =	60	—	—	—	—	—
	Mean =	2.1					
	STD =	0.1					

Source: DTN: SN0203L2210196.007 [DIRS 158322].

NOTES: Air dried. Lithostratigraphic unit: Tptpmn, except for HDFR1-97.5-C, which may be from TptplI (see Section 6.3.1.3.1).

N = Number of samples; STD = Standard deviation.

Table 6.3-4. Thermal Conductivity as a Function of Saturation State

Lithostratigraphic Unit	Number of Specimens	Linear Fit: $K=K_d+Slope \cdot S_1$				Fit to $K=K_d+(K_w-K_d) \cdot \sqrt{S_1}$		
		Intercept or $K_d$ W/(m-K)	Slope	$K_w$ W/(m-K)	Sum of Squared Errors	$K_d$ W/(m-K)	$K_w$ W/(m-K)	Sum of Squared Errors
Tptpmn	6	1.79	0.414	2.20	0.46	1.71	2.14	0.53
Tac4	1	0.52	0.54	1.06	0.007	0.42	0.98	0.011
Tac3	1	0.53	0.55	1.08	0.004	0.43	1.00	0.013
Tac2	2	0.52	0.59	1.11	0.020	0.39	1.03	0.056
Tacbs	2	0.71	0.59	1.31	0.007	0.59	1.21	0.062

Source: DTN: SN0203L2210196.007 [DIRS 158322].

NOTE: Refer to SNL 1998 [DIRS 118788] and DTN cited in Table 4-3.  $K_w$  = thermal conductivity for saturated specimen;  $K_d$  = thermal conductivity for oven-dried specimen;  $S_1$  = liquid saturation

### 6.3.1.3.2 Measurement Uncertainty: Thermal Conductivity

The uncertainty in DST thermal conductivity is similar to that discussed for the SHT in Section 6.2.1.3.2.

### 6.3.1.4 Field Parameters (REKA–Thermal Conductivity and Thermal Diffusivity)

A thermal probe was developed at the University of Nevada, Reno, to determine in situ thermal conductivity and thermal diffusivity. The probe is called Rapid Evaluation of K and Alpha (REKA) (K represents thermal conductivity; Alpha represents thermal diffusivity). REKA is a self-contained probe consisting of a heat source and 16 temperature sensors. During measurements, a small amount of heat, about 2 watts, was transferred to the rock, and temperature differences were measured. Assembled, a REKA probe is a rigid cylinder approximately 0.5 cm in diameter and about 60 cm in length. The REKA probe was grouted in a borehole of approximately 1.2 cm in diameter. The borehole had to be sufficiently straight to allow probe insertion.

For characterization during the preheating phase, five locations were selected based on the competency of the wall rock at this site, including minimal fracturing, sufficient separation from rock bolts, and similarity of density (as determined by drilling rate). All five locations chosen for analysis appear to have similar characteristics based on these criteria. The boreholes were drilled in random directions to average the effects of unseen physical phenomena. Detailed discussion of the REKA measurements and methodology can be found in *Ambient Characterization of the DST Block* (CRWMS M&O 1997 [DIRS 101539], pp. 10-4 to 10-8) and the study by Danko and Mousset-Jones (1993 [DIRS 134360]).

During the heating phase, measurements were made in boreholes 151, 152, and 153 (see Table 6.3-2). The REKA thermal conductivity and thermal diffusivity data during the heating phase may be found in the following input DTNs:

- LL980411004244.060 [DIRS 159107]
- LL980411104244.061 [DIRS 159111]
- LL980902104244.070 [DIRS 159109]

- UN0106SPA013GD.003 [DIRS 159115]
- UN0106SPA013GD.004 [DIRS 159116]
- UN0109SPA013GD.005 [DIRS 159117]
- UN0112SPA013GD.006 [DIRS 159118]
- UN0201SPA013GD.007 [DIRS 159119].

#### 6.3.1.4.1 Results: Field Thermal Conductivity and Thermal Diffusivity

Results of thermal conductivity and thermal diffusivity measurements using the REKA probe during the preheating phase are taken from Section 10.2 of *Ambient Characterization of the DST Block* (CRWMS M&O 1997 [DIRS 101539]) and presented in Tables 6.3-5 and 6.3-6. These results are shown for corroborative purposes to compare with the laboratory measurements presented in Section 6.3.1.3. Table 6.3-5 shows the REKA evaluation results using a constant rock-mass temperature (no rock-mass temperature correction performed). Table 6.3-6 shows the REKA results for a changing rock-mass temperature over the 12-hour measurement period.

Table 6.3-5. REKA Results with No Background Temperature Correction

REKA Location	Thermal Conductivity, K (W/(m-C))	Thermal Diffusivity, Alpha (m <sup>2</sup> /s)
1	1.69	$0.76 \times 10^{-6}$
2	1.95	$0.77 \times 10^{-6}$
3	1.86	$0.91 \times 10^{-6}$
4	1.88	$0.82 \times 10^{-6}$
5	1.70	$0.85 \times 10^{-6}$

Source: CRWMS M&O 1997 [DIRS 101539], Section 10.2.

NOTE: Values in this table derived from in situ measurements are used for corroborative purposes with laboratory measurements discussed in Section 6.3.1.3.

Table 6.3-6. REKA Results with Background Temperature Correction

REKA Location	Thermal Conductivity, K (W/(m-C))	Thermal Diffusivity, Alpha (m <sup>2</sup> /s)
1	1.72	$0.93 \times 10^{-6}$
2	1.92	$0.90 \times 10^{-6}$
3	1.89	$1.04 \times 10^{-6}$
4	1.93	$1.09 \times 10^{-6}$
5	1.76	$0.97 \times 10^{-6}$

Source: CRWMS M&O 1997 [DIRS 101539], Section 10.2.

NOTE: Values in this table derived from in situ measurements are used for corroborative purposes with laboratory measurements discussed in Section 6.3.1.3.

#### **6.3.1.4.2 Measurement Uncertainty: Field Thermal Conductivity and Thermal Diffusivity**

The REKA probe assumes that the rock will behave in a homogenous, isotropic manner, which may not be the case. Nonetheless, its application is valid, and historical correlation of predicted and measured temperatures is sound using in situ thermal properties. The accuracy of the measured thermal conductivity and thermal diffusivity is estimated to be about 5% using the REKA probe (CRWMS M&O 1997 [DIRS 146917]).

### **6.3.2 DST Hydrological Measurements**

To assess the thermal-hydrologic processes in the DST, the spatial distribution and the temporal variations of the moisture content in the rock mass were monitored. Electrical resistivity tomography (ERT), ground penetrating radar (GPR), and neutron logging were used to monitor the moisture content. Air permeability was measured periodically to assess the changes in the fracture permeability during the test. Core samples collected from the DST region were analyzed in the laboratory for hydrologic properties such as porosity, density, gravimetric water content, and electrical properties such as resistivity and relative permittivity. These will be presented in the following corresponding sections.

#### **6.3.2.1 Electrical Resistance Tomography**

ERT surveys made during the DST heating phase show the changes in moisture content caused by heating. Of particular interest are the formation and movement of condensate within the fractured rock mass. Figure 6.3-8 shows the location of the ERT boreholes in the DST. The ERT in the DST was conducted in four imaging planes: two vertical cross sections from the observation drift to the heated drift and two vertical planes along the axis of the heated drift. The two vertical cross sections from the observation drift to the heated drift are located at  $Y = 4.6$  m, formed by boreholes 45 and 46, and at  $Y = 24.7$  m, formed by boreholes 62 and 63. Borehole lengths are about 40 m. The two vertical planes along the axis of the heated drift include: one in the crown of the heated drift formed by boreholes 135, 145, 166, and 176; and one in the invert of the heated drift formed by boreholes 136, 146, 167, and 177. The two vertical planes along the axis of the heated drift cover a length of the drift from  $Y = 2.7$  m to 39.3 m. The borehole lengths are about 20 m in the crown and about 16 m in the invert. The electrode spacing in the DST ERT is about 1 m. The electrodes were grouted in the boreholes.

Near the end of the heating phase, the vertical cross section image plane at  $Y = 24.7$  m malfunctioned because of the increased contact impedance between the electrodes and the rock. Otherwise, the ERT functioned well. DST ERT data can be found in the TDMS under the following input DTNs:

DST ERT preheating-phase data can be found under the following DTN:

- LL980108804244.052 [DIRS 158332] (10/18/1997 to 10/18/1997).

DST ERT heating-phase data can be found under the following DTNs:

- LL980406404244.057 [DIRS 113782] (10/1/1997 to 3/18/1998)
- LL980808604244.065 [DIRS 113791] (2/25/1998 to 6/3/1998) (unqualified)
- LL990702704244.099 [DIRS 113872] (9/30/1998 to 6/14/1999)
- LL000804023142.009 [DIRS 158325] (11/16/1999 to 7/20/2000)
- LL020307723142.018 [DIRS 177795] (8/1/2001 to 12/31/2001).

DST ERT cooling-phase data can be found in the TDMS under the following DTNs:

- LL030606723142.035 [DIRS 177798] (2/5/2002 to 10/1/2002)
- LL030906923142.038 [DIRS 177803] (3/5/2003 to 5/21/2003)
- LL040307423142.072 [DIRS 177806] (11/20/2003 to 3/19/2004)
- LL041000223142.045 [DIRS 177807] (1/12/2004 to 6/30/2004)
- LL050902223142.048 [DIRS 177809] (1/1/2005 to 6/30/2005)
- LL060303223142.051 [DIRS 177810] (7/1/2005 to 12/31/2005) (unqualified).

Some of the wires connected to the electrodes were damaged accidentally during a video survey of the heated drift, conducted in January 2002, which was after the heaters were turned off. Also, beginning in October 2001, the vertical cross section image plane at  $Y = 4.6$  m shows substantially distorted anomalies caused by the increased contact impedance between the borehole 46 electrodes and the rock. As a result, cross-section imaging at  $Y = 4.6$  m from that date forward produced inconclusive results and was not displayed in the corresponding figures.

#### **6.3.2.1.1 Results: ERT**

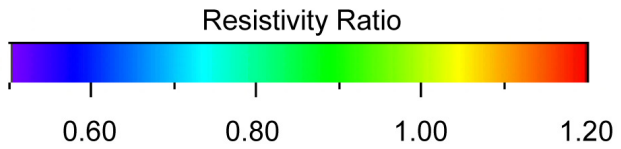
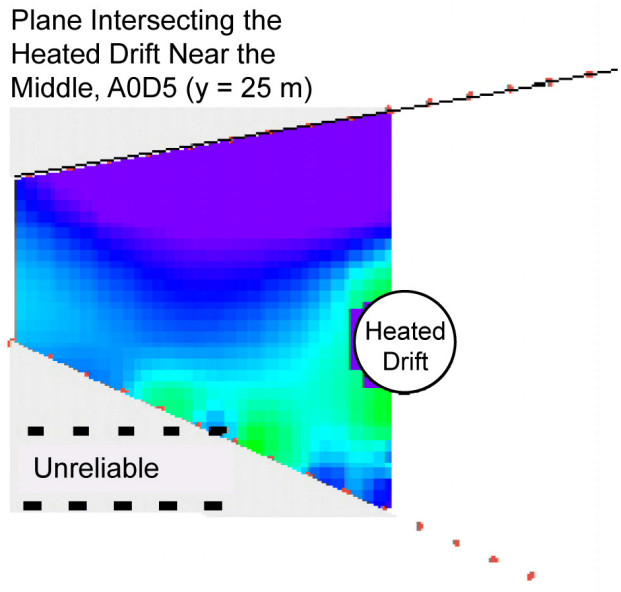
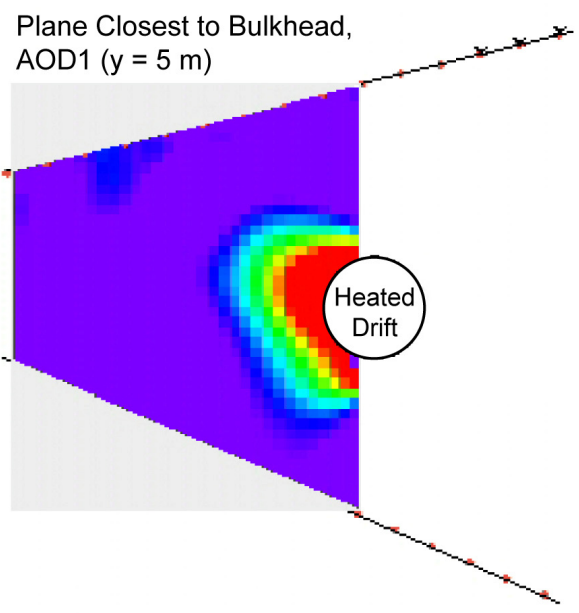
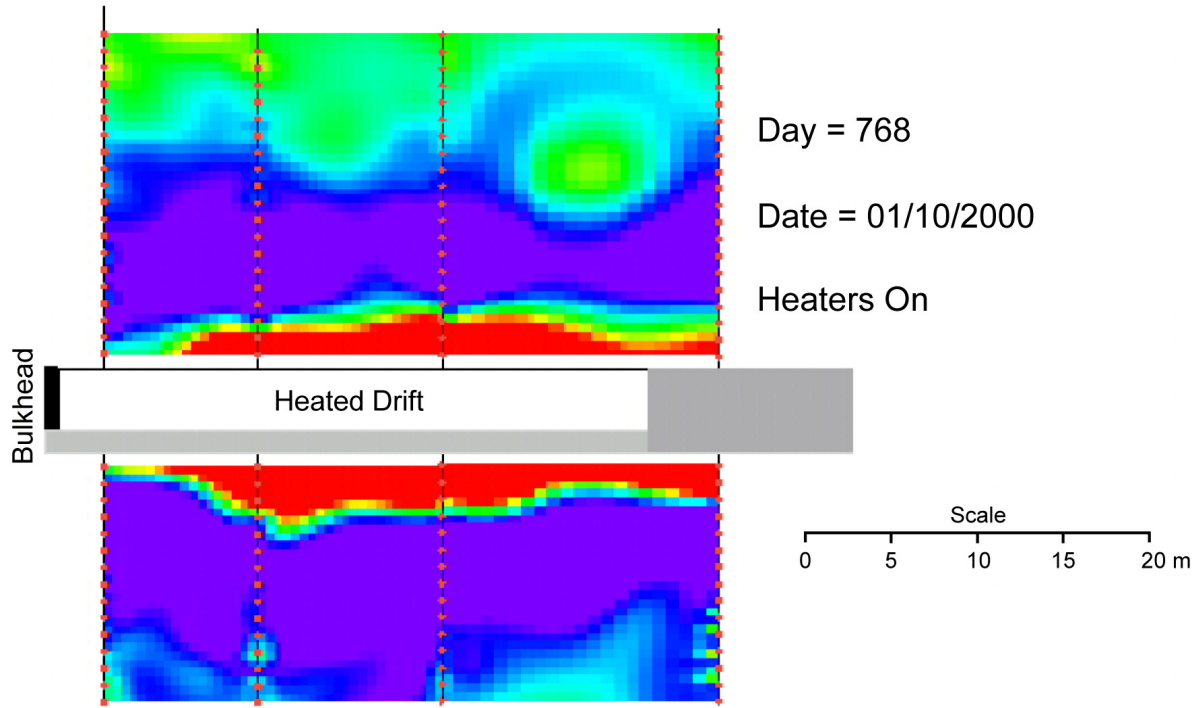
The saturation estimates produced by data reduction model 2 (as presented in Section 6.1.2.1.1) are presented here. As examples of the DST ERT results, Figures 6.3-17 and 6.3-18 show the resistivity image as measured on January 10, 2000, during the middle of the heating phase, and the saturation image produced from it, respectively. Images are presented as a ratio to the preheating baseline values. The vertical image planes along the longitudinal axis of the heated drift started at about 2.7 m from the bulkhead. The vertical cross section imaging plane intersects the heated drift at about 4.6 m from the bulkhead. These figures are examples of the ERT results in the DST. For the rest of the heating phase, ERT results can be found in the TDMS under the input DTNs listed above. As shown in Figure 6.3-18, the drying of rock started in regions near the heaters. Tomograms for the different vertical planes along the heated drift indicate that the end effect is apparent at the bulkhead at  $Y = 0$ , but not as obvious at the far end of the heated drift. Aside from the end effects, the drying along the heated drift was uniform. Some localized increases of moisture (saturation ratios  $>1.0$ ) were observed in regions both above and below the heated drift, but seemed to be more pronounced in the region below the heated drift, just below the edge of the lined section of the heated drift at  $Y = 22.0$  m (Figure 6.3-18). The vertical extent of the drying region near the wing heaters seemed to be greater than that near the floor heaters in the heated drift. This was probably a result of two

factors: (1) greater heating effects in the wing heater plane than in the heated drift, and (2) lower ERT resolution due to longer distances between the electrodes and the heated zone near the wing heaters.

Figures 6.3-19 through 6.3-22 are contour plots of saturation ratio for three snapshots during the post-heating (i.e., cooling) period. A comparison of Figures 6.3-19 and 6.3-20 indicates that the volume of the dryout zone around the heaters continued to increase slightly for several months after the heaters were turned off. This effect was most pronounced along the vertical cross section imaging plane that intersects the heated drift at about 4.6 m from the bulkhead. The wet region observed in Figure 6.3-18 below the heated drift at  $Y = 22$  m disappeared during the first six months of cooling (Figures 6.3-19 and 6.3-20), and later reappeared in October 2002 (Figure 6.3-21). Above the heated drift, other wetting zones developed near the top of boreholes 135 and 145 during the early cooling period (Figures 6.3-19 and 6.3-20).

As the cooling progressed, additional wetting zones developed above and below the heated drift as shown in Figure 6.3-22. Figure 6.3-22 shows an interesting vertical structure that extends above and below the heated drift, between boreholes 145 and 166, and boreholes 146 and 167. Finger-like low saturation regions extend vertically away from the very dry zone near the heated drift. There is also a wet zone just above the top finger-like drier zone. These features may be evidence of refluxing within a fracture zone.

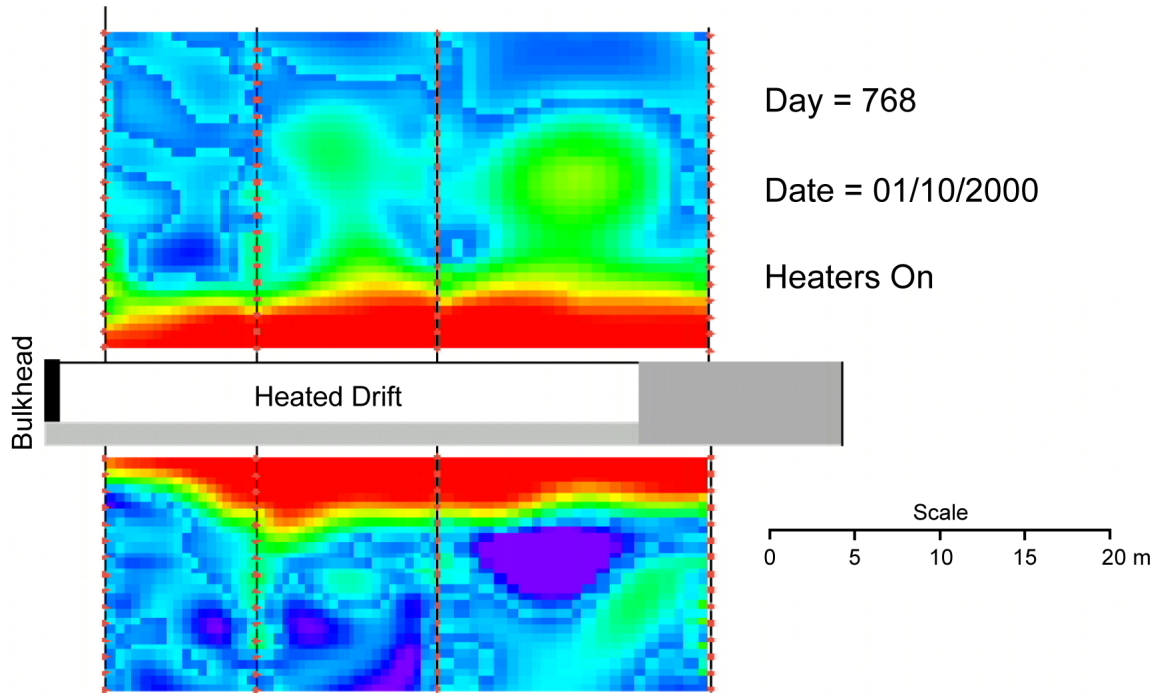




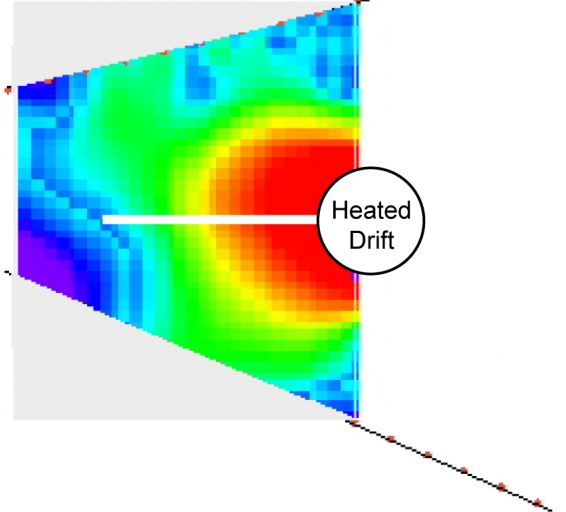
00668DC\_008a.ai

Source: DTN: LL00804023142.009 [DIRS 158325].

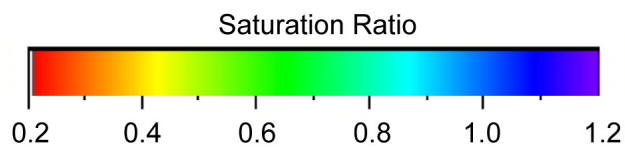
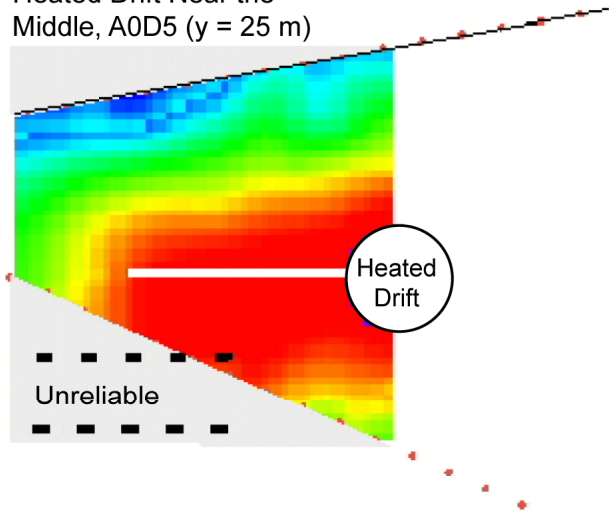
Figure 6.3-17. DST ERT Resistivity Ratios of the 1/10/00 Measurement to the Preheating Measurement



Plane Closest to Bulkhead,  
AOD1 (y = 5 m)



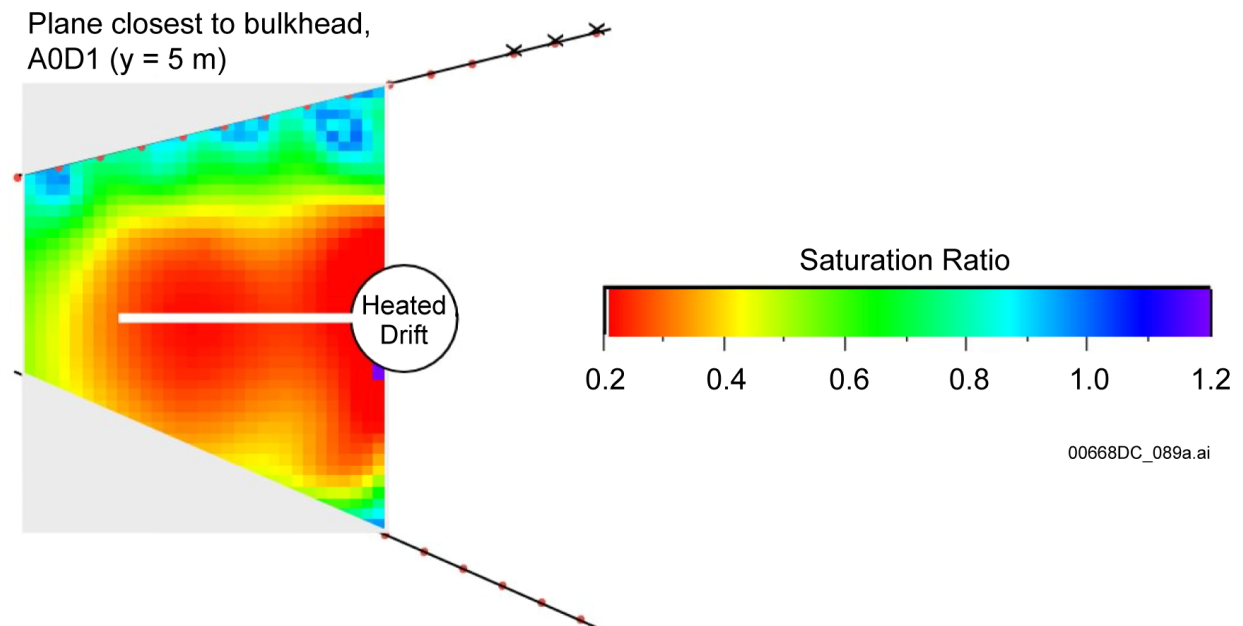
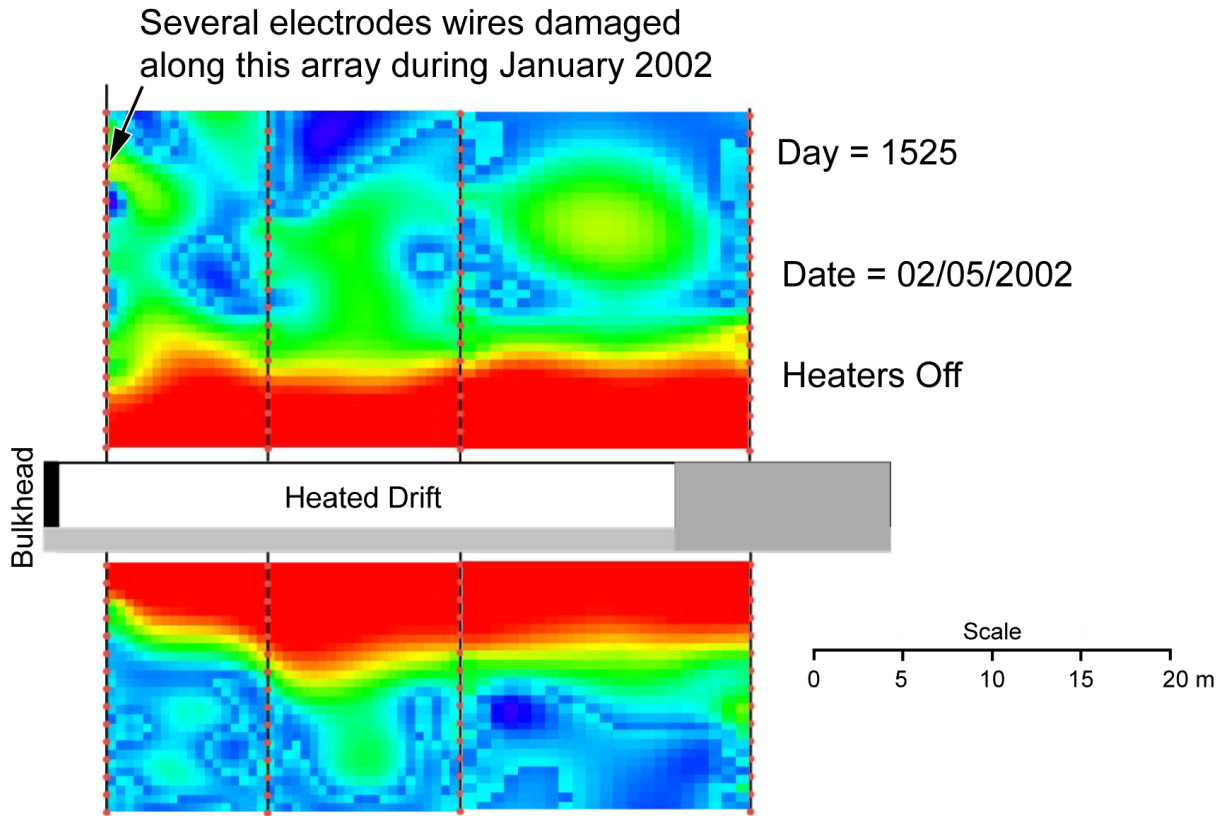
Plane Intersecting the  
Heated Drift Near the  
Middle, AOD5 (y = 25 m)



00668DC\_009a.ai

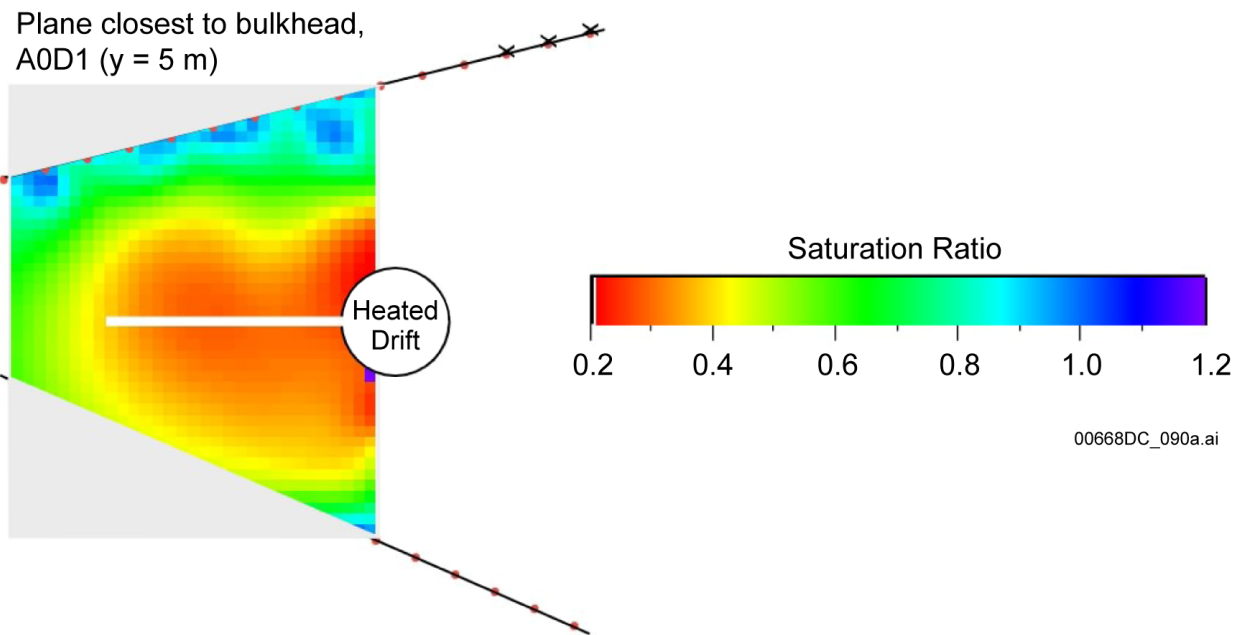
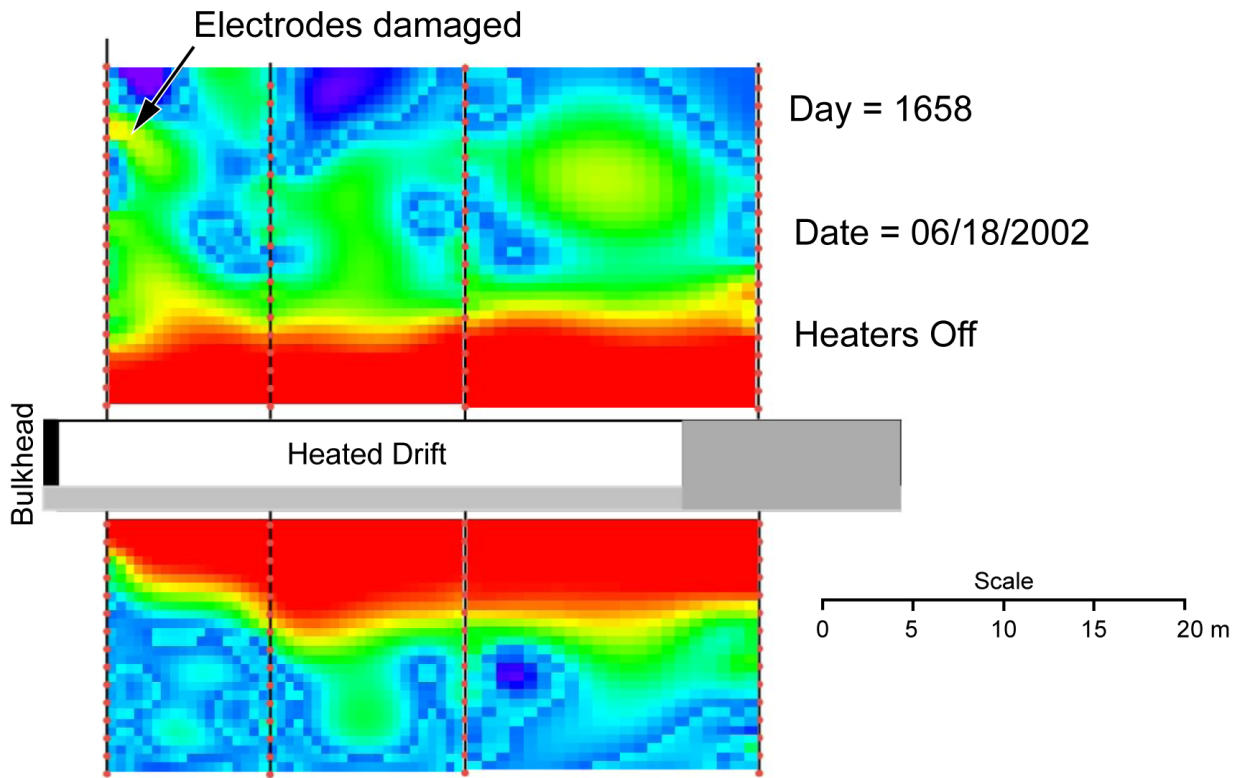
Source: DTN: LL000804023142.009 [DIRS 158325].

Figure 6.3-18. DST Saturation Ratio Calculated from the 1/10/00 Resistivity Ratio



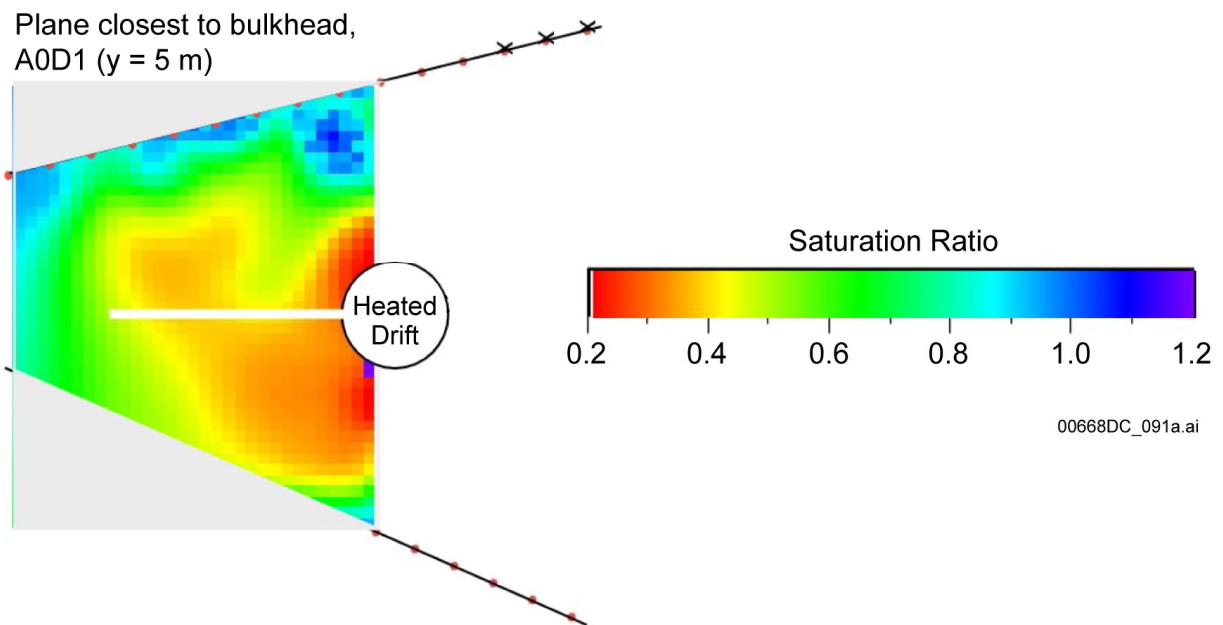
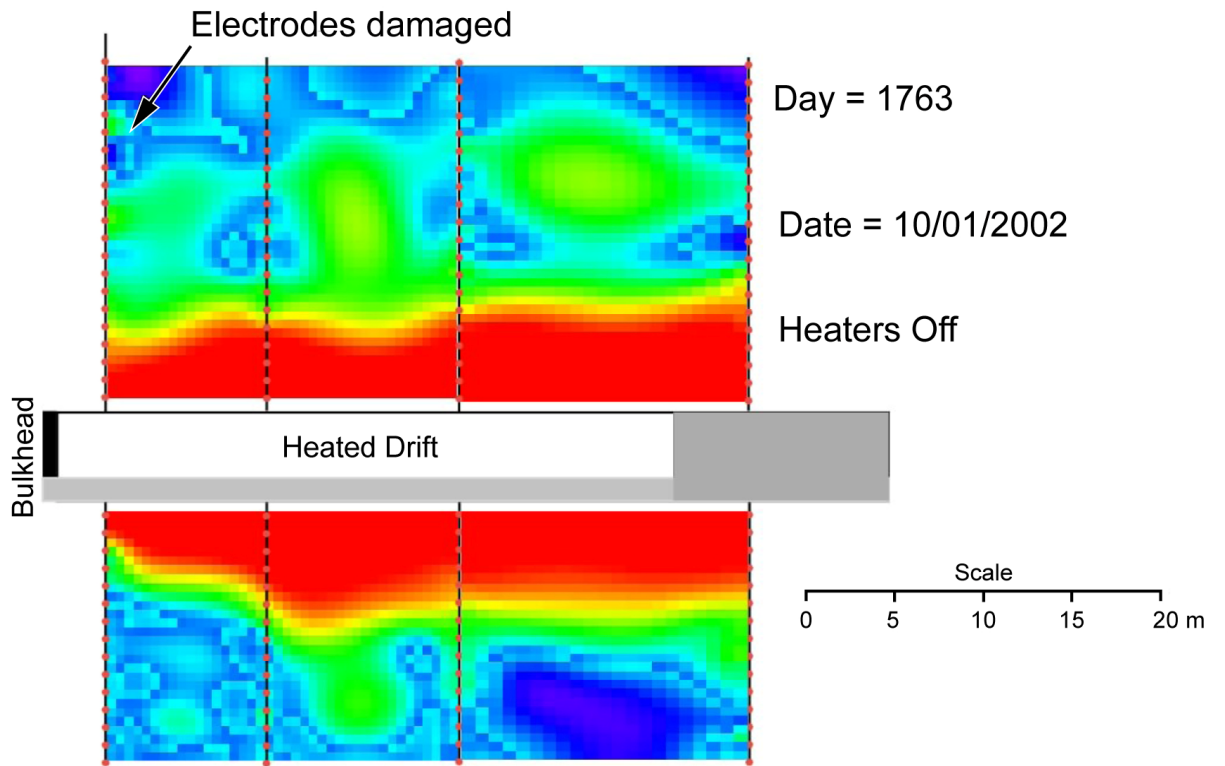
Source: DTN: LL030606723142.035 [DIRS 177798].

Figure 6.3-19. Saturation Estimates Corresponding to February 2002, Shortly after Heating Phase Ended



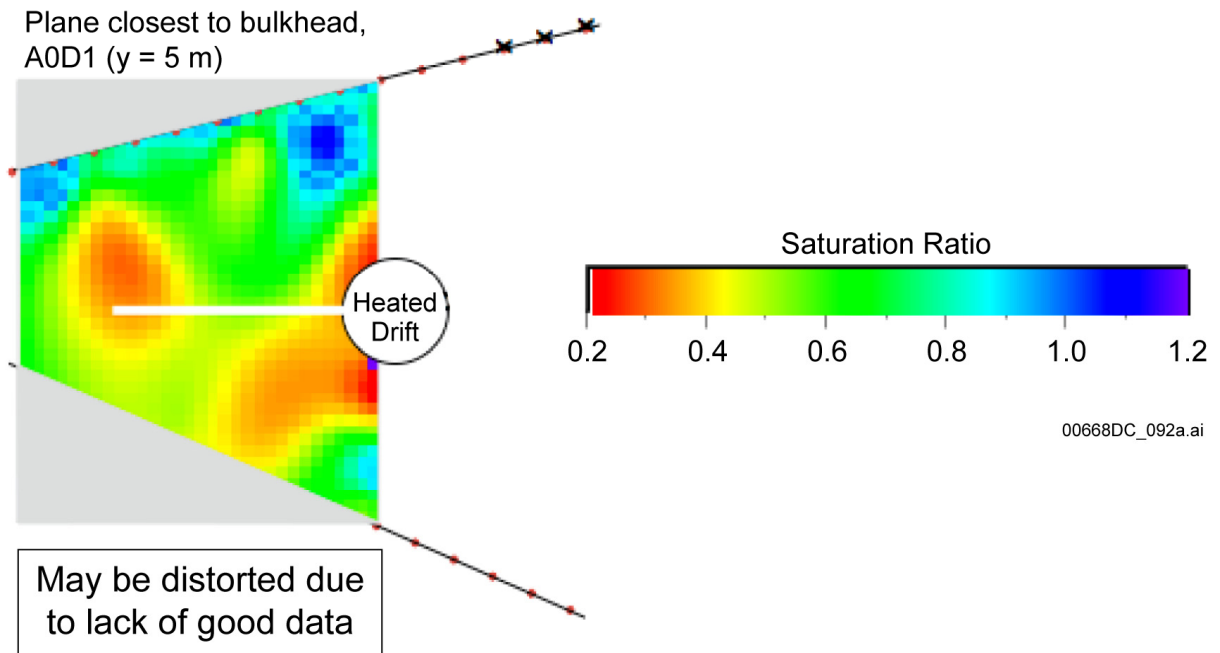
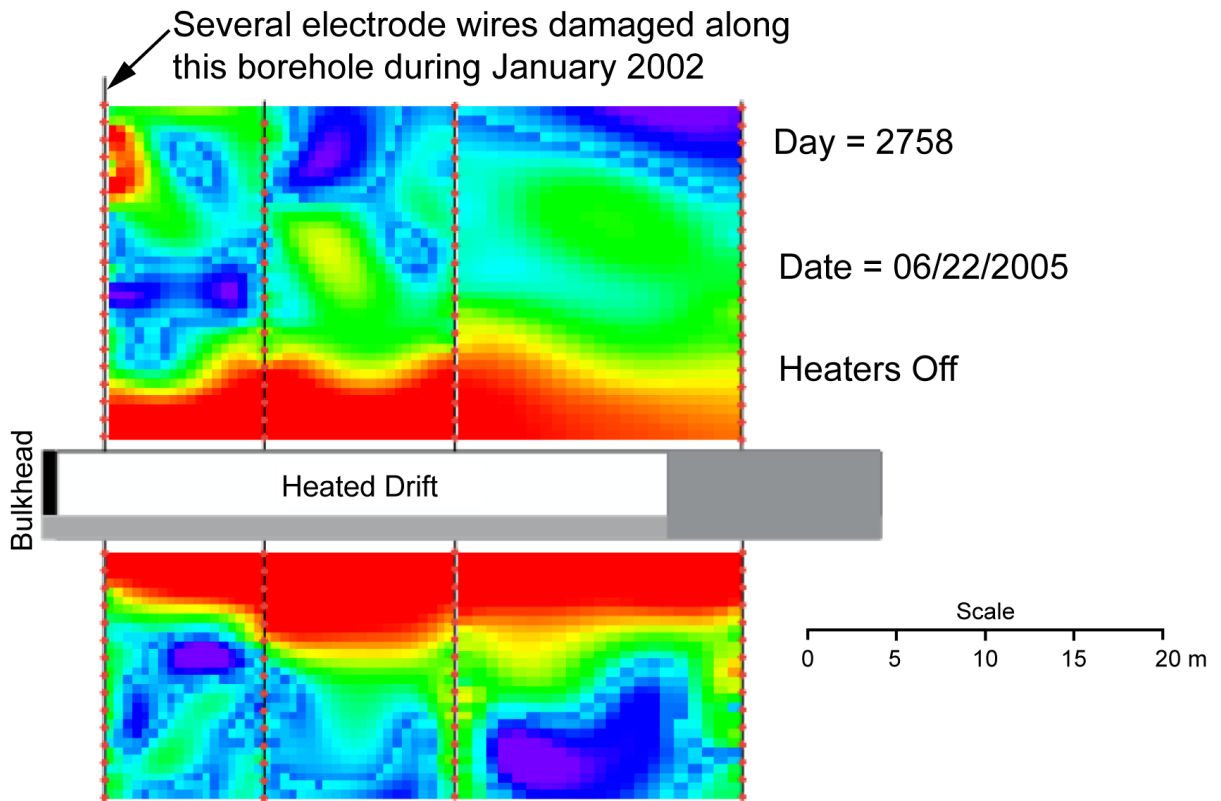
Source: DTN: LL030606723142.035 [DIRS 177798].

Figure 6.3-20. Saturation Estimates Corresponding to June 2002, Approximately Five Months after Heating Phase Ended



Source: DTN: LL030606723142.035 [DIRS 177798].

Figure 6.3-21. Saturation Estimates Corresponding to October 2002, When a Large Region of Increased Saturation Reappeared below the Heated Drift



Source: DTN: LL050902223142.048 [DIRS 177809].

Figure 6.3-22. Saturation Estimates Corresponding to June 2005, Approximately 3.5 Years after the End of the Heating Phase

### **6.3.2.1.2 Measurement Uncertainty: ERT Saturation Changes**

Based on laboratory calibration, ERT precision in determining water level saturation is about 10% to 20% when the saturation level is below 40%, and 20% to 30% when the saturation level is greater than 40% (CRWMS M&O 1997 [DIRS 146917]). There are many factors that could contribute to the uncertainty in the estimated saturation changes in the rock mass by using ERT:

- The accuracy of the temperature maps in the vertical cross section imaging planes near the observation drift is limited by the sparse coverage of the temperature sensors. Errors in the extrapolated temperature maps will result in erroneous saturation estimates.
- The procedure used to convert resistivity change to saturation change relates resistivity changes to changes in temperature and/or water saturation. If the quantity or types of ions in the pore water changes, the bulk resistivity will change, and the saturation estimates will be in error.

The other uncertainty factors that impact the ERT in general can be found in Section 6.1.2.1.3. Interpretation of ERT results is aided when ERT is used in combination with other methods such as ground penetrating radar and neutron logging.

### **6.3.2.2 Ground Penetrating Radar**

The feasibility of the cross-hole radar profiling method to monitor the saturation changes due to thermal hydrological processes was proven for the SHT and discussed in Section 6.2.2.2. The same data acquisition and data analysis methods discussed in 6.2.2.2 were applied to the DST. Detailed discussion of the data acquisition and data processing specific to the DST can also be found in three Level 4 milestone reports (Peterson and Williams 1998 [DIRS 159128]; Peterson and Williams 1998 [DIRS 159120]; Williams and Peterson 1998 [DIRS 159121]).

The radar data were acquired in ten boreholes (47 to 51, 64 to 68) as shown in Figure 6.3-6. These boreholes are collared from the observation drift and are the same boreholes used for neutron logging. These ten boreholes form two arrays of five boreholes each in two vertical planes. Cross-hole tomographic data were collected between adjacent borehole pairs (transmitter and receiver) using two acquisition modes: the zero offset profile and multiple offset profile, as discussed previously in Section 6.2.2.2. The severity of the borehole inclination in the borehole pairs 47-48 and 64-65, however, limited the data acquired between these boreholes to zero offset profile data only. Full multiple offset profile data coverage, necessary for subsequent tomographic processing, could not be accomplished. Since these borehole pairs represent data coverage that is far enough away from the heated drift intersection that few thermally induced changes in the radar data were anticipated, the impact of data acquisition limitation is minimal.

GPR data were acquired in phases according to a schedule calling for measurements every 4 to 6 months during the heating phase.

After acquisition of Phase 1 data, the borehole temperatures became so great that the cables used in the measurements melted. It took many months to redesign and manufacture cables that were more heat resistant for Phase 2. Furthermore, owing to the extreme heat encountered in borehole 67 (due to its proximity to a wing heater), accurate measurements could no longer be

taken. Hence, all data acquisition for borehole pairs involving this borehole (66-67 and 67-68) was halted after Phase 5. However, because of the similarity in spatial positioning of the well pairs, the data acquired between well pairs 49-50 and 50-51 acted as sufficient proxy for the well pairs 67-68 and 66-67.

Radar wave travel times have been submitted to the TDMS periodically over the course of the experiment. The DTNs (referenced according to the phase numbers: PRE for Preheating; P1 for Phase 1 of heating) are listed as follows:

- LB990630123142.005 [DIRS 129274] (PRE, P1, P2, P3)
- LB000121123142.004 [DIRS 158338] (P4)
- LB000718123142.004 [DIRS 153354] (P5)
- LB0101GPRDST01.001 [DIRS 158346] (P6)
- LB0108GPRDST05.001 [DIRS 158440] (P7)
- LB0203GPRDSTEH.001 [DIRS 158350] (P8, P9, P10)
- LB0210GPRDSTHP.001 [DIRS 160895].

DTNs for the cooling phase are listed as follows:

- LB0209GPRDSTCP.001 [DIRS 177817]
- LB0210GPRDSTCP.001 [DIRS 160896]
- LB0303GPRDSTCP.001 [DIRS 177822]
- LB0309GPRDSTCP.001 [DIRS 177823]
- LB0403GPRDSTCP.001 [DIRS 177824]
- LB0509GPRDSTCP.001 [DIRS 177825]
- LB0603GPRDSTCP.001 [DIRS 177826].

The XYZ coordinates of the transmitter and receiver positions were determined from the borehole collar and bottom as-built coordinates and are in input DTN: LB990630123142.005 [DIRS 129274].

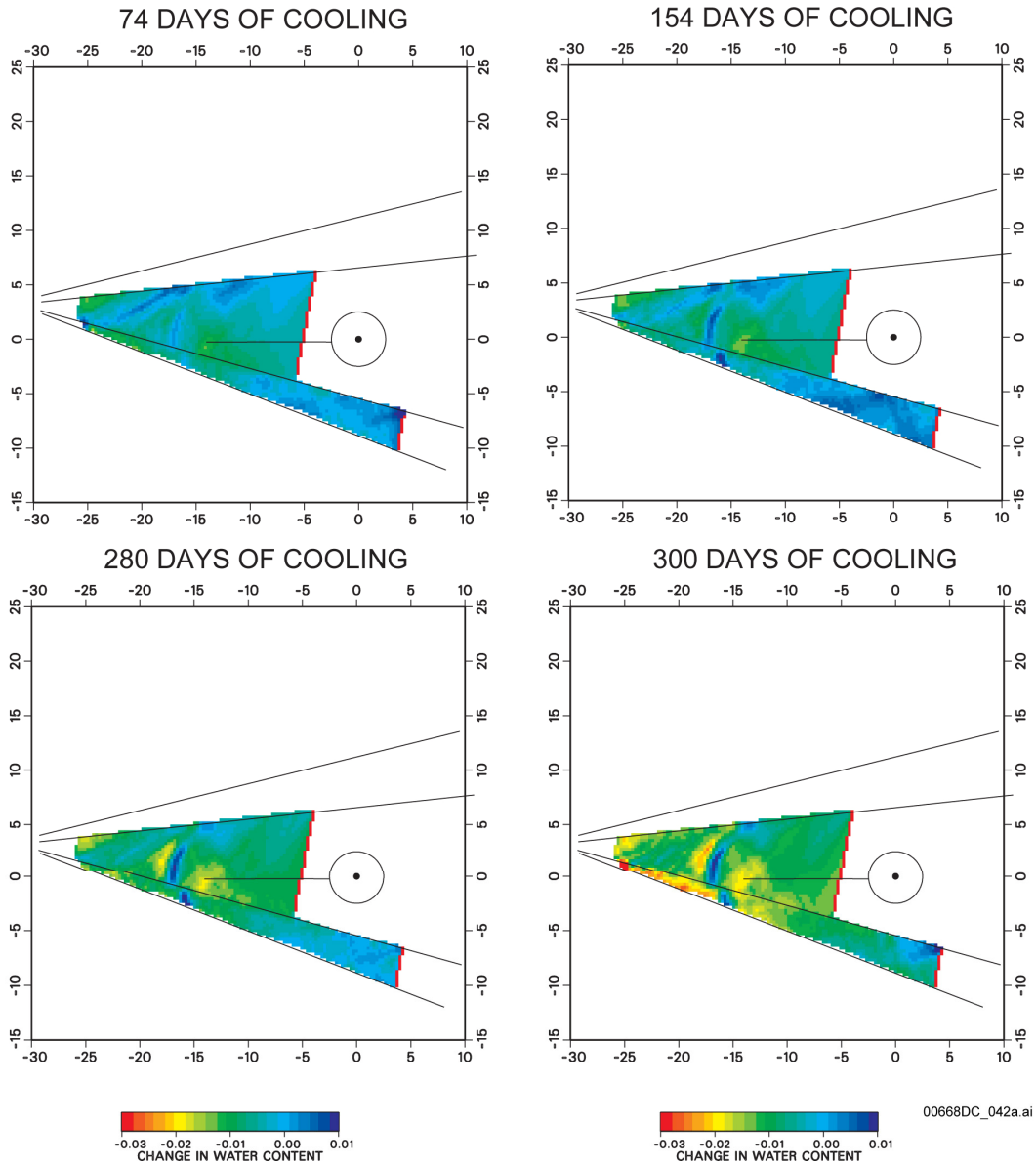
#### **6.3.2.2.1 Results: GPR**

To perform the travel-time inversion, a 40-m  $\times$  40-m field in each plane of boreholes was divided into a grid of 160  $\times$  160 pixels producing a pixel dimension of 0.25 m  $\times$  0.25 m, which corresponds to the antenna-station spacing of 0.25 m. The multiplicity of source and receivers resulted in a dense sampling of the inter-borehole area; over 4,000 arrival times were available for each tomographic inversion. The inverted times produce the velocity fields for each of the 11 surveys (PRE, and P1 through P10).

The velocity differences are highlighted by subtracting the travel time values between two successive surveys and inverting these differenced data. The P1 values are differenced from the PRE values, the P2 values are differenced from the P1 values, and so on, until P10 is differenced from the P9 travel times. Difference tomograms for the 51-50 and 50-49 well pairs are shown in Figure 6.3-23. The tomograms all show significant velocity increases and decreases. In general, radar velocities increase with water content decrease, as seen near the heated drift and the wing



heaters. The derived tomograms are submitted under summary DTN: LB0208GPRDSTHP.001, as identified in Table 6.3-1.



Source: DTNs: LB0208GPRDSTHP.001 [DIRS 170577]; LB0209GPRDSTCP.001 [DIRS 177817]; LB0210GPRDSTCP.001 [DIRS 160896]; LB0303GPRDSTCP.001 [DIRS 177822]; LB0309GPRDSTCP.001 [DIRS 177823]; LB0403GPRDSTCP.001 [DIRS 177824]; LB0509GPRDSTCP.001 [DIRS 177825]; LB0603GPRDSTCP.001 [DIRS 177826].

NOTE: Horizontal distance (m) from the heated drift axis center is plotted on the x-axis; vertical distance is plotted on the y-axis

Figure 6.3-23. GPR Difference Velocity Tomograms for DST Borehole Pairs 51-50 and 50-49

### 6.3.2.2.2 Measurement Uncertainty: GPR

Data uncertainty associated with picking the travel times and inversion errors are as discussed in Section 6.2.2.2.2 for the SHT.

### 6.3.2.3 Neutron Logging

Neutron logging is used to determine moisture content in rocks and soils. Neutron logging was conducted to monitor moisture content in boreholes 47 to 51, 64 to 68, and 79 and 80 (see Figure 6.3-6) during the DST. For the DST, Teflon tubes, with RTD bundles mounted on the outside, were inserted into boreholes 79 and 80, and grouted into place. In the other neutron boreholes (47 to 51 and 64 to 68), a Teflon tube was grouted in the boreholes without the RTDs. The Teflon tube permits easy insertion, placement, and removal of the tool, as well as preventing rockfall damage and loss of the tool. The neutron probe used for the preheating baseline measurements and the very early in-heat measurements of the DST was a Campbell Pacific Nuclear model 503DR, serial number H37067677, 3.81-cm (1.5-in.) diameter probe. Starting from February 1998, a probe (Comprobe model 1905-07EF, serial number 4751, 4.13-cm (1.625-in) diameter) designed for operating at temperatures up to 200°C became available, and was used in the DST for the remainder of the DST heating phase. To evaluate the possible impact of changing tools, the baseline measurement in borehole 47 conducted on October 27, 1997, using the Campbell Pacific tool, was compared with the Comprobe measurement in the same borehole on February 17, 1998. As shown in Figure 6.3-6, borehole 47 was one of the farthest neutron boreholes from the heaters. No moisture content change was expected in this borehole at this early stage of the heating. A relationship of Comprobe count =  $0.11387 \times$  CPN count was established to convert the Campbell Pacific counts to Comprobe counts. All the holes were logged monthly for the first year, when holes showing little activity were dropped to quarterly logging. Immediately after the heating was turned off on 1/14/02, the holes were logged twice within about two weeks to capture any changes due to the turnoff. Since then, logging has been approximately semiannually.

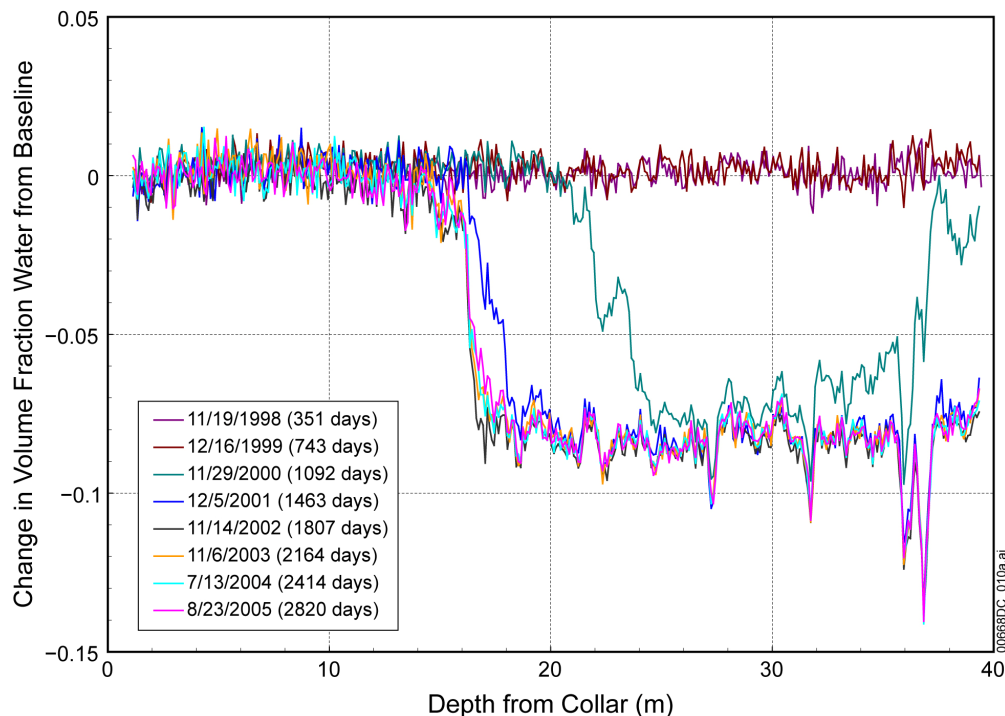
The data are recorded as “counts” or “Counts per second” in the field and later developed into volumetric water content. The developed data can be found in the TDMS under the following DTNs:

- LL020710223142.024 [DIRS 159551]
- LL030309723122.022 [DIRS 165700]
- LL030709023122.032 [DIRS 165701]
- LL040308623122.043 [DIRS 177827]
- LL041001623122.052 [DIRS 177831]
- LL050206323122.057 [DIRS 177829]
- LL060101523122.066 [DIRS 177833]
- LL060302423122.067 [DIRS 177834].

#### 6.3.2.3.1 Results: Neutron Logging

A very small subset of the DST neutron results that reside in the TDMS is presented here. The neutron results are shown as the difference in fraction volume water content between the

heating-phase measurements and the preheating baselines. Therefore, in the following figures, a positive difference fraction volume water means gaining moisture content, and a negative difference fraction volume water means drying. To calculate water saturation, one can simply divide the fraction volume water content by the porosity. As an example of the DST neutron logging results, Figure 6.3-24 shows the difference fraction volume water in borehole 66 as a function of depth from the collar during the heating phase. Borehole 66 extends from the observation drift to above the heated drift at about 26.5 m from the bulkhead. This borehole is near the crown of the heated drift, but not close to the wing heaters. Figure 6.3-24 shows snapshots of the difference fraction volume water content, approximately annually for the eight years since heating started. The traces are identified by the data collection date and the corresponding number of days since the heaters were turned on. The water content was virtually unchanged at the end of the first two years of heating. During the third year of heating, the drying was most significant, both in spatial extent and amount of moisture loss. As shown in Figure 6.3-24, a “dry region,” corresponding to a reduced volume fraction water of about 0.08 units below baseline, formed along an 8-m interval of borehole. During the fourth year of heating, the moisture content in the dry region did not change much, but the dry region extended significantly along the borehole to an interval of about 20 m. Neutron logging results in the DST showed that the moisture content in boreholes 47, 48, 64, and 65 did not change significantly during the four-year heating phase. The drying in a neutron borehole was a strong function of its distance to the heaters (either to the wing heaters or to the floor heaters in the heated drift).

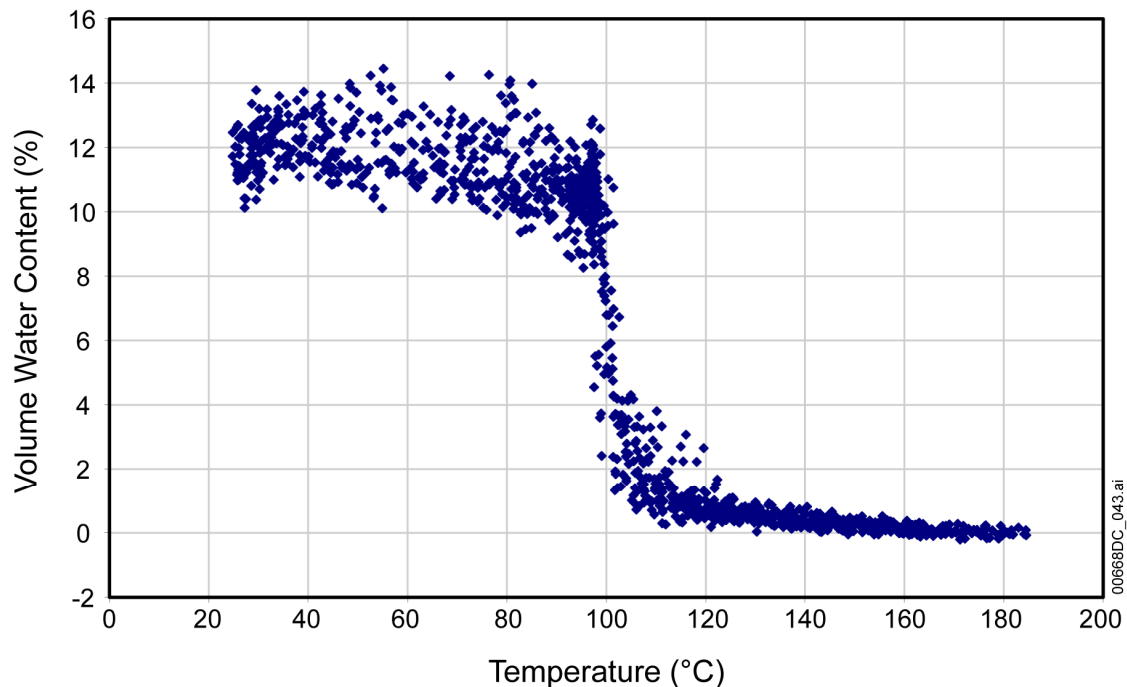


Source: DTNs: LL020710223142.024 [DIRS 159551]; LL030309723122.022 [DIRS 165700]; LL030709023122.032 [DIRS 165701]; LL040308623122.043 [DIRS 177827]; LL041001623122.052 [DIRS 177831]; LL050206323122.057 [DIRS 177829]; LL060101523122.066 [DIRS 177833]; LL060302423122.067 [DIRS 177834].

Figure 6.3-24. Difference Fraction Volume Water Content Measured in DST Borehole 66 Using Neutron Logging (November 19, 1998, to December 11, 2001)

The heaters were turned off on January 14, 2002 (day 1503). By day 1807, the dry region had advanced further along the hole by nearly two more meters. During the last three years of data (days 2164, 2414, and 2820), the dry region receded somewhat as moisture returned to the dry region's margins.

Figure 6.3-25 shows the relationship between volume water content and temperature during the heating phase, based on neutron and temperature measurements from boreholes 79 and 80. This plot shows that the water content in the rock changes little until temperatures near boiling are reached and most drying occurs between 90°C and 105°C.



Source: DTN: MO0406SEPTVDST.000 [DIRS 170616].

Figure 6.3-25. Rock Moisture Content as a Function of Temperature as Measured from Neutron Logging of Boreholes 79 and 80 during the DST Heating Phase

### 6.3.2.3.2 Measurement Uncertainty: Moisture Content Determined by Neutron Logging

The neutron tool was calibrated to the liner-grout and liner-RTD bundle-grout systems as used in the DST borehole. However, variations in the grout volume along a borehole, possibly caused by changes in the borehole diameter, breakout regions, etc., will introduce uncertainty in the measured results. One particularly severe case was in borehole 80, where the preheating baseline measurements were conducted before grouting and after grouting. The baseline measurements showed that the deepest 6-m section of the borehole was not grouted. Calibration results without grout were used for reducing the data in the ungrouted section of the borehole. The amount of grout in the region between the grouted and the ungrouted sections of the borehole (between 50 and 53 m from the collar) was unknown. Therefore, the moisture content in that portion of the borehole is associated with a greater degree of uncertainty.

The other factors that contribute to measurement uncertainty associated with neutron logging are as discussed in Section 6.2.2.3.2.

### **6.3.2.4 Active Pneumatic Testing and Passive Hydrological Monitoring Measurements**

#### Preheating Air Injection

Preheating characterization by air permeability tests was performed in DST boreholes as they became available for testing. The preheating air-injection tests provide an estimate of the fracture permeability in the test block and establish baseline values for tracking changes arising from thermally driven coupled processes. Single-hole air permeability tests were performed in November and December 1996, and in February and March 1997, in 14 boreholes (boreholes 45 to 48, 51 to 53, 56 to 57, 69 to 70, 73, 75, and 78). Locations of these boreholes in the test block are shown in Figures 6.3-4, 6.3-6, 6.3-7, and 6.3-8. Pressure and flow data for these tests can be found in DTN: LB970600123142.001 [DIRS 105589] and are documented by Tsang and Cook (1997 [DIRS 100646]). In addition, 24 boreholes were tested in July 1997. These are boreholes 158 through 167, 170 through 174, and 176 through 177 (Figure 6.3-3), intended for temperature measurements, and several wing heater boreholes (boreholes 98 to 100, and 115 to 118). Pressure and flow data for the July 1997 tests can be found in DTN: LB980120123142.005 [DIRS 114134] and are documented by Tsang and Freifeld (1998 [DIRS 159097]).

#### Hydrology Borehole Configuration

For each of the 12 hydrology boreholes (57 to 61, 74 to 78, and 185 to 186, as shown in Figure 6.3-4), a string of custom-designed high-temperature packers was installed to divide the 40-m-long borehole typically into four isolated zones of approximately 8 m each. For boreholes 58 and 77, only a string of three packers could be installed because of obstruction caused by fallen rocks from the fractures and lithophysal cavities. After installation of the pneumatic packer strings in the baseline, air permeability measurements were performed in the 46 isolated intervals. Air was injected at a constant flow rate in a zone isolated either by two packers or by a packer and the bottom of borehole, while the pressure responses in this and all other packed-off zones were monitored. The air-injection pressure and flow data from the hydrology boreholes prior to initiation of heating can be found in DTN: LB980120123142.004 [DIRS 105590] and are documented by Tsang and Freifeld (1998 [DIRS 105774]). After the collection of the initial DST preheating air-injection data, the entire process of selecting injection intervals was automated, using computer-controlled gas delivery manifolds installed near the collars of each cluster of boreholes. The new combination of hardware and software makes the entire process of air permeability measurement fully automated, allowing for more consistent collection of data with minimum need for onsite field personnel to oversee the testing. Detailed information on the setup of the air-injection equipment can be found in the report by Freifeld and Tsang (1998 [DIRS 159098]).

The DST active hydrologic testing program consists of periodic (approximately quarterly) air-injection tests conducted in these same 46 isolated intervals in the 12 hydrology boreholes. These tests are to monitor the changes in the fracture permeability as a result of coupled processes.

### Heating Phase Air Injection

Periodic air-injection test data containing measured pressures and flow rates collected during the heating have been submitted to the TDMS in the following DTNs:

- LB980420123142.002 [DIRS 113706]
- LB981016123142.002 [DIRS 129245]
- LB990630123142.001 [DIRS 129247]
- LB000121123142.002 [DIRS 158337]
- LB000718123142.002 [DIRS 158341]
- LB0101AIRKDST1.001 [DIRS 158345]
- LB0108AIRKDST5.001 [DIRS 158438]
- LB980715123142.002 [DIRS 113742]
- LB0203AIRKDSTE.001 [DIRS 158348].

### Cooling Phase Air Injection

Air injection testing was carried out throughout the cooling phase of the DST, although at a rate less frequent than quarterly as hydrological changes became less obvious. The data have been submitted to the TDMS in the following DTNs:

- LB0209AIRKDSTC.001 [DIRS 177869]
- LB0303AIRKDSTC.001 [DIRS 177870]
- LB0309AIRKDSTC.001 [DIRS 177871]
- LB0403AIRKDSTC.001 [DIRS 177872]
- LB0410AIRKDSTC.001 [DIRS 177886]
- LB0509AIRKDSTC.001 [DIRS 177887]
- LB0603AIRKDSTC.001 [DIRS 178559].

### Passive Hydrological Monitoring Data of Pressure, Temperature, and Humidity

In addition to active air injection tests, passive monitoring of pressure, temperature, and humidity is being conducted on an hourly basis by the DCS. Locations (XYZ coordinates) of these sensors can be found in DTN: MO0002ABBLSLDS.000 [DIRS 147304]. Because of the slow rate of change for these parameters, the data are parsed to 4 points per day by the DCS manager. This reduced data set is then reviewed and submitted in three data reports, containing time-stamped pressure, temperature, and humidity data. Each file contains a sequential list of data for all 46 monitored locations within the DST hydrology boreholes. Passive monitoring data for the heating phase of the DST can be found in the following input DTNs:

- LB0401PRTDSTHP.001 [DIRS 169251]
- LB0401PRTDSTHP.002 [DIRS 169252]
- LB0401PRTDSTHP.003 [DIRS 169253]
- LB0401PRTDSTHP.004 [DIRS 169255]
- LB0401PRTDSTHP.005 [DIRS 169246]
- LB0401PRTDSTHP.006 [DIRS 169247]

- LB0401PRTDSTHP.007 [DIRS 169248]
- LB0401PRTDSTHP.008 [DIRS 169249]
- LB0401PRTDSTHP.009 [DIRS 169250].

The summary DTN for the heating phase pressure and temperature data is listed in Table 6.3-1.

Passive pressure and temperature monitoring data for the cooling phase of the DST can be found in the following input DTNs:

- LB0401PRTDSTCP.001 [DIRS 170568]
- LB0401PRTDSTCP.002 [DIRS 170569]
- LB0309H2ODSTCP.001 [DIRS 177905]
- LB0403PRTDSTCP.001 [DIRS 177906]
- LB0410PRTDSTCP.001 [DIRS 177907]
- LB0609PRTDSTCP.001 [DIRS 177908]
- LB0609PRTDSTCP.002 [DIRS 177909].

Readings from the downhole humidity sensors function only to provide corroborative evidence of drying, as tracked by geophysical methods such as electrical resistivity tomography, cross-hole radar tomography, and neutron logging. The humidity data are designated corroborating and non-Q.

Passive humidity data for the heating and cooling phases of the DST can be found in the following input DTNs:

- LB0401RHMDSTHP.001 [DIRS 177911]
- LB0401RHMDSTHP.002 [DIRS 177914]
- LB0401RHMDSTHP.003 [DIRS 177915]
- LB0401RHMDSTHP.004 [DIRS 177916]
- LB0401RHMDSTHP.005 [DIRS 177918]
- LB0401RHMDSTHP.006 [DIRS 177920]
- LB0401RHMDSTHP.007 [DIRS 177921]
- LB0401RHMDSTHP.008 [DIRS 177922]
- LB0401RHMDSTHP.009 [DIRS 177924]
- LB0401RHMDSTCP.001 [DIRS 177929]
- LB0401RHMDSTCP.002 [DIRS 177930]
- LB0311RHMDSTCP.001 [DIRS 177932]
- LB0403RHMDSTCP.001 [DIRS 177933]
- LB0410RHMDSTCP.001 [DIRS 177935]
- LB0509RHMDSTCP.001 [DIRS 177937]
- LB0603RHMDSTCP.001 [DIRS 177938].

### Gas Tracer Tests

Tracer tests were performed in boreholes 75 and 76 to estimate fracture porosity in the test block. The gas tracer data can be found in DTN: LB980420123142.002 [DIRS 113706]. Estimated fracture porosity from the gas tracer data can be found in DTN: LB980912332245.002 [DIRS 105593]. Freifeld and Tsang (1998 [DIRS 159098]) provide detailed discussion of this testing.

Tracer tests were performed with the hardware and software used for performing DST quarterly air-injection tests, with additional hardware to perform the mixing of a tracer gas into the air-injection stream and to control and analyze gas withdrawn from an extraction interval. A quadruple mass spectrometer gas analyzer was set up in the field to perform the quantitative analysis of tracer gas concentration in real time.

#### **6.3.2.4.1 Results: Active Pneumatic Testing and Passive Hydrological Monitoring**

##### Preheating Air Injection

Steady-state analysis of the data was performed using Equation 5.1-1. Estimated permeability values from preheating characterizations conducted in November and December of 1996 and in February and March of 1997 are shown in Table 6.3-7. Estimated permeability values for the 24 boreholes tested in July 1997 are shown in Table 6.3-8. Estimated preheating baseline permeabilities for the 46 isolated intervals tested in November 1997 are shown in Table 6.3-9.

Table 6.3-7. Estimated Local Permeability for 41 Packed-off Zones in 14 Boreholes during DST Preheating (November/December 1996 and February/March 1997)

<b>Borehole ID</b>	<b>k(m<sup>2</sup>) in Zone 1</b>	<b>k(m<sup>2</sup>) in Zone 2</b>	<b>k(m<sup>2</sup>) in Zone 3</b>
45 ESF-HD-ERT- 1	5.8E-14	2.4E-14	4.5E-13
46 ESF-HD-ERT-2	4.1E-15	6.2E-15	9.0E-14
47 ESF-HD-NEU-1	6.1E-14	4.4E-13	4.7E-13
48 ESF-HD-NEU-2	2.4E-14	3.5E-14	3.4E-13
51 ESF-HD-NEU-5	8.8E-16	4.4E-13	4.1E-14
52 ESF-HD-CHE-1	1.0E-13	1.2E-13	2.0E-12
53 ESF-HD-CHE-2	1.1E-13	1.3E-12	N/A
56 ESF-HD-CHE-5	1.9E-15	3.4E-14	4.8E-13
57 ESF-HD-HYD-1	2.7E-13	6.1E-14	1.4E-13
69 ESF-HD-CHE-6	2.1E-13	9.5E-15	4.9E-13
70 ESF-HD-CHE-7	1.9E-14	4.5E-14	4.2E-13
73 ESF-HD-CHE-10	6.6E-14	6.8E-15	1.0E-13
75 ESF-HD-HYD-7	4.9E-13	1.4E-13	3.0E-13
78 ESF-HD-HYD-10	15.5E-14	1.1E-14	7.8E-14

Source: DTN: LB970600123142.001 [DIRS 105589].



Table 6.3-8. Parameters Used in Equation 5.2-1 for the Estimation of Local Permeability during DST Preheating (July 1997)

Borehole ID_Data File	L (m)	Q (SLPM)	P <sub>2</sub> -P <sub>1</sub> (kPa)	P <sub>1</sub> (kPa)	k(m <sup>2</sup> )
177_02JUL19	12.822	10	30.67	89.24	7.01E-15
158_02JUL08	16.076	99	16.68	90.14	1.12E-13
159_02JUL07	16.062	99	8.48	89.38	2.33E-13
160_01JUL03	16.012	499	0.83	89.45	1.26E-11
160_01JUL04	12.964	499	4.20	89.52	2.89E-12
161_01JUL01	16.312	299	11.09	89.52	5.22E-13
161_01JUL02	13.264	199	15.99	89.45	2.79E-13
162_01JUL01	17.822	54	27.01	89.45	3.32E-14
163_02JUL01	16.312	99	32.60	89.38	5.29E-14
164_02JUL02	16.012	299	15.99	89.45	3.59E-13
164_02JUL03	12.964	299	17.99	89.52	3.76E-13
165_02JUL05	16.012	299	16.61	89.52	3.44E-13
166_02JUL06	16.038	99	21.36	89.59	8.63E-14
167_01JUL06	12.822	199	35.56	89.52	1.17E-13
170_02JUL21	16.012	99	5.38	89.72	3.72E-13
171_02JUL20	16.012	99	22.88	89.45	8.02E-14
172_02JUL18	16.312	99	6.34	89.45	3.10E-13
173_02JUL17	17.822	21	33.15	89.52	1.02E-14
174_02JUL16	16.312	21	21.50	89.45	1.79E-14
176_02JUL22	16.012	199	5.72	89.38	7.05E-13
100_02JUL15	7.512	99	7.37	93.24	4.61E-13
115_02JUL12	7.512	99	4.69	93.17	7.36E-13
116_02JUL11	7.512	199	6.68	93.24	1.03E-12
117_02JUL10	7.512	299	12.13	93.31	8.26E-13
118_02JUL09	7.512	299	8.13	93.17	1.26E-12
98_02JUL13	7.512	499	1.17	93.24	1.51E-11
99_02JUL14	7.512	299	4.62	93.24	2.26E-12

Source: DTN: LB980120123142.005 [DIRS 114134].

Table 6.3-9. Parameters Used in Equation 5.2-1 for the Estimation of Local DST Permeability during Preheating (November 1997)

Borehole-Zone (data file ID)	L(m)	Q(SLPM)	(P <sub>2</sub> -P <sub>1</sub> ) (kPa)	P <sub>1</sub> (kPa)	k(m <sup>2</sup> )
57-1 (11797544PM)	8.84	20	4.58	89.2	1.46E-13
57-2 (11897401AM)	6.10	100	18.5	89.5	2.26E-13
57-3 (11897218PM)	7.62	2	39.9	89.3	1.58E-15
57-4 (119971235AM)	10.55	200	12.6	89.7	4.37E-13
58-1 (111697133AM)	6.10	20	5.12	90.2	1.74E-13
58-2 (1116971151AM)	8.54	20	3.18	90.4	2.15E-13
58-3 (1116971008PM)	17.98	171	3.74	89.9	8.45E-13
59-1 (111097610PM)	10.06	100	22.1	86.9	1.27E-13
59-1 (111097610PM)	10.06	20	4.25	86.9	1.45E-13
59-2 (111197427AM)	7.62	100	8.95	90.8	4.04E-13
59-3 (111197244PM)	8.54	100	10.8	88.0	3.11E-13
59-4 (111297101AM)	7.19	200	7.8	91.6	9.69E-13
60-1 (111097101PM)	5.49	20	2.75	88.8	3.62E-13
60-1 (111097101PM)	5.49	100	21.2	88.8	2.13E-13
60-2 (1110971118PM)	10.67	100	5.8	87.7	4.98E-13
60-3 (111197936AM)	5.49	2	7.2	88.5	1.35E-14
60-4 (111197753PM)	11.19	20	45.5	89.5	9.85E-15
61-1 (117971235PM)	7.01	200	34	89.5	2.04E-13
61-1 (117971235PM)	7.01	100	14.6	89.5	2.61E-13
61-2 (117971052PM)	8.54	100	3.85	88.8	8.99E-13
61-3 (11897909AM)	6.10	20	16.3	100.0	4.68E-14
61-4 (11897727PM)	12.63	100	26.9	89.4	8.23E-14
74-1 (11497749PM)	10.37	100	10.6	90.0	2.65E-13
74-2 (114971139PM)	6.71	20	12.9	90.3	6.12E-14
74-3 (11597330AM)	4.27	20	8.04	90.4	1.44E-13
74-4 (111797308PM)	14.09	100	17.3	90.9	1.21E-13
75-1 (11597140PM)	8.23	100	11.3	91.4	2.95E-13
75-2 (11597450PM)	7.32	100	23.7	90.8	1.46E-13
75-3 (115978PM)	10.67	100	17.3	89.9	1.53E-13
75-4 (111797129PM)	8.48	100	4.68	90.8	7.24E-13
76-1 (116971106AM)	7.93	100	13.1	90.0	2.64E-13
76-2 (11697216PM)	8.54	20	5.27	89.8	1.29E-13
76-3 (11697526PM)	8.54	20	9.89	89.0	6.76E-14
76-4 (11697836PM)	10.00	20	6.82	90.5	8.62E-14
77-1 (111597825PM)	8.84	100	21.5	91.0	1.40E-13

Table 6.3-9. Parameters Used in Equation 5.2-1 for the Estimation of Local DST Permeability during Preheating (November 1997) (Continued)

Borehole-Zone (data file ID)	L(m)	Q(SLPM)	(P <sub>2</sub> -P <sub>1</sub> ) (kPa)	P <sub>1</sub> (kPa)	k(m <sup>2</sup> )
77-1 (11697351PM)	8.84	20	1.87	90.6	3.57E-13
77-1 (111397341PM)	8.84	20	1.72	89.9	3.91E-13
77-2 (111697642AM)	5.49	20	21.2	90.0	4.21E-14
77-2 (11697701PM)	5.49	20	33.1	89.3	2.56E-14
77-2 (111397828PM)	5.49	20	31.4	88.7	2.74E-14
77-2 (110797729AM)	5.49	20	31.1	89.4	2.75E-14
77-3 (111697459PM)	22.70	100	3.83	90.5	3.94E-13
78-1 (1117971013AM)	6.10	20	4.4	90.4	2.02E-13
78-2 (11797419AM)	8.23	20	14.3	90.4	4.64E-14
78-3 (11797554AM)	5.79	20	16	89.9	5.49E-14
78-4 (1115971008AM)	14.49	20	4	91.1	1.09E-13
185-1 (115971204PM)	5.79	20	2.75	89.5	3.46E-13
185-2 (11597315PM)	8.54	100	15.6	89.4	2.07E-13
185-3 (11597625PM)	15.24	100	20.9	90.2	9.26E-14
185-4 (11597935PM)	6.65	20	4.18	89.6	2.01E-13
186-1 (11497553PM)	5.79	20	2.47	90.4	3.80E-13
186-2 (11497944PM)	8.54	20	22.1	93.9	2.71E-14
186-3 (11597134AM)	13.11	20	51.9	89.9	7.34E-15
186-4 (1117971151AM)	5.09	2	11.4	90.6	8.68E-15

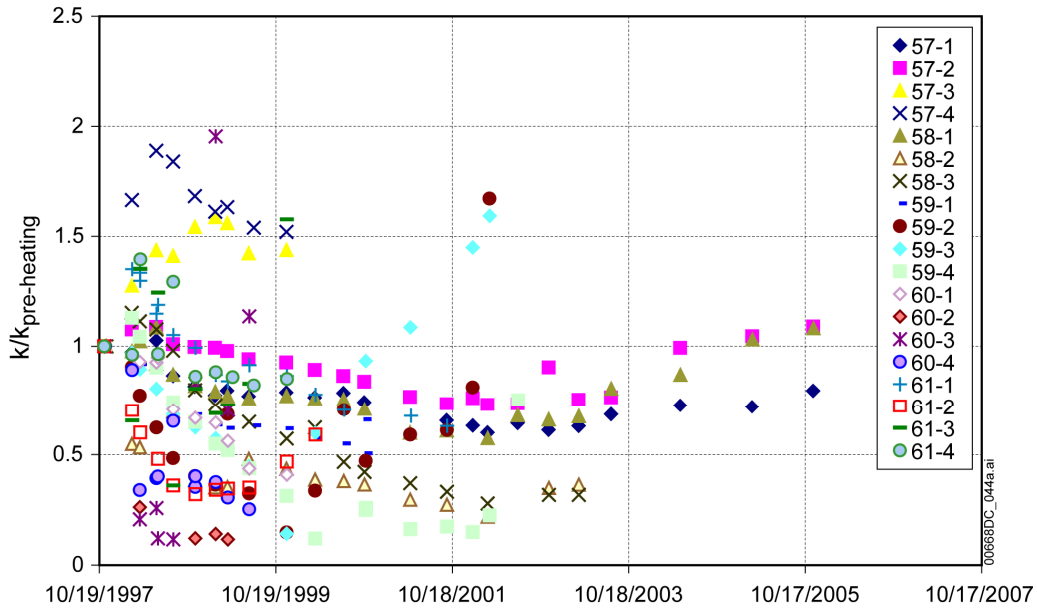
Source: DTN: LB980120123142.004 [DIRS 105590].

### Heating and Cooling Phase Air Injection

The air injection test data submitted to the TDMS contained measured pressures and flow rates only. Pressure data appeared as absolute pressure. To estimate permeability for the injection interval, the pressure values measured prior to the start of the injection, and the steady-state value obtained late in the injection period, are used in Equation 5.1-1.

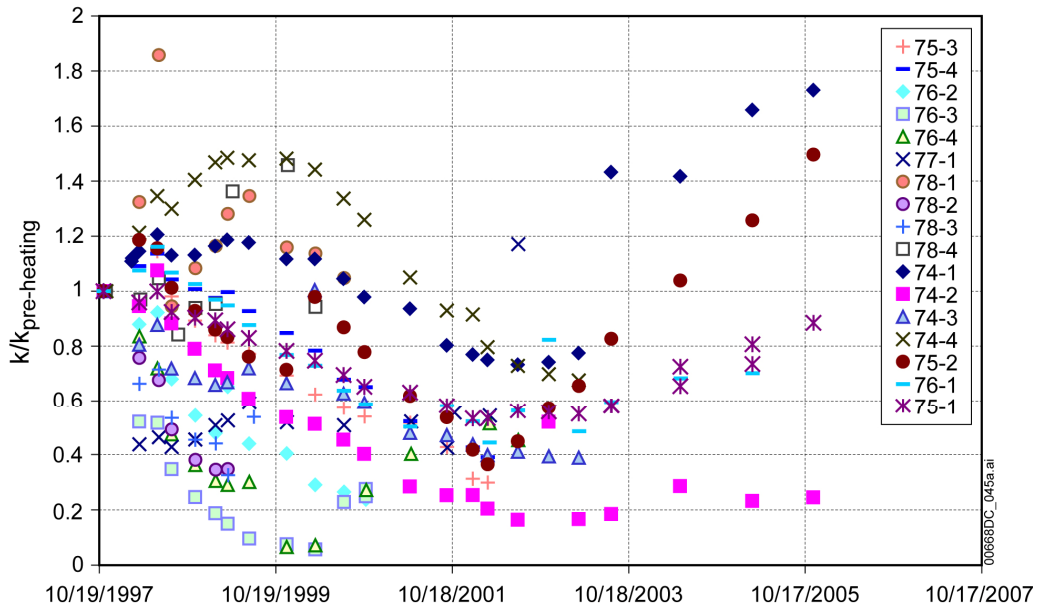
Throughout the DST, changes in permeability as a ratio to baseline permeability estimates could be used to indicate changes in fracture liquid saturation. These are shown in Figures 6.3-26, 6.3-27, and 6.3-28 for boreholes 57 to 61, 74 to 78, and 185 and 186, respectively. Permeability ratio as a function of time through the heating phase for the packed-off zones in the hydrology boreholes as shown in these figures are the content of summary DTN: LB0208AIRKDSTH.001 [DIRS 160897].

Changes in the borehole 57-2 permeability can be used to demonstrate the use of these figures in interpreting changes in fracture saturation throughout the DST. As shown in Figure 6.3-26, the borehole 57-2 permeability gradually declined from its baseline value. This decrease in air permeability indicates a gradual buildup in fracture liquid saturation during the heating phase of the DST. During cooling, the permeability values are seen to slowly return to the baseline value.



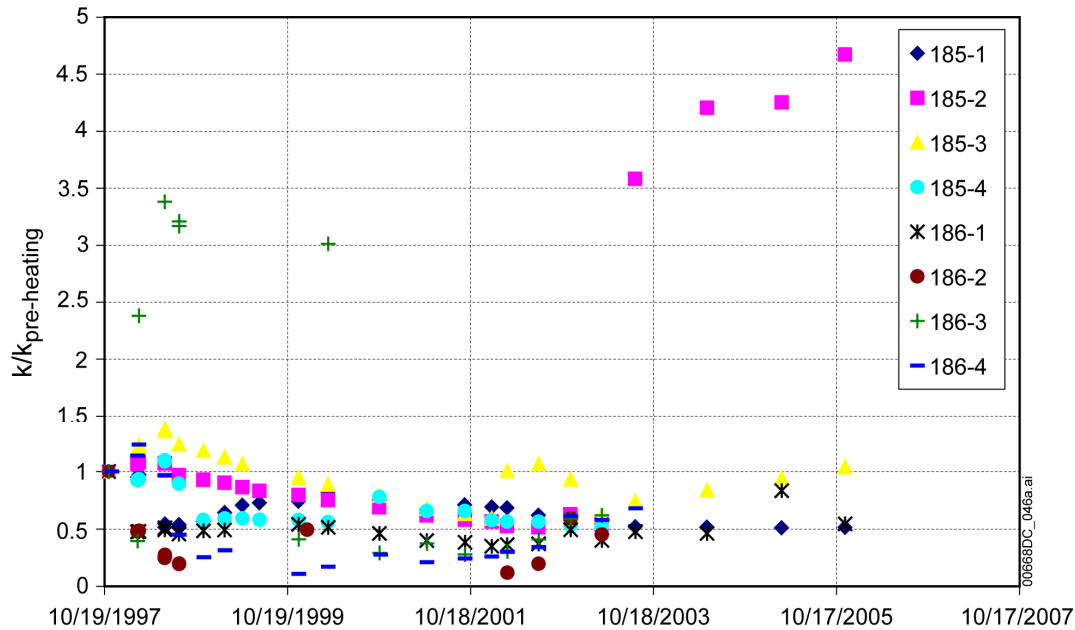
Source: DTNs: LB0208AIRKDSTH.001 [DIRS 160897]; LB0209AIRKDSTC.001 [DIRS 177869]; LB0303AIRKDSTC.001 [DIRS 177870]; LB0309AIRKDSTC.001 [DIRS 177871]; LB0403AIRKDSTC.001 [DIRS 177872]; LB0410AIRKDSTC.001 [DIRS 177886]; LB0509AIRKDSTC.001 [DIRS 177887]; LB0603AIRKDSTC.001 [DIRS 178559].

Figure 6.3-26. Changes in Permeability Displayed as a Ratio to the Preheating Permeability Estimate for DST Boreholes 57 through 61



Source: DTNs: LB0208AIRKDSTH.001 [DIRS 160897]; LB0209AIRKDSTC.001 [DIRS 177869]; LB0303AIRKDSTC.001 [DIRS 177870]; LB0309AIRKDSTC.001 [DIRS 177871]; LB0403AIRKDSTC.001 [DIRS 177872]; LB0410AIRKDSTC.001 [DIRS 177886]; LB0509AIRKDSTC.001 [DIRS 177887]; LB0603AIRKDSTC.001 [DIRS 178559].

Figure 6.3-27. Changes in Permeability Displayed as a Ratio to the Preheating Permeability Estimate for DST Boreholes 74 through 78



Source: DTNs:LB0208AIRKDSTH.001 [DIRS 160897]; LB0209AIRKDSTC.001 [DIRS 177869]; LB0303AIRKDSTC.001 [DIRS 177870]; LB0309AIRKDSTC.001 [DIRS 177871]; LB0403AIRKDSTC.001 [DIRS 177872]; LB0410AIRKDSTC.001 [DIRS 177886]; LB0509AIRKDSTC.001 [DIRS 177887]; LB0603AIRKDSTC.001 [DIRS 178559].

Figure 6.3-28. Changes in Permeability Displayed as a Ratio to the Preheating Permeability Estimate for DST Boreholes 185 and 186

Some of the zones, such as 76-3, 76-4, and 59-3, show rapid decreases in air-permeability during heating followed by equally rapid increases attributed to the dryout of the zone. These trends usually terminated prior to the end of the DST due to packer failures caused by thermal degradation of the rubber packer glands. This is consistent with the conceptual model that drying of the fractures will lead to greater air-permeability. Other zones, such as 57-1, 58-1, and 75-1, display gradual decreases in air-permeability followed by a gradual rebound once the cooling phase started. These zones did not go through dryout and the gradual decrease in permeability is thought to be caused by water vapor being transported away from the heaters, where it is able to condense and collect in the fractures. During cooling this trend is reversed and the fractures are able to dry out. It can also be possible that the change in the rock stress state is causing mechanical changes in the fracture system and that the rebound in permeability is an elastic response of the rock mass.

There are other behaviors exhibited in the air injection responses that are potentially caused by abrupt mechanical changes in the hydrologic system. Boreholes 74-1, 75-2, and 185-2 show distinct changes in estimated permeability values that form a discontinuity from the more gradual underlying trends. While there is not sufficient data to attribute any distinct rapid change in permeability to a distinct event, the changes in permeability do indicate a complex response of the rock mass to the changes induced.

As heating of the test block continued, many air-injection tests showed responses that were considered anomalous. Most of the unusual behavior was attributable to two-phase processes,

such as vapor condensation or evaporation. An anomalous response to an air injection was observed in borehole zone 60-3. The unusual response was attributed to the injection of cool dry air into a saturated hot environment. In these cases, the data cannot be used for the estimation of formation permeability, because no meaningful steady state values are obtained.

Another type of anomalous response was observed during air injection into 78-4. In this test, borehole zones 78-1, 78-2, and 78-3 all recorded decreases in pressure. This is counter-intuitive, since mass is being added to the system and pressure should increase. However, the observed pressure declines are the result of cold gas being transported in the 78-4 injection tube which needs to go through the sealed-off packer intervals 78-1, 78-2, and 78-3. This cooling can lead to condensation of vapor in these zones and thereby reduces pressure during the injection test.

The failure of some of the pneumatic packers as heating progresses is another factor affecting analysis of the DST air-injection tests. Because a deflated packer changes the injection interval length, the data collected from the zones before and after the packer deflates were not amenable to comparison with the baseline data. Hence, the estimated permeabilities for zones next to deflated packers were not amenable to comparison with baseline permeability values. The deflated packers and the dates that they became deflated are shown in Table 6.3-10.

Table 6.3-10. Date of Pneumatic Packer Deflation in the DST Hydrology Boreholes

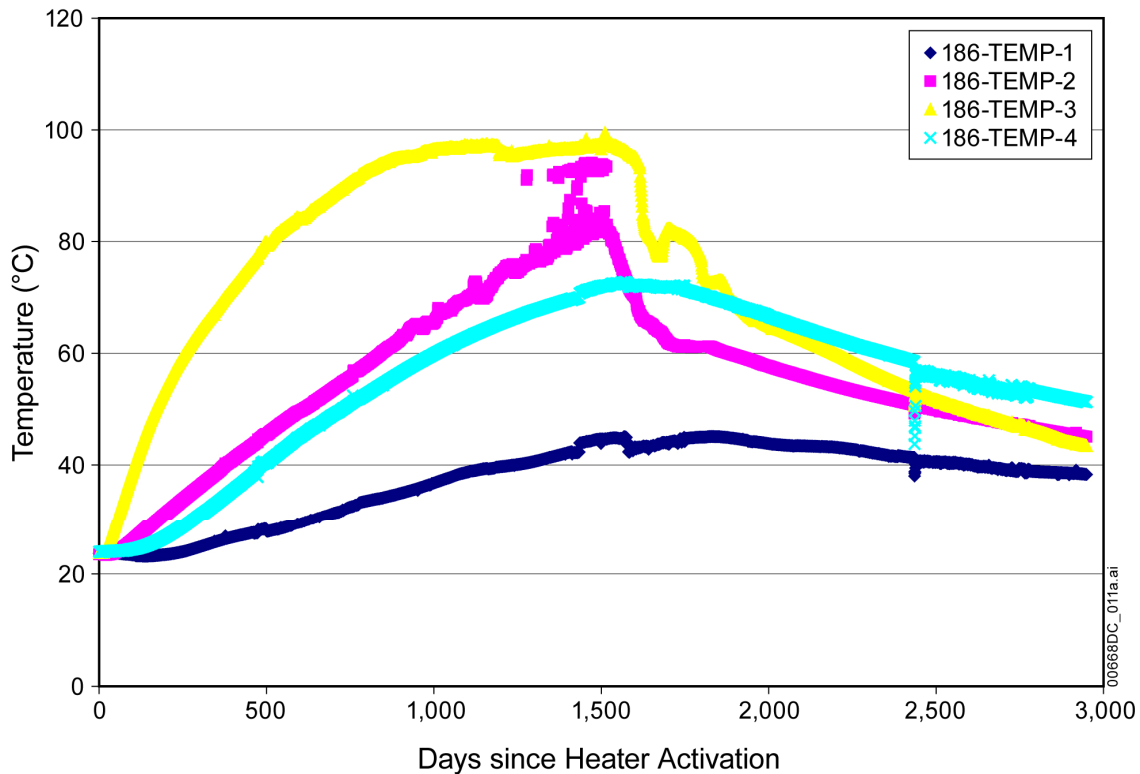
Packer Location	Date
57-4	March 22, 2000
59-1	February 6, 2001
60-1	November 14, 2001
60-2	January 1, 2000
60-3	November 30, 1999
60-4	August 27, 1999 <sup>a</sup>
61-2	November 7, 2001
61-3	July 24, 2000
61-4	February 6, 2001
76-3	December 24, 2000
77-3	January 7, 1998
78-2	December 24, 2000
78-3	December 1, 1999
78-4	September 9, 2000

Source: DTN: LB0208AIRKDSTH.001 [DIRS 160897].

<sup>a</sup> Reinflated February 16, 2000; deflated again August 15, 2000.

*Passive Hydrological Monitoring Data of Pressure, Temperature, and Humidity*

Time history of the passive monitoring data in the hydrology holes may be plotted from the data files submitted to the TDMS as listed above. As an example, Figure 6.3-29 shows the temperature data for the sensors located in borehole 186.



Source: DTNs: LB0208H2ODSTHP.001 [DIRS 170579]; LB0309H2ODSTCP.001 [DIRS 177905]; LB0401PRTDSTCP.001 [DIRS 170568]; LB0401PRTDSTCP.002 [DIRS 170569]; LB0403PRTDSTCP.001 [DIRS 177906]; LB0410PRTDSTCP.001 [DIRS 177907]; LB0609PRTDSTCP.001 [DIRS 177908]; LB0609PRTDSTCP.002 [DIRS 177909].

Figure 6.3-29. Passive Monitoring Temperature Data for DST Borehole 186

### Gas Tracer Tests

Three convergent weak dipole flow field tracer tests were performed between boreholes 75 and 76 in the DST. Air with a sulfur hexafluoride tracer was injected into borehole 76, and gas was withdrawn from borehole 75 for analysis. Gas tracer tests in the DST area were conducted in boreholes 75 and 76, zones 2 and 4. Two different-strength dipoles were used in zone 2, 10:1 and 30:1. A 10:1 dipole was used to test zone 4. The strength of the dipole refers to the ratio of withdrawal gas flux to injected gas flux. The data for each test are provided in DTN: LB980420123142.002 [DIRS 113706].

The injection air and withdrawal gas flow rates and zone pressures were monitored prior to the injection of any tracer to ensure that a steady-state flow field was achieved. After a steady state pressure field was obtained, the air-injection flow rate was reduced to 0.90 of the original value. A makeup gas stream of tracer equal to 0.10 of the original injection air stream was added from a 10,000 ppm cylinder of SF<sub>6</sub>. The final injection gas stream had a concentration of 1,000 ppm SF<sub>6</sub>. After a limited injection period, the injection of tracer was halted, and the injection air stream was returned to its original flux rate. Throughout the entire duration of the experiment, the withdrawal gas stream was maintained at a steady flux rate, and SF<sub>6</sub> concentration measurements were performed by the mass spectrometer every 30 seconds.

#### **6.3.2.4.2 Measurement Uncertainty: Active Pneumatic Testing and Passive Hydrological Monitoring Measurements**

Since the same types of measurements were performed for the SHT, readers are referred to the discussion of the SHT in Section 6.2.2.4.2. Measurement uncertainty in analysis has been considered. For example, although the estimate of air permeability may not be as accurate as desired because of the assumptions involved, restricting the use of only the ratio of permeability to its respective preheating value, while keeping all other experimental parameters identical throughout the test, minimizes the impact of measurement uncertainty.

#### **6.3.2.5 Laboratory Hydrological Parameters**

Laboratory testing of saturation, porosity, bulk density, particle density, and gravimetric water content was conducted for both dry-drilled cores and wet-drilled cores from the DST block at Alcove 5 of the ESF. The measurements were carried out according to the technical implementation procedure YMP-LBNL-TIP/AFT 2.0. Data can be found in the TDMS under DTNs: LB970500123142.003 [DIRS 131500] and LL020506123142.021 [DIRS 169256].

Similar to those discussed in Section 6.2.2.5 for the SHT, moisture retention curves were measured at elevated temperatures to about 94°C for samples taken from the DST block. In preparation for the moisture retention measurements, the dry bulk density, saturated bulk density, and porosity for these samples were determined. The moisture retention curves and the related densities and porosity data measurements have been documented by Lin et al. (2002 [DIRS 159099]).

In addition to the above, electrical resistivity and relative permittivity were also measured as a function of water saturation at 35°C, 50°C, 70°C, and 95°C, over a range of frequency from  $10^{-2}$  to  $10^6$  Hz. These properties are useful for the processing of geophysical imaging data. The measurements were made using either an HP4274A LCR meter, an HP4284A LCR meter, or a Solartron 1260 frequency response analyzer. Measurements made over a range of frequencies verify measurements made at a single frequency and provide additional information about conduction mechanisms and microstructural parameters. The electrical property data can be found in the TDMS under DTNs: LL981109904242.072 [DIRS 118959] and LL020502523142.020 [DIRS 159105]. Reporting can be found in Section 11.1 of *Drift Scale Test As-Built Report* (CRWMS M&O 1998 [DIRS 111115]).

##### **6.3.2.5.1 Results: Laboratory Hydrological Parameters**

###### *Saturation, Porosity, Density, and Gravimetric Water Content*

The data from two sets of core measurements are tabulated in Table 6.3-11 for the dry-drilled cores and in Table 6.3-12 for the wet-drilled cores from the DST area. Summaries of the averages and standard deviations of the measured values are presented at the end of each table to facilitate comparison between different data sets. The first data set in Table 6.3-11 is based on the cores from boreholes 182, 183, and 184 dry-drilled from an elevated platform at the end of the connecting drift across from the DST block. Included in the second set in Table 6.3-12 are wet-drilled cores from boreholes 52, 53, 56, and 81 within the DST block.



Table 6.3-11. Laboratory Measurement of Dry-Drilled Cores from DST Permeability Boreholes (182, 183, and 184)

<b>Borehole 182, ESF-HD-PERM-1</b>					
<b>Sample Location (m)</b>	<b>Saturation (%)</b>	<b>Porosity (%)</b>	<b>Bulk Density (g/cc)</b>	<b>Particle Density (g/cc)</b>	<b>Gravimetric Water Content (g/g)</b>
5.5	86.67	9.61	2.27	2.51	0.037
9.9	89.67	11.02	2.24	2.52	0.044
15.5	85.08	10.27	2.25	2.51	0.039
19.8	86.72	10.27	2.25	2.51	0.039

<b>Borehole 183, ESF-HD-PERM-2</b>					
<b>Sample Location (m)</b>	<b>Saturation (%)</b>	<b>Porosity (%)</b>	<b>Bulk Density (g/cc)</b>	<b>Particle Density (g/cc)</b>	<b>Gravimetric Water Content (g/g)</b>
5.2	83.84	9.62	2.27	2.51	0.035
10.1	82.86	12.02	2.21	2.51	0.045
15.3	76.61	13.35	2.19	2.53	0.046
19.9	79.21	10.89	2.24	2.51	0.038

<b>Borehole 184, ESF-HD-PERM-3</b>					
<b>Sample Location (m)</b>	<b>Saturation (%)</b>	<b>Porosity (%)</b>	<b>Bulk Density (g/cc)</b>	<b>Particle Density (g/cc)</b>	<b>Gravimetric Water Content (g/g)</b>
5.1	81.40	9.87	2.25	2.50	0.035
10.0	86.61	10.91	2.24	2.51	0.042
15.5	85.80	9.43	2.27	2.51	0.035
18.9	81.76	10.17	2.26	2.52	0.037

<b>Borehole Summary</b>					
	<b>Saturation (%)</b>	<b>Porosity (%)</b>	<b>Bulk Density (g/cc)</b>	<b>Particle Density (g/cc)</b>	<b>Gravimetric Water Content (g/g)</b>
<b>Average</b>	83.85	10.62	2.25	2.51	0.039
<b>Standard Deviation</b>	3.67	1.14	0.02	0.01	0.004

Source: DTN: LB970500123142.003 [DIRS 131500].

Table 6.3-12. Laboratory Measurement of Wet-Drilled Cores from DST Boreholes (81, 52, 53, and 56)

<b>Borehole 81, ESF-HD-MPBX-1</b>					
<b>Sample Location (m)</b>	<b>Saturation (%)</b>	<b>Porosity (%)</b>	<b>Bulk Density (g/cc)</b>	<b>Particle Density (g/cc)</b>	<b>Gravimetric Water Content (g/g)</b>
4.6 <sup>a</sup>	96.43	10.15	2.25	2.50	0.043
6.8	84.97	9.73	2.27	2.51	0.036
12.3 <sup>b</sup>	96.02	10.16	2.26	2.52	0.043
17.8 <sup>c</sup>	96.80	9.46	2.26	2.49	0.040
20.8 <sup>d</sup>	103.77	15.34	2.14	2.53	0.073
24.1	94.10	8.77	2.28	2.50	0.036
32.0	95.42	9.67	2.28	2.52	0.040
35.1 <sup>e</sup>	92.97	11.81	2.21	2.51	0.050
39.4	92.82	10.31	2.26	2.52	0.042
45.3	94.57	9.27	2.28	2.51	0.038

<sup>a</sup> Entire surface of core was wet.

<sup>b</sup> Closed vertical fracture along core axis.

<sup>c</sup> Two fractures with small aperture.

<sup>d</sup> Two open fractures + "crushed zone" + porous looking calcite inclusion.

<sup>e</sup> Large open fracture down center of upper half.

<b>Borehole 52, ESF-HD-CHE-1</b>					
<b>Sample Location (m)</b>	<b>Saturation (%)</b>	<b>Porosity (%)</b>	<b>Bulk Density (g/cc)</b>	<b>Particle Density (g/cc)</b>	<b>Gravimetric Water Content (g/g)</b>
15.3 <sup>a</sup>	87.56	11.73	2.22	2.52	0.046
18 <sup>b</sup>	95.91	17.32	2.09	2.52	0.079
26.5 <sup>a</sup>	87.89	11.04	2.24	2.51	0.043
29.9 <sup>c</sup>	97.32	13.98	2.16	2.51	0.063
35.0	96.98	18.19	2.07	2.53	0.085
38.2 <sup>d</sup>	98.58	16.57	2.11	2.53	0.077

<sup>a</sup> Water drop loss during transfer.

<sup>b</sup> Large fracture exposed on surface.

<sup>c</sup> Contains large open vug on side surface.

<sup>d</sup> Contains fracture on side surface.

<b>Borehole 53, ESF-HD-CHE-2</b>					
<b>Sample Location (m)</b>	<b>Saturation (%)</b>	<b>Porosity (%)</b>	<b>Bulk Density (g/cc)</b>	<b>Particle Density (g/cc)</b>	<b>Gravimetric Water Content (g/g)</b>
10.7 <sup>a</sup>	95.31	11.67	2.22	2.51	0.050
16.7 <sup>a</sup>	96.84	12.94	2.19	2.51	0.057
22.2	94.96	11.52	2.22	2.51	0.049
28.2 <sup>b</sup>	74.03	15.62	2.11	2.50	0.055
36.5 <sup>b</sup>	95.47	12.80	2.21	2.53	0.055

<sup>a</sup> Contains fracture on side surface.

<sup>b</sup> Large amount of water condensed in container.

Table 6.3-12. Laboratory Measurement of Wet-Drilled Cores from DST Boreholes (81, 52, 53, 56)  
(Continued)

<b>Borehole 56, ESF-HD-CHE-5</b>					
<b>Sample Location (m)</b>	<b>Saturation (%)</b>	<b>Porosity (%)</b>	<b>Bulk Density (g/cc)</b>	<b>Particle Density (g/cc)</b>	<b>Gravimetric Water Content (g/g)</b>
10.6	94.99	14.57	2.15	2.52	0.064
18.0 <sup>a</sup>	94.34	12.33	2.20	2.51	0.053
23.2	95.58	16.02	2.11	2.51	0.072
29.6	92.79	15.91	2.14	2.54	0.069
35.7	86.21	11.65	2.21	2.51	0.045
38.9	82.40	10.09	2.25	2.51	0.037

<sup>a</sup> Contains fracture on side surface.

<b>Borehole Summary</b>					
	<b>Saturation (%)</b>	<b>Porosity (%)</b>	<b>Bulk Density (g/cc)</b>	<b>Particle Density (g/cc)</b>	<b>Gravimetric Water Content (g/g)</b>
<b>Average</b>	93.15	12.54	2.20	2.51	0.053
<b>Standard Deviation</b>	5.93	2.75	0.06	0.01	0.015

Source: DTN: LB970500123142.003 [DIRS 131500].

The average saturation value compiled from all surface-based boreholes for Topopah Spring crystal-poor middle nonlithophysal tuff (266 samples) is  $85 \pm 12\%$  (Flint 1996 [DIRS 100673]). The average value for the dry-drilled cores is 84%, and that for the wet-drilled cores is 93%. The corresponding surface-based borehole porosity value is  $11 \pm 2\%$ , as compared to the average values from 11% for dry cores to 13% for wet cores. Therefore, the 11% difference in liquid saturation between the dry-drilled and the wet-drilled data sets in the thermal test area is within the standard deviation of 12% for all the surface-based samples.

### Moisture Retention Curves

Identical to the procedures discussed in Section 6.2.2.5, moisture retention curves were determined for core samples taken from boreholes 52 (CHE-1), 53 (CHE-2), 56 (CHE-5), 69 (CHE-6), 70 (CHE-7), and 73 (CHE-10), whose locations are shown in Figure 6.3-7. In preparation for the moisture-retention determinations, hydrological properties were determined.

Moisture-retention curves of the DST samples were performed at temperatures of 25.1°C, 49.6°C, and 93.7°C. Similar to the SHT data (Section 6.2.2.5), there is very little hysteresis observed between the wetting and drying curves at all temperatures. The temperature cycle has a very small effect on moisture retention. The post-temperature cycle room temperature data show a slightly smaller moisture retention than the initial room temperature data.

The DST samples show less moisture retention than the SHT samples (Section 6.2.2.5) at all temperatures. However, they show greater moisture retention than that of USW G-4 (Roberts and Lin 1995 [DIRS 159100]; 1995 [DIRS 159048]) and the Fran Ridge samples

(Section 6.1.2.5). The data of the DST samples are at the high end of the results of the USW H-1 samples (Section 6.1.2.5). The data of the DST samples are at the lower bound of that shown by Flint (1998 [DIRS 100033]).

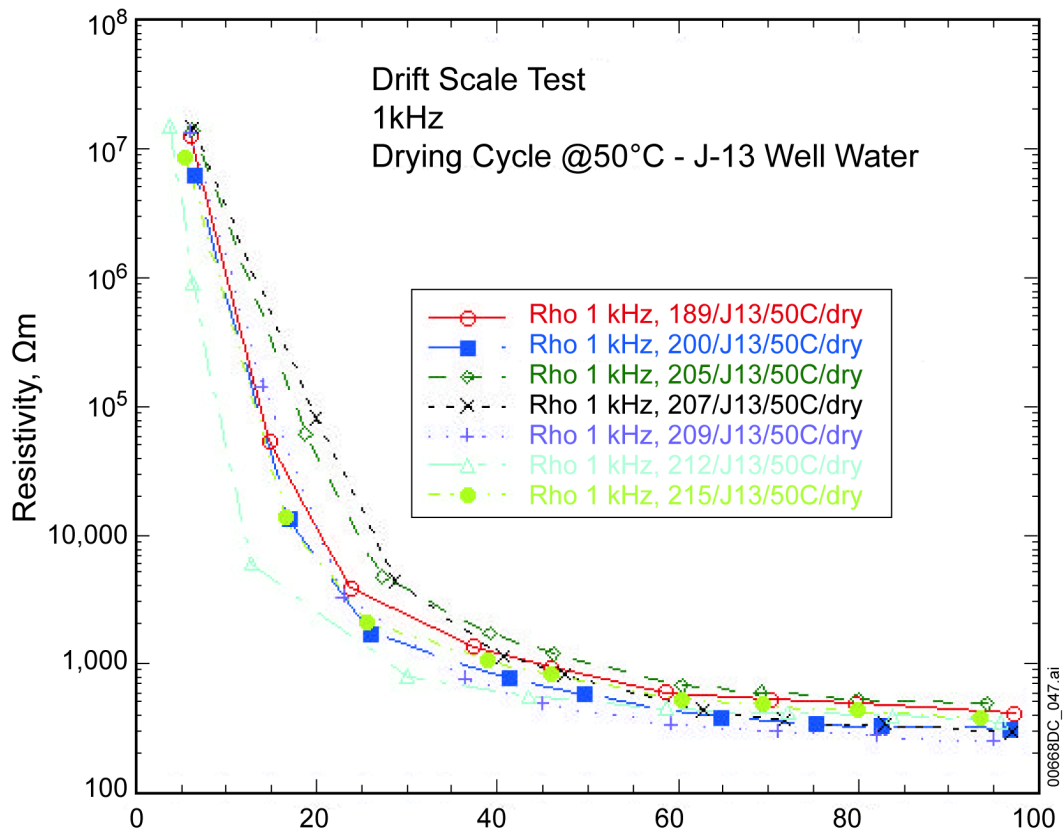
### Electrical Resistivity and Relative Permittivity

Resistivity measurements are reported for one frequency, 1 kHz, because this frequency was determined to be free of electrode contamination (contact impedance) and represents the electrical properties of the material. Relative permittivity measurements are reported at 1 MHz, the highest frequency in the measurements. Samples were prepared from cores obtained from chemistry boreholes 69, 70, and 73 of the DST (Figure 6.3-7). Samples with obvious large cavities and inhomogeneous inclusions were avoided. Prior to the electrical property measurement, hydrological properties were obtained (DTN: LL981109904242.072 [DIRS 118959]). The samples are disk-shaped, with a diameter-to-thickness aspect ratio of 10:1 (dime shaped). The diameter of the samples is approximately 5.1 cm. All samples were prepared with the bedding direction perpendicular to the direction of measurement.

Electrical measurements began on samples that were dry. Water from well J-13 was added to the samples in small amounts and allowed to distribute throughout the sample. The length of time for this to occur was typically 3 to 4 hours, as verified by examining the resistivity of a sample as a function of time. Saturations were determined by weighing the samples immediately after electrical measurements were completed. Each sample was placed in a custom built holder made of Lucite or Lexan and separated from the atmosphere by an o-ring seal. Despite these precautions, water was sometimes lost from samples when measurements at relatively high saturations were attempted at high temperatures. The holders were placed in a standard oven and allowed time to equilibrate to the temperature (typically overnight). Upon reaching maximum saturation, the drying portion of the measurements began. The maximum saturation achieved was between 95% and 100%. Some samples were damaged (chipping and cracking) because of the cooling and heating, and the handling. Those samples were reshaped when necessary and the holders modified to accept the new shape. Samples were no longer used when indicators, such as noise in the data or mechanical flaws, demonstrated that the electrical-properties measurements were unreliable.

Figure 6.3-30 shows the electrical resistivity of the DST samples as a function of water saturation in the drying cycle at 50°C. This is just one example to illustrate the variation of electrical resistivity with water saturation. The rest of the resistivity data can be found in the TDMS. The characteristics of the variation of resistivity with water saturation at other temperatures are similar. This type of resistivity saturation dependence is similar to that observed for other tuff samples. For all temperatures, the dry resistivity is between  $10^7$  and  $10^8$   $\Omega\text{m}$  and drops rapidly to between approximately 3,000 and 1,000  $\Omega\text{m}$  (depending on temperature) as saturation increases. This is interpreted as an indication that the adsorption of water and surface conduction dominate this region of saturation. At approximately 30% saturation, there is a change in the slope of  $\log \sigma$  versus saturation. Between 30% and 100% saturation, the resistivity decreases by only one-half to one order of magnitude.

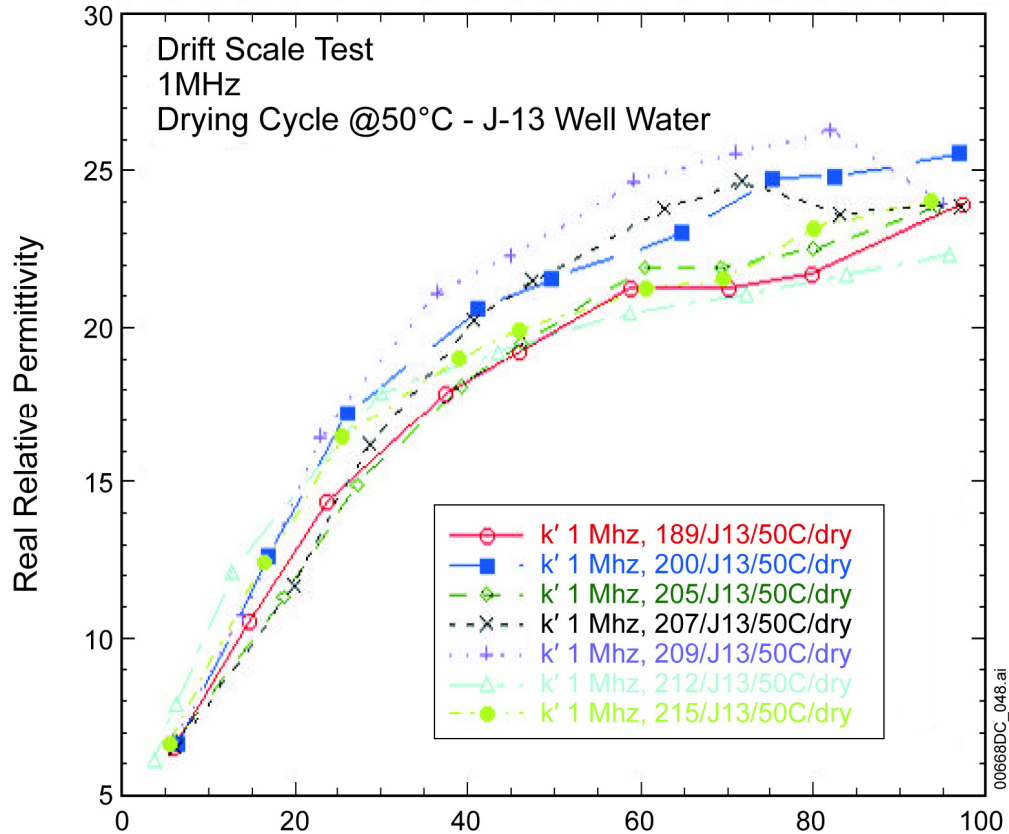
A small amount of hysteresis is observed between wetting and drying cycles. There are small increases in resistivity during the wetting phase, similar to previous measurements utilizing distilled water as the saturating fluid (Roberts and Lin 1997 [DIRS 101710]).



Source: DTN: LL981109904242.072 [DIRS 118959].

Figure 6.3-30. Electrical Resistivity of DST Samples as Function of Saturation in the Drying Cycle at 50°C

Figure 6.3-31 shows the relative permittivity of the DST samples as a function of water saturation in the drying cycle at 50°C. This example illustrates the variation of the relative permittivity with water saturation. The rest of the permittivity data can be found in the TDMS under the DTNs listed above. At low saturations, permittivity is insensitive to temperature. The dry samples all have a dielectric constant (relative permittivity) between five and six. The near-saturated samples have a range of values between 22 and 26. This range of relative permittivity values at one temperature is fairly typical above approximately 40% saturation for all temperatures. The scatter in the data increases as temperature increases and is more noticeable for the 70°C wetting cycle above approximately 60% saturation. One possible explanation for the scatter in the data is that capacitance measurement noise at the highest frequencies of measurement (up to 1 MHz) increases with temperature.



Source: DTN: LL981109904242.072 [DIRS 118959].

Figure 6.3-31. Relative Permittivity of the DST Samples as a Function of Saturation in the Drying Cycle at 50°C

### 6.3.2.5.2 Measurement Uncertainty: Laboratory Hydrological Parameters

#### *Saturation, Porosity, Density, and Gravimetric Water Content*

The main source of error for saturation measurement is in the estimate of the weight of water condensed in the walls of the core container. This is evaluated by absorbing the water from the container with a paper cloth and weighing the cloth. When large amounts of fragments and powder are observed on the surfaces of the container, this measurement overestimates the water loss because it includes the weight of fine solids. Although the reason for this physically meaningless value of saturation over 100% is understood, there is no clearly better measurement to arrive at a more accurate value. Observations of factors that may potentially affect the results are included in footnotes to Table 6.3-12. This “soft” information forms the basis for distinguishing cores that yield reliable weight measurements from cores that give potentially abnormal and inaccurate measurement. Discussions in Section 6.3.2.5.1 also indicate that the liquid saturation of the wet-drilled cores can differ from that of the dry-drilled cores by 11%. The difference may be attributed in part to different drilling methods and in part to spatial heterogeneity.

### Moisture Retention Curves

Section 6.2.2.5.2 contains a discussion of the measurement accuracy and data uncertainty in moisture-retention measurements.

### Electrical Properties

The accuracy of the instruments for the electrical property measurement was within 5% at the highest impedance limits (greater than 100 M $\Omega$ ). Each instrument was checked using a set of 1% tolerance resistors and capacitors. The instruments were found to yield consistent results. Sample variations, as can be seen in the data, are greater than the instrument error. There were some uncertainties in the water saturation level during the measurement, especially at elevated temperatures and high saturation levels. Anisotropy in the electrical properties was not assessed for the DST samples. During the measurements, the path of the electric current was perpendicular to the bedding plane of the rock, which was not well established. Obvious heterogeneity in the test samples was avoided. The heterogeneity may cause great variation in electrical properties.

#### **6.3.2.6 Heat and Mass Flow through the Bulkhead**

The following discussion involves investigations of heat and mass flow through the DST bulkhead. The subject matter was discussed in a white paper entitled "Heat and Mass Flow Through the Bulkhead in the Drift Scale Test" (Pannell 2001 [DIRS 159514]). The white paper satisfied an agreement (TEF 2.1) reached between DOE and the U.S. Nuclear Regulatory Commission (NRC) at the January 2001 Technical Exchange on Thermal Effects on Flow. The white paper covers both measurements and modeling. A brief summary will be presented here pertaining only to the measurements. These measurements were conducted for informative and complementary purposes and are not intended to be a requisite for the understanding of heat and mass loss through the bulkhead. The bulkhead separating the hot side of the heated drift from the unheated section is not completely sealed because bundles of power cable and instrument wiring pass through the bulkhead (CRWMS M&O 1998 [DIRS 111115], pp. 8-2 and 8-5), and the bulkhead is set against uneven and fractured rock.

The issue of heat and mass loss through the DST bulkhead has been ongoing since the design of the DST, a design in which the primary purpose of the bulkhead was to act as a thermal barrier (CRWMS M&O 1996 [DIRS 101375], pp. 3-17 and 3-18) as well as a personnel safety barrier. Preheating numerical simulations of the DST resulted in concerns about unmonitored heat and mass loss through the thermal bulkhead (Buscheck and Nitao 1995 [DIRS 100657]). Recommendations included isolating the DST heated drift from direct pneumatic interference with the ESF tunnel system. This precaution was in itself problematic, since personnel safety concerns would develop if the pressure within the DST heated drift were allowed to increase.

On December 3, 1997, the heating of the DST was initiated. Within 40 days of the start of heating, moisture started to flow out of the bulkhead, as evidenced by condensation on various surfaces on the cool side of the bulkhead. This behavior was consistent with the heating of a large volume of rock that is highly fractured and approximately 90% saturated. As water in the rock boiled and turned to steam, the vapor moved under pressure gradient into cooler rocks, as

well as into the heated drift and through the bulkhead. Also, the observed wetting on the cool side of the bulkhead alternated with drier conditions, with the latter coinciding with low relative humidity readings in the heated drift. Upon investigation, it appeared that barometric pumping was the cause for the intermittent wetting. Gas phase flow from the rock to the heated drift is driven by pressure gradient. Superimposed on the positive pressure gradient from the rock to the heated drift are the barometric pressure fluctuations. Therefore, as barometric pressure decreased, more vapor flowed from the rock into the heated drift and out the permeable bulkhead, increasing the relative humidity in the heated drift. Conversely, as the barometric pressure increased, less vapor flowed from the rock into the heated drift and the relative humidity decreased. Indeed, the relative humidity measurements in the heated drift vary inversely with the barometric pressure.

Between July 1998 and May 1999, several measurements of conductive and convective heat loss through the bulkhead were performed (CRWMS M&O 1998 [DIRS 159512], p. 3-1; 1999 [DIRS 154585]; 1999 [DIRS 159513]). A summary listing of field efforts to address the issue of mass and heat loss through the bulkhead is provided below:

- (1) Determination of conductive heat flux by applying a heat-flux meter to seven locations on the bulkhead (five measurement locations were steel and two were glass)
- (2) Estimation of convective heat loss by considering how much water vapor was removed from a small diameter pipe in the bulkhead during a 60-minute sampling period
- (3) Attempt to utilize the relative humidity data in the cool side of the bulkhead from the Moisture Monitoring Program to estimate the moisture loss from the DST. However, the operational ventilation flow rates (between 50 and 150 million liters per hour) imposed just outside of the heated drift were too large to allow a direct measurement of changes in the monitored humidity data.

As mentioned above, these measurements were conducted for informative and complementary purposes. For example, these measurements provided much insight into the difficulty of obtaining useful measurements of conductive and convective losses. Problems with obtaining an accurate measurement of conductive losses as attempted in item (1) involved the irregular and multiple-material surface of the bulkhead. Complications with measuring convective heat losses in items (2) and (3) mainly stemmed from the intrinsic difficulty of measuring a highly heterogeneous moisture and heat flux from a diffuse source. Also, considerable uncertainty was involved in item (2) because it was not possible to reasonably estimate the fraction of moisture loss captured in the measurement system as a result of the inherent leakage through bundles of power cables and instrument-wiring pathways.

After the “white paper” was prepared (which references measurements (1) and (2) above), the thermal test team initiated a final field experiment to determine whether a heat and mass measurement was feasible. The basic approach involves measuring the temperature and the relative humidity, on the cool side of the heated drift, as a function of time and discrete spatial locations. Then the integral moisture increase in the drift volume on the cool side of the bulkhead was used to estimate the mass loss from DST convective heat flow. This measurement



is nontrivial because of the substantial ventilation on the cool side of the bulkhead and the limitations of relative humidity measuring devices. In the July 2001 scoping study, the measured temperature and relative humidity in 38 installed Rotronic HygroClip relative humidity temperature sensors were used to estimate the changes in vapor mass and energy. The preliminary estimates of heat loss (for “nonrepresentative” conditions because the airflow from the ventilation system was necessarily reduced) yielded a total heat loss of approximately 0.5 to 2.6 kW. This is at least one order of magnitude less than what was expected from the numerical modeling of the DST. This final experiment demonstrated that the vapor loss through the bulkhead of the heated drift was too complex to measure directly.

### **6.3.3 DST Mechanical Measurements**

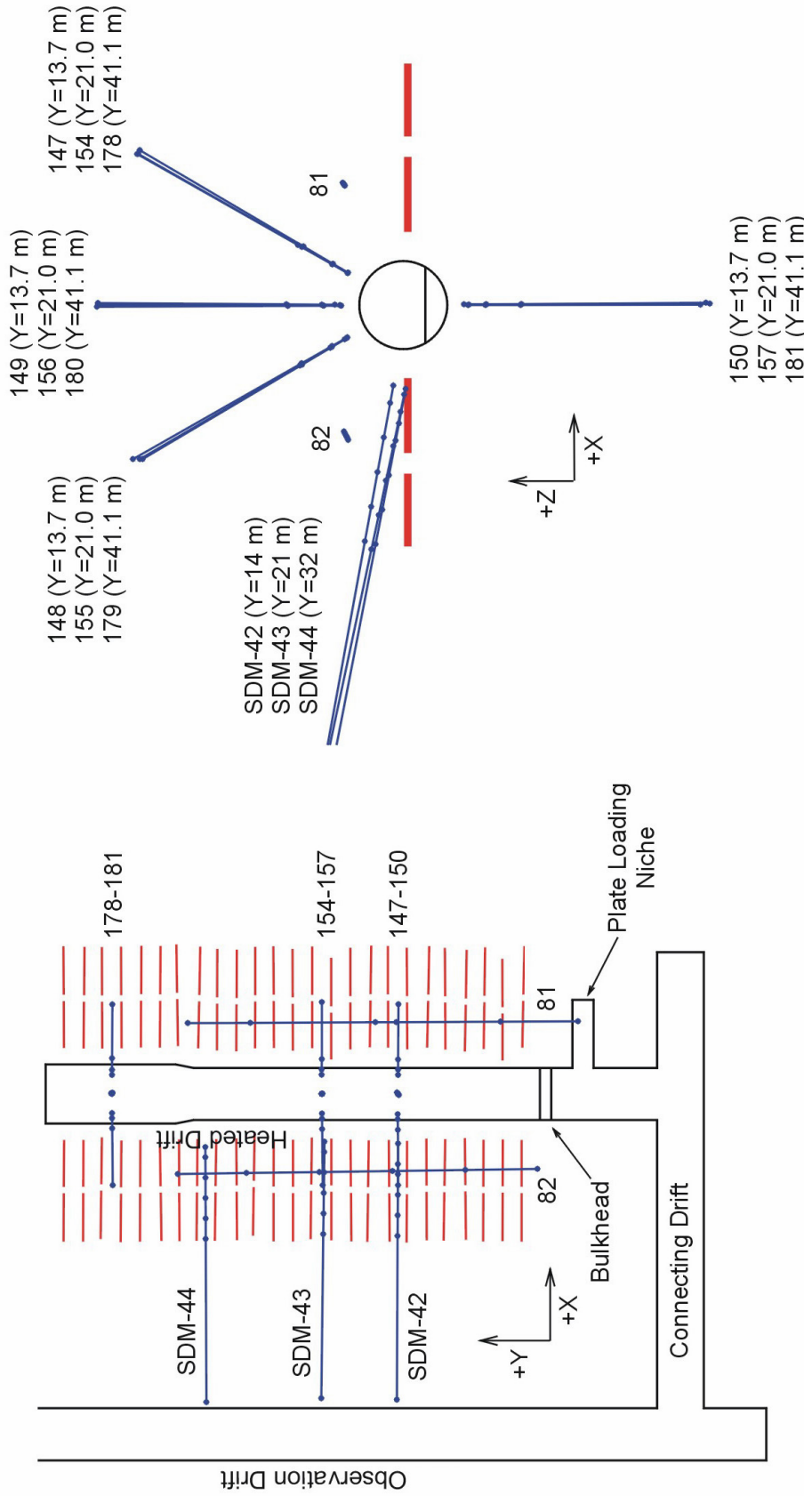
The discussion of mechanical measurements for the DST has been divided into several subsections based on the type of measurement:

- Multipoint borehole extensometer displacement data
- Cross-drift extensometers displacement data
- Strains measured on the inner surface of the cast-in-place liner
- Acoustic emission
- Laboratory parameters such as elastic modulus, Poisson’s ratio, and thermal expansion for intact rock and concrete
- Plate loading test
- Additional measurements, including rock scaling and acoustic emissions.

Detailed discussion of the mechanical measurements is documented in Section 6.3 in *Drift Scale Test Design and Forecast Results* (CRWMS M&O 1997 [DIRS 146917]), in Section 5.1.2 of *Drift Scale Test As-Built Report* (CRWMS M&O 1998 [DIRS 111115]), and in Sections 4 and 8 of *Ambient Characterization of the Drift Scale Test Block* (CRWMS M&O 1997 [DIRS 101539]). DST mechanical measurement input and summary DTNs are listed in Tables 4-3 and 6.3-1, respectively.

#### **6.3.3.1 Multipoint Borehole Extensometers**

Figure 6.3-32 shows the layout of the MPBX boreholes. The as-built location coordinates of the collars and anchors are provided in Table 6.3-2. Displacements reported in this document followed the convention of extension being positive. Displacements were measured within the rock-mass surrounding the heated drift and between the heated drift and the observation drift. These measurements were used to evaluate numerical models related to thermal-hydrological-mechanical coupling as well as to provide data for determination of rock-mass thermal expansion. MPBXs were installed in 17 boreholes both within and outside the heated drift to monitor rock-mass movement during the DST.



Source: DTN: MO0002ABBLSLDS.000 [DIRS 147304].

NOTE: Schematics are prepared from translated coordinates based on an origin located at the center of the heated drift bulkhead. Wing heaters are plotted in red; MPBX boreholes and anchors are plotted in blue.

Figure 6.3-32. MPBX Layout for the Drift Scale Test

Two of the MPBXs (designated ESF-HD-81-MPBX1 and ESF-HD-82-MPBX2, with 81 and 82 referring to the borehole numbers) were installed in two long horizontal boreholes drilled parallel to the heated drift from the connecting drift. Twelve MPBXs (MPBX3 through MPBX14) were installed in three four-borehole arrays (numbers 147 to 150, 154 to 157, and 178 to 181) drilled into the surrounding rock mass from within the heated drift itself. The array containing MPBXs 3, 4, 5, and 6 (boreholes 147 to 150) is located in the heated drift at Y = 13.7 m; the array with MPBXs 7, 8, 9, and 10 (boreholes 154 to 157) is located at Y = 21.0 m; and the array with MPBXs 11, 12, 13, and 14 (boreholes 178 to 181) is located at Y = 41.1 m, in the concrete liner test section of the heated drift. For the three MPBXs in each array collared in the crown of the drift, the four anchors for each were located nominally at 1, 2, 4, and 15 m from the collar. For the fourth MPBX in each array, which was collared at the top of the invert, the anchors were installed so as to put them in the same relative position in the surrounding rock mass as the other MPBXs (i.e., approximately 2.2, 3.2, 5.2, and 16.2 m from the collar).

The remaining three borehole MPBXs were drilled for sequential drift mine-by monitoring. These MPBXs were installed in November and December of 1996 in boreholes 42, 43, and 44, drilled slightly downward from the observation drift toward the heated drift. Boreholes 42, 43, and 44 are located at heated drift stations 0+13.7, 0+20.8, and 0+32.2 m, respectively (each station refers to the Y-axis distance from the heated drift bulkhead).

The displacement data can be found in the following input DTNs:

- SNF39012298002.002 [DIRS 159114]
- SN0203F3912298.033 [DIRS 158361]
- SNF39012298002.010 [DIRS 158367]
- SN0001F3912298.014 [DIRS 153841]
- SN0007F3912298.018 [DIRS 158374]
- SN0101F3912298.024 [DIRS 158400]
- SN0107F3912298.029 [DIRS 158408]
- SNF39012298002.006 [DIRS 158419]
- SN0209F3912298.040 [DIRS 178009]
- SN0303F3912298.044 [DIRS 178010]
- SN0308F3912298.050 [DIRS 178011]
- SN0403F3912298.055 [DIRS 178012]
- SN0410F3912298.061 [DIRS 178013]
- SN0601F3912298.065 [DIRS 178014]
- SN0608F3912298.069 [DIRS 178015].

The displacement data corrected for thermal expansion can be found in the following input DTNs:

- SNF39012298002.012 [DIRS 153840]
- SNF39012298002.008 [DIRS 153839]
- SN0203F3912298.035 [DIRS 158363]
- SN0001F3912298.016 [DIRS 153842]
- SN0007F3912298.020 [DIRS 158388]

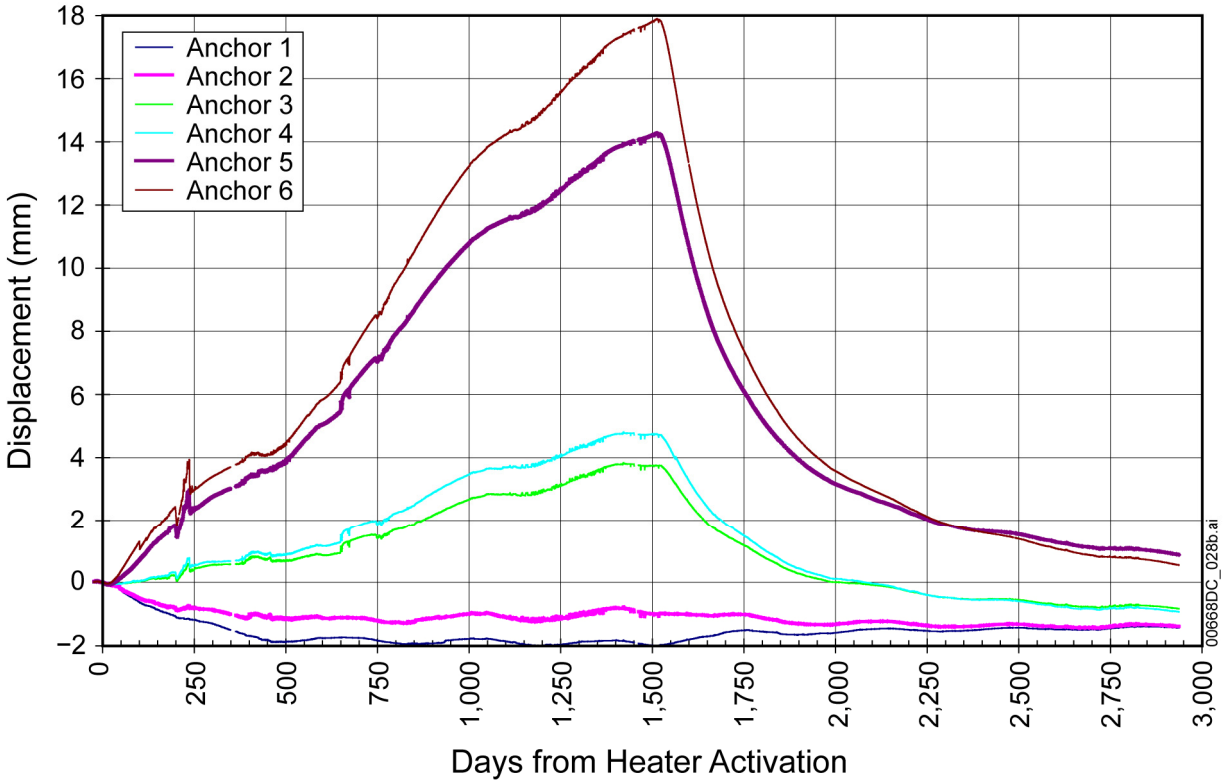
- SN0101F3912298.026 [DIRS 158402]
- SN0107F3912298.031 [DIRS 158413]
- SNF39012298002.004 [DIRS 153837]
- SN0209F3912298.042 [DIRS 177941]
- SN0303F3912298.046 [DIRS 177945]
- SN0308F3912298.052 [DIRS 177946]
- SN0403F3912298.057 [DIRS 177948]
- SN0410F3912298.063 [DIRS 177973]
- SN0601F3912298.067 [DIRS 178005]
- SN0608F3912298.071 [DIRS 177975].

The thermal expansion of carbon fiber and Invar rods can be found in input DTN: SNL22100196001.003 [DIRS 111068].

#### **6.3.3.1.1 Results: MPBX Displacements**

Because of the abundance of DST MPBX displacements, only representative discussion and graphics are provided. All MPBX displacement data and graphics can be accessed in the summary DTN identified in Table 6.3-1. The following discussion provides a cross section of MPBX measurements of displacements within the DST block.

MPBX1 is located in borehole 81, which runs parallel to and is collared outside the heated drift. This borehole is on the north side of the drift (the anchor is located in the Data Acquisition System niche). A time history plot of temperature-corrected displacement is shown in Figure 6.3-33. The overall performance of MPBX1 is good, meaning the data appear relatively stable with few oscillations when graphed. The data for the heating phase of the DST show thermal-mechanical responses consistent with elastic model predictions. Upon cooling, the measurements indicate that the rock mass contracts to nearly its original state. The rock temperatures are not yet back to ambient; however, the displacements at the end of the recording period are nearly the same as they were at ~125 days of heating, when the temperatures are at similar values to the final measurements. This behavior would indicate that the rock mass section unaffected by damage created by drift construction behaves nearly elastically.

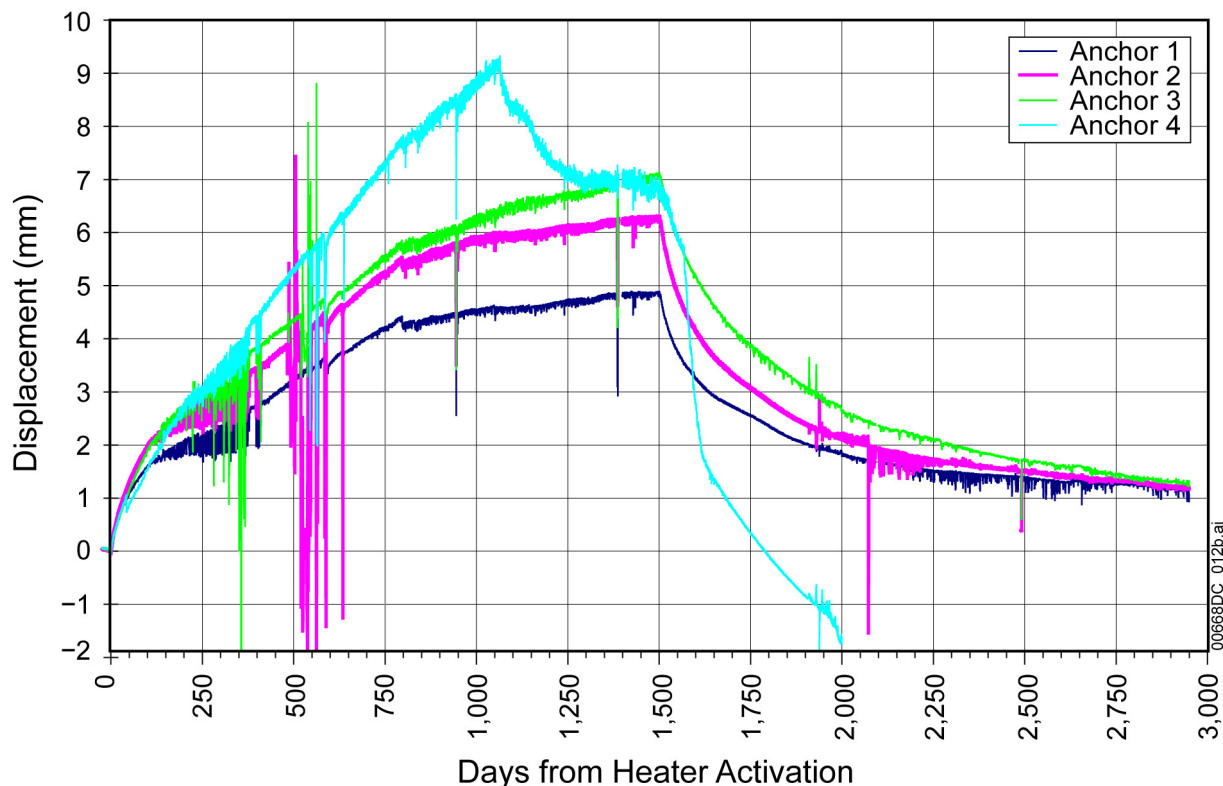


Source: DTNs: SN0407F3912298.060 [DIRS 170627]; SN0209F3912298.042 [DIRS 177941]; SN0303F3912298.046 [DIRS 177945]; SN0308F3912298.052 [DIRS 177946]; SN0403F3912298.057 [DIRS 177948]; SN0410F3912298.063 [DIRS 177973]; SN0601F3912298.067 [DIRS 178005]; SN0608F3912298.071 [DIRS 177975].

Figure 6.3-33. Corrected Displacements Measured for ESF-HD-81-MPBX1

MPBX3 is located at Y = 13.7 m in borehole 147 anchored in the crown of the heated drift, and angled 30° from the vertical towards the north (away from the observation drift). A time history plot of temperature-corrected displacement is shown in Figure 6.3-34. The overall quality of the data from MPBX3 is good, with the exception of the data trace produced by Anchor 4 starting after about three years of heating. The results of MPBX3 are probably the most “typical” of the results, in that the behaviors in general agree with pretest elastic model analyses. Two observations of the MPBX3 data will be used as the basis for discussions of other MPBX results. First, the maximum displacement for anchor 3, which was approximately 4 m from the MPBX collar, at the end of the heating period was approximately 7 mm. This seems to be a typical value for anchor 3 for the MPBXs collared in the crown of the heated drift; anchor 3 for MPBXs 3, 4, 5, 8, and 11 all had maximum displacement values of 6.5 to 7.5 mm. Second, the displacements tend to gradually decrease toward zero during the cooling phase. An actual value of zero displacement at ambient temperatures would be indicative of an elastic expansion/contraction cycle. At the end of the data reporting period (12/31/2005), the temperatures in the rock surrounding the Heated Drift were in the range of 55°C to 60°C throughout the entire region including the MPBX anchors. Using a rock mass thermal expansion coefficient of 2.5  $\mu\epsilon/^\circ\text{C}$  (see Section 6.3.3.6.3), and an initial rock temperature of 21°C, some approximate values for displacement for anchors 1 through 4 at this time based on pure thermal

expansion would be 0.1, 0.2, 0.4, and 1.4 mm respectively. Note for MPBX3 how the values for anchors 1, 2, and 3 range from 1.1 to 1.3 mm at the final time. The nearly equal values indicate elastic behavior between the anchors, and the 1-mm difference from overall elastic contraction may indicate effects due to fractures near the crown created in the drift construction process. The behaviors for working gages for MPBX4 and MPBX5 were similar to MPBX3.

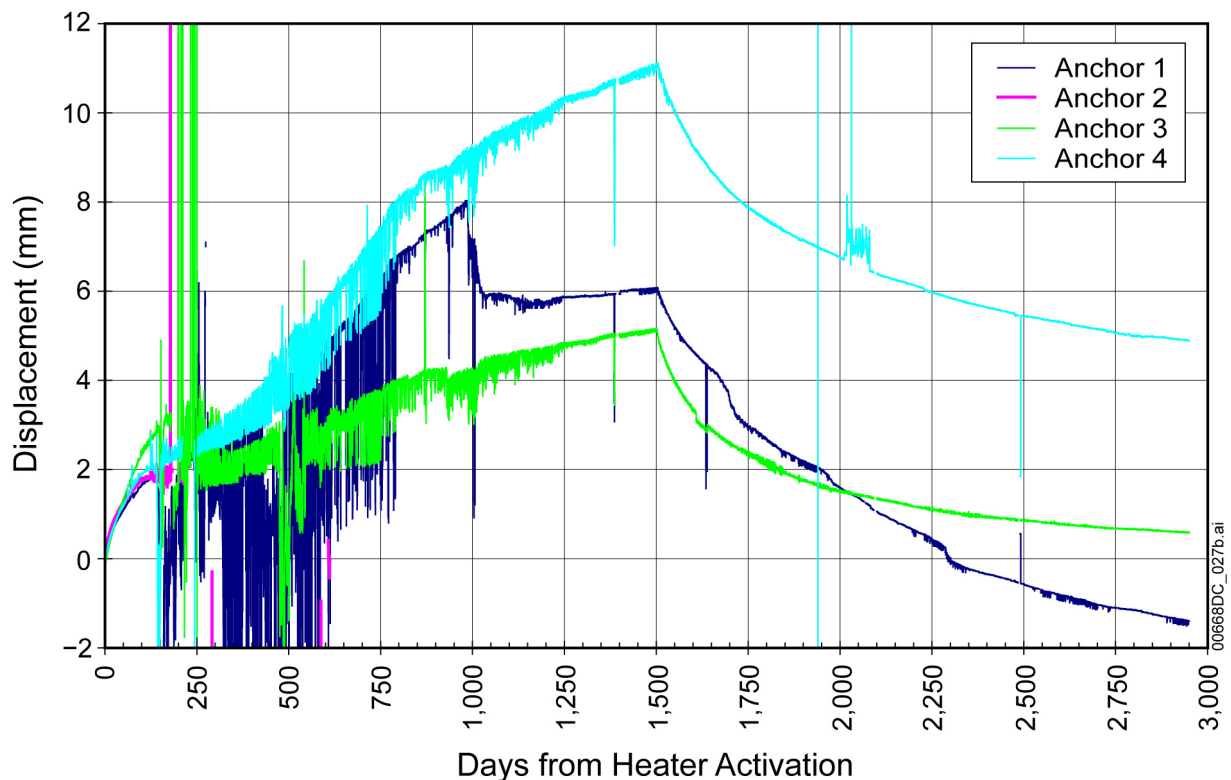


Source: DTNs: SN0407F3912298.060 [DIRS 170627]; SN0209F3912298.042 [DIRS 177941]; SN0303F3912298.046 [DIRS 177945]; SN0308F3912298.052 [DIRS 177946]; SN0403F3912298.057 [DIRS 177948]; SN0410F3912298.063 [DIRS 177973]; SN0601F3912298.067 [DIRS 178005]; SN0608F3912298.071 [DIRS 177975].

Figure 6.3-34. Corrected Displacements Measured for ESF-HD-147-MPBX3

MPBX7 is located at Y = 21.0 m in borehole 154 anchored in the crown of the heated drift, and angled 30° from the vertical towards the north (away from the observation drift). A time history plot of temperature-corrected displacement is shown in Figure 6.3-35. Thermocouple data (DTNs: MO9807DSTSET01.000 [DIRS 113644]; MO9810DSTSET02.000 [DIRS 113662]; MO9906DSTSET03.000 [DIRS 113673]; MO0001SEPDSTPC.000 [DIRS 153836]), recorded at or near boiling, indicate the formation of heat pipes along an interval of borehole, as evidenced by temperature oscillations through day 750. These oscillations influence the displacement measurements because of thermal expansion. The overall quality of the data from MPBX7 is good, although the data are noisy during the first two years of heating because of the temperature oscillations. The level and frequency of noise make this data usable only for evaluating general thermal-mechanical behavior, and not determination of specific events. Three observations can be made about the displacement data during the heating phase: (1) the displacement at anchor 3 is much less than might be expected from elastic analyses; (2) the displacements shown for

anchors 1 (1 m from the collar) and 4 (15 m from the collar) are much closer to each other than would have been expected; and (3) a 2-mm drop in displacement occurred for anchor 1 at around three years of heating. When looking at the displacement for anchor 1 at the end of the cooling phase, that 2-mm displacement appears again, as the final ambient displacement is approaching -2 mm. Also note that anchor 3 is at ~0.6-mm displacement, indicating that the 4 m of rock between it and the collar may be behaving elastically. It is possible that an event happened at anchor 1 which did not effect the linkage between anchor 3 and the collar. The displacement at anchor 4 at the end of the cooling phase is ~5 mm, significantly higher than what would be expected by elastic behavior, indicating that fracturing between 4 and 15 m from the crown may be more significant than for MPBX3, 4, and 5.

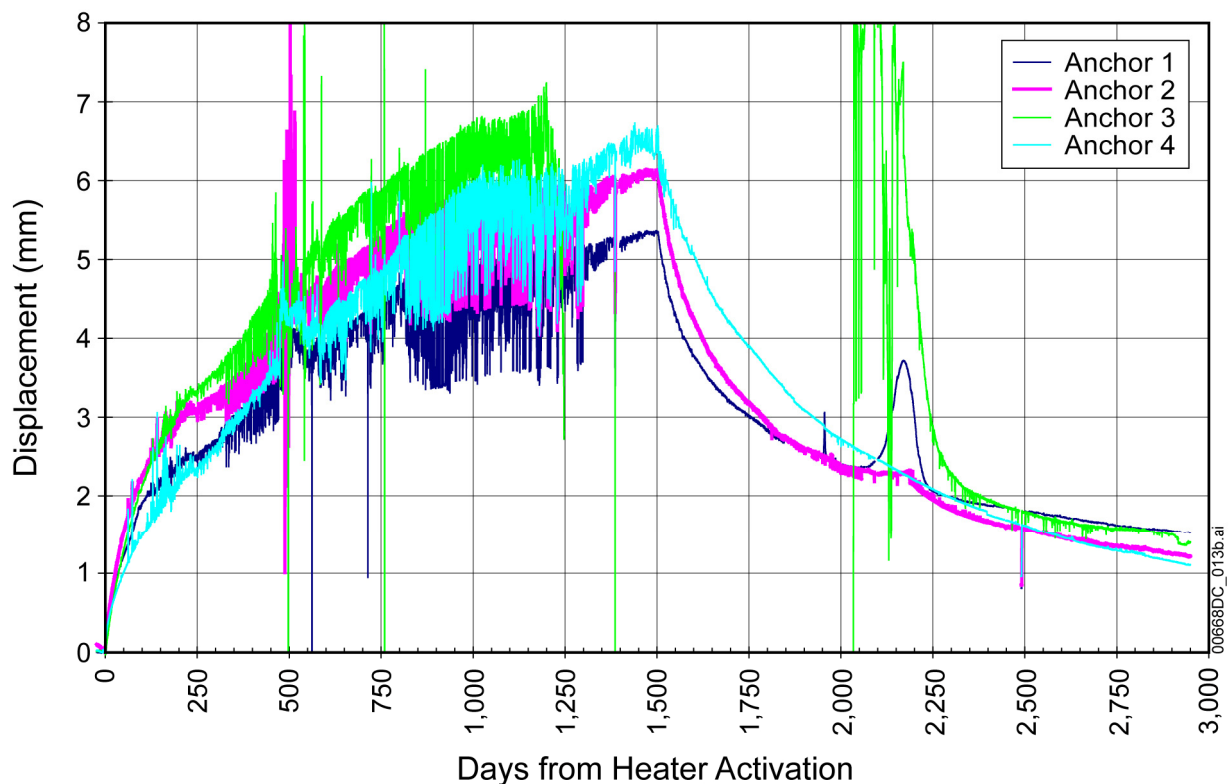


Source: DTNs: SN0407F3912298.060 [DIRS 170627]; SN0209F3912298.042 [DIRS 177941]; SN0303F3912298.046 [DIRS 177945]; SN0308F3912298.052 [DIRS 177946]; SN0403F3912298.057 [DIRS 177948]; SN0410F3912298.063 [DIRS 177973]; SN0601F3912298.067 [DIRS 178005]; SN0608F3912298.071 [DIRS 177975].

Figure 6.3-35. Corrected Displacements Measured for ESF-HD-154-MPBX7

MPBX8 is located at Y = 21.0 m in borehole 155, anchored in the crown of the heated drift, and angled 30° from the vertical towards the south (towards the observation drift). A time-history plot of temperature-corrected displacement is shown in Figure 6.3-36. The overall quality of the displacement data from MPBX8 is good. There are two sources of moisture-induced noise: (1) temperature fluctuations in borehole 155 (days 300 to 500), for which the displacement data reflect real thermal-mechanical response; and (2) at later times (after day 800), fluctuations of MPBX9-TC-1, which introduce artificial noise into the conversion and thermal correction of MPBX8 data. Some evidence of moisture-related temperature oscillation is seen at other

thermocouples for MPBX8. A large temperature perturbation event for all the thermocouples at days 475 to 545 (3/23/1999 to 6/1/1999) is similar in nature and timing to temperature events for MPBX9, as well as farthest sections of MPBX12 and 13, located 20 m further down the drift. This event may indicate connectivity between these four boreholes. The linear variable displacement transducer (LVDT) for anchor 3 apparently failed on day 1,247 (5/2/2001), but recovered later on during the cooling phase and eventually began to produce reasonable-looking data. An unexplained rise and fall in displacement occurred for anchor 1 during the cooling phase between days 2100 and 2250. The behavior represented by the data must be assumed to be real, as there is no noise of temperature anomaly associated with the data. Also, note at the end of cooling that the four anchors are in the 1.1 to 1.5 mm range again, perhaps indicating near-elastic behavior in the rock mass away from the damage zone in the crown.



Source: DTNs: SN0407F3912298.060 [DIRS 170627]; SN0209F3912298.042 [DIRS 177941]; SN0303F3912298.046 [DIRS 177945]; SN0308F3912298.052 [DIRS 177946]; SN0403F3912298.057 [DIRS 177948]; SN0410F3912298.063 [DIRS 177973]; SN0601F3912298.067 [DIRS 178005]; SN0608F3912298.071 [DIRS 177975].

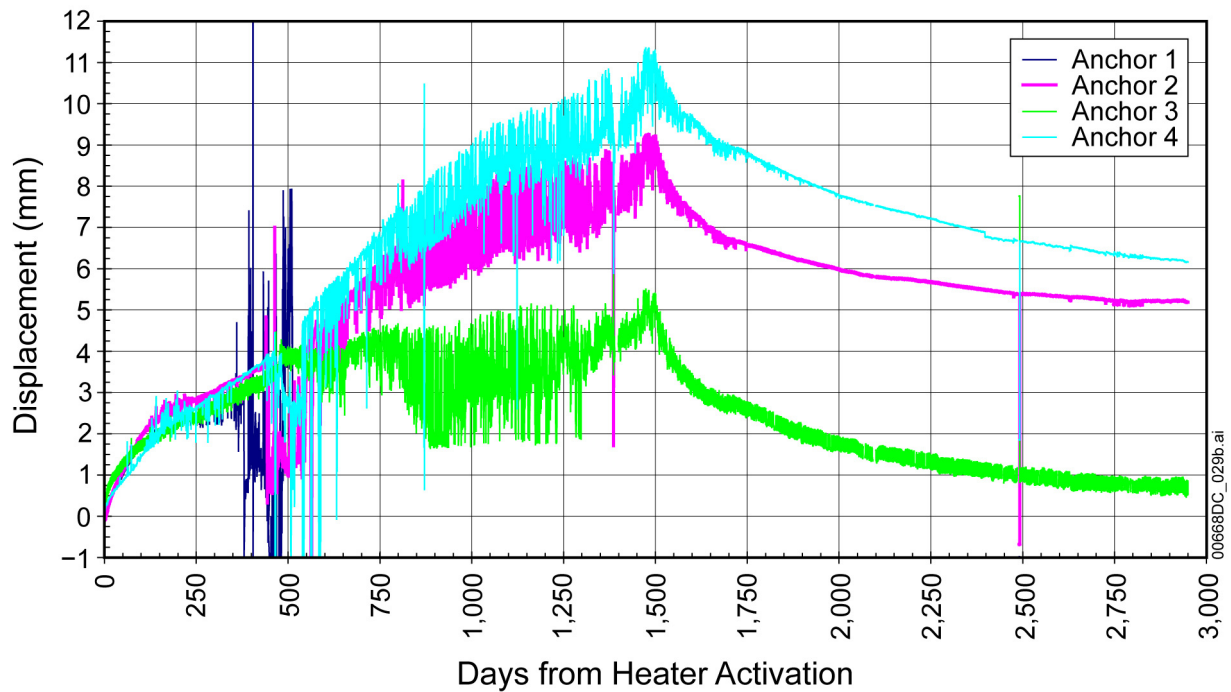
Figure 6.3-36. Corrected Displacements Measured for ESF-HD-155-MPBX8

MPBX9 is located at Y=21.0 m in borehole 156 anchored in the crown of the heated drift, and angled vertically upward. A time-history plot of temperature-corrected displacement is shown in Figure 6.3-37. The displacement data from anchors 2, 3, and 4 of MPBX9 are good. The displacement data from anchor 3 level off unexpectedly (that is, when compared with an elastic model) at around 500 days. The most noticeable feature is the onset of large-scale moisture-induced temperature perturbations, which eventually affect all the thermocouples except those already near boiling. These perturbations cease shortly after the end of the heating



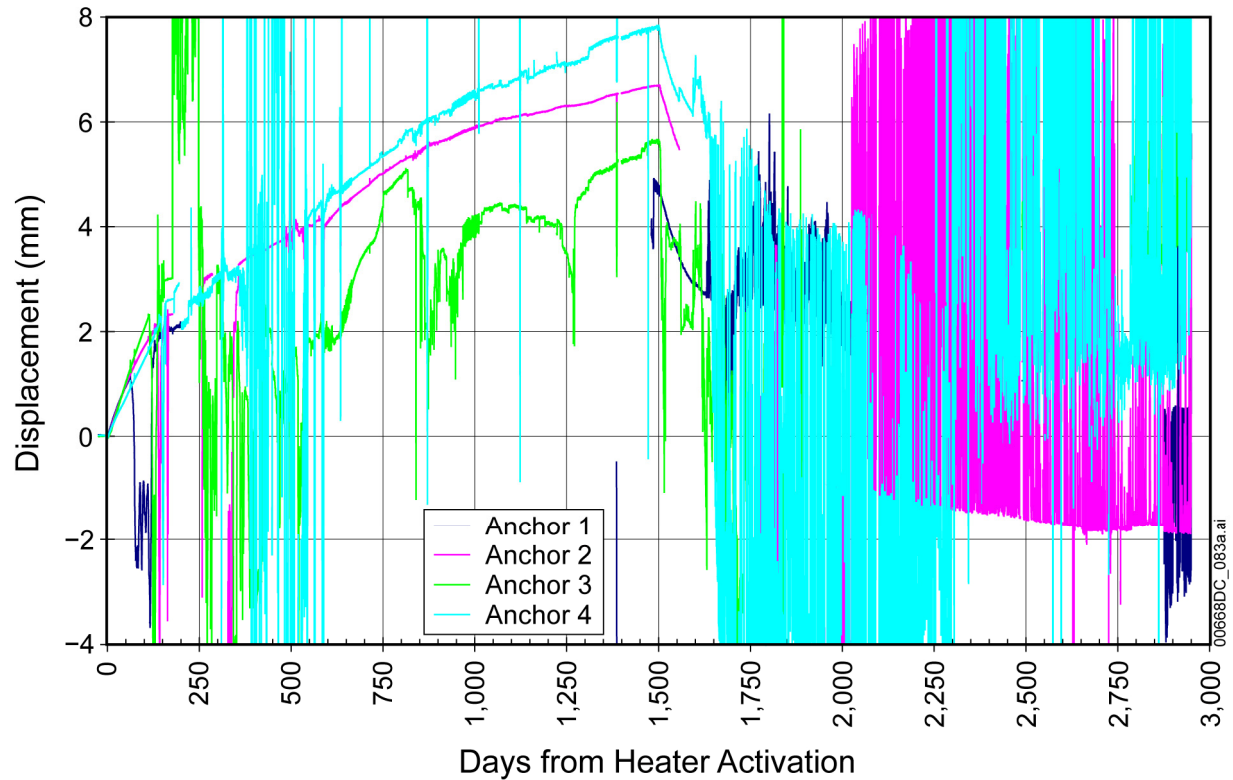
phase. Note how anchor 3 returns to near-ambient displacement, whereas anchors 2 and 4 are 5 to 6 mm away from that level.

MPBX10 is located at Y=21.0 m, anchored in the top of the invert of the heated drift, and angled vertically downward. A time history plot of temperature-corrected displacement is shown in Figure 6.3-38. The displacement data for MPBX10 are anomalous for all the anchors: anchor 1 failed early in the test; anchor 2 is erratic for the first year, then looks sound for the remainder of the test; anchor 3 is erratic throughout the entire test; and anchor 4 has regions of good data interspersed with large-scale noise that is not moisture-induced (because the thermocouples are clean throughout the test). This erratic behavior increases in the cooling phase until the data are no longer usable. Because of the erratic nature of the MPBX10 data, it is hard to identify any events that may be related to non-elastic or microseismic phenomena.



Source: DTNs: SN0407F3912298.060 [DIRS 170627]; SN0209F3912298.042 [DIRS 177941]; SN0303F3912298.046 [DIRS 177945]; SN0308F3912298.052 [DIRS 177946]; SN0403F3912298.057 [DIRS 177948]; SN0410F3912298.063 [DIRS 177973]; SN0601F3912298.067 [DIRS 178005]; SN0608F3912298.071 [DIRS 177975].

Figure 6.3-37. Corrected Displacements Measured for ESF-HD-156-MPBX9



Source: DTNs: SN0407F3912298.060 [DIRS 170627]; SN0209F3912298.042 [DIRS 177941]; SN0303F3912298.046 [DIRS 177945]; SN0308F3912298.052 [DIRS 177946]; SN0403F3912298.057 [DIRS 177948]; SN0410F3912298.063 [DIRS 177973]; SN0601F3912298.067 [DIRS 178005]; SN0608F3912298.071 [DIRS 177975].

Figure 6.3-38. Corrected Displacements Measured for ESF-HD-157-MPBX10

### 6.3.3.1.2 Measurement Uncertainty: MPBX Displacements

The uncertainty of the DST MPBX measurements is similar to comparable SHT MPBX measurements, as discussed in Section 6.2.3.1.2. As shown in Table 6.3-13, the gage range and accuracy of the LVDTs for the MPBXs are  $\pm 25.4$  mm and 0.5% of the measured value, respectively. Other, less quantifiable sources of uncertainty also exist in the data. Many of these uncertainties manifest themselves in unusual behaviors in the data. Oscillating noise was observed in the data histories for several of the MPBX gages. One source of this noise, due to temperature fluctuations caused by circulating water vapor and condensation, was identified for many of these gages. The cause of the other instances of oscillating noise is unknown, but could be related to electrical problems or to defective gages. Several gages displayed a sudden shift in displacement over a period of one day to two weeks. The instantaneous changes may be related to sudden slippage along fractures, creation of new fractures, or seismic events. The changes occurring over longer times may be related to stress redistribution due to the opening or closing of fractures, or the shift or rotation of large rock masses in a fractured field. There are some instances where the relative magnitudes of displacements between anchors on the same MPBX (e.g., MPBX9) do not correlate to expected patterns of behavior. Finally, there are unusual long-term oscillations in the data (e.g., the rise and fall in displacement for MPBX8-1 between days 2100 and 2250) that apparently represent a real event but are not correlated with

the observed responses. Table 6.3-14 lists all the MPBX gages, grades the quality of data for each gage (either “Excellent”, “Good”, “Fair”, or “Poor”), and offers additional descriptions of events for each gage.

Table 6.3-13. Summary of SNL-Installed Measurement System Specifications for the DST

Measurement System	Manufacturer	Gage Range, Accuracy	Comments
Type-K Thermocouples	Watlow ARI, Inc. (probes)	Range: max 1280°C Accuracy: $\pm 2.2^\circ\text{C}$	Chromel-Alumel
Vibrating Wire Displacement Transducers	GEOKON	1 in. ( $\pm 25.4$ mm) full range Accuracy: 0.02% of full range	—
CIP Strain Gages	BLH Electronics	Karma Foil 4-in gages with gage factor of 2 Temperature range limited by bonding epoxy and extension wire	—
High Temperature LVDTs (Heated Drift)	RDP Electrosense, Inc.	$\pm 1$ in. ( $\pm 25.4$ mm) full range Accuracy of 0.5% linearity full range (linear within range; i.e., 0.5% of measured value) Calibrated from ambient to 350°C	AC-LVDTs

Source: CRWMS M&O 1998 [DIRS 108306], Table 6-1.

Table 6.3-14. Data Quality Grades for Each MPBX Displacement Gage

MPBX Gages	Grade	Comment
CDEX-1 (vertical closure gage)	Poor	Appeared to fail between day 550 and 650, with continuing high level of displacement (18 to 20 mm); observation that time-averaged oscillation matches annual climatic cycle.
CDEX-2 (horizontal closure gage)	Excellent	—
SDM-42-MPBX1-ANC-1	Excellent	—
SDM-42-MPBX1-ANC-2	Good	Excellent until apparent gage failure at day 2143 (10/17/2003)
SDM-42-MPBX1-ANC-3	Good	Excellent until apparent gage failure at day 1393 (9/27/2001)
SDM-42-MPBX1-ANC-4	Good	Excellent until apparent gage failure at day 2015 (6/11/2003)
SDM-42-MPBX1-ANC-5	Good	Excellent until about day 1732, apparent gage failure at day 2039 (7/5/2003)
SDM-42-MPBX1-ANC-6	Good	Excellent until apparent gage failure at day 1502 (1/14/2002)
SDM-43-MPBX2-ANC-1	Good	Excellent until apparent gage failure at day 2159 (11/1/2003)
SDM-43-MPBX2-ANC-2	Excellent	—
SDM-43-MPBX2-ANC-3	Excellent	—
SDM-43-MPBX2-ANC-4	Excellent	—
SDM-43-MPBX2-ANC-5	Good	Excellent until apparent gage failure at day 1825 (12/3/2002)
SDM-43-MPBX2-ANC-6	Excellent	—
SDM-44-MPBX3-ANC-1	Excellent	Some noise during the heating phase that appeared to be related to oscillating temperatures induced by moisture recirculation
SDM-44-MPBX3-ANC-2	Excellent	Some noise during the heating phase that appeared to be related to oscillating temperatures induced by moisture recirculation. Also, data show several instantaneous changes which may indicate fracture slippage.

Table 6.3-14. Data Quality Grades for Each MPBX Displacement Gage (Continued)

MPBX Gages	Grade	Comment
SDM-44-MPBX3-ANC-3	Good	See comment for anchor 2. Apparent gage failure at day 2045 (7/10/2003).
SDM-44-MPBX3-ANC-4	Good	See comment for anchor 2. Apparent gage failure at day 1645 (6/6/2002).
SDM-44-MPBX3-ANC-5	Excellent	Some noise during the heating phase that appeared to be related to oscillating temperatures induced by moisture recirculation
SDM-44-MPBX3-ANC-6	Excellent	Significant ~4 mm slip at about day 717
HD-81-MPBX1-ANC-1	Excellent	—
HD-81-MPBX1-ANC-2	Excellent	—
HD-81-MPBX1-ANC-3	Excellent	—
HD-81-MPBX1-ANC-4	Excellent	—
HD-81-MPBX1-ANC-5	Excellent	—
HD-81-MPBX1-ANC-6	Excellent	—
HD-82-MPBX2-ANC-1	Excellent	—
HD-82-MPBX2-ANC-2	Excellent	—
HD-82-MPBX2-ANC-3	Excellent	—
HD-82-MPBX2-ANC-4	Excellent	—
HD-82-MPBX2-ANC-5	Excellent	—
HD-82-MPBX2-ANC-6	Excellent	—
HD-147-MPBX3-ANC-1	Excellent	Some noise during the heating phase that appeared to be related to oscillating temperatures induced by moisture recirculation
HD-147-MPBX3-ANC-2	Excellent	Some noise during the heating phase that appeared to be related to oscillating temperatures induced by moisture recirculation
HD-147-MPBX3-ANC-3	Excellent	Some noise during the heating phase that appeared to be related to oscillating temperatures induced by moisture recirculation
HD-147-MPBX3-ANC-4	Good	Excellent through day 1065. Sudden change in data (apparently real) with precipitous decreasing displacements at that time and immediately after heater shutdown. Apparent gage failure at day 1999 (5/25/2003).
HD-148-MPBX4-ANC-1	Good	Excellent through day 1888, with some moisture-induced noise in the heating phase. Heavy noise in LVDT readings after day 1888, although general data trend still apparent.
HD-148-MPBX4-ANC-2	Good	Excellent through day 1888, with some moisture-induced noise in the heating phase. Heavy noise in LVDT readings after day 1888, although general data trend still apparent.
HD-148-MPBX4-ANC-3	Good	Excellent through day 1888, with some moisture-induced noise in the heating phase. Heavy noise in LVDT readings after day 1888, although general data trend still apparent.
HD-148-MPBX4-ANC-4	Poor	Good data until day 494 (4/11/1999), then unusable data afterward
HD-149-MPBX5-ANC-1	Fair	Bad data until day 225, then excellent-looking data trace but displaced ~6 mm from expected – data trend considered valuable, actual values unreliable.
HD-149-MPBX5-ANC-2	Fair	Bad data until day 225, then excellent-looking data trace but displaced ~6 mm from expected – data trend considered valuable, actual values unreliable.
HD-149-MPBX5-ANC-3	Excellent	Some moisture-induced noise in heating phase
HD-149-MPBX5-ANC-4	Excellent	Some moisture-induced noise in heating phase; slip of ~3 mm at day 2118

Table 6.3-14. Data Quality Grades for Each MPBX Displacement Gage (Continued)

MPBX Gages	Grade	Comment
HD-150-MPBX6-ANC-1	Poor	Inconsistent data during heating phase; noisy data from the LVDTs, unrelated to temperature fluctuations. Data appears bad from 1635 to the end of the test.
HD-150-MPBX6-ANC-2	Fair	Mostly excellent data during heating phase; noisy data from the LVDTs, unrelated to temperature fluctuations. Data appears bad from 1635 to the end of the test.
HD-150-MPBX6-ANC-3	Poor	Inconsistent data during heating phase; noisy data from the LVDTs, unrelated to temperature fluctuations. Apparent gage failure at day 2062 (7/28/2003).
HD-150-MPBX6-ANC-4	Fair	Mostly excellent data during heating phase; noisy data from the LVDTs, unrelated to temperature fluctuations. Apparent gage failure (also TC-8) at day 2062 (7/28/2003).
HD-154-MPBX7-ANC-1	Good	Significant moisture-induced noise in heating phase; 2-mm drop in displacement at ~day 1000
HD-154-MPBX7-ANC-2	Poor	Apparent gage failure at day 231 (7/22/1998)
HD-154-MPBX7-ANC-3	Good	Significant moisture-induced noise in heating phase; ~1.5-mm drop in displacement about day 260; excellent data during cooling phase
HD-154-MPBX7-ANC-4	Excellent	Some moisture-induced noise in heating phase
HD-155-MPBX8-ANC-1	Good	Significant moisture-induced noise in heating phase; unexplained rise and fall in displacement during the cooling phase between days 2100 and 2250
HD-155-MPBX8-ANC-2	Good	Significant moisture-induced noise in heating phase; excellent during cooling phase
HD-155-MPBX8-ANC-3	Fair	Significant moisture-induced noise in heating phase; apparent gage failure at day 1247. Gage appears to recover on day 2300 and data appears to be reasonable with some associated noise.
HD-155-MPBX8-ANC-4	Good	Significant moisture-induced noise in heating phase; excellent during cooling phase
HD-156-MPBX9-ANC-1	Poor	Apparent gage failure at day 513
HD-156-MPBX9-ANC-2	Good	Significant moisture-induced noise in heating phase; excellent during cooling phase
HD-156-MPBX9-ANC-3	Good	Significant moisture-induced noise in heating phase; excellent during cooling phase
HD-156-MPBX9-ANC-4	Good	Significant moisture-induced noise in heating phase; excellent during cooling phase
HD-157-MPBX10-ANC-1	Poor	Apparent gage failure at day 199; gage appears to have "recovered" on day 1480. Noisy data from the LVDT; does not appear to be related to temperature fluctuations; data considered bad.
HD-157-MPBX10-ANC-2	Fair	Mostly good data through heating phase; apparent gage failure at day 1556. Later, gage data continue with extreme noise, data considered bad.
HD-157-MPBX10-ANC-3	Poor	Basically worthless data the entire test
HD-157-MPBX10-ANC-4	Fair	Mostly good data through heating phase; noisy, worthless data after day 1655
HD-178-MPBX11-ANC-1	Poor	Basically worthless data the entire test
HD-178-MPBX11-ANC-2	Fair	Significant moisture-induced noise in heating phase; excellent data through much of cooling phase; noisy data starting at day 2526, no corresponding temperature oscillations.

Table 6.3-14. Data Quality Grades for Each MPBX Displacement Gage (Continued)

MPBX Gages	Grade	Comment
HD-178-MPBX11-ANC-3	Fair	Significant moisture-induced noise in heating phase; good data through early cooling phase; noisy data starting at day 1900, no corresponding temperature oscillations – data from this point on are unusable.
HD-178-MPBX11-ANC-4	Fair	Significant moisture-induced noise in heating phase; good data through early cooling phase; slip of ~2 mm on day 1934; apparent gage failure at day 2132 (10/6/2003).
HD-179-MPBX12-ANC-1	Fair	Significant moisture-induced noise through day 1630 (thermocouples showing same noise patterns), making data difficult to use; excellent data for the remainder of the test.
HD-179-MPBX12-ANC-2	Fair	Significant moisture-induced noise through day 1630, making data difficult to use; excellent data for the remainder of the test.
HD-179-MPBX12-ANC-3	Fair	Significant moisture-induced noise through day 1630, making data difficult to use; excellent data for the remainder of the test.
HD-179-MPBX12-ANC-4	Poor	Bad data nearly the entire test
HD-180-MPBX13-ANC-1	Poor	Excellent data through day 379, then gage apparently fails; data seem to follow annual climatic cycle.
HD-180-MPBX13-ANC-2	Good	Bad data between days 330-550; some moisture-induced noise in heating phase; excellent cooling phase data.
HD-180-MPBX13-ANC-3	Poor	Excellent data thorough day 446, then gage apparently fails; data seem to follow annual climatic cycle.
HD-180-MPBX13-ANC-4	Good	Bad data between days 330 and 550; some moisture-induced noise in heating phase; ~2-mm slip on day 1574; excellent cooling phase data.
HD-181-MPBX14-ANC-1	Excellent	Just a few locations of mild noise
HD-181-MPBX14-ANC-2	Good	Bad data between days 260 and 560, otherwise excellent data
HD-181-MPBX14-ANC-3	Good	Bad data between days 260 and 560, otherwise excellent data
HD-181-MPBX14-ANC-4	Good	Bad data between days 260 and 560, significantly more noise during cooling phase, but data still usable

Source: DTNs: SN0209F3912298.042 [DIRS 177941]; SN0303F3912298.046 [DIRS 177945]; SN0308F3912298.052 [DIRS 177946]; SN0403F3912298.057 [DIRS 177948]; SN0410F3912298.063 [DIRS 177973]; SN0601F3912298.067 [DIRS 178005]; SN0608F3912298.071 [DIRS 177975]; SN0407F3912298.060 [DIRS 170627].

### 6.3.3.2 Cross-Drift Extensometers

Two CDEXs were installed in the section of the heated drift with a cast-in-place concrete liner to measure cross-drift convergence. Convergence meters CDEX-1 and CDEX-2 were located nominally at approximately Y = 42.3 m (between the eighth and ninth canister heaters). CDEX-1 measures vertical closure, and it is anchored in the top of the invert of the heated drift and to the crown of the liner. CDEX-2 measures horizontal closure and is anchored to the liner on each rib. As for the MPBXs, displacements from the CDEXs reported in this document follow the convention of extension being positive.

The cross-drift extensometer data can be found in the following input DTNs:

- SNF39012298002.002 [DIRS 159114]
- SN0203F3912298.033 [DIRS 158361]
- SNF39012298002.010 [DIRS 158367]
- SN0001F3912298.014 [DIRS 153841]

- SN0007F3912298.018 [DIRS 158374]
- SN0101F3912298.024 [DIRS 158400]
- SN0107F3912298.029 [DIRS 158408]
- SNF39012298002.006 [DIRS 158419]
- SN0209F3912298.040 [DIRS 178009]
- SN0303F3912298.044 [DIRS 178010]
- SN0308F3912298.050 [DIRS 178011]
- SN0403F3912298.055 [DIRS 178012]
- SN0410F3912298.061 [DIRS 178013]
- SN0601F3912298.065 [DIRS 178014]
- SN0608F3912298.069 [DIRS 178015].

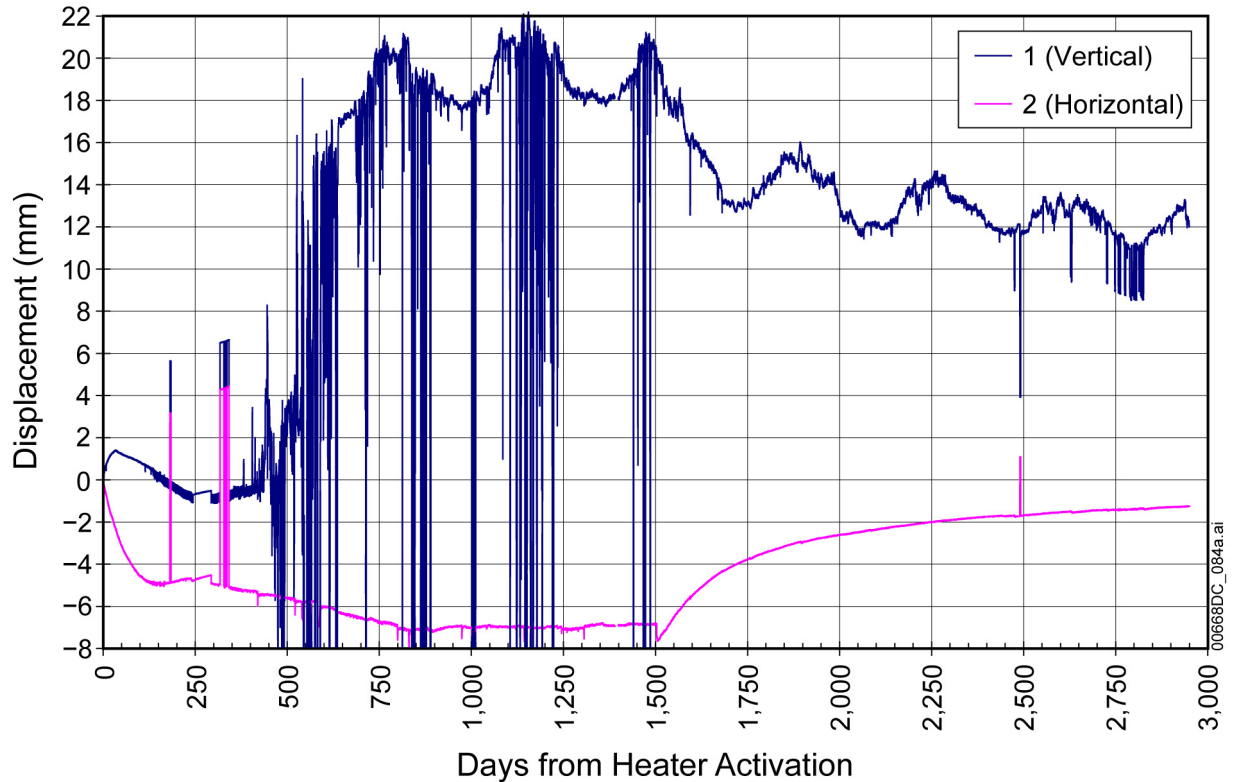
The cross-drift extensometer data corrected for thermal expansion can be found in the following input DTNs:

- SNF39012298002.012 [DIRS 153840]
- SNF39012298002.008 [DIRS 153839]
- SN0203F3912298.035 [DIRS 158363]
- SN0001F3912298.016 [DIRS 153842]
- SN0007F3912298.020 [DIRS 158388]
- SN0101F3912298.026 [DIRS 158402]
- SN0107F3912298.031 [DIRS 158413]
- SNF39012298002.004 [DIRS 153837]
- SN0209F3912298.042 [DIRS 177941]
- SN0303F3912298.046 [DIRS 177945]
- SN0308F3912298.052 [DIRS 177946]
- SN0403F3912298.057 [DIRS 177948]
- SN0410F3912298.063 [DIRS 177973]
- SN0601F3912298.067 [DIRS 178005]
- SN0608F3912298.071 [DIRS 177975].

The data for thermal expansion of carbon fiber and Invar rods is found in input DTN: SNL22100196001.003 [DIRS 111068].

### **6.3.3.2.1 Results: CDEX Displacements**

A time history plot of temperature-corrected displacement from CDEX-1 and CDEX-2 is shown in Figure 6.3-39. In general, ovalization takes place during the heating phase in which horizontal closure and vertical extension occur. This deformation reflects increasing horizontal stresses as temperatures increase during the heating phase. Vertical stresses tend to remain constant during heating, since in an elastic regime their magnitudes are limited by the overburden. The vertical extensometer CDEX-1 apparently fails around day 550, after which a continuing high level of displacement (18 to 20 mm) oscillates and matches the annual climatic cycle. The horizontal gage shows a return to zero displacement during the cooling phase.



Source: DTNs: SN0407F3912298.060 [DIRS 170627]; SN0209F3912298.042 [DIRS 177941]; SN0303F3912298.046 [DIRS 177945]; SN0308F3912298.052 [DIRS 177946]; SN0403F3912298.057 [DIRS 177948]; SN0410F3912298.063 [DIRS 177973]; SN0601F3912298.067 [DIRS 178005]; SN0608F3912298.071 [DIRS 177975].

Figure 6.3-39. Corrected Displacements Measured for ESF-HD-CDEX-1 and -2

### 6.3.3.2.2 Measurement Uncertainty: CDEX Displacements

There are several potential sources for measurement uncertainty in the displacement measurements presented in Sections 6.3.3.1.2 and 6.2.3.1.2 for the MPBXs. Much of that same discussion pertains as well to the CDEXs. The only exception to that discussion would be any effects caused by being inside a borehole, which obviously the CDEXs are not. The gage range and accuracy of CDEX-related instrumentation are presented in Table 6.3.3-6 in Section 6.3.3.1.

### 6.3.3.3 Strains

Strain gages were installed on the surface of the cast-in-place (CIP) concrete sections located at the west end of the heated drift to monitor the concrete behavior during heating and cooling of the DST. A total of 45 four-inch-long Karma foil resistive strain gages were installed in 15 rosettes (three gages per rosette) in a circumferential-axial-45° pattern at three Y stations. The five strain gage rosettes at each station were located at the crown, to the left and right above the springline, and to the left and right near the concrete invert; this layout is shown in Figure 6.3-40. The rosette strain gages are designated by rosette number and orientation (AXL = axial, CIR = circumferential, DIA = diagonal); for example, ESF-HD-RSG-5-AXL is the axial strain gage for rosette number 5. In addition to the 45 strain gages (15 rosettes) bonded to the CIP



liner, there were five additional strain gages bonded to concrete and 304 stainless steel “coupons” placed near Canister Heater 8 in the heated drift. These “coupons” are prisms of concrete and steel that are used to provide baseline data on the strain-gage response and some indication of unconstrained concrete material response. Gage and anchor locations (as-built) for strain-gage measurements made for the DST are presented in DTN: SNF38040197001.001 [DIRS 159130].

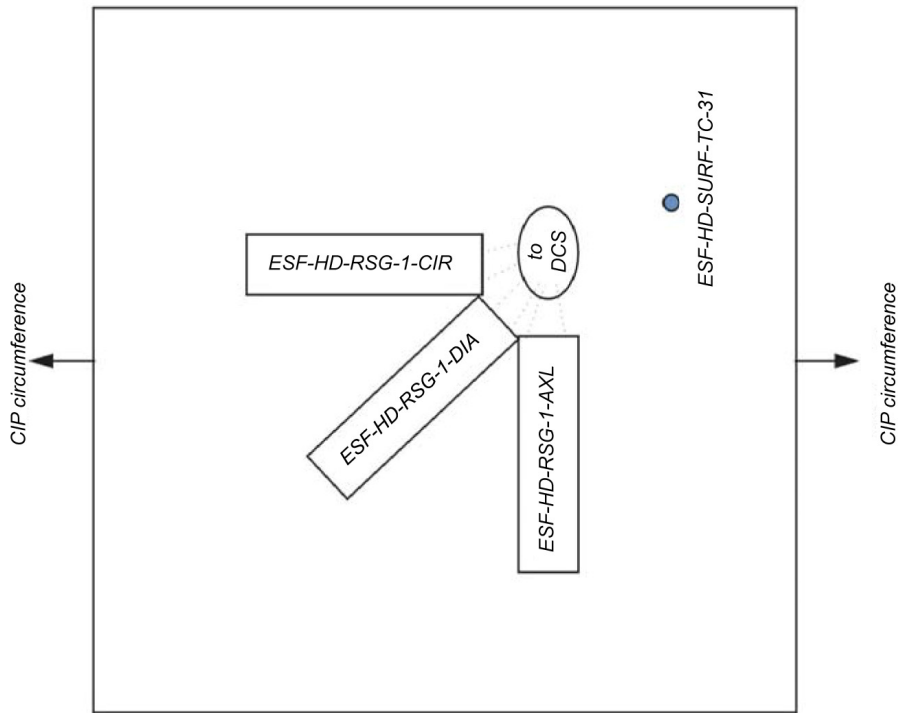
The strain data can be found in the following input DTNs:

- SN0203F3912298.034 [DIRS 158362]
- SNF39012298002.011 [DIRS 158368]
- SNF39012298002.007 [DIRS 158365]
- SN0001F3912298.015 [DIRS 158372]
- SN0007F3912298.019 [DIRS 158387]
- SN0101F3912298.025 [DIRS 158401]
- SN0107F3912298.030 [DIRS 158409]
- SNF39012298002.003 [DIRS 158417]
- SN0209F3912298.041 [DIRS 178019]
- SN0303F3912298.045 [DIRS 178020]
- SN0308F3912298.051 [DIRS 178021]
- SN0403F3912298.056 [DIRS 178022]
- SN0410F3912298.062 [DIRS 178023]
- SN0601F3912298.066 [DIRS 178024]
- SN0608F3912298.070 [DIRS 178025].

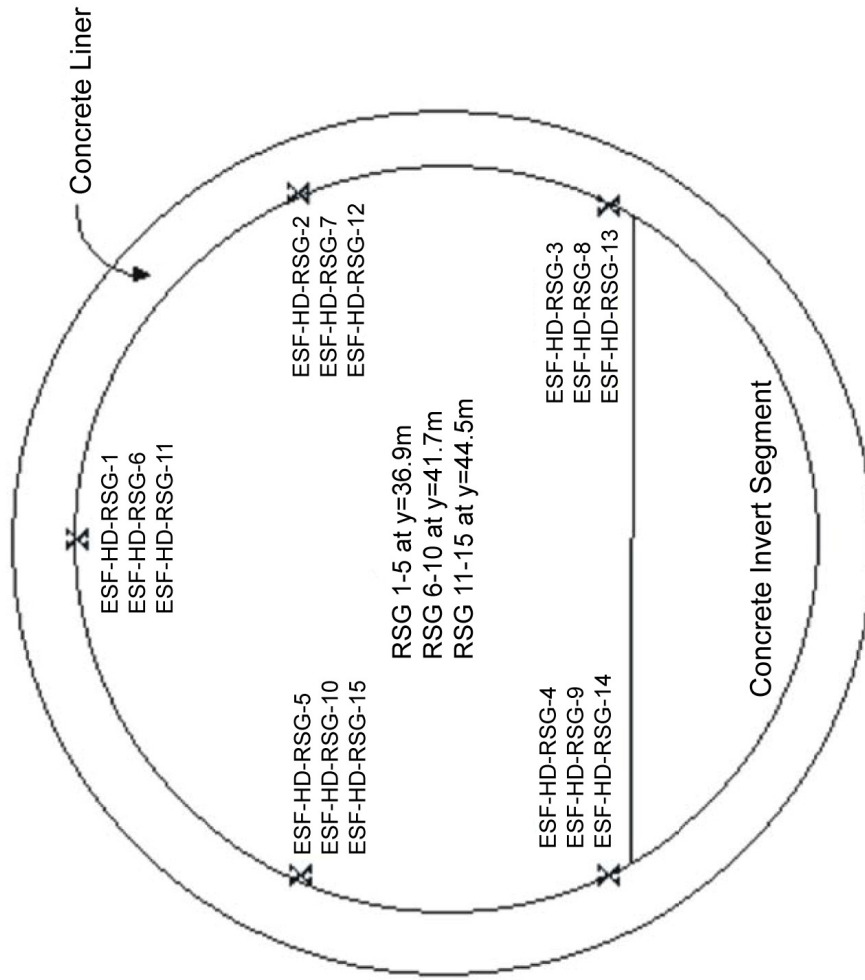
The strain data corrected for thermal expansion can be found in the following input DTNs:

- SN0203F3912298.036 [DIRS 158364]
- SNF39012298002.009 [DIRS 158366]
- SNF39012298002.013 [DIRS 158369]
- SN0001F3912298.017 [DIRS 158373]
- SN0007F3912298.021 [DIRS 158391]
- SN0101F3912298.027 [DIRS 158407]
- SN0107F3912298.032 [DIRS 158414]
- SNF39012298002.005 [DIRS 158418]
- SN0209F3912298.043 [DIRS 178027]
- SN0303F3912298.047 [DIRS 178028]
- SN0308F3912298.053 [DIRS 178029]
- SN0403F3912298.058 [DIRS 178030]
- SN0410F3912298.064 [DIRS 178031]
- SN0601F3912298.068 [DIRS 178032]
- SN0608F3912298.072 [DIRS 178033].

Typical Strain Gage and Surface Thermocouple CIP Layout



View Looking from Bulkhead



00668DC\_050.ai

Source: CRWMS M&O 1998 [DIRS 108306].

Figure 6.3-40. Layout and Location of Strain Gage Rosettes on the Concrete Liner

### 6.3.3.3.1 Results: Strains

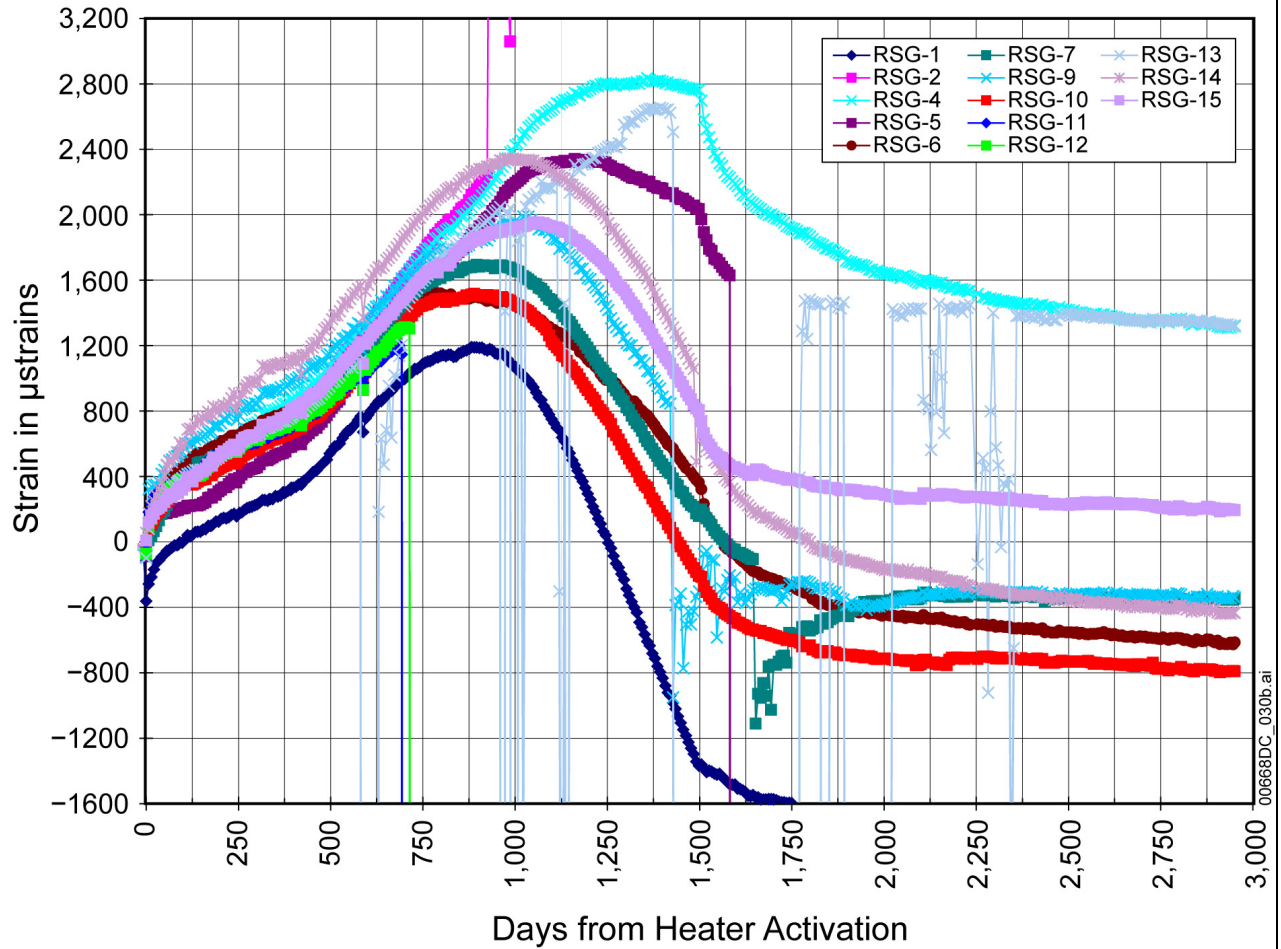
Because of the abundance of DST strain data, only representative discussion and graphics are provided. All strain data and graphics can be accessed in the summary DTN identified in Table 6.3-1.

Figure 6.3-41 shows a time history plot of the strains measured by the axial strain gages on the liner surface. The strain gages placed on the concrete liner and on unconstrained concrete samples (not shown here) in the heated drift indicate the combined effects of thermal expansion, dehydration-induced shrinkage, and mechanical stress imposed by the interaction of the concrete with the heated rock surrounding the drift. The results from the strain gages on the unconstrained samples exhibit behavior indicative of drying shrinkage caused by dehydration, a phenomenon seen elsewhere in engineering literature.

The circumferential, or hoop, strains begin as compressive strains as the surrounding rock expands inward and compresses the liner. The axial and diagonal strains are nearly always in extension, because there is far less interference with thermal expansion of the liner in the axial direction. All of the strain gages on the liner surface went into extension by approximately day 325 on account of combined thermal and mechanical effects. A mechanical component of the strain can be estimated by subtracting the strains measured from the unconstrained coupons (the thermal component) from the total strains. The mechanical component of the circumferential strain gages on the liner consistently shows that the crown of the liner is in compression, while the rest of the liner experiences smaller magnitudes of compression and tension. Note in the strain plots the beginning of the creep degradation of the epoxy beginning at around 950 days. There were six gages that appeared to continue to work past the 950-day, 200°C epoxy degradation point; the data from these gages are presented in Figure 6.3-42. Thermal expansion coefficients for  $T > 96^{\circ}\text{C}$  have been estimated for the unconstrained concrete coupons that lay on the floor of the heated drift. The coupons reveal information regarding the thermal expansion of concrete at elevated temperatures. The data reveal four distinct temperature regimes, each with its own characteristics for the thermal expansion coefficient  $\alpha$ :

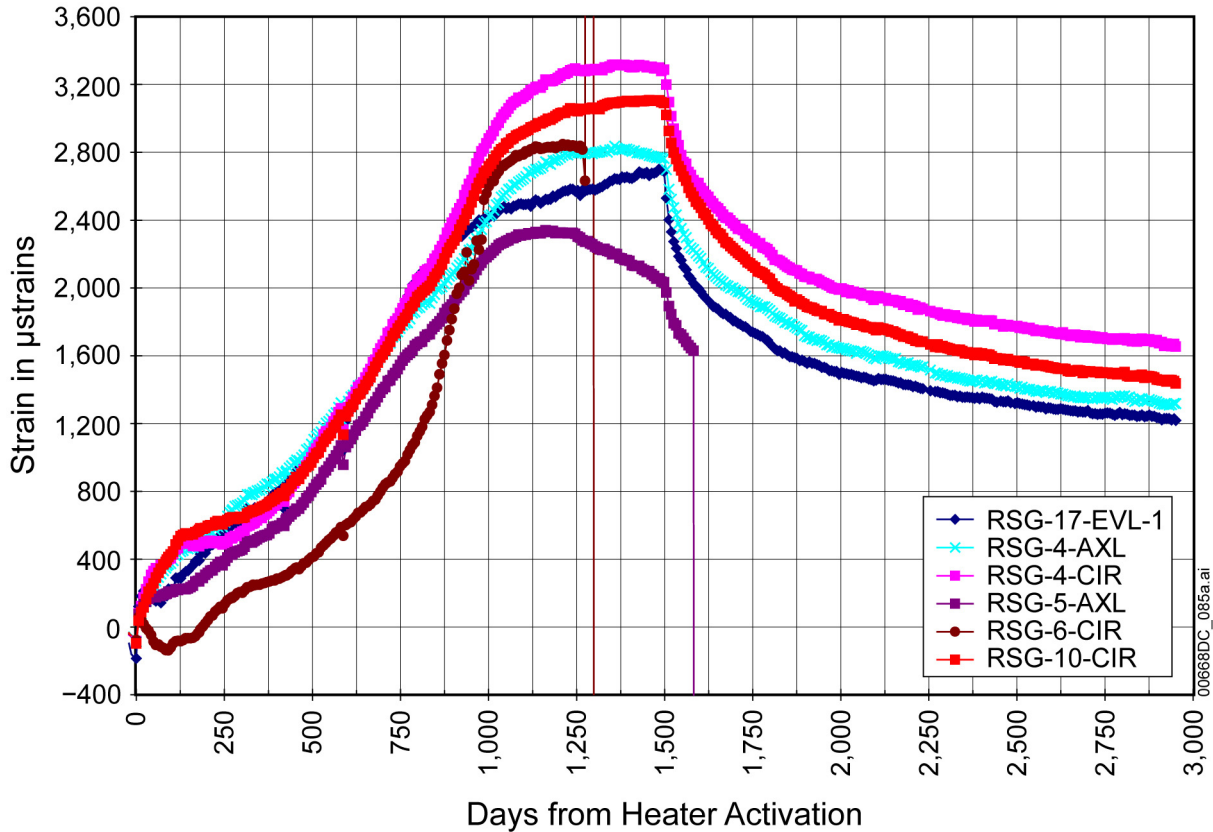
1.  $T < 100^{\circ}\text{C}$ , fast temperature rise: 8 to 12  $\mu\epsilon/^{\circ}\text{C}$
2.  $T < 100^{\circ}\text{C}$ , slow temperature rise: approximately 0 due to coincident drying shrinkage
3.  $100^{\circ}\text{C} < T < 165^{\circ}\text{C}$ : 10 to 14  $\mu\epsilon/^{\circ}\text{C}$
4.  $T > 165^{\circ}\text{C}$ : 31 to 37  $\mu\epsilon/^{\circ}\text{C}$ .

This behavior is within the same range as the laboratory thermal expansion data for SHT and DST intact rock samples (SNL 1997 [DIRS 117471]). When the strain for each coupon is plotted as a function of temperature, the coupons all exhibit a precipitous change in slope (i.e., thermal expansion) at about 165°C. Also, hysteresis in the strain data can be observed when temperature drops due to power outages.



Source: SN0208F3912298.038 [DIRS 170610] (unqualified); SN0209F3912298.043 [DIRS 178027]; SN0303F3912298.047 [DIRS 178028]; SN0308F3912298.053 [DIRS 178029]; SN0403F3912298.058 [DIRS 178030]; SN0410F3912298.064 [DIRS 178031]; SN0601F3912298.068 [DIRS 178032]; SN0608F3912298.072 [DIRS 178033].

Figure 6.3-41. Axial Strains Measured by the Strain Gages on the DST Concrete Liner



Source: SN0208F3912298.038 [DIRS 170610] (unqualified); SN0209F3912298.043 [DIRS 178027]; SN0303F3912298.047 [DIRS 178028]; SN0308F3912298.053 [DIRS 178029]; SN0403F3912298.058 [DIRS 178030]; SN0410F3912298.064 [DIRS 178031]; SN0601F3912298.068 [DIRS 178032]; SN0608F3912298.072 [DIRS 178033].

Figure 6.3-42. Strain Gages Operating Past Epoxy Degradation Point

### 6.3.3.3.2 Measurement Uncertainty: Strains

The following list includes all the known sources of measurement uncertainty for the strain data:

#### Quantifiable

- The accuracy of the instrumentation itself. The gage range and accuracy of strain gage-related instrumentation are presented in Table 6.3-13.
- The conversion of the electrical output to engineering units. The uncertainty from these equations, and the computational (round-off) error inherent in the DCS data conversion software, are negligible.

### Nonquantifiable

- Electrical interference, such as spurious signals from power surges, can cause low-magnitude noise, unexplained meandering in the data, or high-magnitude spikes.
- Problems caused by elevated temperature leading to epoxy degradation.

#### **6.3.3.4 Acoustic Emission**

Passive seismic monitoring was used to monitor changes in acoustic emission (AE) activity and wave propagation characteristics. Microseismic events can be attributed to cracking of the rock or movement along preexisting fractures or joints from thermal expansion. The methods, concepts, and instrumentation that were developed and tested in the early 1980s at the Climax Stock spent nuclear fuel test (Majer and McEvilly 1985 [DIRS 159101]) were closely followed here for the DST. The microseismic monitoring measurements were governed by technical implementing procedure YMP-LBNL-TIP/TT 4.0. Detailed discussions of experimental set-up and data processing can be found in three level 4 milestone reports (Peterson and Williams 1998 [DIRS 159102]; Williams et al. 1998 [DIRS 159104]; Williams and Peterson 1998 [DIRS 159121]).

Sixteen accelerometers were placed in DST boreholes 138 to 140, 142 to 144, 159 to 161, 163 to 165, 171, 172, 174, and 175 (see Table 6.3-2). There were two different types of sensors depending on maximum temperature rating: Wilcoxon Research Model 793-6 (rated to 150°C) and Model 728-T (rated to 125°C). These were selected based on anticipated temperatures from preheating modeling. All ratings are at least 20°C higher than the maximum temperature anticipated. The sensors were connected to the Data Collection Shed by high-temperature (Teflon) coaxial wire so that sensor measurements could be recorded. The desired bandwidth was in the range of 1,000 to 10,000 Hz. Data recordings of the microseismic activity in the test block have been submitted to the TDMS periodically over the course of the heating phase under the following input DTNs:

- LB980120123142.007 [DIRS 158352] (for background measurements)
- LB980420123142.004 [DIRS 113717] (for time period 01/1998 to 03/1998)
- LB000121123142.005 [DIRS 158339] (for time period 12/1998 to 10/1999)
- LB000718123142.005 [DIRS 158343] (for time period 10/1999 to 03/2000)
- LB0101ACEMDST1.001 [DIRS 158344] (for time period 04/2000 to 07/2000)
- LB0108ACEMDST5.001 [DIRS 158437] (for time period 09/2000 to 06/2001).

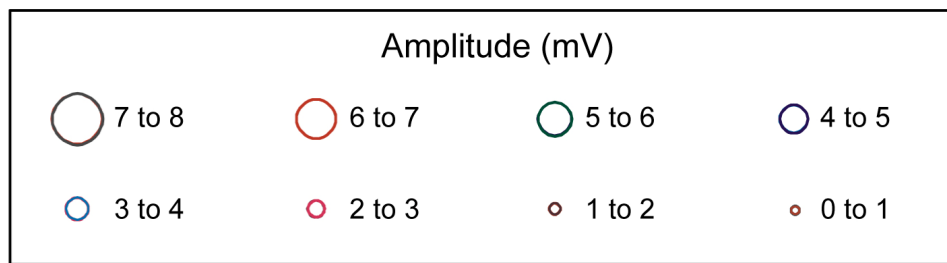
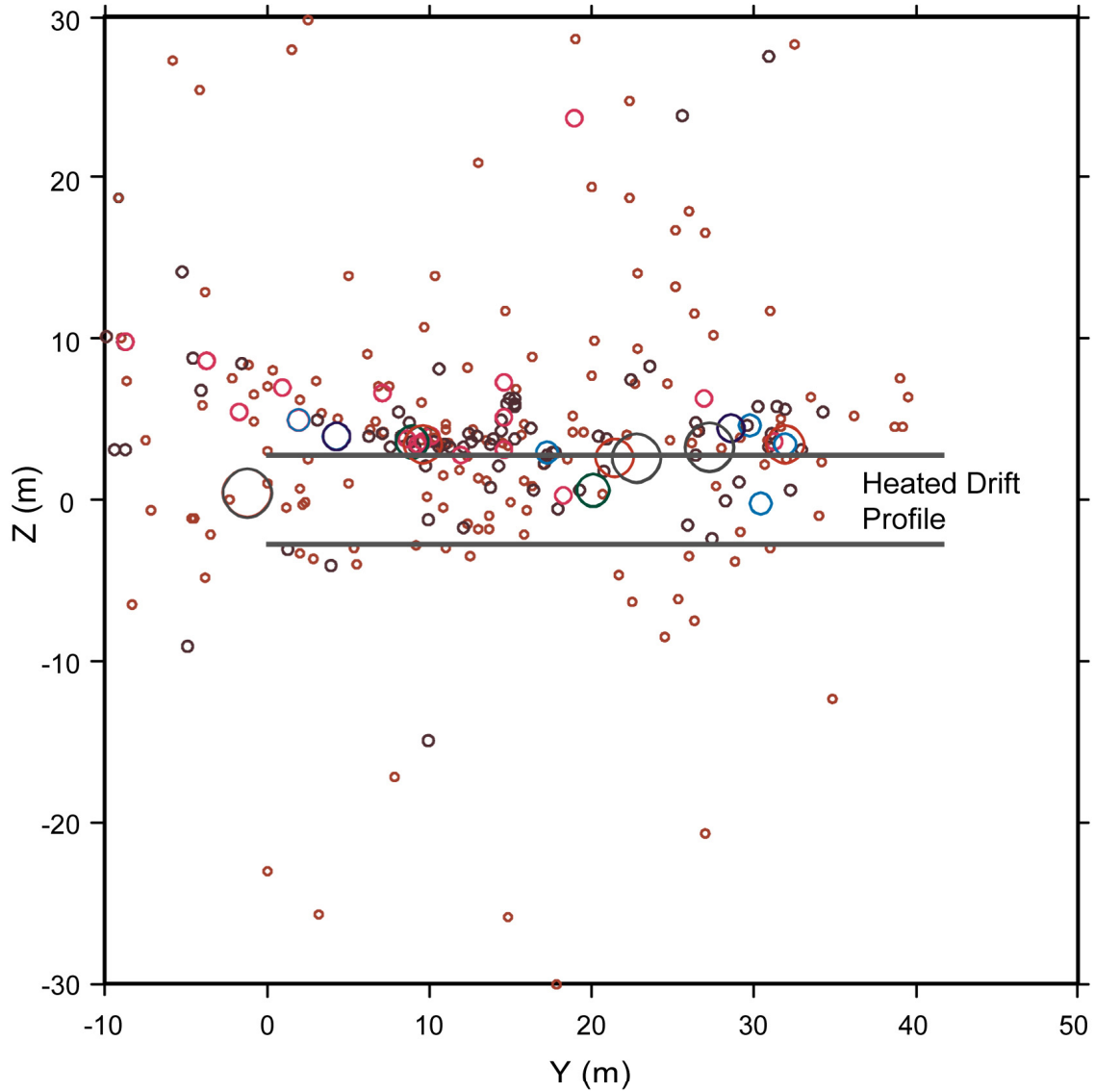
##### **6.3.3.4.1 Results: Acoustic Emissions**

Although the monitoring system was designed to operate continuously over the duration of the experiment, numerous problems occurred. Because of high-voltage noise spikes conducted along the accelerometer coaxial connections, the acquisition system initially experienced false triggering memory buffer errors. Efforts to reduce these problems were finally completed by December 1998, a full year after initiation of the heating phase. Enhancements to the recording system (bandpass filters) resulted in greatly improved data quality (i.e., increased signal/noise) starting in late December 1998. From this period until late October 2000, the system recorded

microseismic events at a roughly uniform rate. After October 2000, however, a period of low activity followed. Although deterioration in accelerometer sensitivities (resulting from thermal exposure, corrosive fluids, etc.) may be one potential cause for the decrease in recorded activity, the system was judged to be operating properly during this time, according to the accelerometer and recording system check procedures detailed in YMP-LBNL-TIP/TT 4.0.

The data recorded in the seismic monitoring consist of the microseismic waveform and the time and date that it was recorded. To determine the location of the source of energy causing the seismic event, the data were processed as follows. The first arrival times were determined by the arrival of the initial burst of energy at each of the 16 monitoring stations. After the first arrival times are picked, the location of the seismic energy source can be estimated by inversion. Figure 6.3-43 shows the locations of all the seismic events (collapsed to the YZ plane) through the heating phase. The data in the TDMS contain the following:

EVENT#:	Represents the sequential order in which the acoustic emission/microseismic event was recorded by the recording system
DATE:	Represents the date on which the event was recorded
TIME:	Represents the time when the event was recorded
X(M):	Represents the 'X' coordinate for the located event
Y(M):	Represents the 'Y' coordinate for the located event
Z(M):	Represents the 'Z' coordinate for the located event
OTIME(MS):	Represents the origin or "zero" time or first-arrival time of the event by the recording system
ERROR:	Root Mean Square (RMS) error in travel time
AMPLITUDE:	Represents the amplitude of the recorded event.



Source: DTN: LB0208ACEMDSTH.001 [DIRS 170575].

Figure 6.3-43. Location of DST Microseismic Activity (Acoustic Emissions) between December 21, 1998, and July 2, 2000



#### 6.3.3.4.2 Measurement Uncertainty: Acoustic Emissions

Hammer blows to the wall of the observation drift are periodically recorded during the experiment. These data are included with transmittals to the TDMS and represent the primary means by which system repeatability and, in a sense, measurement error is assessed. Because the hammer blows always occur at the same location along the observation drift wall, the postprocessing of the hammer “event” should result in the proper spatial location of this event. However, given the greatly elevated accuracy of locating events *within* the array of accelerometers, the hammer blows are not an ideal means of measurement error assessment: the hammer blow occurred outside of the array. Therefore, comparing the location of the hammer blow events over time should result in consistent locations within some reasonable error envelope. The acceptable envelope was determined to be a region of  $2 \times 2 \times 2$  m. The actual microseismic events should have a much higher degree of accuracy because they fall within the array boundaries. Postprocessing of the microseismic events also results in the determination of an RMS error in the seismic-wave travel times. This error may be used to assess the accuracy of the resulting microseismic event location.

#### 6.3.3.5 Laboratory Mechanical Parameters

Several preheating laboratory investigations were done to gather intact rock mechanical and thermal-mechanical properties/parameters of the TSw2 middle nonlithophysal tuff in the DST area, and to assess the concrete used in the invert and liner in the heated drift. This section describes the results of the following three suites of laboratory testing of parameters:

- Thermal expansion of intact rock (archived in input DTN: SN0203L2210196.007 [DIRS 158322])
- Elastic constants and strength properties of intact rock (archived in input DTN: SNL02100196001.001 [DIRS 158420])
- Elastic constants and strength properties of concrete samples (archived in input DTN: SNL23030598001.001 [DIRS 158370]).

Detailed discussions of rock parameters are presented in Section 4 of *Ambient Characterization of the Drift Scale Test Block* (CRWMS M&O 1997 [DIRS 101539]).

##### 6.3.3.5.1 Results: Thermal Expansion

The mean coefficients of thermal expansion (MCTEs) are summarized in Tables 6.3-15 and 6.3-16 for heating and cooling, respectively, during the first thermal cycle. The mean MCTEs and standard deviations about the mean are given at each temperature for each borehole. Summary data for the entire test suite are given with standard deviations and 95% confidence limits at the bottom of each table. The data obtained during the first heating cycle show similar behavior for most MCTEs. With the exception of three, most specimens show steep increases in MCTE, beginning at approximately 200°C and continuing until approximately 300°C. This steep increase is attributed to phase changes in the silica mineral phases because of the presence of cristobolite and tridymite. The increase in MCTE at elevated temperatures is not attributed to

thermally induced fracturing or differential expansion, since these behaviors would not be significant during the second heating phase. The test data indicates sharp increases for both sets of heating/cooling cycles. The decrease in MCTE at 300°C suggests that the phase changes have been completed. Also, hystereses are linked with phase changes. The three specimens showed behavior different from the remainder of the suite partly because of different concentrations of cristobolite and tridymite. These minerals vary substantially from their respective mean values for two of the three samples that exhibited anomalous behavior. Two of these specimens (MPBX2-85.0-B and MPBX1-40.4) appeared to initiate phase changes below 200°C, and one specimen (HDFR1-97.9-B) appeared to undergo essentially no phase change.

Table 6.3-15. Summary of Thermal Expansion Data for Specimens from the DST Block for the First Heating Cycle

Temperature (°C)	MCTE on Heatup ( $10^{-6}/^{\circ}\text{C}$ )											
	25 to 50	50 to 75	75 to 100	100 to 125	125 to 150	150 to 175	175 to 200	200 to 225	225 to 250	250 to 275	275 to 300	300 to 325
N =	17	17	17	17	17	17	17	17	17	17	17	13
Mean =	7.34	8.99	9.73	10.22	10.91	12.20	14.74	22.31	27.34	33.88	54.13	52.28
STD =	0.57	0.47	0.54	0.58	0.79	1.04	4.79	18.09	15.70	6.94	12.18	13.42
95%	0.27	0.22	0.26	0.28	0.38	0.49	2.28	8.60	7.46	3.30	5.79	7.29

Source: DTN: SN0203L2210196.007 [DIRS 158322].

NOTE: N = number of samples; STD = standard deviation; 95% = 95% confidence limit.

Table 6.3-16. Summary of the Mean Thermal Expansion Coefficients for Specimens from DST Block for the First Cooling Cycle

Temperature (°C)	Mean CTE on Cooldown ( $10^{-6}/^{\circ}\text{C}$ )											
	325 to 300	300 to 275	275 to 250	250 to 225	225 to 200	200 to 175	175 to 150	150 to 125	125 to 100	100 to 75	75 to 50	50 to 30
N =	13	17	17	17	17	17	17	17	17	17	16	15
Mean =	15.74	24.07	35.63	36.01	26.50	24.19	18.30	14.14	12.36	11.05	10.24	9.67
STD =	1.88	5.70	8.39	8.32	4.69	9.82	7.37	2.61	1.76	0.84	1.24	0.66
95%	1.02	2.71	3.99	3.96	2.23	4.67	3.50	1.24	0.84	0.40	0.61	0.33

Source: DTN: SN0203L2210196.007 [DIRS 158322].

NOTE: N = number of samples; STD = standard deviation.

### 6.3.3.5.2 Results: Elastic Constants and Strength Parameters of DST Intact Rock

The experimental data for the 16 specimens tested in unconfined compression are summarized in Table 6.3-17. Mean values, standard deviations, and 95% confidence limits are given in Table 6.3-17 for Young's modulus, Poisson's ratio, unconfined compressive strength, and axial strain at peak stress. One specimen, MPBX1-1.0-A (test UCDST001), was unloaded after force began to drop at approximately 53 MPa. The specimen was later reloaded (test UCDST017) to a peak stress of 179 MPa. Data from the first loading of this specimen were used to calculate the mean elastic moduli to be consistent with the other tests. Data from the second loading were

used in calculations of mean unconfined compressive strength and mean axial strain at peak stress.

Young's modulus ranged from 28.9 GPa to 43.1 GPa, with a mean value of 36.8 GPa. The standard deviation was  $\pm 3.5$  GPa, and the 95% confidence limit was  $\pm 1.7$  GPa. The high Young's modulus value (43.1 GPa) corresponds to the first loading of MPBX1-1.0-A. Because this specimen was unloaded at a low stress difference, the modulus was calculated over a lower stress range than for the other specimens.

Poisson's ratio ranged from 0.17 to 0.34, with a mean value of 0.20. The standard deviation was  $\pm 0.04$ , and the 95% confidence limit was  $\pm 0.02$ . The three specimens with the highest Poisson's ratios were the only specimens that had preexisting open fractures.

Strengths ranged from 71 MPa to 324 MPa, with a mean value of 176 MPa. The standard deviation was  $\pm 66$  MPa, and the 95% confidence limit was  $\pm 32$  MPa. The highest and lowest strengths were obtained on specimens from MPBX2 that were in relatively close proximity (4 m apart). Neither specimen had notable surface features that might indicate anomalous behavior. No analyses were performed to determine the best fitting distribution curves for Young's modulus, Poisson's ratio, or unconfined compressive strength.

Table 6.3-17. Tabulation of DST Unconfined Compression Tests

All Specimens TSw2, Ttpmn	Statistical Summary			
	Mean	Standard Deviation	Count	95% Confidence Limit
Static Young's Modulus (GPa)	36.8	3.5	16	1.7
Static Poisson's Ratio	0.201	0.040	16	0.020
Unconfined Compressive Strength (MPa)	176.4	65.8	16	32.3
Axial Strain at Peak Stress	0.005209	0.002048	16	0.001004

Source: DTN: SNL02100196001.001 [DIRS 158420].

NOTES: Test specimen ESF-SDM-MPBX1-1.0-A was tested twice. Mean Young's modulus and mean Poisson's Ratio were calculated using data from the first loading only (UCDST001). Mean unconfined compressive strength was calculated using data from the second loading only (UCDST017).

Test Conditions: Nominally 38.1 mm in diameter, 76.2 mm in length, ambient temperature and pressure, nominal strain rate of  $10^{-5} \text{ s}^{-1}$ .

### 6.3.3.5.3 Results: Elastic Constants and Strength Properties of Cast-in-Place Concrete Samples

Six concrete specimens were tested to failure in unconfined compression, and four specimens were cycled to approximately 40% of the failure strength. Mean values and standard deviations of unconfined compressive strength, Young's modulus, and Poisson's ratio are given in Tables 6.3-18 and 6.3-19 for reinforced and nonreinforced concretes, respectively. Separate Poisson's ratio values are given for the two ( $0^\circ$  and  $90^\circ$ ) radial gages. Average failure strengths were  $56.6 \pm 3.2$  MPa for reinforced concrete and  $54.3 \pm 13.8$  MPa for nonreinforced concrete. When an outlier was removed, the failure strength for nonreinforced concrete was increased to

62.2 ± 0.9 MPa. Mean Young's modulus (determined during all loading cycles) was 33.3 ± 2.1 GPa for the reinforced concrete and 38.8 ± 3.9 GPa for the nonreinforced concrete. Mean Poisson's ratio (also determined during all loading cycles) was 0.25 ± 0.03 for the reinforced concrete and 0.24 ± 0.04 for the nonreinforced concrete.

Table 6.3-18. Summary of Results for DST Reinforced Concrete

	Strength (MPa)	Young's Modulus (GPa)		Poisson's Ratio (0°)		Poisson's Ratio (90°)	
		Loading	Unloading	Loading	Unloading	Loading	Unloading
<b>Tests to Failure</b>							
CIP11	58.2	31.4	—	N/A <sup>a</sup>	—	0.197	—
CIP13	58.6	37.3	—	0.293	—	0.253	—
CIP17	52.9	34.4	—	0.247	—	0.233	—
<b>Cyclic Loading Tests</b>							
CIP14							
Cycle 1:	—	31.3	34.9	0.301	0.276	0.292	0.267
Cycle 2:	—	32.2	34.4	0.254	0.281	0.244	0.274
Cycle 3:	—	31.5	34.1	0.254	0.278	0.242	0.269
Cycle 4:	—	31.7	33.3	0.252	0.250	0.238	0.217
CIP18							
Cycle 1:	—	32.3	34.5	0.222	0.208	0.261	0.261
Cycle 2:	—	35.2	34.3	0.228	0.210	0.255	0.266
Cycle 3:	—	35.3	32.8	0.230	0.205	0.255	0.257
Mean	—	33.3	34.0	0.253	0.244	0.247	0.259
Standard Deviation	—	2.1	0.7	0.027	0.036	0.024	0.019
No. of Measurements	—	10	7	9	7	10	7
Mean (All Data)	56.6	33.6		0.249		0.252	
Standard Deviation	3.2	1.7		0.031		0.022	
No. of Measurements	3	17		16		17	

Source: DTN: SNL23030598001.001 [DIRS 158370].

<sup>a</sup> Radial gage did not function properly so data are omitted.

Table 6.3-19. Summary of Results for Nonreinforced Concrete

	Strength (MPa)	Young's Modulus (GPa)		Poisson's Ratio (0°)		Poisson's Ratio (90°)	
		Loading	Unloading	Loading	Unloading	Loading	Unloading
<b>Tests to Failure</b>							
CIP7	62.89	36.8	—	N/A <sup>a</sup>	—	0.210	—
CIP8	61.60	36.8	—	N/A <sup>a</sup>	—	0.235	—
CIP10	38.33	45.0 <sup>b</sup>	—	0.153	—	0.288	—
<b>Cyclic Loading Tests</b>							
CIP9							
Cycle 1:	—	38.4	38.6	0.252	0.236	0.243	0.260
Cycle 2:	—	41.7	41.1	0.272	0.256	0.278	0.284
Cycle 3:	—	42.2	42.2	0.297	0.264	0.306	0.289
Cycle 4:	—	42.3	42.8	0.274	0.271	0.271	0.307
CIP3							
Cycle 1:	—	32.0	34.5	0.226	0.238	0.179	0.177
Cycle 2:	—	36.2	34.3	0.239	0.242	0.205	0.171
Cycle 3:	—	36.5	32.5	0.233	0.231	0.206	0.180
Mean	—	38.8	38.0	0.243	0.248	0.242	0.238
Standard Deviation	—	3.9	4.2	0.043	0.016	0.042	0.060
No. of Measurements	—	10	7	8	7	10	7
Mean (All Data)	54.3	38.5		0.246		0.241	
Standard Deviation	13.8	3.9		0.032		0.049	
No. of Measurements	3	17		15		17	

Source: DTN: SNL23030598001.001 [DIRS 158370].

<sup>a</sup> Radial gage did not function properly so data are omitted.

<sup>b</sup> CIP10 had a lower strength than CIP7 and CIP8. Because moduli are calculated between 50 microstrain and 40% of the failure strength, the moduli for CIP10 were determined over a lower stress range than CIP7 and CIP8.

#### 6.3.3.5.4 Measurement Uncertainty: Laboratory Mechanical Parameters

The uncertainty in the unconfined compressive test of rock and concrete includes the accuracy of the load cell, the accuracy of the LVDT, specimen alignment, changes in the specimen cross section area during the test, specimen variation, and anisotropy of the rock. Among these factors, the greatest uncertainty is with the specimen variation. The heterogeneity in the rock-mass will have significant effects on its compressive strength and moduli. Many of these uncertainties also apply to thermal expansion and creep testing of intact samples. In addition, temperature and stress control contribute to uncertainties in thermal expansion and creep testing, respectively.

### 6.3.3.6 Field Mechanical Parameters

The following mechanical field measurements are presented in the subsections below:

- Plate loading test
- In situ stress
- Rock-mass thermal expansion.

#### 6.3.3.6.1 Results: Plate Loading Test

The Plate Loading Tests (PLTs) were conducted as part of the DST. The purpose of the PLT was to obtain rock-mass elastic-modulus measurements under ambient and hot conditions for the middle nonlithophysal tuff. Two earlier tests were conducted in 1998, after which design changes were made to ensure a stiffer loading frame for improved measurements. These improved measurements, from the October 2000 test, are summarized in Table 6.3-20. A detailed discussion of the setup, testing procedure, raw test data, and rock-mass modulus calculation from the raw data may be found in the documentation for two input DTNs: SN0011F3912298.022 [DIRS 158392] and SN0011F3912298.023 [DIRS 158399]. A post-heating PLT was performed in April 2003, the results of which are also included in Table 6.3-20. The results differ slightly from the 2000 PLT, with some moduli increasing and some decreasing, but not enough to indicate major changes to the rock during the peak temperature and subsequent cooldown periods. The DTNs for the raw data and calculated moduli for the 2003 PLT are: SN0306F3912298.048 [DIRS 165416] and SN0310F3912298.054 [DIRS 168527].

Table 6.3-20. DST PLT Results from October 2000 and April 2003

	Maximum Displacement (mm)	Secant Moduli (GPa)	Elastic Moduli (GPa)
	October 2000; April 2003	October 2000; April 2003	October 2000; April 2003
Ambient Side			
Deep Anchor	1.69; 1.10	17.3; 26.3	41.0; 60.8
Medium Anchor	1.49; 1.45	19.6; 19.9	49.5; 41.0
Shallow Anchor	1.21; 1.31	24.2; 22.1	59.4; 51.3
Elevated Temperature			
Deep Anchor	LVDT malfunctioned	LVDT malfunctioned	LVDT malfunctioned
Medium Anchor	0.68; 0.65	43.0; 44.4	62.5; 62.1
Shallow Anchor	0.55; 0.46	53.2; 62.7	99.0; 92.1

Source: DTNs: SN0011F3912298.022 [DIRS 158392]; SN0011F3912298.023 [DIRS 158399]; SN0306F3912298.048 [DIRS 165416]; SN0306F3912298.049 [DIRS 168527].

NOTE: Maximum pressure equals 31.75 MPa.

#### 6.3.3.6.2 Results: In Situ Stress Measurements

A series of five successful hydraulic fracturing tests, used to determine in situ stress states, were conducted. The measured in situ stress state is small, which is consistent with the dominant local normal faults. The north-northeastern maximum horizontal stress direction is subparallel to the average strike of these faults and is supported by previous measurements in the Yucca Mountain

area. Detailed discussion is presented in *Unconfined Compression Tests on Specimens from the Drift Scale Test Area of the Exploratory Studies Facility at Yucca Mountain, Nevada* (SNL 1997 [DIRS 117471]) and in Section 10.4 of *Ambient Characterization of the DST Block* (CRWMS M&O 1997 [DIRS 101539]).

### 6.3.3.6.3 Results: Rock Mass Thermal Expansion

Rock mass thermal expansion has been calculated from the DST in situ heating phase data, including temperature change for a given axial length from ambient, gage length, and measured thermal displacement over the gage length. The rock mass thermal expansion coefficient was calculated for the DST using selected data from displacement measurement boreholes 81 and 82. These boreholes run roughly parallel to the heated drift, and extend over a distance of 45 m. Much of that distance is in a high temperature region of relatively constant temperature. A discussion of the thermal expansion coefficient data reduction process may be found in the documentation for summary DTN: SN0407F3912298.060 [DIRS 170627].

Table 6.3-21 lists the rock mass thermal expansion coefficients calculated from the DST MPBX data from boreholes 81 and 82. It also lists intact rock values from laboratory measurements made on DST and SHT samples. These intact rock values are used for comparison with rock-mass values and are identified in the following DTNs:

- SNL22080196001.001 [DIRS 109722]
- SNL22080196001.003 [DIRS 119042]
- SN0203L2210196.007 [DIRS 158322].

Below boiling, the average rock-mass coefficient ranges from approximately 2.0 to  $4.5 \times 10^{-6}/^{\circ}\text{C}$ , approximately half of the intact values. As the temperatures approach  $200^{\circ}\text{C}$ , the rock mass coefficient values approach the intact values, with a maximum average rock-mass coefficient of  $12.55 \times 10^{-6}/^{\circ}\text{C}$  in the highest temperature range. The calculated values for rock mass thermal expansion are, as expected, lower than the values from intact laboratory specimens, because of the ubiquitous presence of vertical fractures in the Ttpmtnuff. The fractures would tend to accommodate some of the thermal expansion in the joint stiffness, particularly during early heating, because the thermal displacement would be insufficient to mechanically close fractures. Also, the three-dimensional effects of heated rock bounded by lower temperature rock would decrease the net effect of thermal expansion by resisting the thermal displacements in adjacent volumes of rock.

Table 6.3-21. Rock Mass Thermal Expansion Coefficients from DST MPBX Data

	T <sub>max</sub> , °C	Thermal Expansion Coefficients in $\mu\text{strain}/^\circ\text{C}$						
		25°C to 50°C	50°C to 75°C	75°C to 100°C	100°C to 125°C	125°C to 150°C	150°C to 175°C	175°C to 200°C
DST MPBX data through 1/14/2002								
HD-81-MPBX1 Anchor 4-Anchor 5	178.02	1.94	3.27	4.61	3.98	7.02	9.47	12.55
HD-81-MPBX1 Anchor 5-Anchor 6	171.74	3.65	1.19	0.46	4.37	7.04	10.34	—
HD-82-MPBX2 Anchor 2-Anchor 3	158.24	0.48	2.78	6.84	4.89	7.21	8.40	—
HD-82-MPBX2 Anchor 3-Anchor 4	163.03	2.82	1.36	4.52	6.12	8.15	10.23	—
HD-82-MPBX2 Anchor 4-Anchor 5	168.72	0.55	3.31	4.66	6.17	7.81	9.79	—
HD-82-MPBX2 Anchor 5-Anchor 6	171.48	2.76	2.57	4.03	0.85	7.38	10.60	—
Avg., DST MPBX	—	2.03	2.41	4.19	4.40	7.43	9.80	12.55
Std. Dev., DST MPBX	—	1.29	0.93	2.07	1.95	0.46	0.80	—
Avg., DST MPBX (no outliers)	—	2.03	2.41	4.45	5.11	7.43	9.80	12.55
Std. Dev., DST MPBX (no outliers)	—	1.29	0.93	0.29	1.00	0.46	0.80	—
SHT Pretest Heat. (TDIF 305593)	300	7.47	8.88	9.64	10.01	10.72	11.26	12.78
SHT Post-Test 1st Heat. (TDIF 307123)	331	8.64	9.87	8.95	9.64	10.68	11.77	12.34
SHT Post-Test 2nd Heat. (TDIF 307123)	323	8.53	9.67	9.01	10.21	11.13	12.23	14.10
DST Pretest 1st Heat. (TDIF 312864)	327	7.34	8.99	9.73	10.22	10.91	12.20	14.74
DST Pretest 2nd Heat. (TDIF 312864)	331	7.22	8.87	9.63	10.24	11.28	13.22	19.37

Source: DTN: SN0407F3912298.060 [DIRS 170627].

NOTE: TDIF = Technical Data Information Form.

#### 6.3.3.6.4 Measurement Uncertainty: Field Mechanical Parameters

Measurement uncertainties are numerous because of the various types of measurements. The uncertainty of the MPBX measurements used for the PLTs and for determination of rock mass thermal expansion coefficients are similar to comparable SHT MPBX measurements, as discussed in Section 6.2.3.1.2. As shown in Table 6.3-13, the gauge range and accuracy of the LVDTs for the MPBXs are  $\pm 25.4$  mm and  $\pm 0.5\%$ , respectively. The type 'K' thermocouples installed with the MPBXs and the PLT have a typical range maximum of 1,280°C and accuracy of  $\pm 2.2^\circ\text{C}$ . Pressure transducers used for the PLT had a range of up to 69 MPa (10,000 psi) with a reported accuracy of 0.5% of the full range. In situ stress measurements obtained from hydraulic fracturing were accurate to within  $\pm 14\%$ , based on instrumentation and displacement



measurement accuracies. Fracture mapping and rock mass classification are subject to uncertainties based on interpretation of the observed fractures in the field. Additionally, for all the field parameters, subjective interpretations, high-pressure complications, fracture spacing, fracture aperture, and inelastic time-dependent deformation represent primary uncertainties.

### **6.3.3.7 Scaling along the Roof of the Heated Drift**

Scaling has been observed in the Heated Drift in four zones within 14 m of the bulkhead and a large area of scaling near the concrete liner between 27 and 33 m from the bulkhead. Associated with each of these scaling zones are many small pieces of rock on the floor that have dropped through the 7.5-cm × 7.5-cm openings in the welded wire fabric of the ground support system. For the most part, these scaling zones have been contained by the existing ground support system in the manner designed. The scaling is summarily discussed herein in terms of background, observations, and conclusions.

#### **6.3.3.7.1 Background**

As shown in *Drift Scale Test As-Built Report* (CRWMS M&O 1998 [111115]), the Heated Drift was isolated from workers and visitors with a bulkhead to provide safety from the high temperatures and to isolate the test from external conditions. The planned thermal management strategy included maintaining the drift wall temperature at approximately 200°C.

The ground support system for the roof consists of rock bolts and welded wire fabric through the first 35 m of the Heated Drift. The support system for the remaining 12.5 m consists of a concrete liner, which covers the rock bolts and welded wire fabric, and extends to the far end of the Heated Drift.

#### **6.3.3.7.2 Observations**

Visual observations documented on November 16, 1999, indicated the presence of small rock chips on the floor located 5 to 20 m from the bulkhead. This observation triggered further investigation with the DST remote camera. Although small rock chips were present on the floor, there was no evidence of accumulated larger rock fragments retained in the welded wire fabric. During a subsequent cleaning and re-installation of the DST bulkhead windows on April 23, 2001, loose rock was observed at several locations above the welded wire fabric attached to the roof of the Heated Drift. Cables from two instrumented boreholes located 2.7 m and 11.9 m from the bulkhead along the longitudinal axis of the Heated Drift were observed to have pulled loose from the welded wire fabric. These cables were originally fastened to the wire fabric during installation and remained fastened, as observed in the video imaging in October 2000. This suggests that much of the scaling occurred since that time. To better characterize the extent of the loose rock, remote video imaging of the inside of the Heated Drift was done at large intervals in 2001 and many times in 2002.

On May 2, 2001, a video was made in order to examine the extent of scaling along the entire length of the Heated Drift roof. Video images were recorded with the DST's remote video camera and with an additional video unit mounted at the bulkhead. In addition, photographs

were taken using a 35-mm camera with a telephoto lens. The 7.5-cm squares in the welded wire fabric provide a usable reference scale in the images.

The video equipment was prepared and installed through the camera door in the bulkhead. One of the cameras recorded roof, wall, and floor images by rotating the lens about the longitudinal axis of the Heated Drift. However, this camera did not image most of the scaling zones because the camera's blind spot (created by rotational limitations of 320° and the mounting rail) does not allow it to view that part of the roof. The second remote camera is aimed forward. It was not intended to record images along the roof of the Heated Drift. Initially, the insulated camera box, which contains two video cameras, successfully traveled the full length of the rail mounted to the roof of the Heated Drift. At the far end of the Heated Drift (35 to 47.5 m from the bulkhead), the drift periphery is covered with a concrete liner. In the early runs, the traveling remote camera clearly showed that this concrete liner remained intact, with no evidence of fractures or damage from heating. However, the video runs in 2002 were stopped at station 51 (a little over 32 m from the bulkhead, before the concrete liner), because the scaled rock at that location blocked the camera's ability to travel any further down the rail at the crown of the drift.

In addition to the remote video runs, the YMP project photographer set up digital video and still photography equipment on the door platform for the remote camera. From that vantage point, high-resolution images of the loose rocks held by the rockbolts and welded wire fabric at several of the zones close to the bulkhead were obtained. Photographs of the roof suggest that most of these observed scaling zones are associated with uneven surfaces or ridges left by the alpine mining machine during excavation of the Heated Drift.

From all of the observations, sketches were developed of the scaling zones in the roof close to the bulkhead. The three zones closest to the bulkhead showed scaling concentrated along the drift crown (i.e., the apex). A fourth zone was located about at the two-o'clock position relative to the crown (i.e., on the right side of the roof, relative to observations made looking down the drift), about 13 m into the Heated Drift. For the scaling zone closest to the bulkhead (about 3 m from the bulkhead), the elongated area is estimated to be 1.0 m<sup>2</sup>. The existing ground support system consists of 3-m-long Super Swellex rockbolts installed on a one-meter square pattern and 3 × 3 × W1.9 × W1.9 welded wire fabric. This ground support was installed from the springline to the crown of the excavation. For the scaling zone located about 7 m from the bulkhead, the lens-shaped area is estimated to be 0.7 m<sup>2</sup>. At 12.5 m from the bulkhead, a somewhat circular zone is estimated to cover an area of about 1.6 m<sup>2</sup>. Located close to the collar or instrument head of a multipoint borehole extensometer referred to as MPBX-3, the fourth scaling zone covers an area of approximately 0.6 m<sup>2</sup>. The loose rock fragments being held up by the welded wire fabric appear to have linear dimensions ranging from 3 to 45 cm.

Since these original observations were made, other scaling zones farther from the bulkhead have been partially observed in the subsequent videos (starting with the video obtained on August 16, 2001). The most intense roof scaling seems to have occurred in the drift at distances from the bulkhead ranging from 27 to 33 m. This large area of fractured rock is close to the concrete liner. Detailed measurements of this area will have to be made first hand as the drift cools enough for direct observations to be made.

In spite of the observed scaling zones, the ground support system installed during the Heated Drift excavation in 1997 appears to be functioning as designed. The rock chips that have been observed on the canisters and/or on the drift floor are quite small in size (generally from dust-sized particles up to 1 cm across). In addition, there has not been any evidence of failed components or deep fractures to date; however, further observations and measurements need to be made in order to complete a more thorough evaluation. All pieces of rock that were of significant size (about 3 to 45 cm) were held up by the welded wire.

### 6.3.3.7.3 Conclusions

The occurrence of scaling along the roof of the Heated Drift of the DST was not unexpected. To begin with, many fractures have been observed in multiple locations of the middle nonlithophysal rock (Tptpmn) in situ. In addition, this rock type is brittle (i.e., susceptible to fracturing in response to stress), and further fracturing was created during drift construction (drill-and-blast mining technique).

The total volume and individual piece size of the observed fallen rock is relatively small, which would indicate that the rock damage has been successfully contained by the existing ground support system in place in the drift (i.e., rock bolts and welded wire fabric). And finally, to date, test equipment, instrumentation, and sensors have not been damaged. As a result, the occurrence of the observed scaling zones does not appear to be an adverse condition in the conceptual understanding of the thermal-mechanical behavior of the rock-mass involving preclosure and postclosure performance of the repository.

### 6.3.3.7.4 Records

Many of the videos of the Heated Drift have been submitted to the YMP Records Center. Tables 6.3-22 and 6.3-23 contain the dates, accession numbers, and records titles for the submitted videos, and special instruction sheets for the videos, respectively.

Table 6.3-22. Video Tapes in the YMP Records Center

Date	Accession Number	Title
02/18/1998	MOL.20020918.0202	Heated Drift Video – Videotape of the Heated Drift in Alcove 5 of the ESF, February 18, 1998, Master (C)
11/17/1999	MOL.20020918.0203	Heated Drift Video – Videotape of the Heated Drift in Alcove 5 of the ESF, November 17, 1999, Master (C)
05/02/2001	MOL.20020918.0204	Heated Drift Video – Videotape of the Heated Drift in Alcove 5 of the ESF, May 2, 2001, Master (C)
08/16/2001	MOL.20020918.0205	Heated Drift Video – Videotape of the Heated Drift in Alcove 5 of the ESF, August 16, 2001, Master (C)
01/09/2002	MOL.20020918.0206	Heated Drift Video – Videotape of the Heated Drift in Alcove 5 of the ESF, January 9, 2002, Master (C)
01/16/2002	MOL.20020918.0207	Heated Drift Video – Videotape of the Heated Drift in Alcove 5 of the ESF, January 16, 2002, Master (C)
01/23/2002	MOL.20020918.0209	Heated Drift Video – Videotape of the Heated Drift in Alcove 5 of the ESF, January 23, 2002, Master (C)

Table 6.3-22. Video Tapes in the YMP Records Center (Continued)

<b>Date</b>	<b>MOL Number</b>	<b>Title</b>
01/30/2002	MOL.20020918.0210 MOL.20020918.0215	Heated Drift Video – Videotape of the Heated Drift in Alcove 5 of the ESF, January 30, 2002, Master (C)
02/06/2002	MOL.20020918.0213	Heated Drift Video – Videotape of the Heated Drift in Alcove 5 of the ESF, February 6, 2002, Master (C)
02/27/2002	MOL.20020918.0216	Heated Drift Video – Videotape of the Heated Drift in Alcove 5 of the ESF, February 27, 2002, Master (C)
03/06/2002	MOL.20020918.0220	Heated Drift Video – Videotape of the Heated Drift in Alcove 5 of the ESF, March 6, 2002, Master (C)
03/20/2002	MOL.20020918.0222	Heated Drift Video – Videotape of the Heated Drift in Alcove 5 of the ESF, March 20, 2002, Master (C)
04/17/2002	MOL.20020918.0225	Heated Drift Video – Videotape of the Heated Drift in Alcove 5 of the ESF, April 17, 2002, Master (C)
05/01/2002	MOL.20020918.0228	Heated Drift Video – Videotape of the Heated Drift in Alcove 5 of the ESF, May 1, 2002, Master (C)
06/05/2002	MOL.20020918.0229	Heated Drift Video – Videotape of the Heated Drift in Alcove 5 of the ESF, June 5, 2002, Master (C)
07/10/2002	MOL.20020918.0231	Heated Drift Video – Videotape of the Heated Drift in Alcove 5 of the ESF, July 10, 2002, Master (C)
10/29/2003	MOL.20040520.0230	Drift Scale Test Heated Drift Video, DST HD Video October 29, 2003 (C)
01/13/2004	MOL.20040520.0231	Drift Scale Test Heated Drift Video, DST HD Video January 13, 2004 (C)

Table 6.3-23. Special Instruction Sheets for Video Tapes in the YMP Records Center

<b>Date</b>	<b>MOL Number</b>	<b>Title</b>
08/15/2002	MOL.20030826.0072	Special Instruction Sheet for Heated Drift Video - Videotape of the Heated Drift in Alcove 5 of the ESF; video was produced by the DST Remote Video Camera Unit on August 15, 2002 by Jim Aamodt, Fred Homuth and Bob Sievert of the TCO; color, hue and exact position of the video does not affect quality; a summary of the camera run can be found in the field record package for the FWP-ESF-96-003 (C)
09/18/2002	MOL.20030826.0073	Special Instruction Sheet for Heated Drift Video - Videotape of the Heated Drift in Alcove 5 of the ESF; video was produced by the DST Remote Video Camera Unit on September 18, 2002 by Jim Aamodt, Kean Finnegan, and Fred Homuth of the TCO; color, hue and exact position of the video does not effect quality; a summary of the camera run can be found in the field record package for FWP-ESF-96-003 (C)
10/23/2002	MOL.20030826.0074	Special Instruction Sheet for Heated Drift Video - Videotape of the Heated Drift in Alcove 5 of the ESF; video was produced by the DST Remote Video Camera Unit on October 23, 2002 by Jim Aamodt, Fred Homuth and Bob Sievert of the TCO; color, hue and exact position of the video does not affect quality; a summary of the camera run can be found in the field record package for FWP-ESF-96-003 (C)

Table 6.3-23. Special Instruction Sheets for Video Tapes in the YMP Records Center (Continued)

Date	MOL Number	Title
10/23/2002	MOL.20040209.0061	Special Instruction Sheet for Drift Scale Test Heated Drift Video, October 23, 2002 (C)
02/18/2003	MOL.20040209.0063	Special Instruction Sheet for Drift Scale Test Heated Drift Video, Disk 1, February 18, 2003 (C)
02/18/2003	MOL.20040209.0064	Special Instruction Sheet for Drift Scale Test Heated Drift Video, Disk 2, February 18, 2003 (C)
03/27/2003	MOL.20040209.0062	Special Instruction Sheet for Drift Scale Test Heated Drift Video, March 27, 2003 (C)
05/29/2003	MOL.20040209.0065	Special Instruction Sheet for Drift Scale Test Heated Drift Video, May 29, 2003 (C)
07/30/2003	MOL.20040209.0066	Special Instruction Sheet for Drift Scale Test Heated Drift Video, July 30, 2003 (C)
03/31/2004	MOL.20041110.0077	Special Instruction Sheet for Drift Scale Test Heated Drift Video/DST HD Video March 31, 2004 (C)
08/04/2004	MOL.20041110.0076	Special Instruction Sheet for Drift Scale Test Heated Drift Video/DST HD Video August 4, 2004 (C)
04/12/2005	MOL.20060427.0145	Special Instruction Sheet for Drift Scale Test Heated Drift, HD DST Video Camera Run 4/12/05 (C)
11/16/2005	MOL.20060427.0146	Special Instruction Sheet for Drift Scale Test Heated Drift, HD DST Video Camera Run 11/16/05 (C)

### 6.3.4 DST Chemical Measurements

This section presents chemical data that have been collected from the DST and intended for the validation of thermal-hydrological-chemical processes by numerical modeling. The following sections will discuss, respectively, aqueous chemistry (6.3.4.1), gas chemistry and isotopic compositions (6.3.4.2), mineralogical and petrologic analyses (6.3.4.3), strontium and uranium isotopic compositions of water samples (6.3.4.4), and special investigations of waters with high fluoride concentrations (6.3.4.5).

#### 6.3.4.1 DST Aqueous Chemistry

Water samples were collected periodically during the heating phase from multiple locations throughout the DST block and analyzed in the laboratory for concentrations of metals, anions, and certain isotopes. Aqueous sampling was conducted from boreholes instrumented to include water and gas sampling capabilities. The boreholes were (by design) drilled to intersect regions of the thermally perturbed rock that would be undergoing different thermal-hydrological-chemical processes (boiling, drying, condensing, dissolving, and precipitating) at different times. For preheating baseline data, pore water was obtained from centrifuged cores of boreholes 182 to 184 (ESF-HD-PERM1 to PERM3) on the right side of the connecting drift across from the DST block. The concentrations of inorganic ions have been measured and reported. Otherwise, all of the analytical data reported in this section are from water samples obtained during heating from boreholes constructed for water sampling within the DST block.

The water-sampling activity continued during the cooling phase, starting at about two-week intervals. Amounts of water recovered gradually diminished, and the last substantial samples

were collected about six months into the cooling phase. Sampling attempts continued on an irregular schedule every few months.

A series of boreholes were equipped with two types of fluid sampling systems. First, ten boreholes were instrumented with FLUTE (Flexible Liner Underground Technologies, Ltd.) liners designed specifically for sampling water and gas for chemical analyses (liners installed for the different thermal field tests were manufactured by both SEAMIST and by FLUTE; although FLUTE provided all of the liners used in the DST, in some documents they continued to be referred to as SEAMIST liners: e.g., in Section 5.1.4 of CRWMS M&O 1998 [DIRS 111115]). These are the chemistry boreholes, ESF-HD-CHE-(1 through 10) (or boreholes 52 to 56 and 69 to 73, as shown in Figure 6.3-7). Second, boreholes instrumented with inflatable packer strings were designed with air permeability testing as the primary function (see Section 6.3.2.4). Observations during the SHT (see Section 6.2.4.1) demonstrated how the system could be effectively implemented in fluid sampling. These are the hydrology boreholes, ESF-HD-HYD-1 through -12 (or boreholes 57 to 61, 74 to 78, 185 and 186, as shown in Figure 6.3-4).

Both the chemistry and the hydrology boreholes were expected to provide opportunities for water collection throughout thermal testing. The chemistry boreholes, with proper spacing of high absorbency pads, would yield appropriate spatial and temporal coverage of geochemical data even with small volumes of water. The hydrology boreholes, with inflated packers that straddle highly fractured regions of rock, would potentially accumulate water as moisture entered along the 5 to 10 m of opening. Generally, although both systems employed proven technology, the high temperatures of the DST would place somewhat unusual requirements on materials used for their construction.

For the FLUTE liners, a high-temperature silicone rubber was selected to ensure flexibility and durability for the often-repeated liner installation and retrieval processes. Unfortunately, the liners themselves never performed to expectations, either under the thermal load of the DST or with sufficient strength to survive repeated manipulations against the irregular and sharp features of the borehole walls. For the inflatable packers, two high-temperature rubbers were selected. Within the cooler regions of rock, a neoprene rubber was employed, and in the hottest boreholes, a fluorocarbon rubber was employed. Both proved to be mechanically sound, but not chemically inert in the hotter boreholes. In this section, the geochemistry of water samples that have been collected in the DST will be discussed. Attempts to salvage the installed liner systems of the chemistry boreholes were unsuccessful. Consequently, the aqueous sampling role of the hydrology boreholes has been critical, and the analyses of waters collected from them form the aqueous geochemistry database of the DST.

The field-measurement data for the heating phase are contained in the following DTNs:

- MO0207AL5WATER.001 [DIRS 159300]
- MO0101SEPFDDST.000 [DIRS 153711]
- SN0203F3903102.001 [DIRS 159133].

Field-measurement data for the cooling phase, including documentation of non-collection of water, are contained in the following DTNs:

- SN0210F3903102.004 [DIRS 170573]
- SN0211F3903102.005 [DIRS 170574]
- SN0303F3903102.006 [DIRS 178034]
- SN0311F3903102.007 [DIRS 178035]
- SN0411F3903102.009 [DIRS 178036]
- SN0507F3903102.010 [DIRS 178037]
- SN0510F3903102.012 [DIRS 178038]
- SN0511F3903102.013 [DIRS 178039].

Analytical data acquired by Inductively Coupled Plasma (ICP) and Atomic Emission Spectroscopy (AES) and Ion Chromatography (IC) for metals and anions respectively are performed under the control of the technical implementation procedures: TIP-AC-02 for metal concentrations and TIP-AC-03 for anion analyses. The standard metals suite includes Al, B, Ca, Fe, K, Li, Mg, Na, S, Si, and Sr; trace metals analyses are available upon request. The standard anion suite includes F, Cl, Br, NO<sub>2</sub>, NO<sub>3</sub>, PO<sub>4</sub>, and SO<sub>4</sub>. The analytical results are in the TDMS identified with data in the following DTNs:

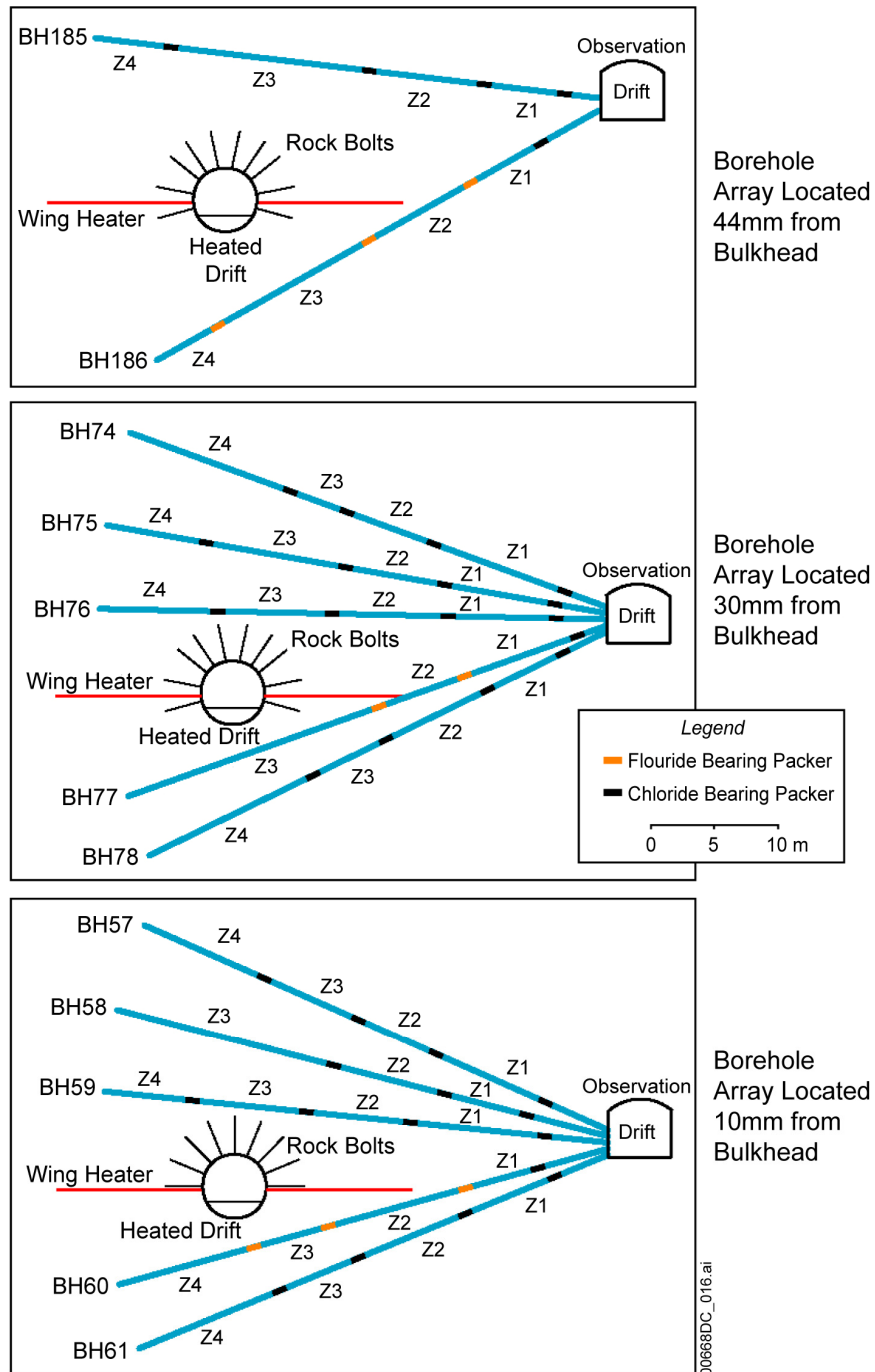
- MO0005PORWATER.000 [DIRS 150930]
- LL001100931031.008 [DIRS 153288]
- LL001200231031.009 [DIRS 153616]
- LL020302223142.015 [DIRS 159134]
- LL021107623121.014 [DIRS 169257]
- LL030107523142.031 [DIRS 169258]
- LL990702804244.100 [DIRS 144922].

Note that DTNs: LL001200231031.009, LL030107523142.031, and LL990702804244.100 are unqualified and should only be used for corroborative purposes.

#### **6.3.4.1.1 Sampling Procedures**

This section discusses water sampling in the hydrology boreholes. The 12 hydrology boreholes instrumented with strings of inflatable packers were located in three arrays (Figure 6.3-44). When inflated, the packers formed isolated open intervals that are referred to as test zones. Test zone 1 for a given borehole is defined to be the interval between the packer closest to the observation drift, and the next closest packer. All the zones are numbered sequentially, with the deepest zone (zone 3 or 4) defined by the deepest packer and the borehole bottom. To implement the packer system as a water collection device in the DST, the air injection lines used in the air permeability testing become the sampling tubes to pump water out into the observation drift. The air injection tubing opens to the lowest elevation of each zone. If fluids enter the zone by fracture flow, they would potentially drain to the bottom, where access to the tube opening would be possible. The provisions for water capture and retention, however, would be somewhat dubious, since the boreholes would be expected to act as capillary barriers to liquid flow. Nevertheless, experience in the SHT demonstrated that fluid would enter into some of the

intervals, collect in the lowest end, and remain until pumping could be conducted. Water samples obtained from these zones were potentially derived from the entire open interval, a length of approximately 5 to 10 m.



Source: DTNs: MO0002ABBLSLDS.000 [DIRS 147304]; SN0208F3903102.002 [DIRS 161246].

Figure 6.3-44. Three Arrays of DST Hydrology Boreholes Showing Relative Packer Positions and Fluid Sampling Zones



Water sampling was conducted by peristaltic pumping of individual zones on a regular and on an as-needed basis. In addition, a couple of opportunities to collect DST borehole waters presented themselves to other thermal test personnel; water samples collected opportunistically were done so without the benefit of standard sampling instrumentation, analytical field testing, and field preservation. These miscellaneous waters are not represented in Figure 6.3-44 or in the compilation of field data to follow. During water sampling activities, all zones were pumped for at least five minutes. Thus, zones that may have been well above the boiling temperature, approximately 96°C, were pumped along with lower temperature zones. In these boreholes, heated water vapor that was pumped through the sample tubing condensed as it was pulled away from the hot sampled area to the cooler vicinity of the observation drift. The condensed water vapor was then collected in the field as a sample of water. Water sampling from boreholes in the relatively dry host rock of the DST precluded practices that are common to sampling in saturated formations from an essentially unlimited water supply. Water volumes typically collected from a borehole zone were approximately 100 to 1,500 mL. As a consequence, conservation measures were generally followed to maximize the information that may be gained from analytical tests. To collect water from individual zones in the hydrology boreholes, a peristaltic pump located in the observation drift was connected to an air-injection line through a manifold located outside each borehole array. Before sampling a zone, the peristaltic pump was prepared with clean sample tubing for the intake and the output lines, or the installed tubing might be thoroughly flushed with de-ionized water. Pumping was initiated once the hoses from the pump to the manifold and from the pump to the collection vessel were in place. An optional vacuum gauge might be inserted into the intake line to indicate whether the air injection line from the borehole was submersed in water or was open.

The collected samples were designated for field testing and various analytical suites. Samples designated for analyses were prioritized based on acquired sample volumes. Field testing included temperature and temperature-dependent measurements of pH, total dissolved solids (TDS), and electrical conductivity (EC). When a sufficient sample was available, an alkalinity titration could be performed. From the measured alkalinity, the sample's carbonate, bicarbonate, and hydroxide concentrations could be calculated. Samples designated for laboratory analysis were filtered in the field ( $\leq 0.45 \mu\text{m}$ ), collected into certifiably clean sample bottles, and preserved. The samples to be collected for analysis included: (1) a metals sample filtered into a polyethylene bottle and acidified to  $\text{pH} \leq 2$  using Ultrapure nitric acid; (2) an anion sample filtered, collected in a polyethylene bottle, and preserved in cold storage; (3) isotope samples for Sr and U analyses filtered into plastic bottles and acidified to  $\text{pH} < 2$  using Ultrapure nitric acid; and (4) stable-isotopes sample (carbon, hydrogen, and oxygen), filtered and collected in glass sample bottles.

#### **6.3.4.1.2 Results: Aqueous Chemistry**

##### *Field Measurements and Observations*

Aqueous samples collected for chemical analyses have been acquired from several hydrology boreholes during the four years of heating. The first samples were collected six months after heating began, with subsequent sampling activities about every two to three months (more or less frequently as indicated). A summary of the water samples, the field data, and important observations for samples collected up to December 31, 2005, is presented in Table 6.3-24.

Samples are reported and tracked by the Sample Management Facility (SMF) code assigned in the field (an 8-digit number, generally preceded by “SPC”). The borehole numbers used in Table 6.3-24 are the sequentially numbered DST boreholes (Figure 6.3-4).

Each row in Table 6.3-24 is a tabulation of relevant information recorded for a single sample. The information may include collection date, start and stop pumping times, total approximate volume, location by borehole number and zone (BH#-zone), field data, sample number (SMF ID), sample temperature (measured in the field at time of collection), and comments and observations. The information represented derives from different personnel (with varying degrees of experience), different field test equipment, and differences in working instrumentation and supplies. The table does not present sampling efforts in which no water was collected.

In Table 6.3-24, temperature entries represent those values measured in the field during sampling and do not represent the in situ borehole temperatures (which are recorded by the DST DCS). Furthermore, the temperature-dependent field properties, (i.e., pH, TDS, and EC) were determined for the measured temperature reported. A multiparameter field test meter measures and automatically compensates for temperature, using the known thermal sensitivity of the glass electrode. The pumping start and stop times are included whenever the information was noted. The stated pumping times by themselves are not important, but, together with the estimated volume, they give an approximate sample flow rate. It has been observed that zones with accumulated water exhibited generally higher flow rates than ones that, for example, were produced by steam condensing in the sampling line. Note, finally, that some CO<sub>2</sub> degassing and exchange with the ambient drift atmosphere occurred during sample pumping and sampling, potentially affecting the pH and the alkalinity in the samples relative to the in situ values. Although alkalinity is a field measurement, it is incorporated with the table of analytical results that follow. Measured alkalinity was an important addition incorporated in the revised sampling procedure, but the titration requires approximately 100 mL of sample. Consequently, for zones that produce low water volumes, alkalinity is not generally measured because of insufficient sample volumes.

Finally, in reviewing Table 6.3-24, an attempt to interpret the *lack* of water from different borehole zones, as suggested by gaps in the data, should be avoided. Field personnel generally allowed several minutes pumping time from each interval. However, the fact that no water was acquired does not necessarily indicate a dry zone; it may also reflect a failed packer seal (see Table 6.3-10 for a list of failed packers), clogged sampling tube, or inadequate pump pressure.

Table 6.3-24. Summary of DST Water Samples, Field Data, and Observations through December 31, 2005

Date	Approx. Start Time	Approx. Finish Time	Estimated Volume (mL)	Collection Hole/Zone	pH	Electrical Conductivity (mS/cm)	Total Dissolved Solids (ppm)	Sample Number	Solution Temperature (°C)	Comments
06/04/98	9:30	—	500	60/2	7.5	—	—	SPC00527968	—	Anion
06/04/98	9:30	—	500	60/2	7.5	—	—	SPC00527969	—	Metals
06/04/98	9:30	—	500	60/2	7.5	—	—	SPC00527970	—	O, H, and C
06/04/98	9:30	—	500	60/2	7.5	—	—	SPC00527971	—	Tritium
06/04/98	9:30	—	500	60/2	7.5	—	—	SPC00527972	—	U, Sr
06/04/98	9:30	—	500	60/2	7.5	—	—	SPC00527973	—	U, Sr
06/04/98	9:30	—	500	60/2	7.5	—	—	SPC00527974	—	<sup>36</sup> Cl
06/04/98	9:30	—	2200	60/2	7.5	—	—	SPC00527975	—	Surplus H <sub>2</sub> O
06/04/98	10:45	—	250	60/3	7.7	—	—	SPC00527977	—	—
08/12/98	8:23	8:50	125	60/2	6.9	—	—	SPC00527915	—	—
08/12/98	8:51	9:10	900	60/3	6.8	—	—	SPC00527916	—	—
08/12/98	9:49	10:07	200	77/3	5.5	—	—	SPC00527917	—	—
11/12/98	9:53	10:04	100	59/4	6.6	—	—	SPC00541803	25	Color noted as yellow by lab report.
11/12/98	10:22	11:42	4000	60/3	6.9	—	—	SPC00541804	26.5 to 49.6	—
11/12/98	13:37	14:04	3000	186/3	6.8	—	—	SPC00541805	34.3 to 35.1	—
01/26/99	10:20	10:29	25	59/4	—	—	—	SPC00504397	—	Not filtered
01/26/99	9:11	9:14	2000	60/3	7.36 to 7.44	—	140 to 141	SPC00504396	52	Estimated 3.5 L pumped, not filtered
01/26/99	11:33	11:50	800	186/3	7.24 to 7.17	—	320	SPC00527961	—	Not filtered
03/30/99	9:50	10:10	700	60/3	8.0	—	—	SPC00529637	—	—
03/30/99	12:40	—	200	77/3	7.0	—	—	SPC00529634	31	—
04/20/99	9:00	9:32	175	60/3	4.19 to 4.50	—	30	SPC00551100	32 to 41	—
04/20/99	12:00	13:45	500	60/3	4.8	—	10	SPC00551103	40	—
04/20/99	9:15	10:07	375	BH 80	6.39 to 6.72	—	30-50	SPC00551102	64	—

Table 6.3-24. Summary of DST Water Samples, the Field Data, and Important Observations through December 31, 2005 (Continued)

Date	Approx. Start Time	Approx. Finish Time	Estimated Volume (mL)	Collection Hole/Zone	pH	Electrical Conductivity (mS/cm)	Total Dissolved Solids (ppm)	Sample Number	Solution Temperature (°C)	Comments
05/10/99	10:20	—	40*	60/3	4.78 to 4.80	12.4	7.98	SPC00551104	21.1 to 24.0*	—
05/10/99	10:24	—	40*	60/3	4.68	11.37	7.09	SPC00551105	34.8 to 36.3*	—
05/10/99	10:10	10:29	175*	60/3	4.68 to 4.80*	—	—	SPC00551106	21.1 to 36.3*	100 mL used for alkalinity.
05/10/99	11:04	—	40*	60/3	4.84	8.72 / 9.67	5.38 / 6.01	SPC00551107	35.3 to 41.3*	Conductivity and TDS represent pre- / post-filtration.
05/25/99	9:40	—	40*	60/3	4.75	11.74	7.43	SPC00551111	26.4 to 27.3*	—
05/25/99	9:23	—	40*	60/3	4.68	16.07	10.18	SPC00551110	24.1 to 25.6*	—
05/25/99	9:10	9:50	150*	60/3	4.68 to 4.75*	—	—	SPC00551151	24.1 to 27.3*	100 mL used for alkalinity.
05/25/99	10:04	—	40*	60/3	4.75	9.37	5.92	SPC00551112	24.8*	—
06/24/99	9:17	—	40*	60/3	5.02	8.84	—	SPC00551154	27.5*	—
06/24/99	9:25	9:55	170*	60/3	5.08*	—	—	SPC00551157	28.9*	100 mL used for alkalinity.
06/24/99	9:25	9:27	40*	60/3	5.08	—	—	SPC00551156	28.9*	—
10/27/99	12:54	—	150*	59/2	5.93	113.4	—	SPC00557028*	43.4*	—
10/27/99	13:03	—	50*	59/2	6.08	110.2	—	SPC00557029*	52*	—
10/27/99	13:27	—	250*	59/3	6.64	203.1	—	SPC00557035*	60.2*	—
10/27/99	13:45	—	40*	59/3	6.81	192.3	118.1	SPC00557036*	62.3*	—
10/27/99	14:27	—	50*	76/3	6.14 to 6.46	—	—	SPC00557039*	28.7*	—
11/30/99	10:21	—	50*	59/2	7.53	80.8	52.84	SPC00557082*	39.5*	—
11/30/99	10:24	—	150*	59/2	7.24	69.14	43.9	SPC00557080*	46.6*	—
11/30/99	10:30	—	—	59/2	6.8	67.04	42.3	—	—	—
11/30/99	10:38	—	40*	59/2	—	70.3	44.36	SPC00557083*	55.9*	—
11/30/99	10:47	—	50*	59/3	7.06	105.2	65.86	SPC00557042*	47.3*	—

Table 6.3-24. Summary of DST Water Samples, the Field Data, and Important Observations through December 31, 2005 (Continued)

Date	Approx. Start Time	Approx. Finish Time	Estimated Volume (mL)	Collection Hole/Zone	pH	Electrical Conductivity (mS/cm)	Total Dissolved Solids (ppm)	Sample Number	Solution Temperature (°C)	Comments
11/30/99	10:50	—	150*	59/3	7.27	106.8	65.4	SPC00552575*	60*	—
11/30/99	10:55	—	40*	59/3	7.47	112	63.8	SPC00557043*	68.4*	—
11/30/99	11:59	—	50*	76/3	7.04	307.2	198.6	SPC00552577*	37.7*	—
11/30/99	12:03	—	150*	76/3	6.91	312.3	201.3	SPC00557085*	48.9*	—
11/30/99	12:10	—	125*	76/3	6.86	317.7	199.4	SPC00552576*	57.9*	—
11/30/99	12:20	—	40*	76/3	6.94	326.2*	207.3	SPC00552579*	53.2*	—
11/30/99	13:10	—	50*	77/3	4.68	156.4	9.99	SPC00557084*	45.2*	Reported conductivity and TDS values are suspect.
01/25/00	9:30	—	150*	59/2	7.43	104.7	67.1	SPC00550668*	27.1*	—
01/25/00	9:33	—	150*	59/2	7.07	62.03	39.35	SPC00550669*	38.5*	—
01/25/00	9:36	—	150*	59/2	6.85	63.01	39.31	SPC00550671*	51.5*	—
01/25/00	9:45	—	—	59/2	6.68	61.21	37.89	—	57.5*	—
01/25/00	11:35	—	50*	77/2	4.63	61.24	40.24	SPC00550672*	37*	—
01/25/00	12:00	—	50*	77/3	3.47	224.9	145.5	SPC00550674*	36.8*	—
05/23/00	11:58	—	150*	59/2	6.96	96.13	61.27	SPC00550680*	30.5*	—
05/23/00	12:00	—	150*	59/2	6.95	98.55	61.91	SPC00550682*	42.6*	—
05/23/00	12:15	—	—	59/2	6.96	99.73	61.76	—	60.4*	—
05/23/00	12:26	—	120*	59/3	5.19	5.2	3.14	SPC00550687*	46.4*	—
05/23/00	9:11	—	160*	76/3	6.92 to 6.96	134.8	86.86	SPC00550697*	21-40.8*	—
06/29/00	11:20	—	—	59/2	6.81 to 6.92	100.3	62.73	—	47.2*	—
06/29/00	11:24	—	—	59/2	7	111.7	68.4	—	58.4*	—
06/29/00	11:27	—	—	59/2	6.99 to 7.08	79.9	49.12	—	50.9*	—
06/29/00	11:45	—	—	59/3	5.39	4.39	2.74	—	40.4*	—
06/29/00	11:50	—	—	59/3	5.6	4.7	2.91	—	45.9*	—
06/29/00	12:00	—	—	59/4	4.6	13.72	8.48	—	50.2*	—

Table 6.3-24. Summary of DST Water Samples, the Field Data, and Important Observations through December 31, 2005 (Continued)

Date	Approx. Start Time	Approx. Finish Time	Estimated Volume (mL)	Collection Hole/Zone	pH	Electrical Conductivity (mS/cm)	Total Dissolved Solids (ppm)	Sample Number	Solution Temperature (°C)	Comments
06/29/00	12:03	—	—	59/4	4.74	14.83	9.21	—	49.2*	—
06/29/00	9:35	—	—	76/3	5.75	13.81	8.64	—	35.8*	—
06/29/00	9:46	—	—	76/4	4.74 to 4.77	12.85	7.99	—	34.4*	—
06/29/00	10:10	—	—	78/2	4.12	35.64	20.44	—	32.8*	—
06/29/00	10:18	—	—	78/3	4.22	28.54	17.78	—	42.1*	—
08/21/00	10:46	10:52	20*	76/3	6.27 to 5.04	—	—	—	—	—
08/21/00	10:52	11:02	15*	76/4	5.01 to 4.99	—	—	—	—	—
08/21/00	11:03	11:10	10*	78/3	5.05 to 5.21	—	—	—	—	—
01/23/01	12:00	12:03	100*	59/2	—	—	—	SPC00530399*	—	Ultrameter problem, no pH, TDS
01/23/01	12:00	12:03	100*	59/2	—	—	—	SPC00529636*	—	Ultrameter problem, no pH, TDS
01/23/01	12:00	12:03	100*	59/2	—	—	—	SPC00529635*	—	Ultrameter problem, no pH, TDS
01/23/01	12:00	12:03	90*	59/2	—	—	—	SPC00530398*	—	Ultrameter problem, no pH, TDS
01/23/01	12:13	12:15	60*	59/3	—	—	—	SPC00530316*	—	Ultrameter problem, no pH, TDS
01/23/01	12:13	12:15	60*	59/3	—	—	—	SPC00530314*	—	Ultrameter problem, no pH, TDS
01/23/01	12:13	12:15	60*	59/3	—	—	—	SPC00530313*	—	Ultrameter problem, no pH, TDS
01/23/01	12:13	12:15	60*	59/3	—	—	—	SPC00530397*	—	Ultrameter problem, no pH, TDS
01/23/01	12:30	12:35	30*	60/4	—	—	—	SPC00530318*	—	Ultrameter problem, no pH, TDS
04/17/01	10:10	10:25	120	59/2	4.9	6.6	10.4	SPC00559467	32	Preserved with HNO <sub>3</sub>

Table 6.3-24. Summary of DST Water Samples, the Field Data, and Important Observations through December 31, 2005 (Continued)

Date	Approx. Start Time	Approx. Finish Time	Estimated Volume (mL)	Collection Hole/Zone	pH	Electrical Conductivity (mS/cm)	Total Dissolved Solids (ppm)	Sample Number	Solution Temperature (°C)	Comments
04/17/01	10:10	10:25	100	59/2	5.3	6.7	4.2	SPC00559468	35	Preserved with HNO <sub>3</sub>
04/17/01	10:40	10:50	200	59/3	6.0	54.2	34.7	SPC00559463	30	Preserved with HNO <sub>3</sub>
04/17/01	10:40	10:50	100	59/3	5.8	30.6	19.0	SPC00559465	38	Preserved with HNO <sub>3</sub>
04/17/01	11:15	11:30	200	59/4	5.2	9.8	6.1	SPC00559466	33	Preserved with HNO <sub>3</sub>
04/17/01	12:40	12:45	200	76/2	5.7	40.1	25.8	SPC00559460	29	—
04/17/01	12:45	12:50	500	76/2	7.7	41.5	25.8	SPC00559464	43	Preserved with HNO <sub>3</sub>
04/17/01	12:50	12:55	500	76/2	7.9	40.2	24.8	SPC00559461	48	—
04/17/01	12:55	13:00	500	76/2	8.1	38.9	24.7	SPC00559462	33	—
04/17/01	13:00	13:09	500	76/2	8.2	38.4	24.4	SPC00559459	29	—
04/17/01	13:09	13:20	250	76/2	8.2	37.8	24.1	SPC00559458	30	—
04/17/01	13:20	13:25	120	76/2	8.3	33.5	22.5	SPC00559456	33	—
04/17/01	13:25	13:33	120	76/2	8.3	37.3	24.0	SPC00559457	31	—
06/26/01	—	—	10	76/3	5.3	—	3.7	—	32	—
06/26/01	11:40	11:55	80	76/4	5.5	11.2	6.7	SPC00559493	42	—
06/26/01	12:10	12:20	25	78/2	5.3	5.2	3.2	SPC00559494	44	—
06/26/01	12:25	12:35	25	78/3	5.0	5.2	3.4	SPC00559495	47	—
06/26/01	12:40	12:50	25	78/4	5.0	6.7	4.0	SPC00559496	44	—
06/27/01	10:40	10:50	240	59/2	5.2	6.1	3.6	SPC00559497	57	Preserved with HNO <sub>3</sub>
06/27/01	10:50	11:25	500	59/2	5.1	4.5	2.6	SPC00559498	58	—
06/27/01	11:25	12:10	500	59/2	5.2	4.2	2.5	SPC00559499	56	—
06/27/01	12:10	12:40	100	59/2	5.6	6.4	3.8	SPC00559471	49	—
06/27/01	12:40	13:15	500	59/2	5.1	4.6	2.7	SPC00559472	54	—
06/27/01	13:15	13:35	25	59/2	5.5	4.5	3.1	SPC00559473	48	—
06/27/01	13:35	14:20	500	59/2	5.2	4	2.4	SPC00559474	42	—
06/28/01	12:30	12:50	100	59/3	4.9	8.3	5.1	SPC00559476	44	—
06/28/01	9:20	12:00	400	BH 72	4.8	14.6	8.9	SPC00559475	55	Using flex-tubing and rods
06/28/01	13:30	13:50	40	60/3	3.3	189	115.0	SPC00559477	35	—

Table 6.3-24. Summary of DST Water Samples, the Field Data, and Important Observations through December 31, 2005 (Continued)

Date	Approx. Start Time	Approx. Finish Time	Estimated Volume (mL)	Collection Hole/Zone	pH	Electrical Conductivity (mS/cm)	Total Dissolved Solids (ppm)	Sample Number	Solution Temperature (°C)	Comments
06/28/01	13:55	14:05	10	60/4	5.1	10.5	8.8	—	39	—
08/07/01	—	—	5	76/3	5.2	4.1	2.5	—	48	—
08/07/01	11:55	12:05	60	76/4	5.4	7.8	4.7	SPC00559454	61	—
08/07/01	11:55	12:05	15	76/4	5.4	7.8	4.7	SPC00575214	61	—
08/07/01	12:15	12:25	100	77/2	3.3	284	173.0	SPC00559455	61	—
08/07/01	12:15	12:25	15	77/2	3.3	284	173.0	SPC00575218	61	—
08/07/01	12:35	12:45	60	77/3	3.3	231	138.0	SPC00559484	60	—
08/07/01	12:35	12:45	15	77/3	3.3	231	138.0	SPC00575213	60	—
08/07/01	12:55	13:05	30	78/2	4.5	8.8	5.2	SPC00559485	47	—
08/07/01	—	—	5	78/3	5.2	9.1	5.6	—	40	—
08/07/01	—	—	10	78/4	5.5	14.3	8.8	—	38	—
08/08/01	10:30	10:50	500	59/2	5.4	2.2	1.3	SPC00559486	38	—
08/08/01	10:30	10:50	15	59/2	5.4	2.2	1.3	SPC00575215	38	—
08/08/01	11:00	11:40	200	59/3	4.9	6	3.6	SPC00559487	58	—
08/08/01	11:00	11:40	15	59/3	4.9	6	3.6	SPC00575212	58	—
08/08/01	11:50	12:05	200	59/4	5.1	2.8	1.6	SPC00559488	51	—
08/08/01	11:50	12:05	15	59/4	5.1	2.8	1.6	SPC00575217	51	—
08/08/01	—	—	5	60/1	4.8	25	15.0	—	35	—
08/08/01	12:20	12:35	100	60/2	3.1	309	194.0	SPC00559490	52	—
08/08/01	12:20	12:35	15	60/2	3.1	309	194.0	SPC00575216	52	—
08/08/01	13:30	13:50	15	60/3	3.4	186	114.0	SPC00559491	56	—
08/08/01	13:55	14:05	10	60/4	4.4	14.5	8.8	—	41	—
10/22/01	10:30	10:40	50	76/3	5.2	8.4	5.1	SPC00575220	42	—
10/22/01	10:45	10:55	30	76/4	5.1	5.2	3.0	SPC00575222	62	—
10/22/01	11:05	11:15	100	77/2	3.1	403	245.0	SPC00575226	53	—
10/22/01	11:20	11:30	30	77/3	3.2	344	208.0	SPC00575223	58	—
10/22/01	—	—	5	78/1	4.2	11.6	6.9	—	57	—
10/22/01	—	—	5	78/2	4.8	5.6	3.3	—	52	—



Table 6.3-24. Summary of DST Water Samples, the Field Data, and Important Observations through December 31, 2005 (Continued)

Date	Approx. Start Time	Approx. Finish Time	Estimated Volume (mL)	Collection Hole/Zone	pH	Electrical Conductivity (mS/cm)	Total Dissolved Solids (ppm)	Sample Number	Solution Temperature (°C)	Comments
10/22/01	—	—	10	78/3	5.0	7.7	4.5	—	59	—
10/22/01	—	—	10	78/4	5.4	10	6.0	—	53	—
10/22/01	10:30	10:50	100	59/2	4.9	8.5	5.2	SPC00575227	52	—
10/22/01	—	—	10	59/3	5.0	5.2	3.0	—	57	—
10/22/01	—	—	10	59/4	4.9	6	3.5	—	61	—
10/22/01	12:50	13:00	80	60/2	3.2	406	252.0	SPC00575225	56	—
10/22/01	13:10	13:20	30	60/3	3.5	151	90.0	SPC00575221	56	—
10/22/01	13:25	13:35	40	60/4	3.8	63	38.0	SPC00575224	49	—
10/22/01	—	—	5	61/1	4.4	14.6	8.7	—	51	—
10/22/01	—	—	10	61/3	4.9	7.9	4.8	—	45	—
10/22/01	—	—	10	61/4	5.0	7.1	4.3	—	52	—
11/08/01	14:45	15:10	50	BH 72	5.1	20.0	12.5	SPC00575228	28	HF experiment
11/08/01	—	—	—	BH 72	5.5	17.5	10.8	—	27	HF experiment
11/15/01	11:00	12:15	20	BH 55	7.5	279.0	176.0	SPC00575231	23	HF experiment
11/21/01	—	—	100	—	—	—	—	SPC00559482	—	HF experiment, rinse of flex tubing
11/21/01	—	—	4	BH 55	—	—	—	SPC00559483	—	HF experiment, not filtered
11/26/01	9:50	10:30	100	BH 72	5.3	13.8	8.6	SPC00575219	25	HF experiment
11/26/01	13:10	15:10	20	BH 55	5.0	20.5	12.8	SPC00575229	24	HF experiment
11/29/01	10:30	11:00	100	BH 72	3.8	39.7	24.3	SPC00559478	39	HF experiment
11/29/01	10:30	11:00	—	BH 72	3.8	41.4	25.3	—	40	HF experiment
11/29/01	11:30	14:30	13	BH 55	5.2	—	—	SPC00559479	—	HF experiment
12/05/01	12:00	13:00	200	BH 72	3.5	111.5	70.6	SPC01016065	21	HF experiment
12/05/01	12:00	13:00	—	BH 72	3.4	167.3	106.0	—	32	HF experiment
12/05/01	12:00	13:00	500	BH 72	3.4	135.0	85.4	SPC01016066	20	HF experiment
12/05/01	11:00	15:10	10	BH 55	—	—	—	SPC01016067	—	HF experiment
01/07/02	—	—	2	BH 55	—	—	—	SPC01016084	—	HF experiment
01/07/02	11:30	11:40	500	76/2	7.8	30.2	18.0	SPC01016082	52	—

Table 6.3-24. Summary of DST Water Samples, the Field Data, and Important Observations through December 31, 2005 (Continued)

Date	Approx. Start Time	Approx. Finish Time	Estimated Volume (mL)	Collection Hole/Zone	pH	Electrical Conductivity (mS/cm)	Total Dissolved Solids (ppm)	Sample Number	Solution Temperature (°C)	Comments
01/07/02	11:30	11:40	15	76/2	7.8	30.2	18.0	SPC01014151	52	—
01/07/02	11:40	11:50	50	76/3	4.9	7.3	4.3	SPC01016076	56	—
01/07/02	11:40	11:50	15	76/3	4.9	7.3	4.3	SPC01014154	56	—
01/07/02	11:50	12:00	30	76/4	4.8	5.5	3.2	SPC01016074	55	—
01/07/02	11:50	12:00	15	76/4	4.8	5.5	3.2	SPC01016071	55	—
01/07/02	12:15	12:25	30	78/2	5.1	4.9	2.9	SPC01016075	44	—
01/07/02	12:15	12:25	15	78/2	5.1	4.9	2.9	SPC01016070	44	—
01/07/02	12:25	12:35	30	78/3	4.9	5.1	3.1	SPC01016078	43	—
01/07/02	12:25	12:35	15	78/3	4.9	5.1	3.1	SPC01014147	43	—
01/07/02	12:40	12:50	40	78/4	4.9	5.4	3.2	SPC01016072	40	—
01/07/02	12:40	12:50	15	78/4	4.9	5.4	3.2	SPC01014149	40	—
01/07/02	13:05	13:20	400	59/2	5.2	3.3	2.0	SPC01016083	30	—
01/07/02	13:05	13:20	15	59/2	5.2	3.3	2.0	SPC01014150	30	—
01/07/02	13:20	13:35	250	59/3	5.3	2	1.2	SPC01016079	34	—
01/07/02	13:20	13:35	15	59/3	5.3	2	1.2	SPC01014153	34	—
01/07/02	13:40	13:50	40	59/4	4.8	5.7	3.5	SPC01016073	35	—
01/07/02	13:40	13:50	15	59/4	4.8	5.7	3.5	SPC01014152	35	—
01/07/02	14:00	14:10	50	61/2	5.5	6.5	4.0	SPC01016081	32	—
01/07/02	14:00	14:10	15	61/2	5.5	6.5	4.0	SPC01014148	32	—
01/07/02	14:15	14:25	40	61/3	5.2	4.8	2.9	SPC01016080	28	—
01/07/02	14:15	14:25	15	61/3	5.2	4.8	2.9	SPC01016068	28	—
01/07/02	14:30	14:40	50	61/4	5.1	7.7	4.5	SPC01016077	33	—
01/07/02	14:30	14:40	15	61/4	5.1	7.7	4.5	SPC01016069	33	—
01/09/02	9:30	9:50	120	77/2	3.7	49.8	30.6	SPC01014156	41	—
01/09/02	9:30	9:50	15	77/2	3.7	49.8	30.6	SPC01014159	41	—
01/09/02	10:00	10:20	100	77/3	3.4	176	106.0	SPC01014155	54	—
01/09/02	10:00	10:20	15	77/3	3.4	176	106.0	SPC01014158	54	—

Table 6.3-24. Summary of DST Water Samples, the Field Data, and Important Observations through December 31, 2005 (Continued)

Date	Approx. Start Time	Approx. Finish Time	Estimated Volume (mL)	Collection Hole/Zone	pH	Electrical Conductivity (mS/cm)	Total Dissolved Solids (ppm)	Sample Number	Solution Temperature (°C)	Comments
01/09/02	10:20	10:50	150	BH 72	3.3	85.8	54.9	SPC01014157	16	HF experiment. Field analysis done on 1/16/02.
01/09/02	10:20	10:50	15	BH 72	3.3	85.8	54.9	SPC01014160	16	HF experiment. Field analysis done on 1/16/02.
01/16/02	11:20	11:40	500	76/2	8.3	35.3	22	SPC01015559	37	—
01/16/02	11:20	11:40	30	76/2	8.3	35.3	22	SPC01015560	37	—
01/16/02	11:20	11:30	60	76/3	5.2	9.3	5.7	SPC01015558	29.2	—
01/16/02	11:20	11:30	30	76/3	5.2	9.3	5.7	SPC01015566	29.2	—
01/16/02	11:40	11:50	60	76/4	5.2	4.2	2.6	SPC01015551	23	—
01/16/02	11:40	11:50	30	76/4	5.2	4.2	2.6	SPC01015565	23	—
01/16/02	11:50	12:00	60	77/2	3.8	34.2	21.4	SPC01015555	26	—
01/16/02	11:50	12:00	30	77/2	3.8	34.2	21.4	SPC01015561	26	—
01/16/02	12:05	12:15	60	77/3	3.5	181	112	SPC01015553	41	—
01/16/02	12:05	12:15	30	77/3	3.5	181	112	SPC01015562	41	—
01/16/02	12:15	12:25	60	78/2	4.9	6.5	4.0	SPC01015549	26	—
01/16/02	12:15	12:25	30	78/2	4.9	6.5	4.0	SPC01015569	26	—
01/16/02	12:25	12:35	60	78/3	4.9	7.2	4.4	SPC01015556	23	—
01/16/02	12:25	12:35	30	78/3	4.9	7.2	4.4	SPC01015568	23	—
01/16/02	12:35	12:45	60	78/4	4.9	6.6	4.0	SPC01015557	37	—
01/16/02	12:35	12:45	30	78/4	4.9	6.6	4.0	SPC01015570	37	—
01/16/02	13:20	13:30	60	59/3	5.0	7.7	4.6	SPC01015550	55	—
01/16/02	13:20	13:30	30	59/3	5.0	7.7	4.6	SPC01015564	55	—
01/16/02	13:30	13:40	60	59/4	5.1	4.7	2.8	SPC01015554	53	—
01/16/02	13:30	13:40	30	59/4	5.1	4.7	2.8	SPC01015563	53	—
01/16/02	14:00	14:20	60	61/4	4.9	9.4	5.8	SPC01015552	27	—
01/16/02	14:00	14:20	30	61/4	4.9	9.4	5.8	SPC01015567	27	—
01/23/02	10:00	10:10	30	75/3	4.4	14.5	9.1	SPC01015580	18	—

Table 6.3-24. Summary of DST Water Samples, the Field Data, and Important Observations through December 31, 2005 (Continued)

Date	Approx. Start Time	Approx. Finish Time	Estimated Volume (mL)	Collection Hole/Zone	pH	Electrical Conductivity (mS/cm)	Total Dissolved Solids (ppm)	Sample Number	Solution Temperature (°C)	Comments
01/23/02	10:20	10:50	1000	76/2	8.1	33.6	20.8	SPC01015588	48	—
01/23/02	10:20	10:50	250	76/2	5.9	29.2	17.2	SPC01015587	61	—
01/23/02	10:20	10:50	30	76/2	5.9	29.2	17.2	SPC01015578	61	—
01/23/02	10:25	10:35	60	76/3	4.9	7.8	4.7	SPC01015582	48	—
01/23/02	10:25	10:35	30	76/3	4.9	7.8	4.7	SPC01015573	48	—
01/23/02	10:40	10:50	60	76/4	5.0	5	2.9	SPC01015583	53	—
01/23/02	10:40	10:50	30	76/4	5.0	5	2.9	SPC01015574	53	—
01/23/02	11:00	11:10	60	77/2	4.1	43.6	26.9	SPC01015585	44	—
01/23/02	11:00	11:10	30	77/2	4.1	43.6	26.9	SPC01015576	44	—
01/23/02	11:05	11:15	60	77/3	3.6	207	130	SPC01015584	32	—
01/23/02	11:05	11:15	15	77/3	3.6	207	130	SPC01015575	32	—
01/23/02	11:20	11:30	10	78/2	5.6	9	5.7	—	17	Sample consumed doing field analyses
01/23/02	11:40	11:50	10	78/3	5.5	5.8	3.6	—	18	Sample consumed doing field analyses
01/23/02	11:45	11:55	10	78/4	5.0	5.9	3.6	—	24	Sample consumed doing field analyses
01/23/02	13:00	13:10	60	59/2	4.5	7.4	4.4	SPC01015581	50	—
01/23/02	13:00	13:10	30	59/2	4.5	7.4	4.4	SPC01015572	50	—
01/23/02	13:20	13:30	60	59/3	4.5	5.4	3.2	SPC01015579	49	—
01/23/02	13:20	13:30	30	59/3	4.5	5.4	3.2	SPC01015571	49	—
01/23/02	13:30	13:40	120	59/4	4.3	3.8	2.3	SPC01015586	49	—
01/23/02	13:30	13:40	30	59/4	4.3	3.8	2.3	SPC01015577	49	—
02/05/02	10:00	10:30	120	76/2	7.8	50.0	30.9	SPC01014169	45	—
02/05/02	10:00	10:30	120	76/2	7.8	50.0	30.9	SPC01014170	45	—
02/05/02	10:00	10:30	30	76/2	6.7	32.0	21	SPC01014179	48	—
02/05/02	10:15	10:30	60	76/3	5.0	3	1.9	SPC01014172	23	—
02/05/02	10:15	10:30	15	76/3	5.0	3	1.9	SPC01014182	23	—
02/05/02	10:40	10:55	60	76/4	5.0	2.7	1.6	SPC01014173	42	—

Table 6.3-24. Summary of DST Water Samples, the Field Data, and Important Observations through December 31, 2005 (Continued)

Date	Approx. Start Time	Approx. Finish Time	Estimated Volume (mL)	Collection Hole/Zone	pH	Electrical Conductivity (mS/cm)	Total Dissolved Solids (ppm)	Sample Number	Solution Temperature (°C)	Comments
02/05/02	13:40	13:50	60	77/2	3.9	51	32	SPC01014163	33	—
02/05/02	13:40	13:50	30	77/2	3.9	51	31	SPC01014176	33	—
02/05/02	13:45	14:00	60	77/3	3.7	138	85	SPC01014164	42	—
02/05/02	13:45	14:00	30	77/3	3.7	138	85	SPC01014177	42	—
02/05/02	11:00	11:10	60	78/2	5.1	6.5	4	SPC01014167	29	—
02/05/02	11:00	11:10	30	78/2	5.1	6.5	4	SPC01014181	29	—
02/05/02	11:05	11:15	10	78/3	4.7	6.8	4.2	—	21	Sample consumed doing field analyses
02/05/02	11:50	12:00	60	59/2	5.0	3.2	1.9	SPC01014165	38	—
02/05/02	11:50	12:00	30	59/2	5.0	3.2	1.9	SPC01014178	38	—
02/05/02	12:20	12:30	60	59/3	5.1	2.3	1.3	SPC01014168	56	—
02/05/02	12:20	12:30	30	59/3	5.1	2.3	1.3	SPC01014174	56	—
02/05/02	12:40	12:50	60	59/4	5.0	3.7	2.2	SPC01014166	43	—
02/05/02	12:40	12:50	30	59/4	5.0	3.7	2.2	SPC01014180	43	—
02/05/02	13:00	13:10	60	61/2	5.3	6.7	4.2	SPC01014171	28	—
02/05/02	13:00	13:10	30	61/2	5.3	6.7	4.2	SPC01014175	28	—
02/05/02	13:05	13:15	10	61/3	5.1	6.2	3.9	—	25	Sample consumed doing field analyses
02/05/02	13:20	13:30	60	61/4	4.9	6	3.7	SPC01014162	25	—
02/19/02	11:00	11:30	60	75/2	4.8	>994	>663	SPC01016608	25	Values exceeded calibrated range.
02/19/02	11:00	11:30	60	75/2	4.8	>994	>663	SPC01016607	25	Sample is yellow.
02/19/02	11:00	11:30	30	75/2	4.8	>994	>663	SPC01016615	25	—
02/19/02	10:50	11:10	30	76/2	4.7	6.1	4	SPC01016600	22	—
02/19/02	10:55	11:10	60	76/4	4.8	3.5	2.2	SPC01016601	24	—
02/19/02	10:55	11:10	30	76/4	4.8	3.5	2.2	SPC01016609	24	—
02/19/02	10:15	10:30	60	77/2	4.3	6.5	4.3	SPC01016605	22	—
02/19/02	10:15	10:30	30	77/2	4.3	6.5	4.3	SPC01016613	22	—
02/19/02	10:25	10:40	60	77/3	3.4	121	79.3	SPC01016606	30	—
02/19/02	10:25	10:40	30	77/3	3.4	121	79.3	SPC01016614	30	—

Table 6.3-24. Summary of DST Water Samples, the Field Data, and Important Observations through December 31, 2005 (Continued)

Date	Approx. Start Time	Approx. Finish Time	Estimated Volume (mL)	Collection Hole/Zone	pH	Electrical Conductivity (mS/cm)	Total Dissolved Solids (ppm)	Sample Number	Solution Temperature (°C)	Comments
02/19/02	12:50	13:10	120	59/2	5.0	2.9	1.8	SPC01016602	38	—
02/19/02	12:50	13:10	30	59/2	5.0	2.9	1.8	SPC01016610	38	—
02/19/02	13:20	13:30	60	59/3	5.0	2.4	1.5	SPC01016603	28	—
02/19/02	13:20	13:30	30	59/3	5.0	2.4	1.5	SPC01016611	28	—
02/19/02	13:40	13:50	60	59/4	4.7	6.1	3.9	SPC01016604	34	—
02/19/02	13:40	13:50	30	59/4	4.7	6.1	3.9	SPC01016612	34	—
03/06/02	9:35	11:15	10	72	—	—	—	SPC01016550	—	—
03/06/02	12:40	12:55	25	60	3.8	83	54.6	SPC01016552	23	At 74 feet
03/06/02	13:20	13:35	30	60	4.3	22.4	14.6	SPC01016552	23	At 132 feet
03/06/02	10:30	11:00	150	75/2	4.9	>994	>663	SPC01016554	25	Values exceeded calibrated range.
03/06/02	10:30	11:00	30	75/2	4.9	>994	>663	SPC01016555	25	Sample is yellow.
03/06/02	11:30	11:40	60	76/3	5.1	12.5	8.3	SPC01016553	20	—
03/12/02	10:20	10:30	90	75/2	4.8	>994	>663	SPC01016619	22	Values exceeded calibrated range.
03/12/02	10:20	10:30	30	75/2	4.8	>994	>663	SPC01016627	22	Sample is yellow.
03/12/02	9:10	9:20	10	76/3	4.6	7.6	4.7	—	23	Sample consumed doing field analyses
03/12/02										
03/12/02	9:25	9:40	100	76/4	4.5	9.5	5.8	SPC01016621	23	—
03/12/02	9:25	9:40	30	76/4	4.5	9.5	5.8	SPC01016628	23	—
03/12/02	8:45	9:00	60	77/2	4.1	32.3	20	SPC01016622	30	—
03/12/02	8:45	9:00	30	77/2	4.1	32.3	20	SPC01016629	30	—
03/12/02	9:05	9:20	60	77/3	3.5	109	67.6	SPC01016623	38	—
03/12/02	9:05	9:20	30	77/3	3.5	109	67.6	SPC01016630	38	—
03/12/02	9:30	9:40	10	78/2	4.7	8.7	5.5	—	22	Sample consumed doing field analyses
03/12/02	9:40	9:50	10	78/3	4.8	8.4	5.3	—	21	Sample consumed doing field analyses

Table 6.3-24. Summary of DST Water Samples, the Field Data, and Important Observations through December 31, 2005 (Continued)

Date	Approx. Start Time	Approx. Finish Time	Estimated Volume (mL)	Collection Hole/Zone	pH	Electrical Conductivity (mS/cm)	Total Dissolved Solids (ppm)	Sample Number	Solution Temperature (°C)	Comments
03/12/02	9:10	9:20	10	78/4	4.6	7.3	4.6	—	22	Sample consumed doing field analyses
03/12/02	12:30	12:45	120	59/2	5.1	4.2	2.5	SPC01016616	45	—
03/12/02	12:30	12:45	30	59/2	5.1	4.2	2.5	SPC01016624	45	—
03/12/02	12:50	13:00	60	59/3	5.3	3	1.8	SPC01016617	52	—
03/12/02	12:50	13:00	30	59/3	5.3	3	1.8	SPC01016625	52	—
03/12/02	13:05	13:07	200	59/4	5.2	2	1.2	SPC01016618	40	—
03/12/02	13:05	13:07	30	59/4	5.2	2	1.2	SPC01016626	40	—
03/12/02	13:15	13:30	50	61/2	5.1	15.9	10	SPC01016620	40	—
04/04/02	10:30	10:50	250	75/2	5.0	>994	>663	SPC01016632	27	Sample is yellow. Values exceeded calibrated range.
04/04/02	10:30	10:50	30	75/2	5.0	>994	>663	SPC01016637	27	Sample is yellow. Values exceeded calibrated range.
04/04/02	9:40	9:50	10	76/3	4.6	13.6	8.5	—	24	Sample consumed doing field analyses
04/04/02	9:50	10:00	60	76/4	4.5	7.1	4.4	SPC01016633	26	—
04/04/02	9:10	9:30	60	77/3	3.8	62.7	39.6	SPC01016634	28	At start of sampling
04/04/02	9:10	9:30	20	77/3	3.7	103	65	SPC01016638	25	At end of sampling
04/04/02	10:00	10:10	10	78/3	4.8	5.1	3.2	—	24	Sample consumed doing field analyses
04/04/02	9:50	10:00	60	78/4	4.7	5.2	3.2	SPC01016635	23	—
04/04/02	12:40	12:55	60	59/4	5.4	6.3	3.9	SPC01016636	40	—
04/04/02	12:40	12:55	30	59/4	5.4	6.3	3.9	SPC01016639	40	—
04/04/02	13:20	13:40	20	61/3	4.9	7.7	4.8	SPC01016631	25	—
04/04/02	13:40	14:00	10	61/4	4.9	9.7	6.1	—	24	Sample consumed doing field analyses
04/25/02	10:00	10:20	40	75/2	5.0	1089	732	SPC01016643	23	Sample is yellow.
04/25/02	11:10	11:20	5	76/3	4.5	25.5	15.8	—	23	Sample consumed doing field analyses
04/25/02	11:50	12:05	40	77/3	3.8	54	34.1	SPC01016644	25	—

Table 6.3-24. Summary of DST Water Samples, the Field Data, and Important Observations through December 31, 2005 (Continued)

Date	Approx. Start Time	Approx. Finish Time	Estimated Volume (mL)	Collection Hole/Zone	pH	Electrical Conductivity (mS/cm)	Total Dissolved Solids (ppm)	Sample Number	Solution Temperature (°C)	Comments
04/25/02	13:15	13:25	5	59/2	5.0	4.9	3	—	26	Sample consumed doing field analyses
04/25/02	13:40	13:50	300	59/4	4.9	2.9	1.7	SPC01016641	28	Fast sample collection rate. Field analyses are of first part of sample stream.
04/25/02	13:40	13:50	30	59/4	4.9	4.3	2.5	SPC01016642	52	Field analyses are of last part of sample stream.
05/29/02	12:05	12:15	40	76/4	5.3	12.1	7.5	SPC01016640	27	—
05/29/02	11:29	11:35	5	78/4	6.4	10	6.2	—	25	Sample consumed doing field analyses
05/29/02	12:56	13:05	5	59/2	5.9	8	5	—	26	Sample consumed doing field analyses
05/29/02	13:06	13:20	5	59/3	5.6	4.2	2.6	—	26	Sample consumed doing field analyses
05/29/02	13:21	13:35	200	59/4	5.2	3.5	2.1	SPC01016645	32	—
06/26/02	9:48	10:10	10	75/2	6.0	278	176	SPC01016652	27	—
06/26/02	10:12	10:22	5	75/3	6.1	12.6	7.8	—	26	Sample consumed doing field analyses
06/26/02	10:55	11:08	15	76/3	4.7	14.2	8.8	SPC01016648	28	—
06/26/02	11:10	11:27	30	76/4	5.3	8.4	5.2	SPC01016649	29	—
06/26/02	10:66	11:09	5	78/3	5.8	10.3	6.4	—	27	Sample consumed doing field analyses
06/26/02	11:10	11:29	5	78/4	5.5	7.6	4.7	—	27	Sample consumed doing field analyses
06/26/02	13:07	13:20	40	59/2	6.7	11.3	6.9	SPC01016650	29	—
06/26/02	13:22	13:32	5	59/3	6.4	8.5	5.2	—	29	Sample consumed doing field analyses
06/26/02	13:36	13:45	30	59/4	6.2	6.5	4	SPC01016651	29	—
11/13/02	10:02	10:10	1	74/4	5.2	—	—	—	—	Insufficient sample for further analyses



Table 6.3-24. Summary of DST Water Samples, the Field Data, and Important Observations through December 31, 2005 (Continued)

Date	Approx. Start Time	Approx. Finish Time	Estimated Volume (mL)	Collection Hole/Zone	pH	Electrical Conductivity (mS/cm)	Total Dissolved Solids (ppm)	Sample Number	Solution Temperature (°C)	Comments
11/13/02	10:24	10:31	1	76/3	5.1	—	—	—	—	Insufficient sample for further analyses
02/18/03	10:03	10:15	25	57/4	4.8	20.4	12.7	SPC01016653	21	—
08/16/04	12:00	12:06	5	57/4	4.6	20.8	12.6	—	28	Sample consumed doing field analyses

Source: DTNs: SN0208F3903102.002 [DIRS 161246] (06/04/98 to 01/09/02); SN0210F3903102.004 [DIRS 170573] (01/16/02 to 04/04/02) ; SN0211F3903102.005 [DIRS 170574] (4/25/02 to 8/28/02); SN0303F3903102.006 [DIRS 178034] (10/7/02 to 2/18/03); SN0411F3903102.009 [DIRS 178036] (5/11/04 to 8/16/04).

NOTES: A single set of field measurements, in conjunction with multiple samples from a single borehole/zone, indicates that samples were split.

Volumes and temperatures listed are included for information only.

Small fluid volumes (<10mL) were depleted after conducting field measurements and not saved as samples.

Blank cell indicates no measurement recorded.

Asterisk (\*) indicates information source from Cho 2001 [DIRS 159473].

### Laboratory Analyses

Water samples collected from the hydrology boreholes are prioritized for several analytical tests including major ion chemistry and certain isotope analyses. Metal and anion concentrations measured by ICP/AES and IC, respectively, are reported in this section. The major ion data compiled for the samples analyzed are presented in Table 6.3-25; values for pH and HCO<sub>3</sub> (measured in the field) are included for convenience.

In Table 6.3-25, the SMF sample identifications are traceable to the field activities recorded in Table 6.3-24 (the exception is for baseline water acquired from pore water centrifuged from boreholes 182 (ESF-HD-PERM1) through 184 (ESF-HD-PERM3)). Different conventions have been followed for assigning the unique SMF identification number used in both tables. Water samples are pumped during a sampling trip, and collected into different bottles designated for analyses. Entries in Table 6.3-25 reflect two conventions that have been followed. First, in a given sampling trip all sample bottles filled from one zone have been assigned a single SPC number; additional descriptions may record a date and time that the sample was acquired for distinguishing the order. Second, a unique SMF identifier is assigned to each of the bottles collected from a single zone, and the relevant date and time are recorded. It is worth noting that samples for metal and anion analyses identified with the same SPC number are not more closely related than samples identified with a different SPC number (entries in Table 6.3-25 might appear to suggest otherwise). This is important because several samples collected one after another have exhibited increasingly dilute chemistries with continued pumping. Similar evidence is also observed in field data when multiple samples from a zone are tested and recorded.

Chemical analyses have been reported from water samples collected from each of the three borehole arrays (see Figure 6.3-44) and from boreholes located both above and below the heated drift. Most of the aqueous samples collected and analyzed would appear to fall into two main groups: (1) Water samples for which chemistries have been consistent with mineral/water interactions, particularly fracture lining minerals such as silica polymorphs and calcium carbonate. Intervals from which these waters derive are below and up to boiling (approximately 96°C) temperatures. (2) Dilute water samples obtained from intervals near or above boiling that were consistent with derivation from condensed moisture in the sampling line. From the beginning, these samples were not considered to add value to the aqueous geochemistry study and were thought unnecessary for collection. However, it has been up to individual field personnel, working in concert with the aqueous sampling procedure, whether to collect and save the samples. Generally, all zones were pumped during the field collection trips, and no distinctions were made for samples derived from condensed water vapor.

Table 6.3-25. Chemical Analyses of DST Borehole Water Samples

SMF No. (SPC0...) Collection Date Collection Time Sample ID	1002488 Preheating PERM-1 <sup>b</sup>	1002586 Preheating PERM-2 <sup>b</sup>	1002525 Preheating PERM-3 <sup>b</sup>	1527969 <sup>a</sup> 06/04/98 BH 60-2	0527968 <sup>a</sup> 06/04/98 BH 60-2	0527977 <sup>a</sup> 06/04/98 BH 60-3	0527915 <sup>a</sup> 08/12/98 BH 60-2	0527916 <sup>a</sup> 08/12/98 BH 60-3	0527917 <sup>a</sup> 08/12/98 BH 77-3
Field pH <sup>c</sup>	7.79	8.32	8.31	7.5	N/A	7.7	6.9	6.8	5.5
Metals/Cations									
Na (mg/L)	60.5	61.0	61.5	20.0	N/A	24.0	20.4	17.2	2.4
Si (mg/L)	37	31	35	56	N/A	41	51.8	43.5	1.48
Ca (mg/L)	98.17	106.17	96.67	20	N/A	25	19.9	18.7	2.09
K (mg/L)	6.0	7.0	9.0	6.0	N/A	4.5	5.4	4.5	1.4
Mg (mg/L)	26.65	16.55	17.35	2.9	N/A	5.7	1.21	4.0	0.21
Al (mg/L)	<0.06	<0.06	<0.06	0.12	N/A	0.017 <sup>b</sup>	<0.06	0.003 <sup>b</sup>	<0.06
B (mg/L)	3.05	2.75	2.75	1.2	N/A	0.92	1.84	1.14	0.13
S (mg/L)	42.25	38.6	38.65	5.5	N/A	9.2	4.5	5.2	1.4
Fe (mg/L)	<0.02	<0.02	<0.02	0.04	N/A	<0.02	0.02	0.12	<0.02
Li (mg/L)	0.1	0.45	0.05	0.07	N/A	0.07	0.03	0.040	<0.01
Sr (mg/L)	1.4	1	1.05	0.18	N/A	0.34	0.11	2.21	0.05
Anions									
HCO (mg/L) <sup>d</sup>	N/A	N/A	N/A	N/A	N/A	N/A	N/A	N/A	N/A
F (mg/L)	0.36	0.96	0.76	N/A	1.00	0.82	0.71	0.43	0.41
Cl (mg/L)	122.73	109.93	123.13	N/A	10	16	6.14	5.52	2.15
Br (mg/L)	0.6	0.76	1.2	N/A	0.84	0.73	0.05	0.21	0.03
SO <sub>4</sub> (mg/L)	124.18	111.38	119.78	N/A	17	30	4.88	8.81	1.86
PO <sub>4</sub> (mg/L)	<0.07	<0.07	<0.07	N/A	<0.07	<0.07	0.25	0.16	1.06
NO <sub>2</sub> (mg/L)	<0.04	<0.04	<0.04	N/A	<0.01	<0.01	<0.04	<0.04	<0.04
NO <sub>3</sub> (mg/L)	21.72	2.52	10.40	N/A	3.00	3.6	0.46	0.60	0.22

Table 6.3-25. Chemical Analyses of DST Borehole Water Samples (Continued)

SMF No. (SPC0...) Collection Date Collection Time Sample ID	0541803 <sup>a</sup> 11/12/98 BH 59-4	0541803 <sup>a,f</sup> 11/12/98 BH 59-4	0541804 <sup>a</sup> 11/12/98 BH 60-3	0541804 <sup>a,f</sup> 11/12/98 BH 60-3	0541805 <sup>a</sup> 11/12/98 BH 186-3	0541805 <sup>a,f</sup> 11/12/98 BH 186-3	0504397 <sup>a</sup> 01/26/99 BH 59-4	0504396 <sup>a</sup> 01/26/99 BH 60-3	0527961 <sup>a</sup> 01/26/99 BH 186-3
Field pH <sup>c</sup>	6.63	6.63	6.92	6.92	6.83	6.83	N/A	7.4	7.2
<b>Metals/Cations</b>									
Na (mg/L)	22.6	135	10.1	20.3	105	17.0	219	19.1	25.9
Si (mg/L)	33.5	44.2	60.0	53.8	16.0	27.2	12.0	65.0	49.3
Ca (mg/L)	476	450	15.3	13.9	11.5	20.2	429	5.93	2.92
K (mg/L)	29.5	37.8	8.7	7.8	3.5	3.9	29.7	4.1	5.9
Mg (mg/L)	64.1	83.9	3.35	3.00	5.1	5.68	164	1.17	6.32
Al (mg/L)	0.01 <sup>d</sup>	<0.06	0.033 <sup>d</sup>	0.033 <sup>d</sup>	0.003 <sup>d</sup>	0.003 <sup>d</sup>	0.086 <sup>d</sup>	<0.06	<0.06
B (mg/L)	4.47	4.13	1.58	1.41	0.51	0.58	6.68	1.75	0.84
S (mg/L)	50.7	64.8	11.6	10.5	8.47	9.42	109	6.4	7.9
Fe (mg/L)	<0.02	<0.02	0.02	<0.02	0.02	<0.02	<0.02	<0.02	0.09
Li (mg/L)	0.21	0.20	0.040	0.040	0.05	0.05	0.33	0.02	0.05
Sr (mg/L)	4.02	3.71	0.22	0.20	0.30	0.34	5.84	0.09	0.37
<b>Anions</b>									
HCO <sup>-</sup> (mg/L) <sup>e</sup>	N/A	N/A	N/A	N/A	N/A	N/A	N/A	41	116
F (mg/L)	0.8	4.3	0.49	0.50	0.56	0.62	0.51	1.27	1.20
Cl (mg/L)	1,130	1,250	19.5	19.6	18.7	18.6	1,160	10.3	23.3
Br (mg/L)	1.13	<0.07	0.6	0.51	0.67	0.60	1.51	0.15	0.32
SO <sub>4</sub> (mg/L)	226	213	30.6	30.8	26.3	26.2	240	13.5	21
PO <sub>4</sub> (mg/L)	<5	<0.2	<0.2	<0.2	<0.2	<0.2	<0.5	<0.05	<0.1
NO <sub>2</sub> (mg/L)	<3	<10	<.10	<.10	<.1	<.1	<.3	<.03	<0.05
NO <sub>3</sub> (mg/L)	3.12	7.81	3.38	3.17	7.47	7.27	11.6	2.56	6.73

Table 6.3-25. Chemical Analyses of DST Borehole Water Samples (Continued)

SMF No. (SPC0...) Collection Date Collection Time Sample ID	0529637-#1 <sup>a</sup> 03/30/99 9:50 AM BH 60-3	0529637-#2 <sup>a</sup> 03/30/99 9:55 AM BH 60-3	0529637-#3 <sup>a</sup> 03/30/99 10:10 AM BH 60-3	0529634 <sup>a</sup> 03/30/99 BH 77-3	0551100 <sup>a</sup> 04/20/99 9:32 AM BH 60-3	0551103 <sup>a</sup> 04/20/99 1:45 PM BH 60-3	0551104 <sup>a</sup> 05/10/99 10:20 AM BH 60-3	0551105 <sup>a</sup> 05/10/99 10:24 AM BH 60-3	0551106 <sup>a</sup> 05/10/99 BH 60-3
Field pH <sup>c</sup>	8.0	N/A	N/A	4.8	4.19-4.50	4.77	4.78-4.80	4.68	N/A
<b>Metals/Cations</b>									
Na (mg/L)	11.2	11.0	2.2	<0.2	0.14	<0.05	1.8	2.5	0.15
Si (mg/L)	62.8	59.8	12.1	1.03	0.7	<0.5	1.1	1.2	0.6
Ca (mg/L)	2.06	2.27	1.22	0.41	0.14	0.10	0.14	0.09	0.22
K (mg/L)	2.4	2.4	0.5	<0.5	<0.5	<0.5	<0.5	<0.5	<0.5
Mg (mg/L)	0.27	0.26	0.01	0.02	<0.005	<0.005	<0.005	<0.005	<0.005
Al (mg/L)	0.36, 0.27 <sup>d</sup>	0.36, 0.27 <sup>d</sup>	0.08, 0.07 <sup>d</sup>	0.005 <sup>d</sup>	<0.2	<0.2	<0.2	<0.2	<0.2
B (mg/L)	2.10	2.11	1.23	0.09	1.7	1.0	2.3	2.6	0.9
S (mg/L)	1.83	1.82	0.42	<0.02	<0.5	<0.5	<0.5	<0.5	<0.5
Fe (mg/L)	<0.02	<0.02	<0.02	0.05	0.02	0.01	<0.01	<0.01	<0.01
Li (mg/L)	0.02	<0.01	<0.01	<0.01	<4	<4	<4	<4	<4
Sr (mg/L)	0.02	0.02	0.01	<0.01	<0.05	<0.05	<0.05	<0.05	<0.05
<b>Anions</b>									
HCO <sup>-</sup> (mg/L) <sup>e</sup>	25.0	N/A	N/A	1.25	N/A	N/A	N/A	N/A	8.1
F (mg/L)	1.02	0.97	0.11	0.01	<0.005	<0.005	<0.005	<0.005	<0.005
Cl (mg/L)	4.15	3.92	0.72	0.3	0.05	0.08	0.06	0.05	0.11
Br (mg/L)	<0.04	<0.04	<0.04	<0.04	<0.03	<0.03	<0.03	<0.03	<0.03
SO <sub>4</sub> (mg/L)	3.83	3.75	0.79	0.13	0.1	0.09	0.09	0.09	0.08
PO <sub>4</sub> (mg/L)	<0.05	<0.05	<0.05	<0.05	<0.02	<0.02	0.92	0.84	0.62
NO <sub>2</sub> (mg/L)	<0.03	<0.03	<0.03	<0.03	<0.007	<0.007	<0.007	<0.007	<0.007
NO <sub>3</sub> (mg/L)	0.92	0.84	0.17	0.065	<0.02	<0.02	<0.02	<0.02	<0.02

Table 6.3-25. Chemical Analyses of DST Borehole Water Samples (Continued)

SMF No. (SPC0...) Collection Date Collection Time Sample ID	0551107 05/10/99 11:04 AM BH 60-3	0551110 <sup>a</sup> 05/25/99 9:23 AM BH 60-3	0551111 <sup>a</sup> 05/25/99 9:40 AM BH 60-3	0551154 <sup>a</sup> 06/24/99 9:17 AM BH 60-3	0551155 <sup>a</sup> 06/24/99 9:23 AM BH 60-3	0551159 <sup>a</sup> 08/09/99 BH 59-2 (AC)	0551160 <sup>a</sup> 08/09/99 BH 59-2 (BC)	0551169 <sup>a</sup> 08/10/99 BH 61-3	0557029 <sup>a</sup> 10/27/99 BH 59-2
Field pH <sup>c</sup>	4.84	4.68	4.75	5.02	N/A	N/A	N/A	N/A	N/A
Metals/Cations									
Na (mg/L)	2.8	1.8	1.6	1.87	2.26	30	24	19	N/A
Si (mg/L)	1.4	2.1	0.7	6.30	3.22	78	81	67	N/A
Ca (mg/L)	0.15	0.13	0.09	0.69	0.23	47	39	14	N/A
K (mg/L)	<0.5	<0.5	<0.5	0.5	<0.5	8	6	5	N/A
Mg (mg/L)	<0.005	<0.005	<0.005	0.012	<0.005	13	11	3.2	N/A
Al (mg/L)	<0.2	<0.2	<0.2	<0.04	<0.04	<0.2	<0.2	<0.2	N/A
B (mg/L)	2.8	2.0	1.9	0.62	1.85	0.8	0.6	1.5	N/A
S (mg/L)	<0.5	<0.5	<0.5	<0.1	<0.1	22	17	3.1	N/A
Fe (mg/L)	0.31	<0.01	<0.01	<0.01	<0.01	0.41	0.32	1.2	N/A
Li (mg/L)	<4	<4	<4	<1	<1	<4	<4	<4	N/A
Sr (mg/L)	<0.05	<0.05	<0.05	<0.01	<0.01	0.54	0.45	0.14	N/A
Anions									
HCO <sup>-</sup> (mg/L) <sup>d</sup>	N/A	8.6	8.6	N/A	N/A	N/A	N/A	N/A	23.5
F (mg/L)	<0.005	<0.005	<0.005	0.685	0.195	0.725	0.575	0.835	0.27
Cl (mg/L)	0.09	0.20	0.06	0.615	0.305	88.3	71.0	24.1	9.5
Br (mg/L)	<0.03	<0.03	<0.03	<0.03	<0.03	0.515	0.46	0.35	0.61
SO <sub>4</sub> (mg/L)	0.12	0.09	0.07	<0.03	0.325	64.2	53.5	9.13	6.2
PO <sub>4</sub> (mg/L)	<0.02	0.69	0.33	<0.02	<0.02	<0.02	<0.02	<0.02	<0.02
NO <sub>2</sub> (mg/L)	<0.007	<0.007	<0.007	<0.007	<0.007	<0.007	<0.007	<0.007	<0.007
NO <sub>3</sub> (mg/L)	<0.02	<0.02	<0.02	N/A	<0.02	3.79	2.83	0.825	1.32

Table 6.3-25. Chemical Analyses of DST Borehole Water Samples (Continued)

SMF No. (SPC0...) Collection Date Sample ID	0557032 10/27/99 BH 59-2	0557033 <sup>a</sup> 10/27/99 BH 59-2	0557036 <sup>a</sup> 10/27/99 BH 59-3	0557038 <sup>a</sup> 10/27/99 BH 59-3	0557040 <sup>a</sup> 10/27/99 BH 76-3	0557080 11/30/99 BH 59-2	0557081 11/30/99 BH 59-2	0557083 11/30/99 BH 59-2	0552575 11/30/99 BH 59-3	0557043 11/30/99 BH 59-3
Field pH <sup>c</sup>	5.93	6.08	N/A	6.64	6.14–6.46	6.86	7.24	N/A	7.47	N/A
Metals/Cations										
Na (mg/L)	9.2	9.2	N/A	19.3	64.5	6.6	7.7	N/A	15.6	N/A
Si (mg/L)	44.5	44.9	N/A	84.2	133.4	38.0	39.9	N/A	92.5	N/A
Ca (mg/L)	7.53	7.47	N/A	13.2	59.5	4.33	5.63	N/A	2.86	N/A
K (mg/L)	3.4	3.6	N/A	5.6	13.4	2.6	3.0	N/A	3.9	N/A
Mg (mg/L)	1.81	1.72	N/A	1.49	13.8	1.02	1.38	N/A	0.29	N/A
Al (mg/L)	0.033 <sup>g</sup>	0.033 <sup>g</sup>	N/A	0.040	0.010	0.030	0.030	N/A	0.071	N/A
B (mg/L)	0.27	0.21	N/A	0.86	2.38	0.14	0.17	N/A	1.06	N/A
S (mg/L)	2.52	2.50	N/A	14.48	34.55	0.76	1.33	N/A	3.25	N/A
Fe (mg/L)	0.20	0.19	N/A	< 0.02	< 0.02	0.09	0.14	N/A	< 0.02	N/A
Li (mg/L)	0.16	0.01	N/A	0.02	0.13	0.01	0.01	N/A	0.02	N/A
Sr (mg/L)	0.11	0.08	N/A	0.13	0.78	0.06	0.08	N/A	0.03	N/A
Anions										
HCO (mg/L) <sup>e</sup>	N/A	23.5	12.4	12.4	N/A	N/A	N/A	22.3	N/A	20.7
F (mg/L)	N/A	0.27	0.64	0.73	1.11	N/A	N/A	0.35	N/A	1.3
Cl (mg/L)	N/A	9.1	12.9	12.9	81.9	N/A	N/A	5.0	N/A	8.8
Br (mg/L)	N/A	0.58	0.89	0.51	0.97	N/A	N/A	< 0.03	N/A	< 0.03
SO <sub>4</sub> (mg/L)	N/A	6.3	40.7	40.3	94.6	N/A	N/A	2.8	N/A	8.2
PO <sub>4</sub> (mg/L)	N/A	< 0.02	< 0.04	< 0.04	< 0.02	N/A	N/A	< 0.02	N/A	< 0.02
NO <sub>2</sub> (mg/L)	N/A	< 0.007	< 0.01	< 0.01	< 0.007	N/A	N/A	0.007	N/A	< 0.007
NO <sub>3</sub> (mg/L)	N/A	1.40	3.06	3.05	6.42	N/A	N/A	< 0.02	N/A	2.4

Table 6.3-25. Chemical Analyses of DST Borehole Water Samples (Continued)

SMF No. (SPC0...) Collection Date Collection Time Sample ID	0552578 11/30/99 BH 76-3	0552579 11/30/99 BH 76-3	0557081 <sup>a</sup> 11/30/99 BH 77-3	0557084 <sup>a</sup> 11/30/99 BH 77-3	0557022 01/25/00 BH 59-2	0550671 01/25/00 BH 59-2	0550673 01/25/00 BH 59-2	0550698 <sup>a</sup> 01/25/00 BH 77-2	0550674 <sup>a</sup> 01/25/00 BH 77-3	0550674 <sup>a</sup> 01/25/00 BH 77-3
Field pH <sup>c</sup>	6.94	N/A	N/A	4.68	7.07	6.68	N/A	4.63	3.47	N/A
Metals/Cations										
Na (mg/L)	28.2	N/A	N/A	0.6	8.1	6.6	N/A	< 0.3	< 0.3	N/A
Si (mg/L)	92.8	N/A	N/A	2.45	42.8	41.7	N/A	2.0	2.5	N/A
Ca (mg/L)	22.3	N/A	N/A	1.27	7.54	2.89	N/A	0.17	< 0.005	N/A
K (mg/L)	7.4	N/A	N/A	< 0.2	3.6	2.8	N/A	< 0.2	< 0.2	N/A
Mg (mg/L)	4.71	N/A	N/A	0.19	1.78	0.72	N/A	0.01	< 0.005	N/A
Al (mg/L)	0.031	N/A	N/A	0.334	< 0.05	0.043	N/A	0.049	0.023	N/A
B (mg/L)	0.81	N/A	N/A	0.09	0.29	0.21	N/A	0.05	0.04	N/A
S (mg/L)	9.46	N/A	N/A	0.24	6.44	0.65	N/A	< 0.05	< 0.05	N/A
Fe (mg/L)	0.10	N/A	N/A	0.37	0.07	< 0.02	N/A	0.25	0.07	N/A
Li (mg/L)	0.04	N/A	N/A	< 0.01	< 0.01	< 0.01	N/A	< 0.01	< 0.01	N/A
Sr (mg/L)	0.26	N/A	N/A	0.02	0.091	0.036	N/A	< 0.005	< 0.005	N/A
Anions										
HCO <sup>-</sup> (mg/L) <sup>e</sup>	N/A	82.3	N/A	N/A	N/A	N/A	22.8	N/A	N/A	N/A <sup>h</sup>
F (mg/L)	N/A	1.3	15	N/A	N/A	N/A	0.73	6.7	19.9	20.8 <sup>h</sup>
Cl (mg/L)	N/A	19	3.5	N/A	N/A	N/A	3.8	0.6	0.8	0.29 <sup>h</sup>
Br (mg/L)	N/A	< 0.03	< 0.03	N/A	N/A	N/A	< 0.1	< 0.1	< 0.1	< 0.1 <sup>h</sup>
SO <sub>4</sub> (mg/L)	N/A	26.0	1.6	N/A	N/A	N/A	1.8	0.39	< 0.1	< 0.1 <sup>h</sup>
PO <sub>4</sub> (mg/L)	N/A	< 0.02	< 0.02	N/A	N/A	N/A	0.62	0.64	4.0	2.9 <sup>h</sup>
NO <sub>2</sub> (mg/L)	N/A	< 0.007	< 0.007	N/A	N/A	N/A	< 0.05	< 0.05	< 0.05	< 0.06 <sup>h</sup>
NO <sub>3</sub> (mg/L)	N/A	2.5	< 0.02	N/A	N/A	N/A	0.77	< 0.1	0.20	0.18 <sup>h</sup>



Table 6.3-25. Chemical Analyses of DST Borehole Water Samples (Continued)

SMF No. (SPC0...) Collection Date Collection Time Sample ID	0550681 05/23/00 BH 59-2	0550682 05/23/00 BH 59-2	0550684 05/23/00 BH 59-2	0550687 05/23/00 BH 59-3	0550697 05/23/00 BH 76-3	0550679 05/23/00 BH 76-4	0550693 06/29/00 BH 59-2	0550694 06/29/00 BH 59-2	0550691 06/29/00 BH 59-2
Field pH <sup>c</sup>	6.96	6.96	6.95	5.19	6.92-6.96	N/A	6.99-7.08	6.99-7.08	7.00
Metals/Cations									
Na (mg/L)	17	18	17	<2.4	29	<2.4	16	15	<4.8
Si (mg/L)	59.4	59.2	59.3	<0.46	96.0	3.4	62.7	57.5	36.3
Ca (mg/L)	4.7	4.4	4.5	<0.17	7.1	1.5	4.3	3.8	2.0
K (mg/L)	4.3	4.4	4.4	<0.095	6.5	0.70	4.7	4.2	2.5
Mg (mg/L)	1.1	1.1	1.1	<0.042	1.4	0.14	1.1	1.0	0.54
Al (mg/L)	<0.053	<0.053	<0.053	<0.053	<0.053	<0.053	<0.053	0.053	<0.11
B (mg/L)	N/A	N/A	N/A	N/A	N/A	N/A	N/A	N/A	N/A
S (mg/L)	N/A	N/A	N/A	N/A	N/A	N/A	N/A	N/A	N/A
Fe (mg/L)	<0.038	<0.038	<0.038	<0.038	<0.038	<0.038	<0.038	<0.038	<0.076
Li (mg/L)	0.021	0.022	0.021	<0.0007	0.045	0.0037	0.019	0.018	0.010
Sr (mg/L)	<0.013	<0.013	<0.013	<0.013	<0.013	<0.013	<0.013	<0.013	<0.026
Anions									
HCO <sup>-</sup> (mg/L) <sup>a</sup>	31.4	31.4	31.4	N/A	N/A	N/A	N/A	N/A	N/A
F (mg/L)	0.58	0.55	0.49	0.15	0.76	0.13	N/A	N/A	N/A
Cl (mg/L)	10.15	10.6	10.15	0.07	14.5	2.75	N/A	N/A	N/A
Br (mg/L)	<0.1	0.38	<0.1	<0.1	<0.1	<0.1	N/A	N/A	N/A
SO <sub>4</sub> (mg/L)	2.9	3.18	3.1	<0.1	4.98	2.24	N/A	N/A	N/A
PO <sub>4</sub> (mg/L)	<0.2	<0.2	<0.2	<0.2	<0.2	<0.2	N/A	N/A	N/A
NO <sub>2</sub> (mg/L)	<0.06	<0.06	<0.06	<0.06	<0.06	<0.06	N/A	N/A	N/A
NO <sub>3</sub> (mg/L)	0.56	0.54	0.71	0.38	1.47	0.85	N/A	N/A	N/A

Table 6.3-25. Chemical Analyses of DST Borehole Water Samples (Continued)

SMF No. (SPC0...) Collection Date Collection Time Sample ID	0550689 06/29/00 BH 59-2	0550690 06/29/00 BH 59-2	0550685 06/29/00 BH 59-4	0550686 06/29/00 BH 59-3	0530300 06/29/00 BH 76-3	0530302 06/29/00 BH 76-3	0550678 06/29/00 BH 76-4	0530303 06/29/00 BH 76-4	0550688 06/29/00 BH 78-2
Field pH <sup>c</sup>	N/A	N/A	4.60-4.74	5.60	5.75	5.75	4.74-4.77	N/A	4.12
Metals/Cations									
Na (mg/L)	N/A	N/A	< 2.4	< 2.4	N/A	< 2.4	< 2.4	N/A	< 2.4
Si (mg/L)	N/A	N/A	< 0.46	< 0.46	N/A	3.1	< 0.46	N/A	< 0.46
Ca (mg/L)	N/A	N/A	< 0.17	< 0.17	N/A	< 0.17	< 0.17	N/A	0.5
K (mg/L)	N/A	N/A	< 0.095	< 0.095	N/A	< 0.095	< 0.095	N/A	< 0.095
Mg (mg/L)	N/A	N/A	< 0.042	< 0.042	N/A	0.29	< 0.042	N/A	< 0.042
Al (mg/L)	N/A	N/A	< 0.053	< 0.053	N/A	0.17	0.18	N/A	< 0.053
B (mg/L)	N/A	N/A	N/A	N/A	N/A	N/A	N/A	N/A	N/A
S (mg/L)	N/A	N/A	N/A	N/A	N/A	N/A	N/A	N/A	N/A
Fe (mg/L)	N/A	N/A	< 0.038	< 0.038	N/A	< 0.038	< 0.038	N/A	< 0.038
Li (mg/L)	N/A	N/A	< 0.0007	< 0.0007	N/A	< 0.0007	< 0.0007	N/A	< 0.0007
Sr (mg/L)	N/A	N/A	< 0.013	< 0.013	N/A	< 0.013	< 0.013	N/A	< 0.013
Anions									
HCO <sup>-</sup> (mg/L) <sup>a</sup>	29.4	29.4	N/A	N/A	N/A	N/A	N/A	N/A	N/A
F (mg/L)	0.18	0.15	N/A	N/A	< 0.007	N/A	N/A	< 0.007	0.11
Cl (mg/L)	0.90	0.32	N/A	N/A	0.67	N/A	N/A	0.94	2.79
Br (mg/L)	0.62	0.48	N/A	N/A	0.47	N/A	N/A	0.57	1.15
SO <sub>4</sub> (mg/L)	0.5	0.42	N/A	N/A	1.54	N/A	N/A	< 0.1	< 0.1
PO <sub>4</sub> (mg/L)	< 0.2	< 0.2	N/A	N/A	< 0.2	N/A	N/A	< 0.2	< 0.2
NO <sub>2</sub> (mg/L)	< 0.06	< 0.06	N/A	N/A	< 0.06	N/A	N/A	< 0.06	< 0.06
NO <sub>3</sub> (mg/L)	0.65	0.48	N/A	N/A	0.49	N/A	N/A	< 0.09	< 0.09

Table 6.3-25. Chemical Analyses of DST Borehole Water Samples (Continued)

SMF No. (SPC...) Collection Date Collection Time Sample ID	0550642 06/29/00 BH 78-3	0530398 01/23/01 BH 59-2	0530316 01/23/01 BH 59-3	0530318 01/23/01 BH 60-4	0559467 04/17/01 BH 59-2	0559463 04/17/01 BH 59-3	0559464 04/17/01 BH 59-4	0559464 04/17/01 BH 76-2	0559458 04/17/01 BH 76-2
Field pH <sup>c</sup>	4.22	N/A	N/A	N/A	4.87	5.96	5.20	7.68	8.22
Metals/Cations									
Na (mg/L)	< 2.4	29	< 2.4	< 2.4	< 2.4	6	< 2.4	9	9
Si (mg/L)	2.3	84.5	< 0.46	46.1	5.2	< 0.46	< 0.46	42.6	44.1
Ca (mg/L)	1.1	7.8	< 0.17	0.68	0.6	3.5	0.57	1.3	1.1
K (mg/L)	0.2	5.8	< 0.053	< 0.095	0.33	0.35	< 0.095	1.6	1.6
Mg (mg/L)	0.15	1.8	< 0.042	< 0.042	0.14	1.40	< 0.042	0.27	0.22
Al (mg/L)	0.31	< 0.053	< 0.053	< 0.053	< 0.053	< 0.053	< 0.053	0.42	0.43
B (mg/L)	N/A	N/A	N/A	N/A	N/A	N/A	N/A	N/A	N/A
S (mg/L)	N/A	N/A	N/A	N/A	N/A	N/A	N/A	N/A	N/A
Fe (mg/L)	< 0.038	< 0.038	< 0.038	< 0.038	< 0.038	< 0.038	< 0.038	0.40	0.40
Li (mg/L)	< 0.0007	0.033	< 0.0007	< 0.0007	< 0.0007	< 0.0007	< 0.0007	0.0098	0.010
Sr (mg/L)	< 0.013	< 0.013	< 0.013	< 0.013	< 0.013	< 0.013	< 0.013	< 0.013	< 0.013
Anions									
HCO <sup>-</sup> (mg/L) <sup>a</sup>	N/A	N/A	N/A	N/A	N/A	N/A	N/A	N/A	N/A
F (mg/L)	< 0.007	0.78	< 0.007	0.35	N/A	N/A	N/A	N/A	0.38
Cl (mg/L)	1.39	25.20	0.26	0.55	N/A	N/A	N/A	N/A	1.9
Br (mg/L)	0.79	< 0.1	< 0.1	< 0.1	N/A	N/A	N/A	N/A	< 0.1
SO <sub>4</sub> (mg/L)	< 0.1	9.5	< 0.1	0.57	N/A	N/A	N/A	N/A	0.89
PO <sub>4</sub> (mg/L)	< 0.2	< 0.2	< 0.2	< 0.2	N/A	N/A	N/A	N/A	< 0.2
NO <sub>2</sub> (mg/L)	< 0.06	< 0.06	< 0.06	0.59	N/A	N/A	N/A	N/A	< 0.06
NO <sub>3</sub> (mg/L)	< 0.09	0.99	< 0.09	0.54	N/A	N/A	N/A	N/A	< 0.09

Table 6.3-25. Chemical Analyses of DST Borehole Water Samples (Continued)

SMF No. (SPC0...) Collection Date Collection Time Sample ID	0559456 04/17/01 BH 76-2	0559481 06/28/01 BH 60-3	0559477 06/28/01 BH 60-3	0559455 08/07/01 BH 77-2	0559455 08/07/01 BH 77-2	0559484 08/07/01 BH 77-3	0559484 08/07/01 BH 77-3	0559490 08/08/01 BH 60-2	0559491 08/08/01 BH 60-3
Field pH <sup>c</sup>	8.29	3.3	3.30	3.3	3.3	3.3	3.3	3.1	3.4
Metals/Cations									
Na (mg/L)	9	< 2.4	N/A	N/A	< 2.4	< 2.4	N/A	< 2.4	< 2.4
Si (mg/L)	45.6	4.9	N/A	N/A	10.7	17.4	N/A	22.7	5.3
Ca (mg/L)	1.3	< 0.17	N/A	N/A	< 0.17	< 0.17	N/A	< 0.17	0.7
K (mg/L)	1.9	< 0.095	N/A	N/A	< 0.095	< 0.095	N/A	< 0.095	0.35
Mg (mg/L)	0.23	< 0.042	N/A	N/A	< 0.042	< 0.042	N/A	< 0.042	< 0.042
Al (mg/L)	0.45	0.67	N/A	N/A	1.0	2.2	N/A	2.5	0.8
B (mg/L)	N/A	N/A	N/A	N/A	N/A	N/A	N/A	N/A	N/A
S (mg/L)	N/A	N/A	N/A	N/A	N/A	N/A	N/A	N/A	N/A
Fe (mg/L)	0.39	0.15	N/A	N/A	0.20	0.19	N/A	1.6	< 0.038
Li (mg/L)	0.0076	< 0.0007	N/A	N/A	< 0.0007	< 0.0007	N/A	< 0.0007	< 0.0007
Sr (mg/L)	< 0.013	< 0.013	N/A	N/A	< 0.013	< 0.013	N/A	< 0.013	< 0.013
Anions									
HCO <sup>-</sup> (mg/L) <sup>a</sup>	N/A	N/A	N/A	< 5	< 5	< 5	< 5	< 5	< 5
F (mg/L)	0.47	N/A	17.7	50.0	41.0	50	57.8	66	8.77
Cl (mg/L)	1.71	N/A	0.90	0.77	< 0.05	< 0.05	1.12	0.76	0.82
Br (mg/L)	< 0.1	N/A	< 0.1	< 0.2	< 0.1	< 0.1	< 0.1	< 0.1	< 0.1
SO <sub>4</sub> (mg/L)	0.85	N/A	< 0.1	0.42	< 0.1	< 0.1	< 0.1	< 0.1	< 0.1
PO <sub>4</sub> (mg/L)	< 0.2	N/A	< 0.2	< 0.3	< 0.2	< 0.2	< 0.2	< 0.2	< 0.2
NO <sub>2</sub> (mg/L)	< 0.06	N/A	< 0.06	< 0.1	< 0.06	< 0.06	< 0.06	< 0.06	< 0.06
NO <sub>3</sub> (mg/L)	< 0.09	N/A	< 0.09	0.69	0.60	0.48	0.21	< 0.09	< 0.09

Table 6.3-25. Chemical Analyses of DST Borehole Water Samples (Continued)

SMF No. (SPC0...) Collection Date Collection Time Sample ID	0575227 10/22/01 BH 59-2	0575225 10/22/01 BH 60-2	0575221 10/22/01 BH 60-3	0575224 10/22/01 BH 60-4	0575222 10/22/01 BH 76-4	0575226 10/22/01 BH 77-2	0575223 10/22/01 BH 77-3	1016082 01/07/02 BH 76-2	1014156 01/09/02 BH 77-2	1014155 01/09/02 BH 77-3
Field pH <sup>e</sup>	4.9	3.2	3.5	3.8	5.1	3.1	3.2	7.8	3.7	3.4
Metals/Cations										
Na (mg/L)	< 2.4	< 2.4	< 2.4	< 2.4	N/A	< 2.4	< 2.4	N/A	N/A	N/A
Si (mg/L)	1.7	10.3	10.9	22.9	N/A	3.6	2.60	N/A	N/A	N/A
Ca (mg/L)	0.49	< 0.17	< 0.17	0.54	N/A	0.36	< 0.17	N/A	N/A	N/A
K (mg/L)	< 0.095	< 0.095	< 0.095	< 0.095	N/A	0.25	< 0.095	N/A	N/A	N/A
Mg (mg/L)	< 0.042	< 0.042	< 0.042	< 0.042	N/A	< 0.042	< 0.042	N/A	N/A	N/A
Al (mg/L)	< 0.053	0.41	0.22	< 0.053	N/A	0.3	0.25	N/A	N/A	N/A
B (mg/L)	N/A	N/A	N/A	N/A	N/A	N/A	N/A	N/A	N/A	N/A
S (mg/L)	N/A	N/A	N/A	N/A	N/A	N/A	N/A	N/A	N/A	N/A
Fe (mg/L)	< 0.038	0.34	< 0.038	0.047	N/A	0.18	0.16	N/A	N/A	N/A
Li (mg/L)	< 0.0007	< 0.0007	< 0.0007	< 0.0007	N/A	< 0.0007	< 0.0007	N/A	N/A	N/A
Sr (mg/L)	< 0.013	< 0.013	< 0.013	< 0.013	N/A	< 0.01	< 0.013	N/A	N/A	N/A
Anions										
HCO <sub>3</sub> (mg/L) <sup>e</sup>	< 5	< 5	< 5	< 5	< 5	< 5	< 5	< 5	< 5	< 5
F (mg/L)	0.27	74	N/A	N/A	< 0.007	51	62	0.4	4.85	19
Cl (mg/L)	< 0.05	2.29	N/A	N/A	0.41	0.75	0.7	2.75	0.63	0.89
Br (mg/L)	< 0.1	< 0.01	N/A	N/A	< 0.1	< 0.1	< 0.1	< 0.2	< 0.2	< 0.2
SO <sub>4</sub> (mg/L)	0.16	0.08	N/A	N/A	0.4	< 0.1	< 0.1	1.02	0.5	0.40
PO <sub>4</sub> (mg/L)	< 0.2	< 0.2	N/A	N/A	< 0.2	< 0.2	< 0.2	< 0.3	< 0.3	< 0.3
NO <sub>2</sub> (mg/L)	< 0.06	< 0.06	N/A	N/A	< 0.06	< 0.06	< 0.06	< 0.2	< 0.2	< 0.2
NO <sub>3</sub> (mg/L)	< 0.09	< 0.09	N/A	N/A	0.06	< 0.09	0.50	< 0.2	< 0.2	0.30

Source: DTN: LL02070923:142.023 (unqualified) [DIRS 161677].

<sup>a</sup> Analytical results are corroborating data (as defined in Section 3.6 of TST-PRO-001) and unqualified.

<sup>b</sup> Pore water samples (baseline): sample ultracentrifuged from borehole core.

<sup>c</sup> See entry in Table 6.3-24 for temperature of pH measurements.

<sup>d</sup> Low detection limit analysis – sample filtered to 0.10 µm and acidified.

<sup>e</sup> HCO<sub>3</sub> – field measurement.

<sup>f</sup> Sample filtered in the field and laboratory (LLNL) prior to analyses.

<sup>g</sup> Sample ID SPC0057028 submitted for low detection for Al analysis.

<sup>h</sup> Anion sample analyzed two different times.

NOTE: N/A = not available; < = not detected (less than “practical reporting limit”); field chemistry of samples for high fluorine de study (11/8/01 to 12/5/01) are reported in Table 6.3-31.

Some trends may be observed among the first group of samples. First, measured pH values range from approximately 6.1 to 8.3. Concentrations for specific analytes were variable, but the trends were similar. In general, SO<sub>4</sub> and Cl were the dominant anions; Si is the principal metal, followed by Ca and Na (having similar concentrations to each other). Present, but in lower concentrations, were K, Mg, Sr, and NO<sub>3</sub>. (These data were different from chemistry of the baseline pore water samples and were unrelated to construction water, which had a bromide tracer of approximately 20 ppm.) This class included a small number of water samples with distinctive, concentrated water. Borehole 59-4 (11/98 and 01/99) in particular appeared to exhibit evaporatively concentrated water, and boreholes 59-2 (08/99) and 76-3 (10/99) had somewhat higher concentrations of the principal analytes observed.

Some samples could be recognized in the field and by laboratory analyses as deriving from condensed vapor and generally showing little or no water–rock interaction. The samples generally had lower pH values (approximately 4.0 to 6.0) and low TDS and EC. These samples were collected from hotter boreholes, at boiling temperatures and higher. The analytical results from the samples indicate that the compositions are consistent with relatively pure water. (These analyses did not represent rock–water interaction and were therefore not routinely submitted to the TDMS.) On the other hand, condensates from the highest temperature intervals (greater than 140°C) exhibited lower pH values (less than 4.0) than might be expected from the effect of CO<sub>2</sub>-bearing steam condensation alone. These samples also exhibit values of TDS and EC that are not negligible and have unusually high fluoride concentrations (5 to 66 mg/L). Further field-testing was carried out to investigate the cause of the unexpected fluoride concentration for these water samples. These investigations are discussed in detail in Section 6.3.4.5.

### **6.3.4.1.3 Measurement Uncertainty: Aqueous Chemistry**

#### *Field Sampling*

The procedures developed for use in the field were intended to support the analytical data that ultimately would be derived from the collected samples. Measures included obtaining field values for some unstable properties on calibrated instruments (e.g., pH, EC, TDS, and alkalinity) and appropriately treating and preserving specific samples (e.g., filtering, acidifying, and storing in appropriate bottles). Reasonable efforts were made to accomplish these goals during each sampling trip. However, occasionally, for reasons outside the field technician's control (e.g., a meter battery was out, replacement bottles and supplies had not arrived before the sampling trip), the protocol could not be followed in its entirety. In those cases, samples were collected (the most important objective) and deviations were described in field notes. These types of issues were not considered to have significant impact on the actual data. Although attempts were made to minimize the time between collection and analysis, delays in getting samples delivered from the SMF were regularly encountered. When redrafting the protocol after the first year of heating, many of the issues were addressed.

The use of peristaltic pumping to acquire water from the hydrology boreholes is generally considered a suitable method for obtaining a representative, in situ DST water sample. However, certain conditions inherent to the thermal test environment may introduce uncertainty into some geochemical parameters. First, because of the relatively dry host rock, most water accumulations are insufficient to achieve and maintain water-filled lines during the sample collection process.

(In the field, this is evidenced by air bubbles in the sample tubing.) Potentially, water passing through the tubing may equilibrate with air in the line and thereby affect the concentrations of dissolved gases (CO<sub>2</sub> for example). Another issue previously mentioned is important when water is pumped to sequentially fill multiple bottles. Water samples clearly marked as to the order in which they become filled (see time notations in Table 6.3-24 and corresponding analyses in Table 6.3-25) may exhibit increasingly dilute concentrations with time. This suggests that as the standing water in the borehole is depleted, the heated vapors present condense and dilute water in the line. This effectively becomes a problem because (for example), if the initial sample is designated and preserved for metals testing, the second sample is designated for anions, and the final sample is used for field measurements (pH, EC, and bicarbonate), then a charge balance calculation and a check of the electrical neutrality would indicate inconsistency. This condition taken to its extreme gives rise to samples derived solely from condensed vapor.

### Laboratory Analyses

For both ICP/AES and IC, method detection limits (MDL) are determined for each analyte. The MDL represents the minimum concentration that can be identified, measured, and reported with 99% confidence that the analyte concentration is greater than zero. Generally, reportable concentrations (as established by laboratory chemists) are required to be greater than 3 to 5 times the MDL. For the concentrations reported in Table 6.3-25, values determined to be less than the “reportable limit” are indicated as nondetected. Therefore, no distinction is made for analytes that are present at some low level and those with no measurable concentration.

An additional uncertainty that may be introduced into analytical results occurs for samples that require some level of dilution. Samples may need to be diluted when concentrations exceed the measurement range for analytes of interest. If the total sample volume is small, reagent grade water may be added to extend the sample. In such cases, the concentration measured, as well as the limits of detection, are multiplied by the dilution ratio. The result is that small errors are exaggerated.

Holding times are another source of uncertainty (and might just as easily be considered in the field-sampling section as in the analytical results). Ideally, all sample analyses should be performed as soon after sample collection as possible to ensure that the analyses are representative of the in situ water chemistry. The U.S. Environmental Protection Agency has established maximum hold times, which are almost universally recognized for drinking water analyses. As guidance for the DST borehole water samples, the established hold times, which typically ranged from 2 to 25 days, were suggested in the protocol (TIP-AC-03). The guidelines have generally been met, with the exception of the holding time recommendations for NO<sub>3</sub>, NO<sub>2</sub>, and PO<sub>4</sub>. The measured concentrations for these less stable anions may be impacted as a result.

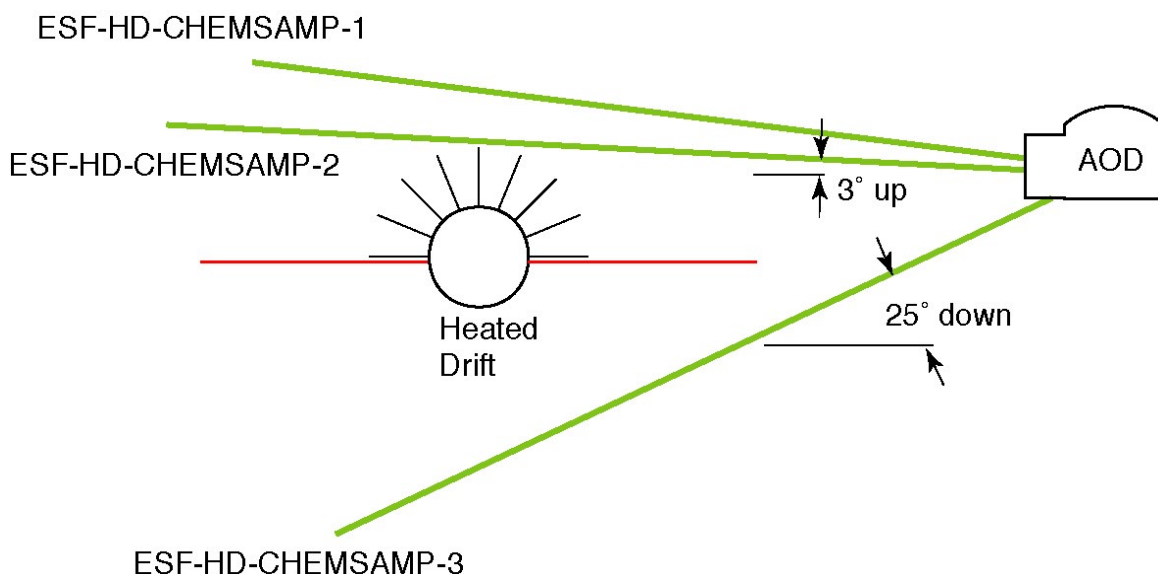
Records indicate that the holding time for samples obtained from centrifuged cores (Section 6.3.4.1) exceeded four months. Water was extracted over a three month period from May 1998 through July 1998. Laboratory analysis was conducted in December 1998 at LLNL by ion chromatography.

Quality control in the analytical laboratories is maintained using reagent blanks, laboratory control samples, and matrix spiked samples submitted in duplicate with sample batches (approximately 10 samples or less). Analytical precision is assessed using the duplicate analyses of both the laboratory control and matrix spiked samples (typically prepared with analyte concentrations approximately midpoint of that expected for the samples). Acceptance limits for measured concentrations in the control samples are  $\pm 10\%$  of the known true value. The accuracy of the results is based upon the percent recoveries for each analyte in the control and matrix spiked samples; the total recoveries of method analytes in the control sample and matrix spiked sample must be within 80% to 120% to be acceptable.

Note that of the six DTNs containing the aqueous chemistry data, the following three are unqualified and should only be used for corroborative purposes: DTNs: LL001200231031.009 [DIRS 153616], LL030107523142.031 [DIRS 169258], and LL990702804244.100 [DIRS 144922].

#### 6.3.4.1.4 CHEMSAMP Water Sample Chemistry

Two boreholes, both continuously cored, were drilled into the heated rock mass of the DST to determine the effects of heating and moisture redistribution on chemistry. ESF-HD-CHEMSAMP-1 was completed to a final depth of 128.99 ft (39.32 m) on November 7, 2001. The collar was located along the left rib of the Access Drift the at  $Y = 15.6$  m. The borehole was angled upward to remain in the below-boiling zone above the heated drift. ESF-HD-CHEMSAMP-3 was completed to a final depth of 130.9 ft (39.90 m) on March 31, 2003. It was also located at  $Y = 15.8$  m, angled downward to penetrate the dryout zone beneath the heated drift (Figure 6.3-45). Approximately half of the recovered core was preserved by wrapping in aluminum foil and sealing in Lexan tubes.

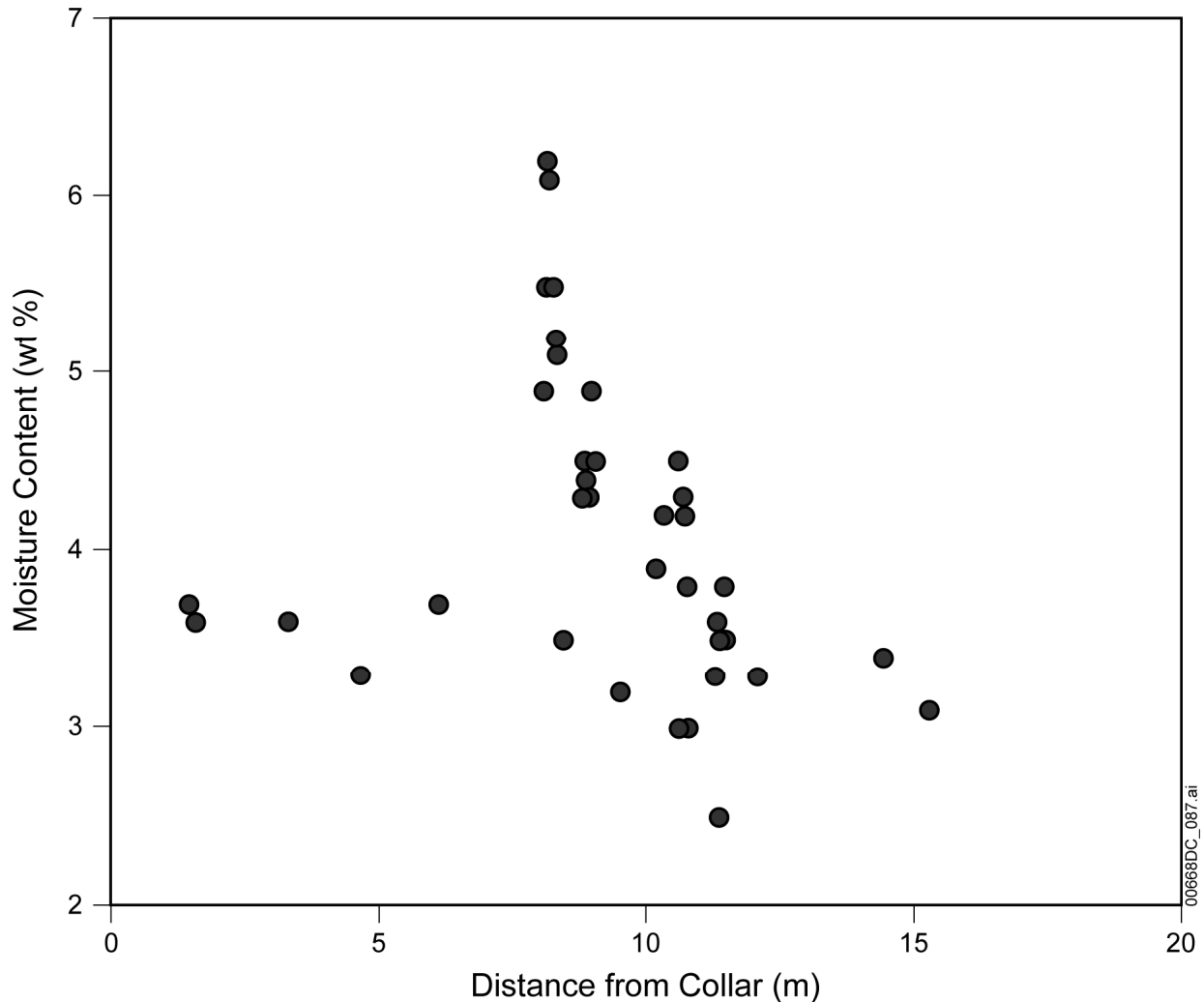


Source: DTN: MO0611ABBHC123.000 [DIRS 178446].

Figure 6.3-45. Cross Section of the Drift Scale Test at the Plane Containing the CHEMSAMP Boreholes



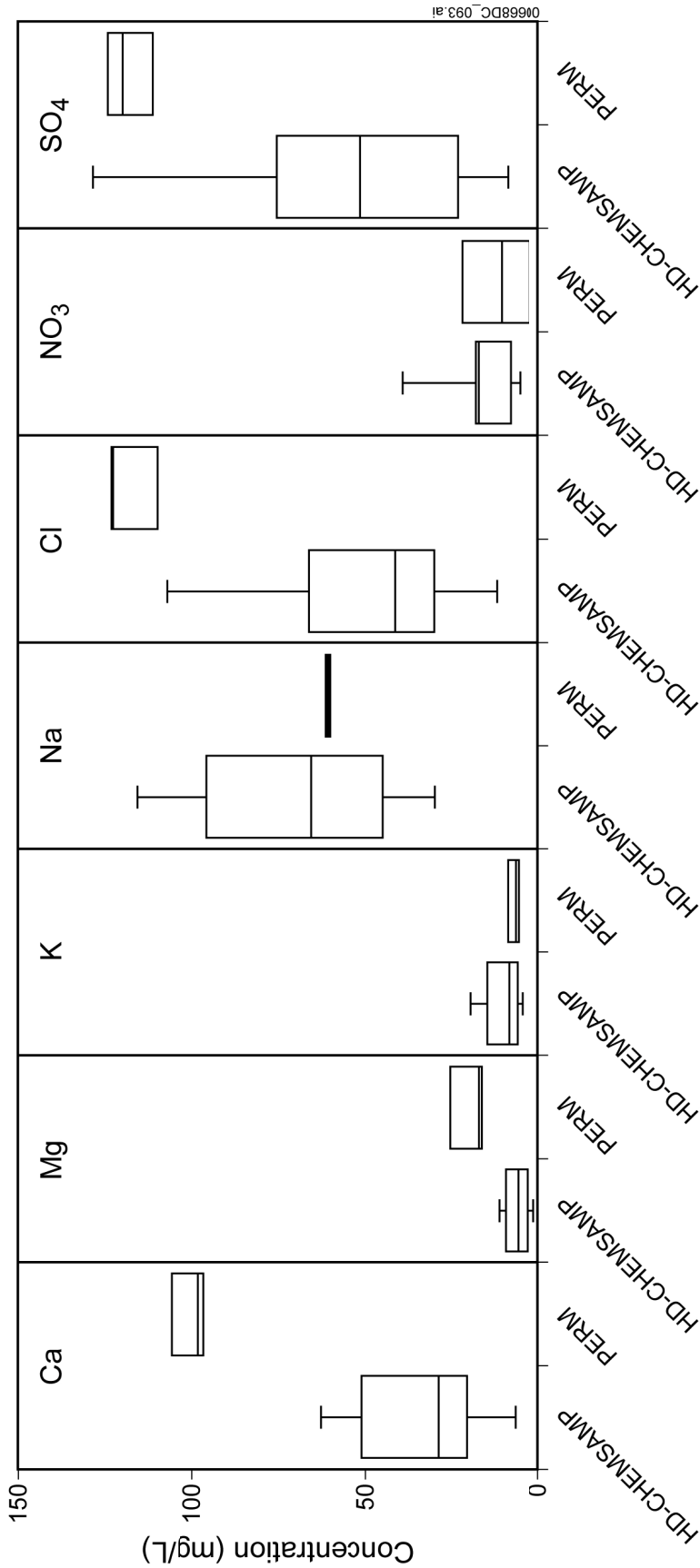
Moisture contents of core samples from CHEMSAMP-1 and CHEMSAMP-3 are listed in Table 6.3-26 and the data are in the TDMS under DTN: GS040308312272.001 [DIRS 178056]. Figure 6.3-46 shows the moisture contents for CHEMSAMP-1 as a function of distance into the borehole. A rather sharp increase in moisture content to values in excess of 6% water by weight was observed at a depth of approximately 8.1 m. Moisture contents of core samples from CHEMSAMP-3 are shown in Figure 6.3-48. In this hole, which penetrated the dryout zone, the moisture contents identify the dryout zone, although none of the samples is entirely dry (the lowest moisture content is 0.3% water by weight).



Source: DTN: GS040308312272.001 [DIRS 178056].

Figure 6.3-46. Moisture Content (wt % water) for Samples from Borehole HD-CHEMSAMP-1

Chemical analyses of extracted pore water from CHEMSAMP-1 and CHEMSAMP-3 are listed in Table 6.3-27 and the data are in the TDMS under DTNs: GS030408312272.002 [DIRS 165226], GS031008312272.008 [DIRS 166570], and GS041108312272.005 [DIRS 178057]. The overall chemistry is similar to that measured in pore water from the HD-PERM core samples from three boreholes drilled adjacent to the DST block prior to heating (Table 6.3-25). The overall comparison between the CHEMSAMP pore water chemistries and those from the PERM water samples is shown as box-and-whisker plots in Figure 6.3-47. The concentration ranges for potassium and sodium (Na) determined for CHEMSAMP pore water encompass those for the PERM pore water. However, calcium (Ca) and magnesium (Mg) concentrations are significantly less in the CHEMSAMP pore water samples than in the PERM pore water. The anions chloride and sulfate often are at lower concentrations in the CHEMSAMP pore water than in the PERM pore water, but there is some overlap in the total range of values. Nitrate concentrations average somewhat larger in the CHEMSAMP pore water.



Source: DTNs: GS030408312272.002 [DIRS 165226]; GS031008312272.008 [DIRS 166570]; GS041108312272.005 [DIRS 178057]; MO0005PORW ATER.000 [DIRS 150930].

NOTE: The boxes represent the 25th through 75th percentiles and the whiskers extend to the complete range of the data.

Figure 6.3-47. Box and Whisker Plots Comparing the Distribution of Chemical Constituents in Water Extracted from HD-CHEMSAMP-1 (N = 4) and HD-CHEMSAMP-3 (N = 13) with Water Extracted from HD-PERM Core (N = 3; Table 6.3-25)

The overall chemistry of the CHEMSAMP pore water indicates dilution (possibly by condensate, especially near the wetting front), but because different constituents were affected to differing extents, addition of pure condensate water or evaporation cannot explain the resulting chemistry. The chemistry of pore water in the unsaturated zone at Yucca Mountain is also heterogeneous on a small scale. Although some fairly dilute samples are evident in the CHEMSAMP pore water, there is no indication of the rather pure condensate water that was sometimes sampled from the hydrology boreholes during the heating phase of the test (Section 6.3.4.1.2). It is possible that the condensate sheds through the fracture network and is not effectively imbibed into the matrix on the time scale of the DST.

Table 6.3-26. Moisture Content of HD-CHEMSAMP Core Samples

<b>Borehole</b>	<b>Interval (ft)</b>	<b>Mid-point (m)</b>	<b>Moisture content (wt %)</b>
HD-CHEMSAMP-1	4.6 to 4.7	1.42	3.7
HD-CHEMSAMP-1	5.0 to 5.1	1.54	3.6
HD-CHEMSAMP-1	10.7 to 10.8	3.28	3.6
HD-CHEMSAMP-1	15.1 to 15.3	4.63	3.3
HD-CHEMSAMP-1	19.9 to 20.0	6.08	3.7
HD-CHEMSAMP-1	26.4 to 26.5	8.06	4.9
HD-CHEMSAMP-1	26.5 to 26.6	8.09	5.5
HD-CHEMSAMP-1	26.6 to 26.7	8.12	6.2
HD-CHEMSAMP-1	26.7 to 26.9	8.17	6.1
HD-CHEMSAMP-1	27.0 to 27.1	8.24	5.5
HD-CHEMSAMP-1	27.1 to 27.2	8.28	5.2
HD-CHEMSAMP-1	27.2 to 27.3	8.31	5.1
HD-CHEMSAMP-1	27.6 to 27.7	8.43	3.5
HD-CHEMSAMP-1	28.8 to 28.9	8.79	4.3
HD-CHEMSAMP-1	28.9 to 29.0	8.82	4.5
HD-CHEMSAMP-1	29.0 to 29.1	8.85	4.4
HD-CHEMSAMP-1	29.1 to 29.2	8.88	4.3
HD-CHEMSAMP-1	29.2 to 29.4	8.93	4.9
HD-CHEMSAMP-1	29.4 to 29.5	8.98	Not determined
HD-CHEMSAMP-1	29.5 to 29.7	9.02	4.5
HD-CHEMSAMP-1	31.0 to 31.2	9.48	3.2
HD-CHEMSAMP-1	33.2 to 33.5	10.17	3.9
HD-CHEMSAMP-1	33.8 to 33.9	10.32	4.2
HD-CHEMSAMP-1	34.6 to 34.7	10.56	4.5
HD-CHEMSAMP-1	34.7 to 34.9	10.61	3.0
HD-CHEMSAMP-1	34.9 to 35.0	10.65	4.3
HD-CHEMSAMP-1	35.0 to 35.1	10.68	4.2
HD-CHEMSAMP-1	35.1 to 35.2	10.71	3.8
HD-CHEMSAMP-1	35.2 to 35.3	10.74	3.0
HD-CHEMSAMP-1	36.9 to 37.0	11.26	3.3

Table 6.3-26. Moisture Content of HD-CHEMSAMP Core Samples (Continued)

<b>Borehole</b>	<b>Interval (ft)</b>	<b>Mid-point (m)</b>	<b>Moisture content (wt %)</b>
HD-CHEMSAMP-1	37.0 to 37.1	11.29	3.6
HD-CHEMSAMP-1	37.1 to 37.2	11.32	2.5
HD-CHEMSAMP-1	37.2 to 37.3	11.35	3.5
HD-CHEMSAMP-1	37.4 to 37.5	11.41	3.8
HD-CHEMSAMP-1	37.5 to 37.6	11.45	3.5
HD-CHEMSAMP-1	39.5 to 39.6	12.05	3.3
HD-CHEMSAMP-1	47.2 to 47.3	14.40	3.4
HD-CHEMSAMP-1	50.1 to 50.2	15.29	3.1
HD-CHEMSAMP-3	29.0 to 29.1	8.85	3.6
HD-CHEMSAMP-3	32.0 to 32.1	9.77	4.4
HD-CHEMSAMP-3	33.9 to 34.0	10.35	4.0
HD-CHEMSAMP-3	34.0 to 34.1	10.38	5.3
HD-CHEMSAMP-3	34.1 to 34.3	10.42	5.3
HD-CHEMSAMP-3	34.3 to 34.4	10.47	5.3
HD-CHEMSAMP-3	34.4 to 34.5	10.50	5.3
HD-CHEMSAMP-3	36.5 to 36.7	11.16	3.9
HD-CHEMSAMP-3	36.7 to 36.8	11.20	3.7
HD-CHEMSAMP-3	36.8 to 36.9	11.23	4.1
HD-CHEMSAMP-3	36.9 to 37.0	11.26	4.1
HD-CHEMSAMP-3	37.0 to 37.1	11.29	3.5
HD-CHEMSAMP-3	37.1 to 37.2	11.32	4.4
HD-CHEMSAMP-3	37.2 to 37.4	11.37	4.5
HD-CHEMSAMP-3	37.4 to 37.5	11.41	4.1
HD-CHEMSAMP-3	38.2 to 38.4	11.67	3.6
HD-CHEMSAMP-3	38.4 to 38.6	11.73	3.5
HD-CHEMSAMP-3	38.6 to 38.8	11.80	3.3
HD-CHEMSAMP-3	38.8 to 38.9	11.84	3.7
HD-CHEMSAMP-3	38.9 to 39.0	11.87	3.8
HD-CHEMSAMP-3	39.0 to 39.1	11.90	3.5
HD-CHEMSAMP-3	41.0 to 41.1	12.51	3.1
HD-CHEMSAMP-3	42.3 to 42.4	12.91	5.1
HD-CHEMSAMP-3	42.4 to 42.6	12.95	5.0
HD-CHEMSAMP-3	42.6 to 42.8	13.01	3.6
HD-CHEMSAMP-3	44.3 to 44.4	13.52	3.3
HD-CHEMSAMP-3	46.0 to 46.1	14.04	4.0
HD-CHEMSAMP-3	46.1 to 46.2	14.07	4.0
HD-CHEMSAMP-3	46.2 to 46.3	14.10	3.8
HD-CHEMSAMP-3	46.3 to 46.5	14.14	4.6
HD-CHEMSAMP-3	46.5 to 46.6	14.19	5.1
HD-CHEMSAMP-3	46.6 to 46.8	14.23	4.7
HD-CHEMSAMP-3	46.8 to 46.9	14.28	4.4

Table 6.3-26. Moisture Content of HD-CHEMSAMP Core Samples (Continued)

<b>Borehole</b>	<b>Interval (ft)</b>	<b>Mid-point (m)</b>	<b>Moisture content (wt %)</b>
HD-CHEMSAMP-3	47.8 to 47.9	14.58	3.3
HD-CHEMSAMP-3	51.4 to 51.5	15.68	1.1
HD-CHEMSAMP-3	54.4 to 54.6	16.61	1.0
HD-CHEMSAMP-3	56.4 to 56.5	17.21	0.6
HD-CHEMSAMP-3	58.3 to 58.4	17.79	0.7
HD-CHEMSAMP-3	60.0 to 60.1	18.30	0.6
HD-CHEMSAMP-3	62.4 to 62.5	19.03	0.7
HD-CHEMSAMP-3	63.3 to 63.4	19.31	0.7
HD-CHEMSAMP-3	64.7 to 64.8	19.74	0.6
HD-CHEMSAMP-3	65.9 to 66.0	20.10	0.5
HD-CHEMSAMP-3	67.8 to 67.9	20.68	0.3
HD-CHEMSAMP-3	70.2 to 70.3	21.41	0.5
HD-CHEMSAMP-3	72.3 to 72.4	22.05	0.5
HD-CHEMSAMP-3	75.9 to 76.0	23.15	0.5
HD-CHEMSAMP-3	79.9 to 80.0	24.37	0.8
HD-CHEMSAMP-3	81.7 to 81.8	24.92	0.8
HD-CHEMSAMP-3	84.2 to 84.3	25.68	0.9
HD-CHEMSAMP-3	88.0 to 88.1	26.84	0.6
HD-CHEMSAMP-3	90.3 to 90.4	27.54	1.9
HD-CHEMSAMP-3	92.8 to 92.9	28.30	2.8
HD-CHEMSAMP-3	95.1 to 95.2	29.00	3.3
HD-CHEMSAMP-3	98.0 to 98.1	29.89	3.3
HD-CHEMSAMP-3	100.7 to 100.9	30.72	3.5
HD-CHEMSAMP-3	104.0 to 104.1	31.71	3.8
HD-CHEMSAMP-3	104.5 to 104.6	31.87	3.9
HD-CHEMSAMP-3	104.6 to 104.7	31.90	4.7
HD-CHEMSAMP-3	104.7 to 104.8	31.93	4.0
HD-CHEMSAMP-3	104.8 to 105.0	31.97	3.0
HD-CHEMSAMP-3	105.0 to 105.2	32.03	3.7
HD-CHEMSAMP-3	105.2 to 105.3	32.08	3.8
HD-CHEMSAMP-3	106.3 to 106.4	32.42	3.1
HD-CHEMSAMP-3	108.2 to 108.4	33.01	3.6
HD-CHEMSAMP-3	108.4 to 108.5	33.06	3.8
HD-CHEMSAMP-3	108.5 to 108.6	33.09	3.8
HD-CHEMSAMP-3	108.6 to 108.7	33.12	3.9
HD-CHEMSAMP-3	108.7 to 108.8	33.15	4.3
HD-CHEMSAMP-3	108.8 to 08.9	33.18	4.0
HD-CHEMSAMP-3	108.9 to 109.0	33.21	4.2
HD-CHEMSAMP-3	109.8 to 109.9	33.48	3.2
HD-CHEMSAMP-3	110.2 to 110.4	33.62	3.6
HD-CHEMSAMP-3	111.2 to 111.3	33.91	3.5

Table 6.3-26. Moisture Content of HD-CHEMSAMP Core Samples (Continued)

<b>Borehole</b>	<b>Interval (ft)</b>	<b>Mid-point (m)</b>	<b>Moisture content (wt %)</b>
HD-CHEMSAMP-3	111.7 to 111.8	34.06	3.4
HD-CHEMSAMP-3	111.8 to 111.9	34.09	3.4
HD-CHEMSAMP-3	111.9 to 112.0	34.12	4.0
HD-CHEMSAMP-3	112.8 to 113.0	34.41	3.6
HD-CHEMSAMP-3	114.6 to 114.9	34.98	3.7
HD-CHEMSAMP-3	115.0 to 115.1	35.07	3.9
HD-CHEMSAMP-3	115.1 to 115.3	35.11	3.7
HD-CHEMSAMP-3	115.3 to 115.4	35.16	3.7
HD-CHEMSAMP-3	115.4 to 115.5	35.19	3.6
HD-CHEMSAMP-3	115.5 to 115.6	35.22	3.4
HD-CHEMSAMP-3	117.8 to 118.0	35.94	3.0
HD-CHEMSAMP-3	118.8 to 118.9	36.23	2.9
HD-CHEMSAMP-3	121.0 to 121.1	36.90	3.3
HD-CHEMSAMP-3	122.8 to 122.9	37.44	3.0
HD-CHEMSAMP-3	124.7 to 124.8	38.02	3.4
HD-CHEMSAMP-3	127.0 to 127.1	38.72	3.6

Source: DTN: GS040308312272.001 [DIRS 178056].

Table 6.3-27. Chemical Analyses of Water Extracted from CHEMSAMP Core Samples

Borehole	Interval (ft)	Mid-point (m)	pH	Conductivity	Ca (mg/L)	Mg (mg/L)	K (mg/L)	Na (mg/L)	SiO <sub>2</sub> (mg/L)	HCO <sub>3</sub> (mg/L)	Cl (mg/L)	Br (mg/L)	NO <sub>3</sub> (mg/L)	SO <sub>4</sub> (mg/L)	F (mg/L)
ESF-HD-CHEMSAMP-1	26.1 to 26.9	8.08	7.6	820	82	18	8.4	53	49	254	71	0.24	22	88	0.91
ESF-HD-CHEMSAMP-1	28.8 to 29.7	8.92	N/M	N/M	84	16.5	10.7	69	49	162	45	N/D	20	70	0.83
ESF-HD-CHEMSAMP-1	34.6 to 35.4	10.67	N/M	N/M	56	12.7	10.9	63	47	63	48	N/D	38	59	1.8
ESF-HD-CHEMSAMP-1	37.1 to 37.2	11.32	N/M	N/M	57	11.6	13.6	66	56	192	79	N/D	29	62	1.7
ESF-HD-CHEMSAMP-3	33.9 to 34.4	10.41	N/M	N/M	29	6.1	6.4	45	45	88	41	0.36	18	51	1.2
ESF-HD-CHEMSAMP-3	34.4 to 34.5	10.50	7.6	420	28	5.4	5.3	40	43	72	41	0.19	18	51	1.2
ESF-HD-CHEMSAMP-3	36.5 to 37.5	11.28	7.9	920	62	8.6	14	96	51	143	107	0.37	39	128	1.7
ESF-HD-CHEMSAMP-3	38.2 to 39.1	11.78	N/M	N/M	51	11	19.7	116	46	145	34	N/D	5.9	17	0.45
ESF-HD-CHEMSAMP-3	42.3 to 42.8	12.97	8.0	530	21	1.5	8.8	66	57	146	30	0.13	10	30	0.79
ESF-HD-CHEMSAMP-3	46.0 to 46.3	14.07	7.8	200	6.9	1.2	4.9	30	33	N/M	12	N/D	5.3	8.8	1.3
ESF-HD-CHEMSAMP-3	46.3 to 46.9	14.20	7.9	300	17	3.4	6.9	51	53	118	27	0.15	7.9	19	1
ESF-HD-CHEMSAMP-3	104.6 to 105.3	31.99	7.9	550	13	2	5.2	39	28	45	27	N/D	6	23	0.84
ESF-HD-CHEMSAMP-3	108.4 to 109.0	33.13	N/M	530	26	4.2	7.9	61	36	104	58	N/D	11	44	0.8
ESF-HD-CHEMSAMP-3	111.8 to 112.0	34.11	N/M	N/M	49	9.6	18.3	108	65	N/M	66	N/D	18	75	1.3
ESF-HD-CHEMSAMP-3	113.1 to 113.8	34.58	N/M	1090	63	11.5	15.2	103	73	212	83	0.61	25	115	1.2
ESF-HD-CHEMSAMP-3	115.0 to 115.6	35.14	N/M	N/M	46	9.2	15.7	89	64	228	66	N/D	17	58	1
ESF-HD-CHEMSAMP-3	127.1 to 128.0	38.88	N/M	820	55	10.8	13.1	85	59	235	63	0.67	18	79	1.4

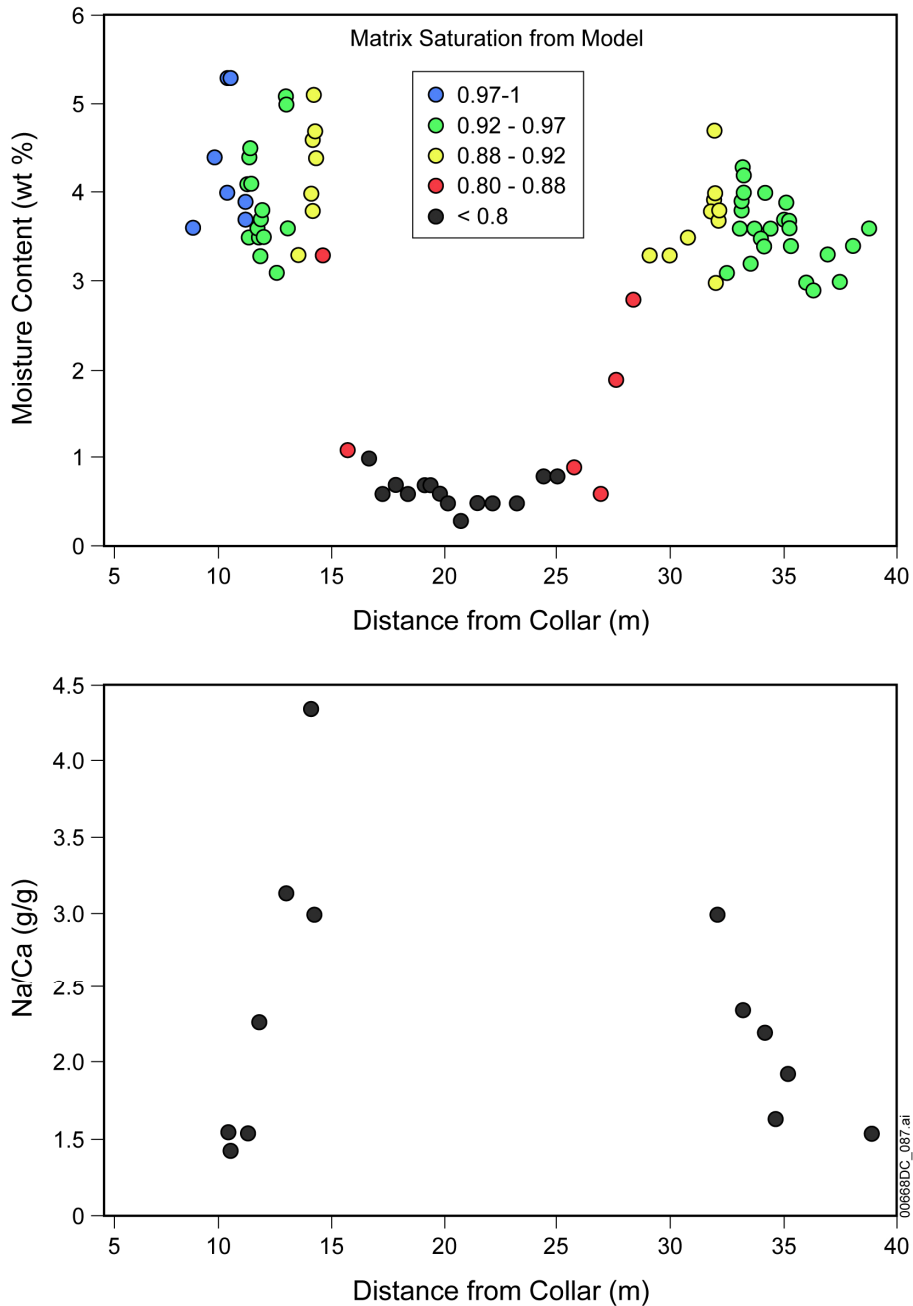
Source: DTNs: GS030408312272.002 [DIRS 165226]; GS031008312272.008 [DIRS 166570]; GS041108312272.005 [DIRS 178057].

NOTE: N/D = not detected; N/M = not measured.



The chemical data for water from borehole CHEMSAMP-3 was examined for trends related to moisture content or location. The extraction of water by ultracentrifuge is limited to rock cores with moisture contents above approximately 3% water (by weight). There are no apparent trends in chemistry with moisture content. Additionally, competing processes such as dilution by condensate, evaporation, and mineral precipitation tend to obscure any trends in concentration for a given constituent. However, the Na/Ca ratio shows significant trends with sample location (Figure 6.3-48). Na/Ca increases toward the dryout zone from both ends of borehole CHEMSAMP-3. The trend is steeper on the near side of the dryout zone as would be predicted by the angle of the borehole with the dryout zone boundary. The most likely cause of the increase in Na/Ca is precipitation of calcite due to both increasing temperature and loss of carbon dioxide. Decreases in both Ca and Mg in the CHEMSAMP pore water can be explained by calcite precipitation when significant amounts of Mg are co-precipitated with calcite.

The CHEMSAMP boreholes, especially CHEMSAMP-3, provide samples of pore water affected by heating and moisture redistribution. The chemistry of the pore water indicates the effects of dilution by condensate and precipitation of calcite. However, not all constituents are affected and the overall chemical compositions of these water samples are not substantially different from ambient pore water. Pore water samples consisting predominantly of condensate are not evident in the samples analyzed from the CHEMSAMP core.



Source: DTNs: GS031008312272.008 [DIRS 166570]; GS040308312272.001 [DIRS 178056]; GS041108312272.005 [DIRS 178057].

NOTE: In the upper plot, the dryout zone is clearly distinguished by moisture contents less than 1%, and the moisture contents correspond well with the predicted matrix saturations estimated for the time that the borehole was drilled. In the lower plot, the increases in Na/Ca in extracted water are an indication of the loss of calcium by precipitation of calcite. The steeper increase on the near side of the dryout zone corresponds to the steeper temperature gradient on this side compared to the far side (Figure 6.3-44).

Figure 6.3-48. Moisture Content (in wt % water) of Core Samples from HD-CHEMSAMP-3 as a Function of Distance into the Borehole (upper plot), and Na/Ca Ratio (by weight), Also as a Function of Distance into the Borehole (lower plot)

### 6.3.4.2 Gas Chemistry

Gas samples were periodically collected from the hydrology boreholes (see Figure 6.3-4) during the heating and cooling phases of the Drift-Scale Heater Test (DST) from December 3, 1997, through December, 2005. The purpose of these samples was to measure the concentration and carbon isotope ratio of CO<sub>2</sub> and the hydrogen and oxygen isotope ratios of water vapor. The concentration and isotopic composition of CO<sub>2</sub> in the heated drift and the observation drift were also measured during the test. In addition, to provide data on the background concentration and isotopic composition of CO<sub>2</sub> in the rock, two gas samples were collected in August 1997 from borehole 182 (one of the ambient testing boreholes drilled on the opposite side of the connecting drift across from the DST block). The CO<sub>2</sub> concentrations and isotope compositions for both the gas samples and the condensate samples collected during 31 sampling trips through the duration of the DST are in the TDMS under the following DTNs:

- LB980420123142.005 [DIRS 111471]
- LB980715123142.003 [DIRS 111472]
- LB0404ISODSTHP.003 [DIRS 169254]
- LB990630123142.003 [DIRS 111476]
- LB0102CO2DST98.001 [DIRS 159306]
- LB000121123142.003 [DIRS 146451]
- LB000718123142.003 [DIRS 158342]
- LB0011CO2DST08.001 [DIRS 153460]
- LB0108CO2DST05.001 [DIRS 156888]
- LB0203CO2DSTEH.001 [DIRS 158349]
- LB0206C14DSTEH.001 [DIRS 159303]
- LB0303ISODSTCP.001 [DIRS 177538]
- LB0309ISODSTCP.001 [DIRS 177539]
- LB0403ISODSTCP.001 [DIRS 177540]
- LB0410ISODSTCP.001 [DIRS 177541]
- LB0509ISODSTCP.001 [DIRS 177542].

#### 6.3.4.2.1 Gas Sampling

Gas samples were pumped from the 12 hydrology boreholes (57 to 61, 74 to 78, 185 and 186). Each hydrology borehole was separated into three or four intervals by strings of high-temperature, inflatable packers. High temperature plastic tubes (that function as conduits for both air injection in permeability measurements and fluid sampling) led from each interval in the boreholes to the observation drift. For gas sampling, the tube leading to the interval to be sampled was isolated and connected to a diaphragm pump with a moisture trap. For higher temperature intervals (greater than approximately 50°C), a 4°C gas chiller unit was placed before the pump to condense the water vapor from the gas before collection.

After purging the interval and sample tubing for 4 to 5 minutes, the gas samples were collected in 1-liter Tedlar bags from the outlet of the diaphragm pump. The normal pumping speed for the pump is 60 L/min; however, airflow rates during sampling varied considerably, depending on factors such as the permeability of the interval, the temperature, and the air moisture content. In

particular, when the temperature in an interval was near the boiling temperature or above, water vapor constituted the major component of the gas phase (greater than 98%). Since most of the water vapor was being stripped from the gas before it entered the pump, the flow of noncondensable gas out of the pump was very low (to less than 1 L/min).

The water vapor condensed in the chiller trap was sampled for oxygen and hydrogen isotope measurements. The condensate in the water trap was composed of all of the water vapor that condensed in the trap throughout the pumping period, including the time during which the sampling interval was being purged. Sampling times for the vapor condensates ranged from approximately 20 minutes for cooler intervals (up to about 80°C) to as little as 5 minutes for the higher-temperature intervals resulting from the high vapor contents of the intervals near the boiling point. After each sample was collected, the chiller trap was thoroughly dried, and the chiller unit was purged with dry tunnel air for at least 5 minutes before collection of the next sample was begun. During two sampling trips (12/16/03 and 4/19/04), the chiller unit was broken, so no condensate samples were collected.

Air samples from the observation drift were collected using the diaphragm pump to fill a 3-liter Tedlar bag. Samples of the heated drift were collected by attaching the pump to a stainless steel tube leading to approximately the mid-point of the drift. The sample was taken after purging the tube for approximately 5 minutes. To determine the initial concentration and isotopic composition of CO<sub>2</sub> in the rock, two gas samples from borehole 182 were collected during August 1998. To take these samples, an inflatable packer was installed approximately 20 m into the borehole. The first sample was collected after the borehole was purged for approximately 5 minutes. The second sample was taken after the interval had been pumped for almost 24 hours.

#### **6.3.4.2.2 Results: CO<sub>2</sub> Concentration**

The CO<sub>2</sub> and isotopic compositions are given in Table 6.3-28. The CO<sub>2</sub> concentrations in the gas samples were measured using two different instruments. Initially, the laboratory measurements of the CO<sub>2</sub> concentrations for these samples were only intended to gain an estimate of the amount of CO<sub>2</sub> that should be produced during separation of the CO<sub>2</sub> from the samples intended for isotopic analyses. The CO<sub>2</sub> concentrations in the rock were supposed to be analyzed in situ with a Columbus Instruments Model 180C Gas Analyzer. However, because of problems with the sampling technique for the in situ measurements and the gas analyzer, the only CO<sub>2</sub> concentration data from the first three years of heating are the laboratory data for the samples listed in Table 6.3-28. Starting in January 2001, the CO<sub>2</sub> concentrations of the isotope samples were analyzed using the Columbus Instruments gas analyzer at the site calibrated with qualified standards. In July of 2004, the computer controlling the Columbus Instruments gas analyzer went down. After replacing the computer, technicians were unable to successfully load the software to run the gas analyzer. Therefore, from that time through the end of the cooling phase (the final four data sets), the samples were analyzed again using the laboratory instrument. Both the laboratory and field analytical techniques are outlined below, and a comparison of the data for samples analyzed by both methods is presented.

For the first three years of the DST, the samples were transported back to a laboratory for analysis. The CO<sub>2</sub> concentrations in the samples are measured using an infrared analyzer (Li-Cor) in the Amundson Laboratory at the University of California, Berkeley. For analyses,

5 cc of gas was injected into the CO<sub>2</sub> analyzer and compared to a 500 ppm standard. At low concentrations ( $\leq 2,000$  ppm or 0.2% v/v), the precision of this technique was approximately  $\pm 1\%$  of the measured value. At higher concentrations, the analyses were out of the range of the standard used to calibrate the instrument, and the precision is not as high (see discussion below). For the final four sets of samples collected from the cooling phase, the gas analyzer at the ESF was no longer functional, so the Li-Cor was also used to measure the CO<sub>2</sub> concentrations in those samples. For these analyses, samples of the qualified gas standards from the site were also measured in order to construct a calibration curve for the full range of values.

Beginning in January 2001, samples were also analyzed using the Columbus Instruments Model 180C gas analyzer at the ESF. For these analyses, approximately 250 cc of gas was fed into the instrument and analyzed after calibration with a qualified standard gas. For samples with lower concentrations ( $\leq 1\%$  v/v), the analyses were done using the low-range sensor calibrated with a 0.504% CO<sub>2</sub> standard. These analyses are accurate to within approximately  $\pm 0.05\%$ . Higher concentration samples (greater than 1% v/v) were measured with the high-range sensor calibrated with a 4.995% CO<sub>2</sub> standard, with an accuracy to within  $\pm 0.3\%$ .

A comparison between the two instruments suggests that lower-end measurements (less than 0.05%), tend to be a bit higher for the Li-Cor analyses than the Columbus Instruments analyses (for the samples analyzed during the first 3 years of the heating phase, not for the samples collected at the end of the cooling phase). For this case, the Li-Cor data are probably better, since the standard used for comparison on this instrument was a 0.05% standard. At higher concentrations, the Li-Cor data are consistently lower than Columbus Instruments data. For these samples, the Columbus Instruments data are more reliable, because they were measured using calibration gases in the same range of concentration. In general, for samples with CO<sub>2</sub> concentrations greater than 0.2%, the early Li-Cor measurements are low by approximately 16%.

Table 6.3-28. Concentration and Isotopic Compositions of CO<sub>2</sub> in Gas Samples Collected during the DST Heating and Cooling Phases

Sample Interval <sup>a</sup> (BH-Zone)	YMP Tracking Number	Date Sampled	<sup>2</sup> CO <sub>2</sub> (v/v-percent) <sup>b</sup>	$\delta^{13}\text{C}$ (‰) <sup>c</sup>	$\delta^{18}\text{O}$ (‰) <sup>d</sup>	<sup>14</sup> C (Fraction Modern Carbon)
57-3	SPC 0052 7911	2/10/98	0.102	-13.8	31.2	—
59-3	SPC 0052 7900	2/09/98	0.084	-10.3	31.9	—
60-3 <sup>e</sup>	SPC 0052 7906	2/09/98	0.100	-8.0	22.9	—
61-3	SPC 0052 7914	2/10/98	0.112	-11.6	30.2	—
74-4	SPC 0052 7903	2/09/98	0.062	-11.2	32.9	—
77-3	SPC 0052 7901	2/09/98	0.644	-5.5	48.3	—
77-3 <sup>e</sup>	SPC 0052 7902	2/10/98	—	-7.4	24.1	—
78-3	SPC 0052 7913	2/10/98	0.244	-11.3	30.7	0.400
Heated Drift	SPC 0052 7909	2/10/98	0.040	-10.3	32.3	—
Observation Drift	SPC 0052 7907	2/10/98	0.043	-10.3	40.0	—
57-3	SPC 0052 7978	6/04/98	0.170	-16.6	29.5	—
58-3	SPC 0052 7979	6/04/98	0.189	-12.0	29.1	—

Table 6.3-28. Concentration and Isotopic Compositions of CO<sub>2</sub> in Gas Samples Collected during the DST Heating and Cooling Phases (Continued)

Sample Interval <sup>a</sup> (BH-Zone)	YMP Tracking Number	Date Sampled	<sup>2</sup> CO <sub>2</sub> (v/v-percent) <sup>b</sup>	δ <sup>13</sup> C (‰) <sup>c</sup>	δ <sup>18</sup> O (‰) <sup>d</sup>	<sup>14</sup> C (Fraction Modern Carbon)
59-3	SPC 0052 7980	6/04/98	0.222	-9.7	26.6	—
59-4	SPC 0052 7988	6/04/98	0.538	-8.9	25.8	—
74-3	SPC 0052 7981	6/04/98	0.143	-13.6	30.1	—
75-3	SPC 0052 7982	6/04/98	0.189	-11.8	29.0	0.416
76-3	SPC 0052 7983	6/04/98	0.687	-5.5	25.2	0.214
77-3	SPC 0052 7984	6/04/98	0.621	-5.5	21.1	—
78-3	SPC 0052 7986	6/04/98	1.494	-8.7	23.4	0.210
185-3	SPC 0052 7987	6/04/98	0.160	-14.7	22.0	—
Observation Drift	SPC 0052 7989	6/04/98	0.046	-10.6	36.4	—
57-3	SPC 0052 7278	8/06/98	0.152	-15.4	29.5	—
58-3	SPC 0052 7279	8/06/98	0.234	-9.3	28.3	—
59-3	SPC 0052 7281	8/06/98	0.342	-7.7	25.4	—
60-3	SPC 0052 7283	8/06/98	14.160	-0.5	24.2	—
61-3	SPC 0052 7285	8/06/98	2.986	-3.7	23.9	—
74-3	SPC 0052 7267	8/05/98	0.133	-12.1	29.9	—
75-3	SPC 0052 7268	8/05/98	0.222	-10.4	29.4	—
76-3	SPC 0052 7269	8/05/98	0.949	-3.5	24.5	—
77-3	SPC 0052 7271	8/05/98	3.330	-4.3	24.0	—
78-3	SPC 0052 7273	8/05/98	2.474	-6.3	23.4	0.156
185-3	SPC 0052 7275	8/06/98	0.186	-12.7	28.8	—
186-2	SPC 0052 7277	8/06/98	1.497	-8.4	25.8	—
182 (56')	SPC 0052 7276	8/06/98	0.092	-13.1	32.4	—
182 (64')	SPC 0052 7266	8/05/98	0.054	-11.9	33.0	—
Observation Drift	SPC 0052 7287	8/06/98	0.038	-9.8	38.0	—
57-3	SPC 0052 7288	10/07/98	0.189	-16.0	29.2	0.492
58-3	SPC 0052 7289	10/07/98	0.414	-7.5	28.0	—
59-3	SPC 0052 7290	10/07/98	0.633	-5.1	22.7	0.200
61-3	SPC 0052 7293	10/07/98	5.335	-2.1	22.6	0.125
74-3	SPC 0052 7295	10/07/98	—	—	—	—
75-3	SPC 0052 7994	10/07/98	0.374	-10.3	27.6	0.322
76-3	SPC 0052 7296	10/07/98	1.611	-3.1	21.3	0.140
77-3	SPC 0052 7990	10/08/98	0.216	-5.1	25.1	—
78-3	SPC 0052 7992	10/08/98	2.702	-3.9	22.1	0.105
185-3	SPC 0052 7995	10/08/98	0.264	-10.5	—	0.369
186-2	SPC 0052 7996	10/08/98	2.239	-7.5	24.0	—
Observation Drift	SPC 0052 7998	10/08/98	0.046	-10.8	37.6	—
Heated Drift	SPC 0052 7999	10/08/98	0.044	-9.5	30.0	—

Table 6.3-28. Concentration and Isotopic Compositions of CO<sub>2</sub> in Gas Samples Collected during the DST Heating and Cooling Phases (Continued)

Sample Interval <sup>a</sup> (BH-Zone)	YMP Tracking Number	Date Sampled	<sup>2</sup> CO <sub>2</sub> (v/v-percent) <sup>b</sup>	δ <sup>13</sup> C (‰) <sup>c</sup>	δ <sup>18</sup> O (‰) <sup>d</sup>	<sup>14</sup> C (Fraction Modern Carbon)
57-1	SPC 0054 1258	12/16/98	0.068	-9.8	31.2	—
57-2	SPC 0054 1259	12/16/98	0.191	-7.9	29.3	—
57-3	SPC 0054 1260	12/16/98	0.220	-16.5	28.7	—
57-4	SPC 0054 1261	12/16/98	0.130	-12.8	29.5	—
58-3	SPC 0054 1262	12/16/98	0.392	-6.1	28.0	—
59-1	SPC 0054 1263	12/16/98	0.087	-7.9	28.0	—
59-3	SPC 0054 1264	12/16/98	0.501	-4.1	22.4	—
59-4	SPC 0054 1267	12/16/98	1.562	-4.2	24.1	—
60-2	SPC 0054 1269	12/16/98	0.099	-5.5	23.7	—
61-1	SPC 0054 1271	12/16/98	0.051	-3.9	32.0	—
61-2	SPC 0054 1272	12/16/98	0.083	-4.4	24.8	—
61-4	SPC 0054 1274	12/16/98	0.331	—	—	—
74-1	SPC 0054 1236	12/14/98	0.047	-10.0	29.8	—
74-2	SPC 0054 1235	12/14/98	0.084	—	—	—
74-3	SPC 0054 1234	12/14/98	0.220	-12.3	29.8	—
74-4	SPC 0054 1233	12/14/98	—	—	—	—
75-3	SPC 0054 1232	12/14/98	0.495	-9.3	27.8	—
76-1	SPC 0054 1231	12/14/98	0.058	-9.6	30.6	—
76-2	SPC 0054 1237	12/15/98	0.308	-5.2	24.5	—
76-3	SPC 0054 1239	12/15/98	1.430	-2.7	20.9	—
76-4	SPC 0054 1241	12/15/98	2.164	-3.5	23.6	—
77-3	SPC 0054 1243	12/15/98	0.115	—	—	—
78-1	SPC 0054 1245	12/15/98	0.100	-11.4	29.1	—
78-2	SPC 0054 1246	12/15/98	2.188	-3.8	24.6	—
78-3	SPC 0054 1248	12/15/98	2.370	-1.5	23.2	0.081
78-4	SPC 0054 1250	12/15/98	0.358	-11.7	28.1	—
185-1	SPC 0054 1252	12/15/98	0.159	-13.2	29.5	—
185-2	SPC 0054 1253	12/15/98	1.387	-10.7	28.6	—
185-3	SPC 0054 1254	12/15/98	0.293	-10.3	27.9	—
185-4	SPC 0054 1255	12/15/98	0.136	-12.4	28.8	—
186-2	SPC 0054 1256	12/15/98	2.043	-6.6	23.5	—
Observation Drift	SPC 0054 1266	12/16/98	0.038	-9.3	39.2	—
Heated Drift	SPC 0054 1276	12/16/98	0.040	-9.7	26.5	0.988
57-3	SPC 0055 0611	3/02/99	0.277	-16.5	26.4	—
58-3	SPC 0055 0612	3/02/99	0.552	-5.7	25.8	—
59-3	SPC 0055 0613	3/02/99	0.746	-3.3	20.1	—
60-2	SPC 0055 0616	3/02/99	0.087	-5.9	22.5	—

Table 6.3-28. Concentration and Isotopic Compositions of CO<sub>2</sub> in Gas Samples Collected during the DST Heating and Cooling Phases (Continued)

Sample Interval <sup>a</sup> (BH-Zone)	YMP Tracking Number	Date Sampled	<sup>2</sup> CO <sub>2</sub> (v/v-percent) <sup>b</sup>	δ <sup>13</sup> C (‰) <sup>c</sup>	δ <sup>18</sup> O (‰) <sup>d</sup>	<sup>14</sup> C (Fraction Modern Carbon)
61-2	SPC 0055 0618	3/02/99	0.097	-3.5	21.5	—
74-1	SPC 0054 1278	3/01/99	0.046	—	—	—
74-2	SPC 0054 1279	3/01/99	0.110	-10.9	27.9	—
74-3	SPC 0054 1280	3/01/99	0.437	-11.2	27.1	—
74-4	SPC 0054 1281	3/01/99	0.302	-11.0	27.6	—
75-3	SPC 0054 1282	3/01/99	1.051	-7.9	25.5	—
76-1	SPC 0054 1283	3/01/99	0.055	-7.9	33.8	—
76-2	SPC 0054 1285	3/01/99	0.324	-4.6	22.7	—
76-3	SPC 0054 1287	3/01/99	1.860	-3.0	19.9	—
76-4	SPC 0055 0600	3/01/99	4.987	-3.0	20.1	—
77-3	SPC 0055 0603	3/02/99	0.119	-6.3	20.5	—
78-1	SPC 0054 1284	3/02/99	0.090	-9.0	28.4	—
78-3	SPC 0055 0605	3/02/99	4.409	-1.8	18.8	—
185-2	SPC 0055 0607	3/02/99	2.020	-9.5	26.1	0.197
185-3	SPC 0055 0608	3/02/99	0.331	-9.8	25.7	0.314
186-2	SPC 0055 0609	3/02/99	2.455	-5.8	20.1	—
Observation Drift	SPC 0055 0602	3/01/99	0.039	-7.8	33.9	—
57-3	SPC 0055 1123	5/25/99	0.333	-15.0	30.7	0.467
58-3	SPC 0055 1121	5/25/99	0.681	-3.5	30.2	—
59-3	SPC 0055 1119	5/25/99	1.101	-1.0	23.5	—
60-2	SPC 0055 1115	5/25/99	0.074	-6.9	26.4	—
60-3	SPC 0055 1113	5/25/99	0.072	-9.3	31.5	—
61-2	SPC 0055 1117	5/25/99	0.073	-4.7	27.3	—
74-1	SPC 0055 1124	5/25/99	0.047	—	—	—
74-2	SPC 0055 1125	5/25/99	0.129	-10.2	29.1	—
74-3	SPC 0055 1126	5/25/99	0.639	-9.9	28.7	0.277
74-4	SPC 0055 1127	5/25/99	0.406	-9.6	29.5	—
75-3	SPC 0055 1128	5/25/99	1.374	-6.3	27.9	0.178
76-1	SPC 0055 1130	5/26/99	0.058	—	—	—
76-2	SPC 0055 1131	5/26/99	0.535	-2.2	24.8	—
76-3	SPC 0055 1133	5/26/99	3.112	-2.0	20.0	0.139
76-4	SPC 0055 1135	5/26/99	13.077	-1.3	22.7	—
77-3	SPC 0055 1137	5/26/99	0.187	-0.2	28.9	—
78-3	SPC 0055 1139	5/26/99	0.288	-0.1	23.1	0.243
185-2	SPC 0055 1142	5/26/99	2.311	-3.5	36.9	—
186-3	SPC 0055 1143	5/26/99	0.426	-8.6	27.1	—
186-2	SPC 0055 1141	5/26/99	0.041	-9.5	37.5	—



Table 6.3-28. Concentration and Isotopic Compositions of CO<sub>2</sub> in Gas Samples Collected during the DST Heating and Cooling Phases (Continued)

Sample Interval <sup>a</sup> (BH-Zone)	YMP Tracking Number	Date Sampled	<sup>2</sup> CO <sub>2</sub> (v/v-percent) <sup>b</sup>	δ <sup>13</sup> C (‰) <sup>c</sup>	δ <sup>18</sup> O (‰) <sup>d</sup>	<sup>14</sup> C (Fraction Modern Carbon)
Observation Drift	SPC 0055 1144	5/26/99	0.042	—	—	—
57-2	SPC 0055 1145	8/09/99	0.362	-4.7	26.7	—
57-3	SPC 0055 1146	8/09/99	0.330	-15.1	27.7	—
57-4	SPC 0055 1147	8/09/99	0.173	-6.4	35.2	—
58-3	SPC 0055 1148	8/09/99	1.209	-4.3	25.5	—
59-2	SPC 0055 1161	8/09/99	1.016	-0.3	19.6	—
59-3	SPC 0055 1163	8/09/99	1.273	-1.0	18.6	0.120
59-4	SPC 0055 1165	8/09/99	6.573	-2.5	22.4	—
60-3	SPC 0055 1167	8/10/99	0.332	-5.5	22.5	—
74-2	SPC 0055 1170	8/10/99	0.158	-10.2	27.6	—
74-3	SPC 0055 1171	8/10/99	0.649	-10.1	27.3	—
74-4	SPC 0055 1172	8/10/99	0.328	-9.0	30.3	—
75-3	SPC 0055 1173	8/10/99	1.315	-7.1	25.1	—
76-3	SPC 0055 1175	8/10/99	2.658	-2.1	21.5	—
77-3	SPC 0055 1177	8/10/99	0.152	—	—	—
78-3	SPC 0055 1179	8/10/99	0.123	-2.5	20.6	—
185-2	SPC 0055 1182	8/10/99	3.214	-7.4	26.3	—
185-3	SPC 0055 1183	8/10/99	0.496	-6.2	29.7	—
186-3	SPC 0055 1184	8/10/99	0.613	-8.2	23.5	—
Observation Drift	SPC 0055 1181	8/10/99	0.038	-8.2	38.3	—
57-3	SPC 0055 1186	11/29/99	0.431	-11.5	31.4	0.427
57-4	SPC 0055 1187	11/29/99	0.275	-7.3	32.1	—
58-3	SPC 0055 1188	11/29/99	1.210	-3.0	26.3	—
59-4	SPC 0055 1191	11/29/99	9.016	-1.6	14.8	—
61-4	SPC 0055 1194	11/29/99	3.551	-3.8	19.9	—
74-3	SPC 0055 1197	11/29/99	1.330	-8.6	26.0	—
74-4	SPC 0055 1198	11/29/99	0.698	-8.7	26.4	—
75-3	SPC 0055 1199	11/29/99	2.779	-5.5	23.1	0.129
76-3	SPC 0055 7071	11/30/99	0.594	-3.0	19.6	0.182
76-4	SPC 0055 7058	11/30/99	6.861	-0.1	14.7	—
77-3	SPC 0055 7060	11/30/99	0.220	-4.3	22.6	—
78-3	SPC 0055 7062	11/30/99	0.619	-0.3	24.1	—
78-4	SPC 0055 7064	11/30/99	1.059	-4.6	25.7	—
185-2	SPC 0055 7067	11/30/99	5.208	-6.3	25.7	0.133
185-3	SPC 0055 7068	11/30/99	0.895	-6.8	24.4	0.190
186-3	SPC 0055 7069	11/30/99	1.796	-7.4	22.6	0.206
Heated Drift	SPC 0055 1196	11/30/99	0.043	-9.9	20.1	—

Table 6.3-28. Concentration and Isotopic Compositions of CO<sub>2</sub> in Gas Samples Collected during the DST Heating and Cooling Phases (Continued)

Sample Interval <sup>a</sup> (BH-Zone)	YMP Tracking Number	Date Sampled	<sup>2</sup> CO <sub>2</sub> (v/v-percent) <sup>b</sup>	δ <sup>13</sup> C (‰) <sup>c</sup>	δ <sup>18</sup> O (‰) <sup>d</sup>	<sup>14</sup> C (Fraction Modern Carbon)
Observation Drift	SPC 0055 7066	11/30/99	0.040	-8.8	37.5	—
57-3	SPC 0055 9314	4/19/00	0.383	-8.8	29.2	—
58-3	SPC 0055 9315	4/19/00	1.672	-4.1	22.0	—
59-3	SPC 0055 9317	4/19/00	0.210	-2.5	24.0	—
60-4	SPC 0055 9319	4/19/00	0.132	-9.7	37.0	—
61-3	SPC 0055 9321	4/19/00	0.075	—	—	—
61-4	SPC 0055 9323	4/19/00	6.308	-3.3	21.8	—
74-3	SPC 0055 9304	4/18/00	1.291	-8.1	23.3	—
74-4	SPC 0055 9305	4/18/00	0.724	-7.3	25.7	—
75-3	SPC 0055 9306	4/18/00	2.430	-3.6	21.8	—
77-3	SPC 0055 9308	4/18/00	0.156	-6.7	21.0	—
78-3	SPC 0055 9310	4/18/00	0.353	-0.5	21.6	0.185
78-4	SPC 0055 9312	4/18/00	1.657	-4.5	22.5	—
185-2	SPC 0055 9300	4/18/00	3.877	-5.8	23.7	—
185-3	SPC 0055 9301	4/18/00	0.823	-5.6	22.7	—
186-3	SPC 0055 9302	4/18/00	1.418	-3.1	35.2	—
Heated Drift	SPC 0055 9326	4/19/00	0.042	-10.7	13.7	—
Observation Drift	SPC 0055 9325	4/19/00	0.042	—	—	—
57-3/4	SPC 0055 9328	8/21/00	0.605	-8.4	15.3	0.201
58-3	SPC 0055 9329	8/21/00	3.262	-3.0	12.1	—
59-3	SPC 0055 9331	8/21/00	0.108	-4.0	17.4	—
60-2/3/4	SPC 0055 9333	8/21/00	0.077	-8.3	18.7	—
61-3/4	SPC 0055 9335	8/21/00	0.056	-8.0	16.6	—
74-3	SPC 0055 9337	8/22/00	1.179	-7.1	13.4	0.154
74-4	SPC 0055 9338	8/22/00	0.978	-5.8	14.7	—
75-3	SPC 0055 9339	8/22/00	1.573	-2.2	10.7	—
76-3	SPC 0055 9341	8/22/00	0.082	-5.2	16.4	—
77-2/3	SPC 0055 9343	8/22/00	0.095	-7.0	13.7	—
78-2/3	SPC 0055 9346	8/22/00	0.355	-2.4	10.9	—
185-2	SPC 0055 9348	8/22/00	5.115	-5.2	14.1	—
185-3	SPC 0055 9350	8/22/00	1.405	-4.5	13.0	—
186-3	SPC 0055 9352	8/22/00	4.408	-3.0	11.0	—
Heated Drift	SPC 0055 9354	8/22/00	0.046	—	—	—
Observation Drift	SPC 0055 9345	8/22/00	0.040	-9.7	27.2	—
57-3/4	SPC 0055 9395	1/22/01	0.67	-7.6	25.8	0.170
58-3	SPC 0055 9397	1/22/01	2.84	-3.4	20.5	—
59-3	SPC 0055 9399	1/22/01	0.11	-5.0	27.4	—

Table 6.3-28. Concentration and Isotopic Compositions of CO<sub>2</sub> in Gas Samples Collected during the DST Heating and Cooling Phases (Continued)

Sample Interval <sup>a</sup> (BH-Zone)	YMP Tracking Number	Date Sampled	<sup>2</sup> CO <sub>2</sub> (v/v-percent) <sup>b</sup>	δ <sup>13</sup> C (‰) <sup>c</sup>	δ <sup>18</sup> O (‰) <sup>d</sup>	<sup>14</sup> C (Fraction Modern Carbon)
60-3/2/4	SPC 0055 9401	1/22/01	0.11	-10.4	24.0	—
61-3/2	SPC 0055 9403	1/22/01	0.54	-7.2	26.4	—
74-3	SPC 0055 9406	1/23/01	1.14	-6.3	23.4	0.144
75-3	SPC 0055 9408	1/23/01	1.65	2.7	32.9	0.166
76-3/2	SPC 0055 9410	1/23/01	0.19	-1.6	—	0.296
77-3/2	SPC 0055 9412	1/23/01	0.09	-7.9	22.2	—
78-3/2/4	SPC 0055 9414	1/23/01	0.68	1.3	35.3	—
185-2	SPC 0055 9416	1/23/01	6.68	-4.8	24.6	—
185-3	SPC 0055 9418	1/23/01	1.94	-4.3	23.2	—
186-3	SPC 0055 9420	1/23/01	7.76	-3.1	20.8	—
Observation Drift 1	SPC 0055 9394	1/22/01	0.04	-10.4	37.6	—
Observation Drift 2	SPC 0055 9422	1/23/01	0.04	-9.8	37.7	—
57-3/4	SPC 0055 9357	4/17/01	0.784	-6.5	26.1	—
58-3	SPC 0055 9359	4/17/01	3.467	-3.7	19.9	—
59-3	SPC 0055 9361	4/17/01	0.108	-3.2	27.8	—
60-3/2/4/1	SPC 0055 9363	4/17/01	0.080	-10.7	26.3	—
61-3/2/4	SPC 0055 9365	4/17/01	0.068	-6.8	24.7	—
74-3	SPC 0055 9367	4/18/01	1.139	-5.6	22.8	—
75-3	SPC 0055 9369	4/18/01	0.941	-0.1	24.8	—
76-3/2	SPC 0055 9371	4/18/01	0.178	-2.7	20.9	—
77-3/2	SPC 0055 9373	4/18/01	0.102	-8.2	23.1	—
78-3/2/4/1	SPC 0055 9375	4/18/01	0.795	-4.9	20.9	0.187
185-2	SPC 0055 9378	4/18/01	7.855	-3.8	25.9	—
185-3	SPC 0055 9380	4/18/01	2.284	-4.6	21.6	—
186-3	SPC 0055 9382	4/18/01	6.413	-2.8	18.7	—
Heated Drift	SPC 0055 9384	4/18/01	0.046	—	—	—
Observation Drift	SPC 0055 9377	4/18/01	0.038	-9.1	38.1	—
57-3/4	SPC 0055 9385	8/07/01	1.011	—	—	0.240
58-3	SPC 0055 9387	8/07/01	6.342	-3.1	20.0	—
59-3/4	SPC 0055 9389	8/08/01	0.178	—	—	—
60-3/2/4/1	SPC 0055 9391	8/07/01	0.096	-10.3	27.6	—
61-3/2/4	SPC 0055 9393	8/07/01	0.557	-5.8	25.6	—
74-3	SPC 0055 9431	8/08/01	0.643	-1.1	35.1	0.326
75-3	SPC 0055 9433	8/08/01	0.821	-3.1	23.7	0.233
76-3/2	SPC 0055 9435	8/08/01	0.130	-4.5	21.4	0.456
77-3	SPC 0055 9437	8/08/01	0.090	-4.1	31.9	—
78-3/2/4	SPC 0055 9439	8/08/01	1.966	1.2	29.3	0.192

Table 6.3-28. Concentration and Isotopic Compositions of CO<sub>2</sub> in Gas Samples Collected during the DST Heating and Cooling Phases (Continued)

Sample Interval <sup>a</sup> (BH-Zone)	YMP Tracking Number	Date Sampled	<sup>2</sup> CO <sub>2</sub> (v/v-percent) <sup>b</sup>	δ <sup>13</sup> C (‰) <sup>c</sup>	δ <sup>18</sup> O (‰) <sup>d</sup>	<sup>14</sup> C (Fraction Modern Carbon)
185-2	SPC 0055 9424	8/07/01	11.522	-4.1	23.1	0.080
185-3	SPC 0055 9426	8/07/01	4.427	-4.7	21.9	0.080
186-3	SPC 0055 9428	8/07/01	8.039	-1.2	21.7	—
Heated Drift	SPC 0055 9356	8/07/01	0.039	-10.0	17.7	0.982
Observation Drift	SPC 0055 9430	8/07/01	0.034	-8.9	38.8	—
57-3/4	SPC 0101 6517	11/27/01	0.88	-7.0	22.8	—
58-3	SPC 0101 6519	11/27/01	2.50	—	—	—
59-3/4	SPC 0101 6522	11/28/01	0.08	-3.4	33.2	—
61-3/2/4	SPC 0101 6524	11/28/01	0.27	-3.6	24.0	—
74-3	SPC 0101 6501	11/27/01	0.64	—	—	—
75-3	SPC 0101 6504	11/27/01	0.85	—	—	—
76-1	SPC 0101 6511	11/27/01	0.37	-4.9	24.1	—
76-3/2	SPC 0101 6509	11/27/01	0.92	-0.1	18.9	—
76-4	SPC 0101 6507	11/27/01	0.07	-6.5	32.3	—
77-3	SPC 0101 6513	11/27/01	0.06	—	—	—
78-3/2/4	SPC 0101 6515	11/27/01	0.71	-8.5	35.5	—
185-1	SPC 0055 9448	11/26/01	0.69	-4.4	26.4	—
185-2	SPC 0055 9445	11/26/01	4.83	-4.5	23.5	—
185-3	SPC 0055 9443	11/26/01	2.90	—	—	—
185-4	SPC 0055 9450	11/26/01	1.49	-6.6	24.0	—
186-3	SPC 0101 6526	11/28/01	7.70	—	—	—
Heated Drift	SPC 0101 6528	11/26/01	0.06	-9.8	36.4	—
Observation Drift	SPC 0055 9452	11/26/01	0.07	-6.9	33.4	—
57-3/4	SPC 0101 6546	1/08/02	0.90	-5.5	26.6	—
59-3/4	SPC 0101 6400	1/08/02	0.15	—	—	—
61-3/2/4	SPC 0101 6402	1/08/02	0.63	3.1	43.8	—
74-3	SPC 0101 6538	1/07/02	1.08	-4.6	24.2	—
75-3	SPC 0101 6540	1/07/02	6.65	-1.5	19.4	—
76-3/2	SPC 0101 6542	1/07/02	0.77	-0.7	17.9	—
78-3/2/4	SPC 0101 6544	1/07/02	0.79	-4.8	19.7	—
185-2	SPC 0101 6532	1/07/02	7.50	-4.5	23.5	—
185-3	SPC 0101 6534	1/07/02	3.43	-4.4	22.5	—
186-3	SPC 0101 6536	1/07/02	3.45	—	—	—
Heated Drift	SPC 0101 6531	1/07/02	0.05	-9.2	25.9	—
Observation Drift	SPC 0101 6530	1/07/02	0.06	-10.1	37.3	—
57-3/4	SPC 0101 6420	1/22/02	0.83	-7.5	21.9	—
58-3	SPC 0101 6422	1/23/02	3.87	-3.4	17.2	—

Table 6.3-28. Concentration and Isotopic Compositions of CO<sub>2</sub> in Gas Samples Collected during the DST Heating and Cooling Phases (Continued)

Sample Interval <sup>a</sup> (BH-Zone)	YMP Tracking Number	Date Sampled	<sup>2</sup> CO <sub>2</sub> (v/v-percent) <sup>b</sup>	δ <sup>13</sup> C (‰) <sup>c</sup>	δ <sup>18</sup> O (‰) <sup>d</sup>	<sup>14</sup> C (Fraction Modern Carbon)
59-3/4	SPC 0101 6424	1/23/02	0.10	-4.6	26.2	—
61-3/2/4	SPC 0101 6426	1/23/02	0.51	-7.8	35.6	—
74-3	SPC 0101 6410	1/22/02	0.86	-0.1	35.9	—
75-3	SPC 0101 6412	1/22/02	4.92	-1.7	17.6	—
76-3/2	SPC 0101 6416	1/22/02	0.82	-0.2	19.0	—
78-3/2/4	SPC 0101 6418	1/22/02	1.22	-4.6	19.1	—
185-2	SPC 0101 6404	1/22/02	6.30	-4.5	22.2	—
185-3	SPC 0101 6406	1/22/02	2.45	-4.4	19.6	—
186-3	SPC 0101 6408	1/22/02	0.17	-5.9	23.6	—
Heated Drift	SPC 0101 6415	1/22/02	0.05	-13.6	33.2	—
Observation Drift	SPC 0101 6414	1/22/02	0.05	-13.6	33.2	—
57-3/4	SPC 0101 6444	2/19/02	0.97	-5.9	25.7	—
58-3	SPC 0101 6446	2/19/02	3.25	-3.3	17.0	—
59-3/4	SPC 0101 6448	2/19/02	0.07	—	—	—
61-3/2/4	SPC 0101 6450	2/19/02	0.74	-4.0	19.1	—
74-3	SPC 0101 6440	2/19/02	0.56	-3.7	21.9	—
75-3/4	SPC 0101 6442	2/19/02	0.42	-2.0	18.7	—
76-3/2	SPC 0101 6436	2/19/02	0.12	-5.6	26.8	—
78-3/2/4	SPC 0101 6438	2/19/02	0.50	-1.5	24.4	—
185-2	SPC 0101 6430	2/19/02	6.09	-3.9	23.1	—
185-3	SPC 0101 6432	2/19/02	2.34	-3.5	23.9	—
186-3	SPC 0101 6434	2/19/02	6.73	-2.2	20.1	—
Heated Drift	SPC 0101 6429	2/19/02	0.04	-10.0	32.8	—
Observation Drift	SPC 0101 6428	2/19/02	0.05	—	—	—
57-3/4	SPC 0101 6474	3/19/02	0.84	—	—	—
58-3	SPC 0101 6476	3/19/02	1.57	—	—	—
59-3/4	SPC 0101 6478	3/19/02	0.08	—	—	—
61-3/2/4	SPC 0101 6480	3/19/02	0.12	-4.9	28.0	—
74-3	SPC 0101 6470	3/19/02	0.35	-3.2	24.3	—
75-3/4	SPC 0101 6472	3/19/02	0.27	-1.4	22.5	—
76-3/2	SPC 0101 6466	3/19/02	0.11	-5.8	29.0	—
78-3/2/4	SPC 0101 6468	3/19/02	0.19	-1.2	31.3	—
185-2	SPC 0101 6458	3/19/02	4.64	-0.5	31.8	—
185-3	SPC 0101 6460	3/19/02	1.82	-3.2	25.9	—
186-3	SPC 0101 6464	3/19/02	4.27	-1.1	24.4	—

Table 6.3-28. Concentration and Isotopic Compositions of CO<sub>2</sub> in Gas Samples Collected during the DST Heating and Cooling Phases (Continued)

Sample Interval <sup>a</sup> (BH-Zone)	YMP Tracking Number	Date Sampled	<sup>2</sup> CO <sub>2</sub> (v/v-percent) <sup>b</sup>	δ <sup>13</sup> C (‰) <sup>c</sup>	δ <sup>18</sup> O (‰) <sup>d</sup>	<sup>14</sup> C (Fraction Modern Carbon)
Heated Drift	SPC 0101 6457	3/19/02	0.04	-10.7	29.4	—
Observation Drift	SPC 0101 6456	3/19/02	0.05	—	—	—
57-3/4	SPC 0101 6482	4/16/02	0.83	-6.5	20.1	—
58-3	SPC 0101 6484	4/16/02	2.57	-3.4	19.4	—
59-3/4	SPC 0101 6486	4/16/02	0.07	—	—	—
61-3/2/4	SPC 0101 6488	4/16/02	0.56	-4.3	20.6	—
74-3	SPC 0101 7202	4/16/02	0.33	—	—	—
75-3/4	SPC 0101 7204	4/16/02	—	—	—	—
76-3/2	SPC 0101 6496	4/16/02	0.04	—	—	—
78-3/2/4	SPC 0101 7200	4/16/02	0.27	-3.7	23.7	—
185-2	SPC 0101 6490	4/16/02	4.70	-3.0	26.0	—
185-3	SPC 0101 6492	4/16/02	2.42	-4.1	21.7	—
186-3	SPC 0101 6494	4/16/02	3.84	-2.4	20.5	—
Heated Drift	SPC 0101 6498	4/16/02	0.03	-10.0	30.0	—
Observation Drift	SPC 0101 6462	4/16/02	0.04	-7.8	36.5	—
57-3/4	SPC 0101 7221	5/14/02	1.13	-1.6	32.9	—
58-3	SPC 0101 7223	5/14/02	1.94	1.5	34	—
59-3/4	SPC 0101 7225	5/14/02	0.06	—	—	—
61-3/2/4	SPC 0101 7227	5/14/02	0.87	-2.9	25.8	—
74-3	SPC 0101 7207	5/14/02	0.41	-2.2	28.7	—
75-3/4	SPC 0101 7209	5/14/02	0.34	-1.5	24.9	—
76-3/2	SPC 0101 7211	5/14/02	0.15	—	—	—
78-3/2/4	SPC 0101 7213	5/14/02	1.11	-2.8	26.2	—
185-2	SPC 0101 7215	5/14/02	6.50	8.3	44.7	—
185-3	SPC 0101 7217	5/14/02	2.55	—	—	—
186-3	SPC 0101 7219	5/14/02	3.94	—	—	—
Heated Drift	SPC 0101 7206	5/14/02	0.05	-10.2	29.2	—
Observation Drift	SPC 0101 7206	5/14/02	0.04	-11.3	33.3	—
57-3/4	SPC 0101 7246	7/24/02	0.297	—	—	—
58-3	SPC 0101 7248	7/24/02	0.092	22.5	45.9	—
59-3/4	SPC 0101 7250	7/24/02	0.079	-9.4	32.3	—
61-3/2/4	SPC 0101 7252	7/24/02	0.223	—	—	—
74-3	SPC 0101 7238	7/24/02	0.292	-5.4	35.3	—
75-3/4	SPC 0101 7240	7/24/02	0.063	—	—	—
76-3/2	SPC 0101 7242	7/24/02	0.065	—	—	—
78-3/2/4	SPC 0101 7244	7/24/02	0.146	30.7	55.2	—

Table 6.3-28. Concentration and Isotopic Compositions of CO<sub>2</sub> in Gas Samples Collected during the DST Heating and Cooling Phases (Continued)

Sample Interval <sup>a</sup> (BH-Zone)	YMP Tracking Number	Date Sampled	<sup>2</sup> CO <sub>2</sub> (v/v-percent) <sup>b</sup>	δ <sup>13</sup> C (‰) <sup>c</sup>	δ <sup>18</sup> O (‰) <sup>d</sup>	<sup>14</sup> C (Fraction Modern Carbon)
185-2	SPC 0103 4442	7/24/02	0.367	-6.0	42.6	—
185-3	SPC 0103 4444	7/24/02	0.293	-7.3	29.5	—
186-3	SPC 0103 4446	7/24/02	—	—	—	—
Heated Drift	SPC 0103 4425	7/24/02	0.044	-10.7	33.6	—
Observation Drift	SPC 0103 4424	7/24/02	0.041	-9.5	37.2	—
57-3/4	SPC 0101 7270	12/4/02	0.642	-6.2	23.5	—
58-3	SPC 0101 7272	12/4/02	0.335	-3.4	24.0	—
59-3/4	SPC 0101 7274	12/4/02	0.093	-6.1	26.9	—
61-3/2/4	SPC 0101 7276	12/4/02	0.219	-5.2	23.6	—
74-3	SPC 0101 7262	12/4/02	0.306	-3.8	23.7	—
75-3/4	SPC 0101 7264	12/4/02	0.129	-3.6	20.4	—
76-3/2	SPC 0101 7266	12/4/02	0.073	-8.7	25.5	—
78-3/2/4	SPC 0101 7268	12/4/02	0.212	-5.7	23.4	—
185-2	SPC 0101 7256	12/4/02	1.503	-1.9	25.5	—
185-3	SPC 0101 7258	12/4/02	1.084	-4.6	21.2	—
186-3	SPC 0101 7260	12/4/02	1.927	-1.7	26.6	—
Heated Drift	SPC 0101 7254	12/4/02	0.048	-9.9	28.5	—
Observation Drift	SPC 0101 7255	12/4/02	0.054	-9.4	36.1	—
57-3/4	SPC 0101 7294	3/11/03	0.711	-7.9	21.8	—
58-3	SPC 0101 7296	3/11/03	0.401	-4.5	22.2	—
59-3/2	SPC 0101 7298	3/11/03	0.158	-6.5	24.0	—
61-3/2/4	SPC 0101 8800	3/11/03	0.469	-5.8	22.1	—
74-3	SPC 0101 7282	3/10/03	0.250	-3.8	23.7	—
75-3/4	SPC 0101 7284	3/10/03	0.097	-4.8	20.3	—
76-3/2	SPC 0101 7278	3/10/03	0.070	-8.2	27.6	—
78-3/2/4	SPC 0101 7280	3/10/03	0.178	-6.0	28.4	—
185-2	SPC 0101 7286	3/10/03	1.230	-3.0	23.5	—
185-3	SPC 0101 7288	3/10/03	0.934	-13.4	19.8	—
186-3	SPC 0101 7290	3/10/03	1.267	-3.0	22.2	—
Heated Drift	SPC 0101 7293	3/10/03	0.051	-10.6	29.0	—
Observation Drift	SPC 0101 7292	3/10/03	0.054	-8.6	34.4	—
57-3/4	SPC 0101 8804	7/15/03	0.614	—	—	—
58-3	SPC 0101 8806	7/15/03	0.431	-7.1	20.4	—
59-3/4	SPC 0101 8808	7/15/03	0.171	-8.3	23.8	—
61-3/2/4	SPC 0101 8810	7/15/03	0.527	-9.4	19.1	—

Table 6.3-28. Concentration and Isotopic Compositions of CO<sub>2</sub> in Gas Samples Collected during the DST Heating and Cooling Phases (Continued)

Sample Interval <sup>a</sup> (BH-Zone)	YMP Tracking Number	Date Sampled	<sup>2</sup> CO <sub>2</sub> (v/v-percent) <sup>b</sup>	δ <sup>13</sup> C (‰) <sup>c</sup>	δ <sup>18</sup> O (‰) <sup>d</sup>	<sup>14</sup> C (Fraction Modern Carbon)
74-3	SPC 0101 8812	7/15/03	0.235	-5.2	23.2	—
75-3/4	SPC 0101 8814	7/15/03	0.096	-7.5	21.4	—
76-3/2	SPC 0101 8816	7/15/03	0.090	-9.4	25.0	—
78-3/2/4	SPC 0101 8819	7/15/03	0.379	-7.0	21.6	—
185-2	SPC 0101 8821	7/15/03	1.235	-4.8	24.0	—
185-3	SPC 0101 8823	7/15/03	0.743	-6.2	21.9	—
186-3	SPC 0101 8825	7/15/03	1.512	-5.9	21.3	—
Heated Drift	SPC 0101 8827	7/15/03	0.051	-10.6	32.4	—
Observation Drift	SPC 0101 8803	7/15/03	0.051	-13.1	37.6	—
57-3/4	SPC 0101 8829	12/16/03	0.446	-8.5	21.2	—
58-3/2	SPC 0101 8831	12/16/03	0.192	-6.3	22.8	—
59-3/2	SPC 0101 8833	12/16/03	0.096	-8.2	24.6	—
61-3/2/4	SPC 0101 8835	12/16/03	0.185	-6.3	24.0	—
74-3/4	SPC 0101 8837	12/16/03	0.253	-6.5	20.6	—
75-3/4	SPC 0101 8839	12/16/03	0.122	-7.2	18.3	—
76-3/2/4	SPC 0101 8841	12/16/03	0.073	-10.3	25.9	—
78-3/2/4/1	SPC 0101 8843	12/16/03	0.109	-8.7	25.9	—
185-2	SPC 0101 8845	12/16/03	0.839	-4.5	24.5	—
185-3	SPC 0101 8847	12/16/03	0.504	-6.1	21.4	—
186-3/2	SPC 0101 8849	12/16/03	0.977	-5.9	21.9	—
Heated Drift	SPC 0101 8851	12/16/03	0.057	-11.1	28.6	—
Observation Drift	SPC 0101 8828	12/16/03	0.048	—	—	—
57-3/4	SPC 0101 8860	4/19/04	0.458	-9.4	21.6	—
58-3/2	SPC 0101 8861	4/19/04	0.263	-7.1	21.0	—
59-3/2	SPC 0101 8862	4/19/04	0.106	-8.1	25.1	—
61-3/2/4	SPC 0101 8863	4/19/04	0.250	-7.7	23.8	—
74-3/4	SPC 0101 8852	4/19/04	0.236	-5.2	34.0	—
75-3/4	SPC 0101 8853	4/19/04	0.188	-7.1	17.8	—
76-3/2/4	SPC 0101 8854	4/19/04	0.119	—	—	—
78-3/2/4	SPC 0101 8855	4/19/04	0.161	-6.8	29.4	—
185-2	SPC 0101 8856	4/19/04	0.458	-9.4	21.6	—
185-3	SPC 0101 8857	4/19/04	0.263	-7.1	21.0	—
186-3/2	SPC 0101 8858	4/19/04	0.106	-8.1	25.1	—
Heated Drift	SPC 0101 8869	4/19/04	0.045	—	—	—
Observation Drift	SPC 0101 8859	4/19/04	0.042	-10.4	37.0	—



Table 6.3-28. Concentration and Isotopic Compositions of CO<sub>2</sub> in Gas Samples Collected during the DST Heating and Cooling Phases (Continued)

Sample Interval <sup>a</sup> (BH-Zone)	YMP Tracking Number	Date Sampled	<sup>2</sup> CO <sub>2</sub> (v/v-percent) <sup>b</sup>	δ <sup>13</sup> C (‰) <sup>c</sup>	δ <sup>18</sup> O (‰) <sup>d</sup>	<sup>14</sup> C (Fraction Modern Carbon)
57-3/4	SPC 0101 8877	8/16/04	0.385	-9.8	24.0	—
58-3/2	SPC 0101 8884	8/16/04	0.183	-7.3	23.4	—
59-3/2	SPC 0101 8886	8/16/04	0.081	-9.0	24.2	—
61-3/2/4	SPC 0101 8868	8/16/04	0.270	-8.6	26.0	—
74-3/4	SPC 0101 8866	8/16/04	0.325	-8.8	30.8	—
75-3/4	SPC 0101 8870	8/16/04	0.108	-2.9	35.3	—
76-3/2/4	SPC 0101 8872	8/16/04	0.067	—	—	—
78-3/2/4	SPC 0101 8879	8/16/04	0.137	-5.3	31.8	—
185-2	SPC 0101 8881	8/16/04	0.653	-4.2	28.9	—
185-3	SPC 0101 8883	8/16/04	0.331	-10.7	25.8	—
186-3/2	SPC 0101 8874	8/16/04	0.371	-4.5	28.0	—
Heated Drift	SPC 0101 8865	8/16/04	0.049	-10.9	36.3	—
Observation Drift	SPC 0101 8864	8/16/04	0.051	-11.7	35.9	—
57-3/4	SPC 0103 4416	1/25/05	0.344	—	—	—
58-3/2/4	SPC 0103 4418	1/25/05	0.056	—	—	—
59-3/2	SPC 0103 4420	1/25/05	0.088	—	—	—
61-3/2/4	SPC 0103 4422	1/25/05	0.252	—	—	—
74-3/4	SPC 0103 4408	1/25/05	0.241	—	—	—
75-3/4	SPC 0103 4410	1/25/05	0.082	—	—	—
76-3/2/4	SPC 0103 4412	1/25/05	0.060	—	—	—
78-3/2/4	SPC 0103 4414	1/25/05	0.153	—	—	—
185-2	SPC 0103 4402	1/25/05	0.496	—	—	—
185-3	SPC 0103 4404	1/25/05	0.322	—	—	—
186-3/2	SPC 0103 4406	1/25/05	—	—	—	—
Heated Drift	SPC 0103 4401	1/25/05	0.040	—	—	—
Observation Drift	SPC 0103 4400	1/25/05	0.042	—	—	—
57-3/4	SPC 0103 4426	8/1/05	0.297	—	—	—
58-3/2/4	SPC 0103 4428	8/1/05	0.092	22.5	45.9	—
59-3/2	SPC 0103 4430	8/1/05	0.079	-9.4	32.3	—
61-3/2/4	SPC 0103 4432	8/1/05	0.223	—	—	—
74-3/4	SPC 0103 4434	8/1/05	0.292	-5.4	35.3	—
75-3/4	SPC 0103 4436	8/1/05	0.063	—	—	—
76-3/2/4	SPC 0103 4438	8/1/05	0.065	—	—	—
78-3/2/4/1	SPC 0103 4440	8/1/05	0.146	30.7	55.2	—
185-2	SPC 0103 4442	8/2/05	0.367	-6.0	42.6	—
185-3	SPC 0103 4444	8/2/05	0.293	-7.3	29.5	—

Table 6.3-28. Concentration and Isotopic Compositions of CO<sub>2</sub> in Gas Samples Collected during the DST Heating and Cooling Phases (Continued)

Sample Interval <sup>a</sup> (BH-Zone)	YMP Tracking Number	Date Sampled	<sup>2</sup> CO <sub>2</sub> (v/v-percent) <sup>b</sup>	δ <sup>13</sup> C (‰) <sup>c</sup>	δ <sup>18</sup> O (‰) <sup>d</sup>	<sup>14</sup> C (Fraction Modern Carbon)
186-3/2	SPC 0103 4446	8/2/05	—	—	—	—
Heated Drift	SPC 0103 4425	8/1/05	0.044	-10.7	33.6	—
Observation Drift	SPC 0103 4424	8/1/05	0.041	-9.5	37.2	—
57-3/4	SPC 0103 7564	11/29/05	0.245	-12.7	23.1	—
58-3/2/4	SPC 0103 7566	11/29/05	0.095	-9.5	35.8	—
59-3/2	SPC 0103 7568	11/29/05	0.034	-9.9	27.8	—
61-3/2/4	SPC 0103 7570	11/29/05	0.167	-8.1	29.8	—
74-3/4	SPC 0103 7556	11/29/05	0.147	-8.0	34.1	—
75-3/4	SPC 0103 7558	11/29/05	0.101	-5.3	33.7	—
76-3/2/4	SPC 0103 7560	11/29/05	0.063	—	—	—
78-3/2/4/1	SPC 0103 7562	11/29/05	0.086	-8.8	37.9	—
185-2	SPC 0103 7550	11/29/05	0.287	-6.3	28.0	—
185-3	SPC 0103 7552	11/29/05	0.170	-4.9	31.7	—
186-3/2	SPC 0103 7554	11/29/05	0.104	0.9	41.9	—
Heated Drift	SPC 0103 7573	11/29/05	0.051	-12.3	27.9	—
Observation Drift	SPC 0103 7572	11/29/05	0.042	-12.8	32.2	—

Source: DTNs: LB980420123142.005 [DIRS 111471]; LB980715123142.003 [DIRS 111472]; LB0404ISODSTHP.003 [DIRS 169254]; LB990630123142.003 [DIRS 111476]; LB000121123142.003 [DIRS 146451]; LB000718123142.003 [DIRS 158342]; LB0011CO2DST08.001 [DIRS 153460]; LB0102CO2DST98.001 [DIRS 159306]; LB0108CO2DST05.001 [DIRS 156888]; LB0203CO2DSTEH.001 [DIRS 158349]; LB0206C14DSTEH.001 [DIRS 159303]; LB0303ISODSTCP.001 [DIRS 177538]; LB0309ISODSTCP.001 [DIRS 177539]; LB0403ISODSTCP.001 [DIRS 177540]; LB0410ISODSTCP.001 [DIRS 177541]; LB0509ISODSTCP.001 [DIRS 177542].

- <sup>a</sup> Sample interval indicates the DST borehole followed by the interval within the borehole from which the sample was collected. Where more than one interval is noted, that means the sample was taken from the first interval given, but the packers between that interval and the others listed were deflated (e.g., 57-3/4 indicates the sample was taken from DST Borehole 57, interval 3, but the packer between intervals 3 and 4 was deflated). Heater drift samples were taken from heater drift gas sampling port #2 (by the bulkhead) and AO drift samples were air samples taken from the access observation.
- <sup>b</sup> CO<sub>2</sub> concentrations reported for samples collected during February of 1997 through August of 2000, April of 2001 through August of 2001, and August 2004 through November 2005 were measured using the Li-Cor in the Amundson laboratory on the UC Berkeley campus. Data reported for samples collected during January of 2001 and November of 2001 through April of 2004 were measured on the Columbus Instruments gas analyzer at the ESF.
- <sup>c</sup> Stable carbon isotope ratios are given as part per thousand or per mil (‰) variations in the ratio of <sup>13</sup>C to <sup>12</sup>C relative to carbon isotope ratio of VPDB (Vienna Pee Dee Belemnite), an internationally accepted standard for reporting carbon isotope data.
- <sup>d</sup> Stable oxygen isotope ratios are given as part per thousand or per mil (‰) variations in the ratio of <sup>18</sup>O to <sup>16</sup>O relative to oxygen isotope ratio of VSMOW (Vienna Standard Mean Ocean Water), an internationally accepted standard for reporting oxygen isotope data.
- <sup>e</sup> Samples collected in 150-cc metal canisters (as opposed to Tedlar bags).

### 6.3.4.2.3 Results: Isotopic Composition of CO<sub>2</sub>

After measuring the CO<sub>2</sub> concentration in the gas samples, the CO<sub>2</sub> was cryogenically separated from the samples for isotopic analyses. The CO<sub>2</sub> isotopic compositions are also given in Table 6.3-28. For large enough yields of CO<sub>2</sub> (greater than 30 μmoles), two aliquots of CO<sub>2</sub> were collected. The stable carbon (δ<sup>13</sup>C value) and oxygen (δ<sup>18</sup>O value) isotope ratios aliquot was analyzed according to the technical implementing procedure YMP-LBNL-TIP/TT-7.0, *Extraction and Analysis of the Stable Isotopic Compositions of CO<sub>2</sub> in Gas Samples for Isotopic Analyses*. If there were problems with the first analysis, then the split was used for a second stable isotope analysis. If there were no problems, then the splits were catalogued and stored for possible radiocarbon (<sup>14</sup>C) analysis.

### 6.3.4.2.4 Results: Isotopic Analyses of Vapor Condensate Samples

The hydrogen and oxygen isotope compositions of the vapor-condensate samples were measured to gain an estimate of the isotopic composition of the pore water in the rock (Table 6.3-29). The hydrogen isotope ratios (δD values) were measured following technical implementing procedure YMP-LBNL-TIP/TT-9.0, *Hydrogen Isotope Analyses of Water*. The oxygen isotope ratios (δ<sup>18</sup>O values) were measured following technical implementing procedure YMP-LBNL-TIP/TT-10.0, *Analysis of the Oxygen Isotopic Composition of Water Samples Using the Isoprep 18*. When the pore water is in isotopic equilibrium with the vapor in the gas samples at the temperature of the rock, the isotopic composition of the pore water can be calculated from the isotopic composition of the vapor (Horita and Wesolowski 1994 [DIRS 159108]). This information can provide valuable insights into the degree of dryout in the rock and the extent of vapor transport.

Table 6.3-29. Hydrogen (δD) and Oxygen (δ<sup>18</sup>O) Isotope Compositions of Steam Condensed from Gas Samples Collected during the DST Heating and Cooling Phases

Sample Interval <sup>a</sup>	YMP Tracking Number	Date Sampled	Isotope Composition	
			Hydrogen δD (‰)	Oxygen δ <sup>18</sup> O (‰) <sup>b</sup>
77-3	SPC 0052 7985	6/04/98	-95	-13.2
58-3	SPC 0052 7280	8/06/98	-128	-18.1
59-3	SPC 0052 7282	8/06/98	-132	-18.6
60-3	SPC 0052 7284	8/06/98	-110	-16.1
61-3	SPC 0052 7286	8/06/98	-152	-21.0
76-3	SPC 0052 7270	8/05/98	-122	-17.5
77-3	SPC 0052 7272	8/05/98	-103	-14.1
78-3	SPC 0052 7274	8/05/98	-127	-18.6
59-3	SPC 0052 7291	10/07/98	-126	-18.3
76-3	SPC 0052 7299	10/07/98	-126	-18.1
77-3	SPC 0052 7991	10/08/98	-86	-10.6
78-3	SPC 0052 7993	10/08/98	—	-18.1
186-2	SPC 0052 7997	10/08/98	-126	-17.9

Table 6.3-29. Hydrogen ( $\delta\text{D}$ ) and Oxygen ( $\delta^{18}\text{O}$ ) Isotope Compositions of Steam Condensed from Gas Samples Collected during the DST Heating and Cooling Phases (Continued)

Sample Interval <sup>a</sup>	YMP Tracking Number	Date Sampled	Isotope Composition	
			Hydrogen $\delta\text{D}$ (‰)	Oxygen $\delta^{18}\text{O}$ (‰) <sup>b</sup>
59-3	SPC 0054 1265	12/16/98	-122	-18.0
59-4	SPC 0054 1268	12/16/98	-119	-16.9
60-2	SPC 0054 1270	12/16/98	-90	-12.2
61-2	SPC 0054 1273	12/16/98	-106	-16.1
61-4	SPC 0054 1275	12/16/98	-119	-16.9
76-2	SPC 0054 1238	12/15/98	-131	-17.6
76-3	SPC 0054 1240	12/15/98	-127	-18.5
76-4	SPC 0054 1242	12/15/98	-110	-16.6
77-3	SPC 0054 1244	12/15/98	-83	-10.1
78-2	SPC 0054 1247	12/15/98	-110	-16.8
78-3	SPC 0054 1249	12/15/98	-132	-18.5
78-4	SPC 0054 1251	12/15/98	-116	-17.2
186-2	SPC 0054 1257	12/15/98	-140	-20.3
Heated Drift 2	SPC 0054 1277	12/16/98	-64	-7.5
59-3	SPC 0055 0614	3/02/99	-118	-17.2
60-2	SPC 0055 0617	3/02/99	-87	-10.9
60-3	SPC 0055 0615	3/02/99	-101	-13.8
61-2	SPC 0055 0619	3/02/99	-95	-14.4
76-2	SPC 0054 1286	3/01/99	-138	-19.0
76-3	SPC 0054 1288	3/01/99	-126	-18.2
76-4	SPC 0055 0601	3/01/99	-110	-16.1
77-3	SPC 0055 0604	3/02/99	-82	-8.2
78-3	SPC 0055 0606	3/02/99	-122	-17.7
186-2	SPC 0055 0610	3/02/99	-130	-19.4
60-2	SPC 0055 1116	5/25/99	-85	-11.2
60-3	SPC 0055 1114	5/25/99	-86	-19.4
61-2	SPC 0055 1118	5/25/99	-91	-11.1
59-3	SPC 0055 1120	5/25/99	-104	-11.0
58-3	SPC 0055 1122	5/25/99	-124	-12.2
75-3	SPC 0055 1129	5/25/99	-128	-17.4
76-2	SPC 0055 1132	5/26/99	-140	-17.1
76-3	SPC 0055 1134	5/26/99	-120	-12.5
76-4	SPC 0055 1136	5/26/99	-110	-11.0
77-3	SPC 0055 1138	5/26/99	-83	-12.8
78-3	SPC 0055 1140	5/26/99	-117	-18.4
58-3	SPC 0055 1149	8/09/99	-126	-17.6
59-2	SPC 0055 1162	8/09/99	-112	-17.1

Table 6.3-29. Hydrogen ( $\delta\text{D}$ ) and Oxygen ( $\delta^{18}\text{O}$ ) Isotope Compositions of Steam Condensed from Gas Samples Collected during the DST Heating and Cooling Phases (Continued)

Sample Interval <sup>a</sup>	YMP Tracking Number	Date Sampled	Isotope Composition	
			Hydrogen $\delta\text{D}$ (‰)	Oxygen $\delta^{18}\text{O}$ (‰) <sup>b</sup>
59-3	SPC 0055 1164	8/09/99	-109	-15.9
59-4	SPC 0055 1166	8/09/99	-107	-16.1
60-3	SPC 0055 1168	8/10/99	-86	-12.1
75-3	SPC 0055 1174	8/10/99	-119	-16.8
76-3	SPC 0055 1176	8/10/99	-122	-17.7
77-3	SPC 0055 1178	8/10/99	-89	-11.2
78-3	SPC 0055 1180	8/10/99	-114	-17.1
186-3	SPC 0055 1185	8/10/99	-94	-13.8
58-3	SPC 0055 1189	11/29/99	-122	-17.4
59-3	SPC 0055 1190	11/29/99	-103	-14.3
59-4	SPC 0055 1192	11/29/99	-125	-18.9
61-3	SPC 0055 1193	11/29/99	-101	-14.2
61-4	SPC 0055 1195	11/29/99	-113	-16.3
75-3	SPC 0055 7056	11/29/99	-121	-17.5
76-3	SPC 0055 7072	11/30/99	-107	-16.3
76-4	SPC 0055 7059	11/30/99	—	-12.6
77-3	SPC 0055 7061	11/30/99	-81	-9.9
78-3	SPC 0055 7063	11/30/99	-104	-13.7
78-4	SPC 0055 7065	11/30/99	-107	-15.8
186-3	SPC 0055 7070	11/30/99	-93	-13.2
58-3	SPC 0055 9316	4/19/00	-117	-17.3
59-3	SPC 0055 9318	4/19/00	-89	-12.0
60-4	SPC 0055 9320	4/19/00	-87	-11.8
61-3	SPC 0055 9322	4/19/00	-101	-14.3
61-4	SPC 0055 9324	4/19/00	-121	-18.3
75-3	SPC 0055 9307	4/18/00	-117	-16.5
77-3	SPC 0055 9309	4/18/00	-83	-11.0
78-3	SPC 0055 9311	4/18/00	-92	-11.6
78-4	SPC 0055 9313	4/18/00	-101	-16.5
186-3	SPC 0055 9303	4/18/00	-90	-13.7
58-3	SPC 0055 9330	8/21/00	—	-17.2
59-3	SPC 0055 9332	8/21/00	-90	-10.9
60-3/2/4	SPC 0055 9334	8/21/00	-89	-12.0
61-3/4	SPC 0055 9336	8/21/00	-89	-12.0
75-3	SPC 0055 9340	8/22/00	-118	-17.1
76-3	SPC 0055 9342	8/22/00	-101	-13.4
77-3/2	SPC 0055 9344	8/22/00	-85	-10.7

Table 6.3-29. Hydrogen ( $\delta\text{D}$ ) and Oxygen ( $\delta^{18}\text{O}$ ) Isotope Compositions of Steam Condensed from Gas Samples Collected during the DST Heating and Cooling Phases (Continued)

Sample Interval <sup>a</sup>	YMP Tracking Number	Date Sampled	Isotope Composition	
			Hydrogen $\delta\text{D}$ (‰)	Oxygen $\delta^{18}\text{O}$ (‰) <sup>b</sup>
78-3/2	SPC 0055 9347	8/22/00	-95	-13.0
185-2	SPC 0055 9349	8/22/00	-139	-17.3
185-3	SPC 0055 9351	8/22/00	-132	-18.1
186-3	SPC 0055 9353	8/22/00	-123	-15.0
57-3/4	SPC 0055 9396	1/22/01	-128	-17.9
58-3	SPC 0055 9398	1/22/01	-126	-19.4
59-3	SPC 0055 9400	1/22/01	-86	-11.2
60-3/2/4	SPC 0055 9402	1/22/01	-81	-11.1
61-3/2	SPC 0055 9404	1/22/01	-88	-11.0
74-3	SPC 0055 9407	1/23/01	-122	-17.4
75-3	SPC 0055 9409	1/23/01	-121	-17.1
76-3/2	SPC 0055 9411	1/23/01	-90	-12.5
77-3/2	SPC 0055 9413	1/23/01	-90	-11.0
78-3/2/4	SPC 0055 9415	1/23/01	-95	-12.8
185-2	SPC 0055 9417	1/23/01	-139	-18.4
185-3	SPC 0055 9419	1/23/01	-132	-18.1
186-3	SPC 0055 9421	1/23/01	-135	-19.1
57-3/4	SPC 0055 9358	4/17/01	-123	-18.0
58-3	SPC 0055 9360	4/17/01	-129	-19.6
59-3	SPC 0055 9362	4/17/01	-85	-11.1
60-3/2/4/1	SPC 0055 9364	4/17/01	-81	-10.1
61-3/2/4	SPC 0055 9366	4/17/01	-86	-11.3
74-3	SPC 0055 9368	4/18/01	-123	-17.7
75-3	SPC 0055 9370	4/18/01	-112	-16.8
76-3/2	SPC 0055 9372	4/18/01	-92	-13.0
77-3/2	SPC 0055 9374	4/18/01	-91	-11.7
78-3/2/4/1	SPC 0055 9376	4/18/01	-91	-12.9
185-2	SPC 0055 9379	4/18/01	-137	-18.2
185-3	SPC 0055 9381	4/18/01	-133	-18.5
186-3	SPC 0055 9383	4/18/01	-111	-16.2
57-3/4	SPC 0055 9386	8/07/01	-121	-17.7
58-3	SPC 0055 9388	8/07/01	-129	-20.1
59-3/4	SPC 0055 9390	8/08/01	-87	-11.3
60-3/2/4/1	SPC 0055 9392	8/07/01	-74	-8.8
61-3/2/4	SPC 0055 9355	8/07/01	-59	-10.7
74-3	SPC 0055 9432	8/08/01	-126	-17.8
75-3	SPC 0055 9434	8/08/01	-115	-16.9

Table 6.3-29. Hydrogen ( $\delta D$ ) and Oxygen ( $\delta^{18}O$ ) Isotope Compositions of Steam Condensed from Gas Samples Collected during the DST Heating and Cooling Phases (Continued)

Sample Interval <sup>a</sup>	YMP Tracking Number	Date Sampled	Isotope Composition	
			Hydrogen $\delta D$ (‰)	Oxygen $\delta^{18}O$ (‰) <sup>b</sup>
76-3/2	SPC 0055 9436	8/08/01	-100	-13.2
77-3	SPC 0055 9438	8/08/01	-89	-11.6
78-3/2/4	SPC 0055 9440	8/08/01	-84	-10.1
185-2	SPC 0055 9425	8/07/01	—	-18.6
185-3	SPC 0055 9427	8/07/01	-117	-18.4
186-3	SPC 0055 9429	8/07/01	-112	-16.2
57-3/4	SPC 0101 6518	11/27/01	-116	-16.9
58-3	SPC 0101 6520	11/27/01	-124	-18.3
59-3/4	SPC 0101 6523	11/28/01	-78	-10.2
61-3/2/4	SPC 0101 6525	11/28/01	-60	-11.5
74-3	SPC 0101 6502	11/27/01	-130	-18.1
75-3	SPC 0101 6505	11/27/01	-114	-16.1
76-1	SPC 0101 6512	11/27/01	-134	-18.2
76-3/2	SPC 0101 6510	11/27/01	-143	-12.6
76-4	SPC 0101 6508	11/27/01	-79	-11.3
77-3	SPC 0101 6514	11/27/01	-95	-12.3
78-3/2/4	SPC 0101 6516	11/27/01	-88	-11.5
185-1	SPC 0055 9449	11/26/01	-133	-17.4
185-2	SPC 0055 9446	11/26/01	-138	-18.3
185-3	SPC 0055 9444	11/26/01	-122	-18.4
185-4	SPC 0055 9451	11/26/01	-149	-17.7
186-3	SPC 0101 6500	11/26/01	-100	-14.2
186-3(II)	SPC 0101 6527	11/28/01	-113	-16.2
57-3/4	SPC 0101 6547	1/08/02	-81	-17.7
58-3	SPC 0101 6549	1/08/02	-84	-18.5
59-3/4	SPC 0101 6401	1/08/02	-79	-10.5
61-3/2/4	SPC 0101 6403	1/08/02	-85	-11.2
74-3	SPC 0101 6539	1/07/02	-117	-17.1
75-3	SPC 0101 6541	1/07/02	-114	-17.0
76-3/2	SPC 0101 6543	1/07/02	-88	-11.9
78-3/2/4	SPC 0101 6545	1/07/02	-82	-10.7
185-2	SPC 0101 6533	1/07/02	-131	-17.3
185-3	SPC 0101 6535	1/07/02	-132	-18.5
186-3	SPC 0101 6537	1/07/02	-109	-15.4
57-3/4	SPC 0101 6421	1/22/02	-117	-17.7
58-3	SPC 0101 6423	1/23/02	-127	-19.9

Table 6.3-29. Hydrogen ( $\delta D$ ) and Oxygen ( $\delta^{18}O$ ) Isotope Compositions of Steam Condensed from Gas Samples Collected during the DST Heating and Cooling Phases (Continued)

Sample Interval <sup>a</sup>	YMP Tracking Number	Date Sampled	Isotope Composition	
			Hydrogen $\delta D$ (‰)	Oxygen $\delta^{18}O$ (‰) <sup>b</sup>
59-3/4	SPC 0101 6425	1/23/02	-76	-10.1
61-3/2/4	SPC 0101 6427	1/23/02	-87	-11.4
74-3	SPC 0101 6411	1/22/02	—	-17.2
75-3	SPC 0101 6413	1/22/02	-117	-17.7
76-3/2	SPC 0101 6417	1/22/02	-89	-12.1
78-3/2/4	SPC 0101 6419	1/22/02	-83	-12.5
185-2	SPC 0101 6405	1/22/02	-139	-18.6
185-3	SPC 0101 6407	1/22/02	-120	-18.4
186-3	SPC 0101 6409	1/22/02	-99	-13.9
57-3/4	SPC 0101 6445	2/19/02	-130	-17.7
58-3	SPC 0101 6447	2/19/02	-129	-18.8
59-3/4	SPC 0101 6449	2/19/02	-90	-10.8
61-3/2/4	SPC 0101 6451	2/19/02	-88	-11.8
74-3	SPC 0101 6441	2/19/02	-119	-17.4
75-3	SPC 0101 6443	2/19/02	-123	-17.2
76-3/2	SPC 0101 6437	2/19/02	-87	-12.7
78-3/2/4	SPC 0101 6439	2/19/02	-83	-11.2
185-2	SPC 0101 6431	2/19/02	-144	-19.0
185-3	SPC 0101 6433	2/19/02	-120	-18.8
186-3	SPC 0101 6435	2/19/02	-102	-14.3
57-3/4	SPC 0101 6475	3/19/02	-122	-17.7
58-3	SPC 0101 6477	3/19/02	-133	-18.9
59-3/4	SPC 0101 6479	3/19/02	-84	-11.6
61-3/2/4	SPC 0101 6481	3/19/02	-97	-13.0
74-3	SPC 0101 6471	3/19/02	-117	-16.3
75-3	SPC 0101 6473	3/19/02	-124	-17.3
76-3/2	SPC 0101 6467	3/19/02	-89	-13.7
78-3/2/4	SPC 0101 6469	3/19/02	-89	-11.7
185-2	SPC 0101 6459	3/19/02	-144	-19.0
185-3	SPC 0101 6463	3/19/02	-132	-18.5
186-3	SPC 0101 6465	3/19/02	-111	-16.4
57-3/4	SPC 0101 6483	4/16/02	-123	-16.2
58-3	SPC 0101 6485	4/16/02	-123	-18.2
59-3/4	SPC 0101 6487	4/16/02	-85	-11.4



Table 6.3-29. Hydrogen ( $\delta D$ ) and Oxygen ( $\delta^{18}O$ ) Isotope Compositions of Steam Condensed from Gas Samples Collected during the DST Heating and Cooling Phases (Continued)

Sample Interval <sup>a</sup>	YMP Tracking Number	Date Sampled	Isotope Composition	
			Hydrogen $\delta D$ (‰)	Oxygen $\delta^{18}O$ (‰) <sup>b</sup>
61-3/2/4	SPC 0101 6489	4/16/02	-87	-11.6
74-3	SPC 0101 7203	4/16/02	-114	-14.7
75-3/4	SPC 0101 7205	4/16/02	-115	-16.1
76-3/2	SPC 0101 6497	4/16/02	-100	-13.9
78-3/2/4	SPC 0101 7201	4/16/02	-79	-10.1
185-2	SPC 0101 6491	4/16/02	-121	-16.1
185-3	SPC 0101 6493	4/16/02	-131	-18.4
186-3	SPC 0101 6495	4/16/02	-120	-17.4
57-3/4	SPC 0101 7222	5/14/02	-124	-16.8
58-3	SPC 0101 7224	5/14/02	-123	-17.5
59-3/4	SPC 0101 7226	5/14/02	-85	-10.0
61-3/2/4	SPC 0101 7228	5/14/02	-93	-11.4
74-3	SPC 0101 7208	5/14/02	-122	-16.6
75-3/4	SPC 0101 7210	5/14/02	-115	-16.2
76-3/2	SPC 0101 7212	5/14/02	-103	-13.6
78-3/2/4	SPC 0101 7214	5/14/02	-96	-12.7
185-2	SPC 0101 7216	5/14/02	-133	-17.3
185-3	SPC 0101 7218	5/14/02	-129	-17.3
186-3	SPC 0101 7220	5/14/02	-121	-16.8
57-3/4	SPC 0101 7247	7/24/02	-118	-16.9
58-3	SPC 0101 7249	7/24/02	-125	-18.8
59-3/4	SPC 0101 7251	7/24/02	-93	-12.3
61-3/2/4	SPC 0101 7253	7/24/02	-101	-14.4
74-3	SPC 0101 7239	7/24/02	-122	-17.6
75-3/4	SPC 0101 7241	7/24/02	-120	-17.3
76-3/2	SPC 0101 7243	7/24/02	-100	-13.4
78-3/2/4	SPC 0101 7245	7/24/02	-96	-13.8
185-2	SPC 0101 7233	7/24/02	-141	-18.7
185-3	SPC 0101 7235	7/24/02	-132	-18.4
186-3	SPC 0101 7237	7/24/02	-142	-20.5
57-3/4	SPC 0101 7257	12/4/02	-115	-17.1
58-3	SPC 0101 7259	12/4/02	-119	-18.4
59-3/4	SPC 0101 7261	12/4/02	-88	-11.3
61-3/2/4	SPC 0101 7271	12/4/02	-95	-13.8

Table 6.3-29. Hydrogen ( $\delta D$ ) and Oxygen ( $\delta^{18}O$ ) Isotope Compositions of Steam Condensed from Gas Samples Collected during the DST Heating and Cooling Phases (Continued)

Sample Interval <sup>a</sup>	YMP Tracking Number	Date Sampled	Isotope Composition	
			Hydrogen $\delta D$ (‰)	Oxygen $\delta^{18}O$ (‰) <sup>b</sup>
74-3	SPC 0101 7273	12/4/02	-126	-18.3
75-3/4	SPC 0101 7275	12/4/02	-108	-16.5
76-3/2	SPC 0101 7277	12/4/02	-105	-14.7
78-3/2/4	SPC 0101 7257	12/4/02	-104	-14.8
185-2	SPC 0101 7257	12/4/02	-140	-18.6
185-3	SPC 0101 7259	12/4/02	-134	-18.4
186-3	SPC 0101 7261	12/4/02	-139	-19.7
57-3/4	SPC 0101 7295	3/11/03	-128	-19.1
58-3	SPC 0101 7297	3/11/03	-129	-18.5
59-3/4	SPC 0101 7299	3/11/03	-102	-13.1
61-3/2/4	SPC 0101 8801	3/11/03	-104	-13.7
74-3	SPC 0101 7283	3/10/03	-118	-16.9
75-3/4	SPC 0101 7285	3/10/03	-113	-16.1
76-3/2	SPC 0101 7279	3/10/03	-104	-14.1
78-3/2/4	SPC 0101 7281	3/10/03	-110	-15.1
185-2	SPC 0101 7287	3/10/03	-128	-13.2
185-3	SPC 0101 7289	3/10/03	-134	-17.1
186-3	SPC 0101 7291	3/10/03	-137	-18.3
57-3/4	SPC 0101 8805	7/15/03	-107	-13.6
58-3	SPC 0101 8807	7/15/03	-132	-18.6
59-3/4	SPC 0101 8809	7/15/03	-84	-9.8
61-3/2/4	SPC 0101 8811	7/15/03	-99	-12.5
74-3	SPC 0101 8813	7/15/03	-106	-14.9
75-3/4	SPC 0101 8815	7/15/03	-103	-14.3
76-3/2	SPC 0101 8817	7/15/03	-95	-12.5
78-3/2/4	SPC 0101 8820	7/15/03	-100	-13.1
185-2	SPC 0101 8822	7/15/03	-109	—
185-3	SPC 0101 8824	7/15/03	-119	-16.1
186-3	SPC 0101 8826	7/15/03	-121	-16.8
57-3/4	SPC 0101 8878	8/16/04	-132	-20.2
58-3/2	SPC 0101 8885	8/16/04	-125	-19.0
59-3/4	SPC 0101 8887	8/16/04	-116	-16.8
61-3/2/4	SPC 0101 8888	8/16/04	-108	-13.1
74-3	SPC 0101 8867	8/16/04	-140	-20.3

Table 6.3-29. Hydrogen ( $\delta D$ ) and Oxygen ( $\delta^{18}O$ ) Isotope Compositions of Steam Condensed from Gas Samples Collected during the DST Heating and Cooling Phases (Continued)

Sample Interval <sup>a</sup>	YMP Tracking Number	Date Sampled	Isotope Composition	
			Hydrogen $\delta D$ (‰)	Oxygen $\delta^{18}O$ (‰) <sup>b</sup>
75-3	SPC 0101 8871	8/16/04	-124	-19.2
76-3/2	SPC 0101 8873	8/16/04	-114	-17.0
78-3/2/4	SPC 0101 8880	8/16/04	-114	-14.3
185-2	SPC 0101 8882	8/16/04	-119	-15.8
185-3	SPC 0101 8818	8/16/04	-136	-19.4
186-3/2	SPC 0101 8876	8/16/04	-125	-17.9
57-3/4	SPC 0103 4417	1/25/05	—	-14.3
58-3/2/4	SPC 0103 4419	1/25/05	—	-17.2
59-3/2	SPC 0103 4421	1/25/05	—	-14.4
61-3/2/4	SPC 0103 4423	1/25/05	—	-11.7
74-3/4	SPC 0103 4409	1/25/05	—	-18.3
75-3/4	SPC 0103 4411	1/25/05	—	-17.0
76-3/2/4	SPC 0103 4413	1/25/05	—	-15.1
78-3/2/4	SPC 0103 4415	1/25/05	—	-12.6
185-2	SPC 0103 4403	1/25/05	—	-13.4
185-3	SPC 0103 4405	1/25/05	—	-17.7
186-3/2	SPC 0103 4407	1/25/05	—	-17.2
57-3/4	SPC 0103 4427	8/1/05	—	-12.9
58-3/2/4	SPC 0103 4429	8/1/05	—	-16.5
59-3/2	SPC 0103 4431	8/1/05	—	-12.9
61-3/2/4	SPC 0103 4433	8/1/05	—	-17.1
74-3/4	SPC 0103 4435	8/1/05	—	-17.1
75-3/4	SPC 0103 4437	8/1/05	—	-17.1
76-3/2/4	SPC 0103 4439	8/1/05	—	-16.0
78-3/2/4	SPC 0103 4441	8/1/05	—	-14.4
185-2	SPC 0103 4443	8/2/05	—	—
185-3	SPC 0103 4445	8/2/05	—	-10.9
186-3/2	SPC 0103 4447	8/2/05	—	-18.2
57-3/4	SPC 0103 7565	11/29/05	—	-15.3
58-3/2/4	SPC 0103 7567	11/29/05	—	-18.4
59-3/2	SPC 0103 7569	11/29/05	—	-13.5
61-3/2/4	SPC 0103 7571	11/29/05	—	-11.4
74-3/4	SPC 0103 7557	11/29/05	—	-17.4
75-3/4	SPC 0103 7559	11/29/05	—	-18.2
76-3/2/4	SPC 0103 7561	11/29/05	—	-14.7

Table 6.3-29. Hydrogen ( $\delta D$ ) and Oxygen ( $\delta^{18}O$ ) Isotope Compositions of Steam Condensed from Gas Samples Collected during the DST Heating and Cooling Phases (Continued)

Sample Interval <sup>a</sup>	YMP Tracking Number	Date Sampled	Isotope Composition	
			Hydrogen $\delta D$ (‰)	Oxygen $\delta^{18}O$ (‰) <sup>b</sup>
78-3/2/4	SPC 0103 7563	11/29/05	—	-12.3
185-2	SPC 0103 7551	11/29/05	—	-16.5
185-3	SPC 0103 7553	11/29/05	—	-18.1
186-3/2	SPC 0103 7555	11/29/05	—	-17.2

Source: DTNs: LB980420123142.005 [DIRS 111471]; LB980715123142.003 [DIRS 111472]; LB0404ISODSTHP.003 [DIRS 169254]; LB990630123142.003 [DIRS 111476]; LB000121123142.003 [DIRS 146451]; LB000718123142.003 [DIRS 158342]; LB0011CO2DST08.001 [DIRS 153460]; LB0102CO2DST98.001 [DIRS 159306]; LB0108CO2DST05.001 [DIRS 156888]; LB0203CO2DSTEHE.001 [DIRS 158349]; LB0303ISODSTCP.001 [DIRS 177538]; LB0309ISODSTCP.001 [DIRS 177539]; LB0410ISODSTCP.001 [DIRS 177541]; LB0509ISODSTCP.001 [DIRS 177542].

<sup>a</sup> Field number corresponds to intervals in hydrology boreholes.

<sup>b</sup> Stable oxygen isotope ratios are given as part per thousand or per mil (‰) variations in the ratio of  $^{18}O$  to  $^{16}O$  relative to oxygen isotope ratio of VSMOW (Vienna Standard Mean Ocean Water), an internationally accepted standard for reporting oxygen isotope data.

#### 6.3.4.2.5 Measurement Uncertainty: Concentration and Isotopic Ratios

##### CO<sub>2</sub> Concentration

Besides the uncertainties associated with the measurements, there were a number of other factors that affected the measured CO<sub>2</sub> concentrations. These are listed below, together with an assessment of the potential impact on the measured CO<sub>2</sub> concentrations:

- (1) Removal of water vapor from the samples. Condensing the water vapor from the samples will lead to measurement of high CO<sub>2</sub> concentrations in the gas relative to the actual concentrations of pore gas in the rock. This is more significant in intervals at or above the boiling point. However, the magnitude of this effect can be calculated for conditions such that the gas in the rock was saturated with water vapor at the temperature of the rock. Using this correction provides a lower bound on the CO<sub>2</sub> concentration in situ, but the actual values must be close to the lower bound because of the observed high humidity in the sampled intervals (Section 6.3.4.2.1).
- (2) Small leaks in the sampling apparatus. This could lead to some contamination of the samples with air from the observation drift. This was probably not significant except in samples where the gas flow rates were very low (e.g., those intervals with high vapor contents in the gas). In those instances, the measured concentrations could be diluted by as much as 50% relative to the actual concentrations.
- (3) Other tests using the hydrology boreholes. The hydrology boreholes were used for a variety of other measurements, including air permeability tests and sampling of water. The impact of water sampling was probably minimal, but the air permeability

measurements (which consisted of injecting N<sub>2</sub> gas into the intervals) could significantly dilute the CO<sub>2</sub>. As much as possible, gas sampling was scheduled just before any air permeability tests were performed to minimize the effects of the air permeability measurements on the CO<sub>2</sub> measurements.

- (4) Deflated packers. Over time, several packers in the hydrology boreholes developed leaks and deflated (see Table 6.3-10 for a list of deflated packers and the dates they became deflated). This was especially prevalent in the higher-temperature intervals. Even when deflated, the packers still formed a barrier between the intervals (their deflated diameter is only slightly less than the diameter of the borehole). However, it is likely that samples taken from intervals with deflated packers contained some gas from the intervals on the other side of the deflated packers. After April 2000 (when the problem became more prevalent), investigators began noting which samples were collected from intervals with deflated packers by including the adjacent intervals in the sample name. For instance, when the packer between interval 3 and 4 in borehole 57 was deflated and a sample was collected from interval 3, the sampling interval was noted as 57-3/4, indicating that the sample was taken from borehole 57, interval 3, but may contain input from interval 4. Several of the packers began leaking before April 2000 and were deflated (most notably in borehole 77), but this was not indicated by the sampling interval.

- (5) Refer to precision and accuracy discussion in Section 6.3.4.2.2.

#### Isotopic Composition of Pore Water Estimated from That of Condensate Isotope Compositions

There are a number of uncertainties that limit the reliability of these measurements:

- (1) Temperature uncertainties. The temperature can vary significantly within an interval, making it difficult to determine the temperature to use for calculating the isotopic composition of the water.
- (2) Condensation in sample tubing. During sampling, the water vapor moves from the hot temperatures in the rock to the cooler temperatures in the observation drift. This can lead to significant condensation of water vapor in the tubing prior to the chiller unit. This effect is believed to have been minimal because of the large volume of air flushed through the tubing and the increase in the temperature of the tubing during sampling. However, this still may account for some loss of vapor prior to the chiller unit. Since the  $\delta D$  and  $\delta^{18}O$  values of the vapor are lower than those of the liquid, this will cause the isotopic composition of the water vapor that reaches the condensate trap to be lower than the composition of the water vapor in the rock.
- (3) Inefficient trapping by the chiller unit. The chiller unit used for this sampling was not capable of completely cooling high-temperature water vapor (greater than 80°C) to 4°C. As a result, a fraction of the water vapor in the higher-temperature samples passed through the chiller unit. The water vapor that does not condense in the trap will have lower  $\delta D$  and  $\delta^{18}O$  values than the water in the trap, which will lead to high values for the condensate. To minimize this effect, any water in the pump trap

(generally less than 10 mL) after the chiller unit was mixed back into the water in the chiller trap. Altogether, the amount of water vapor loss is believed to be less than 5%. For this amount of loss, the net effect on the  $\delta D$  values will be less than 3%; on the  $\delta^{18}O$  values it will be less than 0.5%. It should also be noted that this shift and any shift caused by #2 above would offset each other.

#### 6.3.4.3 DST Mineralogic and Petrologic Analyses

Mineralogic characterization data provide quantitative information on mineral distribution and abundance in the preheating rock under ambient conditions. Mineralogic changes while the test is in process are also documented. These data support the coupled thermal-hydrologic-chemical modeling effort.

As expected, detectable mineralogic changes from the test were restricted to the natural fracture system and the surfaces of preheating boreholes that function as preferential fluid flow paths. Mineralogic changes within the rock matrix were expected to be undetectably minute. These expectations were supported by qualitative examination of the SHT postcooling overcores (see Section 6.2.4.2) and by quantitative X-ray diffraction (XRD) of pre- and post-testing crushed TSw2 samples from a hydrothermal column test (Lowry 2001 [DIRS 157900], p. 29). These studies found no detectable mineralogic alteration of the rock matrix at the conclusion of the hydrothermal tests. Evidence of mineralogic alteration was limited to fractures and borehole surfaces of the SHT and to crushed-tuff fragment surfaces from the column test.

Mineralogic characterization of the natural rock-fracture surfaces was accomplished by study of preheating drill core from the DST block. A decision was made to employ stereoscopic examination of fracture surfaces, supplemented by scanning electron microscope (SEM) and XRD, for mineralogic analysis, so as to characterize as much fracture surface as possible. Compared to the exclusive use of microanalytical techniques, this strategy sacrifices achievable precision and accuracy, but maximizes the representativeness of the data because more fracture surface is examined. The end product is a quantitative mineralogic inventory of the fracture system that can be input to modeling. Mineral abundances of stellerite, manganese minerals, crystalline silica and feldspar, clay, and calcite on the fracture surfaces are in the TDMS under input DTN: LA9912SL831151.002 [DIRS 146449].

Investigators learned from the SHT that mineralogic sampling while a test is in progress would be more valuable than collecting samples only after the test is finished. To realize this goal for the DST, a sidewall sampling tool was designed and built to provide an in-progress sampling capability. The tool operates within existing boreholes, targeting intervals of fractured rock that were identified from borehole video recordings. Two coring sessions have been conducted during the transition from heating to cooling phases of the test.

In November 2000, the sidewall coring tool was used to collect six sidewall cores from inclined boreholes ESF-HD-CHE-2 and ESF-HD-CHE-3 (boreholes 53 and 54 in Figure 6.3-7). In June 2001, eight samples were collected from the two previously sampled boreholes plus borehole ESF-HD-CHE-9 (borehole 72 in Figure 6.3-7). The sidewall cores from these boreholes have provided information on mineralogic changes in the boiling zone. The elemental

abundances and chemical, textural, and mineralogic characteristics of core samples from borehole 54 are in the TDMS under input DTN: LA0201SL831225.001 [DIRS 158426].

### 6.3.4.3.1 Results: Mineralogy of the Preheating Natural Fracture System

Systematic data on natural, preheating fracture-mineral coverage were collected from the drill core of borehole ESF-HD-TEMP-2 (borehole 80 in Figure 6.3-3), a horizontal borehole that runs parallel to the heated drift. The drill core is 195.6 ft (59.62 m) long, but the first 25 ft (7.62 m) of the core are well outside the heated drift and were excluded from study. The number of fractures in the relevant length of core was too large for all to be included in the characterization. Therefore, a conceptual model of fracture attributes was developed to guide the selection of a subset of fractures for mineralogic analysis. The conceptual model is based on a major simplification of the criteria used to define subzones of the middle nonlithophysal zone (Buesch and Spengler 1998 [DIRS 101433], pp. 18, 20).

The rock traversed by ESF-HD-TEMP-2 consists of intervals dominated by vapor-phase features and intervals where vapor-phase features are not prominent. As seen in the drill core, the dominant vapor-phase features are vapor-phase partings and vapor-phase stringers that dip eastward at low angles parallel to the rock foliation. Both partings and stringers are fractures lined with crystalline silica and feldspar fracture coatings, commonly called vapor-phase minerals. In intervals where vapor-phase partings and stringers and associated vapor-phase cavities (lithophysae) are common, the rock-matrix color is light brownish gray. Rock-matrix color in the intervals with only rare vapor-phase features is grayish orange pink to light brown.

Reconnaissance examination of the drill core suggested that the fracture coatings are different in the vapor-phase and nonvapor-phase intervals, an observation that was confirmed by detailed study. Based on this observation, detailed fracture mineral studies were performed in two core sections of approximately equal length representing each type of interval. Mineral abundances on the fracture surfaces were determined for stellerite, manganese minerals, crystalline silica and feldspar (combined), clay (probably also including minor mordenite), and calcite. The results are presented in Table 6.3-30. For the minerals included in the inventory, differences in abundance of crystalline silica plus feldspar, and in calcite between the vapor-phase and nonvapor-phase intervals, were documented. The greater abundance of crystalline silica plus feldspar in the vapor-phase interval is expected because these minerals are among the defining characteristics of vapor-phase void spaces.

Table 6.3-30. Mineral Coverage on Fractures, Drill Core ESF-HD-TEMP-2

Section 1, 25.0 to 29.3 ft, Nonvapor-Phase Interval				
Stellerite	Manganese Minerals	Crystalline Silica/Feldspar	Clay	Calcite
42.3%	1.5%	1.0%	4.3%	0%
Section 2, 62.15 to 66.45 ft, Vapor-Phase Interval				
Stellerite	Manganese Minerals	Crystalline Silica/Feldspar	Clay	Calcite
41.6%	2.0%	3.5%	4.7%	2.2%

Source: DTN: LA9912SL831151.002 [DIRS 146449].

Additional natural minerals observed in very small quantities or in local concentrations by SEM of preheating core include mordenite, pyrite, and possible hematite. Other minerals are also present and will be characterized based on their importance for modeling the test results.

#### **6.3.4.3.2 Results: Evidence of Mineral Deposition**

Sidewall cores collected during the test revealed new mineral deposits on borehole surfaces and on the surfaces of fractures that intersect the boreholes. New mineral deposits are common on the borehole surfaces because the boreholes act as preferential pathways for fluid flow. Deposits are less common and quantities of new minerals less abundant on the natural fractures within the core samples.

Mineral deposition within the boiling zone is documented by samples from borehole ESF-HD-CHE-3 (borehole 54). The three products observed so far are tentatively identified as amorphous silica, gypsum, and calcite (DTN: LA0201SL831225.001 [DIRS 158426]). The presence of amorphous silica on fracture surfaces is documented by sidewall cores collected from boreholes 53, 54, and 59 (input DTN: LA0303WS831151.001 [DIRS 169378]). The tentative identifications of gypsum and calcite are based on identifications of these phases by XRD as products of the SHT (DTN: LA0009SL831151.001 [DIRS 153485]). The silica deposits exhibit considerable textural heterogeneity, perhaps because some were deposited when the collection site was in the condensation zone and others deposited when boiling-zone dryout conditions were reached.

Examples of possible condensation zone silica deposition above the heated drift have been identified. In one example, a fracture surface is completely coated by terrace-like silica deposits up to a few micrometers thick. In another example, several discoid silica deposits (up to about 20 micrometers across) rest on a surface of earlier-deposited discs cemented and largely obscured by silica particles about one or two micrometers across. In both examples, the deposits were built up during multiple episodes of silica deposition, perhaps during the passage of numerous pulses of silica-saturated water.

Very thin (less than 0.5 micrometers thick), curled silica sheets may be products of final dryout in the boiling zone. There is no textural evidence of successive buildup in the silica sheets. Also lying atop the earlier silica deposits or on preheating fracture surfaces are scattered deposits of prismatic gypsum and rounded mounds of calcite.

#### **6.3.4.3.3 Results: Evidence of Mineral Dissolution**

Studies of preheating core from the SHT showed that some of the natural fracture minerals have experienced dissolution caused by ancient or ongoing geochemical processes. This complicates the effort to document mineral dissolution resulting specifically from the DST. To provide documentation of natural alteration, samples of preheating drill core from approximately the same locations as sidewall samples were examined by SEM. Images of the typical morphologies of natural fracture coating minerals and rock fracture surfaces were recorded. The majority of such documentation was devoted to stellerite because it is the single most abundant fracture coating mineral.



The natural stellerite fracture coatings in preheating samples did not show clear evidence of dissolution. Stellerite in the sidewall core samples also showed no evidence of dissolution. The lone exception occurred on one fracture from the 66.5-ft (20.27-m) depth in borehole ESF-HD-CHE-3. In this location, a highly corroded stellerite crystal, several slightly to moderately corroded stellerite crystals, and a moderately corroded silica crystal were adjacent to or within a lobate deposit of amorphous silica (DTN: LA0201SL831225.001 [DIRS 158426]). At the time of sample collection, this sample came from within the boiling zone. However, the sampled rock volume had previously been within the condensation zone before the boiling zone moved to its farthest position away from the heaters. It is possible that the observed mineral dissolution and, perhaps, deposition, occurred when the rock volume was in the condensation zone.

#### **6.3.4.3.4 Results: Mineral Deposition Associated with Man-Made Materials Interactions**

During a video camera run in the heated drift in August, 2002, deposits of reddish, fine-grained material were observed on the tops of several canister heaters and on the floor of the drift. All the material had apparently been deposited sometime between April and August, 2002, during the period of rapid cooling after the heaters were shut off. The material appeared to be iron oxide, and the distribution of the deposits suggested that they could have been derived from corrosion of the Swellex rock bolts. A remote-sampling arm with a new fabric cleaning pad was attached to the camera and used to collect some of the red material.

Qualitative XRD data for the red material include several classes of crystalline material (DTN: LA0609SL831322.001 [DIRS 178052]). Quartz, cristobalite, and feldspar were presumed to be rock dust. These mineral phases are composed of silica, alumina, sodium, and potassium. Hematite ( $\text{Fe}_2\text{O}_3$ , iron oxide), a major constituent of the red material, is an alteration product of iron-rich materials that is present naturally in the rock but may also have been produced by oxidation of introduced materials. Halite ( $\text{NaCl}$ ) and calcite may have been produced by evaporation of rock fluids due to heating of the rock. Halite is present in the unheated natural rock but in quantities undetectable by XRD. Calcite has been identified as a product of the DST (see Section 6.3.4.3.2), but is also a minor constituent of fractures in the unheated natural rock.

Sylvite ( $\text{KCl}$ ) also was present in the data for the red deposit, but the diffraction data for the unused cleaning cloth suggested an even larger sylvite content. Therefore, the sylvite present in the red material is interpreted as contamination from the collection pad. The XRD data for the unused pad also included possible indications of the presence of minor calcite and quartz. However, these two phases are much more abundant in the red material, and their presence in the sample is attributed predominantly to in situ processes in the heated drift.

#### **6.3.4.3.5 Measurement Uncertainty: Mineralogic and Petrologic Analyses**

Estimates of fracture coverage by minerals are the principal numerical data derived from these studies. No formal analysis of the errors of estimation has been performed. It is likely that mineral coverages estimated to be 10% or less have relative errors of 50% to 100% (e.g., the estimated 2% coverage by a mineral could be in the 1% to 3% range). Estimated mineral

coverages greater than 10% probably have estimated relative errors of 20% or less. Uncertainties of these magnitudes are considered adequate for current modeling purposes.

#### 6.3.4.4 Strontium and Uranium in Water Samples

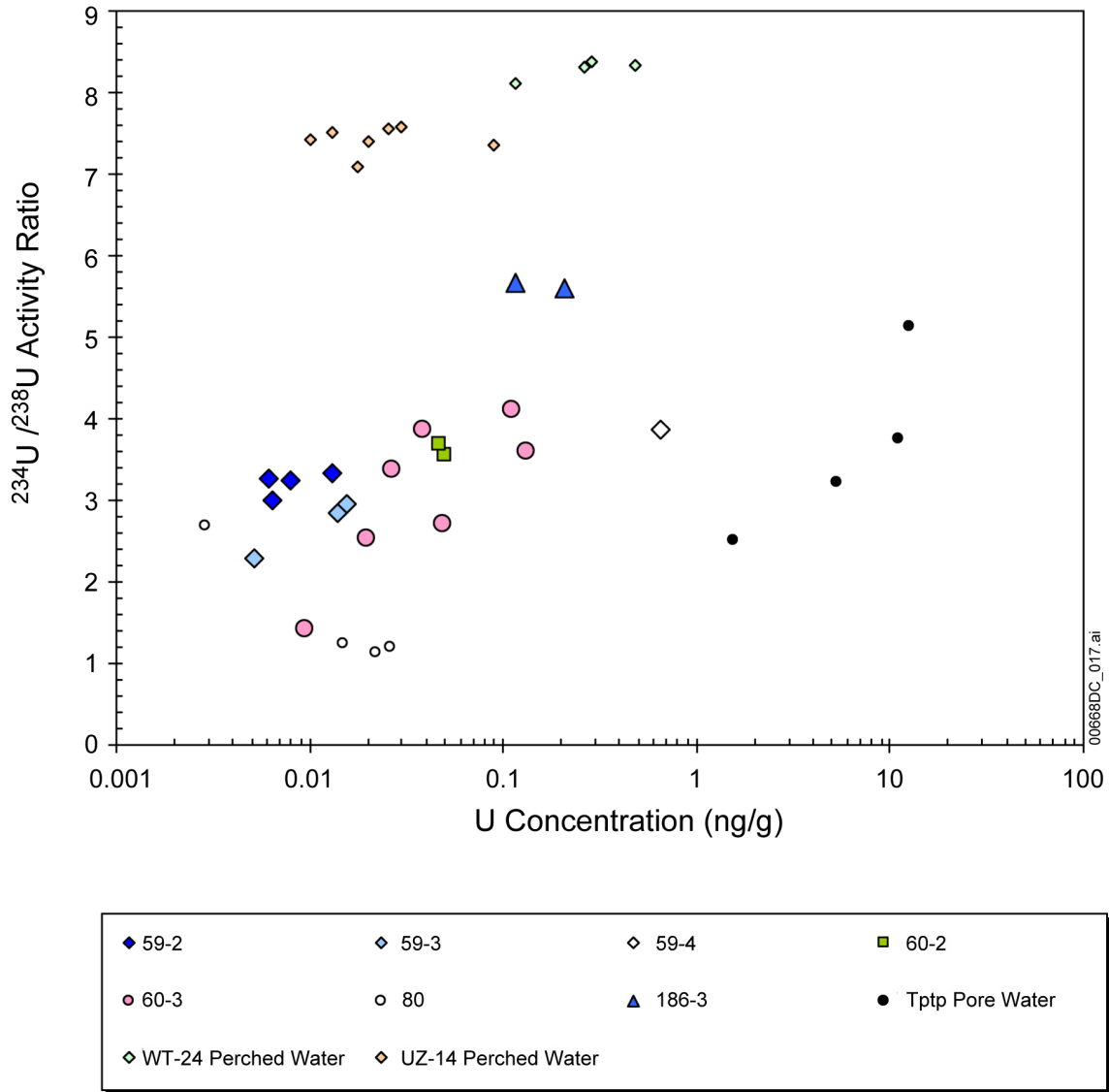
This section discusses strontium and uranium isotopic data obtained from a subset of water samples collected from the DST during the heating phase (Section 6.3.4.1). Measurements of strontium and uranium concentrations and isotopic compositions in water samples may provide information on mineral reactions and water flow paths occurring as the block is heated during the test. In addition, isotopic analyses can provide unequivocal evidence of interaction of test-produced water with the engineered materials introduced into the test block during construction. This section discusses data obtained from waters sampled from five boreholes: 60, 186, 59, 76, and 80. Data were acquired at the USGS in Denver under technical procedures NWM-USGS-GCP-03 and NWM-USGS-GCP-12. Uranium and strontium concentrations were determined by isotope dilution mass spectrometry. Uranium and strontium isotopic ratios were determined by thermal-ionization mass spectrometry. The data have been submitted to the TDMS under the following input DTNs:

- GS011108312322.008 [DIRS 159136]
- GS010608315215.002 [DIRS 156187]
- GS010808312322.004 [DIRS 156007]
- GS011108312322.009 [DIRS 159137]
- GS960908315215.012 [DIRS 169552]
- GS010908315215.005 [DIRS 169553]
- GS990308315215.004 [DIRS 145711]
- GS040508312272.002 [DIRS 169629] (unqualified)
- GS990308315215.003 [DIRS 145707].

##### 6.3.4.4.1 Results: Strontium and Uranium in Water Samples

Figure 6.3-49 shows uranium concentrations and  $^{234}\text{U}/^{238}\text{U}$  activity ratios in DST waters, as well as values obtained for pore water from upper lithophysal and middle nonlithophysal units of the Topopah Spring Tuff (Tptp) and values for water perched in the base of the Tptp. Uranium concentrations in DST samples vary from 0.003 to 0.65  $\mu\text{g}/\text{L}$  and are typically lower than concentrations observed in pore water extracted by ultracentrifugation from the same units. The  $^{234}\text{U}/^{238}\text{U}$  activity ratios in DST samples vary from 1.14 to 5.68, and unlike U concentrations, typically overlap the  $^{234}\text{U}/^{238}\text{U}$  activity ratio values observed in pore water. Samples from individual DST sites obtained at different times during the heating phase of the test have uranium concentrations that show a fairly systematic decrease with time (Figure 6.3-50). Similar to uranium, the strontium concentrations in the test waters approach the values estimated for pore water and decrease with time. Borehole 60-3 water reached a strontium concentration of 0.2  $\mu\text{g}/\text{L}$  in June 1999, about 1,000 times less strontium than this zone produced initially. Figure 6.3-51 shows the variation of strontium isotopic compositions in the test waters compared to various reservoirs of strontium in the DST block. The orange and red bands show the strontium isotopic compositions of the Topopah Spring Tuff (middle nonlithophysal and upper lithophysal zones) today and at the time of their deposition, respectively. The green band is the range of  $^{87}\text{Sr}/^{86}\text{Sr}$  in pore water; these data are from borehole

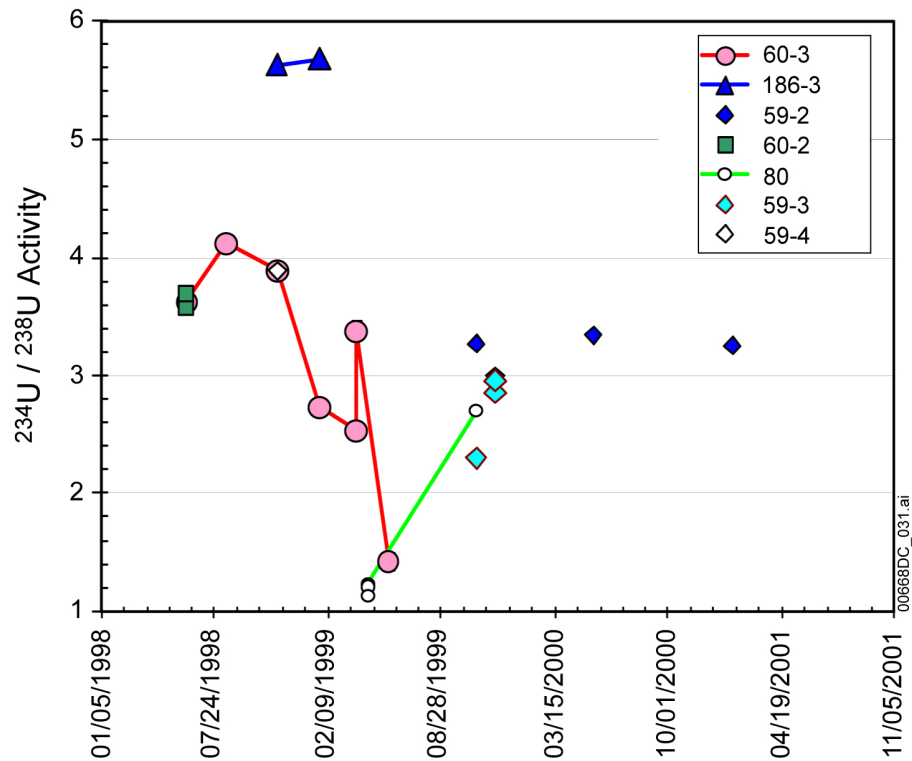
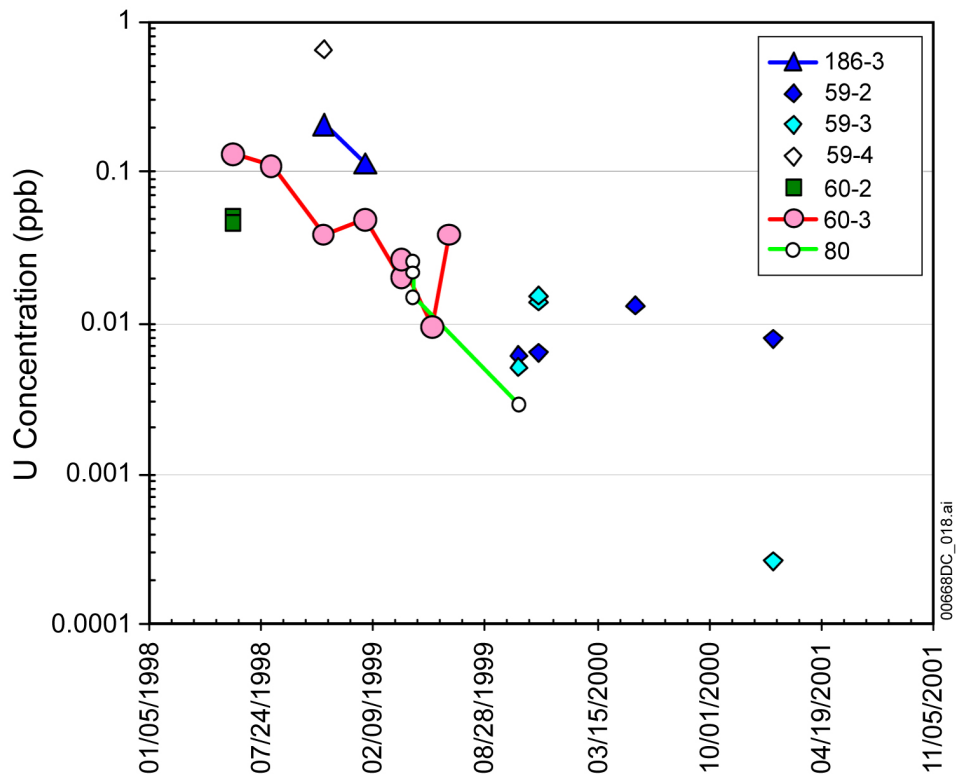
USW SD-9, which is the closest vertical borehole to the DST block. Grout introduced into the DST block during emplacement of borehole instrumentation has also been measured and is shown by the black line at an  $^{87}\text{Sr}/^{86}\text{Sr}$  value of 0.7086. The grout contains over 800 ppm strontium, providing a potentially important added source.



Source: DTNs: GS011108312322.008 [DIRS 159136] (DST and Pore Water); GS010808312322.004 [DIRS 156007] (WT-24 Water); GS010608315215.002 [DIRS 156187] (UZ-14 Water).

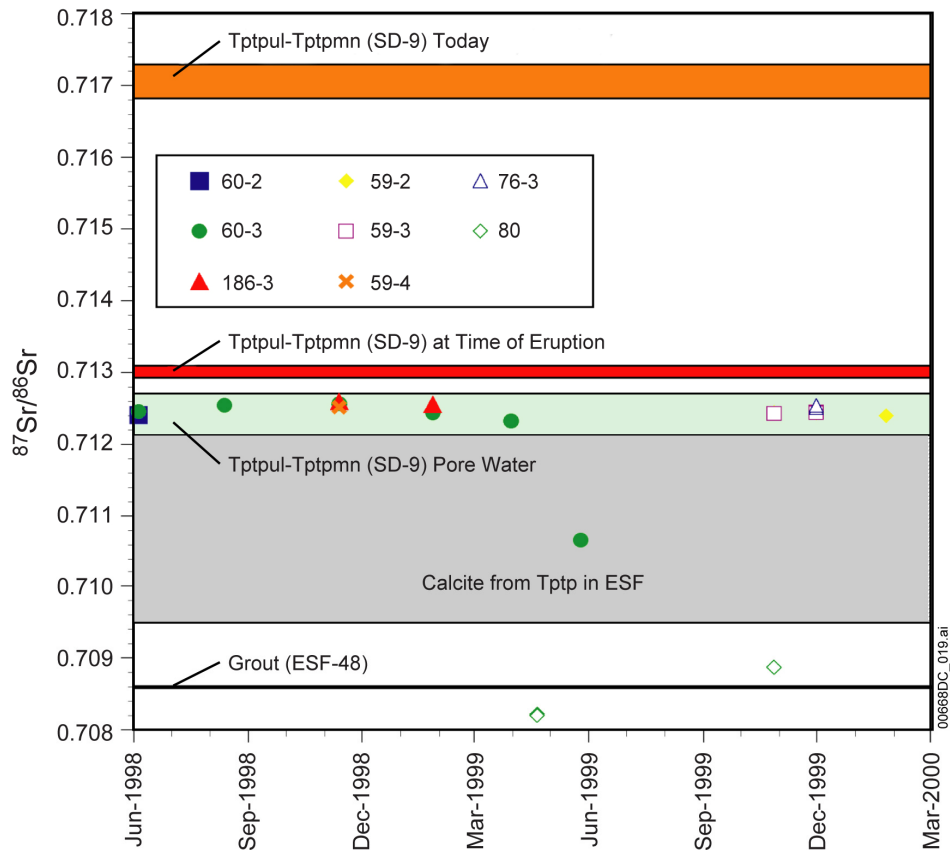
NOTE: Analytical errors are typically smaller than the size of the symbols. Pore waters and perched waters shown for comparison.

Figure 6.3-49. Uranium Concentrations and Isotopic Compositions of Water Samples Collected from the DST



Source: DTN: GS011108312322.008 [DIRS 159136].

Figure 6.3-50. U Concentration (upper) and  $^{234}\text{U}/^{238}\text{U}$  Activity Ratios (lower) in DST Samples Plotted versus Collection Date



Source: DTNs: GS011108312322.009 [DIRS 159137]; GS960908315215.012 [DIRS 169552]; GS010908315215.005 [DIRS 169553]; GS990308315215.004 [DIRS 145711]; GS040508312272.002 [DIRS 169629] (unqualified); GS990308315215.003 [DIRS 145707].

NOTES The calcite field should extend to overlap the pore water field.

“Tptpul-Tptpmn (SD-9) Today” range determined from samples row numbers 47 and 55 in DTN: GS990308315215.004 [DIRS 145711].

“Tptpul-Tptpmn (SD-9) Pore Water” range determined from row numbers 11 and 42 in DTN: GS990308315215.004 [DIRS 145711].

Unqualified data from DTN: GS040508312272.002 [DIRS 169629] are used to plot  $^{87}\text{Sr}/^{86}\text{Sr}$  for grout.

The Tptpul-Tptpmn (SD-9)  $^{87}\text{Sr}/^{86}\text{Sr}$  at the time of eruption (12 Ma before present) was derived from the following equation:

$$\frac{^{87}\text{Sr}}{^{86}\text{Sr}} = \left( \frac{^{87}\text{Sr}}{^{86}\text{Sr}} \right)_t + \frac{^{87}\text{Rb}}{^{86}\text{Sr}} \left( e^{\lambda t} - 1 \right) \quad (\text{Faure 1986 [DIRS 105559], Equation 8.3})$$

where:

$t$  = time before present ( $12 \times 10^6$  years)

$\lambda$  = decay constant of  $^{87}\text{Rb}$  ( $0.0142/1 \times 10^9$  years)

$^{87}\text{Rb}/^{86}\text{Sr}$  determined from the weight ratio of Rb/Sr using equation 8.4 in the study by Faure (1986 [DIRS 105559])

Rb and Sr concentrations from rows 22 and 24 in DTN: GS990308315215.003 [DIRS 145707]; Sr ratios from rows 47 and 53 in DTN: GS990308315215.004 [DIRS 145711].

Figure 6.3-51. Strontium Isotope Ratio Compositions of Water Samples Collected from DST Boreholes Compared to Compositions of Pore Water, Rock, Calcite, and Grout

Most of the water obtained during the DST to date has  $^{87}\text{Sr}/^{86}\text{Sr}$  values within the range of pore water. A very dilute sample obtained from borehole 60-3 falls outside the range of pore water. The most significant deviations from pore water are exhibited by water from borehole 80. These samples, obtained from this neutron borehole, apparently have interacted with the grout used to emplace the liner in this borehole. This statement may be evidence of contamination based on the known isotopic compositions of the grout and the natural system. The chemistry of these samples should be used only as an example of water that has interacted with the engineered materials (Section 6.3.4.5). It is notable that the chemistry of these waters does not show additional evidence of interaction with grout.

Borehole 59, zone 4, was sampled in November 1998 and showed a very unusual chemistry, as reported in Table 6.3-25 (approximately 1,200 mg/L chloride), that was initially interpreted as probable contamination. This sample was analyzed for strontium isotopic composition, and the result plots in the field of pore water (Figure 6.3-51). Similarly, the  $^{234}\text{U}/^{238}\text{U}$  activity ratio for this sample is in the range of observed pore waters and higher than other samples from borehole 59 (Figure 6.3-49), unlike samples with low  $^{234}\text{U}/^{238}\text{U}$  suspected of contamination. Based on these results, the 59-4 sample is not likely contaminated with grout or other anthropogenic materials

#### **6.3.4.4.2 Measurement Uncertainty: Strontium and Uranium in Water Samples**

The accuracy of the isotopic dilution concentration measurements is maintained within the analytical precision by the analysis of known concentration standards; the precision of strontium concentrations is about 1% and the precision of uranium concentrations varies from less than 1% to about 10%, depending on the amount of uranium present. The accuracy of the isotopic measurements is maintained by the frequent analysis of standards with known or assumed isotopic compositions. For uranium, this standard is a material in which the isotopes are in secular equilibrium. For strontium, a standard with a ratio equivalent to modern seawater is analyzed; all  $^{87}\text{Sr}/^{86}\text{Sr}$  ratios are relative to a value of 0.70920 for modern seawater. Absolute precisions at 95% confidence are 0.00005 for  $^{87}\text{Sr}/^{86}\text{Sr}$  and from 0.02 to 0.3 for  $^{234}\text{U}/^{238}\text{U}$ .

#### **6.3.4.5 Chemical Effects of Introduced Materials in the DST**

As noted in Section 6.3.4.1, packers of chloroelastomer (neoprene) were used in hydrology borehole segments where temperatures were not expected to exceed the boiling point. Fluoroelastomer (abbreviated FKM) packers were installed in holes where temperatures well above the boiling point were expected (Figure 6.3-44). Within the data set of water compositions from the hydrology boreholes, two subsets were distinguished based on elevated contents of fluoride or chloride. The water compositions are indications of probable chemical interactions between borehole fluids and introduced materials. Thermal conditions prevailing in the borehole intervals that were sources of high fluoride or high chloride samples have been reconstructed to elucidate the interplay of thermal regime, fluid availability, and introduced packer materials. The water sample compositions taken as indications of geochemical interactions between borehole fluids and packers, plus field and laboratory experiments to test this hypothesis, are described here. Detailed descriptions of the investigations are given in two white papers: *Effects of Introduced Materials in the Drift Scale Test* (Jones 2004

[DIRS 170750]) and *Effects of Neoprene on Water in the Drift Scale Test* (Williams 2003 [DIRS 163765]).

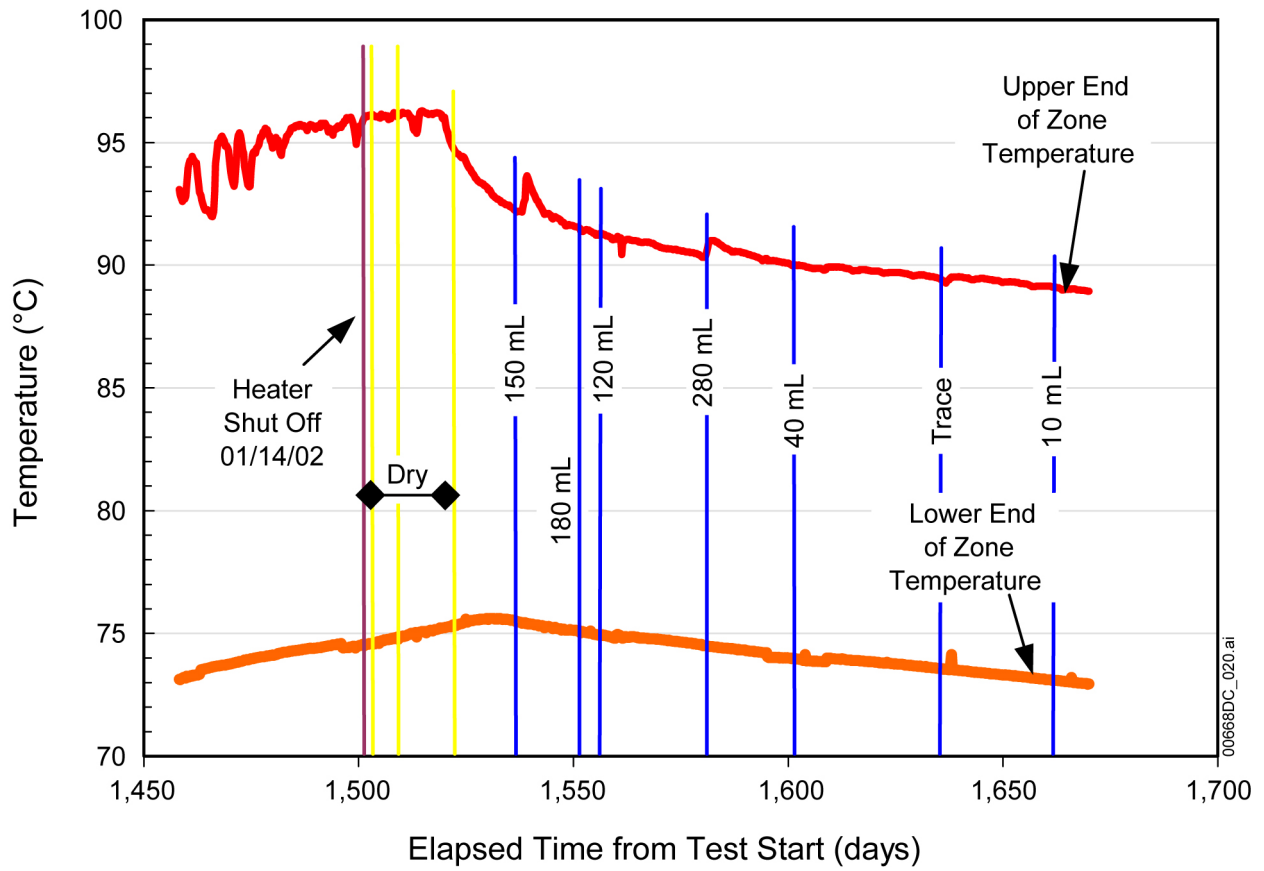
#### **6.3.4.5.1 Thermal Environments of Sample Collection**

The high fluoride, low pH water samples were collected from borehole intervals within superheated (greater than 140°C) zones of the test block. In these high-temperature regions of the rock, about 40°C above the boiling point, water is present only as superheated vapor; liquid water is formed by cooling during the sampling process.

The high chloride water samples were collected from packed-off borehole intervals where temperatures were below the boiling point. Upper-end and lower-end temperatures in the BH 59/4 interval were about 68°C and 70°C, respectively, when the 11/12/98 samples were collected. On 1/26/99, the upper- and lower-end temperatures were 75°C and 77°C, respectively. Thermal data measured in and near BH 75/2 indicate that the top of the zone was near boiling, while the bottom of the zone was much cooler when the first high chloride water was collected. Figure 6.3-52 shows a temperature history for BH 75/2 from shortly before heater shut-off until the interval stopped producing water. Temperature data were taken from the top of zone 75/2 and from the top of zone 75/1, which is the sensor location closest to the bottom of 75/2. A temperature differential of about 15°C existed between the upper and lower ends of zone 75/2.

#### **6.3.4.5.2 Aqueous Geochemistry of Materials Interaction**

The water chemistry information in Tables 6.3-24 (DTN: SN0208F3903102.002 [DIRS 161246]) and 6.3-25 (DTN: LL020709923142.023 [DIRS 161677], unqualified), plus more recent data in Table 6.3-31 (DTNs: LL030305023121.023 [DIRS 170570], unqualified; GS020808312272.004 [DIRS 166569], unqualified; GS030408312272.002 [DIRS 165226]) and DTNs: SN0210F3903102.004 [DIRS 170573], SN0211F3903102.005 [DIRS 170574], and LL030310023121.024 [DIRS 170571] (unqualified), was examined for unusual compositions that probably reflect the chemical influence of introduced materials. The additional data represent samples collected after the heater shut-off and were included to provide the most complete picture of materials interactions. Table 6.3-32 summarizes the information pertinent to the assessment of materials interaction and identifies water samples likely to have been affected. For affected samples, the table lists the criteria for identifying materials interaction and supporting information such as the composition of packers in the sampled borehole intervals.



Source: DTNs: LB0401PRTDSTHP.009 [DIRS 169250]; LB0401PRTDSTCP.001 [DIRS 170568]; LB0401PRTDSTCP.002 [DIRS 170569]; SN0210F3903102.004 [DIRS 170573]; SN0211F3903102.005 [DIRS 170574].

NOTE: The temperature history for the lower end of the zone is derived from a temperature sensor at the upper end of zone 75-1.

Figure 6.3-52. Thermal History and Water Recovery in Borehole 75, Zone 2



Table 6.3-31. Field and Laboratory Analytical Data for Borehole 75-2 Water Samples

Borehole and Zone	75-2 <sup>a</sup>	75-2 <sup>a</sup>	75-2 <sup>a</sup>	75-2 <sup>a</sup>	75-2 <sup>b</sup>	75-2 <sup>b</sup>
Sample Identifier	SPC 01016607	SPC 01016608	SPC 01016554	SPC 01016619	SPC 01016632	SPC 01016652
Collection Date	2/19/2002	2/19/2002	3/6/2002	3/12/2002	4/4/2002	6/26/2002
Field pH	4.8	4.8	4.9	4.8	5.0	6.0
Electrical Conductivity (μS/cm)	2972 <sup>c</sup>	2972 <sup>c</sup>	2040 <sup>c</sup>	1332 <sup>c</sup>	1062 <sup>c</sup>	278
Total Dissolved Solids (ppm)	2253 <sup>c</sup>	2253 <sup>c</sup>	1486 <sup>c</sup>	903 <sup>c</sup>	708 <sup>c</sup>	176
<b>Cations (mg/L)</b>						
Na	174	184	133	103	57.3	19.6
Si	131	130	123	122.0	>98	29
Ca	394	366	209	99.5	73	27
K	18.4	17.8	15.9	8.2	8.7	2.7
Mg	162	162	102	38.9	37	9.5
Al	ND	ND	ND	Trace	0.022	0.283
Fe	1.4	1.5	0.81	0.58	N/A	N/A
Li	0.25	0.26	0.19	0.14	N/A	N/A
Sr	4.8	5.1	2.7	1.0	1.1	0.310
Ag	Trace	Trace	N/D <0.0025	Trace	0.00004	N/A
As	N/D	N/D	N/D	Trace	0.001	N/D <0.003
Ba	0.11	0.12	0.067	0.049	0.046	0.015
Be	N/D	Trace	N/D	Trace	0.0023	N/A
Cd	0.0071	0.0083	0.0037	0.0021	0.0011	N/A
Co	0.090	0.091	0.059	0.037	0.025	0.0058
Cr	0.38	0.40	0.25	0.18	0.094	N/A
Cs	N/A	N/A	N/A	N/A	0.0016	N/A
Cu	Trace	Trace	Trace	0.032	0.121	N/A
Hg	N/A	N/A	N/A	N/A	N/D <0.001	N/D <0.001
Mn	14.7	15.2	9.1	4.7	>3.0	1.340
Mo	0.069	0.072	0.046	0.028	0.0192	0.0093
Ni	3.2	3.3	2.3	1.6	N/A	N/A
Pb	N/D	N/D	N/D	Trace	0.0087	0.0229

Table 6.3-31. Field and Laboratory Analytical Data for Borehole 75-2 Water Samples (Continued)

Borehole and Zone	75-2 <sup>a</sup>	75-2 <sup>a</sup>	75-2 <sup>a</sup>	75-2 <sup>a</sup>	75-2 <sup>b</sup>	75-2 <sup>b</sup>
Sample Identifier	SPC 01016607	SPC 01016608	SPC 01016554	SPC 01016619	SPC 01016632	SPC 01016652
Collection Date	2/19/2002	2/19/2002	3/6/2002	3/12/2002	4/4/2002	6/26/2002
Field pH	4.8	4.8	4.9	4.8	5.0	6.0
Electrical Conductivity (μS/cm)	2972 <sup>c</sup>	2972 <sup>c</sup>	2040 <sup>c</sup>	1332 <sup>c</sup>	1062 <sup>c</sup>	278
Total Dissolved Solids (ppm)	2253 <sup>c</sup>	2253 <sup>c</sup>	1486 <sup>c</sup>	903 <sup>c</sup>	708 <sup>c</sup>	176
<b>Anions (mg/L)</b>						
Rb	N/A	N/A	N/A	N/A	0.0308	0.0066
Sb	N/D	N/D	N/D	Trace	N/A	N/A
Se	0.43	0.46	0.21	0.097	0.005	N/A
Tl	N/D	N/D	N/D	Trace	N/A	N/A
U	N/A	N/A	N/A	N/A	0.001	0.00006
V	N/D	N/D	N/D	Trace	0.0033	N/A
Zn	36.1	38.5	22.8	15.2	>12.0	4.250
HCO <sub>3</sub>	40	40	40	15	N/A	51
Total inorganic carbon	N/A	N/A	17	N/A	N/A	N/A
Total organic carbon	N/A	N/A	142	N/A	N/A	N/A
F	1.28	1.11	1.02	1.11	N/A	0.86
Cl	522	532	418	273	N/A	47
Br	0.84	0.66	0.71	0.45	N/A	ND <0.1
SO <sub>4</sub>	818	821	356	161	N/A	18
PO <sub>4</sub>	N/D <0.3	N/D <0.3	N/D <0.3	N/D <0.3	N/A	N/A
NO <sub>2</sub>	N/D <0.2	N/D <0.2	N/D <0.2	N/D <0.2	N/A	N/A
NO <sub>3</sub>	16.2	16.4	11.8	8.10	N/A	1.8

Source: DTNs: LL030305023121.023 [DIRS 170570] (unqualified); GS020808312272.004 [DIRS 166569] (unqualified); SN0210F3903102.004 [DIRS 170573]; SN0211F3903102.005 [DIRS 170574]; GS030408312272.002 [DIRS 165226].

<sup>a</sup> Analyzed at LLNL.

<sup>b</sup> Analyzed at USGS.

<sup>c</sup> Values are approximate because measurements were outside the calibration range of the instrument.

NOTE: N/D = not detected. N/A = not analyzed. Trace = very low concentration.

Table 6.3-32. Assessment of Effects of Introduced Materials on Water Chemistry

Date	Collection Hole/Zone	pH <sup>a</sup>	Electrical Conductivity (µS/cm) <sup>a</sup>	Total Dissolved Solids (ppm) <sup>a</sup>	Effect of Introduced Materials on Water Chemistry <sup>b</sup>	Comments
06/04/98	60/2	7.5	—	—	Not affected	Large volume of water (5.7 liters) that probably condensed in the sampling zone during early heating in 1998. Part of Zone 60/2 passes within one meter of wing heater holes 87 and 88.
06/04/98	60/3	7.7	—	—	Not affected	—
08/12/98	60/2	6.9	—	—	Not affected	—
08/12/98	60/3	6.8	—	—	Not affected	—
08/12/98	77/3	5.5	—	—	Not affected	The packer between zones 77/3 and 77/2 deflated on 1/7/98. Water collected in 77/3 is down slope from zone 77/2.
11/12/98	59/4	6.6	—	—	Affected	Color noted as yellow by lab report and high chloride content indicates probable contamination from neoprene packer.
11/12/98	60/3	6.9	—	—	Not affected	—
11/12/98	186/3	6.8	—	—	Not affected	—
01/26/99	59/4	—	—	—	Affected	Elevated chloride and sulfate. No field measurements.
01/26/99	60/3	7.36 to 7.44	—	140 to 141	Possibly affected	Collection zone contains fluoride-bearing rubber packer.
01/26/99	186/3	7.24 to 7.17	—	320	Possibly affected	Collection zone contains fluoride-bearing rubber packer.
03/30/99	60/3	8.0	—	—	Possibly affected	Collection zone contains fluoride-bearing rubber packer.
03/30/99	77/3	7.0	—	—	Not affected	Packer deflated between zones 2 and 3.
04/20/99	60/3	4.19 to 4.77	—	10 to 30	Possibly affected	pH and dissolved solids values suggest that much of the sample resulted from condensed steam in the sampling tube.
04/20/99	BH 80	6.39 to 6.72	—	30 to 50	Possibly affected	This hole contains a teflon tube to accommodate neutron logging. The annulus between the tube and borehole wall is grouted. Strontium isotopic composition indicates grout interaction (see Section 6.3.4.4).
05/10/99	60/3	4.68 to 4.80	8.7 to 12.4	5.4 to 8.0	Possibly affected	Condensate in sampling tube, collection zone contains fluoride-bearing rubber packer.
05/25/99	60/3	4.68 to 4.75	9.4 to 16.1	5.9 to 10.2	Possibly affected	Condensate in sampling tube, collection zone contains fluoride-bearing rubber packer.

Table 6.3-32. Assessment of Effects of Introduced Materials on Water Chemistry (Continued)

Date	Collection Hole/Zone	pH <sup>a</sup>	Electrical Conductivity (µS/cm) <sup>a</sup>	Total Dissolved Solids (ppm) <sup>a</sup>	Effect of Introduced Materials on Water Chemistry <sup>b</sup>	Comments
06/24/99	60/3	5.02 to 5.08	8.84	—	Possibly affected	Condensate in sampling tube, collection zone contains fluoride-bearing rubber packer.
08/09/99	59/2	—	—	—	Affected	Elevated chloride (above halite stoichiometry), sulfate. No field measurements.
08/10/99	61/3	—	—	—	Not affected	No field measurements
10/27/99	59/2	5.93 to 6.08	110.2 to 113.4	—	Not affected	—
10/27/99	59/3	6.64 to 6.81	192.3 to 203.1	118.1	Not affected	—
10/27/99	76/3	6.14 to 6.46	—	—	Not affected	—
11/30/99	59/2	6.8 to 7.53	67.0 to 80.8	42.3 to 52.8	Not affected	—
11/30/99	59/3	7.06 to 7.47	105.2 to 112	63.8 to 65.86	Not affected	—
11/30/99	76/3	6.86 to 7.04	307.2 to 326.2	198.6 to 207.3	Not affected	—
11/30/99	77/3	4.68	156.4	9.99	Possibly affected	Reported conductivity and TDS values are suspect. The packer between zones 77/3 and 77/2 failed on 1/7/98. Water collected in 77/3 is down slope from zone 77/2. Sample contains elevated fluoride (15 mg/L).
01/25/00	59/2	6.68 to 7.43	61.21 to 104.7	37.89 to 67.1	Not affected	—
01/25/00	77/2	4.63	61.24	40.24	Possibly affected	Collection zone contains fluoride-bearing rubber packer. Sample contains elevated fluoride (6.7 mg/L).
01/25/00	77/3	3.47	224.9	145.5	Affected	Low pH, elevated conductivity, and increased fluoride indicate condensation of HF acid in sampling tube. Deflated packer between zones 2 and 3.
05/23/00	59/2	6.96	96.13 to 99.73	61.27 to 61.91	Not affected	—
05/23/00	59/3	5.19	5.2	3.14	Not affected	pH and conductivity values suggest that sample condensed from steam in the sampling tube.
05/23/00	76/3	6.92 to 6.96	134.8	86.86	Not affected	—
05/23/00	76/4	—	—	—	Not affected	Low ionic strength. No field measurements.
06/29/00	59/2	6.81 to 7.08	79.9 to 100.3	49.12 to 62.73	Not affected	—
06/29/00	59/3	5.39 to 5.6	4.39 to 4.7	2.74 to 2.91	Not affected	pH and conductivity values suggest that sample condensed from steam in the sampling tube.

Table 6.3-32. Assessment of Effects of Introduced Materials on Water Chemistry (Continued)

Date	Collection Hole/Zone	pH <sup>a</sup>	Electrical Conductivity (µS/cm) <sup>a</sup>	Total Dissolved Solids (ppm) <sup>a</sup>	Effect of Introduced Materials on Water Chemistry <sup>b</sup>	Comments
06/29/00	59/4	4.6 to 4.74	14.83 to 13.72	8.48 to 9.21	Not affected	—
06/29/00	76/3	5.75	13.81	8.64	Not affected	—
06/29/00	76/4	4.74 to 4.77	12.85	7.99	Not affected	—
06/29/00	78/2	4.12	35.64	20.44	Not affected	Packer deflated between zones 2 and 3.
06/29/00	78/3	4.22	28.54	17.78	Not affected	—
08/21/00	76/3	6.27 to 5.04	—	—	Not affected	—
08/21/00	76/4	5.01 to 4.99	—	—	Not affected	—
08/21/00	78/3	5.05 to 5.21	—	—	Not affected	Packer deflated between zones 2 and 3.
01/23/01	59/2	—	—	—	Not affected	Ultrameter problem, no pH, TDS. Chloride below halite stoichiometry.
01/23/01	59/3	—	—	—	Not affected	Ultrameter problem, no pH, TDS. Condensate in sampling tube.
01/23/01	60/4	—	—	—	Not affected	Ultrameter problem, no pH, TDS. Low ionic strength, fluoride <1 mg/L.
04/17/01	59/2	4.87 to 5.27	6.6 to 6.7	4.2 to 10.4	Not affected	Entire sample preserved with HNO <sub>3</sub> ; no anion analysis.
04/17/01	59/3	5.82 to 5.96	30.6 to 54.2	19.0 to 34.7	Not affected	Entire sample preserved with HNO <sub>3</sub> ; no anion analysis.
04/17/01	59/4	5.2	9.8	6.1	Not affected	Entire sample preserved with HNO <sub>3</sub> ; no anion analysis.
04/17/01	76/2	5.7 to 8.3	33.5 to 41.5	22.5 to 25.8	Not affected	Packer deflated between zones 2 and 3.
06/26/01	76/3	5.3	—	3.7	Not affected	pH, total dissolved solids, and conductivity values suggest that sample condensed from steam in the sampling tube for all water collected 6/26/01 and 6/27/01. Packer deflated between zones 2 and 3.
06/26/01	76/4	5.5	11.2	6.7	Not affected	—
06/26/01	78/2	5.3	5.2	3.2	Not affected	Packers deflated between zones 2, 3, and 4.
06/26/01	78/3	5.0	5.2	3.4	Not affected	
06/26/01	78/4	5.0	6.7	4.0	Not affected	
06/27/01	59/2	5.1 to 5.6	4.0 to 6.4	2.6 to 3.8	Not affected	Adjacent zone packer (59/1) deflated 2/6/01, minimal impact to sampling in zone 2.

Table 6.3-32. Assessment of Effects of Introduced Materials on Water Chemistry (Continued)

Date	Collection Hole/Zone	pH <sup>a</sup>	Electrical Conductivity (µS/cm) <sup>a</sup>	Total Dissolved Solids (ppm) <sup>a</sup>	Effect of Introduced Materials on Water Chemistry <sup>b</sup>	Comments
06/28/01	BH 72	4.8	14.6	8.9	Not affected	No packer assembly in borehole, remnants of the SEAMIST liner are present. Condensed water sample acquired using push rods, flex-tubing, and pump to draw steam.
06/28/01	60/3	3.3	189	115.0	Affected	Low pH, elevated conductivity, and increased fluoride (17.7 mg/L) indicate condensation of HF acid in sampling tube. Deflated packers between zones 2, 3, and 4.
06/28/01	60/4	5.1	10.5	8.8	Possibly affected	Collection zone contains fluoride-bearing rubber packer. Packers deflated between zones 2, 3, and 4. No chemical analysis.
08/07/01	76/3	5.2	4.1	2.5	Not affected	pH and conductivity values suggest that sample condensed from steam in the sampling tube for all water collected 6/26/01 and 6/27/01. Packer deflated between zones 2 and 3.
08/07/01	76/4	5.4	7.8	4.7	Not affected	pH and conductivity values suggest that sample condensed from steam in the sampling tube for all water collected 6/26/01 and 6/27/01.
08/07/01	77/2	3.3	284	173.0	Affected	Low pH, elevated conductivity, and increased fluoride indicate condensation of HF acid in borehole 77 sampling tubes. Packer deflated between zones 2 and 3.
08/07/01	77/3	3.3	231	138.0	Affected	
08/07/01	78/2	4.5	8.8	5.2	Not affected	Condensate in sampling tubes. Packers deflated between zones 2, 3, and 4.
08/07/01	78/3	5.2	9.1	5.6	Not affected	
08/07/01	78/4	5.5	14.3	8.8	Not affected	
08/08/01	59/2	5.4	2.2	1.3	Not affected	Condensate in sampling tube
08/08/01	59/3	4.9	6	3.6	Not affected	
08/08/01	59/4	5.1	2.8	1.6	Not affected	Condensate in sampling tube
08/08/01	60/1	4.8	25	15.0	Possibly affected	Condensate in sampling tube, collection zone contains fluoride-bearing rubber packer.
08/08/01	60/2	3.1	309	194.0	Affected	Low pH, elevated conductivity, and increased fluoride indicate condensation of HF acid in sampling tubes for borehole 60. Deflated packers between zones 2, 3, and 4.
08/08/01	60/3	3.4	186	114.0	Affected	

Table 6.3-32. Assessment of Effects of Introduced Materials on Water Chemistry (Continued)

Date	Collection Hole/Zone	pH <sup>a</sup>	Electrical Conductivity (µS/cm) <sup>a</sup>	Total Dissolved Solids (ppm) <sup>a</sup>	Effect of Introduced Materials on Water Chemistry <sup>b</sup>	Comments
08/08/01	60/4	4.4	14.5	8.8	Possibly affected	Condensate in sampling tube, collection zone contains fluoride-bearing rubber packer.
10/22/01	76/3	5.2	8.4	5.1	Not affected	Condensate in sampling tube. Packer deflated between zones 2 and 3.
10/22/01	76/4	5.1	5.2	3.0	Not affected	Condensate in sampling tube
10/22/01	77/2	3.1	403	245.0	Affected	Low pH, elevated conductivity, and increased fluoride indicate condensation of HF acid in borehole 77 sampling tubes. Packer deflated between zones 2 and 3.
10/22/01	77/3	3.2	344	208.0	Affected	
10/22/01	78/1	4.2	11.6	6.9	Not affected	Condensate in sampling tubes. Packers deflated between zones 1, 2, 3, and 4.
10/22/01	78/3	5.0	7.7	4.5	Not affected	—
10/22/01	78/4	5.4	10	6.0	Not affected	—
10/22/01	59/2	4.9	8.5	5.2	Not affected	Condensate in sampling tube
10/22/01	59/3	5.0	5.2	3.0	Not affected	Condensate in sampling tube
10/22/01	59/4	4.9	6	3.5	Not affected	Condensate in sampling tube
10/22/01	60/2	3.2	406	252.0	Affected	Low pH, elevated conductivity, and increased fluoride indicate condensation of HF acid in borehole 60 sampling tubes. Deflated packers between zones 2, 3, and 4.
10/22/01	60/3	3.5	151	90.0	Affected	No anion analysis. Low pH and elevated conductivity suggest condensation of HF acid in borehole 60 sampling tubes. Deflated packers between zones 2, 3, and 4.
10/22/01	60/4	3.8	63	38.0	Affected	No anion analysis. Low pH and elevated conductivity suggest condensation of HF acid in borehole 60 sampling tubes. Deflated packers between zones 2, 3, and 4.
10/22/01	61/1	4.4	14.6	8.7	Not affected	Condensate in sampling tube
10/22/01	61/3	4.9	7.9	4.8	Not affected	Condensate in sampling tube. Deflated packers between zones 2, 3, and 4.
10/22/01	61/4	5.0	7.1	4.3	Not affected	Condensate in sampling tube. Deflated packers between zones 2, 3, and 4.
01/07/02	76/2	7.8	30.2	18.0	Not affected	Packer deflated between zones 2 and 3.

Table 6.3-32. Assessment of Effects of Introduced Materials on Water Chemistry (Continued)

Date	Collection Hole/Zone	pH <sup>a</sup>	Electrical Conductivity (µS/cm) <sup>a</sup>	Total Dissolved Solids (ppm) <sup>a</sup>	Effect of Introduced Materials on Water Chemistry <sup>b</sup>	Comments
01/07/02	76/3	4.9	7.3	4.3	Not affected	Condensate in sampling tube. Packer deflated between zones 2 and 3.
01/07/02	76/4	4.8	5.5	3.2	Not affected	Condensate in sampling tube
01/07/02	78/2	5.1	4.9	2.9	Not affected	Condensate in sampling tubes. Packers deflated between zones 2, 3, and 4.
01/07/02	78/3	4.9	5.1	3.1	Not affected	
01/07/02	78/4	4.9	5.4	3.2	Not affected	
01/07/02	59/2	5.2	3.3	2.0	Not affected	Condensate in sampling tube
01/07/02	59/3	5.3	2	1.2	Not affected	Condensate in sampling tube
01/07/02	59/4	4.8	5.7	3.5	Not affected	Condensate in sampling tube
01/07/02	61/2	5.5	6.5	4.0	Not affected	Condensate in sampling tube. Packers deflated between zones 1, 2, 3, and 4.
01/07/02	61/3	5.2	4.8	2.9	Not affected	Condensate in sampling tube. Packers deflated between zones 1, 2, 3, and 4.
01/07/02	61/4	5.1	7.7	4.5	Not affected	Condensate in sampling tube. Packers deflated between zones 1, 2, 3, and 4.
01/09/02	77/2	3.7	49.8	30.6	Affected	Low pH, elevated conductivity, and increased fluoride indicate condensation of HF acid in borehole 77 sampling tubes. Packer deflated between zones 2 and 3.
01/09/02	77/3	3.4	176	106.0	Affected	
01/16/02	76/2	8.3	35.5	22	Not affected	Packer deflated between zones 2 and 3.
01/16/02	76/3	5.2	9.3	5.7	Not affected	Condensate in sampling tube. Packer deflated between zones 2 and 3.
01/16/02	77/2	3.8	34.2	21.4	Affected	Low pH, elevated conductivity, and increased fluoride indicate condensation of HF acid in borehole 77 sampling tubes. Packer deflated between zones 2 and 3.
01/16/02	77/3	3.5	181	112	Affected	No chemical analysis. Low pH and elevated conductivity suggest condensation of HF acid in borehole 77 sampling tubes. Packer deflated between zones 2 and 3.
01/16/02	78/2	4.9	6.5	4	Not affected	Condensate in sampling tubes. Packers deflated between zones 2, 3, and 4.
01/16/02	78/3	4.9	7.2	4.4	Not affected	
01/16/02	78/4	4.9	6.6	4	Not affected	
01/16/02	59/3	5.0	7.7	4.6	Not affected	Condensate in sampling tube



Table 6.3-32. Assessment of Effects of Introduced Materials on Water Chemistry (Continued)

Date	Collection Hole/Zone	pH <sup>a</sup>	Electrical Conductivity (µS/cm) <sup>a</sup>	Total Dissolved Solids (ppm) <sup>a</sup>	Effect of Introduced Materials on Water Chemistry <sup>b</sup>	Comments
01/16/02	59/4	5.1	4.7	2.8	Not affected	Condensate in sampling tube
01/16/02	61/4	4.9	9.4	5.8	Not affected	Condensate in sampling tube. Packers deflated between zones 1, 2, 3, and 4.
01/23/02	75/3	4.4	14.5	9.1	Not affected	—
01/23/02	76/2	5.9 to 8.1	29.2 to 33.6	17.2 to 20.8	Not affected	Packer deflated between zones 2 and 3.
01/23/02	76/3	4.9	7.8	4.7	Not affected	Condensate in sampling tube. Packer deflated between zones 2 and 3.
01/23/02	76/4	5.0	5	2.9	Not affected	Condensate in sampling tube
01/23/02	77/2	4.1	43.6	26.9	Affected	Low pH, elevated conductivity, and increased fluoride indicate condensation of HF acid in borehole 77 sampling tubes. Packer deflated between zones 2 and 3.
01/23/02	77/3	3.6	207	130	Affected	
01/23/02	78/2	5.6	9	5.7	Not affected	Condensate in sampling tubes consumed doing field analysis. Packers deflated between zones 2, 3, and 4.
01/23/02	78/3	5.5	5.8	3.6	Not affected	
01/23/02	78/4	5.0	5.9	3.6	Not affected	Condensate in sampling tube
01/23/02	59/2	4.5	7.4	4.4	Not affected	
01/23/02	59/3	4.5	5.4	3.2	Not affected	Condensate in sampling tube
01/23/02	59/4	4.3	3.8	2.3	Not affected	
02/05/02	76/2	6.7 to 7.8	32.0 to 50.0	21.0 to 30.9	Not affected	Packer deflated between zones 2 and 3.
02/05/02	76/3	5.0	3	1.9	Not affected	Condensate in sampling tube. Packer deflated between zones 2 and 3.
02/05/02	76/4	5.0	2.7	1.6	Not affected	Condensate in sampling tube
02/05/02	77/2	3.9	51	32	Affected	
02/05/02	77/3	3.7	138	85	Affected	Low pH, elevated conductivity, and increased fluoride indicate condensation of HF acid in borehole 77 sampling tubes. Packer deflated between zones 2 and 3.
02/05/02	78/2	5.1	6.5	4	Not affected	Condensate in sampling tube. Packer deflated between zones 2 and 3.
02/05/02	59/2	5.0	3.2	1.9	Not affected	Condensate in sampling tube
02/05/02	59/3	5.1	2.3	1.3	Not affected	
02/05/02	59/4	5.0	3.7	2.2	Not affected	Condensate in sampling tube
02/05/02	61/2	5.3	6.7	4.2	Not affected	

Table 6.3-32. Assessment of Effects of Introduced Materials on Water Chemistry (Continued)

Date	Collection Hole/Zone	pH <sup>a</sup>	Electrical Conductivity (µS/cm) <sup>a</sup>	Total Dissolved Solids (ppm) <sup>a</sup>	Effect of Introduced Materials on Water Chemistry <sup>b</sup>	Comments
02/05/02	61/3	5.1	6.2	3.9	Not affected	Sampling tube condensate consumed doing field analyses. Packers deflated between zones 1, 2, 3, and 4.
02/05/02	61/4	4.9	6	3.7	Not affected	Condensate in sampling tube. Packers deflated between zones 1, 2, 3, and 4.
02/19/02	75/2	4.8	>994 <sup>c</sup>	>663 <sup>c</sup>	Affected	Yellow color, extremely high conductivity, and increased chloride concentration suggest degradation of neoprene packer.
02/19/02	76/2	4.7	6.1	4	Not affected	Packer deflated between zones 2 and 3.
02/19/02	76/4	4.8	3.5	2.2	Not affected	Condensate in sampling tube
02/19/02	77/2	4.3	6.5	4.3	Affected	Low pH and increased fluoride indicate condensation of HF acid in borehole 77 sampling tubes. Packer deflated between zones 2 and 3.
02/19/02	77/3	3.4	121	79.3	Affected	No chemical analysis. Low pH and elevated conductivity suggest condensation of HF acid in Borehole 77 sampling tubes. Packer deflated between zones 2 and 3.
02/19/02	59/2	5.0	2.9	1.8	Not affected	Condensate in sampling tube
02/19/02	59/3	5.0	2.4	1.5	Not affected	Condensate in sampling tube
02/19/02	59/4	4.7	6.1	3.9	Not affected	Condensate in sampling tube
03/06/02	60	3.8	83	54.6	Affected	Packer assembly removed from borehole on 11/14/01. Sampling tube end placed 74' from collar to acquire sample. Low pH, elevated conductivity, and increased fluoride indicate condensation of HF acid in sampling tube.
03/06/02	60	4.3	22.4	14.6	Affected	Packer assembly removed from borehole on 11/14/01. Sampling tube end placed 132' from collar to acquire sample. Low pH, elevated conductivity, and slightly increased fluoride indicate condensation of HF acid in sampling tube.
03/06/02	75/2	4.9	>994 <sup>c</sup>	>663 <sup>c</sup>	Affected	Yellow color, extremely high conductivity, and increased chloride concentration suggest degradation of neoprene packer.
03/06/02	76/3	5.1	12.5	8.3	Not affected	Packer deflated between zones 2 and 3
03/12/02	75/2	4.8	>994 <sup>c</sup>	>663 <sup>c</sup>	Affected	Yellow color, extremely high conductivity, and increased chloride concentration suggest degradation of neoprene packer.

Table 6.3-32. Assessment of Effects of Introduced Materials on Water Chemistry (Continued)

Date	Collection Hole/Zone	pH <sup>a</sup>	Electrical Conductivity (µS/cm) <sup>a</sup>	Total Dissolved Solids (ppm) <sup>a</sup>	Effect of Introduced Materials on Water Chemistry <sup>b</sup>	Comments
03/12/02	76/3	4.6	7.6	4.7	Not affected	Sampling tube condensate consumed doing field analyses. Packer deflated between zones 2 and 3.
03/12/02	76/4	4.5	9.5	5.8	Not affected	Condensate in sampling tube
03/12/02	77/2	4.1	32.3	20	Affected	Low pH, elevated conductivity, and increased fluoride indicate condensation of HF acid in borehole 77 sampling tubes. Packer deflated between zones 2 and 3.
03/12/02	77/3	3.5	109	67.6	Affected	
03/12/02	78/2	4.7	8.7	5.5	Not affected	Condensate in sampling tubes consumed doing field analysis. Packers deflated between zones 2, 3, and 4.
03/12/02	78/3	4.8	8.4	5.3	Not affected	
03/12/02	78/4	4.6	7.3	4.6	Not affected	
03/12/02	59/2	5.1	4.2	2.5	Not affected	Condensate in sampling tube
03/12/02	59/3	5.3	3	1.8	Not affected	Condensate in sampling tube
03/12/02	59/4	5.2	2	1.2	Not affected	Condensate in sampling tube
03/12/02	61/2	5.1	15.9	10	Not affected	—
04/04/02	75/2	5.0	>994 <sup>c</sup>	>663 <sup>c</sup>	Affected	Yellow color, extremely high conductivity, and increased chloride concentration suggest degradation of neoprene packer.
04/04/02	76/3	4.6	13.6	8.5	Not affected	Sampling tube condensate consumed doing field analyses. Packer deflated between zones 2 and 3.
04/04/02	76/4	4.5	7.1	4.4	Not affected	Condensate in sampling tube
04/04/02	77/3	3.7 to 3.8	62.7 to 103	39.6 to 65	Affected	Low pH, elevated conductivity, and increased fluoride indicate condensation of HF acid. Packer deflated between zones 2 and 3.
04/04/02	78/3	4.8	5.1	3.2	Not affected	Sampling tube condensate consumed doing field analyses. Packers deflated between zones 2, 3, and 4.
04/04/02	78/4	4.7	5.2	3.2	Not affected	Condensate in sampling tube. Packers deflated between zones 2, 3, and 4.
04/04/02	59/4	5.4	6.3	3.9	Not affected	Condensate in sampling tube
04/04/02	61/3	4.9	7.7	4.8	Not affected	Condensate in sampling tube. Packers deflated between zones 1, 2, 3, and 4.
04/04/02	61/4	4.9	9.7	6.1	Not affected	Sampling tube condensate consumed doing field analyses. Packers deflated between zones 1, 2, 3, and 4.

Table 6.3-32. Assessment of Effects of Introduced Materials on Water Chemistry (Continued)

Date	Collection Hole/Zone	pH <sup>a</sup>	Electrical Conductivity (µS/cm) <sup>a</sup>	Total Dissolved Solids (ppm) <sup>a</sup>	Effect of Introduced Materials on Water Chemistry <sup>b</sup>	Comments
04/25/02	75/2	5.0	1089	732	Affected	Yellow color, extremely high conductivity, and increased chloride concentration suggest degradation of neoprene packer.
04/25/02	76/3	4.5	25.5	15.8	Not affected	Sampling tube condensate consumed doing field analyses. Packer deflated between zones 2 and 3.
04/25/02	77/3	3.8	54	34.1	Affected	Low pH, elevated conductivity, and increased fluoride indicate condensation of HF acid. Packer deflated between zones 2 and 3.
04/25/02	59/2	5.0	4.9	3	Not affected	Sampling tube condensate consumed doing field analyses.
04/25/02	59/4	4.9	2.9 to 4.3	1.7 to 2.5	Not affected	Condensate in sampling tube
05/29/02	76/4	5.3	12.1	7.5	Not affected	Condensate in sampling tube
05/29/02	78/4	6.4	10	6.2	Not affected	Sampling tube condensate consumed doing field analyses. Packers deflated between zones 2, 3, and 4.
05/29/02	59/2	5.9	8	5	Not affected	Sampling tube condensate consumed doing field analyses.
05/29/02	59/3	5.6	4.2	2.6	Not affected	Sampling tube condensate consumed doing field analyses.
05/29/02	59/4	5.2	3.5	2.1	Not affected	Condensate in sampling tube
06/26/02	75/2	6.0	278	176	Affected	High conductivity, increased chloride (above halite stoichiometry) suggest degradation of neoprene packer.
06/26/02	75/3	6.1	12.6	7.8	Not affected	Sample consumed doing field analyses
06/26/02	76/3	4.7	14.2	8.8	Not affected	Sampling tube condensate consumed doing field analyses. Packer deflated between zones 2 and 3.
06/26/02	76/4	5.3	8.4	5.2	Not affected	Condensate in sampling tube
06/26/02	78/3	5.8	10.3	6.4	Not affected	Sampling tube condensate consumed doing field analyses. Packers deflated between zones 2, 3, and 4.
06/26/02	78/4	5.5	7.6	4.7	Not affected	
06/26/02	59/2	6.7	11.3	6.9	Not affected	—
06/26/02	59/3	6.4	8.5	5.2	Not affected	Sampling tube condensate consumed doing field analyses
06/26/02	59/4	6.2	6.5	4	Not affected	Condensate in sampling tube
11/13/02	74/4	5.2	—	—	Not affected	Insufficient sample for further analyses

Table 6.3-32. Assessment of Effects of Introduced Materials on Water Chemistry (Continued)

Date	Collection Hole/Zone	pH <sup>a</sup>	Electrical Conductivity (µS/cm) <sup>a</sup>	Total Dissolved Solids (ppm) <sup>a</sup>	Effect of Introduced Materials on Water Chemistry <sup>b</sup>	Comments
11/13/02	76/3	5.1	—	—	Not affected	Insufficient sample for further analyses
02/18/03	57/4	4.8	20.4	12.7	Not affected	—
08/16/04	57/4	4.6	20.8	12.6	Not affected	Sample consumed doing field analyses

Source: DTNs: SN0208F3903102.002 [DIRS 161246]; SN0210F3903102.004 [DIRS 170573]; SN0211F3903102.005 [DIRS 170574]; SN0303F3903102.006 [DIRS 178034]; SN0411F3903102.009 [DIRS 178036]; LL020709923142.023 [DIRS 161677] (unqualified); LL030305023121.023 [DIRS 170570] (unqualified); LL030310023121.024 [DIRS 170571] (unqualified).

<sup>a</sup> Blank spaces indicate that no data were acquired.

<sup>b</sup> All water samples were exposed to introduced materials; the effects may not be detectable through measurement and data assessment.

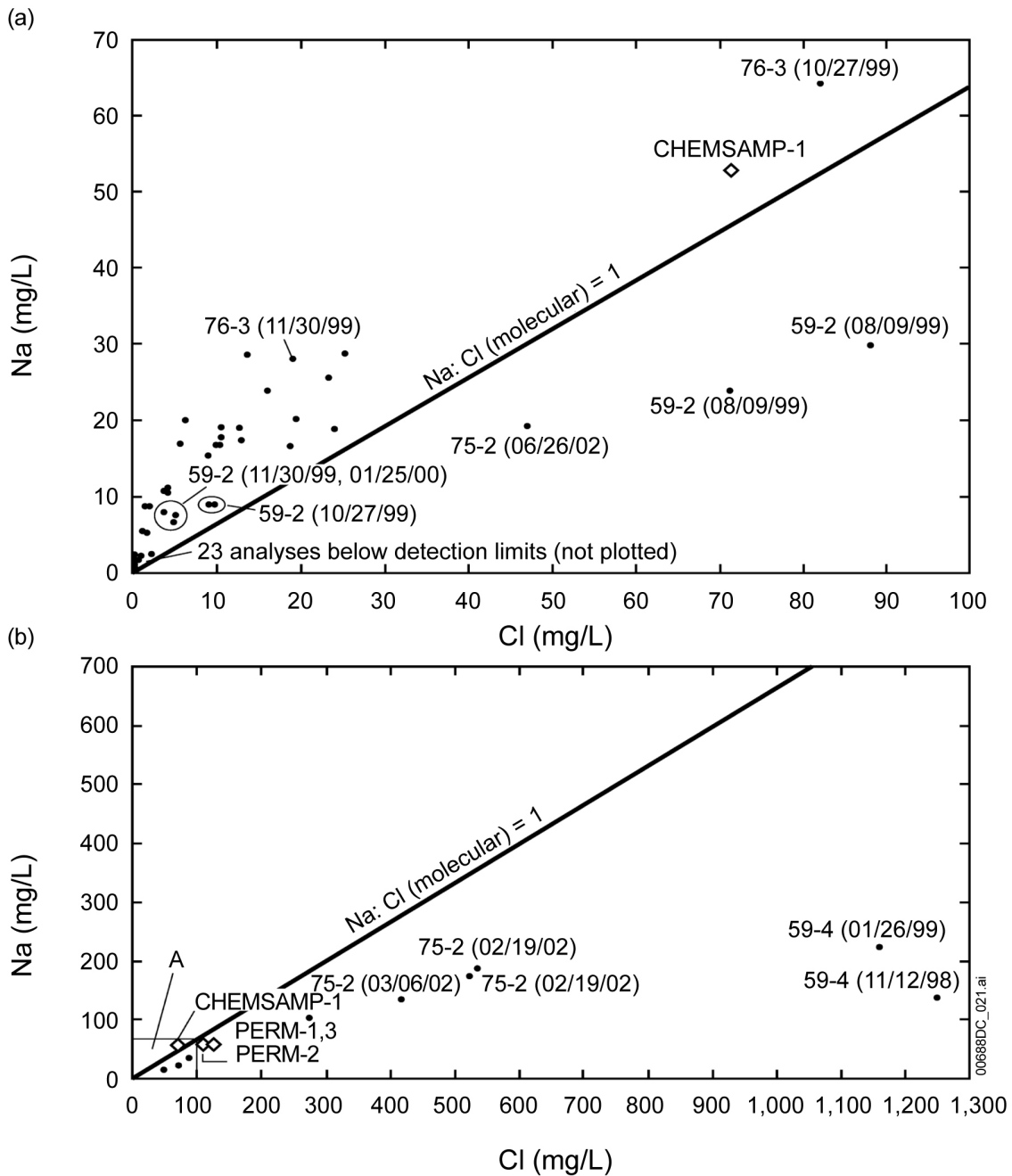
<sup>c</sup> measurement greater than calibrated range of instrument.

### High-Fluoride Samples

Water samples acquired from borehole intervals 77/2, 77/3, 60/2, and 60/3 between 04/20/99 and 04/04/02 had fluoride contents between about 2 and 74 mg/L (Table 6.3-25). All of these samples came from intervals isolated by fluoroelastomer packers. The majority of other water samples have fluoride contents of 1 mg/L or less. The pH values of the high fluoride samples range from 3.1 to 3.7. The range of pH in samples without high fluoride or chloride, including samples from BH 77 and BH 60 that predate the onset of unusual chemistry, is 4.12 to 8.29. The compositions of these samples show near-stoichiometric balance of hydrogen and fluoride ions in waters of low to moderate ionic strength. These characteristics suggest dissolution of hydrogen fluoride (HF) gas into water that condensed from vapor in the sampling tube. Most, but not all, of the high fluoride water samples also have contents of other solutes at levels somewhat higher than their presence in samples of pure condensate.

### High-Chloride Samples

Another subset of water compositions has chloride values substantially higher than about 25 mg/L, which is the most chloride present in the condensate samples, other relatively dilute samples, and the high-fluoride samples. A common characteristic of the high chloride samples is that they contain chloride well in excess of halite stoichiometry with sodium (Figure 6.3-53). High chloride samples include the 11/12/98 and 01/26/99 samplings of BH 59/4 and the 08/09/99 sampling of BH 59/2 (Table 6.3-25). Additional high-chloride samples were collected from BH 75/2 between 02/19/02 and 06/26/02 (six samples analyzed; Table 6.3-31). All of these intervals were isolated by chloroelastomer packers. The first four analyzed samples from the BH 75/2 suite had high chloride values and also had relatively low pH (4.8 to 4.9, with later samples up to 6.0). The BH 59/4 samples and the first four BH 75/2 samples had high sulfate contents and slightly elevated fluoride contents (as high as 4.3 mg/L). The BH 59/4 samples and six of the seven BH 75-2 samples were distinguished by a yellow color whose source has not been determined.



Source: DTNs: GS030408312272.002 [DIRS 165226]; LL020709923142.023 [DIRS 161677] (unqualified); LL030305023121.023 [DIRS 170570] (unqualified).

NOTES: (a) Analyses with low to moderate chloride contents. (b) Analyses with moderate to high chloride contents. Unlabeled points at lower left are 75-2 (6/26/02) and 59-2 (8/9/99, two points), also shown in (a). Range of plot (a) is shown as inset in plot (b).

Data labeled as "75-2 06/26/02" and "CHEMSAMP-1" are from DTN: GS030408312272.002 [DIRS 165226]. Other data points labeled with a 2002 date are from DTN: LL030305023121.023 [DIRS 170570]. All remaining data points are from DTN: LL020709923142.023 [DIRS 161677].

Figure 6.3-53. Sodium versus Chloride for Water Analyses from the DST

### 6.3.4.5.3 Experimental Verification of Materials Interactions

Laboratory and field experiments were designed and conducted specifically to investigate the aqueous chemical effects of heating both introduced and natural materials in the presence of water vapor or liquid water.

#### *Field Experiments Investigating Fluoropolymer Interactions*

A field test was designed to identify the source of fluoride in the BH 77 and BH 60 water samples. The two competing hypotheses were that the fluoride source was introduced materials or that the fluoride source was in the host rock. Introduced materials that are potential sources of HF include fluoroelastomer synthetic rubber and Teflon. The fluoroelastomer was used to make pneumatic packers to isolate test zones and the Teflon tubing was used to draw water and steam from the test zones. The principle of the experiment was to introduce fluoride-containing materials into high-temperature boreholes that had not previously contained such materials .

Two boreholes in the DST array that had not been instrumented for water collection or temperature measurement were selected for the field test. Boreholes 72 and 55 are nearly parallel to BH 77 and BH 60, respectively, and are also close to wing heaters (Figure 6.3-44). The boreholes were prepared for pretest characterization by removing the previously installed SEAMIST liners. The temperature in boreholes 72 and 55 was measured at 5-ft (1.5-m) intervals to determine the ideal (hottest) zone to introduce the test assemblies.

After baseline fluid samples were collected on 11/26/01, a rigid push rod was used to position a Teflon sampling tube and various fluoroelastomer samples in the highest temperature zone of BH 72. The fluoroelastomer samples included sections cut from packer 3 removed from BH 60, sections from an unused SHT packer, and test batch sections of fluoroelastomer produced prior to the full production run for the DST packers. Metal components of the sample string were made of C276 alloy because its corrosion resistance would minimize interference with the test. The sampling port was located at a depth of 78.08 ft (23.8 m).

The sampling apparatus installed in BH 55 was designed to collect control samples and was constructed of C276 alloy steel tube using no packer materials. The sampling port at the end of the tube was located at a depth of 71.75 ft (21.87 m).

Field analyses and laboratory fluoride analyses (DTNs: LL020405123142.019 [DIRS 159307] and SN0208F3903102.003 [DIRS 170620]) are summarized in Table 6.3-33. Additional data for BH 72 and BH 55 that predate the HF field test are also included. Pretest analyses for BH 55 suggest that the test zone was contaminated with remaining SEAMIST materials and residue from the drill rig. The small sample volumes collected during each pretest event made it difficult to thoroughly flush the tubing, increasing the chances of field contamination. The baseline sample collected on 11/26/01 had relatively low fluoride, so BH 55 offered a viable test zone for collection of control samples.



Table 6.3-33. Field Measurements and F-Content of Condensates Sampled during the HF Field Tests

Sample Identification	SMF Number	Collection Date	Field pH	EC / TDS (µS/cm) / (ppm)	F (mg/L)
BH 72 (pretest) <sup>a</sup>	SPC00559475	6/28/2001	4.8	15 / 9	N/D < 0.007
BH 72 (pretest) <sup>a</sup>	SPC00575228	11/8/2001	5.1 to 5.5	19 / 12	0.15
BH 72 baseline <sup>a</sup>	SPC00575219	11/26/2001	5.3	14 / 9	N/D < 0.007
<b>Fluoroelastomer (FKM) and Teflon Installed 11/26/2001</b>					
BH 72 (FKM, PTFE)	SPC00559478	11/29/2001	3.8	41 / 25	2.39
BH 72 (FKM, PTFE)	SPC01016065	12/5/2001	3.4 to 3.5	139 / 88	7.60
BH 72 (FKM, PTFE)	SPC01016066	12/5/2001	3.44	135 / 85	7.23
<b>Fluoroelastomer (FKM) and Teflon Removed 1/9/2002</b>					
BH 55 (pretest) <sup>a</sup>	SPC00575231	11/15/2001	7.5	279/176	0.52
BH 55 (pretest) <sup>a</sup>	SPC00559483	11/21/2001	N/A	N/A	8.56 <sup>b</sup>
BH 55 baseline <sup>c</sup>	SPC00575229	11/26/2001	5.0	21 / 13	1.34
BH 55 <sup>c</sup>	SPC00559479	11/29/2001	5.2	N/A	0.35
BH 55 <sup>c</sup>	SPC01016067	12/5/2001	N/A	N/A	0.08

Source: DTNs: SN0208F3903102.003 [DIRS 170620]; LL020405123142.019 [DIRS 159307].

<sup>a</sup> Sample acquired with Tygon tubing.

<sup>c</sup> Sample acquired using C276 alloy tubing.

<sup>b</sup> Sample likely contaminated; refer to Section 6.3.4.5.5.

NOTE: N/A = not analyzed; N/D = not detected.

### Laboratory Experiments Investigating Fluoropolymer Interactions

Laboratory tests were designed to investigate the tendencies of introduced and natural materials to release HF and to establish which of the materials is the most likely source of HF gas in the DST. Laboratory testing consisted of two parts:

1. A gas flow-through system developed at LBNL which functions in two ways:
  - a. As a recirculation loop in which steam from a boiling reservoir is passed through a reaction chamber containing the materials of interest at the desired temperature, with periodic collection of liquid from the reservoir
  - b. As a single-pass gas-flow system (“air scrubbing”) in which ambient-temperature air passes through the heated reaction chamber and then is bubbled through water at ambient temperature to collect any HF gas. Because HF partitions strongly into the aqueous phase at low temperatures, capture of the HF gas (if present) should be nearly quantitative.
2. Thermogravimetric analysis of fluoroelastomers at LLNL provides a quantitative determination of short-term bulk decomposition rate as a function of temperature.

### Gas Flow-Through Experiments

Laboratory experiments were performed in an array of flow-through reaction chambers containing seven samples of natural and man-made materials. An eighth, empty chamber served as a control. The materials were held in sample chambers at 140°C and 170°C. The seven chambers each contained known quantities of crushed tuff, fluoroelastomer, fluorite, or Teflon. Sample chambers were constructed from one-inch outside diameter tubing and contained a fine wire mesh underlain by a coarse wire mesh at the top and bottom to contain sample materials. A 500-mL water reservoir was located below the sample chamber.

Two sets of experiments were performed. For the first suite of experiments, the water reservoirs were filled with deionized water maintained at 105°C. The top of the chamber and the reservoir were connected by a recirculation tube exposed to ambient temperature. Concern about potential vapor lock in the quarter-inch recirculation tube led to its replacement with a half-inch tube. The tests then were restarted using the same samples in the chambers but with fresh deionized water in the water reservoirs. The initial flow-through test with the quarter-inch tube is referred to as Experiment LBNL-1a, and the subsequent test with the half-inch tube is Experiment LBNL-1b.

A second suite of experiments was conducted using the same equipment except that the recirculation tube at the top of the chamber was replaced with a connection to an air supply. The chamber below the sample chamber contained only air. Air was injected in the top of the sample chamber and allowed to flow across the heated samples maintained at the same temperatures as in the first experiments. The sample valve at the base of the lower chamber controlled the rate at which air flowed through the reaction cell. The air outlet was connected by Tygon tubing to a 30-mL bottle filled with deionized water. Water samples were analyzed for fluoride by ion chromatography, and H was measured with a calibrated pH electrode. This air scrubbing experiment is referred to as Experiment LBNL-2.

Fluoride and pH measurements (DTN: LB0211DSTRBRDG.001 [DIRS 170566]) for the gas flow-through experiments are listed in Table 6.3-34. Experiment LBNL-1a and LBNL-1b data show that in a two-phase water environment at elevated temperatures, levels of aqueous fluoride greater than 1 ppm were generated only in the presence of fluoropolymer or fluorite. The fluoroelastomer and fluoroelastomer + tuff experiments produced up to 4.7 ppm fluoride at 140°C and up to 6.4 ppm fluoride at 170°C. The range of final pH values for the introduced-material samples at both temperatures, 4.2 to 5.9, is significantly lower than for the tuff and tuff and fluorite samples, 7.2 to 9.1.

Experiment LBNL-2, which duplicated the low relative-humidity gas scrubbing that would occur during DST field sampling, showed large differences in aqueous fluoride concentrations and pH between the fluoroelastomer-loaded experiments and all other sample loads (Table 6.3-34). The 170°C fluoroelastomer run generated water with 851 ppm fluoride at pH 2.1 after one day. This concentration is two to four orders of magnitude greater than concentrations obtained for other materials at 170°C and for all materials, including fluoroelastomer, at 140°C, suggesting a strong temperature dependence of HF release.

Table 6.3-34. Fluoride Concentrations (ppm)/pH from Gas Flow-Through Experiments

Date	140°C				170°C			
	Control	Tuff + FKM	FKM	Tuff	Tuff	FKM	Teflon	Tuff + Fluorite
<b>Experiment LBNL-1a: Recirculation with Water (¼" Recirculation Line)</b>								
01/04/02	0.00/6.27	1.11/6.31	1.41/6.03	0.03/6.77	0.18/8.32	0.46/5.36	0.07/8.24	0.28/7.40
01/05/02	0.00/6.85	2.10/6.05	2.51/6.18	0.02/8.34	0.22/8.14	0.48/5.19	0.14/8.35	0.95/8.11
01/06/02	0.00/7.11	2.41/5.68	2.58/6.16	0.03/7.10	0.22/8.27	0.54/5.04	0.15/7.68	1.02/8.13
01/07/02	0.00/6.71	3.63/5.61	4.30/5.70	0.32/8.04	0.18/5.84	1.16/4.97	0.12/5.82	0.99/6.82
01/08/02	0.01/8.38	3.39/5.73	4.53/5.61	0.38/8.45	0.26/6.55	1.07/4.96	0.16/7.62	1.13/8.03
01/09/02	0.00/7.18	3.60/5.83	4.66/5.90	0.30/8.55	0.23/6.88	0.92/5.03	0.16/8.22	0.98/7.93
01/10/02	0.00/7.71	3.44/5.85	4.52/5.66	0.29/8.61	0.21/7.15	1.04/4.38	0.15/7.78	0.91/8.21
<b>Experiment LBNL-1b: Recirculation with Water (½" Recirculation Line)</b>								
01/12/02	0.01/7.24	0.26/6.18	0.35/5.83	0.05/7.40	0.02/6.99	0.50/4.72	0.03/6.94	0.07/7.67
01/13/02	0.01/7.79	0.35/5.90	0.42/5.48	0.09/8.05	0.02/7.23	0.54/4.64	0.03/6.51	0.08/8.11
01/14/02	0.01/8/31	0.34/5.73	0.40/5.44	0.11/8.65	0.02/7.31	1.66/4.34	0.04/6.28	0.08/8.56
01/15/02	0.01/8.40	0.34/5.75	0.45/5.49	0.12/8.72	0.02/7.85	6.35/4.19	0.05/6.39	0.09/9.09
<b>Experiment LBNL-2: Air Scrubbing of Reaction Cell</b>								
01/18/02	0.02/6.38	1.23/3.64	0.03/6.67	0.01/6.53	0.00/6.46	851.2 <sup>a</sup> /2.07	0.02/5.61	0.73/6.87

Source: DTN: LB0211DSTRBRDG.001[DIRS 170566].

<sup>a</sup> Average of four measurements.

### Thermogravimetric Analysis Experiments

Thermogravimetric analysis was performed on BH 72 and BH 60 fluoroelastomers. Dynamic heating experiments were conducted at a heating rate of 20°C/min over the range of 23°C to 600°C to determine general patterns of weight loss with temperature. Multistep isothermal tests were run with argon as the purge gas to conduct gaseous effluents for collection in deionized water. Samples were single pieces of fluoroelastomer with nominal dimensions of 3 mm × 3 mm × 0.8 mm and masses of 15 to 25 mg. Samples were equilibrated at 100°C to evaporate any water present in the samples. They were then heated at variable heating rates to 120°C, 150°C, and 180°C, respectively. Isothermal heating then proceeded at each of these temperatures to probe the longer-term effects of heating on thermal degradation rates.

The results (DTN: LL030605512251.064 [DIRS 170572], unqualified) are summarized in Table 6.3-35. Degradation rates were calculated in terms of micrograms (µg) of material lost per hour per milligram (mg) of original sample. In general, degradation rates increased with increasing temperature. Lower rates were observed for the two larger samples of BH 60 fluoropolymer, indicating a surface area dependence for the degradation rates.

Table 6.3-35. Isothermal Degradation Rates of BH 60 and BH 72 Fluoroelastomer

Sample Material	Initial Sample Weight (mg)	Temperature (°C)	Degradation Rate after 5 hr	Degradation Rate after 10 hr
BH 60 FKM	17.4901	120	0.13 µg/hr/mg	0.10 µg/hr/mg
BH 60 FKM	21.7081	150	0.32 µg/hr/mg	0.17 µg/hr/mg
BH 72 FKM	20.1977	150	0.10 µg/hr/mg	not measured
BH 60 FKM	543.788	150	0.12 µg/hr/mg	0.07 µg/hr/mg
BH 60 FKM	16.3638	180	0.98 µg/hr/mg	0.61 µg/hr/mg
BH 60 FKM	478.548	180	0.26 µg/hr/mg	0.18 µg/hr/mg

Source: DTN: LL030605512251.064 [DIRS 170572] (unqualified).

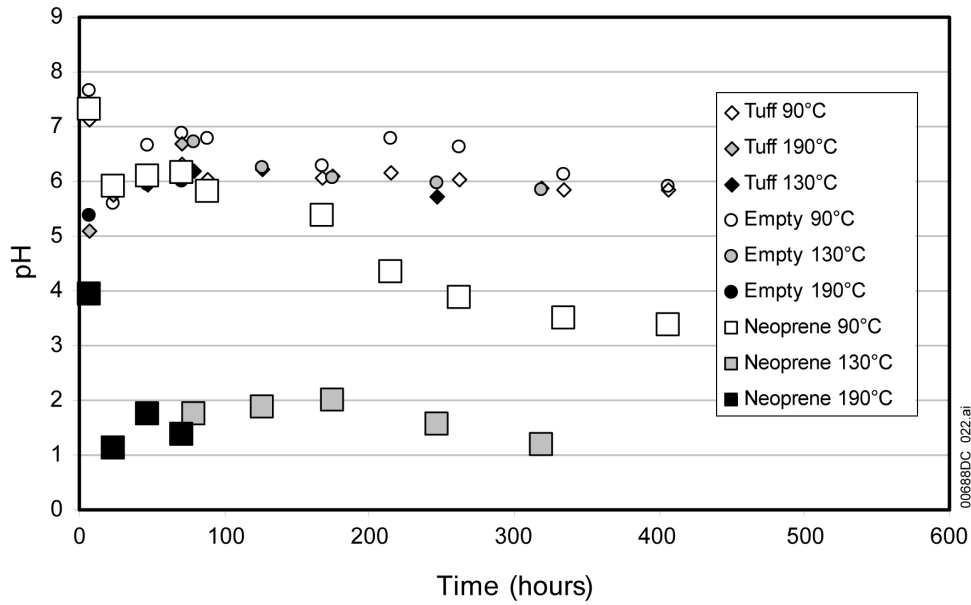
NOTE: Initial sample weight is the weight upon reaching the target temperature.

### Laboratory Experiments Investigating Chloropolymer Interactions

Laboratory investigations of chloropolymer (neoprene) packer material were begun after the fluoroelastomer studies were completed. The design of the laboratory experiments was derived in part from a subset of the experiments with fluoroelastomer, taking into account that the chloride-generating effects in the DST had occurred at or below boiling temperatures.

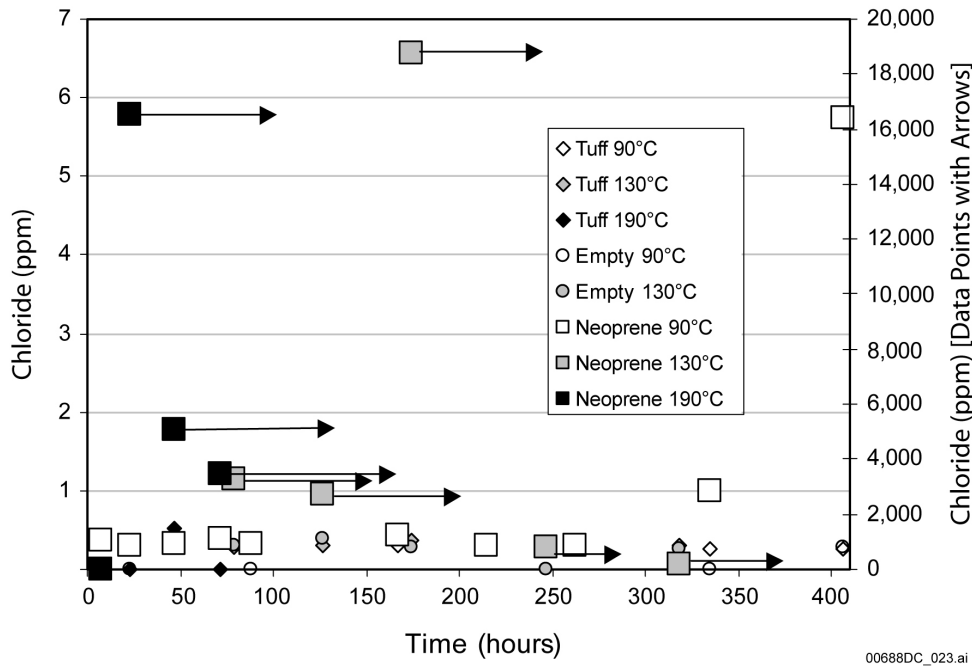
Air flow-through tests with ground chloropolymer (neoprene from a BH 60 packer) and crushed tuff were performed in experimental setups similar to the air-scrubbing experiments with fluoropolymer. Tests were conducted at 190°C (reduced to 150°C after 24 hours, then restarted with new material at 130°C) and 90°C. Similar tests were conducted with crushed tuff and empty test chambers. The tests ran for up to 407 hours. Water samples were collected periodically and analyzed for pH, chloride, fluoride, bromide, nitrate, and sulfate. Follow-up tests were performed to identify a lower-temperature threshold for detectable pH effects. Test chambers with ground neoprene and empty chambers were maintained at 34°C or 47°C for about 577 hours. Then, the test chamber temperatures were raised to 59°C and 71°C and maintained for about 430 hours. Water pH values were measured weekly.

The pH values (DTN: LB0302NEOPDGRD.001 [DIRS 170567]) for water samples from test chambers containing neoprene were lower than for other water samples (Figure 6.3-54). Higher temperatures led to a greater lowering of pH, but the effect was not instantaneous. Similarly, water samples from the higher-temperature test chambers with neoprene had very high chloride concentrations (DTN: LB0302NEOPDGRD.001 [DIRS 170567]) after an initial lag time (Figure 6.3-55). Sulfate was detected in water samples from neoprene tests at 90°C and 130°C, also after a lag time. Neither bromide nor nitrate was detected in any tests.



Source: DTN: LB0302NEOPDGRD.001 [DIRS 170567].

Figure 6.3-54. pH Values of Water Samples from the Flow-Through Test



Source: DTN: LB0302NEOPDGRD.001[DIRS 170567].

NOTE: Values for symbols with arrows are read on right-hand scale. Nondetectable concentrations plotted as zero (some of which do not show) include Neoprene 190°C at 7.67 hours (<500 ppm); Empty 190°C, Tuff 190°C, and Empty 90°C at 23.03 hours (<0.5 ppm); Tuff 190°C at 71.33 hours (<0.5 ppm); Empty 90°C at 88.33 hours (<0.5 ppm); Empty 130°C at 246.33 hours (<0.5 ppm); and Empty 90°C at 334.67 hours (<0.5 ppm).

Figure 6.3-55. Chloride Concentrations for Water Samples from the Flow-Through Test

#### **6.3.4.5.4 Summary and Conclusions**

Water samples from the DST with elevated contents of fluoride or chloride and generally low pH are attributed to fluid interactions with borehole pneumatic packers made of fluoroelastomer or chloroelastomer. Field and laboratory tests with fluoroelastomer and chloroelastomer do not trace fluoride and chloride in DST water samples directly to packer degradation, but the results do support the interpretation that introduced materials have affected the chemistry of some water samples. A general inference from the experiments is that geochemical interactions between packer materials and borehole fluids required specific combinations of introduced materials, thermal environments, and fluid behavior.

Fluoroelastomer packers degrade at temperatures  $\geq 150^{\circ}\text{C}$ , releasing hydrogen fluoride gas. At these temperatures, water is present only as vapor. When the borehole interval is sampled, the water vapor cools and condenses in the sampling tube and the hydrogen fluoride dissolves in the condensate. The resulting liquid contains low to moderate quantities of dissolved tuff constituents, but has high fluoride content and low pH. Water samples affected by this process were collected in borehole intervals 60/2, 60/3, 77/2, 77/3, and possibly 186/3.

Chloroelastomer packers degrade in an oxygen-rich environment (e.g., air), releasing gaseous hydrogen chloride. The hydrogen chloride is scavenged by liquid water and condensing steam in sub-boiling environments, producing water with high chloride and sulfate and moderately low pH. The existence of a temperature gradient along the packed-off interval may enhance the efficiency of this process. Effects of neoprene degradation are most pronounced at temperatures  $\geq 71^{\circ}\text{C}$ . This process may be active only under conditions where liquid water, derived perhaps from draining of fractures, is present in the packed-off borehole interval. Water samples affected by this process were collected in borehole intervals 59/2, 59/4, and 75/2.

Experimental results showed that interactions of tuff and heated water or vapor, without introduced materials, did not produce waters with high fluoride or chloride content. The evidence of introduced-materials effects on the chemistry of water samples underscores the importance of investigating long-term materials stability in heated environments with water or water vapor.

### **6.3.5 DST Miscellaneous Measurements**

This section discusses additional DST measurements not covered in the prior four DST sections. Specifically, fracture mapping and borehole video logging are discussed. Detailed discussion of these measurements is documented in the report entitled *Ambient Characterization of the Drift Scale Test Block* (CRWMS M&O 1997 [DIRS 101539]). Miscellaneous measurement input and summary DTNs are listed in Tables 4-3 and 6.3-1, respectively.

#### **6.3.5.1 Fracture Mapping**

The objective of geologic mapping in the DST block was to determine the vertical and horizontal variability of fracture networks and lithophysal zones and to identify values for parameters to be used for rock-mass classification.

Mapping was done essentially to the same standards used in the ESF main drift, using technical procedure NWM-USGS-G-32 (see DTN: GS970608314224.006 [DIRS 158429]). From these procedures, the USGS/USBR used full-periphery mapping techniques and detailed line surveys to characterize the rock and fractures in the DST area.

#### **6.3.5.1.1 Results: Fracture Mapping**

Full-periphery geotechnical maps for the DST connecting drift are presented in Figures 7-1 through 7-3, and Figures 7-4 through 7-6 for the DST heated drift in *Ambient Characterization of the Drift Scale Test Block Report* (CRWMS M&O 1997 [DIRS 101539]). The lithology of the unit consists of densely welded, devitrified tuff of rhyolitic composition, containing vapor-phase minerals and about 1% phenocrysts, chiefly feldspar and biotite. Matrix colors are a variable mixture of reddish purple (5RP5/2) or pale red (5R4/2) and light brown (5YR5/6) with wisps of very light gray (N8). Pumice (less than 5%) is mostly less than 20 mm, spherulitic, and grayish brown (5YR3/2) to very light gray (N8). Volcanic lithics (1% to 2%) are light gray (N8), less than 10 mm in size, and locally have very light gray (N8) rims. Lithophysae are rare (less than 1%) and range in size up to 80 mm, with vapor-phase minerals and very light gray (N8) rims and spots. Short (10 to 20 cm), discontinuous, subhorizontal vapor phase partings are present throughout the unit, while the more developed subhorizontal partings from bedding-plane features are on the order of meters apart.

#### **6.3.5.1.2 Measurement Uncertainty: Fracture Mapping**

Uncertainty associated with DST fracture mapping is similar to that discussed in Section 6.1.4.1.2.

#### **6.3.5.2 Borehole Video Logging**

The objective of borehole video logs was to provide descriptive visual information from boreholes in the DST block and to supplement other available characterization data. Borehole video logs were also used to help select appropriate depths for packer settings for air permeability testing.

##### **6.3.5.2.1 Results: Borehole Video Logging**

Borehole video logs provide much visual information regarding fractures, including aperture size, fracture frequency, and fracture orientation. Videos can be acquired by referring to the input DTN cited in Table 4-3 (DTN: LARO831422AQ97.002 [DIRS 158431]).

##### **6.3.5.2.2 Measurement Uncertainty: Borehole Video Logging**

These observations are inherently subjective, which results in unquantifiable uncertainty. Also, determination of orientation and location of the video monitor may be flawed.

#### **6.3.5.3 Waste Package Materials**

Coupons of candidate waste package materials (at the time the DST heating phase was started) were placed at strategic locations such as hot/dry locations near heaters and warm/wet regions in

the condensation zones in hydrological boreholes and in the heated drift. These coupons consisted of one of three materials (Alloy 22, carbon steel, and Monel-400). The coupons were tested before the heating phase and will be tested after the cooling phase to evaluate their corrosion potential. Also included in the hydrological boreholes were concrete samples that are not considered waste package materials. Slight corrosion is anticipated in these waste package materials during the DST.

Discussions of these unqualified corrosion measurements of waste package materials are included in this report for completeness.

#### **6.3.5.4 Microbiological Investigations**

The purpose of including the microbial experiments in the DST is to obtain complex process level information about survival and migration of microbes in an environment analogous to a radioactive waste repository. It is considered advantageous to evaluate microbiological response in terms of thermal, hydrological, mechanical and chemical behavior. With the goal of understanding the significance of microbial survival and migration in the repository environment, the following tests were designed:

1. Survival/migration test: borehole emplacement of labeled microbes
2. Survival/migration test: heated drift emplacement of labeled microbes
3. Survival/material-microbe-rock interaction test: carbon steel-microbe-rock and carbon steel-microbe-concrete
4. Sterile collection and freezing of preheating rock sample.

All tests were conducted with microbes that are indistinguishable from the microbes that are present in the rock surrounding the DST block. A nonaltering label was added to the microbes that acts as a tracking device to monitor their progress. The microbes are not pathogenic and have been collected and isolated for the YMP during the excavation of the ESF.

The total number of microbes that have been installed is far less than the number of microbes that have been unintentionally introduced during the construction of the DST. Locations of installation points include the heated drift and select borehole locations.



## 7. SUMMARY

### 7.1 DISCUSSION

As mentioned in Section 1, this report documents the comprehensive set of measurements taken within the YMP Thermal Testing Program since its inception in 1996. This documentation is intended to make data collected readily usable to end users. Only brief discussions are provided for different data sets. These are intended to impart a clear sense of applicability of data, so that they will be used properly within the context of measurement uncertainty. This approach also keeps this report to a manageable size, an important constraint since numerous measurements for three long-term thermal tests are addressed. Furthermore, thermal testing data currently residing in the TDMS have been reorganized and reformatted, as applicable, into new summary DTNs.

The summary of this work, which addresses diverse measurements collected in the YMP Thermal Testing Program, can be grouped into the following two categories:

- The preparation of a single, comprehensive document that provides ready access to key material related to the myriad of thermal testing measurements from each of the three thermal tests
- The development of summary DTNs that facilitate the usage of thermal testing data.

Discussion of key material regarding thermal testing measurements associated with the YMP Thermal Testing Program is presented in Section 6. This discussion is organized by the four processes (thermal, hydrological, mechanical, and chemical) for each of the three thermal tests: the Large Block Test (LBT), the Single Heater Test (SHT), and the Drift Scale Test (DST). Documentation includes an introduction and description, a cross section of behavior for each type of measurement (laboratory and field) for the two main testing phases (characterization and testing), a listing of input DTNs that contain the measurements, discussion of corresponding measurement uncertainties, and a set of germane references that provide additional detail regarding the measurements. In addition, summaries of two in-depth investigations are provided: (1) heat and mass loss through the DST bulkhead, and (2) investigation of DST water samples with elevated concentrations of fluoride and chloride. Summary DTNs have also been restructured, as needed, to be more functional. These summary DTNs for the LBT, SHT, and DST are listed in Tables 6.1-1, 6.2-1, and 6.3-1, respectively. The improved structure of the summary DTNs facilitates the review, understanding, and usage of the thermal testing measurements by providing improved data layout including: consolidation of incremental test data into a single set, graphical descriptions, and coordinates of boreholes and sensors.

Uncertainty associated with most measurements is also discussed. These discussions are restricted to actual measurements and data reduction. If quantifiable uncertainties were cited, then either references to manufacturer's specifications were provided or they were referred to as "estimates." Standard error analyses (mean and standard deviation) were provided for applicable measurements such as repetitive measurements of laboratory or field parameters. Test measurements of a response for a specific location and time are not applicable for standard error analyses. Limitations on data use, if any, are described in the TDMS for the individual data sets and the summary DTNs listed in Tables 6.1-1, 6.2-1, and 6.3-1.

## 7.2 YUCCA MOUNTAIN REVIEW PLAN CRITERIA ASSESSMENT

This report contains a summarization of data obtained during testing for the LBT, SHT, and DST. This report does not contain analyses or modeling activities. This section summarizes the contents of this report as they apply to the following acceptance criteria from Section 2.2.1.3.3.3 of *Yucca Mountain Review Plan, Final Report* (NRC 2003 [DIRS 163274]).

### Acceptance Criterion 1 – System Description and Model Integration Are Adequate

- (4) Spatial and temporal abstractions appropriately address physical couplings (thermal-hydrologic-mechanical-chemical). For example, the U.S. Department of Energy evaluates the potential for focusing of water flow into drifts, caused by coupled thermal-hydrologic-mechanical-chemical processes.

Data associated with coupled processes have been addressed in this report for the field thermal testing program which includes the LBT, SHT, and DST. Data obtained from these tests have been used in downstream analyses and models that address phenomena caused by coupled processes such as the potential for focusing of water flow into drifts.

- (5) Sufficient technical bases and justification are provided for total system performance assessment assumptions and approximations for modeling coupled thermal-hydrologic-mechanical-chemical effects on seepage and flow, the waste package chemical environment, and the chemical environment for radionuclide release. The effects of distribution of flow on the amount of water contacting the engineered barriers and waste forms are consistently addressed, in all relevant abstractions.

Data obtained from the LBT, SHT, and DST programs are used to establish technical bases and justification for some assumptions and approximations in modeling coupled processes in downstream technical products.

- (8) Adequate technical bases are provided, including activities such as independent modeling, laboratory or field data, or sensitivity studies, for inclusion of any thermal-hydrologic-mechanical-chemical couplings and features, events, and processes as documented in the associated reports.

This report provides field and laboratory data from the LBT, SHT, and DST for use in developing and supporting downstream analyses and models that include various couplings and features, events, and processes.

- (9) Performance-affecting processes that have been observed in thermal-hydrologic tests and experiments are included into the performance assessment. For example, the U.S. Department of Energy either demonstrates that liquid water will not reflux into the underground facility or incorporates refluxing water into the performance assessment calculation, and bounds the potential adverse effects of alteration of the hydraulic pathway that result from refluxing water.

Data associated with thermal-hydrologic tests and experiments have been addressed in this report for the LBT, SHT, and DST. Data obtained from these tests have been used in downstream

analyses and models that address performance-affecting processes such as vaporization, condensation, and reflux.

### **Acceptance Criterion 2 – Data Are Sufficient for Model Justification**

- (1) Geological, hydrological, and geochemical values used in the license application are adequately justified. Adequate description of how the data were used, interpreted, and appropriately synthesized into the parameters is provided.

Justification has been provided throughout this report for the geological, hydrological and geochemical data values reported herein. Data use and interpretation in downstream documents are described in those documents.

- (2) Sufficient data were collected on the characteristics of the natural system and engineered materials to establish initial and boundary conditions for conceptual models of thermal-hydrologic-mechanical-chemical coupled processes, that affect seepage and flow and the engineered barrier chemical environment.

Coupled effects associated with the repository natural system have been addressed in this report on the basis of results from the LBT, SHT, and DST. These data assist in establishing initial and boundary conditions for conceptual models of coupled processes discussed in downstream documents.

- (3) Thermo-hydrologic tests were designed and conducted with the explicit objectives of observing thermal-hydrologic processes for the temperature ranges expected for repository conditions and making measurements for mathematical models. Data are sufficient to verify that thermal-hydrologic conceptual models address important thermal-hydrologic phenomena.

The objective of the field thermal testing program is to gain a more in-depth understanding of the various couplings of thermal, hydrological, mechanical, and chemical processes associated with the temperature ranges expected for repository conditions. This report provides a comprehensive set of data used to support the thermal-hydrologic models.

- (4) Sufficient information to formulate the conceptual approach(es) for analyzing water contact with the drip shield, engineered barriers, and waste forms is provided.

The data obtained from the field thermal testing program provides information needed to develop and support conceptual approaches for analyzing water contact as developed in downstream technical products.

### **Acceptance Criterion 3 – Data Uncertainty Is Characterized and Propagated Through the Model Abstraction**

- (4) Adequate representation of uncertainties in the characteristics of the natural system and engineered materials is provided in parameter development for conceptual models, process-level models, and alternative conceptual models. The U.S. Department of Energy may constrain these uncertainties using sensitivity analyses or conservative limits. For

example, the U.S. Department of Energy demonstrates how parameters used to describe flow through the engineered barrier system bound the effects of backfill and excavation-induced changes.

Data associated with measurement uncertainties are quantified throughout this report. Equipment manufacturer's uncertainty data are used when available. Standard error analyses (mean and standard deviation) are provided for applicable measurements such as repetitive measurements of laboratory or field parameters.

### **Acceptance Criterion 5 – Model Abstraction Output Is Supported by Objective Comparisons**

- (3) Accepted and well-documented procedures are used to construct and test the numerical models that simulate coupled thermal-hydrologic-mechanical-chemical effects on seepage and flow, engineered barrier chemical environment, and the chemical environment for radionuclide release. Analytical and numerical models are appropriately supported. Abstracted model results are compared with different mathematical models, to judge robustness of results.

The data obtained from the field thermal testing program, as reported herein, are used either to construct or execute downstream models or to test and support them, as is documented in the associated downstream reports.

## 8. INPUTS AND REFERENCES

### 8.1 DOCUMENTS CITED

- 100653 Brodsky, N.S.; Riggins, M.; Connolly, J.; and Ricci, P. 1997. *Thermal Expansion, Thermal Conductivity, and Heat Capacity Measurements for Boreholes UE25 NRG-4, UE25 NRG-5, USW NRG-6, and USW NRG-7/7A*. SAND95-1955. Albuquerque, New Mexico: Sandia National Laboratories. ACC: MOL.19980311.0316.
- 102003 Brown, E.T., ed. 1981. *Rock Characterization Testing & Monitoring, ISRM Suggested Methods*. New York, New York: Pergamon Press. TIC: 209865.
- 158190 BSC (Bechtel SAIC Company) 2002. *Test Plan for: Drift Scale Test*. SITP-02-UZ-012 REV 00. Las Vegas, Nevada: Bechtel SAIC Company. ACC: MOL.20020204.0143.
- 159051 BSC 2002. *Technical Work Plan for: Unsaturated Zone Sections of License Application Chapters 8 and 12*. TWP-NBS-HS-000003 REV 01. Las Vegas, Nevada: Bechtel SAIC Company. ACC: MOL.20020613.0192.
- 160771 BSC 2002. *Thermal Testing Measurements Report*. ANL-NBS-HS-000041 REV 00. Las Vegas, Nevada: Bechtel SAIC Company. ACC: MOL.20021004.0314.
- 170670 BSC 2003. *Condition Report*. CR No. BSC(B)-03-D-045. Las Vegas, Nevada: Bechtel SAIC Company. ACC: MOL.20031208.0157.
- 170669 BSC 2003. *Unsaturated Zone Flow and Transport Analysis/Model Reports at Lawrence Berkeley National Laboratory, Berkeley, California and Bechtel SAIC Company, LLC Las Vegas, Nevada, Novmbr 12 – 20, 2002*. Audit Report BQAP-BSC-03-02. Las Vegas, Nevada: Bechtel SAIC Company. ACC: MOL.20030430.0222.
- 178055 BSC 2004. *Investigation of Resistance Temperature Device Failures in the Drift Scale Test*. Las Vegas, Nevada: Bechtel SAIC Company. ACC: MOL.20050131.0086.
- 175829 BSC 2005. *Technical Work Plan for: Near-Field Environment Thermal Properties Model and Analysis Reports Integration*. TWP-MGR-PA-000019 REV 01. Las Vegas, NV: Bechtel SAIC Company. ACC: DOC.20051109.0003.
- 178175 BSC 2006. *Technical Work Plan for: Revising the Thermal Testing Measurements Report*. TWP-NBS-HS-000017 REV 00. Las Vegas, Nevada: Bechtel SAIC Company. ACC: DOC.20060731.0006.

- 101433 Buesch, D.C. and Spengler, R.W. 1998. "Character of the Middle Nonlithophysal Zone of the Topopah Spring Tuff at Yucca Mountain." *High-Level Radioactive Waste Management, Proceedings of the Eighth International Conference, Las Vegas, Nevada, May 11-14, 1998*. Pages 16-23. La Grange Park, Illinois: American Nuclear Society. TIC: 237082.
- 100657 Buscheck, T.A. and Nitao, J.J. 1995. *Thermal-Hydrological Analysis of Large-Scale Thermal Tests in the Exploratory Studies Facility at Yucca Mountain*. UCRL-ID-121791. Livermore, California: Lawrence Livermore National Laboratory. ACC: MOL.19960501.0392.
- 159473 Cho, J. 2001. ESF TCO Field Notebook #2 - Borehole Water Collection at ALCOVE 5. Scientific Notebook SN-LANL-SCI-183-V1. ACC: MOL.20010531.0102.
- 101588 Compton, R.R. 1962. *Manual of Field Geology*. New York, New York: John Wiley and Sons. TIC: 209518.
- 101428 CRWMS (Civilian Radioactive Waste Management System) M&O (Management and Operating Contractor) 1996. *Characterization of the ESF Thermal Test Area*. B00000000-01717-5705-00047 REV 01. Las Vegas, Nevada: CRWMS M&O. ACC: MOL.19970116.0187.
- 101375 CRWMS M&O 1996. *Test Design, Plans and Layout Report for the ESF Thermal Test*. BAB000000-01717-4600-00025 REV 01. Las Vegas, Nevada: CRWMS M&O. ACC: MOL.19970114.0166.
- 101539 CRWMS M&O 1997. *Ambient Characterization of the Drift Scale Test Block*. BADD00000-01717-5705-00001 REV 01. Las Vegas, Nevada: CRWMS M&O. ACC: MOL.19980416.0689.
- 146917 CRWMS M&O 1997. *Drift Scale Test Design and Forecast Results*. BAB000000-01717-4600-00007 REV 01. Las Vegas, Nevada: CRWMS M&O. ACC: MOL.19980710.0155.
- 101540 CRWMS M&O 1997. *Single Heater Test Status Report*. BAB000000-01717-5700-00002 REV 01. Las Vegas, Nevada: CRWMS M&O. ACC: MOL.19980416.0696.
- 111106 CRWMS M&O 1997. *Updated In Situ Thermal Testing Program Strategy*. B00000000-01717-5705-00065 REV 01. Las Vegas, Nevada: CRWMS M&O. ACC: MOL.19990526.0296.
- 111115 CRWMS M&O 1998. *Drift Scale Test As-Built Report*. BAB000000-01717-5700-00003 REV 01. Las Vegas, Nevada: CRWMS M&O. ACC: MOL.19990107.0223.

- 108306 CRWMS M&O 1998. *Drift Scale Test Progress Report No. 1.*  
BAB000000-01717-5700-00004 REV 01. Las Vegas, Nevada: CRWMS M&O.  
ACC: MOL.19990209.0240.
- 159512 CRWMS M&O 1998. *Thermal Test Progress Report #1.* Las Vegas, Nevada:  
CRWMS M&O. ACC: MOL.19991104.0269.
- 129261 CRWMS M&O 1999. *Single Heater Test Final Report.*  
BAB000000-01717-5700-00005 REV 00 ICN 1. Las Vegas, Nevada: CRWMS  
M&O. ACC: MOL.20000103.0634.
- 154585 CRWMS M&O 1999. *Thermal Test Progress Report #2.*  
BABEAF000-01717-5700-00001 REV 00. Las Vegas, Nevada: CRWMS  
M&O. ACC: MOL.19991104.0270.
- 159513 CRWMS M&O 1999. *Thermal Test Progress Report #3.* Las Vegas, Nevada:  
CRWMS M&O. ACC: MOL.19991104.0271.
- 159126 Daily, W. and Owen, E. 1991. "Cross-Borehole Resistivity Tomography."  
*Geophysics*, 56, (8), 1228-1235. Tulsa, Oklahoma: Society of Exploration  
Geophysicists. TIC: 253164.
- 134360 Danko, G. and Mousset-Jones, P. 1993. "Modeling of the Ventilation for  
Emplacement Drift Re-Entry and Rock Drying." *High Level Radioactive Waste  
Management, Proceedings of the Fourth Annual International Conference, Las  
Vegas, Nevada, April 26-30, 1993.* 1, 590-599. La Grange Park, Illinois:  
American Nuclear Society. TIC: 208542.
- 100282 DOE (U.S. Department of Energy) 1988. *Site Characterization Plan Yucca  
Mountain Site, Nevada Research and Development Area, Nevada.* DOE/RW-  
0199. Nine volumes. Washington, D.C.: U.S. Department of Energy, Office of  
Civilian Radioactive Waste Management. ACC: HQO.19881201.0002.
- 130104 DOE 1995. *In-Situ Thermal Testing Program Strategy.* DOE/YMSCO-003.  
Las Vegas, NV: YMSCO. TIC: 215726.
- 177092 DOE 2006. *Quality Assurance Requirements and Description.*  
DOE/RW-0333P, Rev. 18. Washington, D.C.: U.S. Department of Energy,  
Office of Civilian Radioactive Waste Management.  
ACC: DOC.20060602.0001.
- 105559 Faure, G. 1986. *Principles of Isotope Geology.* 2nd Edition. New York, New  
York: John Wiley & Sons. TIC: 237212.
- 100673 Flint, L.E. 1996. *Matrix Properties of Hydrogeologic Units at Yucca Mountain,  
Nevada.* Milestone 3GUP603M. Denver, Colorado: U.S. Geological Survey.  
ACC: MOL.19970324.0046.

- 100033 Flint, L.E. 1998. *Characterization of Hydrogeologic Units Using Matrix Properties, Yucca Mountain, Nevada*. Water-Resources Investigations Report 97-4243. Denver, Colorado: U.S. Geological Survey. ACC: MOL.19980429.0512.
- 159098 Freifeld, B. and Tsang, Y.W. 1998. "Active Hydrological Testing." Chapter 2 of *First Quarter TDIF Submission for the Drift Scale Test (Hydrological, Radar, Microseismic), Version 1.0*. Milestone SP2770M4. Berkeley, California: Lawrence Berkeley National Laboratory. ACC: MOL.19980812.0239.
- 100123 Hardin, E.L. 1998. *Near-Field/Altered-Zone Models Report*. UCRL-ID-129179. Livermore, California: Lawrence Livermore National Laboratory. ACC: MOL.19980630.0560.
- 159108 Horita, J. and Wesolowski, D.J. 1994. "Liquid-Vapor Fractionation of Oxygen and Hydrogen Isotopes of Water from the Freezing to the Critical Temperature." *Geochemica et Cosmochimica Acta*, 58, (16), 3425-3437. New York, New York: Elsevier. TIC: 240153.
- 101868 Hvorslev, M.J. 1951. *Time Lag and Soil Permeability in Ground-Water Observations*. AEWES Bulletin 36. Vicksburg, Mississippi: U.S. Army Corps of Engineers, Waterways Experiment Station. TIC: 238956.
- 170750 Jones, R.L. 2004. "Reference Information for the White Paper Entitled: Effects of Introduced Materials in the Drift Scale Test." Interoffice memorandum from R.L. Jones (BSC) to File, July 30, 2004, 0730042608, with attachment. ACC: MOL.20040802.0278; MOL.20020822.0121.
- 170840 Krishna, D.T. 2002. "Issuance of Deficiency Report (DR) BSC(B)-03-043, Resulting from the BSC Quality Assurance (QA) Audit BQAP-BSC-03-02." Letter from D.T. Krishna (BSC) to R.W. Andrews (BSC), December 13, 2002, RFH:ps-1211025420, with enclosure. ACC: MOL.20030227.0225.
- 159047 LaBrecque, D.J.; Ramirez, A.L.; Daily, W.D.; Binley, A.M.; and Schima, S.A. 1996. "ERT Monitoring of Environmental Remediation Processes." *Measurement and Science Technology*, 7, (3), 375-383. Bristol, England: IOP Publishing. TIC: 236228.
- 101393 Lin, W. and Daily, W. 1984. *Transport Properties of Topopah Spring Tuff*. UCRL-53602. Livermore, California: Lawrence Livermore National Laboratory. ACC: NNA.19891026.0025.
- 159069 Lin, W.; Blair, S.C.; Wilder, D.; Carlson, S.; Wagoner, J.; DeLoach, L.; Danko, G.; Ramirez, A.L.; and Lee, K. 2001. *Large Block Test Final Report*. UCRL-ID-132246, Rev. 2. Livermore, California: Lawrence Livermore National Laboratory. TIC: 252918.



- 159099 Lin, W.; Roberts, R.; Carlberg, E.; Ruddle, D.; and Pletcher, R. 2002. *Moisture Retention Curves of Topopah Spring Tuff at Elevated Temperatures*. UCRL-ID-146579. Livermore, California: Lawrence Livermore National Laboratory. TIC: 253211.
- 157900 Lowry, W.E. 2001. *Engineered Barrier Systems Thermal-Hydraulic-Chemical Column Test Report*. TDR-EBS-MD-000018 REV 00. Las Vegas, Nevada: Bechtel SAIC Company. ACC: MOL.20020102.0206.
- 159101 Majer, E.L. and McEvelly, T.V. 1985. "Acoustic Emission and Wave Propagation Monitoring at the Spent Fuel Test: Climax, Nevada." *International Journal of Rock Mechanics and Mining Sciences and Geomechanics Abstracts*, 22, (4), 215-226. New York, New York: Elsevier. TIC: 222776.
- 159518 Mitchell, A. 1996. "Borehole Videos from the Exploratory Studies Facility Thermal Testing Facility-Thermomechanical Alcove." Memorandum from A. Mitchell (LANL) to Distribution, May 21, 1996, LA-EES-13-LV-05-96-021, with attachment ACC: MOL.19960711.0110.
- 163274 NRC (U.S. Nuclear Regulatory Commission) 2003. *Yucca Mountain Review Plan, Final Report*. NUREG-1804, Rev. 2. Washington, D.C.: U.S. Nuclear Regulatory Commission, Office of Nuclear Material Safety and Safeguards. TIC: 254568.
- 159514 Pannell, G. 2001. "Heat Loss White Paper for KTI KTE0201." E-mail from G. Pannell to C. Gardner, April 4, 2001, with attachment. ACC: MOL.20010822.0143.
- 101698 Peterson, J.E. 1986. *The Application of Algebraic Reconstruction Techniques to Geophysical Problems*. LBL-21498. Berkeley, California: Lawrence Berkeley National Laboratory. TIC: 239765.
- 159102 Peterson, J.E., Jr. and Williams, K.H. 1998. "Acoustic Emission/Seismic Wave Monitoring Baseline Data." Chapter 5 of *ESF Drift Scale Test As-Built Data and Baseline Measurements (Hydrological, Radar, and Microseismic)*, Revision 1.0. Milestone SPY193M4. Berkeley, California: Lawrence Berkeley National Laboratory. ACC: MOL.19981016.0046.
- 159128 Peterson, J.E., Jr. and Williams, K.H. 1998. "Pre-Heating Ground Penetrating Radar Baseline Data." Chapter 4 of *ESF Drift Scale Test As-Built Data and Baseline Measurements (Hydrological, Radar, and Microseismic)*, Revision 1.0. Milestone SPY193M4. Berkeley, California: Lawrence Berkeley National Laboratory. ACC: MOL.19981016.0046.

- 159120 Peterson, J.E., Jr. and Williams, K.H. 1998. "Radar Imaging at the Drift Scale Heater Test." Chapter 4 of First Quarter TDIF Submission for the Drift Scale Test (Hydrological, Radar, Microseismic), Version 1.0. Milestone SP2770M4. Berkeley, California: Lawrence Berkeley National Laboratory. ACC: MOL.19980812.0239.
- 101710 Roberts, J.J. and Lin, W. 1997. "Electrical Properties of Partially Saturated Topopah Spring Tuff: Water Distribution as a Function of Saturation." *Water Resources Research*, 33, (4), 577-587. Washington, D.C.: American Geophysical Union. TIC: 239736.
- 159100 Roberts, J.J. and Lin, W. 1995. *Hydrological Property Measurements of Topopah Spring Tuff*. UCRL-ID-119033. Livermore, California: Lawrence Livermore National Laboratory. ACC: MOV.19980504.0004.
- 159048 Roberts, J.J. and Lin, W. 1995. *Report on Laboratory Tests of Drying and Re-Wetting of Intact Rocks*. UCRL-ID-121513. Livermore, California: Lawrence Livermore National Laboratory. ACC: MOL.19960404.0013.
- 117471 SNL (Sandia National Laboratories) 1997. *Unconfined Compression Tests on Specimens from the Drift Scale Test Area of the Exploratory Studies Facility at Yucca Mountain, Nevada*. Albuquerque, New Mexico: Sandia National Laboratories. ACC: MOL.19971120.0014.
- 118788 SNL 1998. *Laboratory Measurements of Thermal Conductivity as a Function of Saturation State for Welded and Nonwelded Tuff Specimens*. Albuquerque, New Mexico: Sandia National Laboratories. ACC: MOL.19980901.0177.
- 100646 Tsang, Y.W. and Cook, P. 1997. *Ambient Characterization of the ESF Drift Scale Test Area by Field Air Permeability Measurements*. Milestone SP9512M4. Berkeley, California: Lawrence Berkeley National Laboratory. ACC: MOL.19971201.0829.
- 105774 Tsang, Y.W. and Freifeld, B. 1998. "Hydrological Baseline Measurements." Chapter 2 of *ESF Drift Scale Test As-Built Data and Baseline Measurements (Hydrological, Radar, and Microseismic)*. Milestone SPY193M4, Rev. 1. Berkeley, California: Lawrence Berkeley National Laboratory. ACC: MOL.19981016.0046.
- 159097 Tsang, Y.W. and Freifeld, B. 1998. "Hydrological Characterization Data." Chapter 3 of *ESF Drift Scale Test As-Built Data and Baseline Measurements (Hydrological, Radar, and Microseismic)*. Milestone SPY193M4, Rev. 1. Berkeley, California: Lawrence Berkeley National Laboratory. ACC: MOL.19981016.0046..

- 101736 Waxman, M.H. and Thomas, E.C. 1974. "Electrical Conductivities in Shaly Sands: I. The Relation Between Hydrocarbon Saturation and Resistivity Index; II. The Temperature Coefficient of Electrical Conductivity." *Journal of Petroleum Technology*, 26, 213-225. Dallas, Texas: Society of Petroleum Engineers. TIC: 239699.
- 159121 Williams, K.H. and Peterson, J.E., Jr. 1998. "Radar Imaging and Acoustic Emission Monitoring: Second Quarter Progress." Chapter 4 of *Second Quarter TDIF Submission for the Drift Scale Test (Hydrological, Radar, Microseismic), Version 0.0*. Milestone SP2790M4. Berkeley, California: Lawrence Berkeley National Laboratory. ACC: MOL.19980812.0240.
- 159104 Williams, K.H.; Majer, E.; and Peterson, J.E., Jr. 1998. "Acoustic Emission Monitoring/Seismic Wave Monitoring: First Quarter Data." Chapter 5 of *First Quarter TDIF Submission for the Drift Scale Test (Hydrological, Radar, Microseismic), Version 1.0*. Milestone SP2770M4. Berkeley, California: Lawrence Berkeley National Laboratory. ACC: MOL.19980812.0239.
- 163765 Williams, N.H. 2003. "Contract No. DE-AC28-01RW1210 – Transmittal of White Paper, Effects of Neoprene on Water in the Drift Scale Test." Letter from N.H. Williams (BSC) to J.D. Ziegler (DOE/ORD), February 4, 2003, 0129035843, with enclosure. ACC: MOL.20030206.0211.

## 8.2 CODES, STANDARDS, REGULATIONS, AND PROCEDURES

033-YMP-QP-3.8, Rev. 1. *Control of the Electronic Management of Information*. Livermore, California: Lawrence Livermore National Laboratory. ACC: MOL.20020108.0169.

- 101786 ASTM D 4971-89. 1989. *Standard Test Method for Determining the In Situ Modulus of Deformation of Rock Using the Diametrically Loaded 76-mm (3-in.) Borehole Jack*. Philadelphia, Pennsylvania: American Society for Testing and Materials. TIC: 245311.

IM-PRO-002, Rev. 0, ICN 0. *Control of the Electronic Management of Information*. Washington, D.C.: U.S. Department of Energy, Office of Civilian Radioactive Waste Management. ACC: DOC.20060927.0023.

IM-PRO-003, Rev. 1, ICN 0. *Software Management*. Washington, D.C.: U.S. Department of Energy, Office of Civilian Radioactive Waste Management. ACC: DOC.20061113.0001.

LANL-YMP-QP-S5.01, Rev. 2. *Electronic Information Management*. Los Alamos, New Mexico: Los Alamos National Laboratory. ACC: MOL.20030421.0134.

LP-2.29Q-BSC, Rev. 0, ICN 2. *Planning for Science Activities*. Washington, D.C.: U.S. Department of Energy, Office of Civilian Radioactive Waste Management. ACC: DOC.20050912.0005

LS-PRO-001, Rev. 2, ICN 0. *Technical Reports*. Washington, D.C.: U.S. Department of Energy, Office of Civilian Radioactive Waste Management. ACC: DOC.20070115.0001.

LS-PRO-0203, Rev. 2, ICN 0. *Q-List and Classification of Structures, Systems, and Components*. Washington, D.C.: U.S. Department of Energy, Office of Civilian Radioactive Waste Management. ACC: DOC.20060927.0016.

NWM-USGS-GCP-03, Rev. 4, Mod. 0. *Uranium-Thorium Disequilibrium Studies*. Denver, Colorado: U.S. Geological Survey. ACC: MOL.19990723.0011.

NWM-USGS-GCP-12 Rev. 4, Mod. 1. *Rb-Sr Isotope Geochemistry*. Denver, Colorado: U.S. Geological Survey. ACC: MOL.19990825.0067.

NWM-USGS-GP-32, Rev. 0. *Underground Geologic Mapping*. Denver, Colorado: U.S. Geological Survey. ACC: MOL.19941102.0023.

SCI-PRO-004, Rev. 1, ICN 0. *Managing Technical Product Inputs*. Washington, D.C.: U.S. Department of Energy, Office of Civilian Radioactive Waste Management. ACC: DOC.20061016.0001.

TIP-AC-02, Rev. 0, CN 4. *Solutions Analysis; Cations by Inductively Coupled Plasma Atomic Emission Spectroscopy (ICP/AES)*. Livermore, California: Lawrence Livermore National Laboratory. ACC: MOL.20020710.0282.

TIP-AC-03, Rev. 0. *Determination of Inorganic Anions by Ion Chromatography (EPA Method 300.00)*. Livermore, California: Lawrence Livermore National Laboratory. ACC: MOL.20010315.0345.

TIP-NF-33, Rev. 0. *Collection and Field Analysis of Water Samples from Boreholes In the Exploratory Studies Facility*. Livermore, California: Lawrence Livermore National Laboratory. ACC: MOL.20010110.0463.

TST-PRO-001, Rev. 0, ICN 0. *Submittal and Incorporation of Data to the Technical Data Management System*. Washington, D.C.: U.S. Department of Energy, Office of Civilian Radioactive Waste Management. ACC: DOC.20060928.0015.

TST-PRO-003, Rev. 0, ICN 0. *Scientific Notebooks*. Washington, D.C.: U.S. Department of Energy, Office of Civilian Radioactive Waste Management. ACC: DOC.20060928.0017.

YMP-LBNL-QIP-6.1, Rev. 8, Mod. 0. *Document Review*. Berkeley, California: Lawrence Berkeley National Laboratory. ACC: 20021024.0322.

YMP-LBNL-QIP-SV.0, Rev. 2, Mod. 1. *Management of YMP-LBNL Electronic Data*. Berkeley, California: Lawrence Berkeley National Laboratory. ACC: MOL.20020717.0319.

YMP-LBNL-TIP/AFT-2.0, Rev. 1, Mod. 0. *Determination of Moisture Content, Bulk Density, Porosity and Particle Density of Rock Samples*. Berkeley, California: Lawrence Berkeley National Laboratory. ACC: MOL.20000710.0494.

YMP-LBNL-TIP/TT-4.0, Rev. 1, Mod. 0. *Acoustic Emission Monitoring/Seismic Wave Monitoring*. Berkeley, California: Lawrence Berkeley National Laboratory. ACC: MOL.20000915.0170.

YMP-LBNL-TIP/TT-7.0, Rev. 0, Mod. 0. *Extraction and Analysis of the Stable Isotope Components of CO<sub>2</sub> in Gas Samples*. Berkeley, California: Lawrence Berkeley National Laboratory. ACC: MOL.19990205.0145.

YMP-LBNL-TIP/TT-9.0, Rev. 0, Mod. 0. *Hydrogen Isotope Analyses of Waters*. Berkeley, California: Lawrence Berkeley National Laboratory. ACC: MOL.19990318.0083.

YMP-LBNL-TIP/TT-10.0, Rev. 0, Mod. 0. *Analysis of the Oxygen Isotopic Composition of Water Samples Using the Isoprep 18*. Berkeley, California: Lawrence Berkeley National Laboratory. ACC: MOL.19990224.0638.

### **8.3 SOURCE DATA, LISTED BY DATA TRACKING NUMBER**

- 156187 GS010608315215.002. Uranium and Thorium Isotope Data for Waters Analyzed Between January 18,1994 and September 14, 1996. Submittal date: 06/21/2001.
- 156007 GS010808312322.004. Uranium and Uranium Isotopic Data for Water Samples from Wells and Springs in the Yucca Mountain Vicinity Collected Between December 1996 and December 1997. Submittal date: 08/29/2001.
- 169553 GS010908315215.005. Strontium Isotope Ratios and Strontium Concentrations in Calcite Samples from the ESF Analyzed from May 25, 2000 to June 5, 2001. Submittal date: 09/12/2001.
- 159136 GS011108312322.008. Uranium Concentrations and <sup>234</sup>U/<sup>238</sup>U Activity Ratios Analyzed between February 1, 1999, and August 1, 2001 for Drift-Scale Heater Test Water Collected between June 1998 and April 2001, and Pore Water Collected between March 1996 and April 1999. Submittal date: 12/19/2001.

- 159137 GS011108312322.009. Strontium Isotope Ratios and Strontium Concentrations in Water Samples from the Drift Scale Test Analyzed from March 16, 1999 to June 27, 2001. Submittal date: 02/07/2002.
- 166569 GS020808312272.004. Analysis of Water-Quality Samples for the Period from July 1999 to July 2002. Submittal date: 09/18/2002.
- 165226 GS030408312272.002. Analysis of Water-Quality Samples for the Period from July 2002 to November 2002. Submittal date: 05/07/2003.
- 166570 GS031008312272.008. Analysis of Pore Water and Miscellaneous Water Samples for the Period from December 2002 to July 2003. Submittal date: 11/13/2003.
- 178056 GS040308312272.001. Gravimetric Moisture Content Measurements for HD-CHEMSAMP Cores for the Period from June 2002 to January 2004. Submittal date: 03/17/2004.
- 169629 GS040508312272.002. Strontium Isotope Ratios and Strontium Concentrations on Introduced Materials to the ESF Tunnel. Submittal date: 06/02/2004.
- 178057 GS041108312272.005. Analysis of Pore Water and Miscellaneous Water Samples for the Period from July 2003 to September 2004. Submittal date: 02/25/2005.
- 169244 GS951108312271.006. Interpretations of Chemical and Isotopic Data from Boreholes in the Unsaturated Zone at Yucca Mountain Nevada. Submittal date: 09/13/2001.
- 169552 GS960908315215.012. Strontium Isotope Ratios and Isotope Dilution Data for Strontium Analyzed 07/06/95 to 08/05/96. Submittal date: 04/10/1997.
- 158429 GS970608314224.006. Provisional Results: Geotechnical Data for Alcove 5 (DWFA), Main Drift of the ESF: Detailed Line Survey Data for the Heated Drift and Cross-Drift. Submittal date: 06/24/1997.
- 145707 GS990308315215.003. X-Ray Fluorescence Elemental Compositions of rock Core Samples from USW SD-9 and USW SD-12. Submittal date: 03/25/1999.
- 145711 GS990308315215.004. Strontium Isotope Ratios and Strontium Concentrations in Rock Core Samples and Leachates from USW SD-9 and USW SD-12. Submittal date: 03/25/1999.
- 158278 LA0002FH6001WP.001. Single Heater Test - Raw Data. Submittal date: 02/25/2000.

153485 LA0009SL831151.001. Fracture Mineralogy of the ESF Single Heater Test Block, Alcove 5. Submittal date: 09/28/2000.

158230 LA0106FH831151.002. Large Block Test Data. Submittal date: 06/06/2001.

158229 LA0106FH831151.003. Large Block Temperature Data. Submittal date: 06/06/2001.

158316 LA0108FH831151.001. Drift Scale Test (DST), Distribution Data Sets: Scientific Notebook SN-LANL-SCI-209-V1. Submittal date: 08/23/2001.

169386 LA0111FH831151.001. Rapid Evaluation of K and Alpha (REKA) in the Drift Scale Test (DST), Distribution Data Sets. Submittal date: 11/06/2001.

158317 LA0111FH831151.002. Drift Scale Test (DST), Raw Data Sets. Submittal date: 11/06/2001.

158318 LA0111FH831151.003. Drift Scale Test (DST), All (Hourly) Data Points. Submittal date: 11/06/2001.

158426 LA0201SL831225.001. Chemical, Textural, and Mineralogical Characteristics of Sidewall Samples from the Drift Scale Test. Submittal date: 01/10/2002.

159515 LA0208FH831151.001. DST DCS Raw Data (All) Includes SNO5 Raw. Submittal date: 08/08/2002.

159308 LA0208FH831151.002. ESF Drift Scale Test, ESF DCS Data TCO Hourly. Submittal date: 08/08/2002.

169378 LA0303WS831151.001. Amorphous Silica in Drift Scale Test Sidewall Samples. Submittal date: 04/09/2003.

178052 LA0609SL831322.001. Mineralogy of Red Spot Deposit from Drift Scale Test. Submittal date: 09/19/2006.

158319 LA9908FH6001WP.001. Drift Scale Test-Raw Data. Submittal date: 08/31/1999.

146449 LA9912SL831151.002. Percent Coverage by Fracture-Coating Minerals in Core ESF-HD-TEMP-2. Submittal date: 01/05/2000.

158431 LARO831422AQ97.002. Exploratory Studies Facility Test Coordination Office Notebook #2 for Borehole Wireline Measurements. Submittal date: 08/27/1999.

158337 LB000121123142.002. Active Hydrology Testing Data (Air Injection) Collected from 12 Hydrology Holes of the ESF Drift Scale Test for the Period June 1, 1999 through October 31, 1999. Submittal date: 01/21/2000.

- 146451 LB000121123142.003. Isotope Data for CO2 Gas Samples Collected From the Hydrology Holes of the ESF Drift Scale Test for the Period August 9, 1999 through November 30, 1999. Submittal date: 01/21/2000.
- 158338 LB000121123142.004. Ground Penetrating Radar Data Collected from Boreholes of the ESF Drift Scale Test for the Period June 1, 1999 to October 31, 1999. Submittal date: 01/21/2000.
- 158339 LB000121123142.005. Acoustic Emission Data Collected from Boreholes of the ESF Drift Scale Test for the Period December 21, 1998 through October 27, 1999. Submittal date: 01/21/2000.
- 158341 LB000718123142.002. Active Hydrology Testing Data (Air Injection) Collected from 12 Hydrology Holes of the ESF Drift Scale Test for the Period November 1, 1999 through May 31, 2000. Submittal date: 07/18/2000.
- 158342 LB000718123142.003. Isotope Data for CO2 Gas Samples Collected from the Hydrology Holes of the ESF Drift Scale Test for the Period April 18, 2000 through April 19, 2000. Submittal date: 07/18/2000.
- 153354 LB000718123142.004. Ground Penetrating Radar Data Collected from Boreholes of the ESF Drift Scale Test on April 13, 2000. Submittal date: 07/18/2000.
- 158343 LB000718123142.005. Acoustic Emission Data Collected from Boreholes of the ESF Drift Scale Test for the Period October 27, 1999 through March 21, 2000. Submittal date: 07/18/2000.
- 153460 LB0011CO2DST08.001. Isotope Data for CO2 from Gas Samples Collected from Hydrology Holes in Drift-Scale Test. Submittal date: 12/09/2000.
- 158344 LB0101ACEMDST1.001. Acoustic Emission Data Collected from Boreholes of the ESF Drift Scale Test for 04/13/00-07/02/00. Submittal date: 01/19/2001.
- 158345 LB0101AIRKDST1.001. Active Air K Testing Data Collected from 12 Hydrology Holes of the ESF Drift Scale Test for 7/24/00-7/28/00 and 10/18/00-10/27/00. Submittal date: 01/19/2001.
- 158346 LB0101GPRDST01.001. GPR Data Collected from Boreholes of the ESF Drift Scale Test on September 27-28, 2000. Submittal date: 01/19/2001.
- 159306 LB0102CO2DST98.001. Concentration Data for CO2 from Gas Samples Collected from Hydrology Holes in Drift-scale Test. Submittal date: 02/28/2001.
- 158437 LB0108ACEMDST5.001. Drift Scale Test Acoustic Emission Data. Submittal date: 10/29/2001.



- 158438 LB0108AIRKDST5.001. Active Air-K Testing. Submittal date: 08/27/2001.
- 156888 LB0108CO2DST05.001. Concentration and Isotope Data for CO2 and H2O from Gas Samples Collected from Hydrology Holes in Drift-Scale Test - May and August 1999, April 2000, January and April 2001. Submittal date: 08/27/2001.
- 158440 LB0108GPRDST05.001. Drift Scale Test Ground Penetrating Radar Data for February 2001. Submittal date: 08/27/2001.
- 158348 LB0203AIRKDSTE.001. Active Air-K Testing, Sept. 2001 - Jan. 2002. Submittal date: 03/13/2002.
- 158349 LB0203CO2DSTE.001. Concentration/Isotope Data for CO2/H2O from Gas Samples Collected from Hydrology Holes in DST up to End of Heating. Submittal date: 03/13/2002.
- 158350 LB0203GPRDSTE.001. Drift Scale Test Ground Penetrating Radar Data for June 2001 - Jan. 2002, Prior to End of Heating. Submittal date: 03/13/2002.
- 159543 LB0204SHAIRK3Q.001. Single Heater Test Air-K (March-May 97). Submittal date: 04/16/2002.
- 159303 LB0206C14DSTE.001. Carbon 14 Isotope Data from CO2 Gas Samples Collected from DST. Submittal date: 06/17/2002.
- 177869 LB0209AIRKDSTC.001. Air Pressure Data for the Cooling Phase of the DST. Submittal date: 09/11/2002.
- 177817 LB0209GPRDSTCP.001. GPR for the Cooling Phase of the DST. Submittal date: 09/12/2002.
- 160896 LB0210GPRDSTCP.001. DST GPR Monitoring of Water Content Over Time (Cooling Phase). Submittal date: 10/31/2002.
- 160895 LB0210GPRDSTHP.001. DST GPR Monitoring of Water Content Over Time (Heating Phase). Submittal date: 10/31/2002.
- 170566 LB0211DSTRBRDG.001. DST Packer Materials Investigation. Submittal date: 11/11/2002.
- 170567 LB0302NEOPDGRD.001. Neoprene Degradation Experiments. Submittal date: 02/23/2003.
- 177870 LB0303AIRKDSTC.001. Air Pressure Data for the Cooling Phase of the DST. Submittal date: 03/28/2003.

- 177822 LB0303GPRDSTCP.001. GPR for the Cooling Phase of the DST: Processed Data. Submittal date: 03/28/2003.
- 177538 LB0303ISODSTCP.001. Isotope Data and CO2 Analysis for the Cooling Phase of the DST. Submittal date: 03/28/2003.
- 177871 LB0309AIRKDSTC.001. Air Pressure Data for the Cooling Phase of the DST. Submittal date: 09/24/2003.
- 177823 LB0309GPRDSTCP.001. GPR for the Cooling Phase of the DST: Processed Data. Submittal date: 09/24/2003.
- 177539 LB0309ISODSTCP.001. Isotope Data and CO2 Analysis for the Cooling Phase of the DST. Submittal date: 09/24/2003.
- 177905 LB0309H2ODSTCP.001. Passive Temperature and Pressure Monitoring Data for the Cooling Phase of the DST. Submittal date: 09/24/2003.
- 177932 LB0311RHMDSTCP.001. Passive Relative Humidity Monitoring Data for the Cooling Phase of the DST. Submittal date: 01/29/2004.
- 170568 LB0401PRTDSTCP.001. Passive Monitoring Data (Temperature and Pressure) for the Drift Scale Test (01/15/2002-06/30/2002). Submittal date: 01/29/2004.
- 170569 LB0401PRTDSTCP.002. Passive Monitoring Data (Temperature and Pressure) for the Drift Scale Test (07/01/2002-12/31/2002). Submittal date: 01/29/2004.
- 169251 LB0401PRTDSTHP.001. Passive Monitoring Data (Temperature and Pressure) for the Drift Scale Test (11/01/1997-02/28/1998). Submittal date: 01/29/2004.
- 169252 LB0401PRTDSTHP.002. Passive Monitoring Data (Temperature and Pressure) for the Drift Scale Test (03/01/1998-05/31/1998). Submittal date: 01/29/2004.
- 169253 LB0401PRTDSTHP.003. Passive Monitoring Data (Temperature and Pressure) for the Drift Scale Test (06/01/1998-08/31/1998). Submittal date: 01/29/2004.
- 169255 LB0401PRTDSTHP.004. Passive Monitoring Data (Temperature and Pressure) for the Drift Scale Test (09/01/1998-05/31/1999). Submittal date: 01/29/2004.
- 169246 LB0401PRTDSTHP.005. Passive Monitoring Data (Temperature and Pressure) for the Drift Scale Test (06/01/1999-10/31/1999). Submittal date: 01/29/2004.
- 169247 LB0401PRTDSTHP.006. Passive Monitoring Data (Temperature and Pressure) for the Drift Scale Test (11/01/1999-05/31/2000). Submittal date: 01/29/2004.
- 169248 LB0401PRTDSTHP.007. Passive Monitoring Data (Temperature and Pressure) for the Drift Scale Test (06/01/2000-11/30/2000). Submittal date: 01/29/2004.

- 169249 LB0401PRTDSTHP.008. Passive Monitoring Data (Temperature and Pressure) for the Drift Scale Test (12/01/2000-05/31/2001). Submittal date: 01/29/2004.
- 169250 LB0401PRTDSTHP.009. Passive Monitoring Data (Temperature and Pressure) for the Drift Scale Test (06/01/2001-01/14/2002). Submittal date: 01/29/2004.
- 177911 LB0401RHMDSTHP.001. Passive Monitoring Data (Relative Humidity) for the Drift Scale Test (11/01/1997-02/28/1998). Submittal date: 01/29/2004.
- 177914 LB0401RHMDSTHP.002. Passive Monitoring Data (Relative Humidity) for the Drift Scale Test (03/01/1998-05/31/1998). Submittal date: 01/29/2004.
- 177915 LB0401RHMDSTHP.003. Passive Monitoring Data (Relative Humidity) for the Drift Scale Test (06/01/1998-08/31/1998). Submittal date: 01/29/2004.
- 177916 LB0401RHMDSTHP.004. Passive Monitoring Data (Relative Humidity) for the Drift Scale Test (09/01/1998-05/31/1999). Submittal date: 01/29/2004.
- 177918 LB0401RHMDSTHP.005. Passive Monitoring Data (Relative Humidity) for the Drift Scale Test (06/01/1999-10/31/1999). Submittal date: 01/29/2004.
- 177920 LB0401RHMDSTHP.006. Passive Monitoring Data (Relative Humidity) for the Drift Scale Test (11/01/1999-05/31/2000). Submittal date: 01/29/2004.
- 177921 LB0401RHMDSTHP.007. Passive Monitoring Data (Relative Humidity) for the Drift Scale Test (06/01/2000-11/30/2000). Submittal date: 01/29/2004.
- 177922 LB0401RHMDSTHP.008. Passive Monitoring Data (Relative Humidity) for the Drift Scale Test (12/01/2000-05/31/2001). Submittal date: 01/29/2004.
- 177924 LB0401RHMDSTHP.009. Passive Monitoring Data (Relative Humidity) for the Drift Scale Test (06/01/2001-01/14/2002). Submittal date: 01/29/2004.
- 177929 LB0401RHMDSTCP.001. Passive Monitoring Data (Relative Humidity) for the Drift Scale Test (01/15/2002-06/30/2002). Submittal date: 01/29/2004.
- 177930 LB0401RHMDSTCP.002. Passive Monitoring Data (Relative Humidity) for the Drift Scale Test (07/01/2002-12/31/2002). Submittal date: 01/29/2004.
- 177872 LB0403AIRKDSTC.001. Air Pressure Data for the Cooling Phase of the DST. Submittal date: 03/16/2004.
- 177824 LB0403GPRDSTCP.001. GPR for the Cooling Phase of the DST: Processed Data. Submittal date: 03/16/2004.
- 177540 LB0403ISODSTCP.001. H2O and CO2 Isotope Analysis for the Cooling Phase of the DST. Submittal date: 03/16/2004.

177906 LB0403PRTDSTCP.001. Passive Monitoring Data (Temperature And Pressure) for the Drift Scale Test. Submittal date: 03/16/2004.

177933 LB0403RHMDSTCP.001. Passive Monitoring Data (Relative Humidity) for the Drift Scale Test. Submittal date: 03/16/2004.

169254 LB0404ISODSTHP.003. Third Submittal of CO2/H2O Isotope Data for the Heating Phase of the DST. Submittal date: 04/15/2004.

177886 LB0410AIRKDSTC.001. Air Pressure Data for the Cooling Phase of the DST. Submittal date: 11/24/2004.

177541 LB0410ISODSTCP.001. H2O and CO2 Isotope Analysis for the Cooling Phase of the DST. Submittal date: 11/24/2004.

177907 LB0410PRTDSTCP.001. Passive Temperature and Pressure Monitoring Data for the Cooling Phase of the DST (01/01/04-06/30/04). Submittal date: 10/19/2004.

177935 LB0410RHMDSTCP.001. Passive Relative Humidity Monitoring Data for the Cooling Phase of the DST (01/01/04-06/30/04). Submittal date: 10/19/2004.

177887 LB0509AIRKDSTC.001. Air Pressure Data for the Cooling Phase of the DST. Submittal date: 09/29/2005.

177825 LB0509GPRDSTCP.001. Ground Penetrating Radar Data for the Cooling Phase of the DST. Submittal date: 09/29/2005.

177542 LB0509ISODSTCP.001. H2O and CO2 Isotope Analysis for the Cooling Phase of the DST. Submittal date: 09/29/2005.

177937 LB0509RHMDSTCP.001. Passive Relative Humidity Monitoring Data for the Cooling Phase of the DST (07/01/2004-06/30/2005). Submittal date: 09/29/2005.

178559 LB0603AIRKDSTC.001. Air Pressure Data for the Cooling Phase of the DST. Submittal date: 10/22/2006.

177826 LB0603GPRDSTCP.001. Ground Penetrating Radar Data for the Cooling Phase of the DST. Submittal date: 03/31/2006.

177938 LB0603RHMDSTCP.001. Passive Relative Humidity Monitoring Data for the Cooling Phase of the DST (07/01/2005-12/31/2005). Submittal date: 03/10/2006.

- 177908 LB0609PRTDSTCP.001. Passive Temperature and Pressure Monitoring Data for the Cooling Phase of the DST (07/01/04-06/30/05). Submittal date: 09/14/2006.
- 177909 LB0609PRTDSTCP.002. Passive Temperature and Pressure Monitoring Data for the Cooling Phase of the DST (07/01/05-12/31/05). Submittal date: 09/14/2006.
- 105587 LB960500834244.001. Hydrological Characterization of the Single Heater Test Area in ESF. Submittal date: 08/23/1996.
- 158287 LB970100123142.001. Air Injections in Boreholes #16 and #18 in the Single Heater Test Area. Submittal date: 01/17/1997.
- 158293 LB970500123142.001. Air Injection Data in Boreholes #16 and #18 in the Single Heater Test Area. Submittal date: 05/23/1997.
- 131500 LB970500123142.003. Laboratory Test Results of Hydrological Properties from Dry Drilled and Wet Drilled Cores in the Drift Scale Test Area and in the Single Heater Test Area of the Thermal Test Facility. Submittal date: 05/30/1997.
- 105589 LB970600123142.001. Ambient Characterization of the ESF Drift Scale Test Area by Field Air Permeability Measurements. Submittal date: 06/13/1997.
- 158295 LB970700123142.002. Third Quarter IR Pictures of the Single Heater Test Area. Submittal date: 07/17/1997.
- 118965 LB971000123142.001. Air Injections in Boreholes #16 and #18 in the Single Heater Test Area. Submittal date: 10/17/1997.
- 158297 LB980120123142.001. First Quarter FY98 IR Pictures of the Single Heater Test Area. Submittal date: 01/20/1998.
- 105590 LB980120123142.004. Air Injections in Boreholes 57 through 61, 74 through 78, 185 and 186 in the Drift Scale Test Area. Submittal date: 01/20/1998.
- 114134 LB980120123142.005. Hydrological Characterization by Air Injections Tests in Boreholes in Heated Drift in DST. Submittal date: 01/20/1998.
- 158352 LB980120123142.007. Data Represents the Measurement of Discrete Acoustic Energy of the Rock Measured Prior to Turning on the Heaters in the SHT. Submittal date: 01/20/1998.
- 158280 LB980120123142.008. Data from "Letter Report on First Quarter Results of Measurements in Hydrology Holes in the Single Heater Test Area, FY1998.". Submittal date: 05/28/1999.

- 113706 LB980420123142.002. Active Hydrology Testing Data in Boreholes 57-61, 74-78, and 185-186; Air Injection Tests and Gas Tracer Tests. Submittal date: 04/20/1998.
- 113717 LB980420123142.004. Acoustic Emission Data (Recorded Events and Calibration Files). Submittal date: 04/20/1998.
- 111471 LB980420123142.005. Isotope Data for CO<sub>2</sub> from Gas Samples Collected from Drift Scale Test February 1998 in First Quarter TDIF Submission for the Drift Scale Test. Submittal date: 11/12/1998.
- 113742 LB980715123142.002. Active Hydrology Testing Data in Boreholes 57-61, 74-78, and 185-186; Air Injection Tests and Gas Tracer Tests in 2ND Quarter TDIF Submission of the Drift Scale Test Heating Phase. Submittal date: 07/15/1998.
- 111472 LB980715123142.003. Isotope Data for CO<sub>2</sub> from Gas Samples Collected from Drift Scale Test June 4, 1998 in 2nd Quarter TDIF Submission of the Drift Scale Test Heating Phase. Submittal date: 07/15/1998.
- 118999 LB980901123142.001. Active Hydrology Testing Data in Boreholes 16 and 18. Submittal date: 08/26/1998.
- 119009 LB980901123142.002. Passive Monitoring Data (Temperature, Relative Humidity, and Gauge Pressure) for the Final TDIF Submittal for the Single Heater Test. Submittal date: 08/26/1998.
- 119016 LB980901123142.003. Ground Penetrating Radar Data for Final TDIF Submittal for the Single Heater Test. Submittal date: 08/26/1998.
- 119029 LB980901123142.006. Laboratory Test Results of Hydrological Properties from Post-Test Dry-Drilled Cores in the Single Heater Test Area for the Final TDIF Submittal for the Single Heater Test. Submittal date: 08/31/1998.
- 105593 LB980912332245.002. Gas Tracer Data from Niche 3107 of the ESF. Submittal date: 09/30/98.
- 129245 LB981016123142.002. Active Hydrology Testing Data (Air Injection) from Boreholes 57-61, 74-78, 185-186 Taken from August 1998 to September 1998 for the Third Quarter TDIF Submission for the Drift Scale Test. Submittal date: 10/16/1998.
- 129247 LB990630123142.001. Fourth, Fifth, and Sixth Quarters TDIF Submission for the Drift Scale Test, September 1998 to May 1999. Submittal date: 06/30/1999.
- 111476 LB990630123142.003. Fourth, Fifth, and Sixth Quarters TDIF Submission for the Drift Scale Test, September 1998 to May 1999. Submittal date: 06/30/1999.

- 129274 LB990630123142.005. Fourth, Fifth, and Sixth Quarters TDIF Submission for the Drift Scale Test, September 1998 to May 1999. Submittal date: 07/20/1999.
- 158325 LL000804023142.009. Liquid Saturation Tomographs for the ESF Drift Scale Test (DST) Determined from ERT Measurements. Submittal date: 08/04/2000.
- 153288 LL001100931031.008. Aqueous Chemistry of Water Sampled from Boreholes of the Drift Scale Test (DST). Submittal date: 11/10/2000.
- 153616 LL001200231031.009. Aqueous Chemistry of Water Sampled from Boreholes of the Drift Scale Test (DST). Submittal date: 12/04/2000.
- 159134 LL020302223142.015. Aqueous Geochemistry of DST Samples Collected from HYD Boreholes. Submittal date: 03/07/2002.
- 177795 LL020307723142.018. Liquid Saturation Tomographs for the ESF Drift Scale Test (DST) Determined from Electrical Resistance Tomography (ERT). Submittal date: 05/16/2002.
- 159307 LL020405123142.019. Aqueous Geochemistry of Condensed Fluids Collected During Studies of Introduced Materials. Submittal date: 05/22/2002.
- 159105 LL020502523142.020. Electrical Properties of Topopah Spring Tuff as a Function of Saturation and Temperature. Submittal date: 07/05/2002.
- 169256 LL020506123142.021. Moisture Retention Curves at Elevated Temperatures. Submittal date: 08/30/2002.
- 159551 LL020710223142.024. Moisture Content of Rock from Neutron Logging Activities in the Drift Scale Test (DST): August 1997 through May 2002. Submittal date: 08/20/2002.
- 169257 LL021107623121.014. Aqueous Geochemistry of DST Samples Collected Between April 20, 1999 and January 25, 2000. Submittal date: 12/03/2002.
- 169258 LL030107523142.031. Anion Concentrations of Two DST Samples Collected Between June 4, 1998 and March 30, 1999. Submittal date: 01/28/2003.
- 170570 LL030305023121.023. Aqueous Geochemistry of DST Water Samples Collected in February and March of 2002 from Borehole 75, Zone 2 (BH 75-2). Submittal date: 03/12/2003.
- 165700 LL030309723122.022. Moisture Content of Rock from Neutron Logging Activities in the Drift Scale Test (DST): July 2002 through November 2002. Submittal date: 05/07/2003.

- 170571 LL030310023121.024. Chemical Composition of Water Samples Collected from Hyd Boreholes of the Drift Scale Test (DST). Submittal date: 03/24/2003.
- 170572 LL030605512251.064. Thermogravimetric Analysis (TGA) Data on the Thermal Decomposition of Fluoroelastomer (Fkm) Samples Taken from Bh-60 and Bh-72 of the Drift Scale Test at Yucca Mountain. Submittal date: 06/12/2003.
- 177798 LL030606723142.035. Saturation and Resistivity Ratio Tomographs from the Drift Scale Test for the Period February 5, 2002 through October 1, 2002. Submittal date: 06/17/2003.
- 165701 LL030709023122.032. Moisture Content of Rock from Neutron Logging Activities in the Drift Scale Test (DST): January 2003 through May 2003. Submittal date: 07/24/2003.
- 177803 LL030906923142.038. Electrical Resistivity and Saturation Ratio Tomographs of the Drift Scale Test (DST), March 4, 2003 through May 21, 2003. Submittal date: 09/16/2003.
- 177806 LL040307423142.072. Electrical Resistivity and Saturation Ratio Tomographs of the Drift Scale Test (DST) for November 18 - 19, 2003. Submittal date: 03/30/2004.
- 177827 LL040308623122.043. Moisture Content of Rock from Neutron Logging Activities in the Drift Scale Test (DST): May 2003 through November 2003. Submittal date: 11/09/2004.
- 177807 LL041000223142.045. Saturation Ratio and Resistivity Ratio Tomographs from the Drift Scale Test for the Period January 1, 2004 through June 30, 2004. Submittal date: 02/13/2005.
- 177831 LL041001623122.052. Moisture Content of Rock from Neutron Logging Activities in the Drift Scale Test (DST): January 1, 2004 through June 30, 2004. Submittal date: 02/15/2005.
- 177829 LL050206323122.057. Moisture Content of Rock from Neutron Logging Activities in the Drift Scale Test (DST): July 1, 2004 through December 31, 2004. Submittal date: 03/23/2005.
- 177809 LL050902223142.048. Saturation Ratio and Resistivity Ratio Tomographs from the Drift Scale Test for the Period January 1, 2005 through June 30, 2005. Submittal date: 11/20/2005.
- 177833 LL060101523122.066. Moisture Content of Rock from Neutron Logging Activities in the Drift Scale Test (DST): February 2005 through September 2005. Submittal date: 01/10/2006.



- 177834 LL060302423122.067. Moisture Content of Rock from Neutron Logging Activities in the Drift Scale Test (DST): October 2005 through December 2005. Submittal date: 03/29/2006.
- 177810 LL060303223142.051. Saturation Ratio Tomographs from the Drift Scale Test for the Period July 1, 2005 through December 31, 2005. Submittal date: 04/05/2006.
- 158237 LL950812704242.017. Report on Laboratory Tests of Drying and Re-Wetting of Intact Rocks. Submittal date: 08/07/1995.
- 158271 LL960400404244.012. Fracture Mapping of the East Side of the Large Block Test. Submittal date: 04/01/1996.
- 158274 LL960400504244.013. Fracture Mapping of the South Side of the Large Block Test. Submittal date: 04/01/1996.
- 158275 LL960400604244.014. Fracture Mapping of the West Side of the Large Block Test. Submittal date: 04/01/1996.
- 158276 LL960400704244.015. Fracture Mapping of the North Side of the Large Block Test. Submittal date: 04/01/1996.
- 158244 LL960905204244.022. Permeability Measurements on an Intact Core Sample from the Large Block Test. Submittal date: 09/24/1996.
- 158281 LL970101004244.026. First Quarter Results of ERT Measurements in the Single Heater Test. Submittal date: 01/08/1997.
- 158309 LL970101104244.027. First Quarter Results of Chemical Measurements in the Single Heater Test. Submittal date: 01/08/1997.
- 111481 LL970409604244.030. Second Quarter Results of Chemical Measurements in the Single Heater Test. Submittal date: 04/17/1997.
- 148609 LL970505404244.031. Second and Third Quarter Results of ERT Measurements for Single Heater Test. Submittal date: 05/23/1997.
- 111482 LL970703904244.034. Third Quarter Results of Chemical Measurements in the Single Heater Test. Submittal date: 07/15/1997.
- 113889 LL970803404244.040. Data on Moisture Content in the Large Block Test (LBT). Submittal date: 08/08/1997.
- 158313 LL970805504244.043. XYZ of Instruments in Single Heater Test (SHT) in RTD Holes 15, 17, 22, and 23; Packer Holes 16 and 18; Chemistry Holes 20 and 21. Submittal date: 08/14/1997.

158286 LL971002904244.044. Fourth Quarter FY97 Results of ERT Measurements in the Single Heater Test. Submittal date: 10/13/1997.

148611 LL971006604244.046. Fourth Quarter FY97 Results of Chemical Measurements in the Single Heater Test (SHT). Submittal date: 10/21/1997.

113894 LL971204304244.047. Neutron Logging Activities at the Large Block Test (LBT). Submittal date: 12/08/1997.

148610 LL980105204244.049. First Quarter FY98 Results of ERT Measurements in the Single Heater Test. Submittal date: 01/13/1998.

118963 LL980106904244.051. First Quarter FY98 Results of the Neutron Logging Report. Submittal date: 01/16/1998.

158332 LL980108804244.052. Electrical Resistivity Tomography (ERT) Monitoring of the Drift Scale Test. Submittal date: 01/22/1998.

158299 LL980109904243.015. Fourth Quarter FY 1997 and First Quarter FY 1998 Data on the O-MPBX at the Single Heater Test (SHT). Submittal date: 01/26/1998.

113782 LL980406404244.057. First and Second Quarter FY98 Results of ERT Measurements in the Drift Scale Test. Submittal date: 04/14/1998.

159107 LL980411004244.060. DST Baseline REKA Probe Measurements. Submittal date: 04/24/1998.

159111 LL980411104244.061. DST Baseline REKA Probe Measurements for Thermal Conductivity and Diffusivity. Submittal date: 04/24/1998.

113791 LL980808604244.065. Second Quarter FY98 Results of ERT Measurements in the Drift Scale Test. Submittal date: 08/21/1998.

159109 LL980902104244.070. DST Baseline REKA Probe Measurements for Thermal Conductivity and Diffusivity. Submittal date: 09/03/1998.

145385 LL980913304244.072. Data Submission Report for Electrical Resistance Tomography Results Obtained During the Large Block Test FY98. Submittal date: 09/24/1998.

135872 LL980918904244.074. Temperature, Relative Humidity and Gas Pressure Results During the Large Block Test FY 98. Submittal date: 09/29/1998.

145099 LL980919304244.075. Neutron Logging Activities at the Large Block Test (LBT). Submittal date: 09/30/1998.

- 148630 LL980919404244.076. Measurement of the Sensor Displacement While Heating the Large Block at the Large Block Test FY98. Submittal date: 09/30/1998.
- 158261 LL981001604244.079. The Imaging of the Resistivity Distribution Between Two Boreholes using an Automatic Data Collection and Switching System. Submittal date: 10/05/1998.
- 118959 LL981109904242.072. Electrical Properties of Tuff from the ESF as a Function of Water Saturation and Temperature. Submittal date: 11/19/1998.
- 169259 LL981110704244.085. Large Block Test Report, Chapter 4, Instrumentation and Monitoring. Submittal date: 11/20/1998.
- 158270 LL981202305912.004. Investigation of Bacterial Transport in the Large Block Test, a Thermally Perturbed Block of Topopah Spring Tuff. Submittal date: 12/03/1998.
- 158263 LL981208404244.092. X-Ray Radiography of Fracture Flow and Matrix Imbibition in Topopah Spring Tuff Under a Thermal Gradient. Submittal date: 12/08/1998.
- 113872 LL990702704244.099. Data for the Drift Scale Test. Submittal date: 07/13/1999.
- 144922 LL990702804244.100. Borehole and Pore Water Data. Submittal date: 07/13/1999.
- 153836 MO0001SEPDSTPC.000. Drift Scale Test (DST) Temperature, Power, Current, and Voltage Data for June 1, 1999 through October 31, 1999. Submittal date: 01/12/2000.
- 147304 MO0002ABBLSLDS.000. As-Built Borehole Locations and Sensor Locations for the Drift Scale Test Given in Local (DST) Coordinates. Submittal date: 02/01/2000.
- 150930 MO0005PORWATER.000. Perm-Sample Pore Water Data. Submittal date: 05/04/2000.
- 153707 MO0007SEPDSTPC.001. Drift Scale Test (DST) Temperature, Power, Current, and Voltage Data for November 1, 1999 through May 31, 2000. Submittal date: 07/13/2000.
- 153708 MO0012SEPDSTPC.002. Drift Scale Test (DST) Temperature, Power, Current, and Voltage Data for June 1, 2000 through November 30, 2000. Submittal date: 12/19/2000.

- 153711 MO0101SEPFDDST.000. Field Measured Data of Water Samples from the Drift Scale Test. Submittal date: 01/03/2001.
- 158321 MO0107SEPDSTPC.003. Drift Scale Test (DST) Temperature, Power, Current, and Voltage Data for December 1, 2000 through May 31, 2001. Submittal date: 07/06/2001.
- 158320 MO0202SEPDSTTV.001. Drift Scale Test (DST) Temperature, Power, Current, and Voltage Data for June 1, 2001 through January 14, 2002. Submittal date: 02/28/2002.
- 159300 MO0207AL5WATER.001. Water Sampling in Alcove 5 (Results from 2/4/1997 through 4/20/1999). Submittal date: 07/11/2002.
- 161767 MO0208SEPDSTTD.001. Drift Scale Test (DST) Temperature Data for January 15, 2002 through June 30, 2002. Submittal date: 08/29/2002.
- 165698 MO0303SEPDSTTM.000. Drift Scale Test (DST) Temperature Data for July 1, 2002 through December 31, 2002. Submittal date: 03/17/2003.
- 165699 MO0307SEPDST31.000. Drift Scale Test (DST) Temperature Data for 01/01/2003 through 06/30/2003. Submittal date: 07/07/2003.
- 177813 MO0403SEPDST32.000. Drift Scale Test (DST) Temperature Data for July 1, 2003 through December 31, 2003. Submittal date: 03/08/2004.
- 177814 MO0408SEPDSTTD.000. Drift Scale Test (DST) Temperature Data for January 1, 2004 through June 30, 2004. Submittal date: 08/18/2004.
- 177815 MO0509SEPDSTTD.000. Drift Scale Test (DST) Temperature Data for July 1, 2004 through June 30, 2005. Submittal date: 09/01/2005.
- 177816 MO0603SEPDSTTD.000. Drift Scale Test (DST) Temperature Data for July 1, 2005 through December 31, 2005. Submittal date: 03/09/2006.
- 178054 MO0603SEPDSTTB.002. Drift Scale Test (DST) Temperature Borehole RTD Status as of December 31, 2005. Submittal date: 03/09/2006.
- 113644 MO9807DSTSET01.000. Drift Scale Test (DST) Temperature, Power, Current, Voltage Data for November 7, 1997 through May 31, 1998. Submittal date: 07/09/1998.
- 113662 MO9810DSTSET02.000. Drift Scale Test (DST) Temperature, Power, Current, Voltage Data for June 1 through August 31, 1998. Submittal date: 10/09/1998.

- 113673 MO9906DSTSET03.000. Drift Scale Test (DST) Temperature, Power, Current, and Voltage Data for September 1, 1998 through May 31, 1999. Submittal date: 06/08/1999.
- 153841 SN0001F3912298.014. Measurements of Displacement Data for the Drift Scale Test (with Results from 6/1/1999 through 10/31/1999). Submittal date: 01/18/2000.
- 158372 SN0001F3912298.015. Measurements of Strain Data for the Drift Scale Test (with Results from 6/1/1999 through 10/31/1999). Submittal date: 01/18/2000.
- 153842 SN0001F3912298.016. Measurements of Displacement Data for the Drift Scale Test Corrected for Thermal Expansion (with Results from 6/1/1999 through 10/31/1999). Submittal date: 01/18/2000.
- 158373 SN0001F3912298.017. Measurements of Strain Data for the Drift Scale Test Corrected for Thermal Expansion (with Results from 6/1/1999 through 10/31/1999). Submittal date: 01/18/2000.
- 158374 SN0007F3912298.018. Measurements of Displacement Data for the Drift Scale Test (with Results from 11/1/1999 through 5/31/2000). Submittal date: 07/17/2000.
- 158387 SN0007F3912298.019. Measurements of Strain Data for the Drift Scale Test (with Results from 11/1/1999 through 5/31/2000). Submittal date: 07/17/2000.
- 158388 SN0007F3912298.020. Measurements of Displacement Data for the Drift Scale Test Corrected for Thermal Expansion (with Results from 11/1/1999 through 5/31/2000). Submittal date: 07/17/2000.
- 158391 SN0007F3912298.021. Measurements of Strain Data for the Drift Scale Test Corrected for Thermal Expansion (with Results from 11/1/1999 through 5/31/2000). Submittal date: 07/17/2000.
- 158392 SN0011F3912298.022. Plate-Loading Measured Displacement and Test Pressure Data (with Results from 10/16/2000 through 10/17/2000). Submittal date: 11/30/2000.
- 158399 SN0011F3912298.023. Plate-Loading Rock Mass Modulus Data (with Results from 10/16/2000 through 10/17/2000). Submittal date: 11/30/2000.
- 158400 SN0101F3912298.024. Measurements of Displacement Data for the Drift Scale Test (with Results from 6/1/2000 through 11/30/2000). Submittal date: 01/18/2001.
- 158401 SN0101F3912298.025. Measurements of Strain Data for the Drift Scale Test (with Results from 6/1/2000 through 11/30/2000). Submittal date: 01/18/2001.

- 158402 SN0101F3912298.026. Measurements of Displacement Data for the Drift Scale Test Corrected for Thermal Expansion (with Results from 6/1/2000 through 11/30/2000). Submittal date: 01/18/2001.
- 158407 SN0101F3912298.027. Measurements of Strain Data for the Drift Scale Test Corrected for Thermal Expansion (with Results from 6/1/2000 through 11/30/2000). Submittal date: 01/18/2001.
- 158408 SN0107F3912298.029. Measurements of Displacement Data for the Drift Scale Test (with Results from 12/1/2000 through 5/31/2001). Submittal date: 07/09/2001.
- 158409 SN0107F3912298.030. Measurements of Strain Data for the Drift Scale Test (with Results from 12/1/2000 through 5/31/2001). Submittal date: 07/09/2001.
- 158413 SN0107F3912298.031. Measurements of Displacement Data for the Drift Scale Test Corrected for Thermal Expansion (with Results from 12/1/2000 through 5/31/2001). Submittal date: 07/09/2001.
- 158414 SN0107F3912298.032. Measurements of Strain Data for the Drift Scale Test Corrected for Thermal Expansion (with Results from 12/1/2000 through 5/31/2001). Submittal date: 07/09/2001.
- 159133 SN0203F3903102.001. Drift Scale Test Water Sampling (with Results from 4/17/2001 through 1/14/2002). Submittal date: 03/29/2002.
- 158361 SN0203F3912298.033. Measurements of Displacement Data for the Drift Scale Test (with Results from 6/1/2001 through 1/14/2002). Submittal date: 03/26/2002.
- 158362 SN0203F3912298.034. Measurements of Strain Data for the Drift Scale Test (with Results from 6/1/2001 through 1/14/2002). Submittal date: 03/26/2002.
- 158363 SN0203F3912298.035. Measurements of Displacement Data for the Drift Scale Test Corrected for Thermal Expansion (with Results from 6/1/2001 through 1/14/2002). Submittal date: 03/26/2002.
- 158364 SN0203F3912298.036. Measurements of Strain Data for the Drift Scale Test Corrected for Thermal Expansion (with Results from 6/1/2001 through 1/14/2002). Submittal date: 03/26/2002.
- 158322 SN0203L2210196.007. Thermal Expansion and Thermal Conductivity of Test Specimens from the Drift Scale Test Area of the Exploratory Studies Facility at Yucca Mountain, Nevada. VA Supporting Data. Submittal date: 03/06/2002.

- 178009 SN0209F3912298.040. Measurements of Displacement Data for the Drift Scale Test (with Results from 1/15/2002 through 6/30/2002). Submittal date: 09/11/2002.
- 178019 SN0209F3912298.041. Measurements of Strain Data for the Drift Scale Test (with Results from 1/15/2002 through 6/30/2002). Submittal date: 09/11/2002.
- 177941 SN0209F3912298.042. Measurements of Displacement Data for the Drift Scale Test Corrected for Thermal Expansion (with Results from 1/15/2002 through 6/30/2002). Submittal date: 09/11/2002.
- 178027 SN0209F3912298.043. Measurements of Strain Data for the Drift Scale Test Corrected for Thermal Expansion (with Results from 1/15/2002 through 6/30/2002). Submittal date: 09/11/2002.
- 170573 SN0210F3903102.004. Drift Scale Test Water Sampling (Results from 1/16/2002 through 4/4/2002). Submittal date: 10/22/2002.
- 170574 SN0211F3903102.005. Drift Scale Test Water Sampling (Results from 4/25/2002 through 8/28/2002). Submittal date: 12/06/2002.
- 178034 SN0303F3903102.006. Drift Scale Test Water Sampling (Results from 10/7/2002 through 2/18/2003). Submittal date: 04/02/2003.
- 178010 SN0303F3912298.044. Measurements of Displacement Data for the Drift Scale Test (with Results from 7/1/2002 through 12/31/2002). Submittal date: 03/19/2003.
- 178020 SN0303F3912298.045. Measurements of Strain Data for the Drift Scale Test (with Results from 7/1/2002 through 12/31/2002). Submittal date: 03/19/2003.
- 177945 SN0303F3912298.046. Measurements of Displacement Data for the Drift Scale Test Corrected for Thermal Expansion (with Results from 7/1/2002 through 12/31/2002). Submittal date: 03/19/2003.
- 178028 SN0303F3912298.047. Measurements of Strain Data for the Drift Scale Test Corrected for Thermal Expansion (with Results from 7/1/2002 through 12/31/2002). Submittal date: 03/19/2003.
- 165416 SN0306F3912298.048. Plate-Loading Measured Displacement and Test Pressure Data for 2003 (with Results from 4/30/2003). Submittal date: 06/25/2003.
- 178011 SN0308F3912298.050. Measurements of Displacement Data for the Drift Scale Test (with Results from 1/1/2003 through 6/30/2003). Submittal date: 08/29/2003.

- 178021 SN0308F3912298.051. Measurements of Strain Data for the Drift Scale Test (with Results from 1/1/2003 through 6/30/2003). Submittal date: 08/29/2003.
- 177946 SN0308F3912298.052. Measurements of Displacement Data for the Drift Scale Test Corrected for Thermal Expansion (with Results from 1/1/2003 through 6/30/2003). Submittal date: 08/29/2003.
- 178029 SN0308F3912298.053. Measurements of Strain Data for the Drift Scale Test Corrected for Thermal Expansion (with Results from 1/1/2003 through 6/30/2003). Submittal date: 08/29/2003.
- 168527 SN0310F3912298.054. Updated Plate-Loading Rock Mass Modulus Data for 2003. Submittal date: 10/27/2003.
- 178035 SN0311F3903102.007. Drift Scale Test Water Sampling in Alcove 5 (Results from 4/3/2003 through 10/7/2003). Submittal date: 01/13/2004.
- 169262 SN0401F3511695.012. Evaluation and Comparative Analysis of Single Heater Test Thermal and Thermomechanical Data: First Quarter FY98 Results (8/26/96 through 11/30/97), Revised January 2004. Submittal date: 01/08/2004.
- 169263 SN0401F3511695.013. Thermal and Thermomechanical Data for the Single Heater Test Final Report, Revised January 2004. Submittal date: 01/08/2004.
- 178030 SN0403F3912298.058. Measurements of Strain Data for the Drift Scale Test Corrected for Thermal Expansion (with Results from 7/1/2003 through 12/31/2003). Submittal date: 04/09/2004.
- 178022 SN0403F3912298.056. Measurements of Strain Data for the Drift Scale Test (with Results from 7/1/2003 through 12/31/2003). Submittal date: 04/09/2004.
- 178031 SN0410F3912298.064. Measurements of Strain Data for the Drift Scale Test Corrected for Thermal Expansion (with Results from 1/1/2004 through 6/30/2004). Submittal date: 10/14/2004.
- 178012 SN0403F3912298.055. Measurements of Displacement Data for the Drift Scale Test (with Results from 7/1/2003 through 12/31/2003). Submittal date: 04/09/2004.
- 177948 SN0403F3912298.057. Measurements of Displacement Data for the Drift Scale Test Corrected for Thermal Expansion (with Results from 7/1/2003 through 12/31/2003). Submittal date: 04/09/2004.
- 178013 SN0410F3912298.061. Measurements of Displacement Data for the Drift Scale Test (with Results from 1/1/2004 through 6/30/2004). Submittal date: 10/14/2004.



- 178023 SN0410F3912298.062. Measurements of Strain Data for the Drift Scale Test (with Results from 1/1/2004 through 6/30/2004). Submittal date: 10/14/2004.
- 177973 SN0410F3912298.063. Measurements of Displacement Data for the Drift Scale Test Corrected for Thermal Expansion (with Results from 1/1/2004 through 6/30/2004). Submittal date: 10/14/2004.
- 178036 SN0411F3903102.009. Drift Scale Test Water Sampling in Alcove 5 on May 11, 2004 and August 16, 2004. Submittal date: 11/22/2004.
- 178037 SN0507F3903102.010. Drift Scale Test Water Sampling in Alcove 5 on January 27, 2004. Submittal date: 07/19/2005.
- 178038 SN0510F3903102.012. Drift Scale Test Water Sampling in Alcove 5 on January 25, 2005 and June 2, 2005. Submittal date: 10/24/2005.
- 178039 SN0511F3903102.013. Drift Scale Test Water Sampling in Alcove 5 on November 8, 2005. Submittal date: 11/16/2005.
- 178024 SN0601F3912298.066. Measurements of Strain Data for the Drift Scale Test (with Results from 7/1/2004 through 6/30/2005). Submittal date: 03/01/2006.
- 178014 SN0601F3912298.065. Measurements of Displacement Data for the Drift Scale Test (with Results from 7/1/2004 through 6/30/2005). Submittal date: 03/01/2006.
- 178005 SN0601F3912298.067. Measurements of Displacement Data for the Drift Scale Test Corrected for Thermal Expansion (with Results from 7/1/2004 through 6/30/2005). Submittal date: 03/01/2006.
- 178032 SN0601F3912298.068. Measurements of Strain Data for the Drift Scale Test Corrected for Thermal Expansion (with Results from 7/1/2004 through 6/30/2005). Submittal date: 03/01/2006.
- 178015 SN0608F3912298.069. Measurements of Displacement Data for the Drift Scale Test (with Results from 7/1/2005 through 6/30/2006). Submittal date: 09/08/2006.
- 178025 SN0608F3912298.070. Measurements of Strain Data for the Drift Scale Test (with Results from 7/01/2005 through 6/30/2006). Submittal date: 09/08/2006.
- 177975 SN0608F3912298.071. Measurements of Displacement Data for the Drift Scale Test Corrected for Thermal Expansion (with Results from 7/1/2005 through 6/30/2006). Submittal date: 09/08/2006.

- 178033 SN0608F3912298.072. Measurements of Strain Data for the Drift Scale Test Corrected for Thermal Expansion (with Results from 7/01/2005 through 6/30/2006). Submittal date: 09/08/2006.
- 158315 SNF35110695001.001. Single Heater Test: As-Built Gage Layouts (Thermocouples, Thermistors, MPBX's). Submittal date: 09/25/1996.
- 158300 SNF35110695001.010. Goodman Jack Measurements in the Single Heater Test Block. Submittal date: 05/25/1999.
- 159130 SNF38040197001.001. Heated Drift Test: SNL As-Built Gauge Table (Thermomechanical Gauges Only). Submittal date: 01/06/1998.
- 159114 SNF39012298002.002. Measurements of Displacement Data for the Drift Scale Test (with Results from 11/1/1997 through 5/31/1998). Submittal date: 07/09/1998.
- 158417 SNF39012298002.003. Measurements of Strain Data for the Drift Scale Test (with Results from 11/9/1997 through 5/31/1998). Submittal date: 09/24/1998.
- 153837 SNF39012298002.004. Measurements of Displacement Data for the Drift Scale Test Corrected for Thermal Expansion (Results from 11/9/1997 through 5/31/1998). Submittal date: 09/24/1998.
- 158418 SNF39012298002.005. Measurements of Strain Data for the Drift Scale Test Corrected for Thermal Expansion (Results from 11/9/1997 through 5/31/1998). Submittal date: 09/24/1998.
- 158419 SNF39012298002.006. Measurements of Displacement Data for the Drift Scale Test (with Results from 6/1/1998 through 8/31/1998). Submittal date: 10/08/1998.
- 158365 SNF39012298002.007. Measurements of Strain Data for the Drift Scale Test (with Results from 6/1/1998 through 8/31/1998). Submittal date: 10/08/1998.
- 153839 SNF39012298002.008. Measurements of Displacement Data for the Drift Scale Test Corrected for Thermal Expansion (Results from 6/1/1998 through 8/31/1998). Submittal date: 10/08/1998.
- 158366 SNF39012298002.009. Measurements of Strain Data for the Drift Scale Test Corrected for Thermal Expansion (Results from 6/1/1998 through 8/31/1998). Submittal date: 10/08/1998.
- 158367 SNF39012298002.010. Measurements of Displacement Data for the Drift Scale Test (with Results from 9/1/1998 through 5/31/1999). Submittal date: 06/28/1999.

- 158368 SNF39012298002.011. Measurements of Strain Data for the Drift Scale Test (with Results from 9/1/1998 through 5/31/1999). Submittal date: 06/28/1999.
- 153840 SNF39012298002.012. Measurements of Displacement Data for the Drift Scale Test Corrected for Thermal Expansion (with Results from 9/1/1998 through 5/31/1999). Submittal date: 06/28/1999.
- 158369 SNF39012298002.013. Measurements of Strain Data for the Drift Scale Test Corrected for Thermal Expansion (with Results from 9/1/1998 through 5/31/1999). Submittal date: 06/28/1999.
- 158420 SNL02100196001.001. Unconfined Compression Tests on Specimens from the Drift Scale Test Area of the Exploratory Studies Facility at Yucca Mountain, Nevada. Submittal date: 05/14/1997.
- 109722 SNL22080196001.001. Thermal Properties of Test Specimens from the Single Heater Test Area in the Thermal Testing Facility at Yucca Mountain, Nevada. Submittal date: 08/15/1996.
- 158306 SNL22080196001.002. Unconfined Compression Tests on Specimens from the Single Heater Test Area in the Thermal Testing Facility at Yucca Mountain, Nevada. Submittal date: 08/22/1996.
- 119042 SNL22080196001.003. Posttest Laboratory Thermal and Mechanical Characterization for Single Heater Test (SHT) Block. Submittal date: 08/26/1998.
- 111068 SNL22100196001.003. Thermal Expansion of Carbon Fiber and Invar Rods. Submittal date: 09/16/1997.
- 158213 SNL22100196001.006. Laboratory Measurements of Thermal Conductivity as a Function of Saturation State for Welded and Nonwelded Tuff Specimens. Submittal date: 06/08/1998.
- 158370 SNL23030598001.001. Unconfined Compression Tests on Cast-in-Place Concrete Specimens from the Drift Scale Test in the ESP (Exploratory Studies Facility) at Yucca Mountain, Nevada. Submittal date: 03/10/1998.
- 159115 UN0106SPA013GD.003. Drift Scale Thermal Test (DST) REKA Probe Acquired Data for Thermal Conductivity and Diffusivity for the Period 05/01/1998 to 04/30/2001 (Heated Measurements for Boreholes 151, 152, and 153). Submittal date: 06/13/2001.
- 159116 UN0106SPA013GD.004. Drift Scale Thermal Test (DST) REKA Probe Developed Data for Thermal Conductivity and Diffusivity for the Period 05/01/1998 to 04/30/2001 (Heated Measurements for Boreholes 151, 152, and 153). Submittal date: 06/28/2001.

- 159117 UN0109SPA013GD.005. Drift Scale Test (DST) Rapid Evaluation of K and Alpha (REKA) Probe Acquired Data for Thermal Conductivity and Diffusivity for the Period 05/01/2001 to 08/31/2001 (Heated Measurements for Boreholes 151, 152, and 153). Submittal date: 09/28/2001.
- 159118 UN0112SPA013GD.006. DST REKA Probe Acquired Data for Thermal Conductivity and Diffusivity for the Period 09/01/2001 to 12/31/2001 (Heated Measurements for Boreholes 151, 152, and 153). Submittal date: 12/31/2001.
- 159119 UN0201SPA013GD.007. DST REKA Probe Developed Data for Thermal Conductivity and Diffusivity for the Period 05/01/2001 to 12/31/2001 (Heated Measurements for Boreholes 151 and 152). Submittal date: 01/07/2002.

#### **8.4 SUMMARY DATA, LISTED BY DATA TRACKING NUMBER**

- 170575 LB0208ACEMDSTH.001. Acoustic Emission for the Heating Phase of the DST. Submittal date: 08/09/2002.
- 160897 LB0208AIRKDSTH.001. Air Permeability Data for the Heating Phase of the DST. Submittal date: 08/09/2002.
- 170576 LB0208AIRKSHTC.001. Air Permeability Data for the Heating and Cooling Phases of the SHT. Submittal date: 08/12/2002.
- 170577 LB0208GPRDSTHP.001. GPR for the Heating Phase of the DST. Submittal date: 08/09/2002.
- 170578 LB0208GPRSHTCP.001. GPR for the Heating and Cooling Phases of the SHT. Submittal date: 08/12/2002.
- 170579 LB0208H2ODSTHP.001. Passive Hydrological Data for the Heating Phase of the DST. Submittal date: 08/09/2002.
- 161638 LB0208ISODSTHP.001. Isotope Data and CO2 Analysis for the Heating Phase of the DST. Submittal date: 08/09/2002.
- 161677 LL020709923142.023. Aqueous Geochemistry of Borehole Waters Collected in the Heating Phase of the DST. Submittal date: 07/26/2002.
- 164182 LL020710523142.025. Temperatures, Heater Powers, and Rock Displacements of the Large Block Test. Submittal date: 09/10/2002.
- 170580 LL020801723142.028. Electrical Resistance Tomographs of the Drift Scale Test, November 1997 through December 2001. Submittal date: 08/07/2002.
- 170581 LL020801823142.029. Electrical Resistance Tomographs of the Single Heater Test, August 1996 through December 1997. Submittal date: 08/07/2002.

- 161129 MO0208RESTRDST.002. Restructured Drift Scale Test (DST) Heating Phase Power and Temperature Data. Submittal date: 08/06/2002.
- 170582 MO0208RESTRSHT.002. Restructured Single Heater Test (SHT) Heating Phase Power and Temperature Data. Submittal date: 08/06/2002.
- 170615 MO0406SEPDSTHP.000 Drift Scale Test (DST) Heating Phase Power and Reference Temperature Data. Submittal date: 06/07/2004.
- 170616 MO0406SEPTVDST.000 Temperature and Volume Water Content for Drift Scale Test (DST) Heating Phase for Boreholes 79 and 80. Submittal date: 06/29/2004.
- 161246 SN0208F3903102.002. Summary of Thermal Test Water Samples and Field Measurements through 1/14/2002. Submittal date: 08/16/2002.
- 170620 SN0208F3903102.003. Field Measurements and Fluoride Content from HF (Hydrogen-Fluoride) Tests. Submittal date: 08/16/2002.
- 170610 SN0208F3912298.038. Summary of Smoothed Measurements of Strain Data for the Heating Phase of the Drift Scale Test (with Results from 12/3/1997 through 1/14/2002). Submittal date: 08/16/2002.
- 170627 SN0407F3912298.060. Rock Mass Thermal Expansion Coefficients from the Drift Scale Test (DST) Compared with In Situ Measurements. Submittal date: 07/13/2004.

INTENTIONALLY LEFT BLANK